PROGRAM

LPI CONTRIBUTION NO. 1184

LUNAR AND PLANETARY INSTITUTE

USRA

PROGRAM FOR TECHNICAL SESSIONS

THIRD INTERNATIONAL CONFERENCE ON MARS POLAR SCIENCE AND EXPLORATION

OCTOBER 13–17, 2003
ALBERTA, CANADA

SPONSORS

Lunar and Planetary Institute
National Aeronautics and Space Administration
Canadian Space Agency
International Glaciological Society
Geological Survey of Canada
University of Alberta, Department of Earth and Atmospheric Sciences
NASA Mars Program Office

CONVENERS

Stephen Clifford, *Lunar and Planetary Institute*
Peter Doran, *University of Illinois at Chicago*
David Fisher, *Geological Survey of Canada*
Christopher Herd, *University of Alberta*

SCIENCE ORGANIZING COMMITTEE

Planetary Members

Alain Berinstain, *Canadian Space Agency*
William Boynton, *University of Arizona*
Mike Carr, *U.S. Geological Survey, Menlo Park*
Frank Carsey, *Jet Propulsion Laboratory*
William Durham, *Lawrence Livermore National Laboratory*
Jack Farmer, *Arizona State University*
James Garvin, *NASA Goddard Spaceflight Center*
Rejean Grard, *European Space Agency/ESTEC*
Robert Haberle, *NASA Ames Research Center*
Ken Herkenhoff, *U.S. Geological Survey, Flagstaff*
Hugh Kieffer, *U.S. Geological Survey, Flagstaff*
Pascal Lee, *NASA Ames Research Center*
Daniel McCleese, *NASA Jet Propulsion Laboratory*
Christopher McKay, *NASA Ames Research Center*
Jeffrey Plaut, *NASA Jet Propulsion Laboratory*
James Rice Jr., *Arizona State University*
David Smith, *NASA Goddard Spaceflight Center*
Ken Tanaka, *U.S. Geological Survey, Flagstaff*
Peter Thomas, *Cornell University*
Maria Zuber, *Massachusetts Institute of Technology*

Terrestrial Members

Walter Ammann, *Swiss Federal Institute for Snow and Avalanche Research*
Nobuhiko Azuma, *Nagaoka University of Technology*
Charles Cockell, *British Antarctic Survey*
Dorthe Dahl-Jensen, *University of Copenhagen*
Sigfus Johnsen, *University of Copenhagen*
Shawn Marshall, *University of Calgary*
John Nye, *University of Bristol*
Wayne Pollard, *McGill University*
Todd Sowers, *Pennsylvania State University*
Lonnie Thompson, *Byrd Polar Research Center*
Thorsteinn Thorsteinsson, *National Energy Authority and University of Iceland*
Eske Willerslev, *University of Copenhagen*

** Denotes speaker*

Monday, October 13, 2003
Morning Session I
SETTING THE STAGE
8:15 a.m. Victoria Room

WELCOME, INTRODUCTIONS, AND IMPORTANT ANNOUNCEMENTS

Clifford S. * Parker T.
A Brief Summary of Important Issues in the Hydrologic and Climatic Evolution of Mars

McCleese D. * [INVITED]
Future Exploration of Mars: Opportunities for Polar Investigations

THE LATEST FROM MARS: GRS

Boynton W. V. * Chamberlain M. Feldman W. C. Prettyman T. Hamara D. Janes D. Kerry K. GRS Team [INVITED]
Ice in the Polar Regions of Mars: Evidence for Wet Periods in the Recent Past **[#8133]**

Feldman W. C. * Maurice S. Prettyman T. H. Mellon M. T. Squyres S. W. Karunatillake S. Elphic R. C. Funsten H. O. Lawrence D. J. Tokar R. L.
Association of Measured Distribution of Near-Surface Hydrogen at High Northerly Latitudes with Surface Features on Mars **[#8101]**

Litvak M. L. * Mitrofanov I. G. Kozyrev A. S. Sanin A. B. Tretyakov V. Boynton W. V. Hamara D. K. Shinohara C. Saunders R. S. Drake D.
Comparison Between North and South Near Polar Regions of Mars from HEND/Odyssey Data **[#8020]**

GENERAL DISCUSSION

10:15 – 10:30 a.m. BREAK

Monday, October 13, 2003
Morning Session II
THE LATEST FROM MARS: THEMIS
10:30 a.m. Victoria Room

Plaut J. J. * Christensen P. Bender K. Bell J. Cherednik L. Ivanov A. Kieffer H. McConnochie T. Richardson M. Titus T. [INVITED]
THEMIS Visible Imaging of the South Polar Layered Deposits, Martian Southern Spring, 2003 **[#8130]**

Ivanov A. B. * Byrne S. Richardson M. I. Vasavada A. R. Titus T. N. Bell J. F. McConnochie T. H. Christensen P. R. THEMIS Science Team
Analysis of Properties of the North and South Polar Layered Deposits **[#8084]**

GENERAL DISCUSSION

THE NATURE AND EVOLUTION OF THE SEASONAL POLAR CAPS

Smith D. E. * Zuber M. T. [INVITED]
The Masses of Mars/Seasonal Polar Icecaps **[#8063]**

12:00 – 1:30 p.m. LUNCH

Monday, October 13, 2003
Afternoon Session I
THE NATURE AND EVOLUTION OF THE SEASONAL POLAR CAPS *(Continued)*
1:30 p.m. Victoria Room

Zuber M. T. * Smith D. E. [INVITED]
Observations of the Seasonal Polar Icecaps of Mars at 1064 nm **[#8032]**

Prettyman T. H. * Feldman W. C. Murphy J. R. Funsten H. O. Lawrence D. J. Linn R. R. Maurice S. Tokar R. L.
Seasonal Advance and Retreat of Mars' South Polar Cap as Measured by the Mars Odyssey Neutron Spectrometer **[#8099]**

Calvin W. M. * Titus T. N. Mahoney S. A.
Constraints on the Within Season and Between Year Variability of the North Residual Cap from MGS-TES **[#8036]**

Titus T. N. * Kieffer H. H. Plaut J. J. Christensen P. R. Ivanov A. B. THEMIS Science Team
South Polar Cryptic Region Revisited: THEMIS Observations **[#8081]**

Kieffer H. H. * [INVITED]
Behavior of Solid CO_2 on Mars: Still a Zoo **[#8083]**

Hansen G. B. *
Evolution of Low-Emissivity Spots in the Martian Winter Polar Caps: Mobility of Dust Grains **[#8103]**

GENERAL DISCUSSION

3:30 – 3:45 p.m. BREAK

Monday, October 13, 2003
Afternoon Session II
PANEL DISCUSSION
3:45 p.m. Victoria Room

PANEL DISCUSSION
THE SOUTH POLAR CAP OF MARS: CO_2 MASS BALANCE, CLATHRATES, AND OTHER BIZARRE PROPERTIES

Moderator: Fisher D. A.
Panelists: Kieffer H. H. Haberle R. M. Thomas P. H. Schmidt B.

GENERAL DISCUSSION

Beaty D. W.*

Mars Exploration Program Advisory Group (MEPAG): Prioritized Goals, Objectives, and Investigations related to Mars Polar and Climate Research

Monday, October 13, 2003
POSTER SESSION I
7:00 – 9:30 p.m.

Ansan V. Mangold N.
"Cold" or "Warm" Early Mars: New Analysis of Warrego Valles from THEMIS and MOLA Data **[#8072]**

Ansan V. Mangold N.
Identification of Past Polar Deposits Among Layered Terrains on Mars: Preliminary Results **[#8071]**

Beaty D. W. Miller S. L. Bada J. L. Bearman G. H. Black P. B. Bruno R. J. Carsey F. D. Conrad P. G. Daly M. Fisher D. Hargreaves G. Henninger R. J. Huntsberger T. L. Lyons B. Mahaffy P. R. McNamara K. Mellon M. Papanastassiou D. A. Pollard W. Righter K. Rothschild L. Simmonds J. J. Spray J. G. Steele A. Zent A. P.
An Assessment of the Issues and Concerns Associated with the Analysis of Ice-bearing Samples by the 2009 Mars Science Laboratory **[#8076]**

Benson J. L. James P. B.
Yearly Comparisons of the Mars North Polar Cap: 1999, 2001, and 2003 MOC Observations **[#8097]**

Bonev B. P. James P. B. Bjorkman J. E. Hansen G. B. Wolff M. J.
Effects of Atmospheric and Surface Dust on the Sublimation Rates of CO_2 on Mars **[#8052]**

Byrne S. Ivanov A. B.
The Most Recent Section of the South Polar Layered Deposits **[#8108]**

Cockell C.
Challenges and Solutions for the Human Exploration of the Martian Poles **[#8126]**

Dassas K. Forget F.
Simulations of the Seasonal Variations of the Mars South Polar Cap: Preliminary Results **[#8054]**

Dohm J. M. Fairen A. G. Baker V. R. Ferris J. C. Anderson R. C. Uceda E. R.
Episodic Endogenetic-driven Atmospheric and Hydrologic Cycles and Their Influence on the Geologic Records of the Northern and Southern Hemispheres, Mars **[#8059]**

Eluszkiewicz J. Titus T. N.
A Microphysically-based Approach to Inferring Porosity, Grain Size, and Dust Abundance in the Seasonal Caps from Atmospherically-corrected TES Spectra **[#8068]**

Farrell W. M. Mahaffy P. R.
The Ability to Probe the Martian Polar Subsurface Via Ground-penetrating Radar **[#8014]**

Földi T. Bérczi Sz. Palásti E.
Experimental Instrument on Hunveyor for Collecting Bacteria by Their Electrostatic Coagulation with Dust Grains (FOELDIX): Observation of Electrostatical Precipitated Coagulated Units in a Nutrient Detector Pattern **[#8001]**

Forget F. Haberle R. M. Montmessin F. Cha S. Marcq E. Schaeffer J. Wanherdrick Y.
3D Simulations of the Early Mars Climate with a General Circulation Model **[#8070]**

Fritsen C. H. Priscu J. C. Doran P. T.
Bacterial Distribution and Production Within Lake Ice and Glacial Ice Along the Fringe of the Antarctic Ice Cap **[#8120]**

Haberle R. M. Mattingly B. Titus T. N.
Reconciling the MOLA, TES, and Neutron Observations of the North Polar CO_2 Mass Budget on Mars **[#8035]**

Hale A. S. Bass D. S. Tamppari L. K.
Albedo Variation on the Martian Northern Polar Cap as Seen by MGS **[#8066]**

Hecht M. H.
Speculations on Orbital Forcing of Sublimation from the Polar Caps **[#8092]**

Inada A. Richardson M. I. Toigo A. D.
Modeling Martian Fog Formation in the Northern High Latitudes During the Retreat of the Seasonal North Polar Cap **[#8077]**

Kanner L. C. Bell M. S. Allen C. C.
Prospecting for Martian Ice from Orbit **[#8113]**

Kargel J. S. Molnia B.
ASTER Imagery and Interpretation of Glaciers in Jasper National Park and Elsewhere in the Cordillera **[#8127]**

Kossacki K. J. Markiewicz W. J.
Seasonal Melting of Surface Water Ice Condensing in Martian Gullies **[#8031]**

Koutnik M. R. Byrne S. Murray B. C.
Surface Features of the South Polar Layered Deposits of Mars and Possible Terrestrial Analogues **[#8074]**

Kreslavsky M. A. Head J. W.
Polar Wander in the Geological History of Mars: Constraints from Topography Statistics **[#8085]**

Kronholm K. Johnson J. B. Schneebeli M.
Determining Structural and Mechanical Properties of Snow with a High-Resolution Penetrometer **[#8048]**

Kuhlman K. R. La Duc M. T. Kuhlman G. M. Anderson R. C. Newcombe D. A. Fusco W. Steucker T. Allenbach L. Ball C. Crawford R. L.
Preliminary Characterization of a Microbial Community of Rock Varnish from Death Valley, California **[#8057]**

Tuesday, October 14, 2003
Morning Session I
MARS' PRESENT-DAY ATMOSPHERIC CIRCULATION
8:15 a.m. Victoria Room

REVIEW OF THE DAY'S AGENDA

Montmessin F. * Haberle R. M. Forget F. Rannou P. Cabane M.
Describing the Components of the Water Transport in the Martian Atmosphere **[#8089]**

Tyler D. * Barnes J. R.
Simulation of Atmospheric Circulations Over the Summertime North Pole Using the OSU Mars MM5 **[#8129]**

Keating G. M. * Theriot M. E. Jr. Tolson R. H. Bougher S. W. Forget F. Angelats i Coll M. Forbes J. M.
Recent Detection of Winter Polar Warming in the Mars Upper Atmosphere **[#8033]**

Colaprete A. * Haberle R. M.
Carbon Dioxide Convection in the Martian Polar Night and Its Implications for Polar Processes **[#8064]**

Bridger A. F. C. * Haberle R. M. Hollingsworth J. L.
Interannual Atmospheric Variability Simulated by a Mars GCM: Impacts on the Polar Regions **[#8111]**

PANEL DISCUSSION
PRESENT-DAY INTERANNUAL VARRIATIONS
IN THE TRANSPORT OF CO_2, H_2O, AND DUST INTO THE MARTIAN POLAR REGIONS
Moderator: Haberle R. M.
Panelists: Forget F. James P. Tyler D. Bridger A. F.

GENERAL DISCUSSION

10:15 – 10:30 a.m. BREAK

Tuesday, October 14, 2003
Morning Session II
GEOLOGY OF THE MARTIAN SOUTH POLAR LAYERED DEPOSITS
10:30 a.m. Victoria Room

Head J. W. * Ghatan G. J. Marchant D. [INVITED]
Extensive Hesperian-aged South Circumpolar Ice Sheet on Mars: Dorsa Argentea Formation Synthesis **[#8067]**

Herkenhoff K. E. * Soderblom L. A. Kirk R. L. [INVITED]
Stratigraphy and Structure of the South Polar Layered Deposits on Mars **[#8030]**

Thomas P. C. *
The South Polar Residual Cap of Mars: Layers, Erosion, and Stratigraphy **[#8047]**

Byrne S. * Ingersoll A. P. Pathare A. V. Jiron F. S.
Climactic History from South Polar Residual Cap Geomorphology **[#8037]**

12:00 – 1:30 p.m. LUNCH

Tuesday, October 14, 2003
Afternoon Session I
GEOLOGY OF THE MARTIAN SOUTH POLAR LAYERED DEPOSITS *(Continued)*
1:30 p.m. Victoria Room

Kolb E. J. * Tanaka K. L.
Detailed Geologic Analysis of Part of the South Polar Layered Deposits, Planum Australe, Mars **[#8116]**

van Gasselt S. * Jaumann R.
Chasma Australe, Mars: Formation by Successive Headward Thermo-Erosional Collapses **[#8098]**

GENERAL DISCUSSION

GEOLOGY OF THE MARTIAN NORTH POLAR LAYERED DEPOSITS

Fishbaugh K. E. * Head J. W. III [INVITED]
Amazonian Geologic History of the North Polar Cap of Mars: Stratigraphy, Melting, and Retreat **[#8050]**

Payne M. C. * Farmer J. D.
Using Mars Orbiter Laser Altimeter Data to Detect Subglacial Features at the Residual North Polar Ice Cap **[#8002]**

Ng F. S. L. * Zuber M. T.
Albedo Feedback in the Patterning Mechanisms of Martian Polar Caps **[#8061]**

3:30 – 3:45 p.m. BREAK

Tuesday, October 14, 2003
Afternoon Session II
GEOLOGY OF THE MARTIAN NORTH POLAR LAYERED DEPOSITS *(Continued)*
3:45 p.m. Victoria Room

Milkovich S. M. * Head J. W. III
North Polar Cap of Mars: Correlation of Layers Within and Between Troughs **[#8082]**

Pathare A. V. * Paige D. A.
The Sublimation and Relaxation of Troughs and Scarps Within the Martian North Polar Layered Deposits **[#8087]**

PANEL DISCUSSION
THE MARTIAN POLAR LAYERED DEPOSITS: THE ROLE OF MELTING AND FLOW
Moderator: Fisher D. A.
Panelists: Tanaka K. L. Nye J. F. Kargel J. S. Durham W. B. Fishbaugh K. E.

GENERAL DISCUSSION

PANEL DISCUSSION
THE DEVELOPMENT OF ICE-RICH SOILS ON EARTH:
A TERRESTRIAL PERSPECTIVE ON THE MARS GRS RESULTS
Moderator: Clifford S. M.
Panelists: Marchant D. R. Boynton W. V. Feldman W. C. Litvak M. L. Moorman B.

GENERAL DISCUSSION

Tuesday, October 14, 2003
POSTER SESSION II
7:00 – 9:30 p.m.

Leverington D. W.
Preliminary Results from a Survey of Candidate Permafrost and Periglacial Features on Mars **[#8013]**

Lim D. S. S. Douglas M. S. V.
The Use of Paleolimnology for Tracking Climate Change in the Canadian High Arctic – Analogies for Mars Exploration **[#8004]**

Longhi J.
Some Applications of CO_2-H_2O Phase Equilibria to the Composition and Evolution of the Martian Polar Ice Caps **[#8100]**

Määttänen A. Korhonen H. Lehtinen K. E. J. Vehkamäki H. Kulmala M.
An Investigation of Aerosol Dynamics in the Atmosphere of Mars **[#8045]**

Mangold N.
Distribution and Climatic Control of Small Scale Polygons on Mars **[#8044]**

Mangold N. Maurice S. Feldman W. Costard F. Forget F.
Geographical Relationships Between Small Scale Polygons and Ground Ice Distribution from Neutron Spectrometer on Mars **[#8043]**

Marchant D. R. Head J. W. Kreslavsky M. A.
Tongue-shaped Lobes on Mars: Relation to Rock Glacier Deposits and Long-Term History of Emplacement **[#8106]**

Markiewicz W. J. Kossacki K. J.
CO_2 Ice in Polygonal Troughs in Malea Planum, Mars: Sub-Surface H_2O Ice, MOC Images and TES Surface Temperature **[#8042]**

Matzl M. Schneebeli M.
Combining Micro-Penetrometer and Near-Infrared Photography to Measure Physical Properties in Snow Profiles **[#8062]**

Moersch J. E. Drake D. M.
Neutron Detector for Mars Rover Missions **[#8093]**

Moudden Y. Beagley S. R. Fomichec V. McConnell J. C. Akingunola A. Garcia Munioz A.
Development of a Mars General Circulation Model **[#8034]**

Nieto C. E. Stewart R. R.
Geophysical Investigations at a Mars Analog Site: Devon Island, Nunavut **[#8115]**

Ouvarova T. Caldwell J. Atreya S. Wong A. Renno N. James P.
Hubble Space Telescope Search for Localized Outgassing on Mars **[#8065]**

Pathare A. V. Marchant D. R. Head J. W.
Preservation of Ancient Glacial Ice Below Sublimation Till in the Dry Valleys of Antarctica: Implications for Mars **[#8114]**

Pettinelli E. Burghignoli P. Galli A. Pisani A. R. Ticconi F. Del Vento D. Cereti A.
Electromagnetic Propagation Modelling for GPR Exploration of Martian Subsoil **[#8080]**

Portyankina G. Markiewicz W. J.
Model for Formation of Spider Patterns in the Cryptic Region **[#8026]**

Schmidt K. G.
Investigation of Exchange Processes in the Martian Water Cycle **[#8008]**

Schmitt B. Mulato L. Douté S.
The Formation and Detectability of CO_2 Clathrate Hydrate on Mars **[#8073]**

Siili T. Määttänen A.
Sublimation and Condensation Flows in Chasma Borealis: A Sensitivity Study Using a 2-D Ensemble Mesoscale Circulation Model **[#8046]**

Simoes S. Trautner R. Grard R.
The Application of the Electric Sounding Technique to the Search for Water at Shallow Depths with Planetary Landers and Rovers: A Survey of the RSSD-ESA Activities **[#8010]**

Tamppari L. K. Smith M. D. Hale A. S. Bass D. S.
Interannual Comparison of Water Vapor in the North Polar Region of Mars **[#8119]**

van Gasselt S. Reiß D. Jaumann R.
Distribution and Morphology of Polygons, South Polar Region, Mars **[#8088]**

Vasavada A. R. Richardson M. I. Byrne S. Ivanov A. B. Christensen P. R. THEMIS Team
Thermophysical Properties of Mars' North Polar Layered Deposits and Related Materials from Mars Odyssey THEMIS **[#8095]**

Wentworth S. J. Gibson E. K. Jr. McKay D. S.
Low-Temperature, Aqueous Alteration of Soil in Wright Valley, Antarctica, Compared with Aqueous Alteration on Mars **[#8128]**

Wilson A. T.
Life in Perennially Ice Covered Lakes on Mars — An Antarctic Analogue **[#8039]**

Woodworth-Lynas C. Guigné J. Y.
Ice Keel Scour Marks and Ice Floe Grounding Structures in Kasei Valles and Echus Chasma **[#8012]**

Wyatt M. B. Tanaka K. L.
Origin of MGS-TES Surface Compositions in the Northern Plains and Polar Region of Mars **[#8118]**

Wednesday, October 15, 2003
MID-CONFERENCE FIELD TRIP

Evening Session
SPECIAL SESSION: MARS POLAR AND CLIMATE SCOUT CONCEPTS
7:00 p.m. Victoria Room

McCleese D. *
Scout Missions and Future Exploration of the Martian Poles **[#8090]**

Pascal Team Haberle R. M. * [INVITED]
The Pascal Mars Scout Mission **[#8075]**

Sims M. H. * McKay C. P. [INVITED]
Long Day's Drive: An Alternative Paradigm for Martian Robotic Exploration **[#8053]**

Hecht M. H. * Saunders R. S. [INVITED]
CryoScout: A Descent Through the Mars Polar Cap **[#8078]**

Mahaffy P. R. * Atreya S. A. Fairbrother D. A. Farrell W. M. Gorevan S. Jones J. Mitrofanov I. Scott J. [INVITED]
The Mars POLar Aerobotic Reconnaissance (POLAR) Balloon Scout Mission **[#8038]**

Smith P. H. * [INVITED]
The Phoenix Scout Mission **[#8107]**

GENERAL DISCUSSION

Thursday, October 16, 2003
Morning Session I
RECENT CLIMATE CHANGE ON MARS: MODELING RESULTS
8:15 a.m. Victoria Room

REVIEW OF THE DAY'S AGENDA

Haberle R. M. * Montmessin F. Forget F. Spiga A. Colaprete A. [INVITED]
Obliquity Driven Climate Change in Mars' Recent Past **[#8060]**

Wilson R. J. * Richardson M. I. Smith M. D.
The Polar Regions and Martian Climate: Studies with a Global Climate Model **[#8123]**

Levrard B. Laskar J. Forget F. * Montmessin F.
A GCM Recent History of the Northern Martian Polar Layered Deposits **[#8096]**

Mischna M. A. * McCleese D. J. Richardson M. I. Vasavada A. R. Wilson R. J.
Polar and Non-Polar Layers on Mars: A Single Mechanism for Formation? **[#8007]**

GENERAL DISCUSSION

10:15 – 10:30 a.m. BREAK

Thursday, October 16, 2003
Morning Session II
RECENT CLIMATE CHANGE ON MARS: GEOLOGIC EVIDENCE
10:30 a.m. Victoria Room

Mustard J. F. * Head J. W. Kreslavsky M. A. Milliken R. E. Marchant D. R.
Geological Observations, Climate Modeling, and Ice Stability: Evidence for Recent Martian Ice Ages **[#8055]**

Russell P. S. * Head J. W. Hecht M. H.
Volatile-rich Crater Interior Deposits in the Polar Regions of Mars: Evidence for Ice Cap Advance and Retreat **[#8086]**

Kargel J. S. * Molnia B. Tanaka K. L.
Martian Polar Ice Sheets and Mid-Latitude Debris-rich Glaciers, and Terrestrial Analogs **[#8112]**

Hartmann W. K. *
Upper Latitude Ice Flow, Gullies, and Long-Term Glacial History **[#8110]**

Head J. W. * Shean D. E. Milkovich S. Marchant D.
Tropical Mountain Glaciers on Mars: Evidence for Amazonian Climate Change **[#8105]**

GENERAL DISCUSSION

12:00 – 1:30 p.m. LUNCH

Thursday, October 16, 2003
Afternoon Session I
RHEOLOGY OF MARTIAN ICE-RICH MATERIALS
1:30 p.m. Victoria Room

Greve R. * Mahajan R. A.
Influence of Ice Rheology and Dust Content on the Dynamics of the North-Polar Cap of Mars **[#8003]**

Turtle E. P. * Pathare A. V. Crown D. A. Chuang F. C. Hartmann W. K. Greenham J. C. Bueno N. F.
Modeling the Deformation of Lobate Debris Aprons on Mars by Creep of Ice-rich Permafrost **[#8091]**

Durham W. B. * Kirby S. H. Stern L. A. Circone S. C.
The Rheology of CO_2 Clathrate Hydrate and Other Candidate Ices in the Martian Polar Caps **[#8132]**

PANEL DISCUSSION
NATURE, ORIGIN, AND EVOLUTION OF
MID-LATITUDE DEPOSITIONAL MANTLES AND DEBRIS/FLOW FEATURES
Moderator: Clifford S. M.
Panelists: Mangold N. Hartmann W. K. Turtle E. P. Mustard J. F.

GENERAL DISCUSSION

3:30 – 3:45 p.m. BREAK

Thursday, October 16, 2003
Afternoon Session II
GOING DEEP THROUGH ICE ON EARTH AND MARS
3:45 p.m. Victoria Room

Carsey F. D. * Hecht M. H. [INVITED]
Evolving Technologies for In-Situ Studies of Mars Ice **[#8102]**

Dahl-Jensen D. * Johnsen S. Willerslev E. Miller H. Thorsteinsonn Th.
Basal Water at the NorthGRIP Drill Site **[#8135]**

Thorsteinsson Th. * Jóhannesson T. Larsen G. Sigurdsson O. Schmidt K. G. Forwick M.
Dust Flux into the Grímsvötn Subglacial Lake, Vatnajökull Ice Cap, Iceland, Estimated from Ice Core Data **[#8134]**

Briggs G. A. * McKay C. George J. Derkowski G. Cooper G. Zacny K. Fincher R.
Pollard W. Clifford S.
An Automated, Low Mass, Low Power Drill for Acquiring Subsurface Samples of Ground Ice for Astrobiology Studies on Earth and on Mars **[#8018]**

GENERAL DISCUSSION

6:30 – 9:00 p.m. CONFERENCE DINNER

John Shaw * [INVITED GUEST SPEAKER]
Alberta as Mars
Professor, Department of Earth and Atmospheric Sciences, University of Alberta

Friday, October 17, 2003
Morning Session I
ELECTROMAGNETIC SOUNDING INVESTIGATIONS OF EARTH AND MARS
8:15 a.m. Victoria Room

REVIEW OF THE DAY'S AGENDA

Plaut J. J. * Picardi G. MARSIS Team [INVITED]
Probing the Subsurface of the Martian Polar Regions with MARSIS on Mars Express **[#8131]**

Hamelin M. * Grard R. Berthelier J.-J. Ney R. Trautner R. Simoes F.
Detection and Localization of Mars Sub-Surface Ice by Surface Impedance Measurements from a Rover as Part of the WISDOM/PASTEUR and Other Rover Experiments **[#8006]**

Ori G. G. * Flamini E. Seu R. Marinangeli L.
Testing the SHARAD Experiment of Mars Reconnaissance Orbiter with a Flight Balloon over Polar Regions **[#8058]**

Grant J. A. * Leuschen C. J. Schutz A. E. Rudy J. Williams K. K.
Constraining the Nature and Distribution of Polar Deposits on Mars Using Ground Penetrating Radar **[#8017]**

GENERAL DISCUSSION

10:15 – 10:30 p.m. BREAK

Friday, October 17, 2003
Morning Session II
SPECIAL SESSION IN MEMORY OF DAVID WYNN-WILLIAMS:
LIFE AND ITS DETECTION IN EXTREME POLAR ENVIRONMENTS
10:30 a.m. Victoria Room

McKay C. P. * [INVITED]
The Polar Regions and the Search for Evidence of Life on Mars **[#8056]**

Cockell C. * Lee P. Osinski G. Fike D.
Life in Polar Impact-shocked Rocks — An Analog for Micro-Habitats at the Martian Poles **[#8124]**

Edwards H. G. M. * Moody C. A. Jorge Villar S. E. Wynn-Williams D. D.
Antarctic Analogues for Mars Exploration: A Raman Spectroscopic Study of Biogeological Signatures **[#8009]**

Willerslev E. * [INVITED]
The Preservation of DNA in Ice Sheets and Permafrost

12:00 – 1:30 p.m. LUNCH

Friday, October 17, 2003
Afternoon Session I
SPECIAL SESSION IN MEMORY OF DAVID WYNN-WILLIAMS:
LIFE AND ITS DETECTION IN EXTREME POLAR ENVIRONMENTS *(Continued)*
1:30 p.m. Victoria Room

Doran P. T. * Bar-Cohen Y. Fritsen C. Kenig F. McKay C. P. Murray A. Sherrit S.
Life Detection and Characterization of Subsurface Ice and Brine in the McMurdo Dry Valleys Using an Ultrasonic Gopher: A NASA Astep Project **[#8019]**

Christner B. C. * Priscu J. C.
Earth's Icy Biosphere **[#8121]**

Becker L. * Brinckerhoff W. Cotter R. J.
Detection of Organic Compounds in Polar Ices on Mars Using AP MALDI **[#8122]**

PANEL DISCUSSION
FINDING EVIDENCE OF LIFE IN ICY ENVIRONMENTS
Moderator: Doran P.
Panelists: McKay C. Willerslev E. Christner B. Becker L.

GENERAL DISCUSSION

3:30 – 3:45 BREAK

Friday, October 17, 2003
Afternoon Session II
PANEL AND MODERATED DISCUSSIONS
3:45 p.m. Victoria Room

PANEL DISCUSSION
NEW PERSPECTIVES ON MARS POLAR SCIENCE AND EXPLORATION
Moderator: Head J. W.
Panelists: Lim D. Russel P. Moudden Y. Portyankina G. Ouvarova T.

PANEL DISCUSSION
NEW PERSPECTIVES ON MARS POLAR SCIENCE AND EXPLORATION
Moderator: Clifford S. M.
Panelists: Kieffer H. H. Nye J. F. Head J. W. Haberle R. M.

MODERATED DISCUSSION
HIGH-PRIORITY INVESTIGATIONS AND RECOMMENDED MISSIONS

ANNOUNCEMENT OF CONFERENCE SPECIAL ISSUE, FOURTH INTERNATIONAL CONFERENCE IN 2005, AND CLOSING REMARKS

5:30 p.m. CONFERENCE ADJOURNS

"COLD" OR "WARM" EARLY MARS: NEW ANALYSIS OF WARREGO VALLES FROM THEMIS AND MOLA DATA . V. Ansan and N. Mangold, Orsay-Terre, FRE2566, CNRS et Université Paris-Sud, Bat. 509, 91405 ORSAY Cedex, France, ansan@geol.u-psud.fr.

Introduction: The debate about the Noachian climate is very dependent on the interpretation of geomorphic features like valley networks. Valley networks were first interpreted as surface runoff under warmer climate [1], but surface runoff has been criticized because of the low drainage density [2] and alternative hypothesis have been proposed in cold climate [e.g.3]. Flows sustained by regional hydrothermal activity have been involved especially for the Thaumasia region in which Warrego networks because of the association of runoff sources with old volcanoes and fault zone [4]. In this study we infirm this possibility and we show that fluvial activity due to precipitation is a likely process to form Warrego valleys. Evidences for such processes are taken from new MGS and Odyssey data.

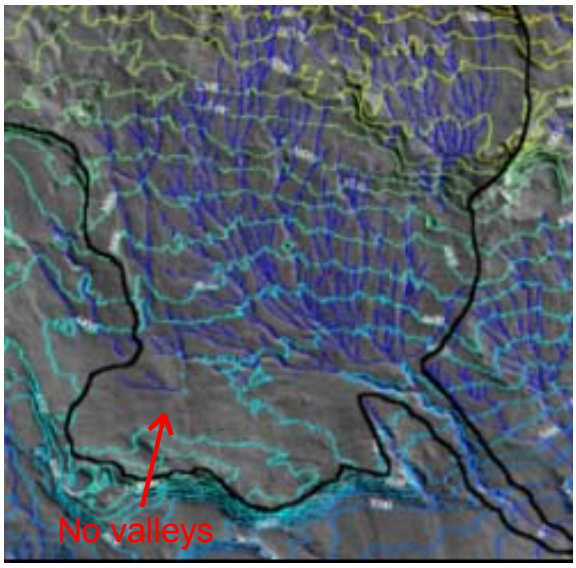

Fig. 1: Viking MDIM with MOLA elevation curves and warrego valles network in blue. Note the apparent absence of valleys on south flank whereas THEMIS data (Fig. 2) permit to identify valleys at this location.

MOC and THEMIS observations: Warrego Vallis is located on the southern part of the Thaumasia region, so the southern part of Tharsis bulge (Fig. 1). Other less developed networks similar in shape also exist on the flank east of Warrego. MOC high resolution images provide local information on the shape of valleys. Valleys are mantled by smooth material, likely dust eolian material. This filling of valleys makes the detection of small tributaries very difficult. New THEMIS IR images can be used to detect valleys that are not visible on Viking imagery. Indeed, THEMIS image south of the networks show several valleys not identified on the Viking images (Fig. 2). Their absence on Viking image (Fig. 1) is likely an effect of the sun incidence. THEMIS image permit to rebuilt a network geometry showing that the flank south of the main valley is involved in the network. The lack of volcanoes or large impact craters at the upper part of this south flank makes the hypothesis of hydrothermally controlled network unlikely. On the contrary, the smaller elevation difference of only 500 m on this flank may explain that valleys are less visible on Viking images.

Topography of the valley network: MOLA data shows that valley heads in the north part of the network occur at height of about 8 km. The average slope is of 0.03 with a total of 6000 m of elevation difference (Fig. 3). A usual criticism to runoff formed by precipitation is that networks are poorly dendritic, this means that intersection between rivers is low and not orthogonal like for dendritic pattern. However, the intersection angle depends strongly on the slope on which runoff forms. Terrestrial studies show that under about 0.026 of slopes (1.5°) the drainage is dendritic with nearly orthogonal intersections and up this value of 0.026 the drainage becomes parallel, with low angle intersections [5]. MOLA data shows that we are in the case of such parallel network, because slopes are of about 0.03 north of the main valley. The observed geometry is consistent with terrestrial parallel drainage due to the slope. On the contrary, the network is dendritic near the main valley where the slope is lower than 1.5°. In addition, we estimate a drainage density of 1.32 km^{-1}. This value is in the range of terrestrial environment by comparison to previous drainage densities usually less than 0.1 km^{-1} found from Viking data [2].

Origin of valley network: Finally, (1) MOC images show that valleys are strongly degraded and that small tributaries are possibly erased, (2) the regional slope measured by MOLA can explain the parallel geometry of the network and (3) THEMIS IR data shows that some valleys exist on the south flank showing that this network is not only controlled by sources on the northern part. Thus, evidences against runoff formed by precipitations are eliminated. On the contrary, it is unlikely that hydrothermal sources explain rivers in the south flank as they have their sources on a structural relief poorly related to any volcanic activity. Sapping is also difficult because it is controlled by layers and the geometry is different than typical sapping valley like Nirgal valleys. Moreover, the sources take place at elevations of up to 8 km which are the highest points

in the regions, making unlikely an underground system at such crest line without refilling by run off.

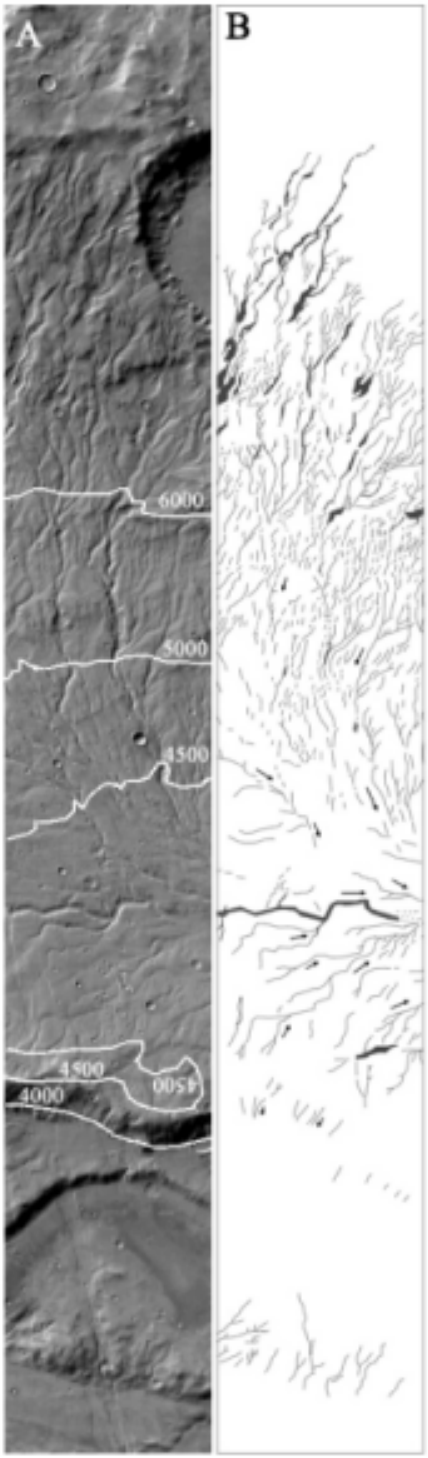

Fig. 2: A. Day-IR themis image I01714004 (100 m/pix) on which the MOLA altimetry is projected with a height interval of 500 m. B. In the lower part of the network, newly observed valleys connect to Warrego main valley with a North downstream. These valleys were not observed on Viking images.

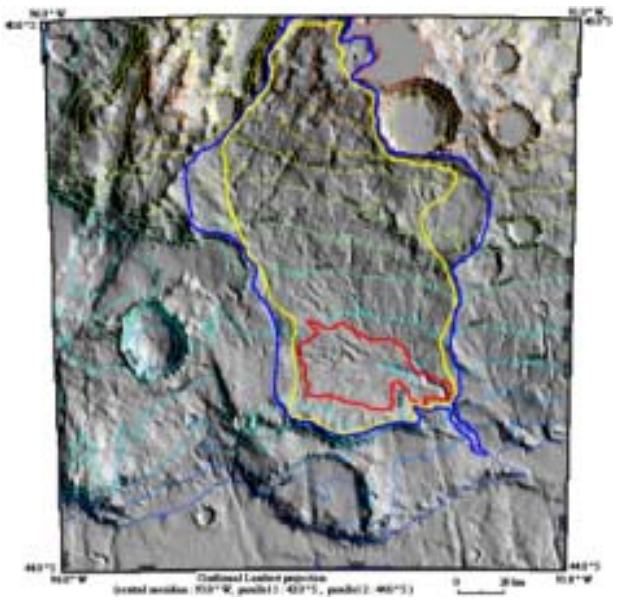

Fig. 3: Warrego Vallis from MOLA shaded relief. The yellow curve shows part of valley network where slopes are over 1.5°. The red curve limits the area where the slope is less than 1.5°. We see from the Themis data (Fig. 2) that the network is parallel in the yellow area and dendritic in the red area.

Conclusion: Using different sets of data, topography, visible and IR images at all possible scale, we show that Warrego valleys have characteristics in favour to surface runoff produced by precipitation. This conclusion favors observation such as those discussed by Craddock and Howard [7]. Warrego is a unique network in terms of density of drainage but the lack of other dense network can be explained because Warrego is one of the rare location with regional slope of more than 2°. Our conclusion, if confirmed by future works, would be useful to constrain climate models of Early Mars which often reject the possibility of warmer climate. It also shows the interest to use THEMIS data to identify valley networks on Mars.

References: [1] Craddock and Maxwell, *J.G.R.*, 102, E6, 13321-13340, 1997 [2] Carr, M. H., *J.G.R.*, 102 (E4), 9145-9152, 1997, [3] Carr, M. H., *Water on Mars*, 1996. [4] Dohm J. M. and K. L. Tanaka et al, *Planet. Spa. Sci*., 47, 411-431, 1999. [5] Schumm, S.A., M. P. Mosley and W. E. Weaver, *Experimental flows*, WileyInterscience, 1987 [6] Tooth., *Earth Science Reviews*, 51, 67-107, 2000, [7] Craddock and Howard, *J.G.R.*, 107, E11, 5111, 2002.

IDENTIFICATION OF PAST POLAR DEPOSITS AMONG LAYERED TERRAINS ON MARS: PRELIMINARY RESULTS V. Ansan and N. Mangold, Orsay-Terre, FRE2566, CNRS et Université Paris-Sud, Bat. 509, 91405 ORSAY Cedex, France, ansan@geol.u-psud.fr.

Introduction: The origin of layered terrains interpreted to be of sedimentary origin on Mars is debated since their discovery from Viking observations [1,2,3]. Lacustrine, fluvial, volcanic ashes, eolian, ancient polar deposition are the usual hypothesis for their origin. Recently, using MOC images, light-toned deposits have been interpreted as old Noachian deposits formed under water [1]. In this study, we focus on the differences in geologic context, age and geomorphic between deposits on the floor of 4 craters (Fig. 1). We conclude that 2 crater deposits are likely due to past processes involving water at surface, but that the 2 others have more debatable origin.

Location and context of 4 crater interiors analyzed:
Holden crater: 27°S, 35°W. 100 km large crater at the mouth of Uzboi valles. Layered deposits are several hundreds of meters thick.
Terby crater: 28°S, 285°W. 100 km large crater north of Hellas. The crater floor is dissected by canyons where layered deposits are observed over 1 km.
Spallanzani crater: 58°S, 274°W. South-East of Hellas crater. The 50 km large crater is filled by deposits of about 1.5 km thick.
Galle crater (not to confound with Gale crater): 52°S, 30°W. Crater east of Argyre. Deposits are 500 m thick on the south of the crater floor.

Geomorphic characteristics: The erosion of these layered deposits is different from one crater to the other. Holden and Terby crater floors are dissected in canyons and cliffs where layers are observed. These layers are strong and homogeneous with no large debris aprons on the foot of scarps. On the contrary, Spallanzani and Galle layers are not so uniform, with numerous interlayers with strong erosion and low strength as visible by lot of small scarps. They do not show the typical light ton but they could be covered by thin layer of dust. Closed pits and large yardangs due to wind action confirm that the material is not very much consolidated. By comparison, light-toned deposits also display yardangs (Fig. 1B) but at a scale very different which implies a more consolidated material.

Age from stratigraphical relationships and crater counts: Holden deposits are overlain by dark material, both in the interior of valleys and on the top of cliffs. This material is probably a crust of eolian material accumulated after erosion of the deposits. These dark deposits are strongly craterized, sometimes nearly saturation, implying that the age of deposits are at least Hesperian, if not older. In Terby, same dark crust blanket the light-toned deposits which are only visible in some natural cross-section where this blanket was eroded. The large surface which is not dissected by canyons gives an age in the Noachian period from crater counts at MOC and Themis visible image scale. The blanket of dark material was probably removed recently explaining the low proportion of craters on the layered deposits. On the contrary, Galle and Spallanzani crater deposits are completely devoid of craters. They are also devoid of dark blanket, except some young dunes which fills pits and throughs. These deposits seem very young by comparison to Holden or Terby. Nevertheless both deposits are submitted to a strong and recent erosion, so it is not possible to know if the surface was exhumed from much older terrains than it appears.

Channels close to deposits: Both Holden and Terby have channels crossing the deposits. Uzboi vallis in the case of Holden, and different small channels going down from crater rims in the case of Terby. Galle is inside the region of Argyre which is supposed to have been dissected by channels in the Hesperian age but we do not see any fresh channels with potential age in agreement with the apparent youth of the layered terrains inside Galle. On the contrary, Spallanzani is apparently not connected with any channels.

Discussion: The 4 craters can be classed in two groups. On one hand, the deposits of Holden and Terby are probably both of Noachian age. They occur in connection with channels and valley networks. They correspond to the same light toned material than the layers of Terra Meridiani or Valles Meridiani analyzed by [1]. Both craters deposits are good candidates for sedimentary deposition under water as already proposed. On the other hand, Spallanzani and Galle deposits are much more desegregated by wind, the material is clearly different than for Holden and Terby. These craters are located at latitudes of 52° and 58° South, thus at latitudes where ice is stable close to the surface, or was stable in a recent past. Recent models show that deposits of ice and dust as polar layered deposits can occur much more equatorward than currently during period of high obliquity [e.g. 4]. They could thus be the result of past period of high obliquity. In such hypothesis, the deposits are quickly eroded by wind action and the closed pits and throughs could correspond to cryokarstic effects of the sublimation of ice which exists currently at these latitude. Alternatively, the deposits could be old and ice could be still present as ice is stable deep in the ground at these latitudes. Then the progressive erosion could have exhumed these terrains progressively and the sublimation would have created the pits and throughs. Finally,

if Spallanzani is a potential candidate for past polar deposits, Galle remains more uncertain because of the geological context in a region where water played a strong role in the past.

Conclusion: The identification of polar deposits on the whole planet may permit to give paleoclimatic informations. This study highlights the necessity to determine geomorphic criteria in order to discriminate between the different hypothesis for the origin of layered deposits. Among the 4 craters studied, Holden and Terby confirm past studies assuming that they are crater lakes, but the deposits of Spallanzani crater could correspond to potential polar deposits which are now eroded by wind.

References: [1] Malin and Edgett, Science, [2] Cabrol and Grin Global Planetary Changes 35, 199-219, 2002 [3] Carr, M. H., *Water on Mars*, 1996. [4] Michna et al., 6th Mars int. Conf. , Pasadena, 2003.

Fig. 1: A: MOC image of Holden crater. Note the cratered surface on the plateau. B MOC image of Terby crater. C. MOC close-up of Galle crater. Layers are freshly dissected. D. MOC image of Spallanzani crater. Closed pits and erosion of scarps imply large wind effects in the erosional process.

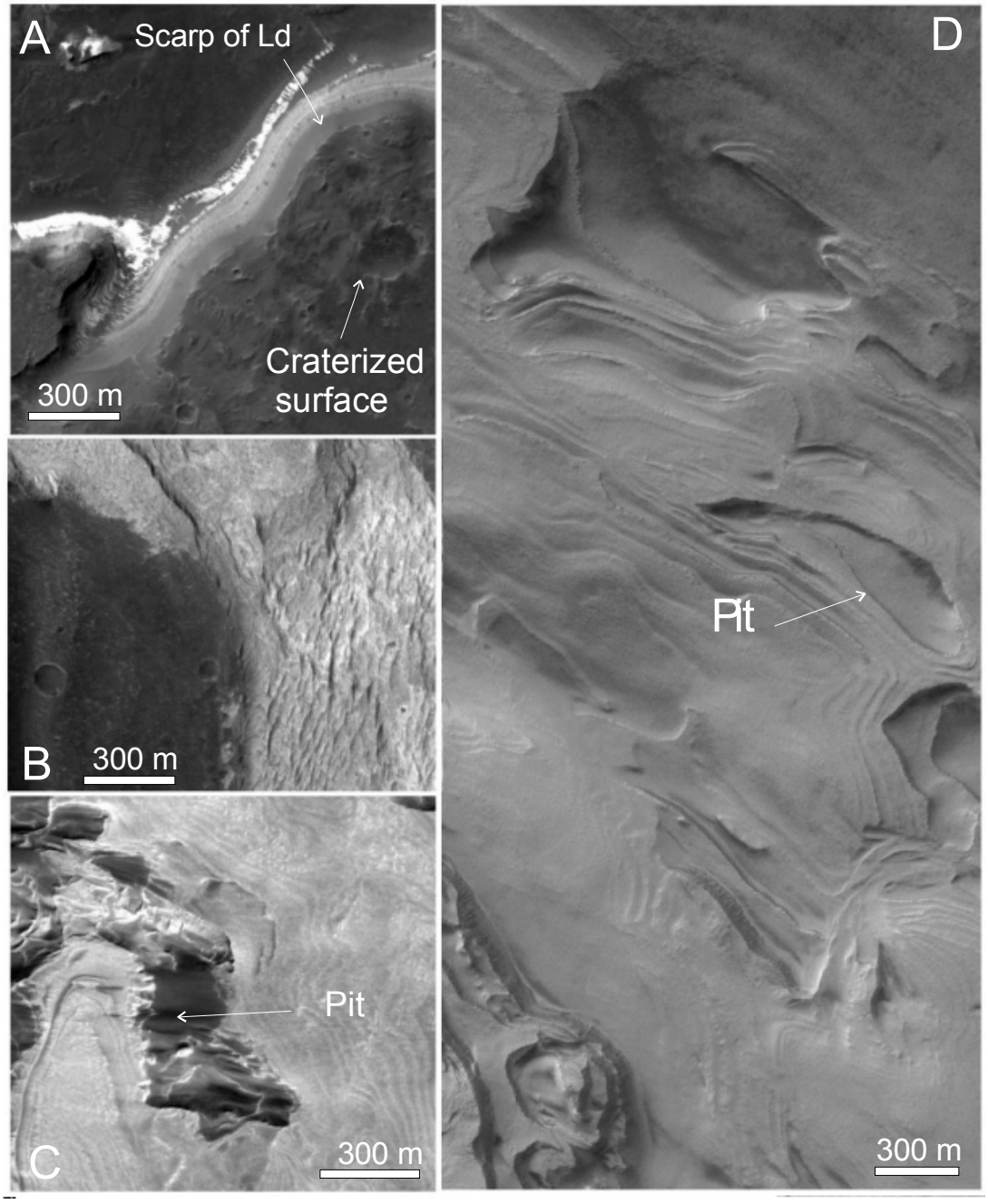

GRAIN GROWTH OF ICE WHICH CONTAINS MICROPARTICLES. N. Azuma, T. Takeda and K. Funaki, Department of Mechanical Engineering, Nagaoka University of Technology,Nagaoka, Niigata, 940-2188, Japan; azuma@mech.nagaokaut.ac.jp

Martian ice-cap ice contains a large number of microparticles (>1%vol.)[1] To estimate grain size in Martian polar ice caps is of vital importance to understand the deformation mechanisms in the ice caps. However, the estimate greatly depends on the microparticle content in ice because microparticles impede grain growth[2]. The dependence of grain growth rate on the concentration of microparticles have not been well investigated experimentally because of the difficulty in preparation of samples containing uniformly distributed microparticles.

We conducted grain growth experiments using artificial ice samples that have various concentrations (0.1-5%) of silica particles with a uniform size of 0.3 μm. Here we discuss the dependence of grain growth rate on concentration of microparticles (Fig 1 and Fig.2) . We also present the effect of the microparticles on the grain size evolution of ice during deformation.

References:

[1] Thomas P.et al. (1992) In Mars, ed. H.Kieffer et. al., Univ. Ariz.Press, 767-795

[2] Alley R.B. et al. (1986) J.Glaciol.,32 (112), 415-433

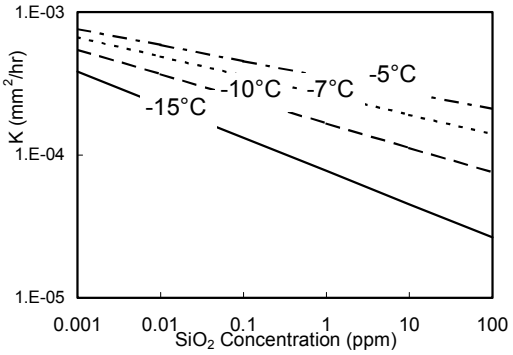

Figure 1 Results of grain growth experiments. K represents the grain growth rate.

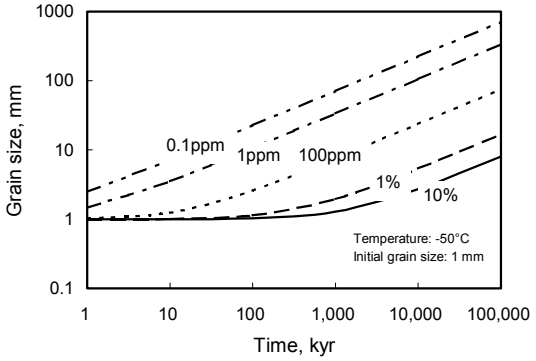

Figure 2 Grain size versus time curves estimated from present results.

AN ASSESSMENT OF THE ISSUES AND CONCERNS ASSOCIATED WITH THE ANALYSIS OF ICE-BEARING SAMPLES BY THE 2009 MARS SCIENCE LABORATORY. D.W. Beaty, (Mars Program Office, Jet Propulsion Laboratory, California Institute of Technology, dwbeaty@jpl.nasa.gov; 818-354-7968), S.L. Miller (JPL/Caltech), J.L. Bada (Univ. of Calif. San Diego), G.H. Bearman (JPL/Caltech), P.B. Black (CRREL, Picatinny Arsenal), R.J. Bruno (JPL/Caltech), F.D. Carsey (JPL/Caltech), P.G. Conrad (JPL/Caltech), M. Daly (MD Robotics), D. Fisher (Geological Survey of Canada), G. Hargreaves (USGS/National Ice Core Laboratory), R.J. Henninger (JPL/Caltech), T.L. Huntsberger (JPL/Caltech), B. Lyons (Byrd Polar Research Center), P.R. Mahaffy (NASA—GSFC), K. McNamara (NASA—JSC), M. Mellon (University of Colorado), D.A. Papanastassiou (JPL/Caltech), W. Pollard (McGill University), K. Righter (NASA—JSC), L. Rothschild (NASA—ARC), J.J. Simmonds (JPL/Caltech), J.G. Spray (University of New Brunswick), A. Steele (Carnegie Institute of Washington), A.P. Zent (NASA—ARC)

Introduction: In early 2003, the Mars Icy Sample Team (MIST) was formed to address several questions related to the acquisition and analysis of ice-bearing samples on the surface of Mars by a robotic mission. These questions were specifically framed in the context of planning for the 2009 Mars Science Laboratory (MSL) lander, but the answers will also also have value in planning other future landed investigations.

Questions:

- Which scientific investigations, in priority order (especially of relevance to an assumed mission theme of habitability), can be addressed using ice-bearing samples and the MSL landed system?
- Which measurements are needed on ice-bearing samples to support these investigations?
- What are the minimum sample collection hardware and processes needed to acquire the necessary ice-bearing samples?
- What are the minimum sample preparation steps required for ice-bearing samples?
- What are the issues associated with preservation of the scientific content of the samples between the time of their collection and the time of their analysis?
- Can common hardware be used to interact with both ice-free and ice-bearing samples? This would allow the decision of where to send the mission (i.e., in terms of a latitude band) to be deferred until very late in the mission development process.

Assumptions: For the purpose of this analysis, we have defined four model sample types: Weakly ice-cemented regolith, ice-saturated regolith, ice-supersaturated samples (up to 100% ice), and ice-bearing rocks. These sample types have different concentrations of ice, different texture, and different resistance to sampling devices.

Ice Science Priorities: The MIST team ranked the scientific objectives of studying an ice-bearing sample (using the potential capabilities of the MSL landed system). The following is a prioritized list, using the impact on astrobiology as the prioritization criterion.

1. Is ice present and in what abundance?
2. Are organic molecules present in the sample, and if so, what is their identity, and what is their relationship to the ice fraction of the sample?
3. Is some fraction of the water present in the sample in the liquid state (e.g., as fluid inclusions, or along grain boundaries)? If so, how much, and what is its composition?
4. How did the ice get into the ground? Was it trapped from the atmosphere? Is it buried surface ice? Did it percolate from surface standing water or from sheetwash?
5. How old is the ground ice?
6. Has the ground ice been processed, melted, or redistributed since deposition? If so, when and how?

In addition, the planetary scientists on the MIST team concluded that several additional high priority investigations (origin of the water, climate at the time the ice formed, exchange rates/processes, planetary modeling, etc.).could be supported by measuring the isotopic properties of the water.

Some assertions regarding ice sample science: Based on the collective experience of the MIST team, we pose the following assertions regarding deriving science value from an ice-bearing sample on the martian surface.

1. For the ice-related investigations described above, well-designed measurements on a small number of ice-bearing samples will be more useful than poorly designed measurements on a large number of samples.

2. None of the high-priority ice-related measurements require that ice-bearing samples be crushed.
3. It is not scientifically necessary to split a sample to make multiple ice-related measurements. Most of the logic for doing this for the refractory portions of geologic samples does not apply to the ice fraction. It is far more important that the samples are fresh than to have statistically equivalent splits.
4. Sample aging is always a problem with ice-bearing samples. An acceptable solution to minimizing these effects is to optimize the operational scenario (e.g., transfer ice samples at night, while it is cold). This will be far simpler than mechanical means of sample preservation (e.g. encapsulation, refrigeration).
5. It is impossible to design a simple sample preparation and distribution system in which dry and wet samples follow the same path. We never do this in Earth labs.
    - If the ice fraction of a sample melts in a system designed for dry samples, there is potential for serious damage (un-removable contaminants, and perhaps worse).
    - Note: It may be possible using thermodynamic arguments to show that the ice will sublimate rather than melt, and if so, an engineering solution is not required.

Discussion:

For the highest-priority astrobiology investigations, non-destructive measurements are essential. Textural relationships between ice crystals, any organic material present, liquid/salt inclusions, and any associated mineral material need to be observed. Microscopy, probably with different kinds of illumination, will be key. For the highest priority planetary science investigations, subliming the ice and running the vapor through a mass spectrometer is essential. Given the priorities of the Mars program, we do not see a good scientific reason to subject an ice-bearing sample to mechanical sample preparation steps such as crushing and splitting. Thus, the mechanical process of interacting with an ice-bearing sample is in some ways simpler than interacting with rocks, which need to be crushed and split for many types of measurements.

The most useful kinds of ice-bearing samples for the scientific objectives described above are ice-saturated regolith and ice-supersatured material. These two sample types cannot be effectively sampled without a drill. We do not have a good way of calculating the depth of penetration necessary to acquire these sample types, but in our judgement a subsurface access capability of 0.3-0.5 m is a minimum.

When a cold ice-bearing sample is moved from its natural state to the warmer environment of the rover, it will progressively degrade, first by addition (freezing of water vapor onto the sample), then by subtraction (sublimation). We were unable to model the rate of this degradation process in the time available to us, but it will be dependent on the integrated exposure to higher temperature over time and air circulation. How much time-temperature is acceptable?--Preliminary calculations suggest that several hours should be acceptable if ΔT is modest.

Recommendations:

1. We recommend including a means of determining whether or not ice is present in the acquired sample either at the site of sample collection, or at the front end of the lab.
2. Minimize the effects of sample degradation by:
    - Placing ice-critical instruments in a cold part of the rover.
    - Collecting and processing samples for ice-related measurements at night.
    - Processing and analyzing ice samples quickly. We recommend that instruments needing to receive raw ice-bearing samples have a "bypass" port, which would allow raw material to be introduced without passing through the sample preparation systems.
3. To protect the principal (dry) sample prep and analysis systems which are at the heart of MSL's scientific objectives, we recommend that samples be dried prior to introduction into crushing, splitting, or sieving operations.
    - The combination of time and temperature necessary to achieve the minimum necessary state of dryness needs more analysis and discussion. A part of this analysis needs to include assessment of the temperature at which one starts to lose information on hydrated phases.

Conclusion:

Our summary conclusion is that it is possible to design a single overall surface system that can interact with both ice-bearing and ice-free samples. However, this system will need to have more complexity than a system designed to interact only with ice-free samples. Such a system could be designed now, and we would be able to send it to a location selected years from now in response to future discoveries (possibly either ice-free or ice-bearing).

Detection of Organic Compounds in Polar Ices on Mars Using AP MALDI Luann Becker[1], William Brinckerhoff[2] and Robert J. Cotter[3], [1]Department of Geology, University of California, Santa Barbara, 1140 Girvetz Hall, Santa Barbara, CA 93106 email: lbecker@crustal.ucsb.edu; [2]Applied Physics Laboratory (APL), Laurel MD, 20723; [3]Johns Hopkins School of Medicine (SOM), Baltimore, MD, 21205

Introduction

With the current and planned missions to Mars and to some outer planetary moons such as Europa and Titan, NASA is now entering a new phase of planetary exploration strongly motivated by *Astrobiology*. Our interest in Mars is, in part, a result of recent studies of martian meteorites that suggest that the early history of the red planet was remarkably similar to that of the Earth, where life apparently arose both quickly and early on (possibly as soon as ~3.85 Ga). If this is indeed the case, then Mars was presumably a much warmer, wetter, planet then it is today. This hypothesis is further supported by the images returned by the Viking, Mariner and Mars Global Surveyor (MGS) orbiter spacecrafts that all show compelling evidence that copious liquid water existed on the surface of Mars in the past. In fact, new images provided by MGS suggest that there may be current sources of liquid water and ice at or near the surface of the red planet. Other MGS images show evidence of an early ocean at the North Pole and extensive underwater channels draining into large valleys (Valles Marineris) near the equator. All of these data support the possibility that life may have arisen on Mars in liquid water environments.

The search for organic matter in rocks, sediments and ices from Mars is critical to the assessment of any extinct or extant life. Our missions to Mars have the potential to further address the question of whether life arises spontaneously, given appropriate planetary conditions, as well as possibly learning more about our own prebiotic evolution that has been all but erased from the Earth's crustal record. The search for life beyond our own planet is one of considerable interest to scientists and the general public alike. Yet, as we learned from the Viking missions, the search for life signs in a complex environment is problematic and requires an appropriate strategy that will maximize our opportunities to properly examine these compelling questions. This strategy must encompass both the selection of appropriate measurement techniques and the careful testing and evaluation of those techniques in an environment with challenges similar to those found *in situ*.

One of the highest technical barriers to obtaining sensitive analyses of solid phase materials (e.g. ices) on Mars is the often complex and resource-intensive process of sampling. Powerful instruments, such as mass spectrometers, typically require solid samples to be cleanly manipulated and vacuum processed in order to achieve their advertised capabilities. We are in the process of developing and testing an integrated mass spectrometer system that uses a direct sampling and ionization method operating at ambient atmospheric pressure, yet achieves the very high sensitivity and discriminatory power required for complex *in situ* samples. The atmospheric pressure matrix assisted laser desorption/ionization (AP-MALDI) method uses a pulsed laser to volatilize and ionize organic compounds from the surfaces of solid samples, which are then immediately drawn into a differentially-pumped miniature mass spectrometer inlet for analysis.

The development of a MALDI source that operates at ambient atmospheric pressure was strongly motivated by the drive toward higher throughput screening analyses in proteomics and chemical/biological agent detection. In the case of AP-MALDI, the ions are formed at ambient pressure and then drawn into the system. By eliminating the sample acquisition and vacuum loading steps, AP-MALDI has the potential to be used on large sample arrays or wide-area collection plates within a robotic monitoring system or directly on rocks and ice in the field. Moreover, there are a number of features of AP-MALDI that are especially advantageous for use on geological samples in a harsh, remote environment such as Mars. **First,** ambient laser desorption maintains the pristine nature of samples, and the capillary inlet does not contact the sample. Therefore, AP-MALDI could be implemented at the end of an articulated robot arm. **Second,** laser desorption is able to perform local analyses of undisturbed samples that are heterogeneous at the grain scale; the focal diameter is typically in the range from 100 microns to 1 mm. Thus highly localized mineralogical "niches" that may contain biomarker organics are more likely to be detected than with a bulk sample. **Third,** the Mars ambient pressure of 5-10 Torr is precisely in the range that has been shown to dramatically increase sensitivity and decrease metastable fragmentation. That is, a method that provides increased performance at a complexity and convenience cost in terrestrial AP-MALDI may be available without those costs on Mars. The lower ambient pressure (5–10 vs. 760 Torr) at Mars also reduces the overall complexity of the instrument inlet and the requirements on the pumping system because of the reduced differential pressure gradient to reach the required base pressure of the analyzer.

Earth Analogs – Antarctica

Since the exploration of Mars will necessitate a highly robust and refined instrument technology testing equipment in the appropriate Earth analog, like the environments encountered in Antarctica, would greatly facilitate the development of *in situ* instrumentation. Exploration of the ice cap and the unique preservation of organic material in the Antarctic environment will provide the testing ground for the development of our AP- MALDI instrument. Several studies of Antarctic ice have revealed both extraterrestrial and terrestrial sources of organic compounds that are concentrated in the surface ice by the natural process of sublimation (Becker et al., 1999, 2002). The cold and dry Antarctic conditions are ideal for evaluating the preservation of organic compounds and the effects of seasonal changes that may lead to the decomposition of biologically relevant compounds. The acquisition of this data set, both through *in situ* field measurements and with samples collected and returned to the laboratory, will be invaluable to our strategy for the search of extinct/extant organic compounds on Mars.

The current expectation of the ability of AP-MALDI to perform these analyses is based upon initial laboratory work with a breadboard, which has been used to detect 10–50 femtomole (fmol) of analyte (liquid) deposited on a target surface in a four-component mixture of peptides in the 800-1700 Dalton (Da) molecular weight range. Recent analyses of portions of Vostok ice cores revealed between 2 x 10^2 and 3 x 10^2 bacterial cells per milliliter and low concentrations of potential growth nutrients (Karl et al., 1999; Priscu et al., 1999) suggesting that Lake Vostok may contain viable microorganisms. We have available, samples of accreted ice from Lake Vostok. We will present preliminary results on these ice samples and other materials (minerals, sediments) using our AP-MALDI functional proto-type instrument. Testing of the prototype instrument in Antarctica will begin in 2003. This initial testing program will be used to implement the design of our brassboard instrument that will be tested again in Antarctica in the 2006 field season.

References: Becker, L. Popp, B., Rust, T. and Bada, J. L. (1999) *Adv. Space Res.* 24, 477-488. Becker, L. (2002) *National Research Council, Signs of Life: A report based on the April 2000 Life Detection Workshop on Life Detection Techniques,* National Academies Press, Washington, D.C. Karl, D. M., Bird, D. F., Bjorkman, K., Houlihan, T., Shackelford, R., Tupas, L. (1999) *Science* 286, 2144-47. Priscu, J.C., E.E. Adams, W.B. Lyons, M.A. Voytek, D.W. Mogk, R.L. Brown, C.P. McKay, C.D. Takacs, K.A. Welch, C.F. Wolf, J.D. Kirstein. R. Avci. (1999) *Science* 286, 2141-2144.

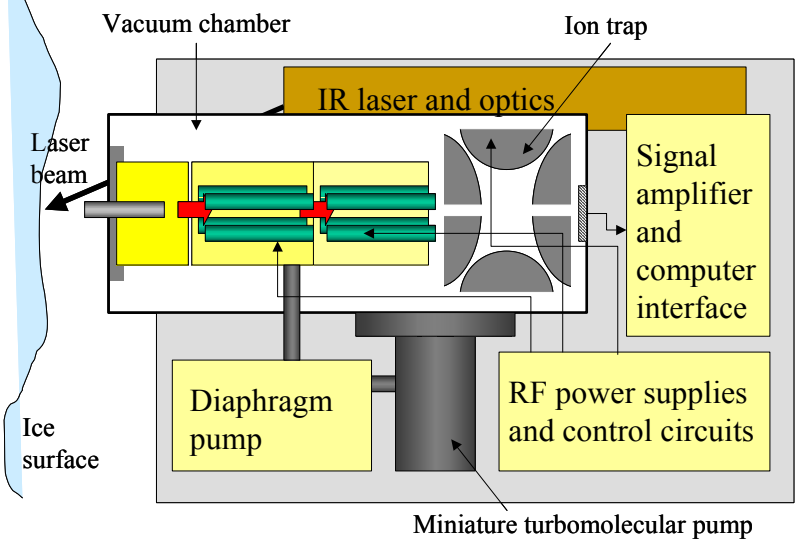

Fig. 1 The envisioned integrated brassboard AP-MALDI-ITMS concept. The instrument analyzes an ice or ice matrix sample deposit in situ, in a non-contact "stand-off" mode. The sample-inlet distance in the mm range depends on a number of factors to be investigated. Laser- sampled ions travel through the inlet stage and focused by a quadrupole/octopole rod assembly to maximize signal. The laser, ion trap, power, and data collection systems are controlled through a user-monitored interface. The asynchronous operation of laser and ion trap permit analyses to be performed in autonomous programmed modes.

YEARLY COMPARISONS OF THE MARS NORTH POLAR CAP: 1999, 2001, AND 2003 MOC OBSERVATIONS. J. L. Benson and P. B. James, Ritter Astrophysical Research Center, Dept. of Physics and Astronomy, Univ. of Toledo, Toledo, OH 43606 (jbenson@physics.utoledo.edu; pbj@physics.utoledo.edu)

Introduction: The seasonal cycle of the martian north polar cap has been studied since the time of William Herschel, who published the first quantitative observations of the seasonal recession of the polar caps in 1784 [1]. Ground-based observations made after Herschel were summarized by Slipher in 1962 [2]. More recent ground-based observations of the north polar cap have been done by Iwasaki et al. [3, 4, 5, 6]. Mariner 9 [7] and Viking [8, 9] also made north polar observations. Cantor et al. used Hubble Space Telescope observations between 1990 and 1997 to determine several north polar recessions and Lambert albedos of the cap [10].

Mars Global Surveyor went into orbit around Mars in September 1997. The wide-angle cameras on the Mars Orbiter Camera (MOC) acquire images of the entire planet every day at a resolution of ~ 7.5 km/pixel in both red (575 nm – 625 nm) and blue (400 nm – 450 nm) bandpasses (WAR and WAB). Some polar cap observations were acquired during the aerobraking (AB) and science phasing (SPO) of MGS before systematic mapping began in March, 1999 at L_S = 110°.

More than two complete Martian years have now been monitored by MGS/MOC, including three summer seasons in the northern hemisphere. Data pertaining to the spring / summer recessions of the north cap during the first year of mapping has been reported previously [11]. The north polar recession in 2000 was very similar to previously observed recessions. The MOC observations confirmed an almost linear cap regression from L_S = 340° until L_S = 60°.

Using WAR images, we have studied the subsequent spring recession of the north seasonal polar cap and also made albedo measurements of the residual cap. We look for interannual variability between this and previous years observed by MOC. This comparison is especially interesting because an extensive planet encircling dust storm occurred in early northern fall of the second Martian year while there was no such large storm in the first year. Therefore, it may be possible to determine the effects of dust on the condensation and sublimation of the carbon dioxide in the cap.

Seasonal North Cap: The late winter and early spring portions of the north cap recession have been phases for which the largest interannual variability has been reported. The extent of the surface cap boundary in late winter has been controversial. Also, a halt in cap regression in early to mid-spring has been reported [3, 8]; that is, the boundary of the cap remains fixed at a latitude of about 65º for several weeks before the recession resumes. A global dust storm during the condensation phase of the north cap is one mechanism suggested to be responsible for this variability. However, it is difficult to separate interannual effects from longitudinal asymmetries in the cap due to the gradual change in the longitudes on Mars seen from a location on Earth.

We have determined the regression curves for the 2000-2001 and 2002-2003 recessions of the north polar cap (Figure 1); a planet encircling dust storm occurred in early fall in the second year. The regression curves from the two years are very similar, however, there are small differences between L_S=10º and L_S=50º. There is no sign of a halt in cap regression in either year.

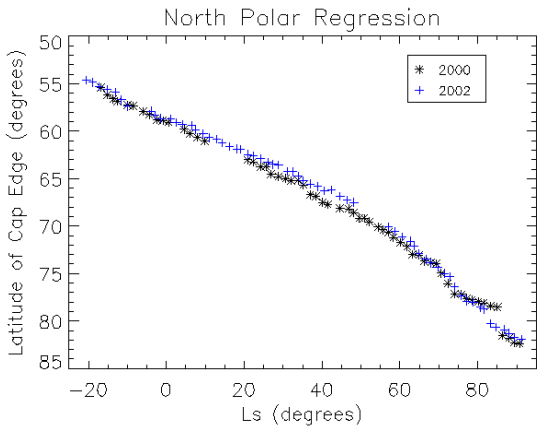

Figure 1: Regression of the north polar cap in 2000 (*) and 2002 (+). The latitude of the cap edge on a sterographic projection is ploted versus areocentric solar longitude. Recessions are similar, however, there are slight variations between L_S=10º and L_S=50º.

Residual North Cap: Mars Global Surveyor mapping began at L_S = 110º in 1999. Detailed comparisons of the caps in different years are complicated by frequent dust storms that may obscure the surface cap; fallout from these storms on the surface cap may also affect the apparent albedo for longer periods.

In Figure 2, the average Lambert albedo of the center (geographic pole) of the RNPC is plotted against L_S

for 1999 (*) and 2003 (Δ). Due to a change in sensitivity of the MOC WA Red Camera during the fall of 2001, those data are not included here, however, James and Cantor have reported these results [12]. The general behaviors of the albedo in this central region of the cap seem to be similar in the two years. The main exceptions are two data points from 1999 near L_S = 135°. There is a gap in the MOC WA red mapping subsequent to these events due to the Geodesy Campaign; so the question of the duration of this suppression is not answered by the red images alone, and additional investigation using the blue filter mapping images, which continued through the period, will be needed. The decrease after L_S > 160° is probably due to the fact that the Lambert approximation fails at the large incidence angles in late summer.

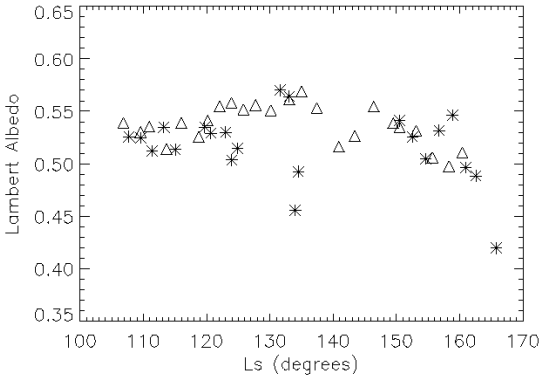

Figure 2: Average Lambert albedo for a 30 × 30 pixel^2 region around the geographic north pole as a function of L_S for 1999 (*) and for 2003 (Δ).

Acknowledgements: The authors were supported by grants from the Mars Data Analysis Program.

References: [1] Herschel, W. (1784) *Phil. Trans*., 24, 233-273. [2] Slipher, E. C. (1962) *The Photographic Story of Mars*, Northland Press. [3] Iwasaki, K. et al. (1979) *JGR*, 84, 8311-8316. [4] Iwasaki, K. et al. (1982) *JGR*, 87, 10265-10269. [5] Iwasaki, K. et al. (1984) *PASJ*, 36, 347-356. [6] Iwasaki, K. et al. (1999) *Icarus*, 138, 20-24. [7] Soderblom, L. A. (1973) *JGR*, 78, 4197-4210. [8] James, P. B. (1979) *JGR*, 84, 8332-8334. [9] James, P. B. (1982) *Icarus*, 32, 565-569. [10] Cantor, B. A. et al. (1998) *Icarus*, 136, 175-191. [11] James, P. B. and Cantor, B. A. (2001) *Icarus*, 154, 131-144. [12] James, P. B. and Cantor, B. A. (2001) *BAAS XXXIII*, Abstract #19.16.

EFFECTS OF ATMOSPHERIC AND SURFACE DUST ON THE SUBLIMATION RATES OF CO_2 ON MARS. B. P. Bonev[1], P. B. James[1], J.E. Bjorkman[1], G. B. Hansen[2], and M. J. Wolff[3], [1]Ritter Astrophysical Research Center, Dept. of Physics and Astronomy, Univ. of Toledo, Toledo, OH 43606, USA (bbonev@kuiper.gsfc.nasa.gov; pbj@physics.utoledo.edu; jon@physics.utoledo.edu), [2]Planetary Science Institute, Northwest Division, Univ. of Washington, Seattle laboratory, Seattle, WA 98195 (ghansen@rad.geology.washington.edu), [3]Space Science Institute, 3100 Marine Street, Boulder, CO 80303-1058, USA (wolff@colorado.edu).

Introduction: We present an overview of our modeling work dedicated to study the effects of atmospheric dust on the sublimation of CO_2 on Mars. The purpose of this study is to better understand the extent to which dust storm activity can be a root cause for interannual variability in the planetary CO_2 seasonal cycle, through modifying the springtime regression rates of the south polar cap. We obtain calculations of the sublimation fluxes for various types of polar surfaces and different amounts of atmospheric dust. These calculations have been compared qualitatively with the regression patterns observed by Mars Global Surveyor (MGS) in both visible [1, 2] and infrared [3] wavelengths, for two years of very different dust histories (1999, and 2001).

Atmospheric modeling: Our approach is to model the radiative transfer through a dusty atmosphere bounded by a sublimating CO_2 surface. Although we have done some preliminary monochromatic calculations [4], our main focus has been to employ a full spectrum model, which incorporates the main effect of atmospheric dust. This is the redistribution of the radiation incident to the surface from visible frequencies to the IR. We have adapted a monte-carlo radiative equilibrium algorithm, initially developed for modeling circumstellar envelopes [5], to the case of a plane-parallel dusty planetary atmosphere. This model was introduced in a case study [1] applied to the regression of the Mountains of Mitchel, one of the brightest regions in south seasonal polar cap. This work points out that although our model atmosphere is one-dimensional, our radiation transfer code is three-dimensional and includes wavelength-dependent dust opacity, anisotropic scattering and thermal dust emission. We have used the most recently calculated dust single scattering properties for both visible and IR wavelengths [6]. An important modification of the original code, has been the treatment of anisotropic scattering in the visible spectral region, which enabled incorporating the phase function appropriate for Martian dust [7].

Surface modeling: The surface albedo spectrum is a major parameter in this study. Its accurate modeling is of primary importance and without it, the effects of atmospheric dust cannot be assessed correctly. There are a number of parameters influencing the surface albedo spectrum [8], the most important of which is the amount of *surface dust intermixed in the frost*. The amount of surface intermixed dust and water, and the grain size of the CO_2 frost, can be constrained by data from at least three spectral regions: the thermal IR near 25 microns [8], the near-IR [9], and the visible ranges of the Mars Orbiter Camera (MOC) on MGS [10]. We initially conducted a limiting case study [1] of the sublimation of surfaces with zero and very high dust content. In [11] we have examined in depth the albedo changes with surface dust-to-ice mixing ratio and CO_2 frost grain size; the variation of the albedo with photon incident angle and the dependence on the ratio of direct/diffuse incident radiation. In monte carlo calculations the albedo dependence on the direction of the reflected photons is also important. This variable has been held as a free parameter by simulating different laws of surface reflection. A good constraint of the best directional distribution of the photons reflected would enable incorporating this factor accurately into our model.

Sublimation fluxes for different amounts of atmosheric and intermixed surface dust: We have calculated sublimation fluxes (SF) for a number of combinations between the total atmospheric dust optical depth and the type of the CO_2 ice surface. The SF have been normalized to the total flux incident on the atmosphere and calculated as a difference between the spectrally integrated fluxes absorbed and emitted by the surface (set to sublimate at 147 K). An example calculation is presented on Figure 1. It corresponds to a particular grain size, but this parameter has been varied as well [11]. The main model results reproduce qualitatively the observational comparison between 1999 (relatively dust free year) and the 2001 (global dust storm) south polar cap regression patterns, observed by MGS and described in [2, 11]:

1. The absorption of surface frost with a high dust content (1 wt% being the upper limit [8]) is dominated by visual photons. Therefore the attenuation of direct solar radiation by atmospheric dust results in retarded sublimation.

2. Conversely, the absorption of regions with low dust content is dominated by IR photons, owing to the

high visual albedos. In this case the visual-to-IR redistribution of the energy incident to the surface, caused by atmospheric dust, leads to increased sublimation rates.

3. There is a wide range of combinations between surface dust content and frost grain size for which the CO_2 sublimation rates show only subtle variations with the amount of atmospheric dust load. In these cases the surface absorption is distributed equally between visual and IR wavelengths, so the overall atmospheric dust effect is not important. It should be emphasized that the discussed region of the parameter space represents a "typical frost" [8] and consequently explains the apparent insensitivity of the *average decay rate* of the south seasonal cap to dust storm activity [2]. Strong coupling between sublimation and atmospheric dust exists primarily on *local scale* for regions with "deviant" surface albedos such as the Mountains of Mitchel (high visual albedo, faster regression in 2001 [1,3]), and the "Cryptic" region [12] (low visual albedo, slower regression in 2001 [3]).

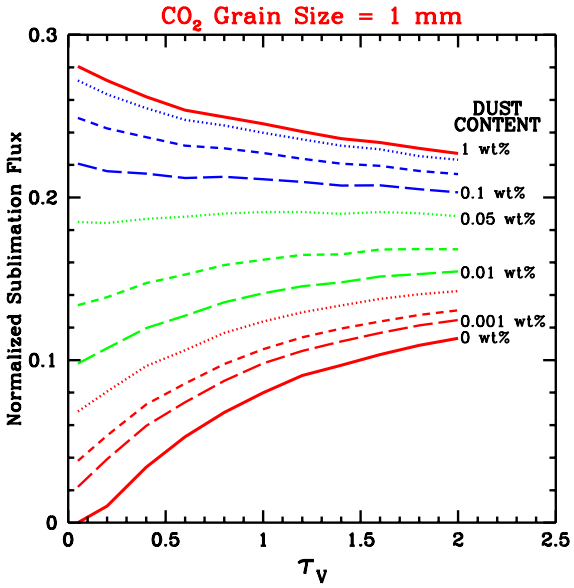

Figure 1. CO_2 Sublimation Flux vs. Total Atmospheric Dust Optical Depth at 550 nm for a frost grain size of 1 mm and various contents of intermixed surface dust.

A note should be made about the possibility that newly deposited surface dust played a role in the faster regression of bright regions (like the Mountains of Mitchel) by lowering the surface albedo and thus increasing the absorbed flux and consequently the sublimation rate. While this scenario cannot be ruled out, it fails to explain the slowing down of the dark regions such as the Cryptic region, which is consistent with the effect of atmospheric dust.

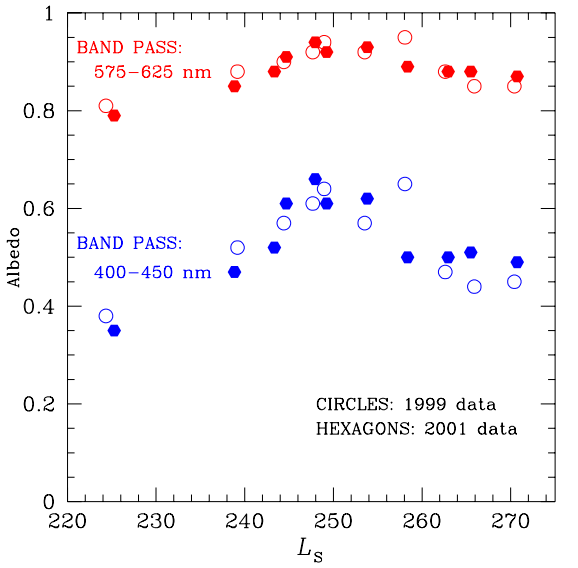

Figure 2. Top-of-the atmosphere Lambert albedos from 1999 and 2001 MOC data, averaged over a region within the perennial residual south polar cap.

In progress: In addition to the presented overview, we will discuss improvements of the atmospheric modeling, and some aspects of the study of the perennial residual south polar cap. The high maximum values of the red visual albedo of the residual cap (Figure 2) suggest small contents of intermixed surface dust and low sublimation rates at dust free conditions. The maximum values of the red and blue albedo measurements (like L_s~148°, 1999) most likely have minimal atmospheric contribution and can be used to constrain the ice properties through models of surface albedo spectra [8]. The likely higher sublimation the cap has undergone in 1972 (Mariner 9 observations) will also be addressed.

Acknowledgement: Four of the authors (BPB, MJW, PBJ, GBH, and JLB) were supported by grants from the Mars Data Analysis Program. JEB was supported by NSF Grant AST-9819928.

References: [1] Bonev, B. P. et al. (2002) *GRL*, *29*, 2017, doi:10.1029/2002GL015458. [2]. James, P. B. et al. (2003), *Intern. Mars Conf. VI,* #3093. [3] Titus, T. N. and Kieffer, H. H. (2002) *LPS XXXIII*, #2071. [4]. James, P. B. et al. (2000) *DPS 32, #51.10.* [5] Bjorkman, J. E. and Wood, K. W. (2001) *ApJ*, *554*, 615-623. [6] Wolff, M J. and Clancy, R. T. (2003) *JGR*, in press. [7] Tomasko et al. (1999) *JGR, 104, 8987-9007*. [8] Hansen, G. B. (1999) *JGR, 104*, 16,471-16,486. [9] Glenar et al. (2002), *DPS 34, #15.23*. [10] James et al. (2001) *JGR, 106, 23,635-23,652*. [11] Bonev, B. P. et al. (2003), *Intern. Mars Conf. VI,* #3111. [12] Kieffer, H. H. et al. (2000) *JGR, 105, 9653-9699*.

ICE IN THE POLAR REGIONS OF MARS: EVIDENCE FOR WET PERIODS IN THE RECENT PAST.

W. V. Boynton[1,2], M. Chamberlain[1], W. C. Feldman[3], T. Prettyman[3], D. Hamara[1], D. Janes[1], K. Kerry[1] and the GRS Team. [1]Lunar and Planetary Lab, Univ. of Arizona, Tucson AZ 85721, [2]Department of Planetary Science, Univ. of Arizona, Tucson AZ 85721, [3]Los Alamos National Laboratory, Los Alamos N.M 87545.

Introduction: In our earlier work [1] we showed that the south polar region of Mars had high contents of subsurface ice. This conclusion was based on a preliminary analysis of data from the Mars Odyssey Gamma-Ray Spectrometer instrument suite. Subject to the assumptions made at the time, the GRS observations in the south-polar region could be fit to a two-layer model consisting of a "dry" upper layer with low hydrogen content and an ice-rich lower layer. The upper layer ranged in H content, expressed as H_2O, from 2% near -45° latitude to 3% near -75°. The thickness of the upper layer, expressed as column density, ranged from >100 g/cm^2 at -55° latitude to 40 g/cm^2 near -75°. The ice content of the lower layer was inferred to be 35 ± 15% with the higher end of the range preferred.

Several necessary assumptions were made in this work, the most significant of which was that we needed to make a normalization for the absolute flux of both gamma rays and neutrons. We now know that both of these assumptions were incorrect, and we have determined better normalization values. For the neutrons, we normalize to the case of the thick CO_2 seasonal frost in the north overlying the water-ice residual cap [3]. For the gamma rays, we normalize to the frost-free northern residual cap [4]. The effect of these re-normalizations is to increase the amount of subsurface ice compared to the earlier work.

Results: The results are shown in the first two maps in fig. 1. In these maps, the gamma-ray flux has been converted to equivalent amount of H_2O assuming that the hydrogen is evenly distributed with depth, *i.e.* there is not an overlying ice-free layer. This assumption is clearly incorrect, but it serves to provide a firm lower limit to the amount of H_2O in the soil. If, as seems clear, the ice-rich regolith is covered by an H_2O-poor layer, the H_2O content in the lower layer must be substantially higher because the overlying layer will attenuate the gamma-ray flux. In both polar regions, away from the residual cap, this lower limit to the H_2O content is around 40%. A similar analysis based on the epithermal neutron flux, again assuming the H_2O is uniformly distributed with depth, shows a minimum limit of around 60% H_2O in the polar regions [5].

Another interesting result is to look at the limit on the thickness of the upper "dry" layer in the case of a two-layer model (fig. 1). These maps have been made by assuming the ice-rich layer is pure ice, and that the gamma-ray signal is attenuated by the overburden of the dry layer (here assumed to be 3% H_2O). Again for both polar regions, we see that the maximum thickness the upper layer could have is about 20 g/cm^2. This result is inconsistent with the results of the data from the GRS Neutron Spectrometer, as the thermal neutron flux clearly shows a minimum in the south around 70 deg latitude [2,1], and this minimum occurs when the H_2O-rich layer is buried by around 50 g/cm^2 of dry material, a result that is nearly independent of the amount of H_2O in the lower layer.

Discussion: We are drawn now to the conclusion that the simple two-layer model does not describe the observations. This result is not surprising considering that the footprint of the GRS is large, about 550 km, and a variety of different H_2O contents and depths could co-exist in our footprint.

Nevertheless, one of the important observations is still the very large quantity of ice found in the polar regions. The minimum amount, about 60% by mass, requires that an emplacement mechanism other than vapor diffusion to fill pore spaces was responsible for depositing the ice in the polar regions. This conclusion follows from consideration of the data in Table 1, which shows the relationship between volume percent and weight percent assuming a bulk grain density of 2.5 g/cm^3. The column "Ice-free density" is the density of the soil without ice assuming the ice was completely filling the pore space. If we allow for some experimental uncertainty on the GRS results, it is still clear that the minimum H_2O content is conservatively between 50% and 65% by mass. When converted to volume %, we require unreasonably low-density soils to have sufficient pore space to accommodate the high concentration of ice found by the GRS.

One mechanism that could emplace with a high ice/dust ratio is the deposition ice in the form of snow

or frost directly onto the surface in the polar regions. In this case the deposition rates of ice and dust would determine the bulk ice/dust ratio. Obviously for this mechanism to satisfy the GRS observations, the rate of ice deposition would have to be higher than the rate of dust deposition.

Table 1. *Relationship between ice content and ice-free soil density.*

Weight % ice	Volume % ice	Ice-free density
35%	59%	1.01
50%	73%	0.67
65%	84%	0.41

Presumably the dust and ice could be deposited at different times over the course of a Mars year, but the ice would have to be present on the surface year round. Any significant seasonal sublimation of ice would leave behind a lag deposit of dust which would dilute the snow or frost deposited the next year. Clearly in order to build up the regolith with a high ice/dust ratio, the lag deposit cannot be greater than the layer of ice which is deposited in any given season.

The current Mars epoch is clearly not conducive to the deposition of snow or frost on the surface to survive throughout the year, but if this kind of process is responsible for emplacing the ice with a high ice/dust ratio, an important question is how long ago did this happen. Even though the amount of ice seems to be inconsistent with its emplacement by vapor deposition, it seems clear that that the process of vapor deposition and ice sublimation [6,7] is operating on Mars. This conclusion is based on the observation that the line marking the beginning of the ice-rich region in the south [1] precisely matches the predictions for where subsurface ice should be stable under current martian conditions. Even though the high content of ice could not be emplaced by vapor deposition, once emplaced under the appropriate wet conditions, it can subsequently sublime away to its stable depth leaving a lag deposit above it when the climate changes to one more like the present.

Since the deposition/sublimation mechanism appears to be viable now, it must also work under other conditions with different obliquities. Under such conditions, the depth to the frost point will change [7]. Because the high ice content is within about 20 g/cm^2 of the surface and because vapor deposition cannot re-emplace ice in the high concentrations observed, it would appear that the maximum depth to the frost point has never exceeded this value of around 20 g/cm^2 after the ice was emplaced in the form of snow or frost. If, as seems likely, conditions in the past were such that the lag deposit could have gotten much thicker, the observation of the near-surface ice-rich deposit implies that the wet conditions for snow or frost deposition occurred more recently.

References: [1] Boynton *W. V. et al.*, (2002) *Science, 297,* 81. [2] Feldman W. C. *et al.*, (2002) *Science, 297,* 75. [3] Feldman W. C. *et al.*, (2003) *GRL*, submitted [4] Boynton W. V. *et al.*, (2002) 6th Mars Conf. Abstract #3259. [5] Feldman W. C. *et al.*, (2002) 6th Mars Conf. Abstract #3218. [6] Leighton R. B. and Murray B. C. (1966) *Science, 153,* 136. [7] Mellon M. T. and Jakosky B. M. (1993) *JGR, 98,* 3345..

Fig. 1. *Polar stereographic views of the minimum H_2O content inferred from the Mars Odyssey GRS (left) and maximum thickness of the upper layer. The dark contour is the residual cap; the light contour is the layered terrain.*

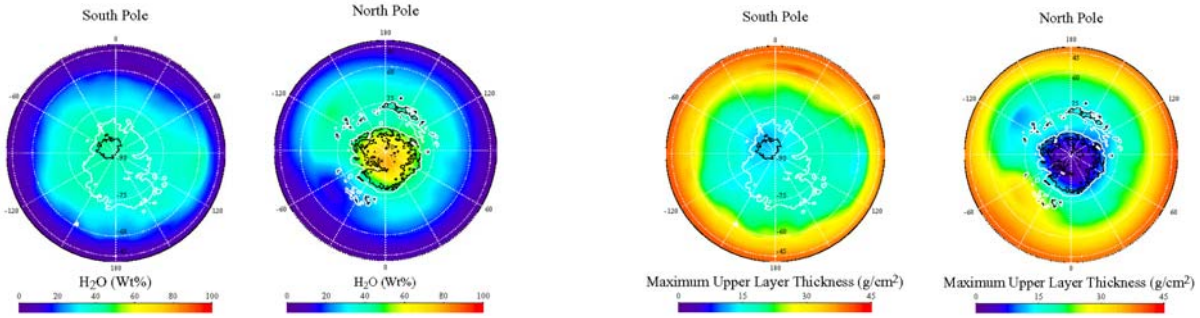

INTERANNUAL ATMOSPHERIC VARIABILITY SIMULATED BY A MARS GCM: IMPACTS ON THE POLAR REGIONS. Alison F.C. Bridger[1], R. M. Haberle[2] and J. L. Hollingsworth[3]: [1]Department of Meteorology, San Jose State University, San Jose CA 95192-0104, USA (bridger@met.sjsu.edu); [2,3]NASA Ames Research Center, MS 245-3, Moffett Field, CA, 94035-1000, USA (robert.m.haberle@nasa.gov, jeffh@humbabe.arc.nasa.gov).

Abstract: It is often assumed that in the absence of year-to-year dust variations, Mars' weather and climate are very repeatable, at least on decadal scales. Recent multi-annual simulations of a Mars GCM reveal however that significant interannual variations may occur with constant dust conditions [1]. In particular, interannual variability (IAV) appears to be associated with the spectrum of atmospheric disturbances that arise due to baroclinic instability. One quantity that shows significant IAV is the poleward heat flux associated with these waves. These variations – and their impacts on the polar heat balance – will be examined here.

Background: The dust loading of the martian atmosphere can vary significantly from location-to-location, from sol-to-sol, and from year-to-year. The surface dust reservoir varies too. However, were the surface and atmospheric dust distributions to remain fixed from one year to the next, it seems likely that the resulting atmospheric circulation at a give season would be repeatable from year-to-year. This follows from the absence of oceans on Mars.

We have recently conducted several multi-annual simulations with the NASA-Ames Mars General Circulation Model (MGCM; [2]). These extend for 10 years beyond a spin-up year (some 40 year simulations have also been performed). Some simulations have fixed dust all year (e.g., with a visible opacity of 0.5), while others have opacities varying through the year (e.g., following Viking observations). In these cases, the dust loading and distribution at a given *Ls* is the same during every year of the simulation. In a new series of simulations, we randomly specify the annual dust variation to fall between a low dust scenario (e.g., 0.3) and a high dust scenario (e.g., Viking)..

Results: In the first set of simulations (opacity fixed at 0.5 for all time), there is significant IAV in a number of parameters. For example, sol-averaged surface pressures at higher latitude sites (e.g., the Viking Lander 2 site) show variations of several tenths of a millibar from the 10-year average during the midwinter season [1]. This is an O(10%) variation from the long-time mean. Likewise, sol-averaged surface temperatures can be as much as 10-20 K above/below the 10-year average at these same sites. Such IAV is typical in the northern winter season at higher northern latitudes; it is far weaker in the corresponding southern winter season.

The region of high IAV is coincident with the location (in space and season) of baroclininc wave activity, suggesting a connection between the baroclinic wave activity and IAV. We have computed the poleward-directed heat flux $\left(\overline{v' T}\right)$ associated with these eddies (on Earth, this is a substantial fraction of the total poleward atmospheric heat flux). Figure 1 shows the resulting distributions of $\overline{v' T}$ computed over a 90 sol period centered on Ls 270 for each of the 10 years in the fixed opacity 0.5 simulation (the north pole is to the right on each plot, and the contour interval is 5 Km/s, with larger values shaded). Clearly, there are significant year-to-year variations in heat transport into the winter polar regions; the eddy heat flux in some years is virtually zero (e.g., years 01 and 08), whereas in other years values are O(30-40 Km/s). By comparison, poleward-directed heat fluxes associated with topographically-forced stationary waves have magnitudes O(10 Km/s) and show much less year-to-year variation [1].

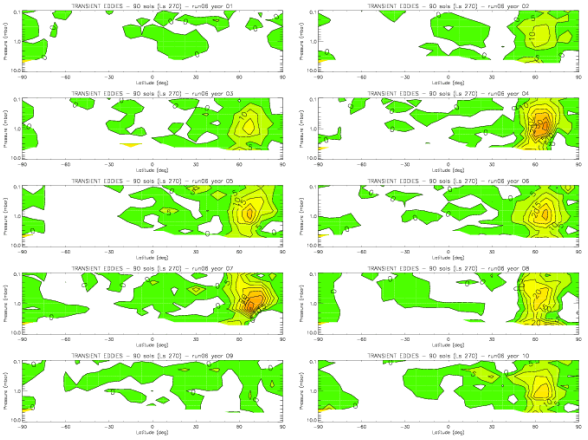

In the light of these variations in eddy heat fluxes into to winter polar region, we examine impacts on the polar heat budget. For example, the total accumulated ice mass in the northern polar region, computed as a function of *Ls*, deviates from the 10 year-average by up to ±O(3%) (Figure 2; each color represents a different year, and time is plotted a sol number, where sol 0 is *Ls* 0).

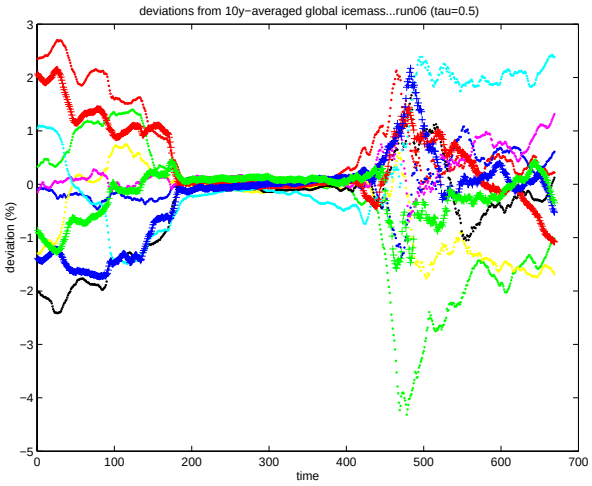

In this talk, we will expand upon the consequences of IAV for the polar region, with attention focussed on those quantities that might be detectable in long-term observations.

References: [1] Bridger,A.F.C., J. L. Hollingsworth, R.M.Haberle and S.R. Rafkin (2003), Granada workshop. [2] Haberle, R.M. *et al* (1999), JGR, 104, p. 8957.

AN AUTOMATED, LOW MASS, LOW POWER DRILL FOR ACQUIRING SUBSURFACE SAMPLES OF GROUND ICE FOR ASTROBIOLOGY STUDIES ON EARTH AND ON MARS.

G. A. Briggs, C. McKay, NASA Ames Research Center, J. George, G. Derkowski, NASA Johnson Space Center, G. Cooper, K. Zacny, University of California, Berkeley, R. Fincher Baker-Hughes International, W. Pollard, McGill University, S. Clifford, Lunar and Planetary Institute

As a project that is part of NASA's Astrobiology Technology & Instrument Development Program (ASTID), we are developing a low mass (~20kg) drill that will be operated without drilling fluids and at very low power levels (~60 watts electrical) to access and retrieve samples from permafrost regions of Earth and Mars. The drill, designed and built as a joint effort by NASA JSC and Baker-Hughes International, takes the form of a down-hole unit attached to a cable so that it can, in principle, be scaled easily to reach significant depths.

A parallel laboratory effort is being carried out at UC Berkeley to characterize the physics of dry drilling under martian conditions of pressure, temperature and atmospheric composition. Data from the UCB and JSC laboratory experiments are being used as input to a drill simulation program which is under development to provide autonomous control of the drill.

The first Arctic field test of the unit is planned for May 2004. A field expedition to Eureka on Ellesmere Island in Spring 2003 provided an introduction for several team members to the practical aspects of drilling under Arctic conditions. The field effort was organized by Wayne Pollard of McGill University and Christopher McKay of NASA ARC. A conventional science drill provided by New Zealand colleagues was used to recover ground ice cores for analysis of their microbial content and also to develop techniques using tracers to track the depth of penetration of contamination from the core surface into the interior of the samples.

VAST ATMOSPHERIC COLD TRAPS WITHIN THE LARGE RINGED TOPOGRAPHIC FEATURES IN NE SIBERIA: IMPLICATION FOR MARS. G. A. Burba, Vernadsky Institute of Geochemistry and Analytical Chemistry, 19 Kosygin St., Moscow 119991, Russia e-mail: burba@online.ru

Introduction: The ridges within the vast mountain country of the NE Siberia have been revealed recently to comprise two giant ring structures (RS), 500 and 400 km in diameter [1] . Such evidence is a new look on the general topographic structure of the area and could be of importance for climatic consequences.The central lower areas of these structures, which are enclosed within a ring wall of mountain ridges, work as giant "cold traps" for the atmospheric air. During the winter seasons the temperature inversion in the near-surface layer of the atmosphere take place there.

Topographic description: The highest area of the North-East Siberia, Russia, consists of the mountain ridges arranged as the two adjacent RS. These RS are located between Lena River Mouth and Magadan Coast of the Sea of Okhotsk. Each of the two rings have circular pattern of mountain ranges, which encircle a plateau area in the central part of the ring. The general topographic shape of each RS is a complex of high mountain rings (altitudes 1000 to 3000 m) with a lower, but still topographically high (400-1200m) plateau inside, and lowland plains outside (50-200 m). The outer diameter of each structure is about 700 km. The rim crest diameters are about 500 km for Yana Ring Structure (YRS), NW in the couple, and 400 km for Oymyakon Ring Structure (ORS), SE one. YRS is located between 63 and 70°N, 125 and 140°E, and ORS – between 61 and 67°N, 136 and 151°E. In general YRS is somewhat lower than ORS, especially with its inner area. The structures are named after the Yana River and Oymyakon settlement, which are located within each of the them.

Air temperature data: The weather observations at Verkhoyansk on Yana River, near the center of YRS, and at Oymyakon on Indigirka River, near the center of ORS, have determined as early as in 1930s that these areas are the coldest places at the Northern hemisphere of the Earth with the minimal records of air temperature as low as – 68° C at Verkhoyansk and – 71° C at Oymyakon. Further long-term meteorological data revealed the areas of Verkhoyansk and Oymyakon as the enclosed regions with very low air temperatures in winter. Both areas have value of the mean monthly air temperature for January defined as "lower than – 48° C" [2]. And over the whole NE Asia such low values are typical ONLY to these two areas, the central parts of YRS and ORS.

Interpretation: Now, after a new look at the topographic structure of the NE Siberia, it could be explained that each of these "cold poles" is located within the lower areas at the central parts of the large ring structures (intermountain basins), which works as a giant cold traps being enclosed within a ring wall of mountain ridges. Such situation could lead to the circumstances of the temperature inversion in the near-surface layer of the atmosphere.

Implication for Mars: Couldn't the similar situation with the air temperature take place during the winter season within the craters and large basins in the polar regions of Mars?

References: [1] Burba G. A. (1995) *LPSC XXVI*, 189-190. [2] Atlas SSSR (1984) Map "Air temperature", 99 (Atlas of the USSR – *In Russian*).

The most recent section of the south polar layered deposits. S. Byrne[1] and A.B. Ivanov[2], [1]Division of Geological and Planetary Sciences, California Institute of Technology, Mail-stop 150-21, Pasadena, CA 91125.. [2]Jet Propulsion Laboratory, MS168-416, Pasadena, CA 91106. **shane@gps.caltech.edu**, **anton.ivanov@jpl.nasa.gov**

Introduction: The polar layered deposits of both hemispheres contain a record of Martian environmental conditions. In this study we will assemble a fully three dimensional stratigraphic sequence for the topmost section of the southern layered deposits.

A prominent layer sticks out as a bench part-way down the section. We will correlate other layers relative to this one in exposures on opposite ends of the section. In this way we hope to learn how this part of the overall southern layered deposits is organized in three dimensions.

The necessary datasets which will be utilized will be hires topographic grids from the Mars Orbiter Laser Altimeter (MOLA) provided by the MOLA team and high resolution Mars Orbiter Camera (MOC) images with spatial resolutions of 1.4 to 12 m/px. Due to continuous repeat coverage of the polar orbiting Mars Global Surveyor and Mars Odyssey (MGS & MO) spacecraft this area has very high coverage. MOC frames almost totally cover the entire exposure which makes it ideal for this kind of study.

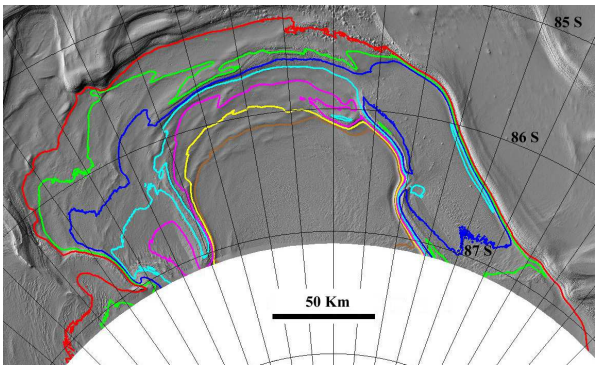

Figure1: MOLA derived shaded relief view of the top of the south polar layered deposits illuminated from the left. The coloured lines represent elevation contours from 4000m to 4600m (red to brown) at 100m intervals.

Regional context and marker bed: The layered sequence in the southern layered deposits can be divided into discrete sections based on elevation (see figure 1). The topmost section is centered on 87° S 5° E and its exposures span elevations of 4300m - 4600m. The highest point of the layered deposits (~4800m) also lies within this area. The top surface is covered with a thin skin of CO_2 ice which comprises part of the southern residual cap.

The layers comprising this section are exposed in scarps to the east and west at 350° E and 20° E as shown in figure 1. The northern edge of this section is not well exposed due to a smooth mantling cover and disruption from the McMurdo secondary crater field. The southern end of this section is well exposed on continuations of the eastern and western scarps however the lack of spacecraft data poleward of 87° S prohibits analysis in this region.

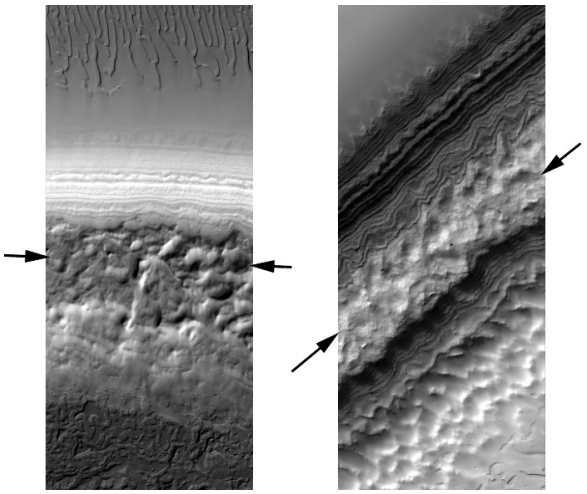

Figure 2: MOC images M08/06301 (left) and M08/02672 (right) from the western and eastern scarps respectively. Scale in both cases is the same (each image 2.8 km wide). Illumination from lower right and upper left respectively. Elevation decreases from top to bottom by 400-500 meters in both cases.

Figure 2 shows an example of two MOC frames separated by ~100 km. The same heavily pitted topographic step is visible part way down the scarp in both cases. This layer will serve as a marker bed by which the position of other layers can be measured.

Work to be presented: We will report on variations in elevations of layers within the topmost section of the south polar layered deposits. We will consider models where the layers are represented as inclined planes and surfaces containing low-order curvature.

We will document changes in strikes and dips as a function of elevation which can be interpreted as erosional unconformities. A lack of erosional unconformities within the section would imply a stable polar environment over the time it took this section to form.

Climactic history from south polar residual cap geomorphology. S. Byrne[1], A.P. Ingersoll[1], A.V. Pathare[1] and F.S. Jiron[1], [1]Division of Geological and Planetary Sciences, California Institute of Technology, Mail-stop 150-21, 1200 East California Blvd., Pasadena, CA 91125, USA. **shane@gps.caltech.edu**, **api@gps.caltech.edu**, **avp@gps.caltech.edu**, **franklin@its.caltech.edu**

Introduction: The southern residual CO_2 cap is a small (88,000 km^2) high-albedo feature which sits atop the much thicker and more extensive southern layered deposits. It persists throughout the year in contrast to the thinner seasonal CO_2 frost which appears and disappears each year. The solid CO_2 which lasts throughout the year both controls circulation patterns regionally and buffers the atmospheric pressure globally. In turn this residual CO_2 deposit is affected by changes in environmental conditions wrought by external forces such as dust storm activity.

This solid CO_2 reservoir has been theorized and observed for decades [1, 2]. Mars Global Surveyor data have revealed this CO_2 residual deposit to contain a rich variety of geomorphic features [3]. One of the most ubiquitous classes of features on the residual cap are the flat-floored quasi-circular pits with steep walls (see Fig. 1), dubbed Swiss-cheese features.

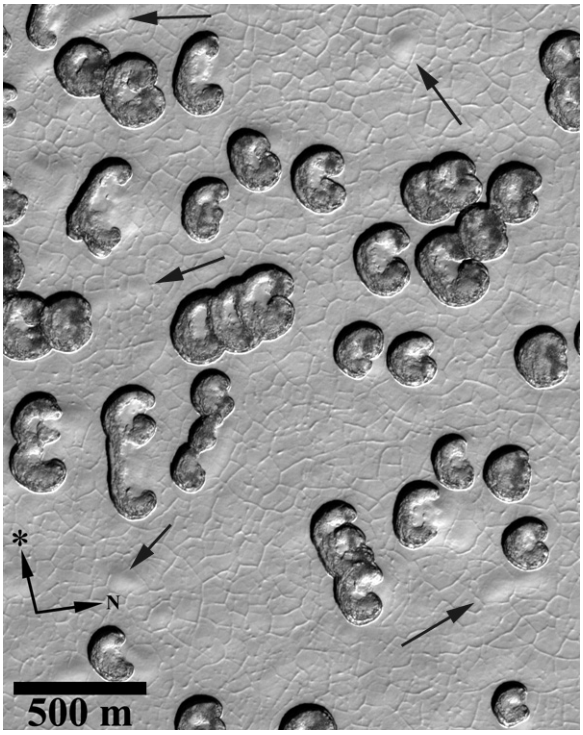

Figure 1. Surface of the Martian residual CO_2 cap showing heart-shaped depressions (Swiss-cheese features). Arrows denote shallow bowls, discussed later. Sub-frame of MOC narrow angle image E13/00663, 87° S, 352° E, L_s 323° (late southern summer), bottom arrows denote direction to sun and north.

Feature description: Swiss-cheese features are characterized by flat floors and steep walls. Features in the region shown in figure 1 and discussed in the next section have a definite symmetry axis found to point in the north-south direction (7). Features in other parts of the cap commonly posses a raised central island in their center surrounded by a moat.

Late in the southern summer when the seasonal covering of CO_2 frost has been removed the walls can be seen to be darker than the surrounding flat upper surfaces.

No changes in shape or size were observed in these features over timescales of a single season (3, 5) but *Malin et al.* (6) observed, using images separated by one Martian year, that the walls of these depressions are expanding laterally at rates of 1-3 m/yr. The rapidity of this expansion is only possible in a medium as volatile as CO_2 ice. *Byrne and Ingersoll* (4) modeled the evolution and growth of these depressions as a hole in a layer of CO_2 ice underlain by water ice and matched their observed expansion rates and morphologic properties, including the flat floors and steep walls.

Swiss-cheese features in local regions all exhibit the same depth, *i.e.*, they all penetrate to the base of the CO_2 deposit, their downward expansion being halted by the involatile nature of the water-ice substrate (4). Different areas on the residual cap exhibit differing thicknesses of the overlying CO_2 slab. The thickest CO_2 deposits appear to be 8-10 meters; however most of the rest of the cap has a much thinner covering. In features which possesses moats and raised central islands it is the moat which penetrates to the underlying water ice layer (7). Modeling results indicate however that the thickness of the overlying CO_2 slab does not affect the retreat rates of the walls.

Environmental history from Swiss-cheese feature populations: The fast rate of wall retreat observed (6) and modeled (4) combined with the small sizes of the depressions indicate that all Swiss-cheese features visible today were created recently (7). Our modeling results indicate that walls should retreat at constant rates once the initial formation phase is over.

In previous work we selected a study region within the residual cap and measured the sizes and orientations of all Swiss-cheese features that it contained (see figure 2). The size distribution is quite narrow indicat-

ing that the measured population has initiated over a very short period of time. We estimate this formation period to have occurred 43-217 Martian years ago. The large spread in age is due to the large spread in modeled wall retreat rates. Values ranging from 0.5-2.5 m/yr are possible with different subsurface albedo conditions (4).

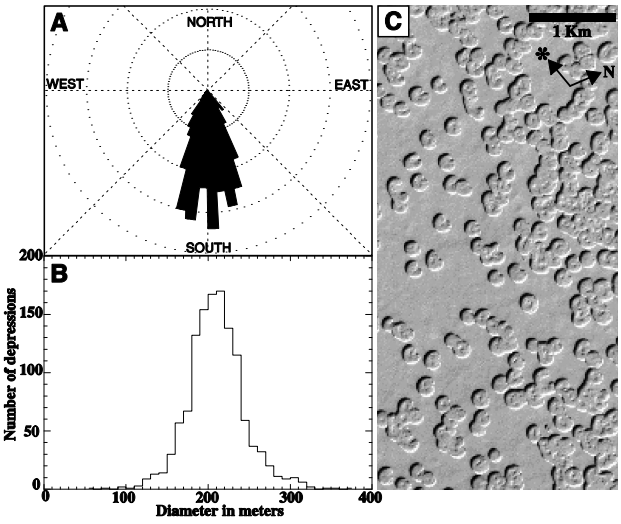

Figure 2. Taken from (7). **A)** Rose diagram of Swiss-cheese feature orientations. Azimuth refers to the direction from the cusp to the opposite wall, through the center of the depression. The total number of features measured was 370, the mean azimuth was within 0.2° of south and the standard deviation was ~17°. Concentric circles indicate number in increments of 10. **B)** Histogram of sizes of identifiable Swiss-cheese features. Diameter here refers to the longest axis for non-circular features. The total number of features measured is 1263, the mean size was 217m and the standard deviation was ~35m. **C)** Many Swiss-cheese features destroying the upper 8m thick layer in a sample view of the study area. Sub-frame of MOC narrow angle image M07/04167, taken at 86.8° S, 355° E, and L_s 211°.

Some change in environmental conditions started this particular population of features growing. Unfortunately we have only begun to observe Mars in detail over the past few decades so understanding what the nature of this event may have been is difficult.

The shallow bowls that are indicated by arrows on figure 1 may be a new generation of Swiss-cheese features. If this is the case we would expect from our modeling that these features would be less than 30 Martian years old. One significant event in Martian history that may have been responsible for their genesis is the 1971 global dust storm. This would lead to increased erosion of the residual cap, but it is unclear why that would initiate the growth of isolated depressions. If the number density of features is an indication of the severity of the event that initiated them, then the event which initiated the main population discussed above and in figure 2 must have been much more severe than this dust storm.

Work to be presented: There are several avenues of research that we are perusing and which will be presented.

- We will report on investigations into the overall mass budget of the CO_2 residual cap. If the Swiss-cheese feature walls are retreating and the mass is not being recondensed elsewhere on the cap then the cap itself will disappear within a few Martian centuries. It seems unlikely that we are observing Mars at such a special time in its history.
- A large range of expansion rates is possible depending on the subsurface albedo profile (4, 7). This is a major obstacle in using our modeling results to date observed Swiss-cheese populations. We will attempt to measure the subsurface albedo profile by examining Mars Orbiter Camera (MOC) images of exposures in the walls of the Swiss-cheese features.
- We have already modeled the initial growth of Swiss-cheese features. However, we always initiated our modeled depressions from pre-existing small surface features. We will report on more detailed investigations into the genesis of Swiss-cheese populations and the possible link to climactic events such as the 1971 dust storm.
- We will continue to catalogue new population statistics for different regions in the residual cap. Each distinct new Swiss-cheese population that we can identify will give us information on previous environmental events that may have occurred.

Investigations into Swiss-cheese features have the potential to describe the last millennia of Martian polar history. It will provide a link from present conditions to longer term variations in Martian climate (due to changing orbital elements) which are perhaps recorded in the layered deposits.

References: [1] Leighton, R. B., and B. C. Murray, *Science* (1966) *153*, 136-144. [2] Kieffer, H. H. (1976) *JGR*, *84*, 8263-8288. [3] Thomas P. C. et al. (2000) *Nature*, *404*, 161-164. [4] Byrne, S., and A. P. Ingersoll (2003) *Science*, *299*, 1051-1053. [5] Malin, M. C., and K. S. Edgett (2001) *JGR*, *106*, 23429-23570. [6] Malin, M. C. et al. (2001) *Science*, *294*, 2146-2148. [7] Byrne, S., and A. P. Ingersoll (2003) *GRL*, *30(13)*.

CONSTRAINTS ON THE WITHIN SEASON AND BETWEEN YEAR VARIABILITY OF THE NORTH RESIDUAL CAP FROM MGS-TES. W.M. Calvin[1], T.N. Titus[2], and S.A. Mahoney[1]. [1]Dept. of Geological Sciences, MS172, University of Nevada, Reno, NV 89557, wcalvin@unr.edu, [2]U.S. Geological Survey, Flagstaff, AZ 86001, ttitus@usgs.gov.

INTRODUCTION: There is a long history of telescopic and spacecraft observations of the polar regions of Mars. The finely laminated ice deposits and surrounding layered terrains are commonly thought to contain a record of past climate conditions and change. Understanding the basic nature of the deposits and their mineral and ice constituents is a continued focus of current and future orbited missions. Unresolved issues in Martian polar science include a) the unusual nature of the CO_2 ice deposits ("Swiss Cheese", "slab ice" etc.) b) the relationship of the ice deposits to underlying layered units (which differs from the north to the south), c) understanding the seasonal variations and their connections to the finely laminated units observed in high-resolution images and d) the relationship of dark materials in the wind-swept lanes and reentrant valleys to the surrounding dark dune and surface materials.

Our work focuses on understanding these issues in relationship to the north residual ice cap. Recent work using Mars Global Surveyor (MGS) data sets have described evolution of the seasonal CO_2 frost deposits [1-5]. In addition, the north polar residual ice cap exhibits albedo variations between Mars years and within the summer season [4-6]. The Thermal Emission Spectrometer (TES) data set can augment these observations providing additional constraints such as temperature evolution and spectral properties associated with ice and rocky materials. Exploration of these properties is the subject of our current study.

MGS-TES DATA SET: Mars Global Surveyor began systematic mapping of the planet in March of 1999. The Mars season was early northern summer, L_s=104. As Kieffer and Titus [2] noted, the seasonal CO_2 frost had disappeared by that time and they observed the growth of higher albedo regions (onset of winter frosting) beginning at $L_s \sim 164$. James and Cantor [4] monitored the seasonal cap recession of 2000 and found the signature of the residual cap emerging under the seasonal CO_2 frost between L_s 60 and 70. We somewhat arbitrarily mark our timeframe of interest as L_s 65 to 165. This allows study of the albedo, temperature and spectral properties of the residual cap through the seasonal cap and the "bare" residual cap. In this regard we can compare variations within the summer season to properties observed under thin or sparse CO_2 frost coverage. The table below illustrates that there are two full and one partial northern summer seasons of data acquired. The data from the first two summers are available via the PDS and the second full summer's data are being released over the next several months.

Northern Summer	L_s 65	L_s 165	Mission Phase
1-partial	4-Dec-98 (pre-mapping)	5-Jul-99	Map
2-full	20-Oct-00	22-May-01	Map/Ext
3-full	8-Sept-02	9-Apr-03	Ext-Ext

PREVIOUS OBSERVATIONS: Earlier workers noted the change in albedo in a number of north pole bright outliers and in the overall coverage by bright ice deposits both between Viking summers and between Viking and Mariner 9 [6-8]. This was possibly attributed to the affects of global dust storms [8]; however Bass et al. [6] showed that significant within season variation occurred among Viking imagery. Cantor et al. [5] also explored this variation in MOC images and noted brightening at the edges within a given Mars summer season and changes in the cap appearance at the same L_s between MGS years (1 and 2 as defined in the table above). The early season appearance was possibly attributed to the occurrence of a large dust storm the previous year, and it was noted that late season ice extent recovers to Viking levels but exhibits small-scale inter-year variations that may not be related to globally repeated weather events [5].

These brightness variations are most extensively observed in the quadrant from 0 to 120 east longitude (lower right) on a polar stereographic projection (see Figures 1 and 2). Typically the large "tail" below the Chasma Boreal and its associated plateau (see Zuber et al. [9] for topography) remain bright while highly sloped cap edges and valleys are defrosted in the early season. Malin and Edgett [10, Figure 76] also call out variations on the end of the southern "tail" (-15 to -40 longitude) and in spiral structures above the Chasma Boreal observed at the same L_s in different Mars years. We note there also appears to be substantial frost variation at the "source" of Chasma Boreal (10 to 25E) from Viking to recent years, being darker in the present epoch in MOC and TES albedos than it was during Viking (Figures 1 and 2).

PRELIMINARY RESULTS: We are examining these seasonal and interannual variations of the north cap in the TES data set. This includes comparison of TES albedo with visible appearance in MOC imagery, merging TES, MOC and Viking data with high-resolution topography, and mapping spectral properties associated with seasonally varying and more constant units within the north residual cap. Figure 2 shows initial results for the early season of MGS "Summer 2" acquired from 12/20/00 to 1/03/01 or L_s ~ 92 to 98. Early season "defrosted" units are seen quite similar to the MOC and Viking results [5, 6, and 10] described in the preceding section. We will present the evolution of TES albedos within this MGS northern summer and the ability to use temperature and slope as a proxy for units which are susceptible to summer and annual changes.

TES spectra are notoriously difficult to work with for these cold polar temperatures. Kieffer et al. [1] show representative examples, but typically use large regional averages to improve the signal-to-noise, especially at higher wavenumbers (>1200 cm-1) where the radiance is dropping rapidly. In an effort to examine seasonal trends they developed several multichannel "bands" and used brightness temperatures (T_b) of these broadband averages and their differences to define surface units. Kieffer and Titus [2] presented data either longitudinally averaged or using these broadband temperatures. We are currently developing methods of handling the spectral variations including use of 2-temperature models to fit mixed pixels of warm rock and cold ice as well as cold surfaces under a warmer atmosphere (e.g. [11]). We will report on the status of various methods and their comparison to previous approaches. We will present preliminary spectral characteristics of ice units that are seasonally variable, seasonally stable and of non-ice units both within and surrounding the residual north cap.

REFERENCES: [1]Kieffer et al, *JGR*, **105**(E4), 9653-9699, 2000. [2]Kieffer and Titus, *Icarus*, **154**, 162-180, 2001. [3]Titus et al. *JGR*, **106**(E10), 23181-23196, 2001. [4]James and Cantor, *Icarus*, **154**, 131-144, 2001. [5]Cantor et al. *JGR*, **107**(E3), 10.1029/2001JE001588, 2002. [6] Bass et al. *Icarus*, **144**, 382-396, 2000. [7] Kieffer, *JGR*, **96**, 1481-1493, 1990, [8] Paige et al. *JGR*, **99**, 25959-25991,1994. [9] Zuber et al. *Science*, **282**, 2053-2060, 1998. [10] Malin and Edgett, *JGR*, **106**(E10), 23429-23570, 2001. [11] Hanel et al., *Exploration of the Solar System by Infrared Remote Sensing*, 1992.

ACKNOWLEDGMENTS: This material is based on work currently supported by NASA under the MDAP Program, Grant: NAG5-12223 to the University of Nevada, Reno and through the 2005 Mars Reconnaissance Orbiter MARCI/CTX Science Team. Viking base image of Mare Boreum courtesy of NASA and obtained through the Planetary Photojournal Web Site at the USGS Flagstaff.

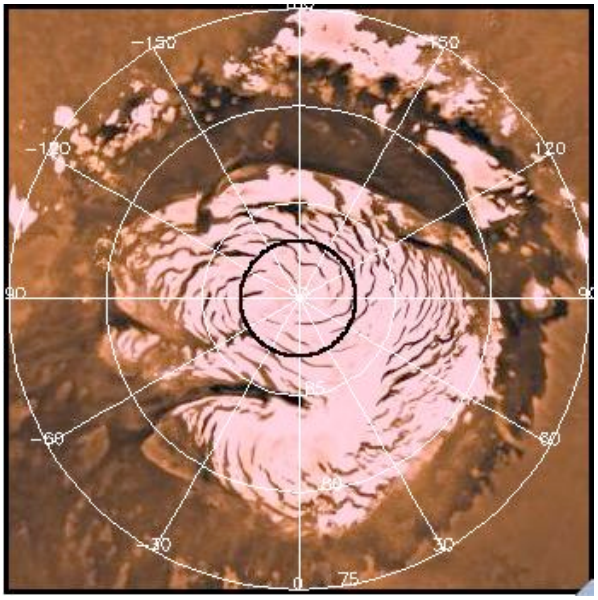

Figure 1: North residual cap as observed by Viking. Black ring denotes area within which TES does not acquire data.

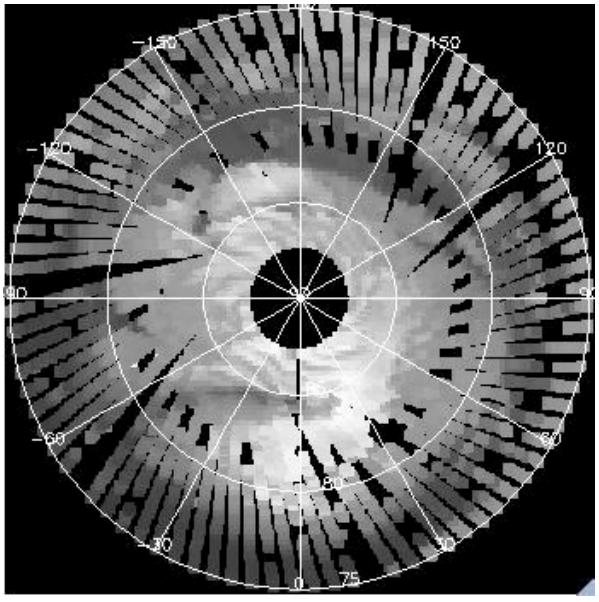

Figure 2: TES albedo map Ls~95 (Dec00/Jan01). Note the lack of bright areas from 30 to 120 E longitude, the extent of Chasma Boreal and the shape of ice surfaces below the Chasma compared with Viking. Squares do not model TES pixel size.

EVOLVING TECHNOLOGIES FOR IN-SITU STUDIES OF MARS ICE F. D. Carsey[1] and M. H. Hecht[2], [1]MS 300-323, Jet Propulsion Laboratory California Institute of Technology, 4800 Oak Grove Dr., Pasadena CA 91109, USA, fcarsey@jpl.nasa.gov, [2]MS 264-255, Jet Propulsion Laboratory California Institute of Technology, 4800 Oak Grove Dr., Pasadena CA 91109, USA, mhecht@jpl.nasa.gov.

Introduction: Icy sites on Mars continue to be of high scientific importance. These sites include the polar caps, the southern mid-latitude subsurface permafrost, and the seasonal frost. These sites have interest due to their roles in climate processes, past climates, surface and near-surface water, astrobiology, geomorphology, and other topics. As is the case for many planetary features, remote sensing, while of great value, cannot answer all questions; in-situ examination is essential, and the motivation for in-situ observations generally leads to the subsurface, which, fortunately, is accessible on Mars. It is clear in fact that a Mars polar cap subsurface mission is both scientifically compelling and practical.

Recent data from orbiting platforms has provided a remarkable level of information about the Mars ice caps; we know, for example, the size, shape and annual cycle of the cap topography as well as we know that of Earth, and we have more information on stratification that we have of, for example, the ice of East Antarctica. To understand the roles that the Mars polar caps play, it is necessary to gather information on the ice cap surface, strata, composition and bed.

In this talk the status of in-situ operations and observations will be summarized, and, since we have conveniently at hand another planet with polar caps, permafrost and ice, the role of testing and validation of experimental procedures on Earth will be addressed.

Exploration Science: The usual Mars scientific topics, life, climate, geophysics and water, are all well connected to Mars ice, and in situ examinations are necessary to obtain the composition, stratification, surface processes, or basal conditions. The primary emphasis for these studies are climate history and processes, on Mars as on Earth. More speculative, but not less interesting, is the prospect that the basal environments of the Mars polar caps, in a climate scenario warmer than the present, would be an excellent habitat, supplied with nutrients and protected from Surficial unpleasantness.

Technologies: In short, Mars polar ice subsurface in-situ missions call for transport to Mars, soft-landing on the polar cap, operations on the surface, power, communication, conduct of surface and near-surface science, access to the subsurface, observing and/or sampling of the subsurface ice cap material, sample management of this material for instrumentation, and planetary protection. It is worth emphasizing that in several of these areas polar science can be accomplished more easily that at other sites. We will proceed here assuming availability of transport to Mars.

Soft landing on a polar cap. The polar caps are characterized by springtime CO_2+H_2O frosts of unknown mechanical properties; we need better information on the response of this frost to landing processes.

Surface operations. The polar caps are benign places in summer with steady temperatures and constant or near-constant sunlight; however, overwintering calls for dedicated development for survival of infrastructure, and this can be accomplished, especially with a nuclear power source. In addition, a mission that lands while the frost is present must accommodate to some decimeters of the landing surface burning off, possibly in nonuniform ways, early in the mission.

Power. A summer mission with low power needs, i.e., one that does not involve deep drilling, has access to ample solar power, although degradation of solar cells in the environment must be examined. Nuclear power from a reactor would solve a host of problems related to high power requirements, as for deep drilling, and to multiyear missions, due to the long life and abundant thermal power produced. This thermal output is also an engineering challenge, since it can both melt away its floor and provide heat that will influence local environmental conditions. Finally, the radiation field of a reactor becomes an engineering issue for electronics. Non-reactor nuclear power occupies a middle ground, with modest power, heat and multiyear capability with fewer difficulties, other than acquiring the radioactive salts.

Communication. Communication from the poles is not challenging. Linkage to orbiters is enhanced by frequent overpasses, and direct communication to Earth is quite simple in the Martian summer.

Surface and near-surface science. Ice cap surface properties and fluxes are likely to be required for any polar cap mission, and the conduct of the measuring programs can be demanding. Key complications are the small variations and fluxes that must be measured accurately, the influence of the spacecraft as an obstacle to windflow and sunlight, operations at the triple point of water, the non-steady surface conditions, and the unknown properties of the surface material.

Access to the subsurface. Drilling even a meter into ice-rich material in the temperature range near –100°C cannot be taken lightly; this material is hard.

Use of thermal methods can be energy intensive and will generate vapor. Thermal methods have received extensive attention and have interesting aspects in their favor at depth, but for shallow penetration with limited power a mechanical approach is favored. Working at depth calls for thermal methods, and both closed-hole (or cryobot) and open-hole strategies have been examined. Power levels become crucial for moderate (10's of meters) and deep (100's of meters) access. It is astonishing to consider that it is within our capability to access essentially any depth of the Mars polar caps.

Scientific observations, sampling and sample management at depth. Once the subsurface has been accessed, sampling must be addressed. Cold ice-rich material is hard and brittle; once a sample is removed and exposed it begins to sublimate if warmed, and if it contains a mix of granular material and salts it may crumble or become mushy or wet; if introduced into instruments, it may adhere to surfaces. Clearly, any observations that can be accomplished non-invasively, e.g., APXS, light scattering, fluorescence, Raman, NMR, etc, are desirable, and some are capable of acquiring data from material within the ice, material not effected by the presence of the drill. On the whole an excellent array of non-invasive scientific instrumentation suitable to subsurface science is in development and requires only adaptation to the specific environment. Sample acquisition and management approaches, of clear value to any in-situ mission, are also in development but have more problems to confront.

Planetary protection. Soon planetary protection requirements for a Mars polar cap mission will be formulated as category IVc, a new (not yet fully documented) category for "special regions" which includes the polar caps. While the specifics of the standards are still in study by the National Research Council, it is clear that rigorous standards of cleanliness will be in force, and these requirements should be integrated into planning early in mission thinking, if possible.

Earth Opportunities for Advancing Mars Polar Exploration Technologies: The high latitudes of Earth contain ice sheets, glaciers, periglacial terrain, permafrost, seasonal snow, rock glaciers and related icy sites in which strong Mars analogs can be developed, as is well known. In the context of climate change, it is of interest to address sites that have changed through cooling, and these are not obvious since Earth seems to be warming now. Some sites worthy of mention:

West Antarctica. The ice streams of West Antarctica (and possibly other locations) are now seen as exhibiting periodic behavior, so called "binge and purge" cycling, in which the bed cools immediately after rapid movement and warms during stagnation.

South Pole "lake". Near South Pole a subglacial flat spot has been observed on airborne radar and identified as a subglacial lake or frozen paleolake or perhaps just a curiously flat spot. Should it be the site where liquid water was present during a previous interglacial, it would today be a fascinating case study in frozen biota, possibly not unlike sites on Mars.

Subglacial volcanoes. At least one active subglacial volcano discovery has been claimed in West Antarctica, and other active volcanoes, with permanent ice and snow covers, can be found in Antarctica and Alaska. Such sites may be highly valuable for comparison with sites in the north polar region of Mars.

Greenland and Antarctica. Substantial regions of both Greenland and Antarctica are at the pressure melting point, and a zone of obvious interest is the transition region between wet and frozen bed areas; these zones can make clear the matter of how this subglacial water alters bed chemistry and biology.

Permafrost. Terrestrial permafrost has long been compared to Mars, and recent Odyssey results certainly encourage this thinking. In the western Arctic, permafrost has been warming, drying, and collapsing, while in Scandinavia there are reports of cooling permafrost. Comparisons of these changes could be useful for Mars thinking. DNA from permafrost has been shown to be well preserved over a few millennia; specific chemical changes to biochemicals over longer time intervals and environments would be interesting for Mars mission planning.

Basal and bed science. For a number of reasons terrestrial glaciology today is strongly interested in bed processes. This is good news for Mars polar science as these projects directly support future Mars polar science in the development of instruments and insights.

Conclusion: Mars polar cap science has received much attention at this, as well as other, scientific meetings, and its high value is well understood among the participants here. An examination of exploration technologies shows us that many of the tools we need to conduct comprehensive scientific studies of the Mars polar caps are available or are in active development. Moreover current work in Earth science is addressing analogous questions in analogous sites; there are effective means to develop, test, validate and assess relevant tools and approaches. In short the scientific questions are mature and the means to address them are maturing quickly. The time is essentially here for significant missions to the polar caps of Mars, and the possibilities are very exciting to contemplate. It is up to us to make these missions happen.

EARTH'S ICY BIOSPHERE. B. C. Christner[1] and J. C. Priscu[1], [1]Montana State University, Department of Land Resources and Environmental Science, Bozeman, MT 59717. mailto: bchristner@montana.edu or jpriscu@montana.edu.

Abstract: Earth's biosphere is cold, with 14% being polar and 90% (by volume) cold ocean <5 ºC. More than 70% of Earth's freshwater occurs as ice (Fig. 1) and a large portion of the soil ecosystem (~20%) exists as permafrost.

Figure 1. Global locations of existing glacial ice sheets and caps (denoted by shading).

Paleoclimate records for the past 500,000 years have shown that the surface temperature on Earth has fluctuated drastically, with strong evidence showing that the Earth was completely ice-covered during the Paleoproterozoic and Neoproterozoic periods [1, 2]. New discoveries of microbial life in cold (-5ºC) and saline lakes, permanent lake ice, cryoconite holes, polar snow, glacial ice, and subglacial environments are extending the known boundaries of the biosphere. Despite the mounting evidence for microbial life in frozen ecosystems, little is know about the psychrophilic or psychrotolerant microorganisms that inhabit them. Molecular-based ecological studies have revealed close phylogenetic relationships between isolates from global locations, with little in common between these environments except that all

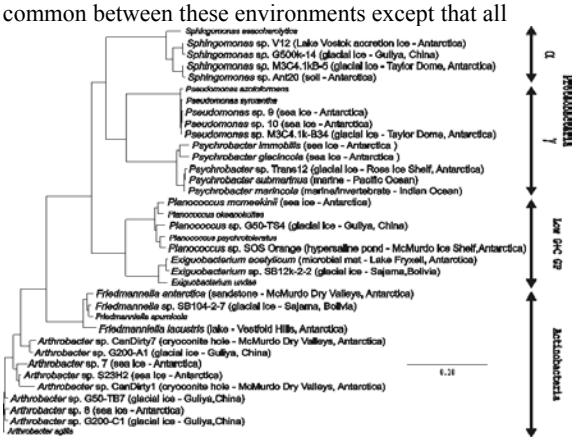

Figure 2. Neighbor-joining tree based on 16S rDNA sequences obtained from isolates (shown in bold) inhabiting permanently cold environments.

are permanently cold (Fig. 2), arguing that microorganisms from these genera evolved under cold circumstances and likely possess survival strategies to survive freezing and remain active at low temperature.

Studies of Earthly ice-bound microbes are also relevant to the evolution and persistence of life on extra-terrestrial bodies. During the transition from a clement environment to an inhospitable environment on Mars, liquid water may have progressed from a primarily liquid phase to a solid phase and the Martian surface would have eventually become ice-covered [3]. Habitats in polar ice may serve as a model for life on Mars as it cooled and may assist us in our search for extinct or extant life on Mars today. Biochemical traces of life or even viable microorganisms may well be protected from destruction if deposited within polar perennial ice or frozen below the planet's surface. During high obliquity, increases in the temperature and atmospheric pressure at the northern pole of Mars could result in the discharge of liquid water that might create environments with ecological niches similar to those inhabited by microorganisms in terrestrial polar and glacial regions. Periodic effluxes of hydrothermal heat to the surface could move microorganisms from the martian subterranean, where conditions may be more favorable for extant life. The annual partial melting of the ice caps might then provide conditions compatible with active life or at least provide water in which these microorganisms may be preserved by subsequent freezing [4].

We propose that the Earth's cryosphere and associated sub-ice lakes should be included as biospheric components of our planet. Here, the cryosphere is defined as that portion of the Earth's surface where water is in a solid form as snow or ice, including solid forms such as sea ice, freshwater ice, snow, glaciers, and frozen ground. Examining permanently ice-covered habitats and microorganisms preserved for extended periods within ice is relevant to astrobiological discussions of past or present life on Mars, and the concept that planetary bodies may not be biologically isolated. Such remote and seemingly inconsequential frozen environments may harbor as yet undiscovered microbial ecosystems that could shed light on the natural history and evolution of life on a frozen Earth, as well as other icy planets and moons in the solar system.

References: [1] Kirschvink, J.L., E.J. Gaidos, L.E. Bertani, N.J. Beukes, J. Gutzmer, L.N. Maepa, and R.E. Steinberger. (2000) *PNAS*, 97, 1400-1405. [2] Hoffman, P.F., A.J. Kaufman, G.P. Halverson, and D.P. Schrag. (1998) *Science,* 281, 1342-1346. [3] Wharton, R.A., Jr., R.A. Jamison, M. Crosby, C.P. McKay, J.W. Rice, Jr. (1995) *J. Paleolimnology,* 13, 267-283. [4] Clifford, S.M. et al., (2000) *Icarus,* 144, 210-242.

CHALLENGES AND SOLUTIONS FOR THE HUMAN EXPLORATION OF THE MARTIAN POLES.

Charles Cockell, SETI Institute, NASA Ames Research Center, Moffett Field, CA 94035-1000.

Introduction: The Martian poles present special challenges for human scientific expeditions that bear similarities to operations in terrestrial polar regions. These challenges include mobility on snows and ices, the problem of accommodation in the deep field, methods for the use of local resources and problems of station maintenance. Because the polar regions are dynamic, substantial volatile sinks, the exploration of the polar regions by humans is a potentially high priority exploration goal. Furthermore, the high astrobiological potential of these regions makes them attractive targets for human exploration.

The exploration of the Martian poles might begin in the earliest stages of a human presence on the planet or missions of exploration might be launched from lower-latitude stations that would avoid the 9-month 24 hr darkness of polar winter, which imposes substantial long-term safety problems.

Mobility: I describe a series of concepts in response to these challenges [1-3]. Mobility on Martian snows and ices can be achieved with pressurized tracked rovers or unpressurized skidoos using methane or other fuels readily made from CO_2 and H_20, both abundantly available at the poles. Materials and supplies can be carried by Nansen sledge in an analogous way to Earth. By heating the underside of the sledges, a sublimed vapor layer can be used to assist in mobility and reduce the chances of freezing to the polar substratum ('polar hover').

Field stations: Field stations, depots and deep-field sites can be realized with pressurized 'ball' tents that allow two scientists to rest within a pressurized, heated environment. Larger versions of such easily assembled stations ('ball field stations') can be used for emergencies and the establishment of short-term camps on the polar ice caps. An augmentation of the ball tent is the Migloo - Martian igloo assembled from a pressurized tent surrounded with blocks of ice that can be used as a Solar Particle Event shelter, the ice reduces the radiation flux. These structures may also find use in deploying robust depots across the polar caps.

In-situ resourse use: Liquid water for drinking and for fuel and oxygen production can be gathered from the poles by two means – either 1) subliming the ice and snow by heating it and gathering the vapor for use in various manfacturing processes. This can be achieved with innovations such as 'sublimation netting' (Figure 1), a network of hollow, heated fibres that heat the ice and snow and draw it into a vacuum system or 2) pressurizing blocks of cut snow and ice and then heating directly into a liquid state, thus avoiding the cost of the latent heat of vaporisation.

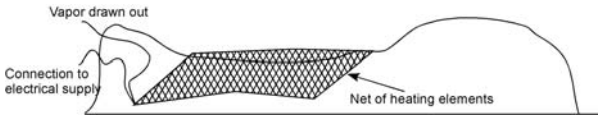

Figure 1. Sublimation netting can be used to gather water for in-situ resource utilization at the Martian poles.

Trans-polar assaults: As well as scientific exploration at specific points on the polar caps, future expeditions might be launched as exploratory trans-polar expeditions across the Martian poles. These expeditions would gather samples across a polar transect and complete traverses that in distance are similar to Trans-polar Antarctic expeditions. I discuss operations at the Martian poles during the 24 hr darkness of polar winter and the challenges presented to overwintering operations.

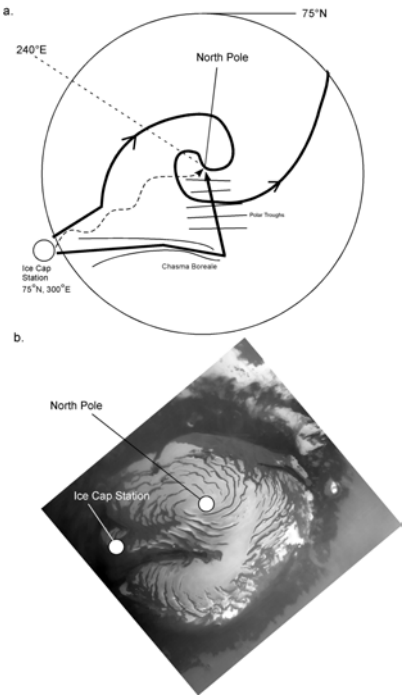

Figure 2. Trans-polar expeditions provide opportunities for polar sampling and purely exploration-driven assaults.

References: [1] C.S. Cockell, (1995) *JBIS*, 48, 359-368. [2] C.S. Cockell, (2001) *Acta Astronautica*, 49, 693-706. [3] C.S. Cockell and A.A. Ellery, (2003) *JBIS*, 56, 33-42.

LIFE IN POLAR IMPACT-SHOCKED ROCKS – AN ANALOG FOR MICRO-HABITATS AT THE MARTIAN POLES. Charles Cockell[1], Pascal Lee[1], Gordon Osinski[2], David Fike[3]. [1] SETI Institute, NASA Ames Research Center, Moffett Field, CA 94035-1000. [2] Planetary and Space Science Centre, Department of Geology, University of New Brunswick, 2 Bailey Drive, Fredericton, NB E3B 5A3, Canada. [3] David A. Fike, Scott Polar Research Institute, Lensfield Road, Cambridge CB2 1ER, England

Introduction: We describe the colonization of shocked gneissic rocks from the Haughton impact structure in the Canadian High Arctic (75°N) [1] as a potential analog for habitats at the Martian poles for speculative indigenous life or contaminants that have already been transferred to Mars by vehicles such as the crashed Mars Polar Lander.

We have used 16s RNA sequencing and SEM to demonstrate the presence of a diverse heterotrophic community of microorganisms throughout the rocks, including spore-forming *Bacillus* spp., which are a known genus of microorganisms to be found on spacecraft surfaces [2]. The low nitrate and phosphate abundances in the polar desert and probably the low leaching rate of organics into the rocks mean that these communities are likely to be nutrient stressed and may spend most of their time in a dormant state. Many of these organisms phylogenetically match psychrophilic species, suggesting adaptation to low growth temperatures.

As well as heterotrophic components, the rocks are also colonized by photosynthetic organisms. Cyanobacteria of the genera *Chroococcidiopsis* and *Dermocapsa* inhabit the rocks as endolithic bands from the surface to a depth of ~5 mm where light levels are sufficient for photosynthesis [1].

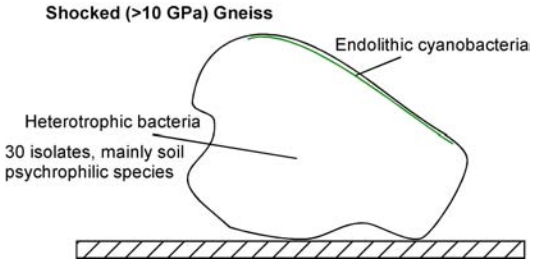

Figure 1. Impact shocked gneiss provides a habitat for a diversity of microorganisms adapted to survival in the terrestrial arctic.

The organisms grow as biofilms on the surfaces of impact fractures and are attached to the rocks in a polysaccharide matrix. The organisms probably enter the rocks after wind deposition onto the surface of the rocks and leach into the subsurface of the rocks with water that penetrates into the inter-connected microfractures. Both phototrophic and heterotrophic components derive their water from snow-melt and rain during the brief ~1.5 month growing season and remain frozen and dormant during the 24 hr darkness of polar winter when temperatures drop to -45°C. We have shown that water can be retained within the rocks for many days after a precipitation event or snow-melt.

During the 24 hr light of polar summer the organisms are protected from UV radiation by the overlying rock and they gain the advantage of thermal heating of the rock [3]. We have shown using sections of rock overlying monolayers of *Bacillus subtilis*, that 0.5mm of rock is sufficient to reduce microbial inactivation by one order of magnitude. The implications of this data are that under 1.5 mm of rock, the damage experienced by micro-organisms entrained into a similar microhabitat on Mars would be similar to that on the exposed surface of present-day Earth under the protection of the ozone column, demonstrating the effectiveness of the endolithic habitat as a refugium from Martian UV radiation.

Using thermisters embedded into the rocks, we found that at a depth of 1 mm the temperatures rose to 10°C higher than the air temperature [3]. Thus, the communities within the rock may experience substantially higher temperatures in the micro-climate than in the external macro-climate, consistent with observations of Antarctic endolithic communities [4].

The similar obliquity of Mars and Earth, and thus the requirement for any potential Martian polar life (indigenous or contaminant microorganisms) to be able to survive the dark Martian polar winter, makes the study of terrestrial polar microorganisms and their modes of survival of special interest as analogs to guide life detection strategies at the Martian poles. Because the Martian surface has a large number of impact craters, which compared to the Earth, are unsubducted and relatively uneroded, understanding the growth and survival of microorganisms within a polar impact structure can yield important insights into the ability of microorganisms to take advantage of impact habitats in the polar regions of Mars.

References: [1] Cockell, C.S., Lee, P., Osinski, G., Horneck, G., Broady, P. (2002). Meteoritics and Planetary Science, 37, 1287-1298. . [2] Fike, D., Cockell, C.S., Pearce, D., Lee, P. (2003). International Journal of Astrobiology, **1**, 311-323. [3] Cockell, C.S., McKay C.P., Omelon, C. (2003). International Journal of Astrobiology, 1, 305-310. [4] McKay, C.P. & Friedmann, E.I. (1985). *Polar Biology* **4**, 19-25.

LIFE IN MARTIAN SNOWS – MEASUREMENTS OF UV PROTECTION UNDER NATURAL ANTARCTIC SNOWS IN THE UVC (254 nm)

Cockell, C.S. British Antarctic Survey, High Cross, Madingley Road, Cambridge. CB1 3AR. UK

Introduction: Ultraviolet radiation down to 195 nm penetrates to the surface of the Martian north polar ice cap during the polar summer on account of the lack of an ozone column, in contrast to the Earth where only radiation above ~290 nm penetrates to the surface (except under ozone depletion, when radiation down to ~280 nm may penetrate). During the winter, spring and fall some ozone production does occur over the Martian poles, but the column abundance is about two orders of magnitude lower than terrestrial stratospheric ozone values. Although this ozone will provide some protection from UVC (200-280 nm) radiation, it is transient. The DNA-damage experienced on the surface of the Martian poles is approximately (under clear, dust-free skies at vernal equinox) three orders of magnitude higher than that experienced by terrestrial polar organisms (under an undepleted ozone column at the same orbital position).

UV in Antarctic and Martian Snows: To investigate the potential of Martian snow to act as a protection mechanism for contaminant microorganisms or organics, the penetration of 254 nm radiation (produced from a field-portable mercury vapor source) into natural snows was measured at Mars Oasis, Antarctica (72°S) during the 2001 austral summer.

Sections of icy snow-pack of approximate dimensions 10 x 10 cm were placed between the cosine-corrected collector of a calibrated Ocean Optics S-2000 spectrometer and the radiation source. A control measurment was taken before each snow-pack measurement and the ratio of the value under the snow-pack to the control was calculated as the attenuation coefficient. The thickness of each snow-pack sample was measured.

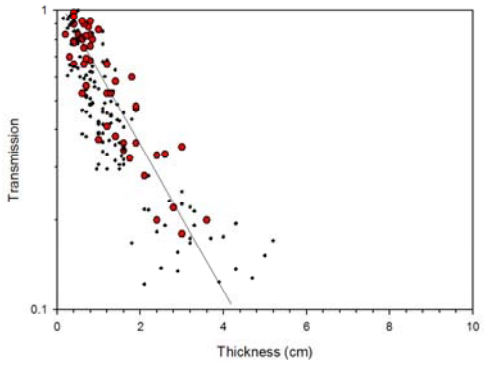

Figure 1. Attenuation of 254 nm radiation (large circles) through snow-pack of different thicknesses. Small dots show attenuation of solar radiation at 310 nm.

The measurements at 254 nm were used as an approximation of the UV-attenuating properties of Martian snows across the whole UVC range. The attenuation of the snow was linearly interpolated between 254 and 310 nm and then linearly extended to 200 nm to make a crude attenuation throughout the Martian UVC range.

For measurements of natural solar radiation between 310 and 400 nm, values were acquired at 1 nm intervals and the collector was held in a clamp directly pointing towards the sun for the control and snow-pack measurement. The penetration of solar radiation from 310 to 400 nm was used for transmission values for the UV ranage common to Earth and Mars [1].

Convolved with a simple Mars radiative transfer model, the data suggests that under ~6 cm of Martian snow, DNA-damage would be reduced by an order of magnitude [2]. Under approximately 30 cm of snow, DNA damage would be no worse than that experienced at the surface of the Earth. Although we do not know the exact characteristics of Martian snows, these first-order data suggest that burial in even modest coverings of Martian snows could allow for the long-term survival (and if water if present, even growth) of contaminant microorgannisms at the Martian polar caps even under the extreme UV fluxes of clear Martian skies. These coverings of snow will also allow for enhanced preservation of organics against UV-degradation.

Intriguingly, at the depth at which DNA damage is reduced to similar levels as those found on the surface of present-day Earth, light levels in the photosynthetically active region (400 to 700 nm) are still two orders of magnitude higher than the minimum required for photosynthesis, showing that within snow-pack on planets lacking an ozone shield, including Mars, UV damage can be mitigated, but light levels are still high enough for organisms that have a requirement for exposure to light for their energy needs. Photosynthetic life is not expected at the Martian poles, but the data reveal the apparently favourable radiation environment for life within the polar caps.

References: [1] Cockell, C.S. and Cordoba-Jabonero, C. Photochem. Photobiol. (in review). [2] Cockell C.S. Abstracts of the 2nd European Exo/Astrobiology Conference, 2002.

Carbon Dioxide Convection in the Martian Polar Night and its Implications for Polar Processes. A. Colaprete[1] and R. M. Haberle[2], [1]SETI (NASA Ames Research Center, Moffett Field, MS 245−3, Mountain View,CA 94035, tonyc@freeze.arc.nasa.gov, [2]NASA Ames Research Center (NASA Ames Research Center, Moffett Field, MS 245−3, Mountain View,CA 94035).

Introduction: Each Martian year nearly 30% of the atmosphere is exchanged with the polar ice caps. This exchange occurs through a combination of direct surface condensation and atmospheric precipitation of carbon dioxide. It has long been thought the amount of condensation within the polar night is maintained by a balance between diabatic processes such as radiative cooling and latent heating from condensing CO_2. This assumption manifests itself in Mars General Circulation Models (GCM) in such a way as to never allow the atmospheric temperature to dip below the saturation temperature of CO_2. However, observations from Mars Global Surveyor (MGS) Radio Science (RS) and the Thermal Emission Spectrometer (TES) have demonstrated this assumption to be, at best, approximate. Both RS and TES observations within the polar nights of both poles indicate substantial supersaturated regions with respect to CO_2. The observed temperature profiles suggest conditionally unstable regions containing planetary significant amounts of potential convective energy. Presented here are estimates of the total planetary inventory of convective available potential energy (CAPE) and the potential convective energy flux (PCEF). The values for CAPE and PCEF are derived from RS temperature profiles and compared to Mars GCM results using a new convective CO2 cloud model that allows for the formation of CAPE.

CO_2 Convection: A rising air parcel will cool along the dry adiabat until saturated (Level of Condensation Lifting) at which time condensation and the release of latent heat force the parcel to cool along the wet adiabat. If the release of latent heat maintains the air parcel temperature above the environment temperature then it can become buoyant and freely convect (Level of Free Convection). Free convection will continue as long as the parcel remains warmer than its surroundings (Level of Neutral Buoyancy). The amount of free convection that can occur depends on the difference in temperature between the ascending air parcel and its environment. One measure of the ability of a parcel to freely convect is the convective available potential energy (CAPE). The CAPE of a parcel can be expressed as

$$CAPE = \int_{z_1}^{z_2} b\,dz \qquad 1.$$

where z_1 and z_2 are the initial and ending altitudes of the rising parcel of air and b is the buoyancy

$$b = g\frac{(T_p - T_e)}{T_e} \qquad 2.$$

with T_p and T_e being the temperature of the parcel and environment respectively. Within the Martian polar night the atmosphere is frequently at or above the CO_2 saturation temperature. If an air parcel near the surface is forced to rise it will very quickly become saturated and cool along the wet adiabat. However, since the surrounding atmosphere is already at the wet adiabat the parcel's buoyancy is nearly zero ($T_p - T_e \approx 0$). Therefore there is very little CAPE (with respect to CO_2 convection) within the Martian polar night and CO_2 convection would be shallow.

Not all of the Mars polar night atmosphere is at or above the saturation temperature, however. RS measurements indicate regions of CO_2 supersaturation in the lower atmosphere below about 1−2 mbar. Examples of RS observations showing supersaturations are shown in Figure 1. In Figure 1 four RS measurements, two for the South polar region and two for the North polar region, are shown with their corresponding CAPE (J kg^{-1}). These supersaturated regions can form if the air in the region is clear of any previously existing CO_2 cloud particles and new cloud particle nucleation has not yet occurred, or if atmospheric cooling rates are so high that the release of latent heat from growing CO_2 cloud particles is insufficient to compensate for the decrease in temperature. Under these conditions a rising parcel may be buoyant and will rise if condensation occurs. The CAPE for the profiles shown in Figure 1 varies from about 35 −250 J kg^{-1}. For comparison moderate to strong terrestrial convective systems have CAPE in the range from 500−1000 J kg^{-1}. Larger terrestrial thunderstorms can have CAPE greater than 2000 J kg^{-1}. On Earth, for similar amounts of CAPE as that calculated from the RS soundings in Figure 1, low to moderate levels of convection resulting in unorganized microbursts would be expected.

RS Observations: In the 6921 RS profiles analyzed thus far, approximately 25% of them show some amount of CAPE (as defined by Eq. 1). Figure 2 shows the location of the RS profiles which

contained CAPE. The highest value of CAPE was in the North and had a value of 421 J kg^{-1}. If all 421 J kg^{-1} of CAPE in this profile was converted to convective motion (neglecting entrainment effects and possibly cloud particle drag) the resulting updraft would have a velocity of almost 30 m s^{-1}. The total integrated CAPE in the profiles shown in Figure 2 is approximately 28 kJ kg^{-1}. Due to the limited spatial and temporal nature of the observations, the temperature profiles studied only constitute a fraction of the total atmospheric volume and time that CAPE is present. An estimate of the total rate of CAPE formation was made by linearly interpolating, in time and space, observed CAPE tendencies between observation points. Assuming all CAPE is converted to heat a total potential convective energy flux (PCEF) was calculated and is shown in Figure 3. The periods of highest PCEF correspond to the mid to late winter periods at both poles. The PCEF magnitude is largest in the North being about twice that of the South. During the late winter period the PCEF constitutes approximately 10% the total latent heating budget, or approximately equal to the total meridional heat transport.

A new CO_2 cloud model recently implemented in the Ames GCM reproduces the observed supersaturated regions. The cloud model includes the microphysical processes of nucleation, condensation, and sedimentation. Proper treatment of ice nuclei (IN) nucleation, assumed here to be dust grains, is critical to reproducing the observed supersaturated regions. The supersaturation at which new CO_2 cloud particles will form was recently measured to be 35%, consistent with the maximum supersaturations observed in the RS temperature profiles. Integrated CAPE and PCEF from simulations utilizing this new CO_2 cloud model are consistent with those estimated from the observations.

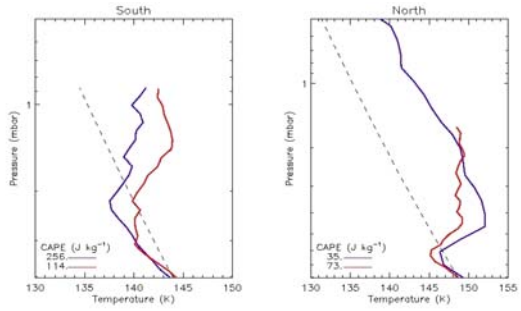

Figure 1. Examples of RS profiles (red and blue curves) showing supersaturated regions and the corresponding CAPE. The dashed curve is the frost temperature for CO2.

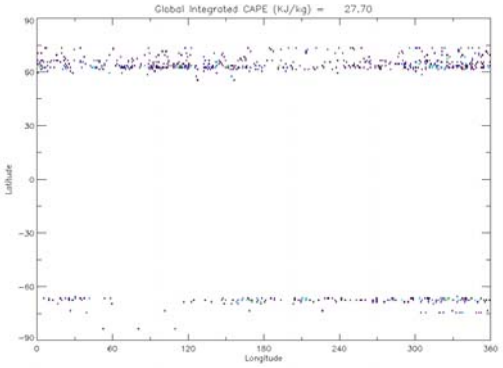

Figure 2: Location of RS profiles having CAPE associated with them.

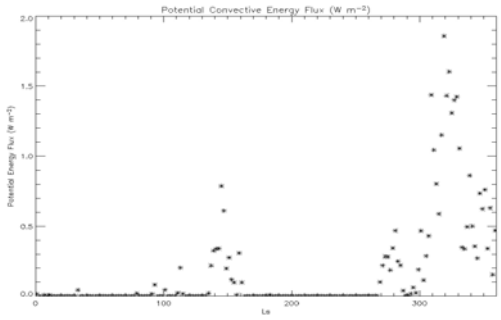

Figure 3. The estimated potential convective energy flux (PCEF) calculated from the total CAPE associated with all RS observations.

BASAL WATER AT THE NORTHGRIP DRILL SITE.

Dorthe Dahl-Jensen[1], Sigfus Johnsen[1], Eske Willerslev[2], Heinz Miller[3], Thorsteinn Thorsteinsonn[4]

[1]Niels Bohr Institute, University of Copenhagen, Juliane Maries Vej 30, DK/2100 Copenhagen OE, Denmark (e-mail: ddj@gfy.ku.dk), [2]Zoological Insitute, University of Copenhagen, [3]Alfred Wegener Istitute, Columbusstrasse, D-27568 Bremerhaven, Germany, [4]University of Iceland.

On July 17 2003, the North GRIP deep ice core drilling program on the Greenland Ice Sheet (75.1 0N, 42.3 0W; 2930 m.a.s.l.), came to a successful end when the drill hit bedrock at 3085 m depth. In the last run the drill was lowered down in the basal water and on surface approximately 10 kg of reddish, bubbly frozen basal water was attached to the drill. A frozen 30 cm long jet of basal water hang from the drill head (www.glaciology.gfy.ku.dk)

The main purpose of the NGRIP project has been to obtain ice dating from the last interglacial period, the Eemian (ca. 115-135 ka BP). A full record of Eemian climate has hitherto not been obtained from a Greenland ice core and the occurrence of rapid climate change during the Eemian, originally inferred from studies of the GRIP ice core, has not been confirmed by other records. Results from airborne radar measurements showed that internal layers, isochrones could be traced from the deep coring sites at Summit in Central Greenland (GRIP and GISP2) to the North GRIP site. However, as the drilling progressed and measurements of ice temperature were made in the borehole, it became clear that the geothermal heat flux was unusually high at NGRIP and that the ice at the bottom was at the melting point.

At present, the bottom ice from the NGRIP core is tentatively estimated to be 127,000 years old. The melt rate at the base is estimated to be 7 mm per year. A study of the internal layers in North Greenland reveal a area of 300 km x 200 km with ice on the melting point. The amount of water produced by the basal melting is enormous and the drainage system must be good as no big lakes are observed under the Greenland Ice Sheet.

The basal water frozen to the NGRIP drill is mainly glacial basal melt water that contains air from the glacial ice. The reddish color however indicates evidence of a content of sediments in the water. Is it possible to find traces of ancient DNA and microbilogical life in the melt water found under the ice which has been closed from the surface for the last 2-5 million years? We hope to return next year and drill cores of the frozen basal water now standing 47 m up in the borehole.

SIMULATIONS OF THE SEASONAL VARIATIONS OF THE MARS SOUTH POLAR CAP: PRELIMINARY RESULTS. K. Dassas , F. Forget , *Laboratoire de Meterologie Dynamique du CNRS, Universite Paris 6, BP99, 75252 Paris Cedex 05, France (dassas@lmd.jussieu.fr).*

Introduction

Every martian year, as much as 30% of the CO_2 atmosphere of Mars condenses in the polar caps of each hemisphere during their respective polar nights. During the spring and summer seasons in a given hemisphere, the seasonal CO_2 cap sublimates back into the atmosphere. While the north polar cap remains roughly circular and centered on the geographic pole during its recession, the south polar cap becomes assymetric with strong variations with space and time. In particular, the preservation of a permanent CO_2 deposit all year long near the south pole raises important issues such as the potential ability of these deposits to buffer the atmosphere. The TES observations of the south polar region during its recession have also confirmed that two regions have different behavior than the rest of the cap in terms of albedo and CO_2 budget. These are the Mountains of Mitchel, a high albedo area where the frost is left behind after the rest of the polar cap recedes each spring, and the Cryptic region, an extended low albedo area which sublimates earlier than the rest of the cap [1]. As of today , the existence and location of the residual cap, the mountains of Mitchel, and the Cryptic region remain poorly understood. No obvious correlations have been found between these areas of interest and topography, geology, thermal inertia or ground albedo [1-2].

Current situation

In the LMD martian general circulation model [3-5], the condensation and sublimation of carbon dioxide on the ground is primarily controlled by relatively simple physical processes. When the surface temperature falls below the condensation temperature, CO_2 condenses, releasing the latent heat required to keep the solid-gas interface at the condensation temperature. Conversly, when CO_2 ice is heated, it partially sublimes to keep its temperature at the frost point temperature. In the atmosphere, condensation may result from radiative cooling on the one hand (especially when the atmosphere is dust laden) and from adiabatic cooling in upward motions on the other hand. The radiative effect of CO_2 snow fall and fresh snow can be taken into account by lowering the emissivity [3]. Although the LMD GCM represents pretty well the boundaries and the total mass of the polar caps, it doesn't reproduce neither the Cryptic region nor the mountains of Mitchell or the residual polar cap. The modeled south polar cap completely sublimes by the beginning of summer.

Investigation

To better understand and simulate polar cap features like the Cryptic region, the mountains of Mitchel or the perenial CO_2 ice cap, different investigations have been done.

What happen's during the polar night?

Using the LMD GCM, simulations have been performed during the polar night (Ls90-120) in order to highlight possible enhanced or reduced CO_2 condensation rate in regions of interest. No obvious correlations between atmospheric or ground condensation rate and neither the Cryptic region nor the mountains of Mitchel have been found. Such a work could be of interest to compare with the Mars clouds detected by the Mars Orbiter Laser Altimeter (MOLA) [6].

New albedo parametrization.

Previously in GCM, the ice albedo parametrization was not dependent on the incident solar flux. According to the observations the CO_2 ice albedo increases as the CO_2 ice is exposed to increasing insolation [6]. We added this parametrization in the GCM. At the same time, we have simulated the fact that slab CO_2 ice becomes transparent when it becomes thin by defining the albedo as a combination of the ice and underlying ground albedos depending on a chosen thickness of the CO_2 ice layer.

Taking account slope orientation.

The previous parametrization of the incident solar flux surface was not taking account the slope (orientation and absolute value). We have performed simulations with a new slope dependent parametrization. Slopes have been calculated using the MOLA topography data (32 pixels / degree).

Future work

In order to better understand the seasonal variations of the south polar cap, we will continue this project and, in particular, perform very high spatial resolution simulations in order to highlight the slope effect or the spatial variations of atmospheric condensation. We also want to improve CO_2 ice microphysic representation, and some work should be done to determine the role of dust. Once all these processes will be taken into account, the GCM should be able to predict features like the Mountain of Mitchel or the Cryptic region. Otherwise, these features will have to be considered as a

major enigma of the martian climate system.

References [1] Kieffer H. et al (2000) JGR, 105, 9653-9699. [2] James P. et al (2001) JGR, 106, NO. E10, 23,635-23,652. [3] Hourdin F. et al (1993) JAS, 50, 3625-3640. [4] Forget F. et al (1998) Icarus, 131, 302-316. [5] Forget F. et al (1999) JGR, 104, 24,155-24,176. [6] Neumann et al (2003) JGR, 108, NO. E4, 5023. [7] Paige D.A (1985) Science, 228, 1160-1168.

EPISODIC ENDOGENETIC-DRIVEN ATMOSPHERIC AND HYDROLOGIC CYCLES AND THEIR INFLUENCE ON THE GEOLOGIC RECORDS OF THE NORTHERN AND SOUTHERN HEMISPHERES, MARS

J. M. Dohm, *Department of Hydrology and Water Resources, University of Arizona, Tucson, Arizona (jmd@hwr.arizona.edu)*, **A. G. Fairén**, *CBM, CSIC-Universidad Autónoma de Madrid, 28049-Cantoblanco, Madrid, Spain,* **V. R. Baker,** *Department of Hydrology and Water Resources, University of Arizona, Tucson, Arizona,* **J. C. Ferris**, *United States Geological Survey, Denver, Colorado,* **R.C. Anderson**, *Jet Propulsion Laboratory, Pasadena, California,* **E. R. Uceda,** *Servicio de Endocrinología, Hospital Ramón y Cajal, Madrid.*

Diverse evidence shows a direct correlation between episodic endogenetic events of the Tharsis magmatic complex (TMC)/Superplume [1], flood inundations in the northern plains [2], and glacial/lacustrine/ice sheet activity in the south polar region, which includes Hellas and Argyre impact basins (**Fig. 1**) [3-5], corroborating the MEGAOUTFLO hypothesis [6,7]. The TMC encompasses a total surface area of approximately 2 X 10^7 km^2, which is slightly larger than the estimated size of the Southern Pacific Superplume [8]. These hydrologic events include (1) a Noachian to possibly Early Hesperian oceanic epoch and related atmospheric and environmental change (a water body covering about 1/3 of the planet's surface area [9]) related to the incipient development of Tharsis Superplume and the northwestern sloping valleys (NSVs) [10,11] and possibly early circum-Chryse development [12-14], the northwest and northeast watersheds of Tharsis, respectively, (2) a smaller ocean [6-7; 15-17] inset within the former larger ocean related to extensive Late Hesperian to Early Amazonian effusive volcanism at Tharsis [18] and Elysium [19-20] and incisement of the circum-Chryse outflow system [e.g.,12-13]. During this time, magmatic/plume-driven tectonic activity transitioned into more centralized volcanism [4,21]. This Late Hesperian water body may have simply diminished into smaller seas and/or lakes [22] during the Amazonian Period, or renewed activity at Tharsis [21] and Elysium [20,23] resulted in brief perturbations from the prevailing cold and dry climatic conditions to later form minor seas or lakes [2]. All of the hydrologic phases transitioned into extensive periods of quiescence [1,2].

Dynamic, pulse-like, magmatic activity, especially at Tharsis [10] is partly the result of a stagnant-lid lithospheric regime where the internal heat of the planet builds over time to catastrophically erupt magmas and volatiles at the martian surface [1,6,7]. This is not to be unexpected, as pulses of activity are also documented for the Southern Pacific Superplume on Earth where present plate tectonism is recorded [8]. On Mars, the primary releases of the stored-up internal heat of the planet occur at dominant vent regions such as at Tharsis and Elysium and along pre-existing zones of weaknesses related to earlier magmatism and tectonism. This may include both impact events and plate tectonism during the earlier stages of planetary development [1,24]. Persistent periods of quiescence transpired between these violent outbursts sending the planet back into a dormant deep freeze [1,25], with the exception of areas where elevated geotherms persist and local hydrologic activity occurs.

Following a persistent deep freeze and ever thickening cryosphere, an Ontong Java-sized event on Mars (especially considering it is unvegetated and less than half the size of Earth, allowing a far greater impact to the climatic system) would trigger enhanced atmospheric conditions and hydrologic dynamics. A prime example of this process is observed during the Late Noachian/Early Hesperian; a time when magmatic-driven activity included the emplacement of older wrinkle ridged materials in the Thaumasia Planum region, the formation of the Thaumasia plateau, and major development of the primary centers of activity, Syria and central Valles (Stage 2 of Tharsis Superplume evolution; see [4,10-11,21]).

Though variation in the orbital parameters of Mars must be considered as a contributing influence on environmental change [26], a direct correlation between endogenic activity at Tharsis (and to a lesser extent Elysium) and global aqueous activity on Mars is observed in the geologic and paleohydrologic records of Mars (schematically portrayed in **Fig. 1**), including: (1) inundations in the northern plains and relatively short-lived climatic perturbations [1,2,6-7,25], (2) growth and retreat of the south polar ice sheet [5], (3) glacial and lacustrine activity in and partly surrounding Hellas [27] and Argyre [3-4], (4) outflow channel activity at NSVs [10-11] and circum-Chryse [e.g.,12-13], (5) formation of the Tharsis Montes aureole deposits [28], and development of impact crater lakes [29,30]. As such, any theoretic modelling of martian atmospheric or surface conditions must take into account endogenetic-driven activity as distinctly expressed in the geologic record.

ATMOSPHERIC CYCLES ON MARS: J.M. Dohm, A.G. Fairén, V.R. Baker, J.C. Ferris, R.C. Anderson, E.R. Uceda.

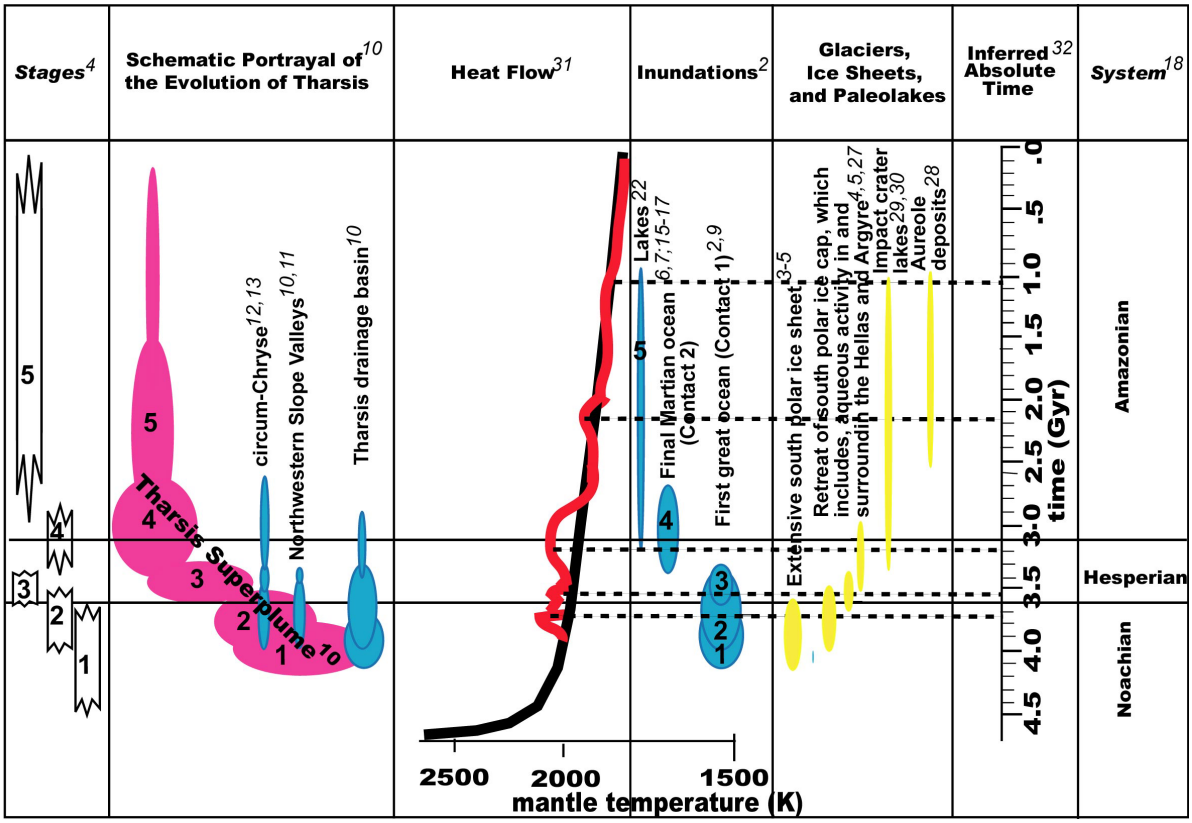

Figure 1. Schematic diagram portraying the spatial and temporal occurrence of major geologic and hydrologic events in martian history.

References. [1] Baker, V.R., *et al*. (2002). A theory for the geological evolution of Mars and related synthesis (GEOMARS). *Lunar Planet. Sci. Conf.*, XXXIII, #1586 (abstract) [CD-ROM]. [2] Fairén, A.G., et al. (2003). Episodic flood inundations of the northern plains of Mars. *Icarus*, in press. [3] Kargel, J.S., and Strom, R.G. (1992). Ancient glaciation on Mars. *Geology*, 20, 3-7. [4] Dohm, J.M., et al., (2001a). Geologic, paleotectonic, and paleoerosional maps of the Thaumasia region of Mars: USGS Misc. Inv. Ser. Map I-2650, scale 1:5,000,000. [5] Milkovich, S.M., et al. (2002). Meltback of Hesperian-aged ice-rich deposits near the south pole of Mars: evidence for drainage channels and lakes. *J. Geophys. Res*., 107, 2001JE001802. [6] Baker, V.R., *et al.* (1991). Ancient oceans, ice sheets and the hydrological cycle on Mars. *Nature*, 352, 589-594. [7] Baker, V.R., *et al.* (2000). Mars' Oceanus Borealis, ancient glaciers, and the MEGAOUTFLO hypothesis. *Lunar Planet. Sci. Conf.*, XXXI, #1863 (abstract) [CD-ROM]. [8] Maruyama, Shigenori, 1994. Plume tectonics, J. Geol. Soc. of Japan, 100, 24-49. [9] Clifford, S. M., and Parker, T. J. (2001). The evolution of the Martian hydrosphere: Implications for the fate of a primordial ocean and the current state of the northern plains. *Icarus*, 154, 40–79. [10] Dohm, J.M., *et al*. (2001b). Ancient drainage basin of the Tharsis region, Mars: Potential source for outflow channel systems and putative oceans or paleolakes. *J. Geophys. Res*., 106, 32,943-32,958. [11] Dohm, J.M., *et al*. (2001c). Latent outflow activity for western Tharsis, Mars: Significant flood record exposed. *J. Geophys. Res*., 106, 12,301-12,314. [12] Rotto, S.L., and Tanaka K.L. (1995). Geologic/geomorphologic map of the Chryse Planitia region of Mars. *U.S. Geol. Surv. Misc. Invest. Ser.* Map I-2441. [13] Nelson, D. M., and Greeley, R. (1999). Geology of Xanthe Terra outflow channels and the Mars Pathfinder landing site. *J. Geophys. Res*., 104, 8653-8669. [14] Zuber, M.T., et al. (2000). Internal structure and early thermal evolution of Mars from Mars Global Surveyor topography and gravity. *Science*, 287, 1788-1793. [15] Parker, T. J., *et al.* (1987). Geomorphic evidence for ancient seas on Mars. In *Symposium on Mars: Evolution of its Climate and Atmosphere, LPI Tech. Rept. 87-01*, 96-98, 1987. [16] Parker, T.J., *et al.* (1993). Coastal geomorphology of the Martian northern plains. *J. Geophys. Res*., 98, 11061-11078. [17] Head, J.W., *et al.* (1999). Possible ancient oceans on Mars: Evidence from Mars Orbiter laser altimeter data. *Science*, 286, 2134-2137. [18] Scott, D.H., and Tanaka, K.L. 1986. Geologic map of the western equatorial region of Mars, *USGS Misc. Inv. Ser. Map I-1802-A (1:15,000,000)*. [19] Greeley, R, and Guest, J. E. 1987. Geologic map of the eastern equatorial region of Mars, *USGS Misc. Inv. Ser. Map I-1802B (1:15,000,000)*. [20] Tanaka, K.L., et al. (2003). Resurfacing history of the northern plains of Mars based on geologic mapping of Mars Global Surveyor data. *J. Geophys. Res*., 108, 8043, doi: 10.1029/2002JE001908. [21] Anderson, R.C., *et al.* (2001). Primary centers and secondary concentrations of tectonic activity through time in western hemisphere of Mars. *J. Geophys. Res.,* **106**, 20,563-20,585. [22] Scott, D.H., *et al.* (1995). Map of Mars showing channels and possible paleolake basins. U.S. Geol. Surv. Misc. Invest. Ser. MAP I-2461. [23] Skinner, J. A., and Tanaka, K. L. (2001). Long-lived hydrovolcanism of Elysium. *Eos. Trans. AGU* ***82***, Fall Meet. Suppl., Abstract P31B-07. [24] Fairén, A.G., et al. (2002). An origin for the linear magnetic anomalies on Mars through accretion of terranes: implications for dynamo timing. *Icarus*, 160, 220-223. [25] Baker, VR. (2001). Water and the Martian landscape. *Nature*, 412, 228-236. [26] Touma, J., and Wisdom, J. 1993. The chaotic obliquity of Mars. *Science*, 259, 1294-1296. [27] Moore, J. M., and Wilhelms, D. E. 2001. Hellas as a possible site of ancient ice-covered lakes on Mars. *Icarus*, 154, 258-276. [28] Scott, D.H., et al. (1998). Geologic map of the Pavonis Mons volcano, Mars: *USGS Misc. Inv. Ser. Map I-2561* (1;2,000,000 scale). [29] Cabrol, N. A., and Grin, E. A. (1999). Distribution, classification and ages of Martian impact crater lakes. *Icarus*, 142, 160-172. [30] Cabrol, N. A., and Grin, E. A. (2001). The evolution of lacustrine environments on Mars: is Mars only hydrologically dormant? *Icarus*, 149, 291-328. [31] Schubert, G., and Spohn, T. 1990. Thermal history of Mars and the sulfur content of its core. *J. Geophys. Res.* 95, 14,095-14,104. [32] Hartmann, W. K., and Neukum, G. 2001. Cratering chronology and the evolution of Mars. *Space Sci. Rew*., 96, 165-194.

LIFE DETECTION AND CHARACTERIZATION OF SUBSURFACE ICE AND BRINE IN THE MCMURDO DRY VALLEYS USING AN ULTRASONIC GOPHER: A NASA ASTEP PROJECT. P. T. Doran[1], Y. Bar-Cohen[2], C. Fritsen[3], F. Kenig[1], C. P. McKay[4] A. Murray[3] and S. Sherrit[2] [1]University of Illinois at Chicago, Earth and Environmental Sciences, 845 West Taylor Street (MC186), Chicago, IL 60607 USA email:pdoran@uic.edu or fkenig@uic.edu, [2]CALTECH, Jet Prop Lab, 4800 Oak Grove Dr, M-S 82-105, Pasadena, CA 91109 USA email: yosi@jpl.nasa.gov or ssherrit@jpl.nasa.gov, [3]Desert Research Instite, 2215 Raggio Parkway, Reno, NV 89512 USA email:cfritsen@dri.edu or alison@dri.edu, [4]NASA Ames Research Center, Divion of Space Science, Moffett Field, CA 94035 USA, email:cmckay@mail.arc.nasa.gov

Introduction: Evidence for the presence of ice and fluids near the surface of Mars in both the distant and recent past is growing with each new mission to the Planet. One explanation for fluids forming spring-like features on Mars is the discharge of subsurface brines. Brines offer potential refugia for extant Martian life, and near surface ice could preserve a record of past life on the planet. Proven techniques to get underground to sample these environments, and get below the disruptive influence of the surface oxidant and radiation regime, will be critical for future astrobiology missions to Mars. Our Astrobiology for Science and Technology for Exploring Planets (ASTEP) project has the goal to develop and test a novel ultrasonic corer in a Mars analog environment, the McMurdo Dry valleys, Antarctica, and to detect and describe life in a previously unstudied extreme ecosystem; Lake Vida (Fig. 1), an ice-sealed lake.

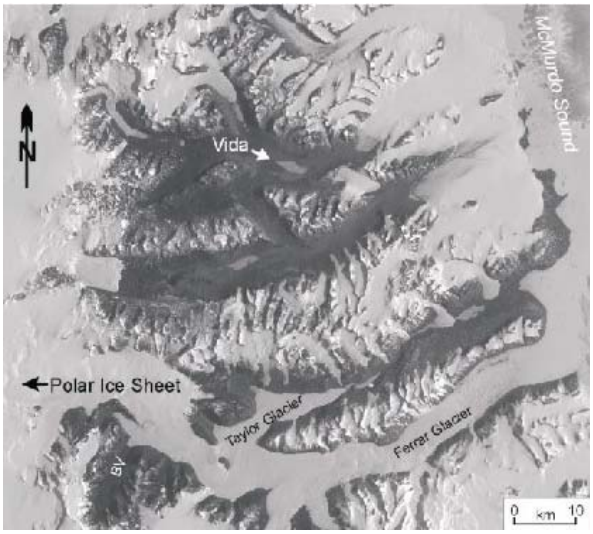

Figure 1: Landsat image of the dry valleys region showing location of Lake Vida. The image is centered at 77.5oS 162oE.

Ice-Sealed Lakes: Lakes in the McMurdo Dry Valleys of East Antarctica have long been studied as extreme environments and potential analogs of purported Martian lakes of the past [e.g. 1, 2]. Commonly studied dry valley lakes have a 2 to 6 m perennial ice cover and 20 to 60 m water column beneath. These lakes also have a range a salinities from fresh to hypersaline, and all allow suffienct sunlight to pass through the ice for photosynthesis to occur in the water column and benthos.

A few lakes in the dry valleys have been largely unstudied until recently because they were believed to be frozen to their beds. One of these lakes (Lake Vida) is also one of the two largest lakes in the dry valleys. Using a combination of ground-pentrating radar and ice coring techniques we have established that Lake Vida comprises a NaCl brine with a salinity seven times sea water and temperature constantly below -10^{o}C lies beneath ~20 m of ice that is at least 2,800 radiocarbon years old [3]. Microbial mats occur throughout the ice column and are viable upon thawing. Sediment layers in the ice effectively block incoming solar radiation (Fig. 2).

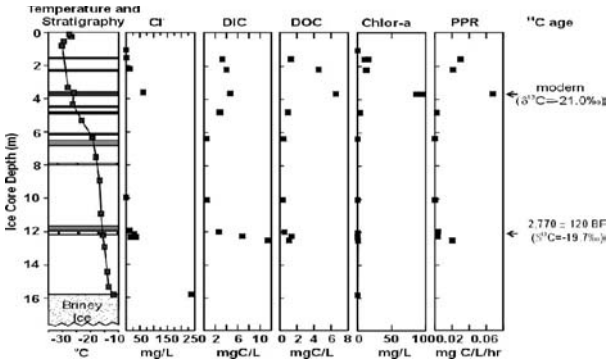

Figure 2: Physical and chemical properties of Lake Vida ice core taken in October 1996. Black horizons on the stratigraphy plot represent sediment layers, gray horizons are sandy ice, and vertically banded horizons contain microbial mat. The temperature profile shown was taken at the time of ice extraction.

Ultrasonic Gopher: Planetary sampling using conventional drilling and coring techniques is limited by the need for high axial force necessitating the use of heavy rovers or anchoring mechanisms. A novel ultrasonic/sonic driller/corer (USDC) mechanism [4] was developed that overcomes these and other limitations

of conventional techniques. The novel element of the USDC is the free-mass that operates as a frequency transformer converting 20 KHz ultrasonic waves to a 60-1000 Hz sonic hammering action (percussion) that is applied onto the drilling/coring bit. The USDC actuator consists of a stack of piezoelectric ceramics with a backing material that focuses the emission of the acoustic energy forward, and a horn that amplifies the displacements generated by the stack. The tip of the ultrasonic horn impacts the free-mass creating a sonic resonance between the horn and the bit.

The USDC has been demonstrated to drill rocks that range in hardness from hard granite and basalt to soft sandstone and tuff. This novel drill is capable of high-speed drilling (2 to 20 mm/Watt·hr for a 2.85mm diameter bit) in basalt and Bishop Tuff using low axial preload (<10 N) and low average power (<5 W). The USDC mechanism has also demonstrated feasibility for deep drilling. The Ultrasonic-Gopher (Fig. 3a) can potentially be used to reach great depths and large diameters (3 and 4.5 cm have been demonstrated) using a low mass rover. Generally, the bit creates a borehole that is larger than the drill bit outer diameter and it also creates a core that is smaller in diameter than the inner diameter of the coring bit. This reduces the chances of bit jamming where hole integrity is maintained, and it eases in the extraction of the core from the bit. Current models suggest that the USDC performance does not change significantly with changes in ambient gravity.

Figure 3: a) Ultrasonic-Gopher and extracted limestone core, b) Recent prototype of ice gopher. Ice chisel bit on the left and actuator on the right.

"Ice Gopher": Ice below 16 m depth in Lake Vida and the brine body have never been sampled directly due to logistical constraints. We are building an ultrasonic "ice gopher" (Fig. 3b) to make in situ ecosystem measurements, and acquire samples to be further analyzed. Early versions of the "ice gopher" suggest that coring through ice may prove a bigger challenge than coring through rock. A large part of our efforts in the early stages of development are focused on the problems of chip handling and ice melt during drilling, both of which can create significant potential for getting the instrument stuck during the mission.

Our field plan is to use the gopher to core through the Lake Vida ice cover, cycling in and out of the hole to retrieve ice cores along the way. The gopher will sample brine as it goes and the brine will be collected at the ice surface under clean and sterile conditions. Using the gopher we will address two main hypotheses

H1. Microbial communities within the brine (include brine pockets in the deep ice) and benthic sediments are currently viable, active and affect the present-day geochemistry of the lake.

H2. The ice, water column and benthos of deeply frozen lakes contain geochemical signatures of past microbiological activity.

Conclusions: Lake Vida provides the unique opportunity to investigate lake ecosystems on the edge of existence to determine what conditions may lead to the eventually complete freezing of a lake and the subsequent development/evolution of microbial communities and geochemical signatures. The combined hypersaline, aphotic, atmospherically isolated and cold conditions in Lake Vida make it potentially among the most extreme aquatic environments on Earth. These conditions were likely to have been present during the last stages of purported lakes on Mars near the end of its water-rich past. Our drilling program will provide useful insight into the challenges of drilling though cold dirt and ice with a low power and light weight instrument to retrieve samples for life detection.

References: [1] McKay C. P. et al. (1985) *Nature, 313,* 561-562. [2] Doran P. T. et al. (1998) *JGR, 103(E3),* 28481-28493. [3] Doran P. T. et al. (2003) *PNAS 100,* 26-31. and Author C. D. (1997) *JGR, 90,* 1151–1154. [4] Bar-Cohen Y. et al. (2001) "Ultrasonic/Sonic Driller/Corer (USDC) With Integrated Sensors," U.S. Patent filed.

THE RHEOLOGY CO_2 CLATHRATE HYDRATE AND OTHER CANDIDATE ICES IN THE MARTIAN POLAR CAPS. W. B. Durham[1], S. H. Kirby[2], L. A. Stern[2], and S. C. Circone, [1]UCLLNL (P.O. Box 808, Livermore, CA 94550; durham1@llnl.gov), [2]USGS (Menlo Park, CA 94025).

Introduction: Modeling the evolution of the Martian polar ice caps requires, among other things, knowledge of the rheologies of their component phases. We review here the known flow laws for water ice and solid CO_2, which are, respectively, the major icy phase, and major CO_2-bearing phase, if conventional wisdom is to be believed. We also present first measurements on the flow of CO_2 clathrate hydrate, whose presence in the south polar cap has been suggested. Earlier measurements of methane clathrate, which is structurally analogous to CO_2 hydrate and which is dramatically harder than water ice suggested that the presence of important volumes of clathrates in the south polar cap were unlikely, owing to the exceedingly high strength of the material. The new measurements show that CO_2 hydrate is significantly weaker than CH_4 clathrate, but still much stronger than water ice. Thus, the rheological basis for dismissing CO_2 hydrate is somewhat weakened, but relaxation models for the south polar cap are still inconsistent with the strength of CO_2 clathrate. Concerning the water ice phase in the polar caps, it is important to consider the balance between grain-size-sensitive (GSS) and grain-size independent (GSI) mechanisms of creep.

Background: Laboratory experimentation on ices is aimed at providing a constitutive rheological law, typically of the form

$$\dot{\varepsilon} = A\sigma^n \exp(-Q/RT) \qquad (1)$$

where $\dot{\varepsilon}$ is the ductile (permanent, volume conservative) strain rate, σ is differential stress, T is temperature, R is the gas constant, and the three parameters A, n, and Q are material-specific constants. It is possible to duplicate Martian temperatures and Martian differential stresses in the laboratory, but it is not possible to duplicate them simultaneously because the resulting Martian strain rates will be too low to measure on the laboratory time scale. While we endeavor to reach ever finer levels of resolution, the current limit on laboratory strain rates, about 2×10^{-8} s^{-1}, is still several orders of magnitude faster than strain rates in the spreading Martian polar caps.

Experimental measurements: The pure phase rheological properties have now been measured in the laboratory for most of the candidate Mars polar cap materials [1-4], and in the case of water ice, a distinction has also been discerned between a GSS and GSI rheology. Conveniently, there are some rather extreme rheological contrasts between some of the phases. In particular, the effective viscosity (proportional to $\sigma/\dot{\varepsilon}$ in Eq. 1) of pure CO_2 ice is several orders of magnitude lower than that of water ice, and the strength of gas hydrates is several orders of magnitude higher than that of water ice. The Mars polar caps are therefore unlikely to hold large reservoirs of CO_2 either as solid CO_2, because the caps would have relaxed far below their current profiles, or as hydrate, because they would not have flowed at all, contrary to what observational evidence suggests.

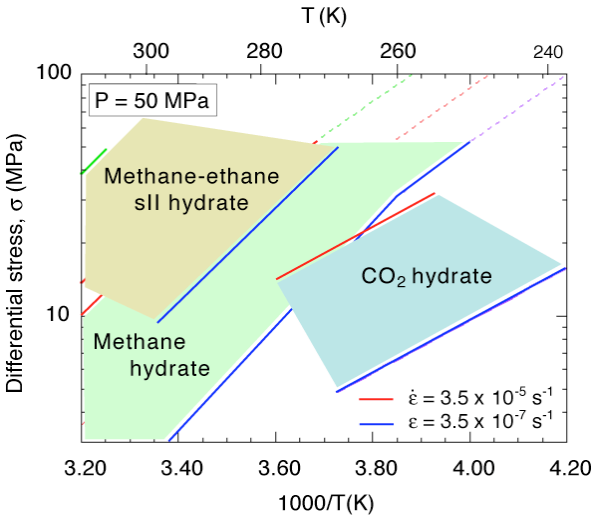

Figure 1. Laboratory measured rheologies of three different gas clathrate hydrates. Methane and CO_2 clathrate are both so-called structure I clathrates, while the methane-ethane clathrate as tested is a structure II material. Fields are bounded by lines of constant $\dot{\varepsilon}$, following Eq. (1)

The latter conclusion was based on the measured strength of methane clathrate, a common earth material with a structure identical to that of CO_2 clathrate. We have now measured the flow of CO_2 clathrate itself (Fig. 1), and found it to be considerably weaker—by about two orders of magnitude in viscosity—than methane clathrate. Although the CO_2 clathrate is still two orders of magnitude more viscous than water ice at similar conditions, the conclusion is now less robust, at least on rheological grounds, that important volumes of CO_2 clathrate cannot exist in the Mars polar caps. We

may have to wait until Mars geology is better understood before we can make additional conclusions.

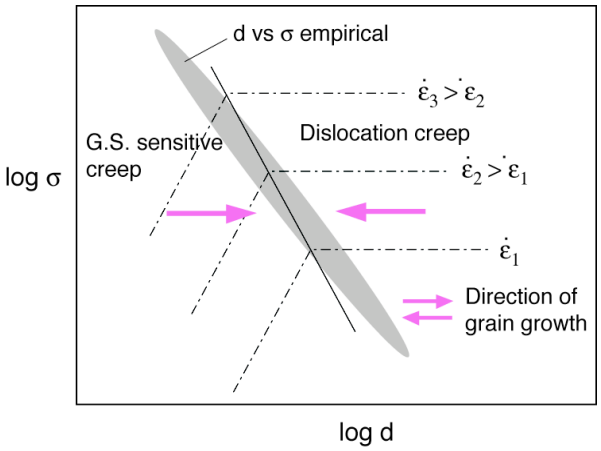

Figure 2. Theoretical evolution of grain size during GSS and GSI (here: dislocation creep) creep, and its effect on steady-state. Grain size tends to increase during GSS creep, but decrease during GSI creep, thus working at cross purposes with respect to the host mechanism. (from [5]).

There is one point we wish to emphasize regarding the rheology of polycrystalline water ice, which is likely to be the major phase in the Mars polar caps. Goldsby and Kohlstedt [1] were able to activate and quantify a GSS rheology in ice, one of the few materials where this has been possible in the laboratory. The finding is quite important to geology and planetary geology because GSS mechanisms are ordinarily less stress sensitive than GSI mechanisms ($n \approx 2$ vs $n \approx 4$ in Eq. 1) and therefore would tend to be favored over GSI mechanisms at the very low stresses and strain rates typical of geological settings.

However, caution should be applied when modeling glacier flow with GSS creep. As pointed out by de Bresser and colleagues [5], one finds many instances in natural settings on Earth (in calcite- and olivine-bearing rocks in particular) where the observed grain size and inferred strain rate imply conditions, following Eq. (1), such that the strain rates contributed by GSS and GSI creep are roughly comparable. Figure 2 offers an explanation for such a phenomenon. Since GSI creep usually involves the movement and growth of dislocations, internal energy of individual grains tends to increase with strain. Since internal energy tends to drive recrystallization, which in turn often results in finer grain sizes, grain size can decrease during GSS creep (the left-pointing red arrow in Fig. 2). GSS creep depends on the presence of grain boundaries in the material, so this action of GSI creep to decrease grain size can have the effect of increasing the proportion of strain rate contributed by GSS creep. On the other hand, deformation by GSI creep takes place by the rigid slip of grain boundaries or by the transport of material along grain boundaries, neither of which changes the internal defect structure or therefore the internal energy of grains. The grains may therefore grow under the motivation of ordinary surface energies (right-pointing arrow in Fig. 2).

The combined result of GSS and GSI creep working at cross purposes with respect to grain growth is that we might expect a balance to eventually be struck, with both mechanisms contributing to flow. In modeling the flow of ice in the Martian polar caps, both flow laws (Eq. 1) for GSS and GSI should be considered.

References: [1] Goldsby D.L. and Kohlstedt, D.L. (1997) *Scripta Mater.*, *37*, 1399-1406. [2] Durham W. B., Stern L. A., and Kirby S. H (1999) *Geophys. Res. Lett.*, *26*, 3493-3496. [3] Durham W. B. and Stern L. A. (2001) *Annu. Rev. Earth Planet. Sci.*, *29*, 295-330. [4] Durham W. B., Kirby S. H., Stern L. A., and Zhang W. (2003) *JGR*, *108*(B4), 2182, doi:10.1029/2002JB001872. [5] de Bresser J. H. P., ter Heege J. H., Spiers C. J. (2001). Grain size reduction by dynamic recrystallization: Can it result in major rheological weakening? *Int. J. Earth Sci., 90,* 28. doi 10.1007/s005310000149

ANTARCTIC ANALOGUES FOR MARS EXPLORATION: A RAMAN SPECTROSCOPIC STUDY OF BIOGEOLOGICAL SIGNATURES.

Howell G..M. Edwards[1], Caroline A. Moody , Susana E. Jorge Villar[1,2] and the late David D. Wynn-Williams[3]

[1] Department of Chemical and Forensic Sciences, University of Bradford, Bradford BD7 1DP, UK.
e-mail: h.g.m.edwards@bradford.ac.uk

[2] Area de Geodinamica Interna, Facultad de Humanidades y Educacion, University of Burgos, Calle Villadiego S/N, 09001 Burgos, Spain.

[3] Antarctic Astrobiology , British Antarctic Survey , High Cross , Madingley Road , Cambridge CB3 0ET , UK.

Introduction: The present conditions at the surface of Mars are not conducive to the survival of life forms, with the thin atmosphere, lack of water, a highly-oxidising regolith and significant UV insolation. The Antarctic provides a terrestrial model with a transect from the maritime, where epilithic colonies can survive through the production of protectant biochemicals, to endolithic systems at the "limits of life" where existence at the surface is impossible [1,2] . In the Antarctic Dry Valleys, the extremely low humidity coupled with low temperatures reaching - 35°C, strong katabatic winds blowing from the Polar plateau and intense UV-radiation exacerbated by atmospheric ozone depletion at higher latitudes provides a putative analogue for the hostile conditions that life must tolerate for survival at or near the Martian surface [3,4].

This extreme terrestrial ecosystem is believed to mirror the conditions under which the evolution of organisms would have had to adapt to the steadily worsening environmental situation on Mars , as exemplified by Epochs III and IV , which effectively describe the Martian surface , subsurface and atmosphere over the last 1.5 million years [4 ,5].]The surface temperatures on Mars range from –123 ^{0}C to + 25 ^{0}C, it's atmosphere is thin and transmits UVB and UVC radiation , and the presence of liquid water at the planetary surface is still conjectural. Clearly , the identification of Antarctic microniches which are amenable to analytical study can provide suitable examples of extremophile terrestrial behaviour of direct relevance to Mars.

Antarctic extremophiles : Special strategies are vital for the adaptation of Antarctic lichens and cyanobacteria to these extreme conditions [6,7]; in addition, the Antarctic provides a gradual change in ecosystem tolerance along a transect from the relatively milder maritime conditions experienced at the coast through to the cryptoendoliths , which are effectively the most adaptable colonies in the Polar region, after which only fossil cyanobacterial evidence is found at the highest latitudes [8,9]. This means that the different strategies being enforced for the survival of these organisms under worsening environmental habitats can be exploredexperimentally and evaluated analytically to assist the predictions of response of organisms to extremes of stress.

To reduce the amount of UVB and UVC radiation reaching the organisms , it is essential that the colonies produce a suite of radiation-protective chemicals for filtering out the low-wavelengths whilst still maintaining their capability for accessing the photosynthetically active wavelengths required for their metabolic processes [10,11]. Hence, it is possible to identify as protective biomolecules complex organic chemicals such as beta-carotene and a range of pigments such as parietin , rhizocarpic acid and calycin --- the former is believed to act as a UV –filter and also function in a DNA-repair mechanism for cell damage caused through radiation exposure, whilst the latter pigments are thought to behave as accessory radiation protectants [11,12,13] . We have carried out some experiments over a two-year period on Antarctic colonies which have been subjected to full radiation exposure at Jane Col , Leonie Island , compared with other colonies at the same site which have been shielded by UVB- and UVC–absorbent plastic cloches. Using nondestructive Raman techniques, it is possible to monitor the production of pigments in response to changes in the environmental situation---in particular , the relative proportions of parietin and beta-carotene in protected and unprotected colonies indicates a possible dualistic role for these pigments [14,15].

The production of hydrated calcium oxalates by colonies under stress is also a key factor of change in other circumstances ; it has been suggested that these oxalates are produced as chelators of heavy metals in the substrate, as water storage devices , acidity controllers and as anti-herbivoral agents. We have recently found evidence for the biogeological modification of iron oxides by extremophilic colonies in the most highly stressed conditions . The importance of this is two-fold , since it not only provides another parameter of knowledge for the understanding of the mechanisms by which terrestrial organisms survive these extremes , but it also gives a clue as to the sort of biogeological changes that have been effected by extremophilic organisms at the limits of life. Hence, in a situation , such as that which probably applied on Mars , any vestiges of extremophilic life would be incapable of tolerating or adapting to the worsening conditions, and they would pass into the fossil record. The clues to their former existence would then be totally found in the geological record and in a suite of unusual relict chemical compounds found there.

Raman spectroscopy : The viability of Raman spectroscopy to identify the key spectral biomarkers of extinct or extant life in the biogeological record has been amply demonstrated for the analysis of Antarctic endoliths [16,17] . The Raman biosignatures of key protectant molecules have been established for the identification of the strategies adopted by cyanobacteria for the colonisation of geological strata . An important requirement here is the ability of the analytical spectroscopic tecnique employed to locate and identify the key biomarkers in the geological systems that might be expected to be encountered in planetary exploration.

The miniaturisation of laboratory-based Raman spectrometers to a size which makes them suitable for part of an instrumentation suite on a robotic lander on a planetary surface has been receiving much attention recently [17-19]. Clearly, the evaluation of prototype instruments for Martian surface or subsurface exploration would be well served by analytical experiments involving Antarctic materials.

In this paper we shall discuss the comparative data obtained from several Raman instruments on Antarctic extremophiles which will include an epilith from Signy Island, a chasmolith from the Lake Hoare LTER site in the Dry Valleys , a cyanobacterial mat from Lake Vanda and an endolith from Mars Oasis (this latter specimen must be considered to be especially relevant to planet Mars !). Some of the advantages of the Raman technique for adoption as analytical instrumentation on a mission to Mars will emerge from this study.

In particular , the capability of the Raman technique for the identification of the spectral biomarkers under different conditions , without special sample preparation and in a micro-sampling mode , giving a specimen "footprint" of only several microns diameter is assessed . A critical factor in this series of experiments is the wavelength selection of the laser excitation employed for the analysis and information from spectra recorded with visible and near-infrared laser sources [20] . This information is relevant for the design of miniaturised Raman instruments that will have the objective of searching for extant or extinct life on planetary surfaces or subsurfaces, especially Mars.

References : [1] Wynn-Williams D.D. et al. (2000) *Biblio. Lichenologica ,75 ,*275-288 . [2] Wynn-Williams D.D. (2000), in *The Ecology of Cyanobacteria : Their Diversity in Time and Space* ,eds. Whitton B.A. , Potts M. , Kluwer, Dordrecht , 341-366 . [3] Wynn-Williams D.D. et al. (2001),in *Proc 1st Euro. Workshop on Exo-Astrobiology, Frascati, May 2000*, eds. Ehrenfreund P. et al., ESA SP 496,225-237 . [4] Wynn-Williams D.D. , Edwards H.G.M. (2000) *Icarus , 144,* 485-503 . [5] McKay C.P. (1997) *Origins Life Evol. Biosphere , 27 ,* 263-289 . [6] Siebert J. et al. (1996 *) Biodiversity Conserv. , 5 ,*1337-1363 . [7] Kappen L. (1993) , in *Antarctic Microbiology ,* ed. Friedmann E.I. , Wiley-Liss , New York , 433-490 . [8] Friedmann E.I. (1982) *Science , 215 ,*1045-1053 . [9] Friedmann E.I. et al. (1988) *Polarforschung , 58 ,* 251-259 . [10] Nienow J.A. et al. (1988) *Microbial Ecology , 16 ,* 271-289 . [11] Cockell C.S. , Knowland J. (1999) *Biol. Revs. Camb. Phil. Soc. , 74 ,*311-345 . [12] Vincent W.F. et al. (1993) *J. Phycology , 29 ,* 745-755 . [13] Wynn-Williams D.D. et al. (1999) *Euro. J. Phycology , 34 ,* 381-391 . [14] Holder J.M. et al. (2000) *New Phytologist , 145 ,* 271-280 . [15] Edwards H.G.M. et al. (1998) *Soil Biol. Biochem., 30 ,* 1947-1953 . [16] Russell N.C. et al. (1998) *Antarctic Sci., 10 ,* 63-73 . [17] Edwards H.G.M. et al. (1999) *,* in *The Search for Life on Mars* , ed Hiscox J.A. , British Interplanetary Soc. , London , 83-88 . [18] Haskin L.A. et al. (1997) *JGR Planets , 102 ,* 19293-19306 . [19] Wang A. et al. (1999) *JGR ,104 ,*27067-27077 . [20] Edwards H.G.M. et al. (2003) *Intl. J. Astrobiology , 1 ,* 333-348 .

A MICROPHYSICALLY-BASED APPROACH TO INFERRING POROSITY, GRAIN SIZE, AND DUST ABUNDANCE IN THE SEASONAL CAPS FROM ATMOSPHERICALLY-CORRECTED TES SPECTRA.

J. Eluszkiewicz[1] and T. N. Titus[2], [1]Atmospheric and Environmental Research, Inc., 131 Hartwell Ave., Lexington, MA 02421, jel@aer.com, [2]U.S. Geological Survey, 2255 North Gemini Dr., Flagstaff, AZ 86001, ttitus@usgs.gov.

Introduction: One of the highlights of the TES observations in the polar regions has been the identification of a "cryptic" region in the south where CO_2 appears to be in the form of a solid slab rather than a fluffy frost [1]. While the exact mechanism(s) by which the cryptic region is formed are still subject of some debate, it appears certain that a type of rapid metamorphism related to the high volatility of CO_2 ice is involved. The high volatility of CO_2 ice under martian conditions has several Solar System analogs (N_2 on Triton and Pluto, SO_2 on Io), thus making the martian cryptic region somewhat less cryptic and certainly non-unique among planetary objects. In an end-member scenario, both the formation and the spectral properties of the cryptic region (and of other areas in the seasonal caps) can be quantitatively modeled by considering sintering of an ensemble of quasi-spherical CO_2 grains [2]. This model includes the special case of instanteneous slab formation, which occurs when the grains are sufficiently small (in the submicron range) so that their sintering timescale is short relative to the deposition timescale (a situation analogous to the "sintering" of water droplets falling into a pond).

Physics of Sintering: Originally, the idea of annealed slabs of CO_2 in the martian seasonal caps was proposed based on an analysis of densification timescales [2]. Recently, we have also evaluated the role played by the non-densifying sintering mechanism caused by vapor transport (Kelvin effect). The main conclusion from this recent work is that the seasonal CO_2 deposits on Mars rapidly metamorphose into an impermeable slab regardless of the initial grain size. The slab forming by this mechanism is expected to contain quasi-spherical voids that then undergo slow elimination by the densifying mechanisms. This densification process *is* strongly grain-size dependent, which can be used to explain the persistence of both low- and high-emissivity areas (e.g., the cryptic region and Mountains of Mitchell, respectively). The proposed texture for the martian CO_2 deposits is consistent with both TES and other observations (in particular, the porous texture of the slab is consistent with the mean density of the seasonal deposits inferred from the MOLA data being less than the theoretical density of solid CO_2 [3]) and it has important consequences for the modeling of the physical properties of the martian seasonal frost. Specifically, the radiative properties of the frost (e.g., albedo and emissivity) are more properly modeled by treating radiative transfer in a slab of solid CO_2 containing spherical voids (and other impurities such as dust grains) rather than by the usual model of spherical CO_2 and dust grains *in vacuo*. In the present study, this problem is tackled by finding the Mie solution for a spherical particle embedded in an absorbing host medium [4]. The Mie solution is then applied in a multiple scattering code [5] to compute the radiative properties of the martian CO_2 deposits.

Application of the New RT Model: The chief advantage of the new RT model is its connection to the microphysical model of the cap texture and, consequently, its predictive capability. In particular, the new model does not require the notion of meter-sized Mie boulders of solid CO_2 in order to explain the high emissivities in the cap spectra (e.g., in the cryptic region) but instead relates them to low porosity. The strong porosity dependence of the computed emissivity suggests that the density evolution obtained from the sintering model can be coupled with the radiative transfer calculations to predict the evolution of emissivities. Preliminary results presented at the 6th Mars Conference [6] have demonstrated the capability of the new model to mimic the observed evolution of the cap emissivity (represented as the depth of the TES 25-μm band, BD_{25}).

Modeling the Shape of TES Spectra: In addition to generating a semi-quantitative agreement with the evolution of BD_{25}, the new model is capable of providing a quantitative match to the shape of the TES spectra. For this more quantitative test, it is important to remove the component of the spectra related to atmospheric dust, which we accomplish using an approach based on the emission phase function (EPF) [7]. To date, 105 EPF-corrected spectra of the caps have been generated. An example of an EPF-corrected spectrum and the model spectra computed using the new RT model are shown in Figure 1. The refractive indices for solid CO_2 used in the calculations are as in [8], while the dusty spectra have been computed using optical constants for palagonite [9]. Application of the new model to match the TES spectra can in principle lead to maps of the porosity, void size, and dust content for the polar caps. In the example shown in Figure 1, a fairly good match to the observed spectrum is obtained for a slab containing 5-μm voids at 1% porosity with a

fractional abundance of 1-µm dust grains of 5 x 10^{-4} by volume (the presence of dust is responsible for the shift of the frequency of mimimum emissivity long-ward of 25 µm). Of course, the RT solution for these parameters is non-unique, and this will necessitate the development of a maximum-likehood inversion method utilizing *a priori* information. The results from the sintering model might in fact be used as an *a priori* constraint (i.e., in a given location, the solution for porosity at different times should be consistent with the porosity evolution predicted by the sintering model). In addition, several important factors neglected so far (e.g., variable cap thickness, nonuniform density distribution with depth, presence of a thermal gradient) should be included, some of which could further improve the agreement between the coupled microphysical/radiative transfer model and TES observations. Ultimately, the new model will provide a powerful observationally-based tool for the modeling of the coupled surface-atmosphere system on Mars.

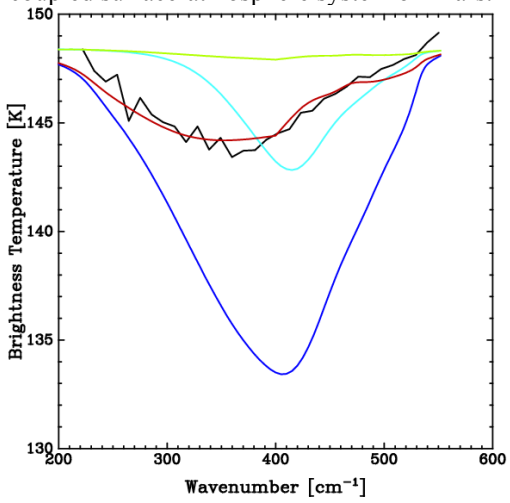

Figure 1: Black line: Observed spectrum. Dark blue line: computed spectrum with 5-µm voids, no dust. Light blue line: computed spectrum with 1-µm voids, no dust. Green line: Computed spectrum with 1-µm voids, 5 x 10^{-4} by volume of dust. Red line: Computed spectrum with 5-µm voids, 5 x 10^{-4} by volume of dust. All computed spectra assume a kinetic temperature of 146 K, slab thickness of 1 meter, 1% porosity, and dust grain size of 1 µm.

Acknowledgement: One of the authors (JE) has been funded by the Mars Data Analysis Program.

References: [1] Kieffer H. et al. (2000) *JGR 105,* 9653. [2] Eluszkiewicz J. (1993) *Icarus 103,* 43. [3] [3] Smith D. E. et al. (2001) *Science 294,* 2141. [4] Yang P. et al. (2002) *Appl. Opt. 41,* 2740. [5] Stamnes K. et al. (1988) *Appl. Opt. 27,* 2502. [6] Eluszkiewicz J. and T. N. Titus (2003) 6th Mars Conference (www.lpi.usra.edu/meetings/sixthmars2003/pdf/3046.pdf). [7] Titus T. N. and H. H. Kieffer (2001) 33rd DPS Meeting. [8] Hansen G. B. (1997) *JGR 102,* 21,569. [9] Roush T. et al. (1991) *Icarus 94,* 191.

THE ABILITY TO PROBE THE MARTIAN POLAR SUBSURFACE VIA GROUND-PENETRATING RADAR. W. M. Farrell and P. R. Mahaffy, NASA/Goddard Space Flight Center, Greenbelt MD 20771, William.Farrell@gsfc.nasa.gov, Paul.R.Mahaffy@gsfc.nasa.gov

Introduction: Ground-penetrating radar (GPR) offers the exciting possibility of remote sensing below the Martian surface for trapped aquifers. A GPR is currently heading to Mars onboard Mars Express (MEX) and a GPR is in consideration to be onboard Mars Reconnaissance Orbiter (MRO) in 2005. While such orbital systems offer great potential for polar stratigraphy studies, their ability to penetrate deep into the Martian polar ice is a function of both the intervening ionospheric density and the overlying ground ice conductivity. The influence of both signal-altering layers will be discussed.

Polar Ice and Water: Clifford[1,2] has suggested that the trapped basal lakes may form at the bottom of the polar cap, along the ice/regolith interface. Such deep aquifers form either due to insulation effects from the overlying ice, local geothermal hot spots, or frictional heating from glacial sliding. Chasma Boreale and Australe have been suggested to be of possible fluvial origin[3], formed by discharging from a past-trapped aquifer within the cap. Basal lakes and deep ice cap melting may ultimately feed a deeper water table that ultimately supplies the cryosphere at lower latitudes[2]. Evidence for this areal extended ice cryosphere has recently been obtained by the GRS experiment onboard Mars Odyssey[4,5]. Similar basal lakes have been found in Antarctica and allegorical discharging lakes are found in Iceland[1,2].

GPR Signal Propagation: In order for orbiting GPR's to examine the polar subsurface for trapped aquifers, their radio signal must first propagate through the attenuating ionosphere. The operating frequency for the MEX/Mars Advanced Radar for Subsurface and Ionospheric Sounding (MARSIS) is 1-5 MHz with a transmitting power of 15 W. The ionospheric plasma frequency, fp, the blocking frequency below which the ionosphere is opaque, extends from about 3 MHz on the dayside of Mars but quickly drops to about ~300 kHz just past (about 10^o from) the terminator. Hence, to minimize the effect of the ionosphere, sounding the polar subsurface from orbit should occur when the overlying polar ionosphere is not illuminated by the sun. Ideal observation periods for MARSIS nighttime polar sounding will be displayed in the presentation.

Besides the ionosphere, the overlying polar ice over a basal lake also attenuates GPR signals. It is demonstrated that the ability of the MARSIS 15 W transmitter to yield a detectable return signal (above the cosmic background level) from an aquifer located at depth, d, varies as $d \sim k\ \sigma^{-1}$, where k is 0.01 S, for a MEX altitudes of 800 km and a transmission frequency of 4 MHz. Consequently, if the polar ice has a consistency comparable to freshwater ice, with $\sigma \sim 10^{-3}$ S/m, a return signal from an aquifer is possible only in the first few meters of the cap. For depths > 10 m, the ice attenuates the signal (both incoming and outgoing) to the extent that the reflected pulse cannot return to the receiver at strengths above the ambient background noise. In contrast, if the cap consistency is more like firm snow, with $\sigma \sim 10^{-5}$ S/m, aquifer detection with a return signal above the noise level is possible to a depth of about 1 km. Clearly, the as-yet-determined character and consistency of the overlying ice will have a significant impact on the successful detection of a polar aquifer.

Future Concepts: There have been other proposed strategies for sounding the polar subsurface. During last year's Scout Mission Opportunity, a multi-institutional team proposed the Mars-POLAR Montgolfier balloon mission to perform a 30-60 day overflight of the north polar region at 4 km altitude. Included in the payload was a 3W Radio Beacon Sounder (RBS) that had the following advantages over their orbital counterparts:

-Proximity to the source by a factor of 100 increases the delivered signal strength to the ground by 30 dB compared to orbital instruments.

-Platform below the shielding, contaminating, and attenuating effects of the ionosphere.

-Ease in deployment of large antenna via direct integration into the balloon, thereby reducing deployment mass and risks that plague orbital sounder antenna deployments.

The feasibility of aquifer detection for a balloon-based system will be compared and contrasted to its orbital counterpart.

References: [1] Clifford, S.M. (1987) *JGR, 92,* 9135. [2] Clifford, S. M. (1993) *JGR, 98,* 10973. [3] Anguita F. et al. (2000) *Icarus, 144,* 302. [4] Mitrofanov, I., et al. (2002), *Science, 297,* 78. [5] Feldman, W. C., et al., *Science, 297,*75.

Association of Measured Distribution of Near-Surface Hydrogen at High Northerly Latitudes with Surface Features on Mars. W.C. Feldman[1], S. Maurice[2], T.H. Prettyman[1], M. T. Mellon[3], S.W. Squyres[4], S. Karunatillake[4], R.C. Elphic[1], H.O. Funsten[1], D.J. Lawrence[1], and R.L. Tokar[1], [1]Los Alamos National Laboratory, Los Alamos, New Mexico, [2] Observatoire Midi-Pyrenees, Toulouse, France, [3] LASP, University of Colorado, Boulder, CO, [4]Cornell University, Ithaca, NY

Introduction: Lower-limit estimates of the global abundance of hydrogen on Mars reveal a remarkable surface distribution [1]. Three discrete reservoirs are apparent. Two of the reservoirs fill large areas that cover much of the northern and southern high-latitude regions, and the third has several components at equatorial to mid latitudes. A map of water-equivalent hydrogen, M_{H2O}, north of +50° latitude derived from epithermal-neutron counting rates measured between areocentric longitudes of 100° and 181° (when the seasonal CO_2 frost cover was completely absent) [1], is shown in Figure 1. M_{H2O} is seen to maximize at 100% by mass, at the north-polar residual cap. This maximum is a component of a generally water-rich region that covers much of the surrounding high-latitude terrain. This region has a local minimum that overlies Olympia Planitia, a secondary maximum that follows a narrow arc at about +75° latitude that connects 100° to 180° east longitude, and a pronounced secondary maximum that is centered at about +70° latitude and –135° east longitude. Whereas the arc-shaped maximum overlies a similar arc of surface water ice that is apparent in visible images of Mars, the secondary maximum has no apparent surface feature. Another feature of the enhanced reservoir of hydrogen at high northerly latitudes is that it is pinched off on one side by a relatively low H_2O-abundance region that is centered on –45° longitude.

Intercomparison with Surface Features: In an attempt to search for physical properties of the Martian surface that are associated with the foregoing hydrogen abundance features, we overlayed contours of M_{H2O} onto maps of thermal inertia, albedo, and rock abundance [2,3,4]. Starting first with the albedo (shown in Fig. 2), we see that the highest albedo, which corresponds to surface water-ice deposits, overlies the central maximum in M_{H2O} and the outlying arc of high M_{H2O}. Additionally, the secondary maximum in M_{H2O} lies within an extended region of relatively high albedo. An extended region of low albedo that is centered on –45° longitude at the mouth of Chasma Boreale, is coincident with the pinched-off portion of the

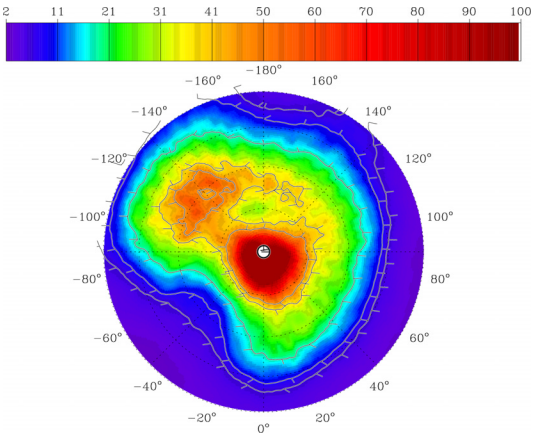

Fig. 1. Map of lower-limit abundances of M_{H2O}, shown in orthographic projection north of +50° latitude. The contours correspond to 7%, 10%, 20%, 40% and 50% M_{H2O}, progressing inward from the outside.

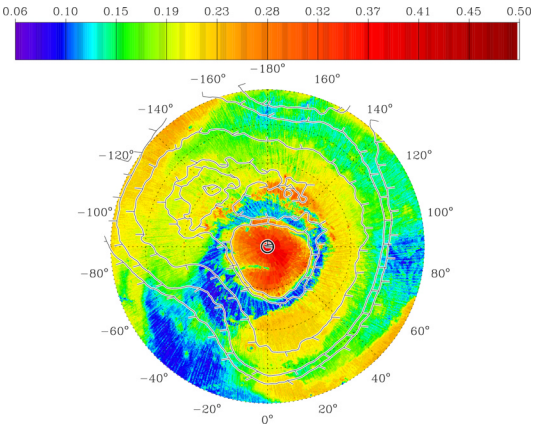

Fig. 2. Map of albedo shown in orthographic projection north of +50° latitude. Contours of mass % H_2O are the same as in Fig. 1.

high-latitude, high M_{H2O} terrain. Extension of this region to lower latitudes is shown in Fig. 3, which intercompares M_{H2O} with rock abundance and albedo. Inspection shows that most regions of high rock abundance and low albedo overlie regions of relatively low M_{H2O}. However, the inverse is not true. There are regions of low rock abundance (and high albedo) that are coincident with regions of low M_{H2O}. In addition, there is a region just south of Arabia Terra, and between

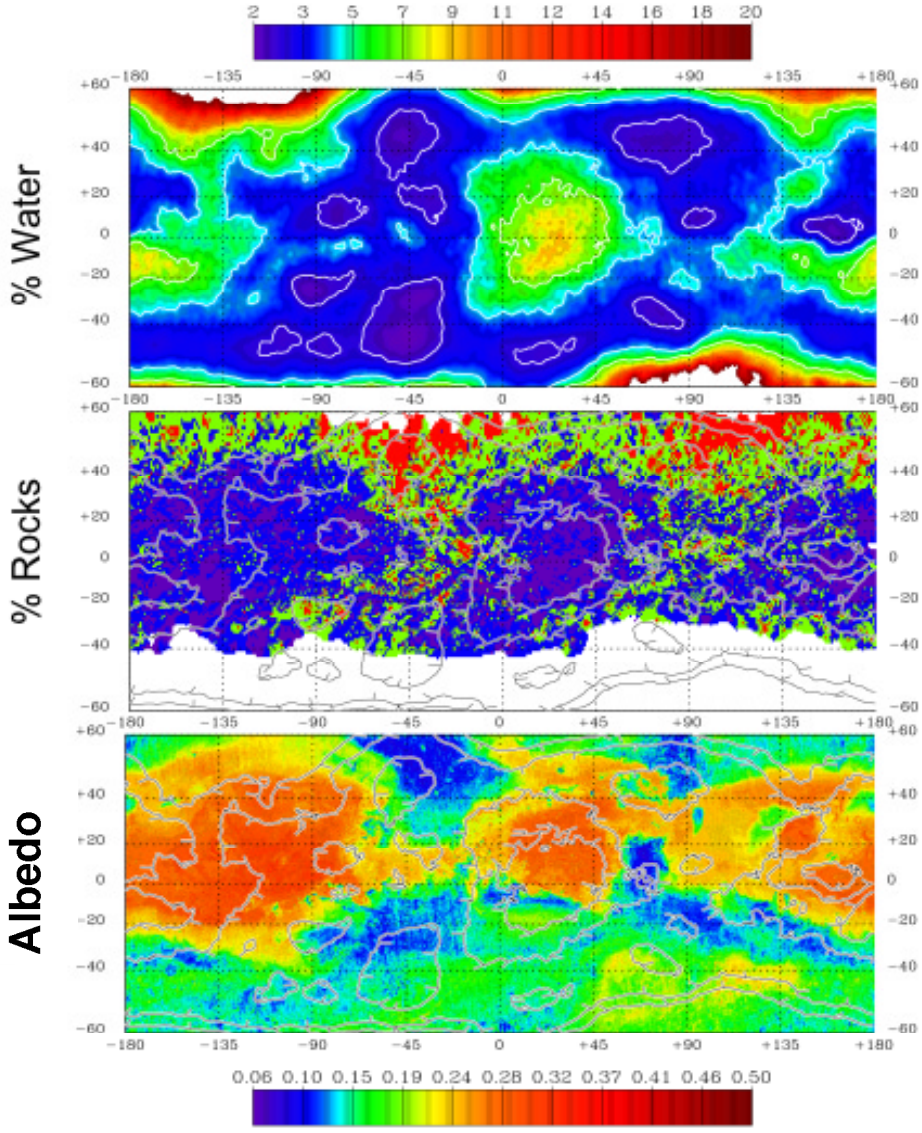

Fig. 3. Maps of M_{H2O}, percent abundance of rocks [4], and albedo [2,3] all in cylindrical projection between ±60°. Contours of M_{H2O} corresponding to 3%, 5%, and 7% are overlayed on all three maps. The colors in the middle panel correspond to 0%-5% [purple], 5%-10% [blue], 10%-17% [green], and >17% [red] rock abundance, respectively.

–20° and –40° latitude near 180° east longitude where the albedo is not high, the rock abundance is low, and M_{H2O} is relatively high. Altogether, these associations suggest that no single process can explain all of the observed structure of enhanced M_{H2O} deposits on Mars. For example, contributing factors could be the physical structure of subsurface soils (such as porosity and permeability), the mineral and chemical composition of these soils, the time dependence of the partial pressure of water vapor in the atmosphere, and the time-dependence of, and insulating properties of the overlying dust cover.

References: **[1]** Feldman, W.C., et al., J.G.R., submitted, 2003, [2] Mellon, M.T., et al., LPSC, XXXIII, Houston, TX, 2002, [3] Christensen, P.R., et al., J. G.R., 106, 23823-23871, 2001, [4] Christensen, P.R., Icarus, 68, 217-238, 1986.

AMAZONIAN GEOLOGIC HISTORY OF THE NORTH POLAR CAP OF MARS: STRATIGRAPHY, MELTING, AND RETREAT Kathryn E. Fishbaugh[1] and James W. Head III[1], [1]Brown University, Dept. Geol. Sci., Box 1846, Providence, RI 02912, kathryn_fishbaugh@brown.edu, james_head_III@brown.edu

Introduction: Mariner 9 [1,2] and Viking era studies [e.g., 3] showed the polar caps to consist of layers with varying amounts of dust and ice, termed the polar layered deposits (Apl), and a residual polar cap (Api) consisting of ice and dust overlying these [4]. In the north, this residual cap consists of water ice and in the south of water and CO_2 ice [4], yet CO_2 clathrate may also compose a percentage of the Apl and residual ice at both poles [5]. Most authors believe that the variability in dust content within the Apl is to some degree controlled by orbital oscillations [6-8]. Only recently have researchers considered the martian polar caps as possibly behaving similarly to terrestrial ice caps, both glaciologically and geologically. *Tanaka and Kolb* [9] and *Kolb and Tanaka* [10] have outlined a possible geologic history of the poles, suggesting that melting and flow have not occurred. Yet, several authors have estimated ice flow rates, of mm to meters/yr [11-13], and Fisher [14] has put forth the idea that ice flow may play a crucial role in the forming of the northern spiraling troughs. Just as terrestrial ice sheets experience meltwater outbursts in the form of jökulhlaups, Chasma Boreale may also have been formed in part by melting of the Apl (possibly due to volcanic eruption) and outflow [15-17]. There is also geologic evidence for at least one stage of retreat of the north polar cap [18,19]. Thus, the martian north polar cap has a much more complex and Earth-like history than simple accumulation of residual ice and dust.

A major outstanding question in the study of the north polar cap is, "When did all of this occur?". *Tanaka and Scott* [4] have placed the beginning of Apl deposition for both caps in the Late Amazonian, and *Herkenhoff and Plaut* [20], based on crater counts, have estimated maximum surface ages of 7-15 x 10^6 yrs. (south) and <100 x 10^3 yrs. (north). The goal of our research thus far has been to piece together a possible history of the north polar cap from the end of Vastitas Borealis Formation (VBF) deposition in the Late Hesperian to the current estimates of the beginning of Apl deposition nearly 3 billion years later in the Late Amazonian. Thus, we have studied the major stratigraphy of the polar deposits, the evidence for growth and retreat of the polar cap, and its melting history.

Stratigraphy: As described above, the polar cap consists of two major units: the polar layered deposits (Apl) and the residual ice (Api) overlying these. *Howard et al.* [21] have described the stratigraphy of the Apl in detail using Viking data. The darker, dustier layers are laterally continuous and contain an unknown percentage of dust. Layer thicknesses vary; Viking images revealed major layers on the order of 5-25 m thick, while MOC has shown layer thicknesses down to the limit of resolution (~2 m) [22,23]. Recently, a darker, layered unit has been found to lie beneath the Apl [22,10,24,25]; *Tanaka et al.* [26] term this unit "polar layered deposits 1" (Apl_1) and give it an Early Amazonian age. We have referred to this unit as the basal unit. Building upon these previous studies of the basal unit, we have continued to investigate its major characteristics [27].

The basal unit consists of alternating light and dark layers. The darker layers are much thicker (10s of meters) and less easily eroded than the thinner ones which may consist of the ubiquitous planetary dust. Steep slopes (some near 40°) indicate possible cementation by water ice. Individual layers also erode at different rates, and some of the lower layers show evidence of eolian erosion. Since the basal unit is exposed in troughs within Olympia Planitia, the sublimation and wind erosion which produced the trough [28] is able to erode the basal unit as well. This erosion has left behind pits, ridges, residual mesas, and yardang-like forms.

The close geographical association of basal unit outcrops with the northern dunes suggests that the basal unit is probably the source for these dunes [24], just as *Thomas and Weitz* [29] found that the lower Apl was probably the dune source (before the basal unit was discovered). The Apl also appear to unconformably overlie the basal unit since the basal unit layers pinch-out along the contact, indicating that major erosion may have taken place between the end of basal unit deposition and the beginning of Apl deposition. It is also possible that deposition of the basal unit occurred in irregular patches, rather than in continuous layers, creating the illusion of an unconformity. Dark lenses found within the lower Apl layers may be dunes which eroded from the basal unit and migrated onto the young, still-forming Apl.

The best exposures of the basal unit lie within the troughs bordering and extending into Olympia Planitia and within the arcuate scarps at the head of Chasma Boreale. At its thickest point, the basal unit is approximately 400 m thick (1100 m, including Olympia Planitia) and pinches out somewhere near Chasma Boreale. According to *Byrne and Murray* [24], Olympia Planitia consists wholly of the basal unit.

We have investigated several theories of formation of the basal unit [30], including 1) eolian deposit, 2) outflow channel/oceanic deposit, 3) incorporation into basal ice, and 4) a remnant of several stages of polar cap retreat, and find that the latter scenario is most likely. Formation of the basal unit accounts for some of the Amazonian history of the north polar cap.

Melting of the Polar Cap: Using Viking data, two different theories on the formation of Chasma Boreale have arisen: katabatic wind erosion and sublimation [28] and melting and outflow [15,16]. We have examined these and formation by glacial flow and ablation using primarily MOLA data and find that the most likely mechanism of formation is a combination of sublimation, katabatic wind erosion, melting, and outflow [17]. The cause of such melting is still unknown but candidate triggers include: 1) volcanic eruption, 2) climate change of a scale large enough to cause melting, 3) incorporation of salts into the

lower layers, and 4) pressure melting due to the presence of a thicker cap. The basal unit may have played a crucial role in the creation of Chasma Boreale as it may have affected placement of water reservoirs and transportation of that water. In addition, much of the basal unit has been eroded by formation of Chasma Boreale; the floor and lobate deposits at the mouth may consist of modified lower layers of the basal unit. If the north polar cap underwent at least one stage of relatively large-scale melting, then this may have contributed in part to polar cap retreat.

Retreat of the North Polar Cap: We have described geologic evidence for at least one stage of polar cap retreat [19,31]. Unusual, rough, knobby depressions south of Olympia Planitia resemble kame-and-kettle topography, formed on Earth by the deposition of englacial sediment and melting of blocks of ice left by glacier retreat. Remnants of polar material (mapped by *Tanaka and Scott* [4]) also lie within and near the kame-and-kettle–like topography. Previously, we described Olympia Planitia as consisting of remnant Apl covered by sublimation lag now reworked into dunes. Based on subsequent studies of the basal unit, we consider it more likely that Olympia Planitia consists of basal unit material which may itself be a remnant of several stages of polar cap retreat.

Retreat of the polar cap plays a crucial role in its history, because it implies that the north polar cap may not have just appeared in the Late Amazonian but instead may have been influencing the hydrologic and climatic cycles of the planet for much longer and may have waxed and waned with changes in climate.

Possible Scenarios of North Polar Cap History: We have outlined four possible scenarios for north polar cap history [32]. (1) Deposition of the polar cap is a recent event, requiring that climate has only just become favorable for polar cap deposition. We find this case unlikely since a climate largely controlled by orbital parameter variations would not have undergone an overall, large-scale change during the Amazonian other than the smaller scale variations caused by the orbital parameter variations [8]. In addition, in this case, triggers needed to cause melting and retreat would be difficult to achieve in such a short time period. (2) Polar wander [33] has recently brought the caps to their present positions. (3) The polar cap is oscillating, waxing and waning with large changes in orbital parameters, the current polar cap being only the latest manifestation of caps that have come and gone since perhaps the Early Amazonian. Ice deposits may even form at lower latitudes during periods of high obliquity [34]. One possibility is that the major layers of the basal unit each represent a lag left by the retreat of one stage of the polar cap. Since the basal unit is exposed in Chasma Boreale and has been eroded by chasma formation, any melting involved in carving the chasma would have occurred after the last major stage of retreat but may also have occurred during previous stages. *Jakosky et al.* [35] modeled sublimation of the polar cap and found that a pure ice cap of the current Apl thickness could sublimate entirely within 50 x 10^3 yrs. at high obliquities (>45°). (4) The lower layers of the polar cap were deposited in the early Amazonian, and deposition has continued since then; crater counting may reveal only their surface age. In this case, the cap may have undergone more than one stage of partial retreat, and processes such as flow and relaxation [36] may be erasing craters and making the surface appear even younger than it is.

Comparison with the South Polar Cap: The south polar cap shares some characteristics with its northern counterpart. Evidence in the form of esker-like ridges, remnant volatile-rich material, and drainage channels indicate possible retreat of southern polar deposits during the Hesperian [37]. Chasma Australe bears a striking large-scale morphological similarity to Chasma Boreale and thus may also have been formed by melting, yet detailed similarities are few, possibly due to the lack of a southern basal unit and thus lack of a significant source for outflow deposits. *Kolb and Tanaka* [10] cite a dearth of features formed by flow and undisturbed layer sequences in the walls of the chasma as evidence against formation by melting and outflow. Our preliminary searches have shown no evidence for a southern basal unit. Possibly, subsequent stages of growth and retreat of the south polar cap during the Amazonian left no basal unit, though there is evidence for small scale growth and retreat during this time [38]. Perhaps early retreat of the southern deposits left such a thick lag that later retreat was significantly retarded. However, there may exist a much smaller southern basal unit that has not yet been exposed. Further studies should include more comparisons with the south polar deposits so that the ideas developed about the north polar cap can be tested.

References: [1] Soderblom, L. et al. (1973), *JGR* 78, 4197-4210. [2] Cutts, J. (1973) *JGR* 78, 4231-4249. [3] Thomas, P. et al. (1992), in *Mars* (ed. By H. Kieffer et al.), 767-795, U of Ariz. Press, Tucson. [4] Tanaka, K. and D. Scott (1987), *U.S.G.S. Misc. Inv. Ser. Map I-1802-C*. [5] Hoffman, N. (2000), *Icarus* 146, 326-342. [6] Blasius, K. et al. (1982), *Icarus* 50, 140-160. [7] Cutts, J. et al. (1982), *Icarus* 50, 216-244. [8] Laskar, J., et al. (2002), *Nature* 419, 375-377. [9] Tanaka, K. and E. Kolb (2001), *Icarus* 154, 3-21. [10] Kolb, E. and K. Tanaka (2001), *Icarus* 154, 22-39. [11] Pathare, A. and D. Paige, *2nd Int. Conf. Mars Polar Sci. and Exp.*, LPI Contrib. 1057, pg. 79. [12] Hvidberg, C. (2003), *Annal. Glaciol.*, in press. [13] Greve, R. et al. (2003), *Planet. and Space Sci.*, in press. [14] Fisher, D. (2000), *Icarus* 144, 289-294. [15] Clifford, S. (1987), *JGR* 92, 9135-9152. [16] Benito, G. et al. (1997), *Icarus* 129, 528-538. [17] Fishbaugh, K. and J. Head (2002), *JGR* 107, 10.1029/2000JE001351. [18] Zuber, M. et al. (1998), *Science* 282, 2053-2060. [19] Fishbaugh, K. and J. Head (2000), *JGR* 105, 22455-22486. [20] Herkenhoff, K. and J. Plaut (2000), *Icarus* 144, 243-255. [21] Howard, A. et al. (1982), *Icarus* 50, 161-215. [22] Malin, M. and K. Edgett (2001), *JGR* 106, 23429-23570. [23] Milkovich, S. and J. Head (2003), *LPSC* 34, #1342. [24] Byrne, S. and B. Murray (2002), *JGR* 107, 10.1029/2001JE001615. [25] Edgett, K. et al. (2003), *Geomorph.* 52, 289-297. [26] Tanaka, K. et al. (2003), *JGR* 108, 10.1029/2002JE001908. [27] Fishbaugh, K. and J. Head (2003), *6th Mars Conf.*, #3137. [28] Howard, A. (2000), *Icarus* 144, 267-288. [29] Thomas, P. and C. Weitz (1989), *Icarus* 81, 185-215. [30] Fishbaugh, K. and J. Head, *6th Mars Conf.* #3141. [31] Fishbaugh, K. and J. Head (2001), *LPSC* 32, #1426. [32] Fishbaugh, K. and J. Head (2001), *Icarus* 154, 145-161. [33] Schultz, P. and A. Lutz (1988), *Icarus* 73, 91-141. [34] Jakoksy, B. and M. Carr (1985), *Nature* 315, 559-561. [35] Jakosky, B. et al. (1995), *JGR* 100, 1579-1584. [36] Pathare, A. and D. Paige (2003), *LPSC* 34, #2051. [37] Head, J. and S. Pratt, *JGR* 106, 12275-12299. [38] Head, J. (2001), *JGR* 106, 10075-10085.

EXPERIMENTAL INSTRUMENT ON HUNVEYOR FOR COLLECTING BACTERIA BY THEIR ELECTROSTATIC COAGULATION WITH DUST GRAINS (FOELDIX): OBSERVATION OF ELECTROSTATICAL PRECIPITATED COAGULATED UNITS IN A NUTRIENT DETECTOR PATTERN. ***T. Földi[1], Sz. Bérczi[2], E. Palásti[1]*** [1]FOELDIX, H-1117 Budapest, Irinyi József u. 36/b. Hungary, [2]Eötvös University, Department G. Physics, Cosmic Materials Space Res. Gr. H-1117 Budapest, Pázmány Péter s. 1/a, Hungary, (berczi szani@ludens.elte.hu)

ABSTRACT

Electrostatic coagulation properties of dust above planetary surfaces [1-5] were studied by FOELDIX-1 instrument of Hunveyor. We developed FOELDIX-1 by a detector unit in order to observe biomarkers on Mars by collecting dust thrown out from dusty regions. The dust collector experiment [6], with the observation capability of the size dependent dust particles [7], was developed by a nutrient containers which forming a pattern can show various types of bacteria in the inner detector-wall of the FOELDIX-1 instrument [8]. Coagulation of electrostatically charged dust particles, rare H_2O molecules and suggested extremophile bacteria from the dusty Martian surface is transported by our experimental assemblage through the space with electrodes and allows to precipitate in the vicinity of some specially charged electrodes [9]. If living units form a community, a consortia of bacteria and fungla spores with the attached soil then the cryptobiotic crust components of Mars may also be found and distinguished by this measuring technology.

INTRODUCTION

Levitating charged dust particles were measured on Surveyors [1], Apollo's LEAM [2] and their models were shown [3-5], and windstorms on Mars are known since old times and were photographed. We also studied levitating dust particle phenomenon in the experiment of FOELDIX-1 where coagulation of lunar quasiatmospheric dust were modelled [6,8]. We placed the FOELDIX-1 instrument to the Hunveyor electrostatic assemblage. To search the possibility of life on Mars we developed our instrument with bacteria and spora detector unit.

The FOELDIX detector unit consists of spots with nutrient containers. They are placed on the inner wall of the dust collector. They form a coordinate system. (In terrestrial conditions the containers can be replaced with other ones.) In principle the detector unit is similar to the Magnetic Properties Experiment of the Mars Pathfinder, where magnetic materials were fixed on a curtain on the surface of the lander. Magnetic materials were arranged in a characteristic pattern of spots. Magnetic forces glued the magnetized particles on the spots. The repeated dust interaction with this curtain amplified the pattern of the colored dust particles attracted on the spots till the visibility of the pattern. Even by camera observation of the curtain the magnetic spot pattern - with various megnetisation strength of the spots in the curtain magnets - allowed estimation of the magnetisation of the dust particles flown by winds [10].

THE SOIL AND BACTERIA TOGETHER

Extremophile bacteria are among the main constituents of the cryptobiotic crust on the Earth. The FOELDIX instrument has a benefit to colllect the fragments of such living consortia in glued units. This way not only dust but the glued bacteria or other living units (i.e. fungla spores) can be collected into the instruments container. Selected detecting mechanism is necessary to distinguish the various components of the cryptobiotic type living unit fragments of the windblown dry powder material. Therefore a detecting surface with a selective nutrient spot arrangement was constructed for the FEOLDIX. On the Hunveyor we measure the CBC collecting capacity of the instrument in the Great Hungarian Plain where dry alkaline grounds can be found, especially in the Hortobágy.

THE MEASURING DETECTOR ARRANGEMENT

In our measuring detector an inner wall-curtain with various nutrients are fixed in the vicinity of special electrodes. These electrodes allow the coagulated dust and bacteria grains (and other complex particles) to precipitate from the streaming particles in the instrument. The coagulated materials with various bacterial components can grow on the nutrient spots with different effectivity. Repeated interaction of the precipitated dust-and-bacteria coagulates will change the color and extent of the nutrient spot regions and amplifies the pattern of the nutrients till the visibility of the arrangement of spots. Microcamera observation of the detector's spot pattern will show the types of bacteria (or fungla spores) existing inside the coagulated dust particles.

COAGULATION OF PARTICLES CONTAINING DUST+BACTERIA+WATER-MOLECULES

On the inner surface of the electron tube, even in the case of hypervacuum, a monomolecular water molecule layer can be found (Tungsram Factory, [11]). These water molecules are small negative ions and have far longer lifetime then that of the small positive ions [12].

In the vicinity of a dusty planetary surface there exist a space charge of electron cloud. The rare water molecules will act as if they were negatively charged and they preserve their charge. The negatively charged water molecules frequently collide with particles of a positively charged dust cloud producing a complex coagulated particle. This particle is a loose aggregate of ions, has great mass and has lower velocity compared to the small mass particles. While colliding with a negatively charged water molecule the water molecule will attach to the larger one. This process enlarges the complex aggregate larger and larger (we measured coagulation up to 450.000 times mass in the FOELDIX instrument). The living units are embraced and included into this coagulated large particles. Living units are shielded by the dust components from UV and other radiations, and presence of water allows to continue life activity, too.

LOCATION OF PROMISFUL OBSERVATION CHANCES FOR MARTIAN LIVING ORGANISMS: SOUTH POLE

On the MOC MGS images there are promisful regions where to land in order to observe Martian life components of bacteria or fungal spores with dust. In winter these dark dunes are covered with frost. Dark dune spots are formed in

late winter and early spring show a structure on the frost covered surface where the soil material is partially exposed on the surface. This uncovered region is the dark spot itself. In these periods wind blows out the dark dune material from the spots and the ejected dark dust forms a thin layer on the surface of the frost cover.

Dark dune spots (DDSs) were estimated as probable sites for biogenic activity [13-15] and the suggested Martian surface organisms (MSOs) were considered as promisful candidates of the recent life on Mars. If the MSOs exist, then they must be flown out from the dark dune spots during the late winter and early spring period of DDS activity.

PRESENCE OF WATER ON DDS SITES

As we referred earlier the water molecule content of the atmosphere helps the electrostatic coagulation of the dust particles [16]. The Southern Polar region of Mars where the DDS sites were found and studied is therefore promisful source for the FOELDIX experiment because Mars Odyssey also found higher concentration of water in this region [17-19]. Although the 2003/2004 Mars missions will not go to the polar regions, a more detailed imaging may reveal special sites with extensive wind activity in the given late winter early spring period [20, 21].

SUMMARY

The new FOELDIX instrument with the bacteria and spore detector unit is capable to observe various Martian living units coagulated by the instrument and deposited by special electrodes on nutrient spots of the detector. The growing spots can be observed by microcamera units built into the FOELDIX instrument. Such detector can measure not only bacteria but the soil type which is glued with the bacteria. Therefore it is probable that components of the cryptobiotical crust units may be discovered by this measuring technology.

ACKNOWLEDGMENTS

This work was supported by the MÜI-TP-190/2002 and 190/2003 funds of the Hungarian Space Office.

REFERENCES:

[1] Criswell, D. R. (1972): Horizon glow and motion of Lunar dust. *Lunar Science III*. p. 163. LPI, Houston; [2] Rhee, J. W., Berg, O. E., Wolf, H. (1977): Electrostatic dust transport and Apollo 17 LEAM experiment. Space Research XVII. p. 627; [3] Horányi M., Walch, B., Robertson, S. (1998): Electrostatic charging of lunar dust. *LPSC XXIX*. LPI, CD-ROM, #1527; [4] Reid, G. C. (1997): On the influence of electrostatic charging on coagulation of dust and ice particles in the upper mesosphere. *Geophysical Res. Letters*, **24,** No. 9. p. 1095; [5] Sickafoose, A. A., Colwell, J. E., Horányi, M. Robertson, S. (2001): Dust particle charging near surfaces in space. In *LPI XXXII*, #1320, LPI, CD-ROM; [6] T. Földi, R. Ezer, Sz. Bérczi, Sz. Tóth. (1999): Creating Quasi-Spherules from Molecular Material Using Electric Fields (Inverse EGD Effect). *LPSC XXX*. LPI, CD-ROM, #1266.; [7] T. Földi, Sz. Bérczi, E. Palásti (2002): Time Dependent Dust Size Spectrometry (DUSIS) Experiment: Applications in Interplanetary Space and in Planetary Atmospheres/Surfaces on Hunveyor. *Meteoritics & Planetary Science,* **37**, No. 7. Suppl., p. A49.; [8] Földi T., Bérczi Sz., Palásti E. (2001): Water and bacteria transport via electrostatic coagulation and their accumulation at the poles on the dusty planet. *LPSC XXXII*, #1059, LPI, CD-ROM; [9] Földi T., Bérczi Sz. (2001): The source of water molecules in the vicinity of the Moon. *LPSC XXXII*, #1148, LPI, CD-ROM; [10] Hviid, S. F.; Knudsen, J. M.; Madsen, M.B.; Hargraves, R. B. (2000): Spectroscopic Investigation of the Dust Attracted to the Magnetic Properties Experiment on the Mars Pathfinder Lander. *LPSC XXXI*, #1641, LPI, CD-ROM; [11] Bródy I., Palócz K. (1953): Lecture on Techn. Univ. Budapest (personal communication); [12] Israel, H. (1957): *Atmospherische Elektricitet*. Leipzig.; [13] Horváth A., Gánti T., Gesztesi A., Bérczi Sz., Szathmáry E. (2001): Probable evidences of recent biological activity on Mars: Appearance and growing of Dark Dune Spots in the South Polar Region. *LPSC XXXII*, #1543, LPI, CD-ROM; [14] A. Horváth, T. Gánti, Sz. Bérczi, A. Gesztesi, E. Szathmáry (2002): Morphological Analysis of the Dark Dune Spots on Mars: New Aspects in Biological Interpretation. *LPSC XXXIII*, #1108, LPI, CD-ROM; [15] A. Horváth, Sz. Bérczi, T. Gánti, A. Gesztesi, E. Szathmáry (2002): The "Inca City" Region of Mars: Testfield for Dark Dune Spots Origin. *LPSC XXXIII*, #1109, LPI, CD-ROM; [16] T. Földi, Sz. Bérczi (2001): Quasiatmospheric Electrostatic Processes on Dusty Planetary Surfaces: Electrostatic Dust and Water molecule Coagulation and Transport to the Poles. *26th NIPR Symposium Antarctic Meteorites*, Tokyo, p. 21-23.; [17] Mitrofanov, I. G. et al., (2003): Global Distribution of Shallow Water on Mars: Neutron Mapping of Summer-Time Surface by HEND/Odyssey. *LPSC XXXIV,* #1104, LPI, CD-ROM; [18] Kuzmin, R. O.; Mitrofanov, I. G.; Litvak, M. L.; Boynton, W. V.; Saunders, R. S. (2003): Mars: Detaching of the Free Water Signature (FWS) Presence Regions on the Base of HEND/ODYSSEY Data and Their Correlation with Some Permafrost Features from MOC Data. *LPSC XXXIV,* #1369, LPI, CD-ROM; [19] A. Horváth, T. Gánti, Sz. Bérczi, A. Gesztesi, E. Szathmáry (2003): Evidence for Water by Mars Odyssey is Compatible with a Biogenic DDS-Formation Process. *LPSC XXXIV*, #1134, LPI, CD-ROM; [20] Córdoba-Jabonero, C.; Fernández-Remolar, D.; González-Kessler, C.; Lesmes, F.; C. Manrubia, S.; Prieto Ballesteros, O.; Selsis, F.; Bérczi, S.; Gesztesi, A.; Horváth, A. (2003): Analysis of geological features and seasonal processes in the Cavi Novi region of Mars. EGS Conference, Nizza, EAE03-A-13011.; [21] Horvath, A.; Manrubia, S. C.; Ganti, T.; Berczi, S.; Gesztesi, A.; Fernandez-Remolar, D.; Prieto Ballesteros, O.; Szathmary, E. (2003): Proposal for Mars Express: detailed DDS-test in the "Inca City" and "Csontváry" areas. EGS Conference, Nizza, EAE03-A-14142.;

3D SIMULATIONS OF THE EARLY MARS CLIMATE WITH A GENERAL CIRCULATION MODEL. F. Forget[1] , R. M. Haberle[2], F. Montmessin[2], S. Cha[2], E. Marcq[1,2], J. Schaeffer[2], Y. Wanherdrick[1], [1] *Laboratoire de Météorologie Dynamique,IPSL, UPMC BP99, place Jussieu, 75252 Paris cedex 05 (forget@lmd.jussieu.fr),* [2] *NASA Ames Research Center, Space Science Division, Moffett Field, California, ..*

Introduction

The environmental conditions that existed on Mars during the Noachian period are subject to debate in the community. In any case, there are compelling evidence that these conditions were different than what they became later in the amazonian and possibly the Hesperian periods. Indeed, most of the old cratered terrains are disected by valley networks (thought to have been carved by flowing liquid water), whereas younger surface are almost devoid of such valleys. In addition, there are evidence that the erosion rate was much higher during the early noachian than later [1]. Flowing water is surprising on early Mars because the solar luminosity was significantly lower than today. Even with the thick atmosphere (up to several bars) that is expected to have existed on Mars at the time, simple 1D models based on a purely gaseous atmosphere predicted climate conditions too cold to allow liquid water to flow [2]. On this basis, some authors have suggested that the difference resulted from a stronger geothermalism during that period, and that a warm climate was not necessary to explain the valley network [3]. However, other authors claim that a warm, wet early climate capable of supporting rainfall and surface runoff is the most plausible scenario for explaining the entire suite of geologic features in the Martian cratered highlands [1].

To help understand this key issue in Mars science, it is important to extend the initial climate simulations that concluded that early Mars must have been cold [2,3], since these calculations were performed with very simple 1D models [4]. Such improvements have been performed by several authors, and in particular it has been suggested that the CO_2 ice clouds that must have formed in such an atmosphere could have produced a strong "scattering" greenhouse effect sufficient to warm the planet above the freezing point of water [5]. However, there again, these simulations were performed with simple 1D models, from which it is difficult to predict the environmental conditions.

A Global Climate model for early Mars

To improve our understanding of the early Mars Climate, we have developped a 3D general circulation model similar to the one used on current Earth or Mars to study the details of the climate today. Our first objective is to answer the following questions : how is the Martian climate modified if 1) the surface pressure is increased up to several bars (our baseline: 2 bars) and 2) if the sun luminosity is decreased by 25account the heat possibly released by impacts during short periods, although it may have played a role [6]

For this purpose, we have coupled the Martian General Circulation model developped at LMD [7] with a sophisticated correlated k distribution model developped at NASA Ames Research Center. It is a narrow band model which computes the radiative transfer at both solar and thermal wavelengths (from 0.3 to 250 microns). The correlated-k's for each bands are generated from a line-by-line code using the HITEMP data base from HITRAN. In addition, pressure induced absorption by CO_2 in included using a simple parameterisation from an analytical formula produced by Moore et al. (1971). This is a major source of uncertainty.

In addition to the radiative transfer and to the parameterisation that are usually included in such a climate models (dynamical core to solve the 3D fluid dynamic equations, subgrid scale turbulent and convective mixing, surface heat balance and subsurface heat conduction, etc...), we have included parameterisations to account for the condensation, transport, gravitational sedimentation and radiative effects of the CO_2 ice clouds that readily form in a thick CO_2 atmosphere. model. Using the correlated k distribution model allowed us to compute the complex radiative transfer processes (scattering in the thermal infrared) that cannot usually be accounted for with the usual GCM's wide band model.

Results

Preliminary results obtained assuming a 2 bars atmosphere suggest that, even without taking into account the radiative effect of CO_2 clouds, temperature near or above the freezing point of water may be obtained seasonally in the summer hemisphere. The diurnal amplitude of surface temperature is small, and therefore warm temperatures may last for long periods. CO_2 ice clouds are found to form almost everywhere on the planet in the upper atmosphere above 40 km. Their radiative effect on the climate is very model dependent but, in most cases, should correspond to a warming of the surface.

Ultimately, such a model may enable us to simulate the water cycle by applying parameterisations currently used in Earth models. It will be interesting to investigate wether snow or rain could have occur on such a planet.

Reference

[1] Craddock and Howard, *J.G.R* 107 [2002]
[2] Kasting, *Icarus* **94**,1 (1991)
[3] Squyres and Kasting, *Science* **265**, 744 (1994).
[4] Haberle, *J.G.R* 103, 28467, (1999)
[5] Forget and Pierrehumbert, *Science* 278, 1273 (1997)
[6] Segura et al. *Science* 298, 1977 (2002)
[7] Forget et al. *J.G.R* 104, 24,155 (1999)

BACTERIAL DISTRIBUTION AND PRODUCTION WITHIN LAKE ICE AND GLACIAL ICE ALONG THE FRINGE OF THE ANTARCTIC ICE CAP. C.H. Fritsen[1], J.C. Priscu[2], P.T. Doran[3], [1]Desert Research Institute, Division of Earth and Ecosystem Science, 2215 Raggio Pkwy, Reno, NV 89512 USA, cfritsen@dri.edu, [2]Montana State University, Bozeman, MT 59717 USA, jpriscu@montana.edu., [3]University of Illinois at Chicago, Earth and Environmental Sciences, 845 West Taylor Street (MC186), Chicago, IL 60607 USA, pdoran@uic.edu.

Introduction: Microbial growth within Earth's icy habitats can help define where microbial consortia may survive and function within similar environments on other planets.

Herein, we report on ice properties, bacterial biomass and rates, of bacterial production within perennial lake ice covers and glacial ice environments within the McMurdo Dry Valleys, Antarctica which lie at the border of the Antarctic polar ice cap along the Victoria land coast (Fig. 1).

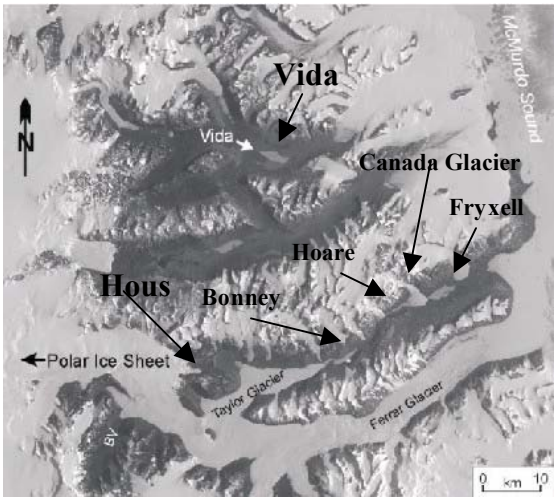

Figure 1: Landsat image of the McMurdo dry valleys region showing location of Lakes Vida, Hoare, Fryxell, Bonney as well as the Taylor, and Canada glaciers. The image is centered at 77.5°S 162°E.

Permanently Ice covered Lakes: Lakes in the McMurdo Dry Valleys of East Antarctica have long been studied as extreme environments and potential analogs of purported Martian lakes of the past [e.g. 1, 2]. Typical, Dry Valley lakes have a 2 to 6 m perennial ice cover overlying 20 to 60 m water columns. These lakes have a range a salinities from fresh to hypersaline, and all allow sufficient sunlight to pass through the ice for photosynthesis to occur in the water column and benthos. Some lakes (e.g. Vida and House) have much thicker ice covers, and it is unknown if the water pockets beneath these ice covers contain viable microbial communities.

Sediment-microbial consortia which are invariably associated with bubble features indicative of liquid water pockets (Fig. 2) are found within the cold ice covers of these lakes [3].

Figure 2. Sediment inclusion from Lake Bonney, with associated arching bubbles indicating the past presence of a melt water pocket. Scale bar is approximately 10 cm.

Glacial Cryoconites: Ablation zones of glaciers also contain sediment inclusions (cryoconites) that harbor microbial consortia [e.g. 4,5]. The sediment-microbiota inclusions are associated with clearer ice created by the melting and refreezing processes which metamorphose the opaque glacial ice by dispersing the small glacial air pockets.

Figure 3: Cryoconite on the Canada Glacier next to author's mitten.

Bacterial numbers: Bacterial cell concentrations range from 4.9e4 to 1.9e7 cells per ml of ice melt water in the lake ice and glacial ice environments. The higher concentrations of bacterial biomass are associated with the ice where sediment inclusions and metamorphosed ice and air inclusions exist (Fig. 3).

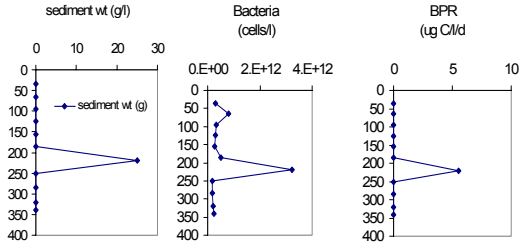

Figure 4. Profiles of sediment content, bacterial cells and bacterial production in the ice cover of Lake Hoare. The coincident peaks of sediment and bacterial abundance and activities are representative of profiles in other lakes as well as enhanced activities in glacial ice with sediment inclusions.

Bacterial Production: Bacterial production rates (BPR) ranged from below levels of detection to 21 ug C l^{-1} d^{-1} in ice melt water. Rates in ice with sediment inclusions averaged ca. 1 ug C l^{-1} d^{-1}.

Rates in ice melt water are not necessarily indicative of *in situ* rates. However, during the summer, these ice habitats experience radiation-induced internal melting [e.g. 6, 7] that creates ice melt water microenvironments. Hence, rates in melt water may be indicative of ice-bound processes. Interestingly, rates of bacterial production relative to measured rates of primary production (PPR) (primarily by cyanobacteria [8]) were comparable (exhibiting rates close to unity) in the samples where BPR and PPR both exceeded 0.1 ug C l^{-1} d^{-1} (Figure 5). Such coincidence in the magnitude of production may be indicative of coupled successional feedback processes that are expected within enclosed systems that reach near steady-state conditions. If these environments do indeed exhibit close coupling we would expect that biomass accrual and biosignature development will be tightly coupled to the ice dynamics that would provide new material to these habitable zones (also see [9]). Recognition of morphological features on the martian polar icescape indicative of such processes may be key to the search for habitable microzones on the Red (and white) Planet.

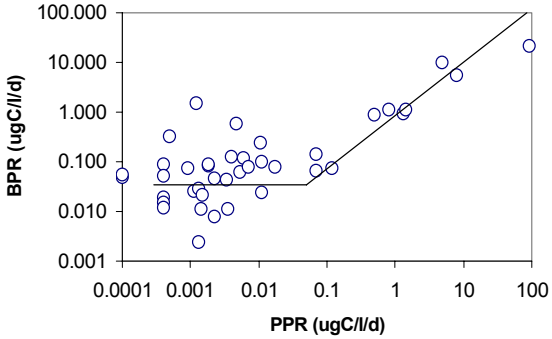

Figure 5: Rates of bacterial production (BPR) relative to primary production (PPR) within lake ice and glacial ice of the McMurdo Dry Valleys.

References: : [1] McKay C. P. et al. (1985) *Nature, 313,* 561-562. [2] Doran P. T. et al. (1998) *JGR, 103(E3),* 28481-28493. [3] Priscu, J.C. et al. (1998) *Science*, 280, 2095-2098. [4] Christner et al. (2002) *Extremophiles*. [5] Muellor D.R. et al. (2001) *Nova Hedwigia*, 123, 173-197. [6] Fritsen, C.H. et al. (1998) *Antarctic Research Series,* 72:269-280. [7] Adams, E.E. et al. (1998) *Antarctic Research Series,* 72:255-268. [8] Fritsen, C.H. et al. (1998) *J. Phycol,* 34, 587-597. [9] Priscu and Christner (In press), *Microbial Diversity and Prospecting.*

ON THE CO_2 HYDRATE PHYSICAL CHEMISTRY AT MARTIAN CONDITIONS. G. Genov and W. F. Kuhs, GZG Abt. Kristallographie, Georg-August-Universität Göttingen, Goldschmidtstr. 1, 37077 Göttingen, Germany (ggenov@gwdg.de; wf.kuhs@geo.uni-goettingen.de)

Introduction: In 1970 Miller and Smythe [1] concluded that the CO_2 hydrate is stable on Mars and that the mixture of pure condensates of CO_2 and H_2O is unstable at the poles. Moreover, some limited kinetic data suggested that the hydrate formation process was fast enough in a meteorological time-scale, which meant, it would lead to a diurnal and annual hydrate cycle. Some authors even put forward the idea that most of the ice in the polar caps was in a hydrate form [2]. Unfortunately, the hydrate and the ice are quite undistinguishable with conventional spectroscopic methods. Moreover, very little is known about the physico-chemical properties of CO_2 hydrates at low temperatures encountered on Mars. We have started to investigate the thermodynamic, physical and kinetic properties of CO_2 hydrate under Martian surface and subsurface p-T conditions.

Possible Importance Of CO_2 Hydrates: Presently is believed that the Martian polar caps consist of water ice, solid CO_2, CO_2 clathrate and dust in unknown proportions, probably different for both caps. The CO_2 clathrate, being the strongest of the three ices could probably affect the rheologic properties of the polar ice layers [3-6] as it was suggested for the north [7] and the south polar caps [8]. If the quantity of the CO_2 hydrate in these regions is large enough it will also influence the process of their basal melting [4, 5]. This is because the hydrates are several times better thermal insulators than water ice and the period needed for establishing a steady-state geothermal gradient in the inner parts of the caps will be much longer.

About The Hydrate Formation: The hydrate formation process is generally believed to start after a certain induction period, needed for some clathrate super nuclei to form. Then the further growth of those nuclei runs in three stages as shown on **Fig. 1**. Guided by the relevance of clathrate hydrate formation from water ice for Mars, a series of kinetic *in-situ* neutron diffraction experiments for CO_2 hydrate formation at higher temperatures were performed. To complement those, a series of pVT formation kinetic experiments were carried out [9]. As a result, applying the model of Salamatin & Kuhs [10, 11], values for the reaction rate coefficients for the different reactions were obtained (**Fig. 2**). A strong bias, of the two points at 272 K and 263 K, from the Arrhenius fit is observed because of the existence of a quasi liquid layer on the surface of the reacting water ice. Thus, two values for the activation energies were obtained – for the high temperature part – 53.5 kJ/mol, and for the low temperature one – 15.5 kJ/mol.

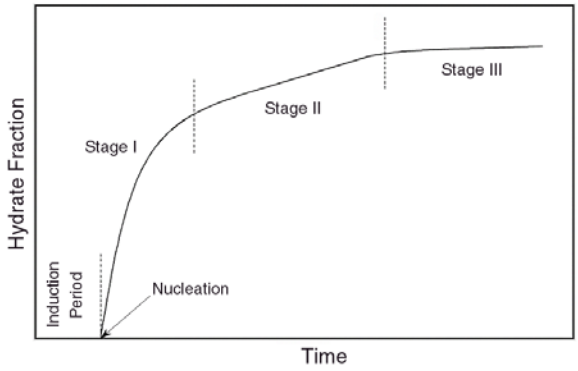

Fig. 1 Stages of the hydrate growth kinetics and induction period.

The delay in formation due to the induction period could be extremely important. Preliminary experiments

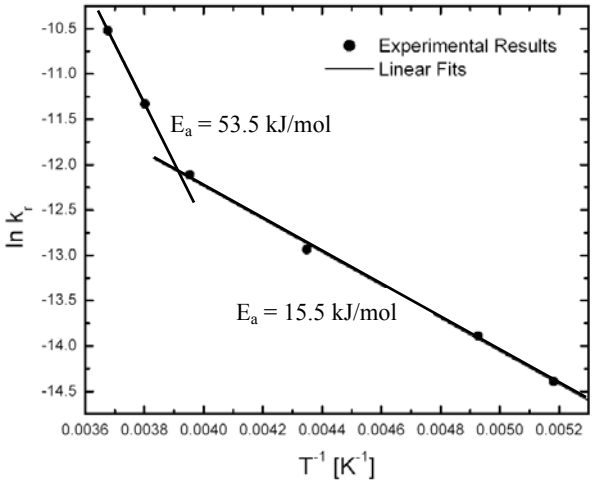

Fig. 2 Plot of the model results for the reaction rate coefficients vs. the temperature.

indicate that the induction period could be several hours up to days at temperatures near 170K and pressures not well exceeding the decomposition pressure of CO_2 hydrate. This may well question the possibility of forming CO_2 hydrate during the Martian night in the diurnal cycle. In our high temperature *in situ* neutron experiments at higher temperatures no induction period was observed within the experimental resolution of 20 s.

Clearly, the induction time depends on temperature and excess pressure and further work is needed to quantify this effect, which is presently under way. Including the effect of induction time in an extended version of the model of Salamatin & Kuhs, we will eventually be in a position to give a realistic prediction for the timescales and kinetics of the hydrate formation at Martian conditions. The kinetics of the growth following the nucleation period is more easily accessible and first estimates will be given in our contribution.

References: [1] Miller S. L. & Smythe W. D. (1970) *Science 170,* 531-533.

[2] Jakosky, B. M. et al. (1995) *J. Geophys. Res., 100, pp. 1579-1584.*

[3] Durham W. B. (1998) *ICMPS, Abstract # 3024*

[4] Kargel J. S. & Tanaka K. L. (2002) *LPS XXXIII, Abstract # 1799*

[5] Kreslavsky M. A. & Head J. W. (2002) *LPS XXXIII Abstract, # 1779*

[6] Kargel J. S. (1998) *ICMPS, Abstract # 3048*

[7] Milkovich S. M. et al. (2002) *LPS XXXIII, Abstract # 171*

[8] Brightwell S. N. et al. (2003) *LPS XXXVI, Abstract # 2077.*

[9] Genov G. & Kuhs W. F. (2003) *VTth ICM, Abstract # 3098.*

[10] Salamatin, A. N. & Kuhs W. F. (2002) *Proc.IV ICGH, pp 766-770*

[11] Staykova, D. K. et al. (2003) *J. Phys. Chem. in press.*

A Radar System for High-Resolution Mapping of Near-Surface Internal Layers in the Polar Ice sheets

S Gogineni, R. Parthasarthy, P. Kanagaratnam, D. Braaten, T. Akins, J Wuite[1] and K. Jezek[1]
The University of Kansas, Radar Systems and Remote Sensing Laboratory
2335 Irving Hill Road, Lawrence, KS 66045-7612, USA
785/864-7734(T) - 785/864-7789 (F) – Gogineni@ittc.ku.edu
[1] BPRC, Ohio State University, Columbus, OH 43210

Accumulation rate is an important variable in determining the mass balance of polar ice sheets. It is currently determined by analyzing ice cores and identifying layers in snow pits, which limits spatial extent over which accumulation rate may be determined. Near-surface internal layers caused by density and conductivity changes can be mapped with a high-resolution radar for estimating accumulation rate. We designed and developed two radars for mapping near-surface internal layers. We developed an airborne radar to operate over the frequency range 600-900 MHz. with a range resolution of about 50 cm to a depth of about 100m. We developed a surface-based system that operates over the frequency range from 500 to 2000 MHz to map layers with 10-cm resolution to a depth of about 100 m. During the 2002 and 2003 field seasons, we collected a large volume of data with the airborne system over the ice sheet in Greenland. We also collected data with the surface-based system at North Greenland Ice Core (NGRIP) drill site in conjunction with detailed in-situ observations from several snow pits and a 15-m firn core. Results from these experiments show that we can map near-surface layers to a depth of atleast 150 m in the dry-snow zone, 120 m in the percolation zone, and 20 m in the melt zone.

In this paper we will discuss the scientific requirements for mapping near-surface internal layers, design considerations and system performance, and present results from airborne and surface-based field experiments. We will also discuss the design of a system for mapping polar-layered deposits in Martian ice caps.

CONSTRAINING THE NATURE AND DISTRIBUTION OF POLAR DEPOSITS ON MARS USING GROUND PENETRATING RADAR. J. A. Grant[1], C. J. Leuschen[2], A. E. Schutz[3], J. Rudy[3], and K. K. Williams[1], [1]Center for Earth and Planetary Studies, National Air and Space Museum, Smithsonian Institution, 6th at Independence SW, Washington, DC, 20560, grantj@nasm.si.edu [2]The Johns Hopkins University, Applied Physics Lab, 11100 Johns Hopkins Road, Laurel, MD, 20723, Carl.Leuschen@jhuapl.edu, [3]Geophysical Surevey Systems, Inc., 13 Klein Drive, North Salem, NH, 03073, alan@geophysical.com.

Introduction: Ground Penetrating Radar (GPR) is capable of addressing a variety of geological problems on the Earth and planets. Terrestrial GPR applications have increased dramatically over the past 30 years and the instrument has become ensconced as an efficient means for non-intrusive definition of radar properties to 10's of meters depth [e.g., 1-3]. Given these capabilities, it is likely that measurements made by a rover-deployed GPR on Mars would help achieve a range of Mars Exploration Program goals including those related to understanding the nature and evolution of polar and near-polar deposits and shallow ground ice [4, 5].

For example, a rover-deployed GPR could penetrate eolian drift or snow masking layered or ground ice-rich units and gullies [6-8] to define the stratigraphy of polar layered deposits [9], the distribution of high latitude ground ice [4, 5], or gully settings. Finally, GPR provides the potential to detect rover hazards (e.g., voids or dust-filled cracks) prior to their engagement. Hence, a GPR could make valuable contributions to rover operations in high latitude settings

Developing a Rover-Deployable GPR for Mars: Careful consideration of the various factors influencing radar performance on Mars instills confidence that a GPR can achieve 10-20 m penetration in high latitude settings [2, 3]. Low ambient temperature and a dry near-surface should reduce electrical losses and mitigate difficulties related to the presence of any fines or salts, thereby enabling radar penetration to on the order of 10 times the wavelength [10]. Magnetic losses may be important in substrates with significant iron-bearing minerals [11, 12], but may be less important in fine-grained, ice-rich polar settings.

Recognizing that a GPR on Mars could constrain stratigraphy and setting to 10-20 m depth is motivation for development of a rover-deployable impulse GPR. Design of our system has focused on development of prototype antennas in parallel with fabrication of a control unit possessing low mass, volume, peak power, and data requirements of 0.5 kg, 3400 cc, 3 W, and ~0.3 MB/day (for 50 meter traverses), respectively. In order to maximize potential penetration and resolution of a Mars GPR, the capability for both high and low frequency investigations has been incorporated. Present designs include a high frequency (600 MHz) bistatic antenna for near-surface high-resolution sounding and a low frequency (100 MHz) monostatic element for deeper probing. Testing of the prototype antennas in terrestrial analog settings confirms the ability to define near-surface stratigraphy that is critical for accurate interpretation of geologic setting (Fig. 1).

Predicting GPR Performance in Polar Settings: Although GPR has been used in high latitude, ice-rich lcoations on the Earth [3], differences in the materials and settings (e.g. dry-ice, more abundant fines) expected in some polar regions of Mars suggest that prediction of GPR performance warrants additional investigation.

A model based on the Finite-Difference Time-Domain (FDTD) method is being used to constrain likely GPR capabilities on Mars and is capable of modeling the complete instrument configuration including antennas, rover, surface roughness, and rocks. The algorithm is a full-wave simulator, is a direct time-domain implementation of Maxwell's curl equations, and can be used to simulate GPR applications as well as process (reverse-time migration) collected data [13]. Simulations highlight the potential value of investing in such models that may enable diagnostic signatures (such as signal attenuation, frequency content, and phase response) to be identified [14], thereby minimizing potential ambiguities associated with detecting an ice rich deposit from radar reflectivity data alone (Fig. 2). Such simulations can facilitate acquisition of dielectric contrasts (from amplitude and phase information), which (with geologic context) could constrain the local geology and setting in polar settings.

Summary: Inclusion of a rover-deployed GPR on a mission targeted to the polar regions of Mars (e.g., 2009 MSL mission) could provide data critical to achieving mission science objectives. Interpretation of GPR data can lead to accurate definition of geologic setting, define the character of stratigraphy associated with layered-terrains, assist in mapping the distribution of near-surface ice, and define the near-surface properties in the vicinity of gullies. As such, data from a GPR could provide context for other rover instruments, and identify sites/samples for in situ analyses.

References: [1] Ulriksen, C.P.F., 1982, Application of Impulse Radar to Civil Engineering: Ph.D. The-

sis, University of Technology, Lund, Sweden, 175p. [2] Grant, J.A., et al. (2003) *J. Geophys. Res*., v. *108*, 10.1029/2002JE001856. [3] Leuschen, C., et al. (2003) *J. Geophys. Res. v. 108*, 10.1029/2002JE001875. [4] Boynton, W. V., et al. (2002), *Science, 297*, 81-85. [5] Feldman, W. C., et al. (2002), *Science, 297*, 75-78, 2002. [6] Christensen, P.R., (1986), J. Geophys. Res., 91, 3533-3545. [7] Ruff, S.W. and Christensen, P.R. (2001) First Landing Site Workshop for the 2003 Mars Exploration Rovers, Ames Research Center, January, 2001. [8] Christensen, P.R., (2003) *Nature, 422*, 45-48. [9] Malin, M. C., and K. S. Edgett (2001), *J. Geophys. Res., 106*, 23,429-23,571. [10] Simpson, R.A., Harmon, et al.(1992), Radar: p. 652-685, in *Mars* (Kieffer, H.H., Jakosky, B.M., Snyder, C.W., and Matthews, M.S., eds.), Univ. Arizona Press, Tucson, AZ, 1498p. [11] Olhoeft, G.R. (1998), Proc. GPR'98, Seventh Int'l Conf. on GPR, University of Kansas, Lawrence, KS, p. 177-182. [12] Paillou, P., et al. (2001), Performances of Ground Penetrating Radars in arid volcanic regions: Consequences for Mars subsurface exploration. [13] Leuschen, C., and R. Plumb, (2001) *IEEE Transactions on Geoscience and Remote Sensing*, *39*, 929-936. [14] Leuschen, C., (2001) *Surface-Penetrating Radar for Mars Exploration*, Ph.D. Dissertation, University of Kansas.

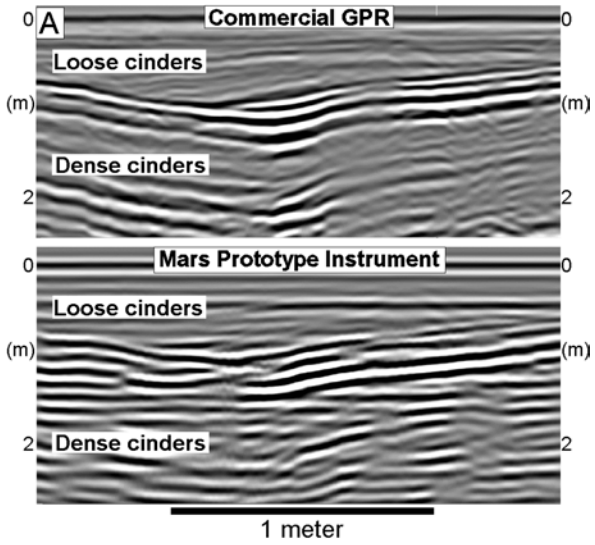

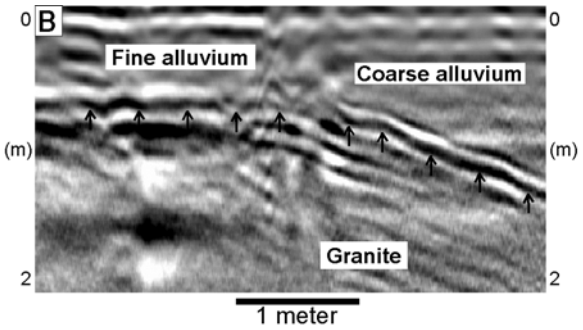

Figure 1. GPR data collected from planetary analog settings using prototype GPR. A) Data from layered volcanic cinders at Sunset Crater, AZ, using commercial 500 MHz antenna (top) and Mars 600 MHz antenna deployed ~15 cm above ground (bottom). B) Data collected using prototype Mars antenna deployed ~15 cm above ground in alluvium over granite bedrock. Arrows show the granite/alluvium contact.

Model: Near-Surface Ice (~2 meters)

top bottom	Lithology	ϕ	*S* ice
0m	atmosphere	100	–
0 m 1.2 m	eolian sediment	50	0
1.2 1.5-2.0	indurated sediment	15	0
1.5-2.0 2.2-2.0	fluvial sediment	30	0
2.2-2.0 6.5-5.5	dirty ice (no rocks)	90	90
6.5-5.5 8.0	non-uniform layered ejecta	10- 20	50

ϕ: porosity (%volume), *S*: saturation

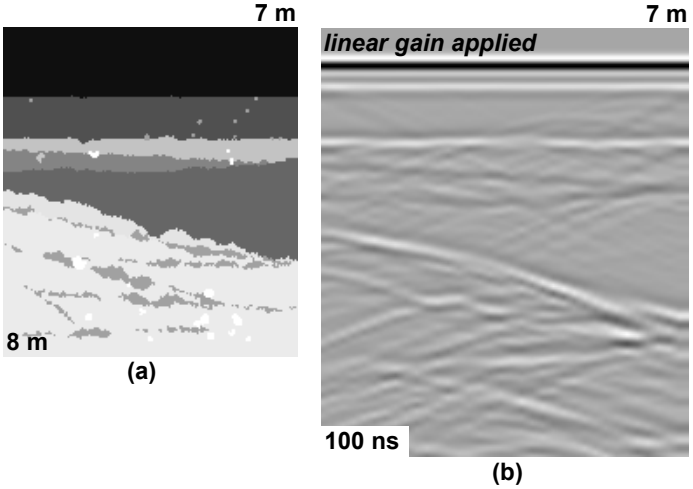

Figure 2 . FDTD simulation of a near-surface ice model. The table describes the stratigraphy, the dielectric distribution is shown in image (a), and the resulting waveforms are in image (b). Numbers in the lower left and upper right of the figure denote simulation depth and distance along the surface, respectively.

INFLUENCE OF ICE RHEOLOGY AND DUST CONTENT ON THE DYNAMICS OF THE NORTH-POLAR CAP OF MARS. Ralf Greve, *Dept. Mechanics, Darmstadt University of Technology, D-64289 Darmstadt, Germany (greve@mechanik.tu-darmstadt.de)*, Rupali A. Mahajan, *Max Planck Institute for Aeronomy, D-37191 Katlenburg-Lindau, Germany*.

Introduction. The Martian poles are both covered by ice caps. The seasonal caps, which can extend down to latitudes of approximately $55^\circ\mathrm{N/S}$, consist of only some ten centimeters of CO_2 snow which sublimes into the atmosphere during the respective summer season. The smaller residual caps poleward of approximately $80^\circ\mathrm{N/S}$ are underlain by massive topographic structures known as the polar layered deposits [11]. The complexes composed of the residual caps and the layered deposits are referred to as the north- and south-polar cap (NPC/SPC), respectively. Owing to the Mars Orbiter Laser Altimeter (MOLA) measurements of the Mars Global Surveyor (MGS) spacecraft, the surface topographies of the NPC and SPC have been mapped very precisely [10,13].

Previous studies [3,4,5] indicate that the NPC is a dynamic ice mass which shows glacial flow of the order of $1\ \mathrm{mm\ a^{-1}}$ at present. Its present topography is the result of the climatic history over the last millions of years, which was probably characterized by climate cycles as a consequence of strong, quasi-periodic variations of the orbital parameters obliquity, eccentricity and precession on time-scales of 10^5–10^6 years [7]. This idea is supported by the light-dark layered deposits of both polar caps indicating a strongly varying dust content of the ice due to varying atmospheric conditions.

In this study, the dynamic and thermodynamic evolution of the NPC will be simulated with the ice-sheet model SICOPOLIS. The boundary conditions of surface accumulation, ablation and temperature are derived directly from the solar-insolation history by applying the Mars Atmosphere-Ice Coupler MAIC developed by Greve et al. [5]. We consider steady-state scenarios under present climate conditions as well as transient scenarios over the last millions of years of climate history. A large uncertainty in model studies of that kind results from the poorly constrained rheological properties of the ice and the unknown dust content. Therefore, we will look systematically into the influence of these two aspects on the evolution of ice topography and glacial flow of the ice body. Some basic considerations for this investigation are given below.

Ice rheology. For terrestrial ice, a well-established non-linear viscous rheology which relates the strain-rate tensor $\boldsymbol{D} = \mathrm{sym\ grad}\,\boldsymbol{v}$ (velocity $\boldsymbol{v}$) to the Cauchy stress deviator $\boldsymbol{t}^{\mathrm{D}}$ is Glen's flow law,

$$\boldsymbol{D} = E A(T') \sigma^{n-1}\, \boldsymbol{t}^{\mathrm{D}}, \tag{1}$$

where $\sigma = [\mathrm{tr}\,(\boldsymbol{t}^{\mathrm{D}})^2/2]^{1/2}$ is the effective shear stress and $n = 3$ the stress exponent. The flow-rate factor depends via the Arrhenius law

$$A(T') = A_0\, e^{-Q/R(T_0+T')} \tag{2}$$

on the temperature relative to the pressure melting point, T', and for $T' \leq -10^\circ C$ suitable values for the constants are $A_0 = 3.985 \times 10^{-13}\ \mathrm{s^{-1}\,Pa^{-3}}$, $Q = 60\ \mathrm{kJ\,mol^{-1}}$ (activation energy), $R = 8.314\ \mathrm{J\,mol^{-1}\,K^{-1}}$ (universal gas constant) and $T_0 = 273.15\ \mathrm{K}$ [9]. The flow-enhancement factor E is equal to unity for pure ice and can deviate from unity due to the softening or stiffening effect of impurities in the ice. A widely used value for terrestrial ice formed during glacial periods is $E = 3$, interpreted as the softening influence of very small amounts of fine dust, approximately $1\ \mathrm{mg\ kg^{-1}}$ with particle sizes of 0.1 to $2\,\mu\mathrm{m}$ [6].

It is not clear whether the flow law (1), which describes the flow mechanism of dislocation creep, is suitable for the low temperatures and low strain rates in the Martian caps. There is strong evidence that other, grain-size-dependent flow mechanisms like grain-boundary sliding become favoured instead [1,2]. These can be described by the flow law

$$\boldsymbol{D} = E A(T') \left(\frac{d_0}{d}\right)^p \sigma^{n-1}\, \boldsymbol{t}^{\mathrm{D}} \tag{3}$$

with the stress exponent $n = 1.8$, the grain size d, the reference grain size $d_0 = 10^{-3}\ \mathrm{m}$ and the grain-size exponent $p = 1.4$. The flow-rate factor $A(T')$ is described by the Arrhenius law (2) with the parameters $A_0 = 9.826 \times 10^{-10}\ \mathrm{s^{-1}\,Pa^{-1.8}}$ and $Q = 49\ \mathrm{kJ\ mol^{-1}}$ [8].

An upper limit for the grain size d can be obtained by assuming that it is a result of normal grain growth only. From a variety of data for terrestrial polar ice masses and theoretical considerations, the growth rate

$$\frac{\mathrm{d}}{\mathrm{d}t}(d^2) = k \tag{4}$$

was derived, where t is the time and $\mathrm{d}/\mathrm{d}t$ is the material time derivative which follows the motion of the ice particles. The growth-rate parameter k depends on the absolute temperature T via the Arrhenius law

$$k(T) = k_0\, e^{-Q_k/RT}, \tag{5}$$

with the activation energy $Q_k = 42.5\ \mathrm{kJ\,mol^{-1}}$ and the constant $k_0 = 9.5\ \mathrm{m^2\,a^{-1}}$ [12]. As an example, for $T = 173\ \mathrm{K}$ this yields a growth rate of $1.40\ \mathrm{mm^2\,Ma^{-1}}$.

Dust content. Satellite imagery shows that parts of the polar caps appear dark, which indicates that they consist of ice with some amount of mixed-in dust. However, for the average volume fraction φ of dust in the ice no quantitative information is available. For modelling studies of the polar caps this is a serious problem because the dust content can affect the ice flow via direct stiffening, an increasing density and a decreasing heat conductivity which leads to basal warming. Therefore, we compute the density, ρ, and heat conductivity, κ, of the ice-dust mixture as volume-fraction-weighed averages of the

values for pure ice and crustal material,

$$\rho = (1-\varphi)\rho_{\rm i} + \varphi\rho_{\rm c}, \quad (6)$$

$$\kappa = (1-\varphi)\kappa_{\rm i} + \varphi\kappa_{\rm c}, \quad (7)$$

with the following parameters: ice density $\rho_{\rm i} = 910\,{\rm kg\,m^{-3}}$, heat conductivity of ice $\kappa_{\rm i} = 9.828\,e^{-0.0057\,T[{\rm K}]}\,{\rm W\,m^{-1}K^{-1}}$, density of crustal material $\rho_{\rm c} = 2900\ {\rm kg\,m^{-3}}$, heat conductivity of crustal material $\kappa_{\rm c} = 2.5\ {\rm W\,m^{-1}\,K^{-1}}$ [4]. Direct stiffening is described by a flow-enhancement factor $E < 1$ based on laboratory measurements of the deformation of ice-dust compounds [1],

$$E = e^{-2\varphi}. \quad (8)$$

This means that a dust content of 10% ($\varphi = 0.1$) leads to an almost 20% stiffer material compared to pure ice.

References. [1] Durham, W. B. (1998). Factors affecting the rheologic properties of Martian polar ice. *First International Conference on Mars Polar Science and Exploration*, LPI Contribution No. 953, pp. 8–9. Lunar and Planetary Institute, Houston. [2] Goldsby, D. L. and D. L. Kohlstedt (1997). Grain boundary sliding in fine-grained ice I. *Scripta Materialia 37* (9), 1399–1406. [3] Greve, R. (2000). Waxing and waning of the perennial north polar H_2O ice cap of Mars over obliquity cycles. *Icarus 144* (2), 419–431. [4] Greve, R., V. Klemann and D. Wolf (2003). Ice flow and isostasy of the north polar cap of Mars. *Planet. Space Sci. 51* (3), 193–204. [5] Greve, R., R. A. Mahajan, J. Segschneider and B. Grieger (2003). Evolution of the north-polar cap of Mars: A modelling study. *Planet. Space Sci.* Submitted. [6] Hammer, C. U., H. B. Clausen, W. Dansgaard, A. Neftel, P. Kristinsdottir and E. Johnson (1985). Continuous impurity analysis along the Dye 3 deep core. In C. C. Langway, H. Oeschger, and W. Dansgaard (Eds.), *Greenland Ice Core: Geophysics, Geochemistry and the Environment*, Geophysical Monographs No. 33, pp. 90–94. American Geophysical Union, Washington DC. [7] Laskar, J., B. Levrard and J. F. Mustard (2002). Orbital forcing of the martian polar layered deposits. *Nature 419* (6905), 375–377. [8] Nye, J. F. (2000). A flow model for the polar caps of Mars. *J. Glaciol. 46* (154), 438–444. [9] Paterson, W. S. B. (1994). *The physics of glaciers*. Third edition. Pergamon Press, Oxford etc. [10] Smith, D. E., and 18 others (1999). The global topography of Mars and implications for surface evolution. *Science 284* (5419), 1495–1503. [11] Thomas, P., S. Squyres, K. Herkenhoff, A. Howard and B. Murray (1992). Polar deposits of Mars. In H. H. Kieffer, B. M. Jakosky, C. W. Snyder, and M. S. Matthews (Eds.), *Mars*, pp. 767–795. University of Arizona Press, Tucson. [12] Thorsteinsson, T. (1996). Textures and fabrics in the GRIP ice core, in relation to climate history and ice deformation. *Reports on Polar Research 205*, 146 pp. Alfred Wegener Institute for Polar and Marine Research, Bremerhaven. [13] Zuber, M. T., and 20 others (1998). Observations of the north polar region of Mars from the Mars Orbiter Laser Altimeter. *Science 282* (5396), 2053–2060.

THE PASCAL MARS SCOUT MISSION. R.M. Haberle[1] and the Pascal Team. [1]Space Science Division, MS 245-3, NASA/Ames Research Center, Moffett Field CA, 94035, Robert.M.Haberle@nasa.gov.

Introduction: Pascal is a Mars Climate Network Mission that is being developed for NASA's Mars Scout Program. The mission would establish a network of 18 science weather stations distributed across the entire surface of Mars that operates for 3-10 Mars years (5.6-18.8 Earth years). Pascal's instrument suite combines entry data from accelerometers and descent cameras, with landed data from pressure, opacity, temperature, wind speed, and water vapor to create a detailed global picture of Martian climate and weather. A panoramic landed camera system acquires images every 30 Sols to monitor changes in the landing environment due to winds. Analysis of data from the science stations, taken as often as once every 15 minutes, will provide a depth of understanding that will vastly increase our knowledge of Mars, and significantly impact site selection for future NASA missions. Pascal is the first mission ever to sample - in situ - the full global diversity of Mars and provide a continuous long-term presence on its surface.

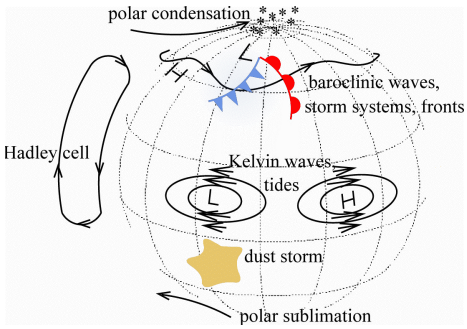

Science goals and objectives: Pascal's primary science goal is to characterize the Martian climate system and ho(Fig. 1). This goal naturally includes the nature of aeolian processes, the role of global and small-scale circulations, and comparative planetary meteorology. Pascal's science objective is to measure the seasonal cycles of dust, water, andCO_2; measure the near surface signature of global and small scale circulation systems; relate those measurements to understanding how these circulation systems control the climate system and modify the surface; and provide a basis for comparative meteorology.

Mission design: The Pascal carrier spacecraft delivers its 18 Probes on direct approach using three separate release events, and propulsive time-of-arrival adjustments to facilitate global coverage. The probes utilize an areoshell for thermal protection and initial deceleration; a parachute and an air bag provide final deceleration for the 9 kg stations. Accelerometers record the deceleration history throughout the entry, descent, and landing phase (Fig. 2), while a descent camera acquires images every 5 seconds while on the parachute. On the

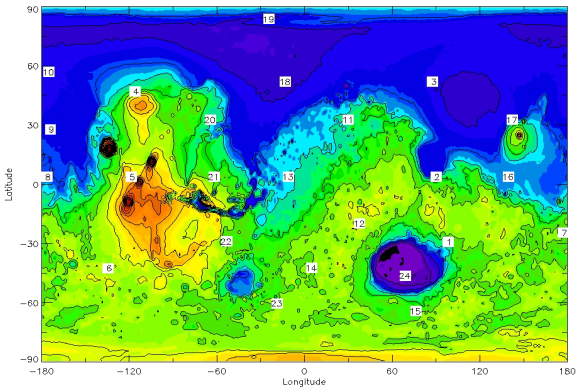

ground, the science stations orient and deploy the camera system and begin autonomous operations. Pascal's long life is enabled by its power system: a lightweight radioisotope-heating unit coupled to a thermoelectric converter. Communication with the Pascal landers occurs through the telecommunication infrastructure of the Mars Exploration Program. A sample network achievable for the 2007 opportunity is shown in Fig. 3.

With this kind of a robust long-lived global network, Pascal will be the first mission ever to sample - in situ - the global diversity of Mars and provide a continuous long-term presence on its surface. In this sense, Pascal is a true "Scout" mission. Humans have long been fascinated with the prospect of an extended stay on Mars, and NASA'S MEP has identified a sample return mission as its ultimate near-term goal. Pascal can provide the information needed to enable such missions. Questions such as where should we land, what are the expected environments, and how can we adapt to them, are all readily addressed by this mission.

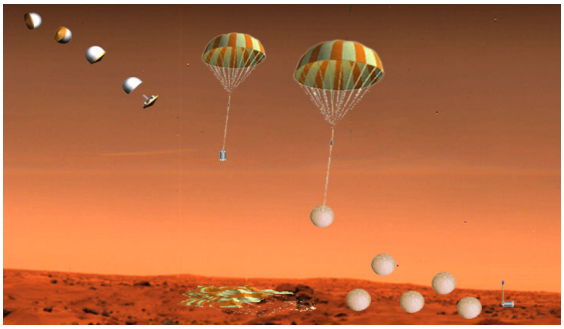

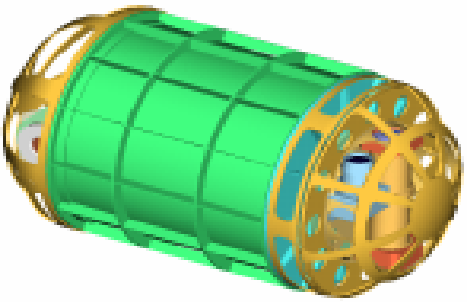

Pascal Science Station

RECONCILING THE MOLA, TES, AND NEUTRON OBSERVATIONS OF THE NORTH POLAR CO_2 MASS BUDGET ON MARS. R.M. Haberle[1], B. Mattingly[2], and T.N. Titus[3]. [1]Space Science Division, MS 245-3, NASA/Ames Research Center, Moffett Field CA, 94035, Robert.M.Haberle@nasa.gov. [2]Dept. Meteorology, San Jose State University, San Jose CA, 95192, bridgemat@yahoo.com. [3]U.S. Geological Survey, 2255 North Gemini Drive, Flagstaff AZ, 86001, ttitus@usgs.gov.

Introduction: There are now three independent observations of the CO_2 polar cap mass budget of Mars' north polar cap. The first is based elevation changes detected by the Mars Orbiter Laser Altimeter (MOLA) on the Mars Global Surveyor (MGS) [1]. The second is based on MGS Thermal Emission Spectrometer (TES) broadband observations of the solar and infrared radiation fields at the top of the atmosphere [2,3]. The third is based on neutron counts measured by the neutron spectrometer (NS) on Odyssey [4]. If one assumes a cap density of 910 kg/m^3 [1], then the peak mass loading poleward of 85°N inferred from the MOLA data is ~1090 kg/m^2, which compares to ~1150 kg/m^2 inferred from TES for the same region, and ~700 kg/m^2 from the NS data. TES and MOLA are in good agreement, but are about 60% higher than the NS data. Is there a way to reconcile these discrepancies?

Role of surface heat storage: The TES data are based on an energy balance. The net radiative loss (gain) in a column is balanced by latent heating due condensation (sublimation) of CO_2. In calculating the mass budget, the other main energy sources, atmospheric heat transport and subsurface conduction, were neglected [2,3]. At the pole, atmospheric heat transport is indeed a small term. However, subsurface heat conduction can be significant because at the North Pole water ice, which has a high thermal conductivity compared to bare soil, is a dominant component of the subsurface. Thus, heat conducted down into the ice during summer will slowly bleed back out during fall and winter reducing the amount of CO_2 that condenses on the pole.

We have taken a first cut at quantifying this effect by fitting a curve to Paige's [5] estimates of the conducted energy flux in his analysis of Viking IRTM data. For a thermal inertia of ~2100 (SI units) this curve shows a peak upward conducted heat flux of about 30 W/m^2 at L_s=180°, which is just after the time CO_2 begins condensing. This then gradually tapers off to less than several W/m^2 near the end of spring just before the CO_2 ice completely sublimes. We then added this term to the TES radiation fields and recalculated the CO_2 mass budget. We find that subsurface heat conduction at the North Pole can reduce the amount of CO_2 that condenses by about 400 kg/m^2, which brings the TES data in close agreement with the NS data.

CO_2 ice density: That leaves the MOLA data much higher the both TES and NS. However, the MOLA data are based on elevation changes and are not direct measurements of the mass loading. To relate the elevation changes to a mass loading requires knowledge of the ice density. The MOLA data can be reconciled with TES and NS if the CO_2 ice density is ~600 kg/m^3. Feldman et al. [4] suggested that low ice densities could be a way to explain the difference between MOLA and NS.

The MOLA combined gravity/elevation measurements infer a mean cap density of 910 ± 230 kg/m^2 [1]. Thus, 600 kg/m^3 is below the lower limit of the MOLA measurements. However, the MOLA-derived density is an average for the entire seasonal cap. It is possible that the density of the north polar deposits is less than the average of the entire seasonal cap. A good physical basis for this is the much more frequent occurrence of "cold spots" at the North Pole compared to lower latitudes [6]. Snowfall is a strong candidate for the origin of these cold spots. If true, it means that a much greater fraction of the north polar deposits originate from the atmosphere as snowfall rather than direct condensation onto the surface. Surface accumulations resulting from snowfall have lower densities than those originating from direct deposition.

Conclusion: Of the three measurements that bear on the north polar CO_2 mass budget, the NS provides the most direct measurement of the mass loading. Yet it shows much less CO_2 accumulating on the pole than initially predicted by either MOLA or TES. These differences can be reconciled by (a) including subsurface heat conduction in the TES calculations, and (b) using a lower ice density to convert MOLA elevation data to a mass loading.

References: [1] Smith D.E., Zuber M.T. and Neumann G.A. (2001) *Science, 294*, 2141-2148. [2] Kieffer, H.H. and Titus, T.N. (2001) *Icarus, 154*, 162-180. [3] Titus, T.N. (2003) *International workshop: Mars atmosphere modelling and observatiions*, Granada, Spain. [4] Feldman W.C., et al. (2003) *JGR*, submitted. [5] Paige, D.A. (1985) *Ph.D. Thesis*, UCLA, 206p. [6] Titus T.N. and Kieffer, H.H. (2003) *6th International Mars Conference*, Pasadena Ca.

OBLIQUITY DRIVEN CLIMATE CHANGE IN MARS' RECENT PAST. R.M. Haberle[1], F. Montmessin[1], F. Forget[2], A. Spiga[3], and A. Colaprete[4]. [1]Space Science Division, MS 245-3, NASA/Ames Research Center, Moffett Field CA, 94035, Robert.M.Haberle@nasa.gov. [2]Laboratoire de Météorolgie Dynamique, Universite Paris, 4 pl. Jussieu, 75252 Paris Cedex 05-FRANCE, forget@lmd.jussieu.fr. [3]Ecole Polytechnique, 91128 Palaiseau, Cedex FRANCE, Aymeric.Spiga@polytechnique.org. [4]SETI Institute, Space Science Division, MS 245-3, NASA/Ames Research Center, Moffett Field CA, 94035, tonyc@freeze.arc.nasa.gov.

Introduction: To explain the equatorial valley networks on Mars, Jakosky and Carr [1] suggested that water ice now stored in the north polar region would be mobilized at high obliquity and precipitate out at low latitudes. Extrapolating the present day latitudinal distribution of water vapor to high obliquity conditions, and noting that the low latitude atmosphere would be saturated, they predicted substantial surface ice deposits would accumulate in the tropics at such times.

The first general circulation model simulations to verify this prediction were reported by Haberle et al. [2] who found that while ice can accumulate at low latitudes at high obliquity, it is distributed regionally depending on orbital conditions. Forget [3], Richardson and Wilson [4], and Mischna et al. [5], subsequently obtained similar results with independent models. Thus, obliquity driven climate change may help explain the many tropical landforms thought to be sculpted by water in one form or another (see, for example, refs [6], [7], and [8]).

While low latitude ice accumulations at high obliquity appears to be a robust result, the major challenge now facing models is predicting ice accumulations in the same places where the geological evidence suggests it occurred. This will depend not only on orbital conditions, but also on what physical processes the models include in the hydrological cycle. For example, none of the models mentioned above include the radiative effects of water vapor or clouds, yet both are expected to be in abundance at high obliquity. And none of the models has a very realistic cloud microphysics scheme, which can have a significant effect on how clouds affect the planet's radiation balance.

Here we extend these early modeling results by including a more sophisticated cloud microphysics package, as well as the radiative effects of water vapor and clouds.

Model description: We use the NASA/Ames C-grid Mars general circulation model with an updated radiation code and cloud microphysics scheme. To speed up the simulations, we run the model at fairly coarse resolution (7.5° latitude x 22.5° longitude). Future efforts will examine the effect of resolution on the results.

Radiation Code Fluxes and heating rates are calculated from a radiation code based on the two-stream solution to radiative transfer that fully accounts for multiple scattering in the presence of gaseous absorption. The model has 12 spectral intervals. Dust and water ice scattering properties are included. For dust, we use the Ockert-Bell [9] values in the visible, and Forget [10] values in the infrared. For ice, we can either compute them online as the cloud evolves, or we can specify them. Gaseous opacities for water vapor and CO_2 are calculated from correlated k-distributions taken from full line-by-line models.

Cloud Microphysics Our cloud scheme is based on a moment/order scheme in which the mass mixing ratio and number density of the cloud ensemble are the advected species. From these we obtain a mean particle size and an estimate or the particle size distribution (assuming a variance) which we then divide into 8 bins. Cloud microphysics is performed in each of these bins and includes nucleation, condensation, and gravitational settling. Dust is treated as a tracer and serves as condensation nuclei. The altered size distribution is then converted back into a mean size, a mixing ratio, and a particle number density.

Results: We have conducted simulations for a variety of different obliquities, all at present solar luminosity. In each case the model is spun up from dry initial conditions with a residual ice cap at the north pole. After several years, depending on obliquity, the atmosphere equilibrates and repeats from year-to-year. A sample result for the 60° obliquity simulation, without the radiative effects of clouds or water vapor, is shown in Fig. 1. The top panel in Fig. 1 is the zonally averaged column water vapor as a function of time for 7 Mars years. The middle and bottom panels are similar, but for cloud mass and surface ice, respectively.

Water ice subliming from the north residual cap during summer is rapidly transported southward. Clouds form in low northern latitudes and ice precipitates to the surface. The remainder is transported into the southern hemisphere and condenses onto the south seasonal CO_2 ice cap which extends almost to the equator at the solstice. When the south cap retreats, water is released into the atmosphere where some precipitates back to the surface and the remainder is transported north. Again clouds form in the low latitudes

and ice precipitates to the surface. At equilibrium, thousands of precipitable microns of water vapor appear in the summer polar regions. There is more water in the south than the north because the south cap is a better trap for water, and because the Southern Hemisphere is warmer during summer than in the north. Cloud abundances also reach the thousand precipitable micron mark with model predicted particle sizes in the 20-30 micron range. These particles are much bigger, and subsequently fall out faster, than those for present obliquity.

Eventually, permanent deposits form (i.e., ice remains on the ground all year long) in the low latitudes of each hemisphere. These deposits are concentrated along the northern flanks of the Tharsis region and to the northeast of the Hellas basin. Topography plays a key role on where the deposits form through its influence on the circulation. The deposits do not necessarily form in locations where the mean annual surface temperatures are a minimum. They form where the saturation state of the atmosphere is highest. This, in turn, is influenced not only by the thermal structure of the atmosphere, but also by the transport characteristics of the atmosphere.

Simulations which include the radiative effects of water vapor show similar results, but with (a) an increase in the amount of surface ice, (b) a slight shift in the location of the deposits, (c) a cooler and cloudier atmosphere, and (d) slightly warmer surface temperatures. We are presently undertaking simulations with the radiative effects of clouds included and will report the results at the meeting. However, off line 1-D simulations using the predicted cloud abundances indicate they will have a much greater influence on the results than water vapor alone. Their abundances (~ 1000 pr-μm), particle sizes (20-30 μm), widespread occurrence, and impact on the solar and infrared radiation fluxes give clouds a much greater role in determining the climate at high obliquity than for present day conditions.

Conclusions: Mars has a natural mechanism for experiencing significant climate change and redistributing surface ice. Obliquity changes alone are quite capable of moving ice into low latitudes and may provide an explanation for the many geological landforms that strongly indicate recent climate change.

References: [1] Jakosky, B.M. and Carr, H.H. (1985) *Nature, 315,* 559-561. [2] Haberle, R.M., et al. (2000) *LPS XXX1,* Abstract #1509. [3] F. Forget (2001), personal communication. [4] Richardson, M.I., and Wilson R.J., *JGR, 107,* 5031-5049. [5] Mischna, et al. (2003) *JGR,* In press. [6] Cabrol, N.A. and Grin, E.A. (2001). Icarus, 149, 291-328. [7] Kargel, J. (2001) DPS Abstract # 48.12. [8] Head, J.W. and Marchant, D.R. (2003) 6th International Mars Conference, Abstract #3807. [9] Ockert-Bell, M.E. et al. (1997). *JGR, 102,* 9039-9050. [10] Forget, F. (1998). *GRL, 25,* 1105-1108.

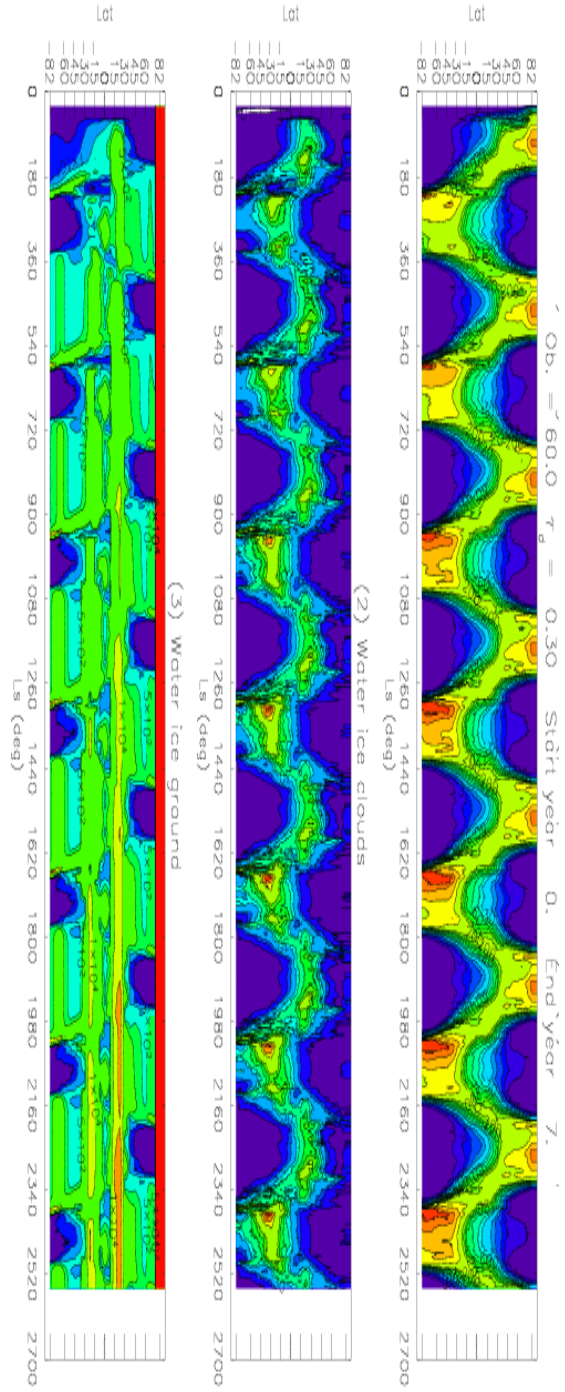

Figure 1

ALBEDO VARIATIONS ON THE MARTIAN NORTHERN POLAR CAP AS SEEN BY MGS. A.S. Hale D. S. Bass, and L. K. Tamppari[3], [1]NASA Jet Propulsion Laboratory (MS 264-235, 4800 Oak Grove Drive, Pasadena, CA 91109 amy.s.hale@jpl.nasa.gov), [2]NASA Jet Propulsion Laboratory (MS T1722, 4800 Oak Grove Drive, Pasadena, CA 91109 deborah.s.bass@jpl.nasa.gov), [3]NASA Jet Propulsion Laboratory (MS 301-422, 4800 Oak Grove Drive, Pasadena, CA 91109 leslie.k.tamppari@jpl.nasa.gov [1]

Introduction The Viking Orbiters determined that the surface of Mars' northern residual cap is water ice. Many researchers have related observed atmospheric water vapor abundances to seasonal exchange between reservoirs such as the polar caps, but the extent to which the exchange between the surface and the atmosphere remains uncertain. Early studies of the ice coverage and albedo of the northern residual Martian polar cap using Mariner 9 and Viking images reported that there were substantial internannual differences in ice deposition on the polar cap [1], a result that suggested a highly variable Martian climate. However, some of the data used in these studies were obtained at differing values of heliocentric solar longitude (L_s). Reevaluation of this dataset in [2] indicated that the residual cap undergoes seasonal brightening throughout the summer, and indicated that this process repeats from year to year. In this study we continue this work with data acquired with Mars Global Surveyor's Mars Orbiter Camera (MOC) and Thermal Emission Spectrometer (TES) instruments.

We use MOC Wide Angel (WA) red filter images of the cap obtained at different values of L_s and different Martian years, and TES albedo data of the north polar region. Previous work in this study has concentrated on MOC images of the cap edge and frost covered outliers [3]; in this phase we systematically investigate images from the cap center (defined for our purposes to be the area northward of 80 degrees latitude) in order to assess any latitudinal trends in seasonal brightening. We have examined data from both instruments from mapping year 1 and 2, though we have ignored MOC data acquired between September 2000 and May 2001, as the MOC camera experienced a state change between those dates that make albedo comparisons with data taken at other times problematic (Cantor, private communication).

Result 1: MOC: Previous work [3] examined brightening of cap edge areas of approximately 40% throughout the northern summer, with the greatest increase occurring in early summer. This result is in agreement with that obtained by [1] for Viking and Mariner 9 data. The region shown in **Figure 1** shows this brightening [3].

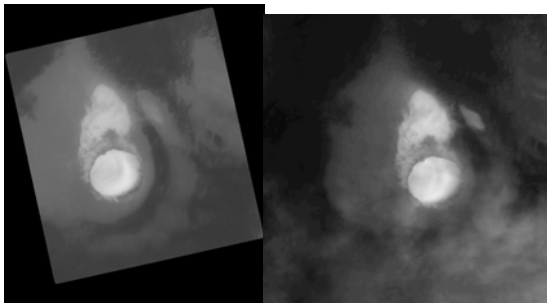

a. b.

. **Figure 1:** MOC images showing the crater at approx. 77 degrees north and 270 degrees west. The left image (a) shows L_s = 108; the image on the right (b) shows L_s =161. An approximate 40% brightening is seen.

In contrast, examination of center cap images to date shows a different trend; center cap images appear to remain at the same albedo as the summer progresses. For example, the region shown in **Figure 2** shows a decrease in brightness of approximately 2.5 % between L_s = 121 and L_s = 155. This change is not within the MOC detectability limits (Malin and Edgett 2001), and so we conclude that this region has experienced no detectable albedo change. This result is in disagreement with that obtained by [1] for Viking and Mariner 9 data that suggested cap edge albedo was controlled by cap center albedo; the reasons for discrepancy are still being explored and will be discussed in our presentation. In all comparisons, the DN values of same pixels of the calibrated processed ISIS level 2 cubes were compared in qview.

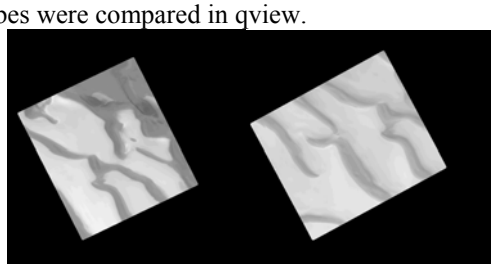

a. b.

Figure 2: MOC images showing the area at approx. 86 degrees north and 141 degrees west. The left image (a) shows L_s = 121, the right one (b) L_s=155. No brightening within reliable detection limits is seen for the same areas

Result 2: TES: The story of north polar water ice frost appears to be even more complex when other datasets are examined. We generated TES lambert albedo maps for the northern polar region; maps were binned in 2 by 2 degrees of latitude and longitude, and 10 degrees of L_s. The spatial resolution of the TES instrument is much less than that of MOC (approximately 3 km per pixel), but larger regional trends can still be seen (**Figure 3**).

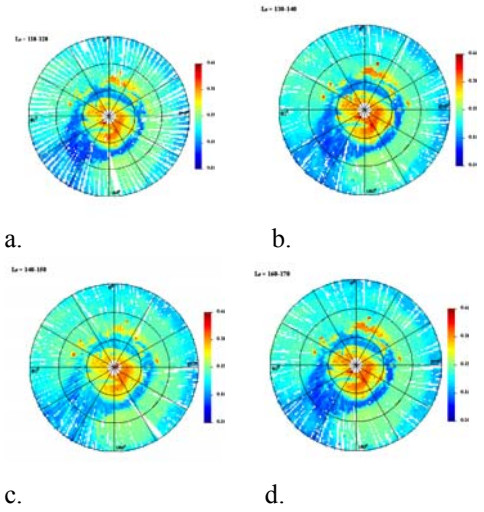

a. b.

c. d.

Figure 3: TES lambert albedo data showing the Martian north polar region. The plot on the top left (a) shows L_s 110-120; the plot on the top right (b.) L_s =120-130. The bottom left image (c) shows L_s 140-150, and image d shows L_s = 160-170 The latitude range shown is from 60 to 90 degrees north. All data from second mapping year.

The TES data show a complex picture, with the cap region appearing to brighten early in the summer, then decrease in albedo later in the season, and then brighten again as the summer ends. This is consistent with behavior documented previously [4]. Work is ongoing correlating TES pixels with areas observed by MOC, as is analysis of how the regional view of TES and the localized view of MOC agree and disagree, and we will present the results in our presentation.

Conclusions: The results reported here describe far more complexity in water ice albedo variability than had previously been appreciated. It is clear that the entire cap may not be treated as a monolithic body, but rather, individual locations show a variety of influences. One possibility is that topographic effects may have an effect; water cycle processes may also have a latitudinal dependence. In other research not presented here we are also investigating is the role of atmospheric effects on surface albedo. Clearly, whatever processes are affecting the cap albedo may have latitudinal dependence, and may have important implications for the Martian water cycle. We will present results regarding the full TES albedo data set, as well as other sites observed by MOC. Additionally we will present out interpretation of regional and local process interaction.

References: [1] Bass D. S et al. (2000) *Icarus, 144,* 382-396. [2] Cantor B. et al. (2002) *JGR., 107*. [3] Hale et al. (2003) 34th LPSC Abstract # 1422. [4] Kieffer and Titus (2001) *Icarus, 154,* 162-180.

DETECTION AND LOCALIZATION OF MARS SUB-SURFACE ICE BY SURFACE IMPEDANCE MEASUREMENTS FROM A ROVER AS PART OF THE WISDOM/PASTEUR AND OTHER ROVER EXPERIMENTS.

M. Hamelin[1], R. Grard[2], J.-J. Berthelier[1], R. Ney[1], R. Trautner[2] and F. Simoes[2], [1]CETP-IPSL, 4 avenue de Neptune, 94107, Saint Maur, France, michel.hamelin@cetp.ipsl.fr, [2]ESA/RSSD, ESTEC, Postbus 299, NL-2200 AG NOORDWIJK ZH, THE NETHERLANDS, rejean.grard@esa.int.

Introduction: Water and ice on Mars are of great interest for geological, biological and engineering issues. The recent Mars Odyssey missions have shown the presence of water ice in the upper subsurface of Mars in polar regions. At lower latitudes or in particular basins ice should be found at larger depths of several meters. The WISDOM experiment (Water Ice and Subsurface Deposit Observations on Mars) is devoted to the exploration of the subsurface and the search for water and ice in medium latitudes where the subsurface ice could be found at even larger depths. For that purpose it combines a mutual impedance measurement to study the upper layers and a Ground Penetrating Radar that allows reaching larger depths down to a few hundred of meters. In the case of medium-high latitude missions where ice is believed to be at a depth of a few meters, the Mutual and Self Impedance techniques to measure the subsurface permittivity can be used as in the WISDOM project. The instrument is a surface electrode array (7 electrodes) deployed or trailed behind a rover. The multiple combinations between electrodes allow to detect ice embedded in the regolith under an upper layer of dry regolith, and to estimate the depth and ice concentration of the icy layer. It would be possible to follow the ice localization along the track of the rover. That would be very useful information to decide where to drill for a direct access to the ice layer.

Ice identification from permittivity measurements: The Permittivity Probe yields the complex permittivity of the ground over the low frequency range (e.g. 1Hz-10 kHz), by measuring the mutual impedance of two antennas, one operating as a transmitter, and the other one as a receiver. At low frequencies, the rotation of polarized molecules contributes the most significantly to the displacement current. Instruments working in the low frequency domain are therefore well suited to the characterization of the electrical properties of ice mixtures. The dielectric constant of water ice embedded in regolith, at temperatures around 200 K, displays indeed a strong dependence on frequency in the 1-100 Hz range. The Permittivity Probe therefore provides a sensitive measure of the water ice content in the sub-surface.

Subsurface ice detection with multiple electrode arrays: When the electrode array is lying on the surface, far away from the rover, the apparent measured permittivity is the mean of vacuum and ground permittivities. So, a flat system of electrodes is ideal to deduce directly the permittivity from self or mutual impedance measurements. For a single quadrupole, the measurement domain is commensurate with the size of the quadrupole. If the subsurface can be considered as layered horizontally, which is likely the case for subsurface icy layers, a multiple array combining several quadrupole sizes, allows determining the parameters of the layered model, layer permittivities and depths of the interfaces. With the system of 7 electrodes that we propose, it would be possible to estimate at least the characteristics of the upper layer and those of the underlying material where ice is expected. A synthetic model of the subsurface is used for this study.

Instrument design: We discuss the design of the instrument, estimate its main characteristics of size and mass that are relative to the desired depth range of the measurements and we point out the particular points to be addressed in an engineering feasibility study.

EVOLUTION OF LOW-EMISSIVITY SPOTS IN THE MARTIAN WINTER POLAR CAPS: MOBILITY OF DUST GRAINS. G. B. Hansen, Planetary Science Institute, Northwest Division, Department of Earth and Space Science, University of Washington, Seattle, WA 98195 (ghansen@rad.ess.washington.edu).

Introduction: Temporally and spatially variable regions of low 20-μm emissivity occur regularly on the winter polar caps of Mars, as first discovered in Viking orbiter observations [1], and subsequently in spectra returned by the Mars Global Surveyor Thermal Emission Spectrometer (TES) [2, 3, 4]. Although many disparate effects were originally offered to explain these features, the current consensus is that they are caused by regions of relatively fine-grained CO_2 frost, probably the result of snowfall [4, 5], and occurring often in regions of high topographic slopes, implying dynamic atmospheric processes [6]. The dynamic nature of these spots has been demonstrated by repeated TES observations of the same locations [7]. The apparent grain coarsening observed has been explained as a process of "continued condensation" [6] or a sintering process starting from micron-sized grains [7] based on theoretical study by Eluszkiewicz [8]. My mapping of the polar cap composition and properties [9] has suggested another possible process: the movement of dust condensation nuclei from the center of newly fallen snow grains (where they are largely optically hidden) to grain boundaries (where they are fully optically active). This process was suggested by the modeling of low-emissivity spots in which the CO_2 ice grain size is little different from, while the apparent dust content is much smaller than in the surrounding regions.

Observation Details and Calibration: The TES spectra shown here are from revolution 214, in the first science phasing orbit period (SPO-1). It took place in April 1998, with $L_S \approx 304°$, roughly halfway between the winter solstice and the spring equinox. The historical polar cap size is near its maximum extent at this time and extends to 55–60° N. The limit of polar night is at ~69° N, and the spacecraft ground track crosses into sunlight at ~67° N. The data sequence starts on the night side at 59.5° N in western Utopia Planitia (70° W). The maximum latitude reached over the elevated residual polar cap is 86.2° N. The seasonal polar cap extends to ~51.5° N on the day side, in Tempe Terra (257° W).

The TES is a Michelson interferometer measuring from 1650 to 200 cm^{-1} (~6–50 μm) with a spectral resolution of either 6 or 12 cm^{-1}, and a two-channel bolometric radiometer measuring solar (0.3–2.7 μm) and thermal (5.5–100 μm) spectral regions [2, 10]. The finest spatial resolution of TES measurements is <3 km. Observations of the winter polar regions are useful only above 8–10 μm.

There are many artifacts in the polar spectra from the PDS supplied dataset. These were corrected by adjusting instrument sensitivity and darks. The sensitivity is set assuming that it does not change rapidly with time, and that later times in the sequence are better calibrated. The darks measured by pointing the mirror up differ from those when pointed to the side or down [10]. The offset is a very significant fraction of typical polar spectra [3]. The dark level can be estimated by inspecting limb scan sequences. They are adjusted at the short wavelength end from the data, since the radiance from a ~150 K surface is essentially 0 for wavenumbers larger than 1300 cm^{-1}. There is an important high-frequency component to the darks as well, which also appears to vary slightly from revolution to revolution. These patterns are determined by assuming that the surface spectrum averaged over the whole polar cap, outside the atmospheric CO_2 band, is smooth. When these new darks are used, both individual spectra and small averages of spectra are much better behaved, in that the remaining variations have all the characteristics of random noise.

Previous Work: The seasonal polar caps of Mars are composed primarily of solid CO_2, likely mixed with some micron-sized Martian dust and water ice. Many of these dust and water ice grains may be brought in as condensation nuclei for CO_2 snow grains. Each polar cap spectra from this revolution has been analyzed by fitting to model spectra of ternary CO_2-H_2O-dust intimate mixtures, including partial spatial coverage, surface temperatures, and water ice clouds [9]. The dust optical properties are poorly known in the important 20–50 μm region. Those used here are derived from analysis of airborne dust in Mariner 9 infrared spectra [11]. They fit a few low-dust observations, assuming that the surface spectrum is a blackbody. The dust study is continuing by looking at a wider variety of spectra and variable surface emissivity.

The results of this analysis show that the central polar cap is 100% covered by CO_2 deposits, and that the temperature varies as expected (as a function of altitude). The CO_2 grain radius varies between 200 μm and 1 cm, averaging ~1 mm, while the dust mass mixing ratio varies from 100 ppm to 1%, averaging 0.1%, and the water ice mass mixing ratio varies from 0 to 0.1%, averaging ~100 ppm.

There are several low-emissivity regions in the central polar cap, normally indicated by a large brightness temperature difference between 25 and 18 μm. A detail

of the brightness temperature difference, CO_2 grain size, and dust mass mixing ratio over one of these regions as shown in Figure 1. The typical behavior shown here is that the large brightness temperature difference is reflected mostly in the dust mixing ratio, and not the CO_2 grain size, as has been assumed previously [4, 7].

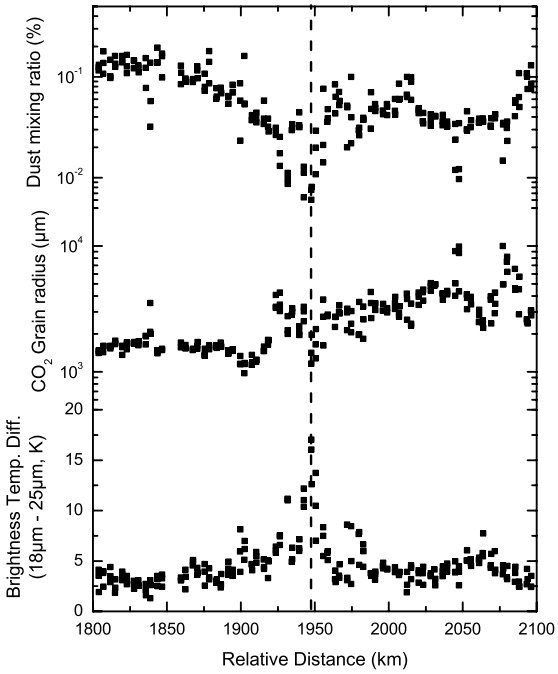

Figure 1

A New Theory: This observation suggests a different process for the temporal and spatial variation of low-emissivity regions. These regions are most likely initiated by fresh CO_2 snowfall from atmospheric dynamic interactions with topographic obstacles. If the CO_2 grains are formed around dust condensation nuclei, the optical properties of the dust are subdued or absent (depending on the ratio of grain size to nucleus size). We will investigate this using layered Mie calculations, but the hiding effect is well known. If the dust nuclei subsequently migrate to the grain boundaries as the deposit matures, the optical effect of the dust will approach the intimate mixing formulation of the models. The effective CO_2 grain size may not change significantly as it matures.

Average spectra from some typical cold spots are shown in Figures 2 and 3. In each case an average from the edges of the low-emissivity region are compared to an average from the center of the region, to show the spectral effect of increased dust at a similar grain size. The background grain sizes is 600 μm, and the dust content varies from 0.01% (center) to 0.1% (edge) in Figure 2, and the background grain size is 2 mm, and the dust content varies from 0.008% (center) to 0.05% (edge) in Figure 3. The background dust mixing ratio is consistent with an original CO_2 grain size of 12–15 μm around a 2-μm dust nucleus.

Figure 2

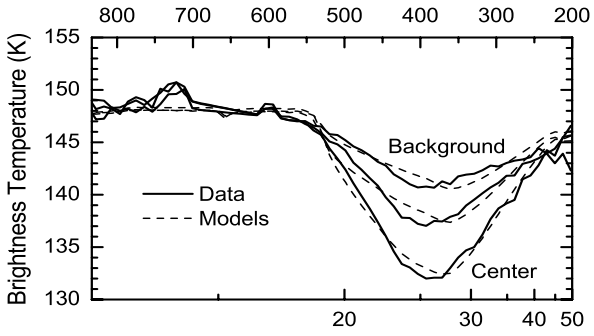

Figure 3

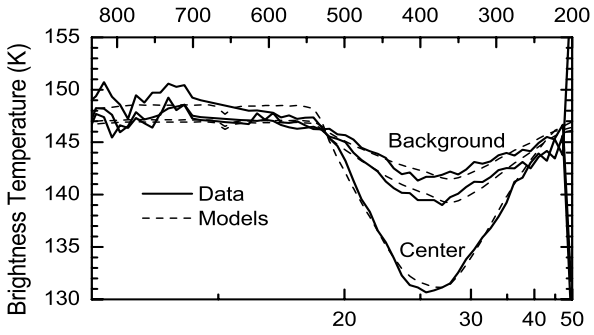

References:

[1] Kieffer *et al.* (1976) *Science, 194*, 1341–1344. [2] Christensen P. R. *et al.* (1992) *JGR, 97*, 7719–7734. [3] Kieffer *et al.* (2000) *JGR, 105*, 9653–9699. [4] Titus *et al.* (2001) *JGR, 106*, 23181–23196. [5] Hansen G. B. (1999) *JGR, 104*, 16471–16486. [6] Forget, F. *et al.* (1998) *Icarus, 131*, 302–316, 1998. [7] Eluszkiewicz, J., and T. N. Titus (2002) *BAAS, 34*, 866. [8] Eluszkiewicz, J. (1993) *Icarus, 103*, 43–48. [9] Hansen, G. B. (2001) *Eos Trans. AGU, 82*, Fall Meet. Suppl., Abstract P12E-09. [10[Christensen P. R. *et al.* (2001) *JGR, 106*, 23823–23871. [11] Hansen, G. B., *BAAS, 34*, 844.

UPPER LATITUDE ICE FLOW, GULLIES, AND LONG-TERM GLACIAL HISTORY. W. K. Hartmann, Planetary Science Institute, 620 N. 6th Ave., Tucson, AZ 85705; hartmann@psi.edu

Ice Flow Features: Varied ice-flow-like features have been found in Mars Global Surveyor (MGS) images of moderate to upper latitudes of Mars. Debris aprons give geomorphological suggestions of flow [1], and numerical modeling by Turtle et al. [2] indicates ice flow could deform ice-rich slopes on timescales of 10^3-10^4 y, reaching highly deformed, more steady-state configurations within 10^6 y. Crater counts by Berman [3] and the author (unpublished) suggest that the surface structures at scales of 10-60 m on debris apron surfaces are young, with ages as low as 10^6-10^7 y. Various aspects of terrain softening, observed in upper latitudes, may also involve ice flow [4]. MGS has shown possible ice-flow softening or viscous relaxation of craters as small as a few km [5].

A dramatic tongue shaped feature on a crater wall at ~38° S latitude is likely example of a recent ice flow down the wall [6]. As seen in Fig. 1, the lower crater wall below the tongue is dissected by gullies somewhat different from the classic Malin-Edgett hillside gullies; they may be result of erosion by runoff water from melting of ice in the observed flowing mass, or earlier such masses. Such tongue-like flow features are very rare, but Berman [3] has identified a few similar examples. The south wall of the same crater (unnamed, east of Hellas near Reull Vallis in a region known for debris aprons) also shows flow features, of different morphology. Here, the valleys are filled with chevron-striated deposits that suggest glacial or rock glacial masses.

Relation to Gullies: Hartmann et al. [6] pointed out that the tongue-like apparent flow feature in Figure 1 has a distal crescentic ridge, with a near-concentric, softer arc-like outer ridge further down slope, and that below many Martian hillside gullies similar crescentic ridges can be seen (Fig. 2). Arfstrom [7] gave examples of similar features formed as moraines in terrestrial glaciers, and proposed that these features are moraines formed as glaciers flowed down crater walls after ice mantling. Thus, some gullies may form underneath, or in association with, such ice masses deposited on crater walls. This is consistent with the hypotheses developed by Mustard [8] and Costard et al. [9] invoking deposition of ice-rich dust mantles during long periods of winter cold and dark, during high-obliquity phases of 10^7 y axial tilt cycles.

An explanation for the rarity of beautifully preserved ice flow features such as seen in Figure 1 may be that the flow is fast (as shown by Turtle et al. [2]), and Martian glaciers self-destruct because of high ice losses from the surface of the flowing mass, due to sublimation as the dusty ice mass flows and churns. They may last no more than a few My.

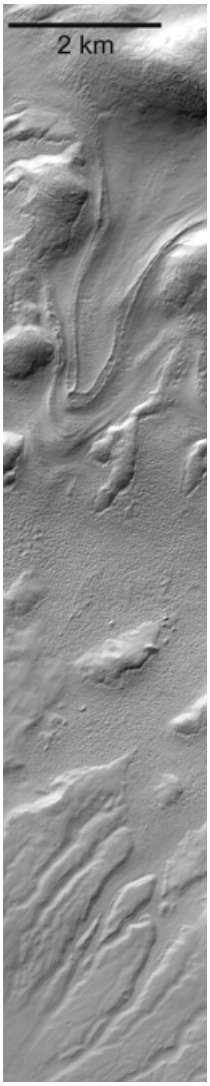

Figure 1. Lobate feature caused by apparent flow down north inner wall of an unnamed crater at 247W 38S. Downhill from the lobate flow, the lower crater wall deposits are dissected by gullying, possibly from runoff associated with ice in previous flows. MOC M18-00897.

In this view, glaciation and gullying at upper latitudes may come in short-lived episodes launched primarily by ice deposition cycles (and less commonly by local water release, creating ice lenses), and even the moderate upper latitudes of Mars may be viewed geomorphologically as parts of the time-varying polar ice cap.

Long-Term Glacial and Polar History: Tanaka et al. [10] tabulated total areas resurfaced by various processes in different epochs. Using early estimates of Martian chronology based on crater counts, he found that resurfacing by periglacial and fluvial processes declined from high Noachian values. Hartmann and Neukum [11] refined the crater chronology, consistent with ages of Martian igneous meteorites from 170 to 1300 My. Using my own subsequent refinement of those data, I updated the estimates of the durations of the Martian epochs, and computed the rate of resurfacing [(Tanaka total km^2 resurfaced by a given process in a given epoch)/(duration of that epoch)]. The result (Fig. 3) confirms that Noachian/Hesperian periglacial resurfacing rates were an order of magnitude or more the modern rate. Fluvial and volcanic resurfacing also show enhanced Noachian/Hesperian rates relative to the present, indicating that early Mars was a more active and Earth-like environment.

References: [1] Pierce T. L. and Crown (2003) *Icarus, 163,* 46-65. [2] Turtle E. P. et al. (2003) 3rd Intl. Polar Sci. Conf. (this meeting). [3] Berman D. C. (2003) M. S. thesis, U. of AZ, in prep. [4] Squyres S. et al. (1992) In *Mars*, U. AZ Press, Tucson, 523-544. [5] Hartmann W. K. and Esquerdo G. (1999) *Meteor. Planet. Sci., 34,* 167-177. [6] Hartmann W. K. et al. (2003) *Icarus, 162,* 259-277. [7] Arfstrom J. (2003) *LPS XXXIV,* Abstract #1174. [8] Mustard J. F. et al. (2001) *Nature, 412,* 411-413. [9] Costard F. et al. (2003) *Science, 295,* 110-113. [10] Tanaka et al. 1987. *Proc. Lunar Planet Sci Conf. 18th,* 665-678. [11] Hartmann W. K. and Neukum G. (2001) *Space Sci. Rev., 96,* 165-194 with modest updated revisions by W. K. Hartmann, in preparation).

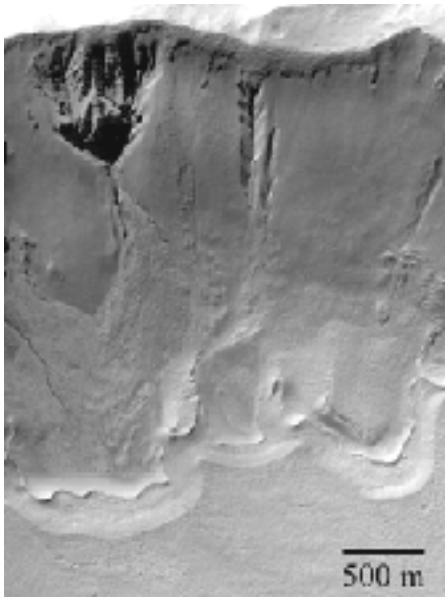

Figure 2. Typical Martian gully system showing sharp arcuate ridge bounded on outside by softer ridges, at the base of the gullied hillside. The arcuate forms, which may be moraines, are similar to those at the foot of the glacier-like mass in image A, suggesting that glacier-like ice rich masses may be associated with gully production. 166W39S MOC M18-00303.

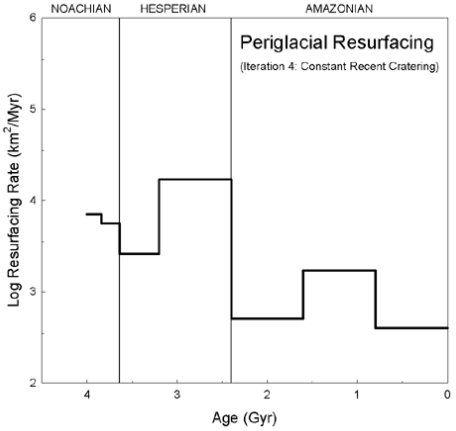

Figure 3. Plot of rate of resurfacing by periglacial processes as a function of time, derived by dividing total area of periglacial resurfacing in each epoch [10] by durations of the epoch [11]. Various timescale by Neukum and by Hartmann agree that Noachian-Hesperian periglacial resurfacing rates were an order of magnitude higher than present values.

EXTENSIVE HESPERIAN-AGED SOUTH CIRCUMPOLAR ICE SHEET ON MARS: DORSA ARGENTEA FORMATION SYNTHESIS: James W. Head[1], Gil J. Ghatan[1] and David Marchant[2], [1]Dept. Geol. Sci, Brown Univ., Providence, RI 02912 USA, [2]Dept. Earth Sciences, Boston Univ., Boston, MA 02215 USA, james_head@brown.edu

Introduction and background: The nature of the climate in early Mars history, and whether pluvial conditions prevailed [e.g., 1] during the Noachian Period (~4.6-3.7 Ga) [2], or if an ocean existed then and/or during the Hesperian Period (~3.7-3.0 Ga) [3], are matters of major debate and investigation. The Dorsa Argentea Formation [4] (DAF) is a south circumplolar deposit of Hesperian age [2] and thus may record the aftermath of Noachian-aged climate and volatile evolution. Here we outline a synthesis of the characteristics of the DAF, and show that these are consistent with the presence of a major water-ice-rich circumpolar deposit during the Hesperian, and its partial melting, sublimation and retreat. We outline interpretations for the source and fate of these volatiles and their significance to polar and hydrological processes and history.

The Dorsa Argentea Formation: Underlying the present Amazonian-aged polar cap (Api, residual ice and Apl, layered terrain) lies the Hesperian-aged Dorsa Argentea Formation, Hd, and related units [4] (Figure 1) (here collectively called the DAF). This deposit covers a surface area that could be as large as 2.94 x 10^6 km^2 (about 2% of the surface of Mars), over twice the area of the present Amazonian-aged deposits. Originally interpreted as largely volcanic in origin [4], this deposit has been reinterpreted on the basis of new MGS data as a volatile-rich ice-sheet-like unit that underwent melting and retreat [5] or, alternatively, a deposit caused by release and emplacement of subsurface volatiles and debris [6]. Here we synthesize the evidence for the DAF and related units representing an extensive south circumpolar glacial-like deposit that underwent significant melting, sublimation and retreat [5].

Sinuous Channels Along the Eastern DAF Margin: Along the eastern margin of the continuous deposit of the DAF (Figure 1; 1) are located a series of sinuous channels that lead away from the margin of the deposit and enter nearby craters, exiting them from downslope margins, crossing intercrater terrain and entering other craters [7]. The channels connecting these craters provide evidence for extensive crater flooding, ponding (minimum volumes of ~10^{12} m^3), overtopping, downcutting, and continuous drainage of material through a series of craters and into the Prometheus Basin near the edge of the current polar cap. Topogrpahy data show that water filled some craters to depths of at least 200 m and possibly as much as 600 m. Water exiting from the edge drained over a lateral distance of ~600 km and a vertical height of ~800 m. These data provide evidence for the water-rich nature of the DAF, its subsequent melting and collapse, and the overland drainage of its meltwater effluent [7].

Concentric Ridges: Nearby these marginal channels but inward of the DAF margin (Figure 1, 2) lies a series of arcuate ridges that are convex-outward from the DAF margin. These have been interpreted to be push moraines derived from bulldozing of ice and sediment at the margins of the DAF [8].

Sisyphi Lobe and Broad Depression: One of two major lobes of the DAF is the Sisyphi Lobe that extends out from the south pole toward 0° (Figure 1). Largely surrounded by Noachian cratered terrain, the deposit in this area is shown by MOLA data to be a topographic low [9], and smooth at small scales, but containing a large-scale pitted texture and a number of unusual mountains.

Unusual Mountains: Located within the Sisyphi Lobe are a number of isolated mountains with average separation distances of ~175 km (Figure 1; 3); these are typically 30-40 km in diameter and ~1-1.5 km high, with their bases falling near an elevation of ~1200 m. The unusual shapes of these mountains as well as the alignment of many, and the sinuous channels emanating from the base of several, has led to the interpretation [10] that they are of volcanic origin, with their unusual morphology and morphometry being accounted for by their eruption under an ice-sheet. Assessment of edifice morphometry led to the conclusion that the overlying ice sheet had a minimum thickness of ~1.4 km [10].

Cavi Sisyphi: Located within the Sisyphi Lobe are a series of irregular and elongate depressions that are typically about 500 m deep and have relatively steep marginal slopes (~11°) (Figure 1; 4). Within several of these are sinuous ridges that have been interpreted to be eskers and are oriented in directions consistent with regional drainage from regions within the DAF that appear to have undergone melting (likely related to the features interpreted as subglacial volcanoes) and drainage toward the margins of the DAF where large channels emerge and wind toward the floor of Argyre [11].

Angusti Lobe: Oriented radially from the south pole toward 70° W is a broad lobe of positive topography which we describe as the Angusti Lobe (Figure 1).

Cavi Angusti: Within the Angusti Lobe lie Cavi Angusti (Figure 1; 5), a series of basins similar to Cavi Sisyphi in surface area and wall steepness, but differeing in several important ways. These basins are typically deeper (~1000 m) and contain centrally located mountains or ridges, which have been interpreted to be volcanic edifices [12]. The terraced interiors and central mountains of many cavi have been interpreted to mean that the basins formed as a result of magmatic intrusion and extrusions causing heating and melting of a water-rich substrate (the overlying DAF) and drainage of the liquid water. Meltwater from basin formation appears to have drained laterally and may also have reentered the subsurface groundwater system [12].

Dorsa Argentea: A series of sinuous and overlapping ridges extend for several hundreds of km from the interior of the DAF toward the margins (Figure 1; 6). A range of different interpretations have been offered in the past [5] but recently terrestrial analogs and topography data have been used to develop detailed criteria for the recongnition of eskers on Mars [13]. Application of these criteria has strengthened the interpretation that these ridges are eskers and that they represent the drainage of meltwater products from the interior of the DAF toward the margins, out into an adjacent lowlying region interpreted to be a lake [14].

Lowlands Around Schmidt Crater: Adjacent to the Angusti Lobe is a low-lying smooth area (Figure 1; 7) interpreted to be a region in which meltwater from the central DAF was delivered and which collected before ultimately draining through a channel in the surrounding topography and down into the Argyre Basin. Informally called Lake Schmidt, this region covers an area of ~270,000 km^2, five times the size of Lake Michigan and may have been in excess of 300 m deep [14]. Also observed is a series of pits in a narrow zone located along the boundary between the Angusti lobe and the adjacent

lowlands; this has been interpreted to be a contact zone between the ice sheet and the lake, in which the pits are comparable to kettle holes formed due to melting of residual ice blocks [15].

Pedestal Craters: Craters with extensive elevated ejecta deposits occur within the DAF with the most prominent one (Figure 1; 8) characterized by marginal ~500 m high scarps [5], suggesting that material removed from below this armoring deposit was at least 500 m thick.

Mountains near South Crater: A series of distinctive mountain peaks occur near South crater (Figure 1; 9) and their morphology suggests that their lower portions were buried by the DAF but that their upper portions were surrounded by the DAF. On the basis of their morphology and unusual structure, we have interpreted these to be nunataks, mountains which rise above surrounding ice sheets.

Hr relationships: Located along the eastern edge of the Sisyphi Lobe (Figure 1; 10), and defining the margin of the DAF is an extensive scarp between the DAF and Hr (ridged plains interpreted to be of volcanic origin). This unusual scarp faces inward toward the DAF and is interpreted to have formed by the emplacement of Hr lavas from sources in Malea Planum up against the DAF, forming a constructional ridge against the ice sheet. Subsequent to the decay of the ice sheet the scarp remains and is now facing inward toward the DAF. The presence of this scarp may help to explain why much of the meltwater appears to have drained into the Prometheus and Argyre Basins, and not out into Hellas.

Channels Marginal to the DAF: Inspection of the DAF along the western margins of the Sisyphi Lobe, as well as along the eastern margins of the Angusti Lobe, reveals the presence of channels that are arrayed radially away from the deposit (Figure 1, white lines). These several large channels begin at and near the margins of the DAF; some can be traced back into the deposit and are continuous with esker-like ridges and elongate cavi in the DAF [16]. These channels lead from the DAF margins northward, draining downslope for distances from 1000-1600 km onto the floor of the Argyre Basin, some 3.5-4.0 km below their origins. The channels do not exhibit tributaries and are sometimes discontinous in flat regions where ponding may have taken place. Their characteristics suggest that a significant portion of the DAF meltwater entered a surface distribution system that transported it to the floor of Argyre [5].

Synthesis: These characteristics of the DAF and adjacent deposits lead us to the interpretation that the unit represents the remnants of a major south circumpolar ice-rich deposit that existed in the Hesperian and that underwent significant melting, sublimation and retreat. Estimates of the present deposit thickness, and the amount of material thought to have been removed suggest that the original volume could have been as much as 5.9 x 10^6 km^3, equivalent to a global layer of water ~20 m deep if the deposit consisted of 50% volatiles. Positive evidence is seen for bottom-up melting (volcanic eruptions); top-down melting may also have occurred. Some of the water from this melting drained laterally overland, but a significant portion may well have entered the groundwater system, potentially recharging the global aquifer [3]. A portion of the volatiles are predicted to have remained in the deposit, representing a net removal from the atmosphere and from the active hydrologic system. Today the DAF forms an accessible record of aqueous conditions and possible biological environments dating from early Mars history.

References: 1) R. Craddock and A. Howard, JGR, 10.1029/2001JE001505, 2002; 2) W. Hartmann and G. Neukum, Space Sci. Rev., 96, 165, 2001; 3) S. Clifford and T. Parker, Icarus, 154, 40, 2001; 4) K. Tanaka and D. Scott, USGS Map 1802-C, 1987; 5) J. Head and S. Pratt, JGR, 106, 12275, 2001; 6) K. Tanaka and E. Kolb, Icarus, 154, 3, 2001; 7) S. Milkovich et al., JGR, 10.1029/2001JE001802, 2002;.8) S. Milkovich and J. Head, Microsymposium 24, 2001;. 9) J. Head and G. Ghatan, LPSC 32, #1062, 2001; 10) G. Ghatan and J. Head, JGR, 10.1029/2001JE001519, 2002; 11) G. Ghatan and J. Head, LPSC 34, #1129, 2003; 12) G. Ghatan et al., JGR, 10.1029/2002JE001972, 2003; 13) J. Head and B. Hallet, LPSC 32, #1366, #1373, 2001; 14) J. Head and S. Pratt, LPSC 32, #1159, 2001; 15) J. Dickson and J. Head, LPSC 34, #1185, 2003; 16) G. Ghatan and J. Head, 6th Mars Conf., #3034.

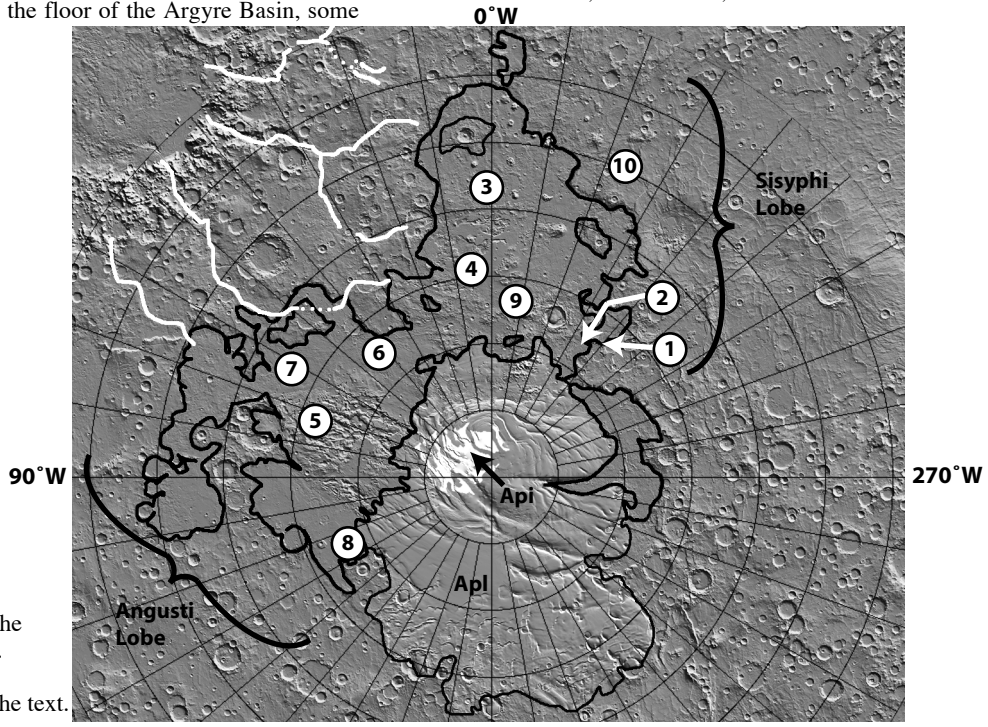

Figure 1. Distribution of the DAF and related deposits. Numbers refer to features and regions described in the text.

TROPICAL MOUNTAIN GLACIERS ON MARS: EVIDENCE FOR AMAZONAIN CLIMATE CHANGE:

James W. Head[1], David E. Shean[1], Sarah Milkovich[1] and David Marchant[2], [1]Dept. Geol. Sci, Brown Univ., Providence, RI 02912 USA, [2]Dept., Earth Sciences, Boston Univ., Boston, MA 02215 USA, james_head@brown.edu

Introduction and background: Polar deposits on Mars represent one of the most significant current volatile reservoirs on the planet and these, together with high-latitude surface and near-surface ground ice, the global cryosphere, possible groundwater, and small amounts of atmospheric water vapor, represent components of the hydrological cycle. Recent Odyssey data have been interpreted to signify the presence of significant amounts of near-surface ice at mid-to high latitudes in both hemispheres [1]. These deposits, together with other topography and morphology data, have been interpreted to mean that volatile-rich deposits have been emplaced from about 30° north and south latitude to the poles during obliquity excursions on the order of <35° [2], perhaps relatively recently, in agreement with predictions from climate models [3].

In this contribution, we outline evidence for the accumulation of ice deposits below 30° north and south latitude during the Amazonian Period. These near-equatorial ice accumulations take the form of tropical glacier deposits that extended outward from the flanks of the Tharsis Montes and Olympus Mons (Figure 1).

Interpretation of Glacial Landforms on Mars: Recent terrestrial studies as well as analysis of landforms on Mars have led to a new understanding of cold-based glacial landforms [e.g., 4]. Although cold-based glaciers do not erode their underlying substrates appreciably, they do deposit characteristic landforms. The material within these landforms originates from supraglacial debris, commonly rockfall and/or volcanic ejecta that falls onto the glacier surface. These rockfall and volcanic particles flow passively through the ice toward glacier margins. During deposition, the resulting landforms (e.g., drop moraines, sublimation till, rock-glacier deposits) are perched on existing topography. Sharp basal contacts and undisturbed underlying strata are hallmarks of cold-based glacier deposits.

The term *drop moraine* is used here to describe ridges that form as supra- and englacial particles are dropped passively at the margins of cold-based glaciers. In the Dry Valleys, such moraines may be cored by glacier ice, owing to the insulating effect of the debris on the underlying glacier. In plan view, drop moraines closely mimic the pattern of former ice margins, though moraine width may vary spatially, owing to the characteristic inhomogeneity in the distribution of supraglacial debris.

Sublimation along the ice-atmosphere interface may bring englacial debris passively to the ice surface. The rate of ice sublimation slows as the evolving sublimation till thickens, eventually insulating the underlying ice by retarding vapor diffusion and thermal change. Many *sublimation tills* in the western Dry Valleys region of Antarctica are underlain by glacier ice, even though some are in excess of a few Ma. Differential flow of underlying glacier ice may result in distinct surface lobes of sublimation till

In the western Dry Valleys region of Antarctica, *rock glaciers* form as sublimation concentrates debris on the surface of active glaciers. Continued flow of the underlying glacier through internal deformation produces ridges and lobes of sublimation till atop the glacier. The thickness of this debris increases down ice flow, as material is continually added to the base of the sublimation till as it moves down valley. In general, rock glacier formation is favored by high debris accumulation rates and low ice velocities, conditions common in an advanced state of glacial retreat. Spoon-shaped hollows that commonly form at the head of many terrestrial rock glaciers likely arise due to excess sublimation in areas with incomplete debris cover as opposed to preservation by the more extensive tills down valley.

Three shield volcanoes, collectively known as the Tharsis Montes, cap the broad Tharsis Rise, a huge center of volcanism and tectonism spanning almost the entire history of Mars. Olympus Mons is located on the flank of the rise (Figure 1). Each of these volcanoes, although largely constructed of effusive and explosive volcanic deposits, contains a distinctive and unusual lobe, or fan-shaped deposit on their west-northwestern flank. These deposits consist of three facies and various hypotheses have been proposed for their origin including one or more of the following: lahars, debris avalanches, landslides, pyroclastic flows, and/or generally related to the advance and retreat of ice [see review in 5].

New Mars Orbiter Laser Altimeter (MOLA) altimetry and Mars Orbiter Camera (MOC) images from the Mars Global Surveyor spacecraft have permitted us to characterize the fan-shaped deposits in much more detail. On the basis of present surface temperatures on Mars and those of the recent past, any mountain glaciers would likely be cold-based and most similar to the slow-moving, cold based glaciers of the Dry Valleys region of Antarctica. We outline here the deposit characteristics and use Antarctic Dry Valley analogs to aid in their interpretation.

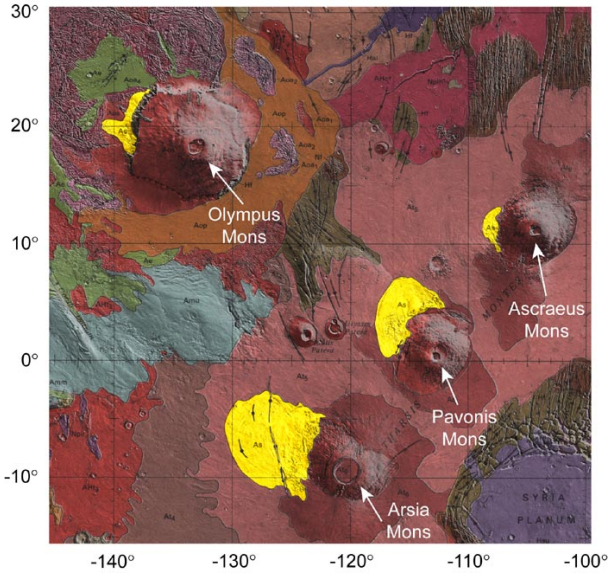

Figure 1. Geologic map of Mars showing the fan-shaped deposits (yellow, unit As) associated with the northwest flanks of the Tharsis Montes and Olympus Mons [8].

Arsia Mons: At Arsia Mons, an outer ridged facies that consists of multiple laterally extensive, arcuate and parallel ridges resting without disturbance on both well-preserved lava flows and an impact crater, is interpreted to be a series of drop moraines formed at the margin of an ablating and predominantly receding cold-based glacier. A knobby facies that consists of equidimensional

knobs, each up to several kilometers in diameter, is present inward of the ridges; this facies is interpreted as sublimation till derived from *in situ* downwasting of ash-rich glacier ice. A third facies comprising distinctive convex-outward lobes with concentric parallel ridges and aspect ratios elongated downslope likely represents rock-glacier deposits, some of which may still be underlain by a core of glacier ice. Taken together, these surficial deposits show that the western flank of Arsia Mons was occupied by an extensive mountain glacial system accumulating on and emerging from the upper slopes of the volcano and spreading downslope to form a piedmont-like fan occupying in excess of 180,000 km^2. We find little evidence for meltwater features in association with any facies, and thus conclude that the glacier ice was predominantly cold based throughout its history and ablation was largely by sublimation.

Pavonis Mons: The Pavonis fan-shaped deposit (Figure 1) extends approximately 250 km northwest of the shield base [6]. The deposit ranges from 3.0-8.5 km above the Mars datum and covers an area of 75,000 km^2, approximately half of the area covered by the Arsia deposit. The ridged facies consists of a series of hundreds of concentric, parallel ridges around the distal margins of the deposit. The ridged facies is also observed in the central regions fan-shaped deposit, with some inner ridges only 70 km from the base of the shield. This geographic distribution of the ridged facies is unique to Pavonis. We interpret these ridges as drop moraines formed at the margins of a retreating cold-based glacier. A knobby or hummocky facies, that lies both inward and outward of the ridged facies, consists of sub-km scale knobs and depressions that are subrounded to elongated downslope in places. The knobby facies appears to superpose underlying features including the ridged facies, and we interpret it to be a sublimation till derived from *in situ* down-wasting of ash-rich glacier ice. There are four isolated regions of the smooth facies within the Pavonis deposit, the largest extends into the central regions of the fan-shaped deposit.

Additional evidence in support of the glacial hypothesis is seen where the Pavonis fan-shaped deposit is bounded to the east by lava flows. A large scarp exists in these regions where the fan-shaped deposit is 200-250 m lower than the adjacent Tharsis plains. It appears that these lava flows were deflected from flowing toward lower topographic areas and instead continue for over 100 km to the north-northwest. The most likely explanation is that a large ice sheet with a relief of at least 250 m blocked westward flow at the time of lava emplacement.

An area of several, high relief, unique flow-like features exists in the western regions of the fan-shaped deposit. These features are morphologically different from subaerial lava flows at higher elevations on the flanks of Pavonis outside the fan-shaped deposit and also from flows on the Tharsis plains beyond the fan-shaped deposit to the west. They consist of elevated plateaus with leveed edges and steep walls, some with relief of over 500 m. Also present in the central regions of the fan-shaped deposit are several linear ridges. These ridges are radial to the base of the shield and have dimensions of approximately 100-200 m high**,** 1 km wide, and 30-60 km long**.** Analysis of high-resolution MOC images and THEMIS Day IR images suggests that these features may be flows and radial dikes, which erupted in a subglacial environment.

Ascraeus Mons: Ascraeus Mons has the smallest fan-shaped deposit of the three Tharsis Montes, which extends approximately 90 km from the base of the shield [7] and covers an area of around 30,000 km^2. The strong westerly trend and small size of the deposit confine the accumulation zone for the glacier on the lower western flanks of Ascraeus Mons. Within the fan-shaped deposit, we see a well-defined ridged facies around the outer margins of the deposit as well as an area of the knobby facies in the central regions. Several flow-like features are also present, similar to those observed at Pavonis. They appear to emanate from a series of fractures to the southwest of the fan-shaped deposit. These flows form a large, 300 m high scarp that is roughly concentric to the outer margin of the Ascraeus fan-shaped deposit, suggesting that they were emplaced at a time when an ice sheet was still present at Ascraeus. The most obvious dissimilarity between the Ascraeus deposit and those at Arsia and Pavonis is the absence of the smooth facies. The lack of a smooth facies at Ascraeus may indicate that it was never present or that underlying volatiles have completely sublimated away due to recent climatic conditions.

Olympus Mons: Extending from the base of the Olympus Mons scarp is a unit consisting of several facies, the most extensive of which are fan-shaped deposits including multiple lobate deposits extending up to 90 km from the base of the scarp. Individual lobes are characterized by regular, arcuate, subparallel ridges up to 60 km long. Many depressions are found in this unit; several are circular and are interpreted as small impact craters while others are irregularly shaped. Depressions tend to be hundreds of meters wide and thousands of meters long with depths on the order of tens of m. One lobe is approximately 700 m high and concave in topographic profile. The margins of the lobes are marked by linear ridges hundreds to thousands of meters long and tens of meters high. This unit is interpreted as the remnants of debris-covered glaciers extending from the basal escarpment. The ridges are interpreted to be moraines. Cross-cutting relations imply several episodes of advance and retreat.

Five lobes on Olympus Mons can be traced back to cirque-like hollows in the basal escarpment. The steep scarps at the heads of these erosional hollows rise approximately 4 km above the fan-shaped deposits, and may have served as the accumulation regions. The characteristics of the Olympus Mons fan-shaped deposits are similar in scale and morphology to features within the Tharsis Montes deposits interpreted to be rock glaciers to rock glaciers in the Antarctic Dry Valleys. The ridges at the outer margins of the deposit lobes are interpreted to be distal moraines and the concentric ridges to be drift ridges typical of Antarctic Dry Valley and may other rock glaciers.

Summary and Conclusions: During the Amazonian, significant climate changes created conditions that permitted accumulation of ice deposits in excess of several hundreds of meters thickness, their spreading away from the base of the volcanoes, and their retreat and readvance. Deposits range up to 180,000 km^2 in area and must have persisted for significant periods of time. These deposits provide evidence for the existence of tropical mountain glaciers and are testimony to the possibility of radical climate changes that might have accompanied orbital parameter perturbations such as obliquity excursions in excess of 45°.

References: 1) W. Feldman et al, *Science*, 297, 75-78, 2002; 2) J. Mustard et al., Mars 6, #3250, 2003; 3) M. Richardson and J. Wilson, *JGR*, 107, 7.1-7.28, 2002; 4) J. Head and D. Marchant, Mars 6, #3087, 2003; 5) J. Head and D. Marchant, *Geology*, 31, 7, 2003; 6) D. Shean and J. Head, Mars 6, #3036, 2003; 7) J. Zimbelman and K. Edgett, LPSC 22, 31, 1992; 8) D. Scott and K. Tanaka, USGS Map #I-1802-A, 1986.

SPECULATIONS ON ORBITAL FORCING OF SUBLIMATION FROM THE POLAR CAPS M. H. Hecht, Jet Propulsion Laboratory, California Institute of Technology (michael.h.hecht@jpl.nasa.gov)

Introduction: Calculation of the periodic variations in the martian orbital parameters by Ward [1] and subsequent refinements to the theory [2,3] have inspired numerous models of variation of the martian water cycle. The limitations of models such as this can not be overstated. Albedo, for example, has a much greater influence on temperature than orbital forcing, and seems to be linked to insolation, possibly via its influence on dust transport [4]. To make further progress, either new constraints must be identified, or additional clues must be obtained from remote sensing and *in situ* exploration.

The MGS and Odyssey missions have provided us with several such critical pieces of information. The discovery of what can only be described as an ice sheet underlying a lag deposit over enormous areas of both hemispheres is one such clue [5], along with indications from surface features of recent, wide-scale modification by water [6]. Another is the observation of mantling of gullied slopes, presumably a vestigial layer of frost and snow protected by a similar lag deposit [7]. More speculative, perhaps, are suggestions from analysis of MOLA data of a net seasonal increase in thickness of the northern cap [8], or correlation of PLD structures with orbital variations dominated by precession of the L_s of perihelion [3]. Speculative implications of these new data are summarized in the sections below.

Critical oscillations: Most orbital forcing models have focused on variations in planetary obliquity (on both a short-term, 110 kyr time scale and larger oscillations occurring over millions of years) [9-11]. The fastest mode of variation, perihelion precession, has generally been deemphasized because it does not change the integrated annual insolation. But as a result of this precession, the asymmetry in peak summer insolation between the poles exceeds 50% today, with the maximum cycling between poles every 25.5 kyrs. Variations in planetary eccentricity also play a role, defining the magnitude of the excursions associated with this perihelion precession.

Fanale, for example, concluded that precession of the longitude of perihelion may be sufficient to increase water removal from the poles by factors of 50-100 [9]. He calculated the peak vapor pressure at the North Pole by assuming a surface of pure water ice or CO_2 ice with distinct optical properties, incorporating only radiative balance and latent heat of CO_2 deposition. It was further assumed that the zonal humidity was proportional to that peak water vapor, which was in turn a simple function of the ice surface temperature. This assumption is reasonable because the energy deposited as sunlight into the polar cap must ultimately be accommodated in the form of sublimation. If advection or vertical transport is insufficient to remove the generated water vapor, for example, it will recondense as fog, pumping heat into the atmosphere and either generating convective currents or increasing the saturation vapor pressure.

Figure 1 shows the results of calculations using a protocol similar to Fanale's, but with the critical addition of tracking latent heat of water condensation and sublimation. All three curves represent an extrapolation back only 150 kyrs. Rather than extrapolating back far enough to reflect large changes in obliquity, the obliquity was forced to specific values. Thus one curve represents the calculated obliquity, a second holds the obliquity at the current value of 25°, and the third holds the obliquity at 40°. The data is expressed in terms of the amount of heat from insolation that is converted to sublimation under these circumstances. It can be seen that, at constant obliquity, the sublimation rate can increase by a factor of 100 with the passage of only 20 kyrs. Changing the obliquity from 25° to 40° adds another factor of only approximately 5.

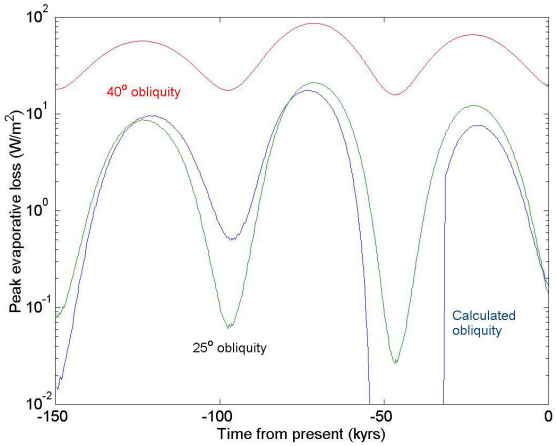

Figure 1: Calculated peak evaporative loss at the North Pole of Mars, expressed as an evaporative heat measure over 150,000 years. The calculation balances radiation, latent heat of CO_2 and H_2O, and insolation using orbital parameters from Ward [1], albedo and emissivity values suggested by Fanale et al [9]. To show the relative effect of precession and obliquity, the three curves represent calculated obliquity and obliquity fixed at 25° or 40°.

Lag deposits and ice cap evolution: Odyssey results suggest that the vast majority of ice on Mars is sequestered beneath either a lag deposit of dust or a buffer layer of CO_2. The reason for this seems straightforward – the water table will retreat to a depth such that the annual thermal wave does not result in temperatures above the dewpoint [12]. In other words, the boundary of the cryosphere will tend to adiabatically adjust to the changing heat balance. The southern hemisphere is currently favored by summer perihelion, and not surprisingly exposed water is scarce. To the extent that cap evolution can track climate change, the boundary of the exposed northern polar cap would represent the latitude above which the surface temperature doesn't exceed the frostpoint.

The appearance of the PLD and the apparent high resurfacing rates of the cap itself [13] suggest that the age of the cap isn't geologically great. There are few polar features suggestive of flow, implying that the cap periodically retreats by other processes, presumably sublimation and transport to lower latitudes or the opposing hemisphere. The time scale for disappearance and reconstruction of the cap has never been resolved, but could range from many millions of years to the rapid 51,000 year cycle of precession.

As the northern hemisphere warms up due to orbital precession, two things may occur. The boundaries of the cap may be encouraged to retreat to higher latitude, and measurable amounts of water may be seasonally removed from the polar cap. If formation of a lag deposit halts the surface erosion of the cap, then further erosion may be limited to the scarps and slopes at the edges of the cap, effectively eroding the cap from the outside. Only by vigorous removal on the perimeter, where gravitational forces remove the residue, could the cap be substantially modified on the timescale suggested by the geological record. Supporting such a view is the observation that as ice sublimates, surface facets will tend to grow normal to the sun direction, maximizing further erosion [14]. We might imagine, therefore, that as the summers become hotter in the north over the next 20,000 years, the diameter of the northern cap will become smaller, with material being vigorously removed from the edges and redeposited on top. Indeed, if the net increase in thickness of the cap suggested by the MOLA data were verified, it would not be inconsistent with such a mechanism. It is also not unreasonable that the cap would bifurcate into two regions – a high latitude, actively growing region with thermally stable exposed ice, and a lower latitude region with suppressed growth, where a lag deposit protects the ice from further erosion.

Conclusions: Models of peak seasonal sublimation from the north polar cap suggest that the important cycle of water injection may be 25.5 or 51 kyrs, depending on whether one or two poles are involved. If the process is limited by hemispheric depletion of available dust-free water, the result may be periodic pulses of water injection. The tendency of the surface to form lag deposits above ice layers is consistent with an equilibrium water table determined by the frostpoint. As temperatures warm, this stability level will retreat below the surface at higher latitudes, encouraging polar cap retreat. The ability of the cap to shrink from the surface may also be limited by lag formation, suggesting that the cap grows and shrinks from the perimeter, with the sublimed material being transported from perimeter to top surface. Favorable geometries with respect to the sun would make this an efficient form of water transport.

References: [**1**] Ward W.R. (1974), *J. Geophys. Res. 79*, 3375-3386. [2] Laskar J. (1990), *Icarus 88,* 266-291. [3] Laskar J., Levrard B., Mustard J.F. (2002), *Nature 419*, 375-377. [4] Kieffer H.H., Zent A.P. (1992), in *Mars*, ed. H. H. Kieffer et al., 1180-1218. [5] Boynton, W. et al. (2002), *Science* **297** 81-85. [6] Kreslavsky M. and Head J. (2000), JGR 105, 26695. [7] Christensen P.R. (2002), *Nature **422***, 45-48. [8] Smith, D. E., M. T. Zuber, G. A. Neumann (2001), *Science* **294**, 2141. [9] Fanale F.P. et al. (1986), *Icarus 67*, 1-18. [10] Carr, M.H. (1982), *Icarus 50*, 129-139. [11] Hecht M. H. (2002), *Icarus 156*, 373-386. [12] Leighton R.B., Murray B.C. [1966], *Science 153* 136-144 [13] Herkenhoff, K. E. and J. J. Plaut (2000), *Icarus* **144**, 243-253. [14] Ingersoll A.P., Svitek T., Murray B.C. (1992), *Icarus 100*, 40-47.

Acknowledgements: This work was performed at the Jet Propulsion Laboratory, California Institute of Technology, under funding from NASA. Useful discussions with Frank Carsey are greatly appreciated.

CRYOSCOUT: A DESCENT THROUGH THE MARS POLAR CAP M. H. Hecht[1] and R. S. Saunders[2], [1]Jet Propulsion Laboratory, California Institute of Technology (michael.h.hecht@jpl.nasa.gov), [2]NASA Headquarters, Washington, D.C. (ssaunde1@hq.nasa.gov)

Introduction: Recent discoveries on Mars—from the numerous gullies seen by Mars Global Surveyor (MGS) to the vast expanses of near-surface ice seen by Odyssey—draw attention to the importance of a modern hydrological cycle and the possibility of extreme climate variations driven by orbital forcing. The surface/atmosphere interactions that define this cycle are presumably reflected in the stratigraphy of the polar layered deposits (PLD), comprising a climate archive that possibly spans many millions of years. If a terrestrial ice sheet were so endowed it would be studied by coring, in order to retrieve the most pristine record of past chemical and physical properties, and to evaluate modification induced by time and stresses within the ice. On Mars' north polar cap, thermal probes are feasible and can provide a reasonable approximation of coring. Optical and spectroscopic analysis of the layers, which are presumably demarcated by embedded dust, would contribute to the reconstruction of a timeline. Meltwater analysis is a convenient way to determine the soluble chemistry of that embedded dust, and to monitor gradients of the isotopic ratios of hydrogen and oxygen that reflect atmospheric conditions at the time the layer was deposited. As on Earth, local thermal measurements can be used to determine bulk mechanical properties of the cap, as well as the geothermal gradient.

CryoScout was proposed as just such a subsurface investigation of the stratigraphic climate record embedded in Mars' North Polar cap (Figure 1). After landing on a gentle landscape in the midst of the mild summer season, CryoScout was to use the continuous polar sunlight to power the descent of a "cryobot," a thermal probe, into the ice at a rate of about 1 m per day. CryoScout would probe deep enough into this time capsule to see the effects of planetary obliquity variations and discrete events such as dust storms or volcanic eruptions. By penetrating tens of meters of ice, the mission would explore at least one of the dominant "MOC layers" observed in exposed layered terrain.

CryoScout's primary objective was to determine the conditions under which the north PLD, the only known unmodified and accessible record of recent Mars climate history, was laid down over the past million years. Secondary objectives were to characterize the present-day polar cap structure and surface conditions. These objectives would be pursued by acquiring data on the present surface mass balance and the variation of compositional, physical, and thermal properties as a function of depth below its surface.

Figure 1: Fueled by continuous sunlight on Mars' North Pole, the cryobot uses heat to sink through undisturbed polar layered deposits.

CryoScout's detailed log of images, temperature, and compositional data, would reflect the influence of meteorology, depositional episodes (volcanic, impact, dust storms), and planetary orbital/axial modulation. Among the questions CryoScout might address are these:

- How has the climate changed with orbital parameters in the past million years? Can such change explain young gullies (MGS) or evidence of ground ice (Odyssey)?
- What is the fine-scale stratigraphy of the North Polar cap?
- What is the inventory of dust, salts, and organic compounds incorporated into the ice?
- What is the inventory of volatiles, including water, CO_2, and clathrate hydrates?
- Has there been recent volcanism on Mars?

Mission Overview: As proposed for the recent Scout competition, a Type 2 trajectory was to deliver a cryobot [1] and surface instruments to the North Polar region of Mars in 2008, arriving at L_s=73, just before the summer solstice. CryoScout would then be in continuous sunlight throughout the 90-day mission, during which the cryobot would penetrate about 80 m into the North PLD. Powered by a large, tracking solar array, the cryobot would descend an average of 4 cm per hour, transmitting data through a tether that slowly unreeled from its aft bay.

Six instruments were selected to accomplish the CryoScout goals. IceCam, the cryobot camera, would record the visible stratigraphy. With 1-mm vertical resolution in nephelometer mode, IceCam would provide a time resolution of months to centuries (assuming deposition rates of 0.01–10 mm per year [2]). In imaging mode, IceCam would acquire full-color stereo images at 10^{-5} m per pixel, probably sufficient for observing annual layers similar to terrestrial varves.

By analyzing the meltwater with a suite of electrochemical sensors, the Mars inorganic chemistry analyzer (MICA) would determine the salt composition and abundance in the embedded dust, providing clues to its origin. The Mars isotopic laser hygrometer (MILH) would measure variations in relative hydrogen- and oxygen-isotope abundance in that same meltwater, reflecting source and climate conditions under which the ice was deposited.

A fiber thermometer incorporated into the tether linking the cryobot to the surface, the Distributed Temperature Sensor (DTS) would measure the time-dependent ice temperature profile, including the thermal wave penetration in the top ~20 m and geothermal heat flux below. The DTS would determine both conductivity and diffusivity, which are needed for macroscopic models of the ice structure and evolution.

The dynamics of the polar cap surface were to be studied through imaging with the stereoscopic surface imager (SSI), which would also measure the thermal balance by recording atmospheric opacity and surface albedo [3]. A surface version of the MILH would record the movement of water vapor, provide a baseline measurement of isotopic ratios, and monitor basic meteorology.

Additional information could be gleaned from various internal sensors, such as detection of inclusions of CO_2 hydrate-clathrates.

Ongoing work: The cryobot approach suffered from two prominent liabilities. First, the cryobot expended large amounts of energy just to compensate for conductive losses in the cold ice of Mars. As a result, it required approximately 500W just to avoid being frozen into the ice, and an average of over 1 kW to achieve the desired descent rate. Second, the meltwater sampling scheme was far from optimal in that the pool of water surrounding the vehicle contained the accumulated solutes of the entire descent.

To remedy these deficiencies, the Subsurface Ice Probe (SIPR) is being tested as a means to perform an "open-hole" descent. The SIPR drill head sits in the bottom of a dry, open hole and melts a small quantity of water at a time, pumping it to the surface for analysis. The tether reel and all analytical instrumentation stay on the surface. By only requiring a small drill-head to be submerged in water, SIPR minimizes thermal losses, and can achieve its mission with less than 100W average power. Second, by returning samples to the surface, SIPR simplifies sidewall imaging (as compared to systems that image through silt-laden water), retains good depth resolution for chemical analysis, and does not require analytical instrumentation to be miniaturized for down-hole use. The only potential drawback to SIPR is the fact that the eventual flow or failure of the ice limits both the depth and duration of the hole. For planetary exploration, this limitation is of marginal importance. On Mars, in particular, SIPR should penetrate up to a kilometer, more than sufficient to study the polar layered deposits.

References: [1] Zimmerman W. et al (2002), Proc. IEEE Aerospace Conf.[2] K.E. Herkenhoff K.E. and Plaut J.J. (2000), Icarus 144, 243–253[3] Smith P. and Lemmon M. (1999) JGR 104, 8975–8986.

STRATIGRAPHY AND STRUCTURE OF THE SOUTH POLAR LAYERED DEPOSITS ON MARS. K. E. Herkenhoff, L. A. Soderblom and R. L. Kirk, U. S. Geological Survey Astrogeology Team, 2255 N. Gemini Dr., Flagstaff, AZ 86001 (kherkenhoff@usgs.gov).

Introduction: The martian polar layered deposits (PLD) are probably the best source of information about the recent climate history of Mars [1-7], but their origin and the mechanisms of accumulation are still a mystery [8]. The polar layers are sedimentary deposits that most planetary scientists believe are composed of water ice and varying amounts of wind-blown dust [2-4], but their composition is poorly constrained [9]. Because climate changes are likely recorded as variations in composition or deposition/erosion rates between layers, the detailed stratigraphy of the PLD is of great interest. Layer thicknesses of ~10 to 50 m were observed in Viking Orbiter images of the north PLD by Blasius *et al*. [10], and Mars Orbiter Camera (MOC) images resolve layers with similar or lesser thicknesses in both polar regions [11]. In order to accurately determine the thickness of layers and interpret PLD stratigraphy and structure, the topography of exposures must be known. Previous studies have identified deformation in the PLD similar to that observed in terrestrial glaciers [12-14], but lack of detailed topography has hindered structural interpretations. Here we describe results of our continuing study to evaluate the topography, structure, and stratigraphy of the south PLD using photoclinometry on MOC images.

Approach: Because the south PLD surface is typically rough (Fig. 1), we used a 2-dimensional photoclinometric technique [15] constrained using simultaneously-acquired MOLA data. This technique is well suited to images taken at high latitudes when the surface was covered by seasonal frost and the solar elevation angle was low so that albedo variations and their effects are minimized and topographic modulation is emphasized (Fig. 1). The high density of MOLA data in the polar regions allows gridded topographic products to be generated at higher spatial resolution (~250 m/pixel) than is possible at lower latitudes. We introduce MOLA topography into the process in five ways [16]: 1) for planimetric control; 2) to precisely model surface and atmospheric reflectance/scattering; 3) to account for subtle variations in surface albedo; 4) as the starting solution for the photoclinometric model; 5) as the DEM base map on which the MOC NA high-resolution DEMs are mosaicked. A sample of the results of this approach is shown in Figure 2.

Results: The photoclinometric models show evidence for folding and faulting of the PLD. Figure 2 shows what appear to be folded beds between relatively planar layers. The planar layers are in some places truncated by the folded layers, either from above or below. These relations suggest that the folds are not simply the result of compression of the entire stack of PLD, although the layers at the bottom of the exposure in Figure 2 may have been folded in this way.

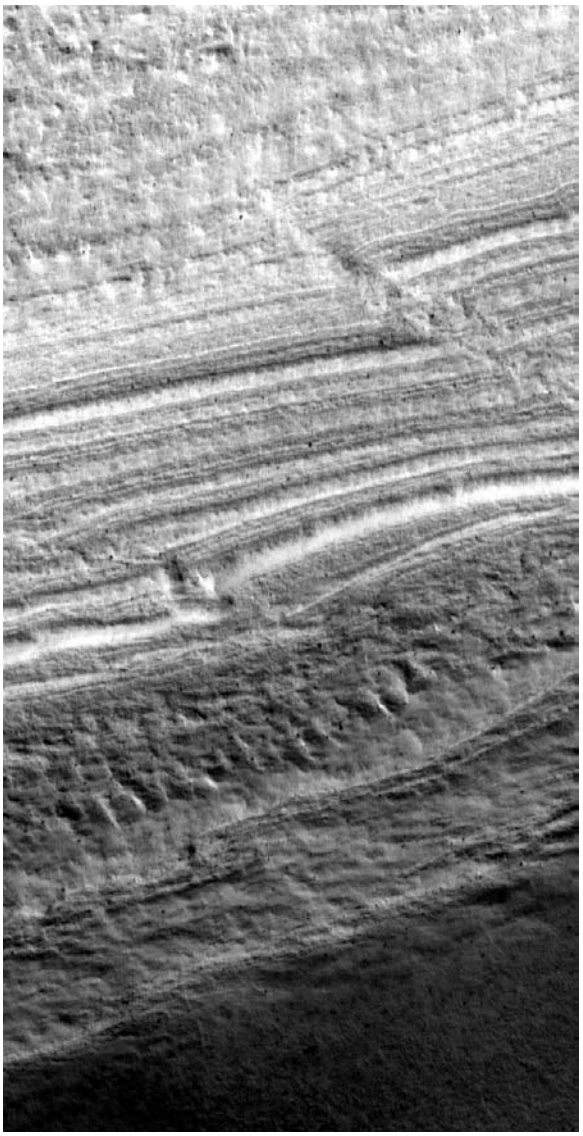

Figure 1. Part of MOC image m0402455 of apparent reverse faults in south PLD. Illumination from bottom left, 2.8 m/pixel.

For the wavy structures near the top of the section, deformation by faulting and/or flow is implied. If the folding was caused by ductile or fluid flow, erosion of the planar beds is required to produce the observed

terminations. The flow process may have caused erosion of the adjacent layers, for example. The feature near the top of the section shown in Figure 2 is consistent with viscous flow down the current topographic slope. Alternatively, the truncations may have been caused by faulting along non-planar surfaces. For example, the wavy structure just above the green plane in Figure 1 may be a fault zone, formed by low-angle normal displacement with the slip vector trending approximately parallel to the present topographic gradient. Analysis of photoclinometric models of other PLD exposures will be discussed at the conference.

References: [1] Murray, B. C., *et al*. (1972). *Icarus* **17**, 328-345. [2] Cutts, J. A., *et al*. (1979). *J. Geophys. Res*. **84**, 2975-2994. [3] Squyres, S. W. (1979). *Icarus* **40**, 244-261. [4] Toon, O. B., *et al*. (1980). *Icarus* **44**, 552-607. [5] Carr, M. H. (1982). *Icarus* **50**, 129-139. [6] Howard, A. D., *et al*. (1982). *Icarus* **50**, 161-215. [7] Plaut, J. J., *et al*. (1988). *Icarus* **76**, 357-377. [8] Thomas, P., *et al.* (1992). In *Mars*, University of Arizona Press, Tucson, pp. 767-795. [9] Clifford, S. M. *et al*. (2000). *Icarus* **144**, 210-242. [10] Blasius, K. R., *et al*. (1982). *Icarus* **50**, 140-160. [11] M. C. Malin and Edgett, K. S. (2001). *J. Geophys. Res.* **106**, 23,429-23,570. [12] Kargel, J. S. (2001). *Eos, Trans. AGU*., **82**, F724. [13] Brightwell, S. N., *et al*. (2003). *LPS XXXIV,* Abstract #2077. [14] Murray, B. C., *et al*. (2002). *Icarus* **154**, 80-97. [15] Kirk, R. L., *et al*. (2003). ISPRS Working Group IV/9 Workshop "Advances in Planetary Mapping 2003", Houston. [16] Soderblom, L. A. and Kirk, R. L. (2003). *LPS XXXIV,* Abstract #1730.

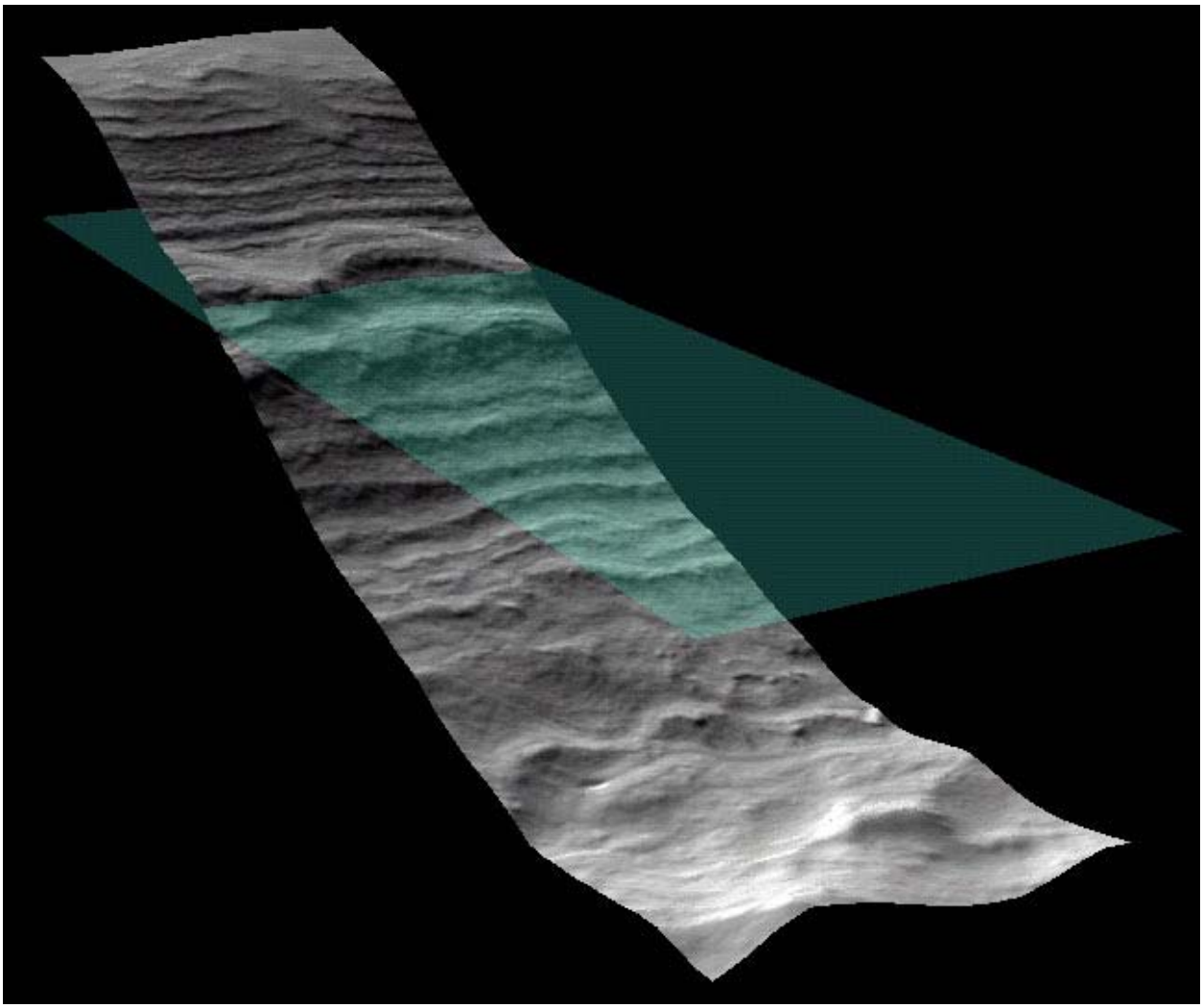

Figure 2. Oblique view of digital elevation model derived from MOC narrow angle image m0905983 (2.7 m/pixel) of south polar layered deposits. Green plane is horizontal reference surface. Note that bedding is not everywhere horizontal, perhaps due to faulting or flow of originally flat-lying layers.

THE MARS IMAGER FOR CLOUD AND AEROSOL (MICA). V. J. Hipkin[1], J. R. Drummond[1], J. Hackett[2], R. Deschambault[2], J. Abbatt[1], G. Besla[1], C. T. McElroy[1], S. M. L. Melo[1], K. Strong[1], J. J. Caldwell[3], J. C. McConnell[3], D. V. Michelangeli[3], P. Bernath[4], J. Sloan[4], W. Ward[5] and B. Tolton[6]. [1]University of Toronto, Toronto, Ontario, [2]COMDEV Ltd, Cambridge, Ontario, [3]York University, Toronto, Ontario, [4]University of Waterloo, Waterloo, Ontario, [5]University of New Brunswick, Fredericton, New Brunswick, [6]Synodon Ltd, Edmonton, Alberta

Introduction: Cloud and dust play an important role in the Mars polar atmosphere. Of particular interest is the evolution of cap-edge dust storms observed during the Mars Global Surveyor mission [1] and the development of the polar hood.

This poster describes the Mars Imager for Cloud and Aerosol (MICA), a four-band visible camera designed to characterize Mars cloud and dust by imaging the limb at sunrise and sunset. It will be capable of producing profiles of Mars aerosol optical properties from 0-75km with a vertical resolution better than 600m. MICA will follow on from Mars Express and MRO cloud and aerosol vertical profile mapping, providing new information, higher vertical resolution and adding to the Mars cloud and dust climatology.

MICA instrument design: Two-band twilight limb images from Viking were analyzed by Jaquin et al [2] and used to produce detailed aerosol extinction profiles. The power of this technique lies in the strong scattering response of small particles to visible light, and in viewing this signal against the dark limb. It allows very thin particle layers to be observed with high signal to noise.

The MICA design uses multiple bands and a new occulting disk technique to provide enhanced dust characterization capabilities. The full dynamic range of the camera is optimized for scattered light. A pinhole in the occulting disk attenuates direct sunlight, reducing its intensity to levels produced by scattering. The resulting composite image contains both a detailed image of the sun and a sensitive wide-angle image of the distribution of thin cloud and aerosol layers (Figure 1). Absolute calibration is possible through viewing the sun at high angle above the atmosphere. The calibrated solar image produces particle extinction measurements directly, while the wide-angle part of the image can be used to fit the scattering phase function in the case of horizontally homogeneous layers. These measurements will provide significant new constraints on Mars aerosol particle size distribution and optical properties.

Proposed mission: This instrument has been proposed as part of the Mars Volcanic Emission and Life (MARVEL) Scout. In the MARVEL mission proposal, MICA's visible observations are complemented by additional aerosol composition information from a bore-sighted high-resolution FTIR instrument. These combined observations produce an extremely powerful data set for the study of Mars dust and cloud latitudinal, seasonal and vertical variability and microphysical processes. The addition of a flip mirror gives MICA the capability to observe the surface.

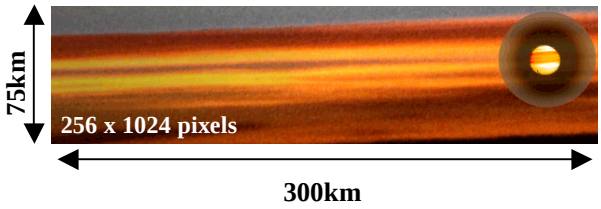

Figure 1: A simulated MICA sunset limb image showing cloud and dust layers. The shadow around the sun is the occulting disk penumbra.

References:
[1] Cantor, B. A. et al (2001) *JGR, 106*
[2] Jaquin et al (1986) *Icarus, 68*

Acknowledgments: This work was supported by the Canadian Space Agency, CREStech and COM DEV LTD.

Further information: Contact Dr. Vicky Hipkin, Dept of Physics, University of Toronto, 60 St. George St, Toronto, Ontario, Canada, M5R 2W3. **Email:** vicky@atmosp.physics.utoronto.ca

ACCURACY OF MARS' POLAR AXIS DETERMINATION BY EARTH-BASED RSDI.

I. V. Holin, Space research institute, Moscow, holin@mail.cnt.ru

Introduction: Radar Speckle Displacement Interferometry (RSDI) is a new Earth-based radar technique to measure instantaneous spin components of inner planets with unprecedented accuracy [1-4]. To avoid mixing with known techniques (VLBI, RORI) note that RSDI is based on the effect of far coherence (speckle displacement) [3-5]. The only right comments on RSDI known to the author until now were given in [6].

RSDI instruments: The hart of RSDI as applied to Radar astronomy needs (Radio astronomy needs are not discussed in this work) is a radar transmitter. At present the only in the world fully steerable and powerful enough radar is the 70m ~450 KW Goldstone transmitting facility in South California, USA. Radar echoes scattered from planetary surfaces can be received by a radio interferometer consisting of two (or more) radio telescopes all over the world, e.g. two-element interferometers are 70m Goldstone – 100m Green Bank, West Virginia (transAmerica ~ 3000 km baseline), 100m Green Bank – 70m Madrid, Spain or 100m Green Bank – 100m Effelsberg, Germany (transAtlantic ~ 6000-7000 km baselines), 100m Goldstone – 70m Kashima, Japan (transPacific ~ 7000 km baseline) and so on.

Limiting accuracy: The limiting RSDI accuracy in instantaneous polar axis orientation of Mars can be written as [7]

$$\sigma = l / qb \sim 1 \text{ arcsec} \qquad (1)$$

where b ~ 3000 km is the baselength (Goldstone – Green Bank), l ~ 3 km is the correlation radius of scattered radar field (size of a speckle), $q = Q^{0.5}$, Q – power signal-to-additive noise ratio (snr) at the correlator output. Eq. (1) presents one-look (measuring time about 1 min) accuracy in instantaneous obliquity or precession angle that can not be overcome by Earth-based monochromatic radar.

Experiments: First RSDI experiment was proposed about Venus in 1992 [7]. Another RSDI experiment on Mercury was analysed in very details in 1999 [8]. Only in May-June 2002 after extensive discussions with S. J. Peale (nobody in Russia except the author believed in success) the first reliable RSDI experiment was carried out on Mercury with the Goldstone – Green Bank radar interferometer by Margot et al. [9]. The May-June 2002 experiments clearly confirmed the theoretical analysis [5]. Now we all know that the technique really works. Also we may hope that a few arcsec final accuracy can be achieved. Most probably RSDI experiments on Mars are upcoming as well. Accuracy on Mars during a single conjunction with Earth can be better than 1 arcsec. Also any variations in Mars'polar axis orientation (nutations) can be measured by the technique. If a new more powerful and more dedicated radar transmitter can be designed and constructed in near future to cover advanced radar astronomy needs in XXI century then after regular observations RSDI accuracy on Mars can be of an order of tens mas (milliarcseconds). We hope future RSDI experiments may help substantially to accelerate extensive theoretical work on creating adequate detailed models of spin dynamics of Mars, Mercury, Venus including all related problems (interiors, dynamics of atmospheres and other).

References: [1] Holin I. V. (2003) *LPS XXXIV,* Abstract # 1109 [2] Holin I. V. (2003) *MetSoc. 66,* Abstract # 5003 [3] Holin I. V. (2003) *Meteoritics & Planet. Sci.* (in revision) [4] Holin I. V. (2002) *Solar System Res. 36,* 206 [5] Holin I. V. (1988) *Radiophys. & Quantum Electron. 31,* 515 [6] Peale S. J. et al. (2002) *Meteoritics & Planet. Sci. 37,* 1269 [7] Holin I. V. (1992) *Radiophys. & Quantum Electron. 35,* 433 [8] Holin I. V. (1999) *Uspekhi Sovr. Radioelektron.,* No. 7, 16 (in russian) [9] Margot J.-L. (2002-2003) private communications.

ECHO SOURCE DISCRIMINATION IN AIRBORNE RADAR SOUNDING DATA FOR MARS ANALOG STUDIES, DRY VALLEYS, ANTARCTICA. J. W. Holt[1], D. D. Blankenship[1], M. E. Peters[1], S. D. Kempf[1], D. L. Morse and B. J. Williams[1], [1]University of Texas Institute for Geophysics, The John A. and Katherine G. Jackson School of Geosciences, University of Texas, 4412 Spicewood Springs Rd., Bldg. 600, Austin, TX 78759, jack@ig.utexas.edu

Introduction: The recent identification of features on Mars exhibiting morphologies consistent with ice/rock mixtures, near-surface ice bodies and near-surface liquid water [1,2], and the importance of such features to the search for water on Mars, highlights the need for appropriate terrestrial analogs in order to prepare for upcoming radar missions targeting these and other water-related features. Climatic, hydrological, and geological conditions in the McMurdo Dry Valleys of Antarctica are analogous in many ways to those on Mars, and a number of ice-related features in the Dry Valleys may have direct morphologic and compositional counterparts on Mars.

We have collected roughly 1,000 line-km of airborne radar data over permafrost, subsurface ice bodies, rock/ice glaciers, ice-covered saline lakes, and glacial deposits in Taylor and Beacon Valleys. These data are being analyzed in order to develop general radar propagation models of features with direct relevance to Mars.

A crucial first step in the data analysis process is the discrimination of echo sources in the radar data. The goal is to identify all returns from the surface of surrounding topography in order to positively identify subsurface echoes. This process will also be critical for radar data that will be collected in areas of Mars exhibiting significant topography, so that subsurface echoes are identified unambiguously.

Data Acquisition Methods: Using a Twin Otter airborne platform, data were collected in three separate flights during the austral summers of 1999-2000 and 2001-2002 using multiple systems, including a chirped 52.5 – 67.5 MHz coherent radar operating at 750 W and 8 kW peak power (with multiple receivers) and 1 - 2 microsecond pulse width, and a 60 MHz pulsed, incoherent radar operating at 8 kW peak power with 60 ns and 250 ns pulse width. The chirped, coherent data are suitable for the implementation of advanced pulse compression algorithms and SAR focusing.

A laser altimeter (fixed relative to the aircraft frame) was also used during both seasons. Post-processing of the positioning data yields accuracies of ~ 0.10 m for samples at ~ 15 m intervals. Precise positioning was accomplished through the use of two carrier-phase GPS receivers on the aircraft and two at McMurdo Station.

Surface and shallow subsurface properties are being supplied by glacial geomorphologists conducting ground-based studies in Taylor and Beacon Valleys.

Data Acquisition Targets: Flight paths for the Dry Valleys flights in late 2001 are shown in Figure 1. Flights in early 2000 achieved approximately the same coverage, excluding Beacon Valley (due to weather). Flight elevation was nominally 500 m above the surface. Radar and laser altimetry data were collected over the following targets relevant to Mars:

Taylor Glacier: The entire length of Taylor Glacier was surveyed. These profiles extend from Taylor Dome on the polar plateau to the terminus in Taylor Valley

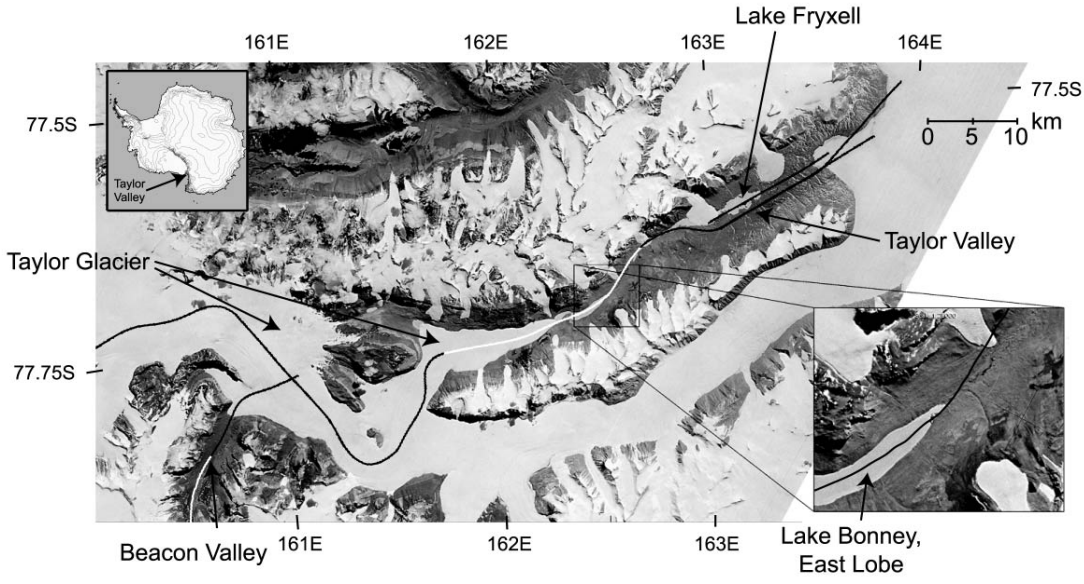

Figure 1. Optical satellite photo of Taylor Valley (center) and Beacon Valley (lower left) within the McMurdo Dry Valleys of Antarctica. UTIG airborne radar profiles (from 2001) are indicated by the solid

black and white alternating lines.

where it is characterized by a high-angle, ice-cored thrust moraine [3]; this profile also includes a lobe that penetrates Beacon Valley. Possible subsurface reflectors in the preliminary data near the terminus appear to be a root of the ice-cored thrust moraine.

Friedman Rock Glacier, upper Beacon Valley: This glacier is 1-2 km wide by 3-4 km long, is heavily debris-covered and is slow moving (max 40 mm/a) [4]. Preliminary data show possible basal reflectors below the glacier where we overflew it.

Debris flows, Taylor Valley: East of Lake Bonney (Fig. 1), a debris flow emanating from the northern wall of Taylor Valley is hypothesized to have occurred in a subaqueous environment [3]. This flow is fairly well defined in the preliminary data (Fig. 2) .

Ancient subsurface ice body, central Beacon Valley: This body is covered by < 1m of glacial drift and hypothesized to be ~ 8 Ma [5].

Permafrost and active layers: In lower Taylor Valley, the Bonney drift includes reworked lake deposits and hummocks thought to be dessicated thrust moraines [3]. Polygonal terrain that we overflew in Beacon Valley is underlain by ice bodies and ice-cemented soil [6].

Lakes Fryxell and Bonney, Taylor Valley: We collected data over both of these ice-covered saline lakes. Permafrost underlies Lake Fryxell [7] and probably Lake Bonney, so we expect a shallow perched water table near the lakes. The reflector underlying the debris flow adjacent to Lake Bonney appears to merge with the lake (Fig. 2).

Data Analysis: The first stage of analysis is the discrimination of subsurface echoes from surface echoes due to surrounding topography. Two techniques are being used in parallel for echo discrimination. Surface returns are being simulated using aircraft position data, the modeled radar antenna pattern, and surface topography from a digital elevation model (DEM) recently acquired by the USGS and NASA in the Dry Valleys with 2-meter postings. These will be compared with the actual data to reveal side echoes.

The second method identifies all echoes in the radar data and maps them into possible correlative surface features to the sides of the aircraft through range estimation. This uses the measured time delay of the echo and known surface topography. We map the echoes onto the DEM (and optical imagery) at the appropriate range in order to identify candidate surface return sources. The two methods should identify all echoes that are not from the subsurface. The comparison of different radar configurations and parallel tracks where they are available will also be utilized to identify the source of any ambiguous echoes.

Once this stage is completed, forward models of the radar properties of these targets will be developed. These can then be applied in a general sense to similar features on Mars, in the context of future radar missions.

Conclusions: Preliminary results of airborne radar sounding in the Dry Valleys of Antarctica indicate penetration of a debris flow, a rock glacier, and massive subsurface ice bodies. Two methods of echo discrimination are being developed in order to confirm apparent subsurface reflectors: (1) forward modeling of echoes using known properties of the radar, antenna pattern and topography, and (2) mapping of radar echoes to the sides of the aircraft to identify features in the topography that could be echo sources.

Acknowledgements: This work is supported by NASA grant NAG5-12693 and the University of Texas at Austin. Data acquisition was supported by NSF grants OPP-9814816 and OPP-9319379. Thanks to Beata Csatho for access to the Dry Valleys DEM.

References: [1] Malin M. C. and Edgett K. S. (2000) *Science, 288,* 2330–2335. [2] Baker V.R. (2001) *Nature, 412,* 228-236. [3] Higgins S. M., Denton G. H., and Hendy, C. H. (2000) *Geogr. Ann., 82A,* 365-389. [4] Rignot E. J., Hallet B. and Fountain A. (2002) *JGR,* submitted. [5] Sugden D. E., Marchant D. R., Potter N., Jr., Souchez R. A., Denton G. H., Swisher C. C., and Tison J.-L., (1995) *Nature, 376,* 412-414. [6] Sletten R. (2002), *pers. comm.*. [7] Harris H. J. H. and Cartwright K. (1981), *Antarctic Res. Ser., 33,* 193-214.

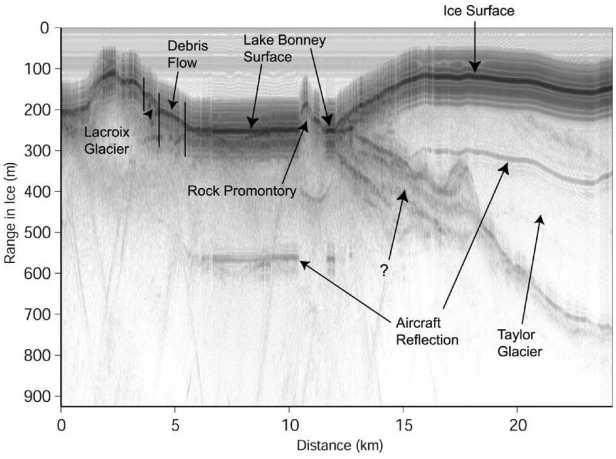

Figure 2. A portion of the radar sounding profile of Taylor Valley (white segment of flight path in center of Figure 1). Up-valley is to the right in this figure. The (?) points to a possible debris-rich layer at the base of Taylor Glacier that may be the source of ice-cored thrust moraines that outcrop at the terminus.

MODELING MARTIAN FOG FORMATION IN THE NORTHERN HIGH LATITUDES DURING THE RETREAT OF THE SEASONAL NORTH POLAR CAP. A. Inada, *Max-Planck-Institut für Aeronomie, Katlenburg-Lindau D37191, Germany (inada@linmpi.mpg.de)*, M. I. Richardson, *Division of Geological and Planetary Sciences, California Institute of Technology, Pasadena, CA, USA (mir@gps.caltech.edu)*, A. D. Toigo, *Center for Radiophysics and Space Research, Cornell University, Ithaca, NY, USA (toigo@astro.cornell.edu)*.

Introduction The early stages of spacecraft exploration of Mars showed that dust plays as important a role in the Martian atmosphere as water vapor does for the Earth. Gierasch and Goody (1972) showed that a model including the radiative effects of suspended dust provided a good fit to the atmospheric temperature structure observed by Mariner 9. The effects of water ice particles in the atmosphere and climate is a more recent concern. The vertical distribution of water vapor varies due to the precipitation of cloud particles (*e.g.*, Kahn 1990; Clancy *et al*., 1996; Richardson *et al*., 2002). The radiative effect of cloud particles has been discussed by Colaprete and Toon (2000). Water vapor condenses at high altitudes of about 80 km as a detached haze, at altitudes (depending on the season and latitude) of 10-50 km as clouds, over the polar caps as polar hoods, and near the surface as fogs. The various clouds, hazes, and fogs make up one component of the the water cycle on Mars (Jakosky, 1983; Richardson and Wilson, 2002). For example, as suggested by Kahn (1990) and demonstrated by Richardson *et al*. (2002), clouds in late northern summer are essential for returning water to the surface at a rate consistent with observations. In addition, the condensed phase of atmospheric water may play a significant role in modifying the spatial distribution of dust, through sequestration, as well as affecting surface temperatures and the atmospheric temperature structure.

Ice particle motions and radiative effects depend on particle size. Additionally, the particle size is sensitive to the manner in which the water ice particle was nucleated (homogeneous or heterogeneous nucleation). This important parameter has been estimated using Mie theory to fit observed infrared spectral data (Curran *et al*., 1973), using one-dimensional haze models to fit Viking limb images (Kahn, 1990), and most recently, using multi-angle thermal and visible observations (R. T. Clancy, private communication, 2003).

These data, combined with morphological information from images (Wang and Ingersoll, 2002), provide important constraints on microphysical models, which seek to provide more detailed insight into the dynamic nature of clouds, hazes, and fogs. One of the earliest explicit models of cloud formation was that of Michelangeli *et al*. (1993), who used the method developed by Toon *et al*. (1988) in a one-dimensional Martian climate model. Recently microphysical processes codes have been included in the Geophysical Fluid Dynamics Laboratory (GFDL) Mars General Circulation Model (GCM) (Rodin *et al*., 2001) and the NASA Ames Mars GCM (Colaprete and Haberle, 2001).

Most previous work modeling atmospheric ice aerosols has focused on clouds. Near-surface water ice particles ("fogs") have been less widely discussed. The boundary layer model of Savijärvi (1995) was used to model fog formation. It showed thin fog formation at the Viking Lander 1 site (22.5° N, 48.0° W). Fogs at the Pathfinder landing site (19.2° N, 33.2° W) and in the Memnonia region (15.0° S, 145.0° W) were simulated with microphysical processes by Inada (2002). Both are one-dimensional models and the simulated locations are in the low-middle latitudes. Fogs imaged by the Viking Orbiter, Mars Global Surveyor, and Mars Odyssey cameras have been observed to form in craters and channels, which motivates the simulation of fogs with models that explicitly treat three-dimensional atmospheric flow in response to high-resolution topographic information. Additionally, the abundance of water vapor sublimated from the northern polar cap leads to a large mixing ratio in high latitudes, and indicates that this may be a place of common fog formation. The purpose of this work is to investigate fog formation in the northern high latitudes during the retreating phase of the seasonal cap.

Figure 1: Fog in canyons seen by Viking Orbiter.

Observations It is generally difficult to identify optically thin clouds and fogs in images taken from orbiters; however, some of these images show brightening in craters, channels, and other depressions (Figure 1). This indicates that the bright feature is related to the surface topography, and is most likely ice aerosol formed near the surface, which can be called fogs. The optical depth of a typical crater fog observed in an orbiter images taken near the Viking Lander 1 site measured by Hoekzema (personal communication, 2003) was 0.92 in the red and 0.93 in violet, while that over the clear surface was about 0.55.

The Mars Atmospheric Water Detector (MAWD) on the Viking Orbiters provided a dataset of the column water vapor abundance that was the primary source of information on the water cycle for many years(Farmer *et al*., 1977; Jakosky and Farmer, 1982). Recently, spectra from the Thermal Emission Spectrometer (TES) on Mars Global Surveyor (MGS)

have been used to determine the annual variation of column-integrated water vapor (Smith, 2002). Both observations show the peak of water vapor amount in the northern high latitudes after the seasonal cap retreat. The maximum column density is over the edge of the northern polar cap in early-to-mid-summer and is more than 75 precipitable microns (pr. μm). This water vapor is contributed to a polar atmosphere which is quite cool, and thus the northern summer pole becomes one of the very few places on Mars when the atmosphere is nearly saturated (Richardson *et al*., 2002). The vapor distribution (the mass mixing ratio) is likely to decrease with height from the surface; elsewhere on the planet, it is likely uniformly distributed with height to at least 10 km. The northern polar atmosphere is thus a likely place for water recondense in the atmosphere due to the diurnal temperature cycle.

Model The simulation of fogs in the polar region is implemented with the Mars MM5 described by Toigo and Richardson (2002). This model is based on the Pennsylvania State University (PSU)/National Center for Atmosphere Research (NCAR) Mesoscale Model Version 5 (MM5) (Dudhia, 1993) and converted for use on Mars. It has been developed to research atmospheric dynamics on scales of a few hundreds meters to a few hundreds of kilometers, so that it is the most suitable model to study fog formation. The surface topography is taken from MGS Mars Orbiter Laser Altimeter (MOLA) high-resolution data set. Boundary conditions are provided by the GFDL Mars GCM (Richardson and Wilson, 2002)

For this study, we add the fog model of Inada (2002) to the Mars MM5. This enables the mesoscale atmospheric model to better simulate the water ice cycle. The microphysical processes of nucleation, condensation, sublimation and sedimentation are included. Coagulation due to sedimentation will be added in the future. Brownian coagulation is negligible because it affects only small particles with r less than 0.01 μm, where r is particle radius. The nucleation rate is a function of the radius of nuclei particles, with nucleation on large dust particles being faster than that on small particles. All dust particles are assumed to act as nuclei. Since there are typically many large dust particles near the surface, little nucleation occurs on particles with $r < 1.0$ μm.

Outlook Fog formation in the northern high latitudes is driven by the retreat of the northern seasonal polar cap. We will present the diurnal time sequence of fog formation, the size distribution of fog particles, water ice amount and the optical depth. The radii of formed ice particles depends on the pre-existing dust particles which are active as nuclei. Since water ice particles are segregated to the surface during the formation phase of the seasonal cap, large dust particles which act nucleation cores of water ice particles are removed from the atmosphere. The seasonal variance of dust size distribution is also simulated. Finally we compare the simulated fogs with observations from the Viking Orbiters cameras, the Mars Orbiter Camera (MOC) and TES on MGS, and the Mars Odyssey THEMIS.

References

Colaprete, A., and R. M. Haberle, A comparison of Mars GCM cloud simulations with observations, American Geophysical Union, Fall Meeting 2001, abstract P31A-0534

Curran R. J., B. J. Conrath, R. A. Hanel, V. G. Kunde, and J. C. Pearl, Mars: Mariner 9 spectroscopic evidence for H_2O ice clouds, 1973

Dudhia, J., A nonhydrostatic version of the Penn State-NCAR mesoscale model: Validation tests and simulation of an Atlantic cyclone and cold font, *Mon. Weather Rev.*, 121, 1493–1513, 1993

Farmer, C. B., D. W. Davies, A. L. Holland, D. D. LaPorte, and P. E. Doms, Mars: Water vapor observations from the Viking Orbiters, *J. Geophysics, Res.*, 82, 4225–4248, 1977

Inada, A., Numerical simulations of Martian fog formation and inflight calibration of Mars Imaging Camera on NOZOMI for its future observations, Doctoral Thesis, Kobe Univ., Kobe, 2002

Jakosky, B. M., and C. B. Farmer, The seasonal and global behavior of water vapor in the Mars atmosphere: Complete global results of the Viking atmospheric water detector experiment, *J. Geophys. Res.*, 87, 2999–3019, 1982

Jakosky, B., The role of seasonal reservoirs in the Mars water cycle–II. Coupled models of the regolith, the polar caps, and the atmospheric transport, *Icarus*, 55, 10–39, 1983

Kahn, R., Ice haze, snow, and the Mars water cycle, *J. Geophys. Res.*, 95, 14677–14693, 1990

Michelangeli, D. V., O. B. Toon, R. M. Haberle, and J. B. Pollack, Numerical simulations of the formation and evolution of water ice clouds in the Martian atmosphere, *Icarus*, 100, 261–285, 1993

Richardson, M. I., and R. J. Wilson, Investigation of the nature and stability of the Martian seasonal water cycle with a general circulation model, *J. Geophys. Res.*, 107(E5), doi:10.1029/2001JE001536, 2002

Richardson, M. I., R. J. Wilson, and A. V. Rodin, Water ice clouds in the Martian atmosphere: General Circulation Model experiments with a simple clouds scheme, *J. Geophys. Res.*, 107(E9), doi:10.1029/2001JE001804, 2002

Rodin, A. V., R. J. Wilson, and M. I. Richardson, GCM simulations of the current Martian water cycle: Clouds and dynamical leverage *Bull. Am. Astro. Soc.*, 33(3), abstract 27.04, 2001

Savijärvi, H., Mars boundary layer modeling: Diurnal moisture cycle and soil properties at the Viking Lander 1 Site, *Icarus*, 117, 120–127, 1995

Smith, M. D., The annual cycle of water vapor on Mars as observed by the Thermal Emission Spectrometer, *J. Geophys. Res.*, 107(E11), doi:10.1029/2001JE001522, 2002

Toigo, A. D. and M. I. Richardson, A mesoscale model for the Martian atmosphere, *J. Geophys Res.*, 107(E7), doi:10.1029/2000JE001489, 2002

Toon O. B., R. P. Turco, D. Westphal, R. Malone, and M. S. Liu, A multidimensional model for aerosols: Description of computational analogs, *J. Atmos, Sci.*, 45, 2123–2143, 1988

Wilson, R. J. and K. P. Hamilton, Comprehensive model simulation of thermal tides in the Martian atmosphere, *J. Atmos, Sci.*, 53, 1290–1326, 1996

ANALYSIS OF PROPERTIES OF THE NORTH AND SOUTH POLAR LAYERED DEPOSITS. A. B. Ivanov[1], S. Byrne[2], M. I. Richardson[2], A. R. Vasavada[3], T. N. Titus[4], J. F. Bell[5], T. H. McConnochie[5], P. R. Christensen[6], THEMIS Science Team, [1]*Jet Propulsion Laboratory, MS168-416, Pasadena, CA, 91106; e-mail : anton.ivanov@jpl.nasa.gov*, [2]*California Institute of Technology, Division of Geological and Planetary Sciences, Pasadena, CA*, [3]*University of California, Los Angeles, CA*, [4]*U.S. Geological Survey, 2255 North Gemini Drive, Flagstaff, AZ*, [5]*Cornell University, Department of Astronomy, Ithaca, NY*, [6]*Arizona State University, Tempe, AZ.*

1 Introduction

One of the many questions of Martian exploration is to uncover the history of Mars, through analysis of the polar layered deposits (PLD). Martian polar ice caps hold most of the exposed water ice on the surface of Mars and yet their history and physical processes involved in their formation are unclear. We will attempt to contribute to our knowledge of the composition and stratigraphy of the PLD.

In this work we present the latest imaging data acquired by the Mars Odyssey THermal EMission Imaging System (THEMIS) [1] and place it into context of the Mars Global Surveyor (MGS) data. We have discussed the North Polar data in [5]. This work concentrates on data acquired over the South pole of Mars and compares properties of North and South PLD.

We are primarily interested in properties of the layers in both ice caps : their continuity, morphology and stratigraphy. These questions can be addressed by THEMIS VIS color images, along with MOC high resolution data and MOLA Digital Elevation Models (DEM). We will investigate thermophysical properties of the layered deposits employing THEMIS IR images. Based on the data obtained by the orbiting spacecraft and described here, we will attempt to expose major directions for modeling and further understanding of the physical processes involved in the formation of the polar layered terrain

2 Available data

2.1 THEMIS VIS

The THEMIS Visible Imaging Subsystem (VIS) is a 5-color, 1024x1024 interline transfer CCD camera that acquires high spatial resolution 18 to 72 m/pixel multispectral images (425 to 860 nm) from Mars orbit ([1, 6]). In order to gain coverage some images are downsampled to a resolution of 36m/pixel. This averaging mode was primarily employed to obtain full coverage of the South Polar Layered Deposits (SPLD) during early spring, when this area is still covered by seasonal frost. A fragment of THEMIS VIS mosaic is shown in Figure 1. This fragment shows a part of residual south polar ice cap between 270E and 320E. Layers are clearly seen in this figure. Since this area is all covered by seasonal frost at this time, brightness variations in this image are primarily due to changes in topography. The staircase structure of the layered deposits is clearly seen. Layers in the North PLD are much smoother and don't exhibit staircase structure. Figure 2 shows a THEMIS 36m/pix image and a MOC high-resolution image of a scarp in the SPLD. Layers are clearly visible in both THEMIS VIS and MOC images. Continuity of the layers can be easily analyzed from the one band THEMIS VIS mosaic, while color images can be taken in selected areas. MOC high-resolution images taken along the trough provide excellent high-resolution morphology.

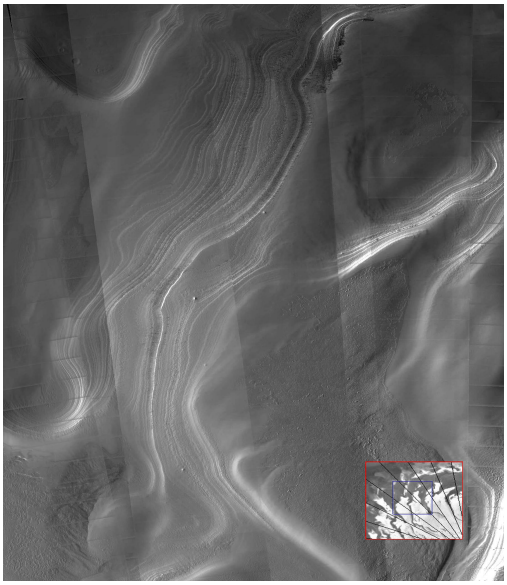

Figure 1: A fragment of THEMIS VIS mosaic of SPLD. The original image resolution is 36 m/pixel. Location of this fragment is shown in the lower right corner on top of the MOC image mosaic. Images were taken in early spring, while ground is still covered by CO_2 frost. Existence of frost on the ground is confirmed by the THEMIS IR data. Context image is shown in the lower-right corner (inside the blue box).

The high quality of the THEMIS VIS data and the high data rate available to download the images will allow us to complete mosaic of the SPLD. We plan to re-image this area during southern summer, when all the seasonal frost will be gone.

2.2 THEMIS IR

The THEMIS IR camera has 10 bands from 6 to 15 μm [1]. Due to to signal-to-noise restrictions the most useful band for polar observations is band 9 (12.57μm). Band 10 (14.88μm) data can be used for atmospheric calibration. High resolution THEMIS IR data allows us to distinguish bulk properties of of layered terrain and ice [5]. We were not able to distinguish between individual layers, however bulk thermophysical properties are under investigation.

2.3 Mars Global Surveyor data

Very interesting details of the polar layered deposits become evident in high resolution MOC Narrow Angle images [4].

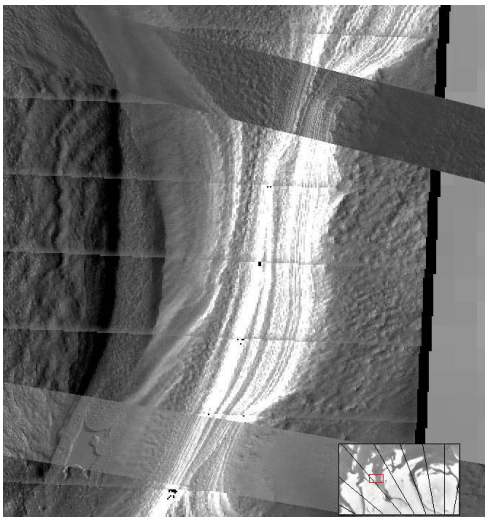

Figure 2: Mosaic of THEMIS VIS and two MOC NA images of a scarp in the SPLD. Images were taken during early southern spring with sun geometry is approximately the same for both MOC and THEMIS images. MOC NA images provide great morphological detail of the layers, while THEMIS VIS images allow to extrapolate this information over much larger areas of SPLD. Context area is shown in the lower-right corner of the figure. Pronounced stripes in the THEMIS image are due to scattered light from adjacent filter in the THEMIS camera.

These images are invaluable for interpreting details of the layered deposits observed with THEMIS. Narrow Angle MOC and THEMIS VIS images are ideal complements for each other An example of a MOC images mosaicked with THEMIS VIS is shown in Figure 2.

3 Discussion

Large spatial and relatively high-resolution coverage provided by the THEMIS visible camera can resolve individual layers in the NPLD over long distances [5]. Higher resolution MOC narrow angle data can be used to characterize these individual layers. Comparing the trace of these layers to topographic data generated by the Mars Orbiter Laser Altimeter (MOLA) yields information in three dimensions about the position of the layer exposure. Strikes and dips of individual layers can be extracted allowing us to predict if this same layer will be exposed in troughs elsewhere in the layered deposits. Testing large-scale continuity of layers in this fashion may help us distinguish between a flowing or non-flowing ice cap. In addition the possibility of extracting a low-resolution version of the topography underlying the icecap from the three dimensional shape of many layers also exists.

The surface appearance of the layered deposits is distinctly different between the two poles [4]. However MOLA data [2] suggests that the general form of the ice caps is roughly the same and they are both composed of water ice mixed with dust [1]. A possible explanation for this difference lies in the timescale of the processes responsible for the formation of the layered deposits. Short-time scale processes are currently eroding the surface of the SPLD, while long-term (compared to obliquity cycle) formation processes are still the same for both caps. We will attempt to probe the internal structure of the cap by collecting vertical positions of selected layers in North and South PLDs.

We have successfully demonstrated the use of THEMIS VIS and MOC data in [5]. We were able to trace a marker bed through a trough and locate the same layer in other troughs.

4 Summary

In this work we present a description of the properties of the South Polar Layered Deposits and compare them with their North counterparts. We employ all available datasets, concentrating on data from Mars Odyssey's THEMIS investigation. Our ultimate goal is to characterize major properties of the polar layered terrains and suggest mechanisms and timescales for their formation. Our approach is to use THEMIS VIS images to investigate continuity of the layers in the layered deposits and their stratigraphic relationships using high-resolution MOLA topography. MOC images will provide important morphological detail. We will also attempt to detect heating or cooling trends in THEMIS Thermal IR imagery for selected troughs in the PLD and interpret these data in terms of thermophysical properties (e.g. thermal inertia) of the layers. The MGS TES atmospheric dataset will provide context and will be important for calibration of THEMIS data.

References

[1] P. R. Christensen, and the THEMIS Science Team. Morphology and Composition of the Surface of Mars: Mars Odyssey THEMIS Results. *Science*, 300(5628):2056–2061, 2003.

[2] D. E. Smith, M. T. Zuber, and et al. Mars Orbiter Laser Altimeter: Experiment summary after the first year of global mapping of Mars. *JGR*, 106:23689–23722, October 2001.

[3] M. D. Smith, and et al. TES results: Mars atmospheric thermal structure and aerosol distribution. *JGR*, 106:23929–23946, October 2001.

[4] M. C. Malin and K. S. Edgett. MGS MOC: Interplanetary cruise through primary mission. *JGR*, 106:23429–23570, October 2001.

[5] A. B. Ivanov, and the Themis Science Team. Analysis of properties of the north polar layered deposits. In *Mars6 Conference Abstracts*, July 2003

[6] J. F. Bell, and the Themis Science Team. High Spatial Resolution Visible Color Units on Mars from the Mars Odyssey THEMIS/VIS Instrument. In *LPSC Conference Abstracts*, March 2003

PROSPECTING FOR MARTIAN ICE FROM ORBIT. L. C. Kanner[1], M. S. Bell[2], and C. C. Allen[3], [1]Carleton College (300 N. College Street, Northfield, MN 55057), [2]Lockheed Martin @ Johnson Space Center (2400 NASA Rd. 1, Mail Code C23, Houston, TX 77058, mary.sue.bell1@jsc.nasa.gov), [3]NASA @ Johnson Space Center (Mail Code ST, Houston, TX 77058)

Introduction: Recent data from the Gamma-Ray Spectrometer (GRS) on Mars Odyssey indicate the presence of a hydrogen-rich layer tens of centimeters thick in high latitudes on Mars [1]. This hydrogen-rich layer correlates to previously determined regions of ice stability. It has been suggested that the subsurface hydrogen is ice and constitutes 35 +/- 15% by weight near the north and south polar regions [2]. This study constrains the location of subsurface ice deposits on the scale of kilometers or smaller by combining GRS data with surface features indicative of subsurface ice.

The most recognizable terrestrial geomorphic indicators of subsurface ice, formed in permafrost and periglacial environments, include thermokarst pits, pingos, pseudocraters and patterned ground. Patterned ground features have geometric forms such as circles, polygons, stripes and nets. This study focuses on the polygonal form of patterned ground, selected for its discernable shape and subsurface implications. Polygonal features are typically demarcated by troughs, beneath which grow vertical ice-wedges. Ice-wedges form in thermal contraction cracks in ice-rich soil and grow with annual freezing and thawing events repeated over tens of years. Ice wedges exist below the depth of seasonal freeze-thaw [3]. Terrestrial ice wedges can be several meters deep and polygons can be tens of meters apart [4, 5, 6], and, on rare occasions, up to 1 km [7]. The crack spacing of terrestrial polygons is typically 3 to 10 times the crack depth [8].

Polygonal terrain is the dominant form of patterned ground seen on Mars [9] and has been recognized in several high resolution Viking Orbiter images [10,11,12,13] and Viking Lander 2 images [14]. High-resolution images from Mars Orbital Camera (MOC) on Mars Global Surveyor reveal Martian surface features in unprecedented detail and meter-sized polygons are more easily discernible and characterized [15]. Martian polygons range in size from 10 m [16] to 10 km [14] or on rare occations up to 20 km [11]. Polygonal terrain is generally grouped based on size and theorized origin into small-scale (~10-250 m) and large-scale (~250 m-20 km) polygons. Small-scale polygons are applicable to this study because it is thought that the origin of small-scale polygons on Mars is the result of permafrost thermal contraction cracking similar to that found on Earth [17,16]. The presence of polygonal ground on the surface generally indicates the presence of ground ice at depths of several meters and can reveal much about the latitudinal distribution of ground ice and ground ice history [17]. Large, multi-kilometer scale polygons likely form by processes unrelated to subsurface ice.

Methods: Using high-resolution narrow-angle MOC images (1.55-12.39 m/pixel), we have noted the presence, absence, and possibility of polygonal terrain around the planet in a latitude band from 30°N to 65°N. Data sets from August 1997-July 2002 were used, less the September 1999-February 2000 set. Polygonal terrain identified in this study can be characterized by the following features: diameter of individual polygons range in size from 25 m - 250 m, polygons are bounded by nearly straight troughs or raised rims and angular joins. Troughs and raised rims frequently show a preferred north-south orientation.

The distribution of polygonal terrain was compared to a mercator projection of GRS relative hydrogen abundance [1,2] as well as a recent geologic map of Mars [18].

Observations: A total of 5,280 images were analyzed and 283 images revealed the presence of polygonal terrain. The distribution of polygonal terrain is scattered throughout the regional band at low elevations (<0m) and nearly all latitudes. The distribution is similar to that found by Seibert and Kargel (2001) [16]. Polygons were identified neither below 35°N nor in the cratered highlands. Particularly high concentrations of polygonal ground are present in the Casius quadrangle between 278°W-258°W and 40°N-50°N. In this region of the Utopia Planitia basin, 74% of the total 132 images analyzed showed the presence of polygonal terrain.

GRS detects hydrogen in high concentrations poleward of 50 +/- 5° [1,2]. The comparision of GRS hydrogen abundance data to the distribution of polygonal terrain shows no correlation (Figure 1). Polygons are present in areas of low concentrations of near subsurface ice as frequently as they are present in areas of high concentrations of near subsurface ice. The high concentration of polygonal ground in western Utopia Planitia correlates to an area of lower concentrations of near subsurface ice.

The majority of polygonal terrain in Utopia Planitia correlates to Hesperian-age units, while there are some occurances to Amazonian-age units [18]. According to Greely and Guest, these units, Hesperian and Ama-

zonian, are of diverse origin – volcanic, tectonic, alluvial, and eolian.

Discussion and Interpretation: What can the anti-correlation between near subsurface ice and presence of polygonal terrain in the Casius quadrangle between 282°W-262°W and 40°N-50°N suggest about the composition of the near and deeper subsurface? One possibility is that the presence of this type of polygonal terrain on Mars is not a response to thermal contraction cracking of ice-rich ground. Ice may be absent at depths of several meters, in turn making the polygonal terrain a response to other contraction processes---desiccation, fracturing of cooling lava, deep-seated horizontal stresses , or stratigraphic control.

On the other hand, ice may exist and do so both as near subsurface ice in the first meter as detected by GRS and as deeper ground ice as seen by the presence of ice-wedging terrain. Data collected in this study suggests the existence of near subsurface and deeper subsurface ice layers which can be explained as a response to climate oscillations. It is likely that hydrogen concentrations in the first meter of the Martian surface are a result of climate conditions at present obliquity. Diurnal termperature occillations affect only the first 2-3 m of the Martian regolith [19]. Ground ice is thought to exist in equatorial regions despite its current instability at the surface [10,20,21]. This conflict can be resolved if deep ground ice is a relic of a colder climate during periods of high obliquity [22]. Theoretical modeling shows that ground ice may have persisted at depths greater than 200 m shortly after the beginning of Mars's geologic history and that ground ice will persist for longer periods of time in regolith of small pore size [23].

If the abundace of Martian small-scale polygons are geomorphically, and structurally similar to terrestrial polygons, their presence should not correlate to hyrdrogen abundance in the first meter for the following reasons: initial propagation of ice wedges occurs below the freeze-thaw layer, or the ice would melt (or sublime), and ice-wedges can extend tens of meters deep. Martian ice-wedge polygons may correlate to thicker layers of ground ice not detected by GRS.

Acknowledgements: We thank William C. Feldman and William V. Boynton for allowing us to use the GRS data and Buck Janes for sending it. Jan Bednarski has provided numerous aerial photos and interpration of Canadian, as well as Martian, permafrost features.

References: [1] Feldman W. C. et al. (2002) *Science., 297,* 75-78. [2] Boynton W. V. et al. (2002) *Science., 297,* 81-85. [3] Williams P. J. and Smith M. W. (1989) *The Frozen Earth: Fundamentals of Geocryology,* p23. [4] Lachenbruch A. H. (1962) *GSA Spec. Pap., 70,* 69p. [5] Kerfoot D. E. (1972) *Arctic, 25,* 142–150. [6] Pewe T. L. (1973) *Geoforum, 15,* 15–26. [7] Pratt W. E. (1958) *AAPG Bulletin, 40,* 2249-2251. [8] Mellon M. T. (1997) *LPS XXVIII,* Abstract #1495. [9] Squyres A. B. et al. (1992) *Mars,* p549. [10] Carr A. B. and Schaber C. D. (1977) *JGR, 82,* 4039–4054. [11] Morris E. C. and Underwood J. R. (1978) *Rep. Planet. Geol. Prog, NASA TM 79729,* 97-99. [12] Evans N. and Rossbacher L. A. (1980) *Rep. Planet. Geol. Prog., NASA TM 82385,* 376-378. [13] Brook G. A. (1982) *Rep. Planet. Geol. Prog., NASA TM 85127,* 265-267. [14] Mutch T. A. et al. (1977) *JGR., 82,* 4452-4467. [15] Malin M. C. et al. (June, July 2003) *Malin Space Center Systems Mars Orbiter Camera Image Gallery* (http://www.msss.com/moc_gallery/). [16] Seibert N. M. and Kargel J. S. (2001) *GRL, 28,* 899-902. [17] Mellon M. T. (1997) *JGR, 102,* 25,617-25,628. [18] Greeley R. and Guest J. E. (1987) *USGS Misc. Inv. Series Map I-1802-B.* [19] Clifford S. M. (2003) *personal contact*. [20] Moughins-Mark P. (1979) *JGR, 84,* 8011-8022. [21] Allen C. C. (1997) *JGR, 84,* 8048-8059. [22] Mellon M. T. and Jackosky B. J. (1993) *JGR, 98,* 3345–3364.

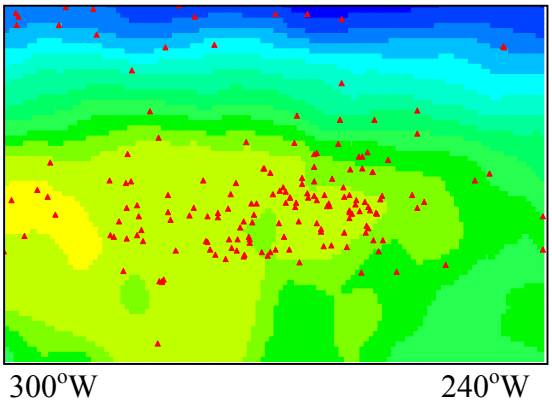

Figure 1. Map of the Casius quadrangle in terms of relative hydrogen abundance (yellow-shaded regions represent areas of low concentrations, blue-shaded regions areas of high) [1,2] and distribution of polygonal terrain marked by the red triangles.

ASTER IMAGERY AND INTERPRETATION OF GLACIERS IN JASPER NATIONAL PARK AND ELSEWHERE IN THE CORDILLERA. J.S. Kargel[1] and B. Molnia[2], [1]U.S. Geological Survey, 2255 N. Gemini Dr., Flagstaff, AZ 86001, U.S.A.; Email: jkargel@usgs.gov; [2]USGS, Reston, Email: bmolnia@usgs.gov.

Fourteen-band ASTER imagery has a spatial resolution of 15 m/pixel in VNIR, one band of which is in stereo; 30 m/pixel in SWIR; and 90 m/pixel in TIR. Variable gain settings selectable for snow and ice targets, high radiometric and geometric fidelity, 60-km scene width, special acquisitions of glacier imagery as a part of the GLIMS project (Global Land Ice Measurements from Space, www.glims.org), and high data downlink rate make ASTER ideal for many glacier studies. Spectacular imagery of glaciers in the Cordillera, including some in Jasper Nat. Park, are being used for detailed assessments of glacier morphology, extent, dynamics, hazards, and value as Mars analogs. A large-format poster will present a sample of ASTER imagery for Jasper Nat. Park and other selected areas of the Cordillera in Alaska and British Columbia.

Fig. 1 (above). Glaciers in South-central Alaska. Portion of ASTER image, VNIR RGB, June 27, 2001.

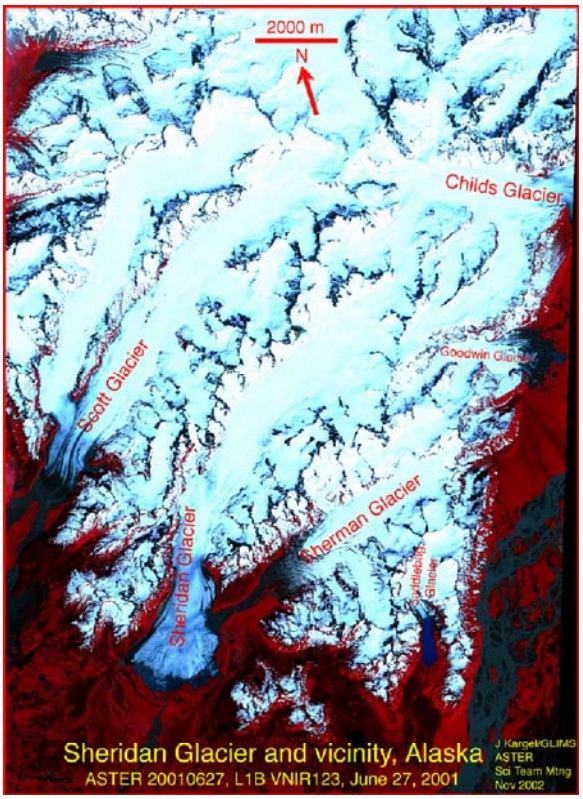

Fig. 3 (next page). Part of the Clemenceau Ice Field, Jasper National Park. Portion of ASTER VNIR R-G-B image July 22, 2002; scene width about 10 km.

Fig. 2. (Below) Sheridan Glacier, SC Alaska, June 27, 2001. Blown up sections of image shown in Fig. 1.

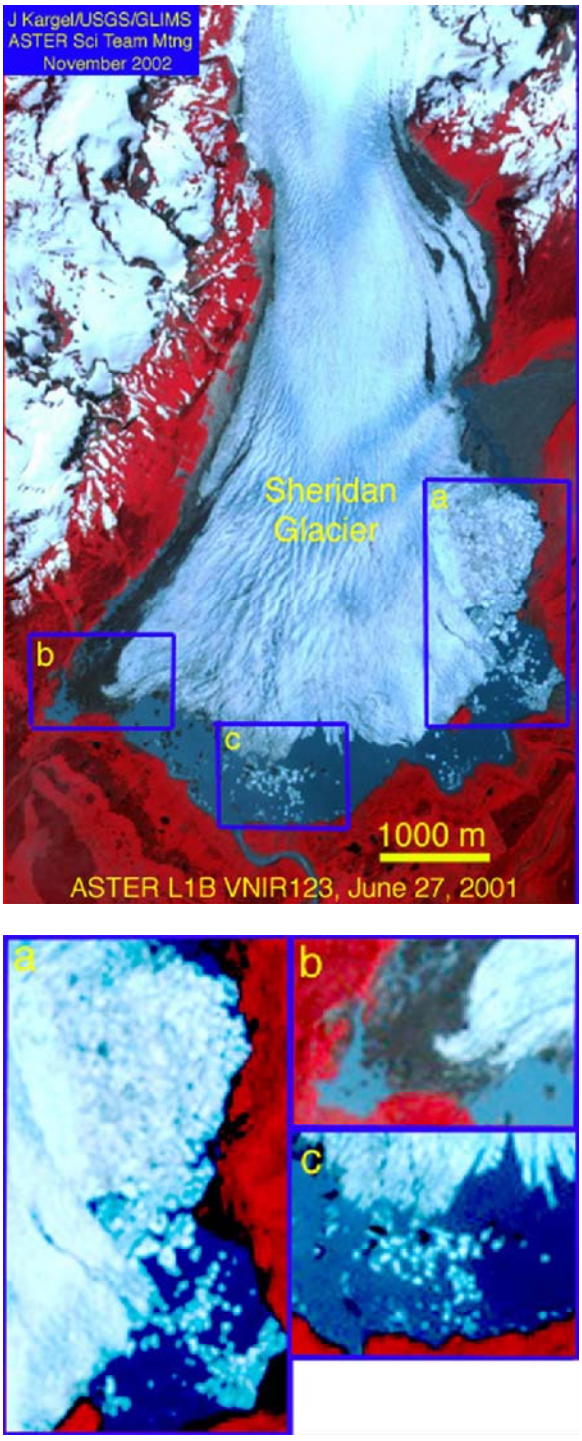

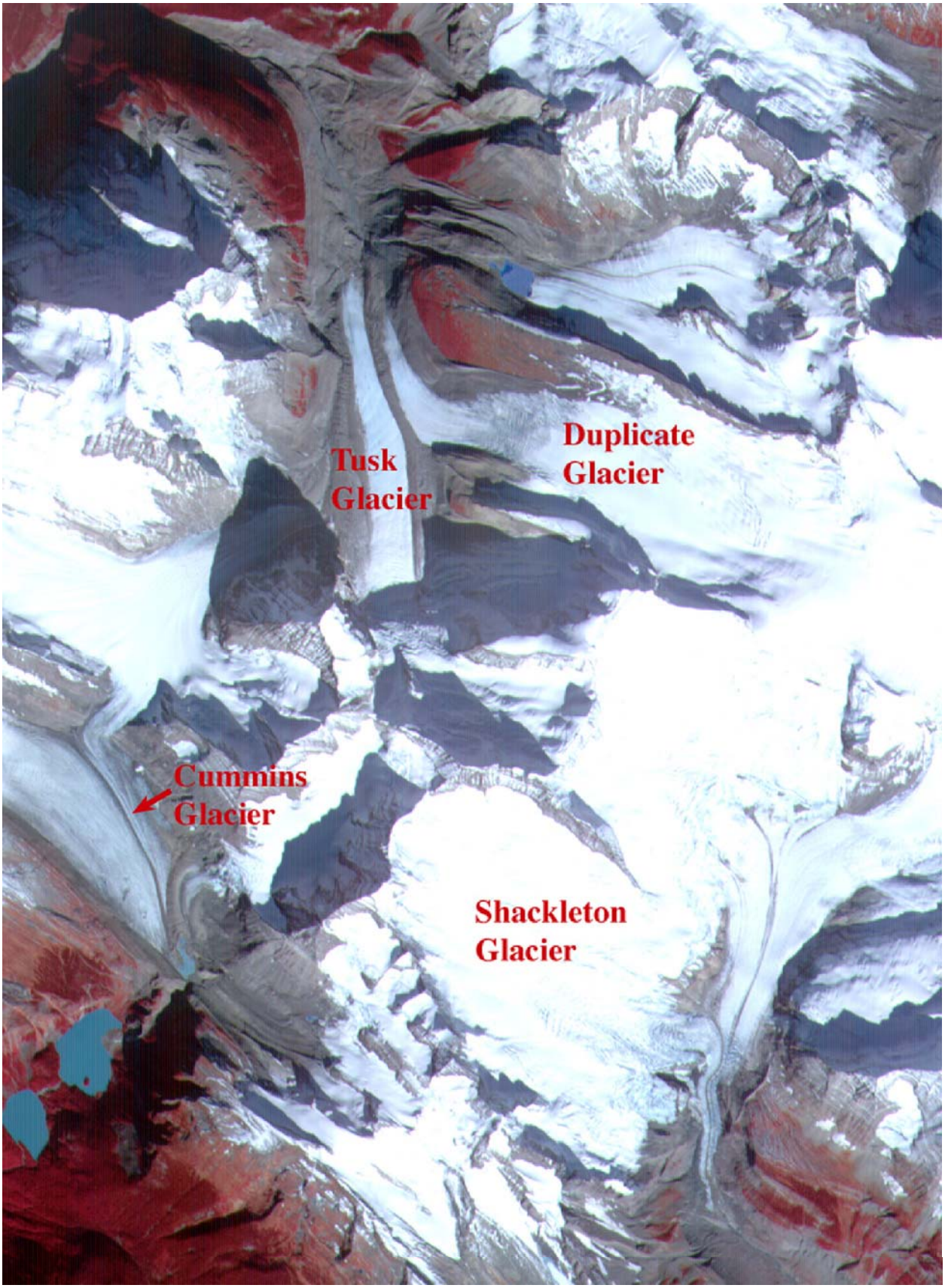
Tusk
Glacier
Duplicate
Glacier
Cummins
Glacier
Shackleton
Glacier

MARTIAN POLAR ICE SHEETS AND MID-LATITUDE DEBRIS-RICH GLACIERS, AND TERRESTRIAL ANALOGS. J.S. Kargel[1], B. Molnia[2], and K.L. Tanaka[3], [1]U.S. Geological Survey, 2255 N. Gemini Dr., Flagstaff, AZ 86001, U.S.A.; Email: jkargel@usgs.gov; [2]USGS, Email: bmolnia@usgs.gov; [3]USGS, Email: ktanaka@usgs.gov.

Introduction: Glaciers are commonly defined as perennial masses of ice and snow that exhibit morphologic indications of significant flow down-slope under its own weight (under the influence of gravity). This definition does not imply a particular origin or flow mechanism, and in the broadest sense it does not even require that the ice is H_2O. Thus, terrestrial rock glaciers are a type of glacier by this definition, as are Earth's snow-fed alpine glaciers, ice caps, and polar ice sheets; Martian lobate debris aprons, lineated valley deposits of the fretted terrain, and the south polar cap are also glaciers. Martian glaciers apparently include both H_2O-dominated and CO_2-rich icy flows; the ones being rich in CO_2-rich are restricted to the south polar cap. Debris-covered snow-fed glaciers and periglacial rock glaciers provide the closest terrestrial analogs to lobate debris aprons and lineated valley deposits of the fretted terrain.

Martian glacier types and terrestrial analogs: Among Martian glaciers and their Earth analogs, we observe many indications of both brittle and ductile flow behavior. Scarps and troughs in Mars' carbon dioxide-covered south polar cap locally expose intense deformation— buckles, folds, boudins, crevasses, thrust faults and elastic flexural bulges; and in outlying areas of polar layered deposits faults are common. Although there are profound differences between the Martian polar caps and terrestrial polar ice sheets, many of the morphologic characteristics of the Martian south polar cap are similar to characteristics of Earth's ice sheets.

Crevasses, faults, folds, medial moraines, and pressure ridges are commonly expressed on Martian valley and alpine glaciers as deeply etched surface structures whose relief is brought out by differential sublimation. These features are directly comparable to those of terrestrial valley and alpine glaciers. Only one good example comparable to braided glacial outwash systems on Earth has been identified on Mars. Small gullies and debris flows associated with Martian glaciers, like those widely observed for Himalayan debris-covered glaciers, are common. Indications of sublimation are widespread in precisely the geographic locations where sublimating ice is most expected based on Mars climate models.

Terrestrial glaciers are the closest landform analogs of the Martian glaciers, but some structural features of the Martian icy flows are mimicked by structures best known from high-grade metamorphic and plate tectonic systems on Earth. Terrestrial high-grade metamorphic complexes, where deep crustal spreading of hot plastic layered rocks occurred, offer insights relevant to boudins, folds, and faults in the south polar cap (Figs. 1 and 2). Ductile compressive shortening and the lobate forms of major polar flow lobes (Fig. 3) have good analogs in glacial ice sheets; pahoehoe lava flows exhibit some of the same morphologies. Also in the south polar cap we observe elastic plate flexure, where good process analogs include oceanic plate flexure due to the loads of ocean islands and magmatic arcs. In lobate debris aprons of Deuteronilus Mensae, wrinkle-ridges (similar to those of lunar maria and Martian volcanic plains) and plate obduction (Fig. 4) are observed, but more common are surface buckles, flowlines, and medial moraines (Fig. 5) similar to those of Earth's rock glaciers and debris-covered glaciers.

Conclusions and Implications: The implications of these analogs, along with insights drawn from analytical models, are that (1) the Martian cryospheric flows are composed of a flowing, faulting, folding substance; (2) it is a substance capable both of sublimating and melting at conditions near the Martian surface; and (3) the flow features are generally rheologically layered. This layering in the subpolar glaciers is probably due to differential debris/ice contents as well as vertical thermal stratification. In the south polar cap rheological layering is probably due both to thermal stratification (offering many orders of magnitude variation in effective viscosity) and differential amounts of water ice, dry ice, clathrate hydrate, and minor constituents (salts, acids, and inert dust components).

In contrast with the southern perennial CO_2-surfaced cap, the north polar cap and icy deposits

around the southern perennial cap have only rare ductile behavior, folding, and other evident indications of a soft, glacier-like rheology.

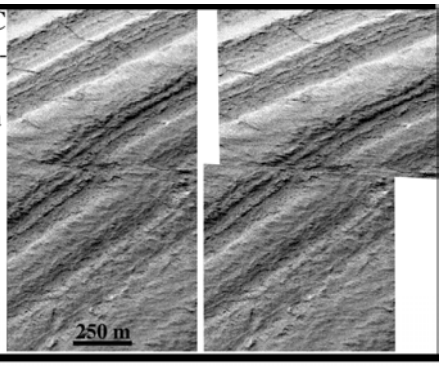

Fig. 1. MOC image M100-3514 shows faulted strata of South Polar Layered Deposits in actual image (left) and recontrsction (right).

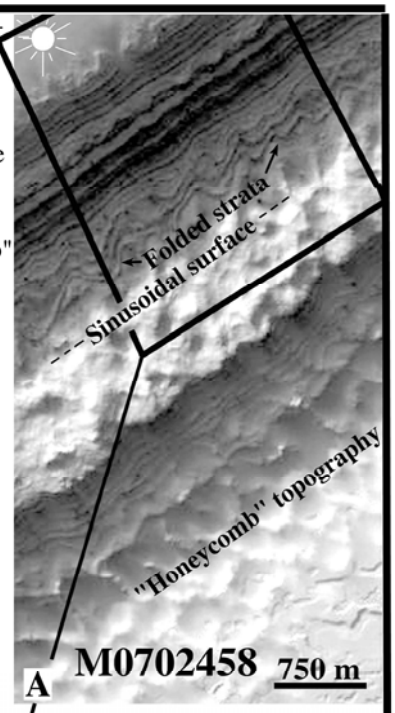

Fig. 2. MOC image M0702458 shows folds exposed in sublimating scarp face of the perennial south polar cap. (A) "Honeycomb" topography may be the eroded expression of boudin structure. (B) Details of folded outcrops (in shaded area) and what may be a folded bedding horizon (in area of direct solar illumination and at the edge of shadow area).

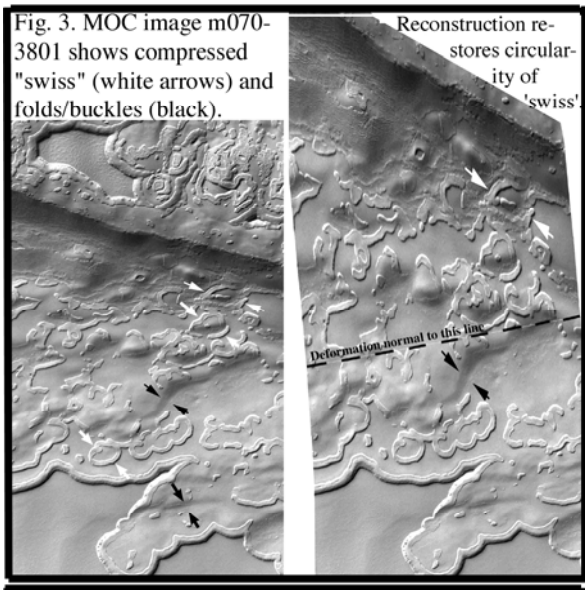

Fig. 3. MOC image m070-3801 shows compressed "swiss" (white arrows) and folds/buckles (black).

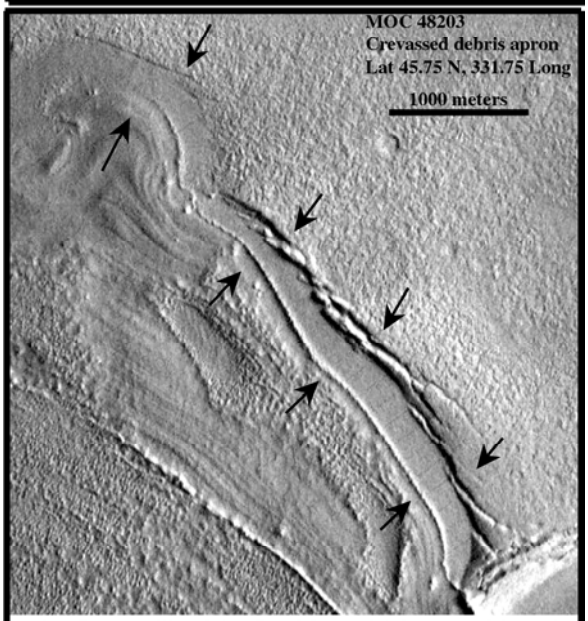

Fig. 4. Mutually obducting lobate debris apron 'plates.'

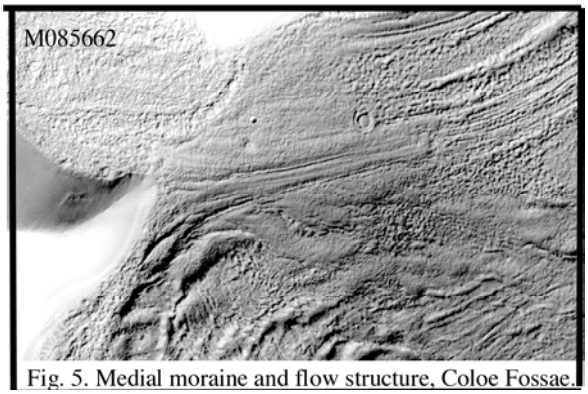

Fig. 5. Medial moraine and flow structure, Coloe Fossae.

RECENT DETECTION OF WINTER POLAR WARMING IN THE MARS UPPER ATMOSPHERE

G. M. Keating, M. E. Theriot, Jr., and R. H. Tolson, *George Washington Univ. Campus at NASA Langley, Hampton, VA 23681 USA (g.m.keating@larc.nasa.gov),* S. W. Bougher, *Univ. of Michigan, Ann Arbor, MI, USA,* F. Forget and M. Angelats i Coll, *Univ. of Paris, Lab. de Meteorologie Dynamique, Paris, France*, and J. M. Forbes, *Univ. of Colorado, Boulder, CO, USA.*

The Mars Global Surveyor (MGS) z-axis accelerometer has obtained over 1600 vertical structures of thermospheric density, temperature, and pressure, ranging from 110 to 170 km, between Sept. 1997 and March 1999, compared to only three previous such vertical structures from Viking 1, 2, and Pathfinder [1]. In November 1997, a regional dust storm in the Southern Hemisphere triggered an unexpectedly large thermospheric response at mid-northern latitudes, increasing the altitude of thermospheric pressure surfaces there by as much as 8 km and indicating a strong global thermospheric response to a regional dust storm [2].

From analysis of the MGS accelerometer data, enormous planetary scale waves have been detected in the Martian thermosphere between 60°N and 60°S. Fourier analysis of the wave structure reveals high amplitude waves 2 and 3 which appear to remain at nearly constant longitude between ± 60° latitude when viewed near 3 PM [3,4]. However, measurements near 3 AM show evidence of essentially a phase reversal in wave 2 [3]. Taking into account the near sun-synchronous orbit it appears that these waves are principally non-migrating tides propagating to the east. Studies by Wilson et al. [5] and Forbes et al. [6] indicate the wave 2 component observed from MGS is principally an eastward propagating diurnal wave 1 which rotates around Mars in the opposite sense of the sun once per day. The wave 1 Kelvin wave principally results from the interaction of tides and topography. Analysis of Thermal Emission Spectrometer (TES) MGS data near 30 km [5] indicates a similar phase to this wave at 30 km [5], which is in accord with the Kelvin wave, and thus the wave appears to propagate up from below into the thermosphere. The observed wave 3 may be a combination of an eastward propagating, semi-diurnal wave 1 and the eastward propagating, diurnal wave 2 (basically the wave 2 Kelvin wave). Both the observed wave 2 and wave 3 maximize near the equator. These results give further evidence of coupling between the lower and upper atmosphere.

The Mars Odyssey 2001 (M01) Spacecraft was placed into orbit about Mars in September 2001. Aerobraking was performed from then until January 2002 to circularize the M01 orbit. The spacecraft carried triaxial accelerometers, which were used to safely perform aerobraking and to continue exploration of the detailed properties of the upper atmosphere, which had begun with the Mars Global Surveyor accelerometer measurements. The accelerometers were used to measure atmospheric density, and from the vertical structures measured on both inbound and outbound trajectories the scale height, temperature and pressure were determined. Altogether 600 vertical structures were obtained ranging from 95 km to above 170 km. Measurements were obtained for the first time near the North Pole. Also, the first measurements were obtained on the night-side in the Northern Hemisphere. Temperatures near 110 km were discovered to increase with latitude maximizing near the North winter pole, apparently due to dynamical heating [7]. This result is contrary to the MarsGram and MTGCM models used for Odyssey aerobraking, where model temperatures are predicted to minimize near the winter pole. For example, maximum temperatures near the North winter pole at 100 km were observed to be near 200 K while MTGCM temperatures were predicted to be near 100 K. However, an upper atmosphere winter polar warming is predicted by the European Mars GCM [8] at both the North and South Poles in local winter at high altitudes. The altitudinal variations and high latitude diurnal variations of temperature near the North Pole also appear to be in fair accord with the Forget et al. model. Apparently, the upper atmosphere North polar winter warmings may result from adiabatic heating from the subsiding branch of the cross-equatorial meridional circulation from the Southern Hemisphere summer. The only measurements of the Southern Hemisphere winter polar upper atmospheric temperatures were obtained from accelerometers aboard the Mars Global Surveyor. These measurements do not show winter polar warmings, but minimum temperatures near the winter South Pole more in accord with radiative equilibrium, and more in

accord with the MTGCM model. Apparently, the summer-to-winter cell supplying dynamical heating to the North winter pole near perihelion is much stronger than the summer-to-winter cell supplying dynamical heating to the South winter pole near aphelion. The stronger dynamical heating during the North polar winter may result from being near perihelion where the closer sun and stronger dust activity may strengthen the meridional cell.

Previously, intense warming of the winter polar atmosphere was observed in the lower atmosphere (~25km) by the Infrared Thermal Mapper Instrument (IRTM) aboard the Viking orbiters during the onset of the 1977b global dust storm at northern hemisphere winter solstice [9,10].

References

[1] R. H. Tolson, G. M. Keating, et al. (1999) Application of accelerometer data to Mars Global Surveyor aerobraking operations, J. of Spacecraft and Rockets, 36, No. 3.

[2] G. M. Keating, et al. (1998) The structure of the upper atmosphere of Mars: In Situ accelerometer measurements from Mars Global Surveyor, Science, 279, 1672.

[3] G. M. Keating, et al. (2001) Persistent planetary-scale wave-2 and wave-3 density variations observed in Mars upper atmosphere from MGS accelerometer experiment, Proceedings of European Geophysical Society, 78, 229.

[4] S. W. Bougher, G. M. Keating, et al. (2001) The upper atmosphere wave structure of Mars as determined from Mars Global Surveyor Accelerometer, EOS, Trans, AGU, supplement, page F717.

[5] R. J. Wilson. (2002) Evidence for nonmigrating thermal tides in the Mars upper atmosphere from the Mars Global Surveyor accelerometer experiment, Geophys Res. Lett., 29, (7), 10.1029 GL013975.

[6] J. M. Forbes, G. M. Keating, et al. (2002) Nonmigrating tides in the thermosphere of Mars, In Press, J. Geophys. Res., Planets.

[7] G. M. Keating, et al. (2002) Detection of North Polar winter warming from the Mars Odyssey 2001 accelerometer experiment, Proceedings of the 34th Scientific Assembly of the Committee on Space Research (COSPAR) and the World Space Congress, 142.

[8] F. Forget, et al. (1999) Improved general circulation models of the Martian atmosphere from the surface to above 80 km, J. Geophys Res., 104, 24155.

[9] B. M. Jakosky and T.Z. Martin. (1987) Mars: North-polar atmospheric warming during dust storms, Icarus,72,528.

[10] R. J. Wilson. (1997) A general circulation model simulation of the Martian polar warming, Geophys. Res. Lett., 24 (2), 123.

BEHAVIOR OF SOLID CO_2 ON MARS: STILL A ZOO. Hugh H. Kieffer, *U. S. Geological Survey [Emeritus], Flagstaff, AZ 86001, USA, (hkieffer@uneedspeed.net).*

Observations of the martian polar caps by TES, THEMIS and MOC have revealed a variety of peculiar patterns: now informally known as **Cryptic material, Dalmatian spots, spiders, oriented fans and fried eggs**. These result from the characteristics and behavior of solid CO_2 on Mars, which is unlike anything on Earth. The proposed model involves the micro-physical interaction of CO_2 and dust with the solar and thermal radiation fields on Mars. This abstract is a shortened version of that for Mars VI, with no citations.

CO_2 Surface Condensation Modes: The condensation of the predominant gas in an atmosphere by radiative cooling yields the prominent seasonal polar caps on Mars. This process has no terrestrial analogy, which limits our intuition. This process is difficult to impossible to simulate in the laboratory because the natural force that allows condensation at a location other than at the coldest boundary (which sets the radiation balance) is gravitation, involving a characteristic scale many km. A practical laboratory scale would require a warm physical barrier that is completely transparent to thermal radiation.

TES observations in many areas in the polar night indicate that most of the condensation occurs at the Martian surface. TES spectra in the 25 μm region indicate that the "**Cryptic**" regions of cold-dark polar material consist of a CO_2 non-scattering slab composed of indeterminately large grains, or a slab. In other regions, fine-grained frost is found.

For condensation of a nearly pure gas by radiative loss there can be two end-member solutions for the form of the solid. If the abundance of non-condensing gases is negligible, so that a diffusion gradient of the condensing material is not involved, then a thick slab can form. On Mars, the dominant radiative loss of the condensate is from inside the bulk material. Growth perturbations outward from a planar solid interface, such as a crystal spike growing upward, have a longer conductive path to the bulk solid which, in turn, can radiate the latent heat of condensation. Lacking a diffusion gradient at the tip of such a spike, the condensation rate is limited by conductive heat loss, and this tip is at a disadvantage for condensation relative to the bulk solid. Thus perturbations do not grow, and the expected steady state form is a thick slab with a smooth surface. Such slabs are observed to grow in laboratory conditions of pure condensing gases, althoughthe thermal gradient internal to the slab results from conduction to a cold substrate rather than by radiative cooling.

In the presence of some amount of non-condensing gas, e.g., the 5% of N_2 plus Ar on Mars, at the micro-physical level there will be some diffusion gradient of the condensing gas toward the condensation sites. Both the temperature gradient and the concentration gradient of the condensate are expected to be linear for steady state conditions. Because of the nonlinear dependence of saturation pressure upon temperature, the partial pressure will be above the saturation pressure throughout this layer. Under this condition,spikes sticking up into this diffusion gradient become the favored site of condensation and they will grow more rapidly than locations deeper into the diffusion gradient. The steady state solution for the form of such a growing deposit is long columnar crystals oriented along the diffusion gradient. Such deposits also are observed to form in laboratory conditions of substrate cooling when small amounts of non-condensing gas are introduced into the chamber . This process of growth in a diffusion gradient gives rise to the beautiful H_2O hoar-frost crystals seen on calm terrestrial winter mornings.

TES observations indicate that both the slab growth and deposition of fine-grain CO_2 condensates occur in the polar night and that different condensation processes are dominant in different locations. The reason for the geographic distribution of the Cryptic material is unknown.

Radiation Balance in a Pure Solid CO_2 Slab: During the polar night, the radiative balance of surface CO_2 will be negative (barring an extraordinarily warm atmosphere). With the Sun above the horizon, solar radiation penetrates deeply into pure CO_2 . The relative absorption lengths for solar and thermal energy become important.

Using the optical properties of solid carbon dioxide, the penetration of both solar energy and ambient thermal radiation into a slab of CO_2 have been calculated. For typical polar summer conditions (incidence angle of 65°, $U = 1.5$), 2/3 of the solar energy penetrates 1m into pure solid CO_2 , whereas thermal flux is reduced to 50% in 3.7 mm. The top 2 mm of the slab are in net radiative loss; below that absorption of insolation results in net heating.

Dirty CO_2 Ice: Mars atmosphere is generally dusty with particles of radius on the order of 2 μm. During the CO_2 condensation season, atmospheric dust grains probably act as condensation nuclei; perhaps first for H_2O and then for CO_2. The proportion of dust in the CO_2 cap has not been measured, but is reasonably assumed to be near the average abundance of dust in the atmosphere. Using an average visual opacity of the atmosphere of 0.5 yields a dust abundance of about 1.5×10^{-3} kg m^{-3} or roughly 2×10^{-5} by mass. Because the particle size is smaller than thermal wavelengths, the presence of embedded dust will make little change to the thermal radiation environment, but will shorten substantially the solar absorption lengths, narrowing or removing entirely the surficial layer with net radiation loss.

Using the above values, and densities of dust grains and solid CO_2 of 2300 and 1600 kg m^{-3}, respectively, corresponds to a mean dust grain separation of $\sim$130 μm. If a seasonal cap budget of 1000 kg m^{-2} is adopted, the mass of dust in the cap is 0.02 kg m^{-2} and the geometric opacity of the dust in the cap is $\sim$1.6. The visual opacity of dust in the slab at sunrise will be roughly the average opacity of the southern atmosphere during the condensation season times the ratio of slab to atmospheric mass, or $\sim$3.3, in agreement with the geometric opacity if the scattering efficiency is taken as 2.0, as expected from Mie theory.

CO_2 Self Cleaning by Entrained Dust Movement: A first approximation is that for a dirty CO_2 slab, all of the solar energy is absorbed by the dust grains. However, because the surrounding CO_2 is isothermal, this radiation absorbed

by the grains must go into sublimation of solid CO_2 . If the local material is impermeable, a high-pressure pocket of gas will form around the grain and local elastic deformation will increase the pressure in the solid CO_2 , allowing some heat to be absorbed without sublimation. The warmer grain cannot be in direct contact with the CO_2 , but must rest on a microscopic layer of gas at the bottom of its vapor prison. If the local gas bubble does not rupture, there will be a downward migration of the bubble through the solid as vapor re-condenses on the roof of the bubble, the location most distant from the grain and hence coolest, and the grain will "burrow" downward as sublimation continues under the grain. Thus, a sealed finite vertical columnar hole will travel downward with the grain. When the grain reaches the bottom of the impermeable layer, it will be ejected downward. This self-cleaning, self-annealing process will tend to reduce the amount of dust in the ice through the spring. Because the net solar flux is greater toward the top of the slab, the uppermost particles will move most rapidly, resulting in concentration of dust as a descending "curtain" in the slab, leaving clean ice above.

Development of Pathways and Vents: The net positive radiation divergence near the surface of pure CO_2 will tend to seal small holes in the surface layer. Porosity will generally be sealed in a region that grows downward from the surface. Thus, the gas formed by springtime sublimation generally cannot diffuse upward through the CO_2 deposit. The gas resulting from net sublimation below the surface must escape somewhere and will hold open some set of larger holes. Because the gases in these vents will have some entrained dust, they can continue to absorb solar radiation, transfer energy to the vent walls, and remain open and grow. Also, gas under an impermeable CO_2 slab could reach pressures several times the atmospheric surface pressure. The saturation temperature under a 1000 kg m^{-2} slab would be 162K, enhancing the ability of venting gas to enlarge the pathways. Because higher velocities are possible and because of the r^2 heat flow versus the r^1 circumference, larger holes/paths will grow at the expense of smaller ones. Gas released beneath the slab must find some path to the open atmosphere. It may travel laterally underneath the slab to vents, cracks, or even to the edge of the seasonal deposit. It is difficult to predict the spacing of such vents, but they collectively must carry the total sublimation gas flux of about 10 kg m^{-2} /day. Vent spacing of tens to hundred meters is observed.

As the effective vents are separated by substantially more than the slab thickness, gas velocities will become far greater than required to suspend dust particles, and any sub-slab lateral transport may begin erosion of underlying loose material. Once the velocity exceeds the fluid threshold, erosion will begin.

The sub-slab lateral gas velocity will depend upon the geometry of the flow; increasing toward a vent. Because the soil thermal inertia of the Cryptic region is low, it is likely that the surface material is incohesive and that channelized flow will develop by scouring, beginning near the vents and progressing outward. Although velocities on the order of 10 m/s are required to initiate transport of fine material by saltation, injection of dust released from the CO_2 into the lateral flow may initiate motion and scouring at lower velocities; 2 mm/s vertical velocity is adequate to maintain atmospheric dust in suspension.

Dark radially converging dendritic patterns are visible in MOC images of some portions of the spring polar cap, these have been termed " **spiders**" by the MOC team. In this model, these patterns represent channels formed by sub-slab channelized flow of the sublimation gas toward the vents. Increasingly large particles could become entrained closer to the vent.

The velocity in the vents will be approximately $.005X^2$ m/s, where X is the ratio of vent separation to vent diameter. For example, for vents 1 m in diameter spaced by 100 m, the gas velocity would be 50 m/s. When the jets exhaust into the atmosphere and velocities decrease, the coarser entrained material will fall out in the prevailing downwind direction. In this model, the oriented dark **fans** seen in the MOC images are caused by this process. This is an exotic model that agrees with observations thus far. It predicts that the dark fans will be oriented into the prevailing wind, that they are seasonal and will disappear with, or shortly after, the CO_2 is gone, and that the "spiders" will be found only in the Cryptic region.

Darks vents are generally, but not exclusively, associated with dunes. Vents can progress into dark spots (**Dalmatian spots**) which grow monotonically until they coalesce. Dark halos commonly develop around the Dalmatian spots; these have been termed "**fried-eggs**" based on their symmetry and proportions. Many MOC images of the seasonal cap in summertime show great variegation of reflectance, interpreted to be incomplete solid CO_2 cover . Sequences of images show the development of evenly-distributed circular darks spots, which may represent the evolution of vents, commonly spaced by order 100 m, that gradually expand to consume the seasonal cap.

This model has been supported by a survey of the location of "spiders" in MOC imaging which shows that they are largely confined to the Cryptic region and their centers generally correlate with the location of fans. Spiders commonly persist as low relief features through the summer.

Most of this story has been developed from observations of the south polar cap. The north and south caps seem to be somewhat different in terms of the abundance of these features; e.g., spiders have not yet been identified in the north.

Summary: Deep in the martian polar night, there is some CO_2 snowfall, but most of the solid CO_2 takes the form of a uniform, continuous, non-scattering slab with embedded dust (and H_2O ice) grains. Following seasonal sunrise, in some areas the ice brightens due to fracture or surficial frosting, but in other areas the slab persists to form the *Cryptic* regions. The solar energy is largely absorbed by the dust grains, which either burrow downward or escape upward, cleaning the CO_2 slab which anneals small holes near its surface. Sunlight then penetrates to the bottom of the slab, warming the soil and subliming ice from the bottom. Widely spaced vents develop that allow the gas to escape. As the sub-slab gas converges toward the vents, it scours the soil surface along ragged channels (*spiders*). Dust entrained in the jetting gas falls out downwind to form *oriented fans*. The vents enlarge to become *Dalmatian spots*, some of which form *fried-egg* halos; these enlarge to consume the seasonal cap. Only the topographic ghosts of the *spiders* persist through the summer.

DETAILED GEOLOGIC ANALYSIS OF PART OF THE SOUTH POLAR LAYERED DEPOSITS, PLANUM AUSTRALE, MARS.
E.J. Kolb[1] and K.L. Tanaka[2], [1]Arizona State University, Dept. of Geological Sciences, Tempe, AZ 85287, eric.kolb@asu.edu, [2]Astrogeology Team, U.S. Geological Survey, 2255 N. Gemini Dr., Flagstaff, AZ 86001, ktanaka@usgs.gov.

Introduction. We have begun geologic mapping of the martian south polar layered deposits (SPLD) as part of a project to map PLD at both poles at 1:1,500,000 scale. In this abstract, we present preliminary geologic mapping results of SPLD exposed in a trough system east of and adjacent to Chasma Australe within Planum Australe (Fig. 1). Our mapping has allowed us to address outstanding SPLD-related issues including: SPLD bedding characterization, relative timing and modes of trough emplacement, and the formation of secondary features such as the north-trending ridged-and-grooved ("wire brush") terrain and the sinuous, generally east-trending ridges ("snakes"). The major goals of the mapping project consist of: (1) Construction of stratigraphic sections of the PLD, including topographic analysis of prominent layers and layer sequences and investigation of intra- and interpolar stratigraphic and topographic variations in the PLD and residual ice caps, (2) detection and interpretation of structural deformation in the PLD, (3) description and interpretation of the erosional history of the PLD. Geologic mapping of the PLD is being performed using a GIS-integrated, multi-dataset approach consisting of current and to-be-released data products including MOLA topography, MOC NA images and THEMIS VIS and IR datasets.

Here, we discuss the geology of the SPLD within a broad trough whose floor dips gently from near the center of the SPLD down toward the margin of Planum Australe. This north-trending, radially orientated trough portrays some diverse and enigmatic landforms (within the region of 100 to 270°W, 80 to 87°S). Data coverage of the trough feature includes 114m/pixel MOLA-derived DEM's and shaded relief maps, 105 mappable MOC NA images and several VIS and IR THEMIS images. We have developed several geologic cross-sections across and along the length of the trough to aid in the characterization of bedding attitude and structure of PLD exposed within the trough.

PLD Sequences. Within the trough, we have identified six distinct, overlapping, mappable sequences of PLD. PLD subdivision is based on the topographic expression (e.g., cliff vs. terrace forming, Fig. 1) of layer sequences. The sequences are bounded by marker beds that are laterally continuous throughout the study area and beyond, extending >150 km along the trough, within both enclosing trough walls, as well as within a trough system east of the mapping area. Marker beds can also be seen extending from PLD exposed within the trough floor into scarps of the adjacent spiral troughs. Individual sequences are 28 to >150 m thick; total thickness of the six sequences is several hundred meters. PLD bedding attitudes and features appear structurally controlled (Fig. 2 and 3), exhibiting syn- and antiformal beds with wavelengths of kilometers to tens of kilometers and maximum bedding dip angles of 1.5°. In Figure 3, large wavelength anti-formal bedding and smaller syn- and antiforms within it control the topographic expression of the PLD sequences.

Morphologic Features. Along the trough floor and on the western trough wall are a series of closely spaced ridges and intervening grooves that are described as "wire brush terrain" by [1]. In some cases, the ridges and grooves occur within single layers, but where there is more relief, they cut across many layers (Figure 1 and 2). Some of the grooves form enclosed, lenticular troughs, whereas other grooves appear to be composed of coalescing pits. Intervening ridges in some cases appear to be capped by narrow ridges of probably relatively resistant material. In one instance, where cliff-forming PLD sequences exposed in the eastern trough wall extend onto areas of the trough floor overprinted with ridges and grooves, the more resistant material forms streamlined outliers orientated parallel to the ridge and groove trend. MOC NA images show large boulder-like mounds in places. Transecting pole-ward regions of the trough are a series of east-trending ridges spaced tens of kilometers apart. They are tens of kilometers long, up to several kilometers wide, and have only several meters of local relief. Some of the ridges exhibit moderate sinuosity. A few ridges can be traced almost continuously across the trough flanks and floor, whereas others appear only within the trough or on trough-enclosing, high-standing SPLD. The ridges are overprinted with the ridge-and-groove features. Where imaged by the MOC NA camera, the ridges commonly exhibit layering only on the ridge's south-facing side. At several locations (most notably on the flanks of the trough), ridges are composed of undisturbed PLD that are traceable on both sides of the ridge. In all instances where this is seen, MOLA topography indicates a gentle northward apparent dip of the PLD that make up the ridges—in parallel with subjacent PLD sequences. PLD surfaces, including the "wire brush" terrain and bedding terraces, appear in MOC NA images to be marked by small irregular, shallow pits and alcoves. These features give the PLD a rugged appearance at meters to tens of meters length scales.

PLD Sculpturing. Proposed trough and ridge-and-groove formation mechanisms include glacial scouring and/or streaming, sub-ice volcanism, and eolian activity whereas the west-trending ridges may indicate deformation episodes or in-filled fractures composed of relatively more resistant material [1 and ref within]. Problems with the glacial hypothesis for the ridge-and-groove features include: (1) The supposed basal surface which the moving ice would have scoured is actually within PLD that is well above the base of Planum Australe, yet the underlying PLD does not appear deformed; (2) the trough would have been planed smooth by glaciers; instead, the PLD beds appear terraced; and (3) based on terrestrial examples, the supposed ice stream (marked by the location and extent of ridge-and-groove terrain) should have occurred at or near the margins of the ice sheet [2], not the higher, interior areas of the SPLD. Large collapse pits and crevasses within PLD that should be overlying any hypothetical calderas had sub-ice volcanism occurred are not seen.

The PLD appear to be composed of beds alternating in competency, given: (1) the stair-step slope profile of the PLD, and (2) the alignment of the tops and bottoms of well-developed ridge-and-groove features with the tops and bottoms of individual layers (Fig. 2). The variable competency of the PLD beds may be related to degree of induration, ice composition and structure, and/or concentration of dust particles within an icy matrix. Thus we conclude that eolian scouring chiefly formed the PLD topography. The occurrence of ridge-and-groove terrain within the trough may be attributable to enhanced intensity and longevity of down-slope winds that have carved dip slopes of friable material. However, the ridge-and-groove terrain does not seem to be actively developing; instead, fine-scale pitting and scarp retreat appears to be the most recent observed landform development, perhaps due to back wasting and sublimation of surface or near-surface ice. An eolian scouring trough-formation mechanism would indicate that several hundred meters of SPLD material has been removed (Fig. 2). In Figure 3, the east-trending ridge occurs at the presumed crest of an anticline. This association, and that PLD is typically only seen on the south side of the ridges indicates that the ridges are the erosional expression of north-dipping SPLD beds.

Relative Timing. Along the length of the radial trough are transecting and evenly spaced topographic swales that connect with and are of the same dimensions and orientations, as that of adjacent spiral trough features within Planum Australe. Within the radial trough, swale crest elevations are 100's of meters lower than their counter parts within the spiral troughs. We postulate that the radial trough post-dates initialization of spiral trough formation and that the swales are the remnants of spiral trough features that had previously extended into regions now occupied by the radial trough. If the spiral troughs have formed by ice-flow processes [3], the undisturbed, continuous bedding contacts that extend from the radial trough into the spiral troughs indicate that since commencement of trough formation, ice flow has not occurred. Erosion of the spiral troughs may be facilitated by along-trough winds (as supported by the streamlined morphology of capping SPLD located on the crest of a spiral trough at 250°W, 83°S) or sublimation of equator-facing slopes. However, we see no evidence for the redeposition of layers on pole-facing slopes [4].

Summary. Our investigation of the trough in Planum Australe that contains distinctive ridge-and-groove ("wire brush") terrain suggests that the PLD:

(1) Consist of layers of variable competency
(2) Include distinctive marker bends traceable for >100 km
(3) Have not been eroded significantly by glacial scour
(4) Do not show deposition of spiral trough wall material on pole-facing slopes
(5) Have experienced significant eolian erosion, including the development of the broad radial trough, the ridge-and-groove terrain, and east-trending ridges by down-slope winds on dip slopes in beds of alternating competency
(6) Radial trough emplacement occurred after spiral trough formation began; their development may include eolian erosion and/or sublimation
(7) Have undergone slope backwasting to reveal beds of variable erosional resistance
(8) Most recently have been dominated by pitting and scarp retreat that may be related to localized removal of ice-rich material

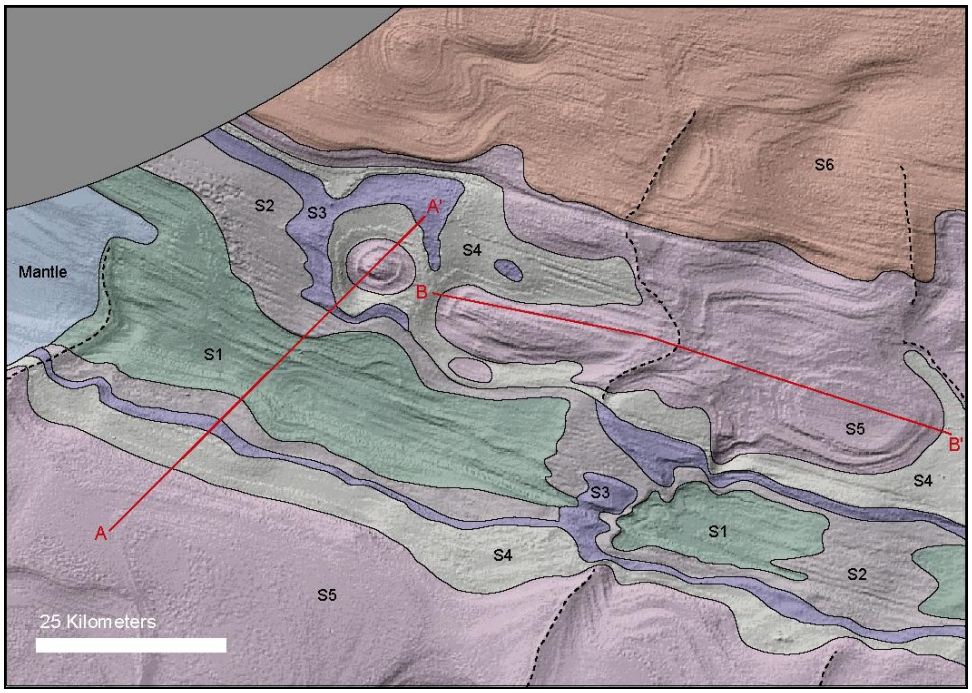

Figure 1. Geologic map of part of the north-trending radial trough east of Chasma Australe. The east-trending ridges are highlighted with a dashed line.

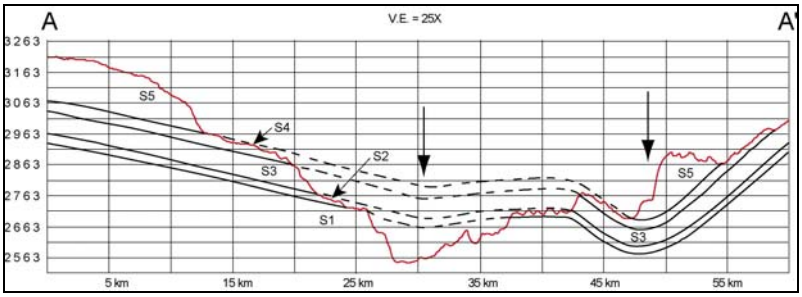

Figure 2. Elevation in meters. Maximum bed dip angle is ~1.5°. The large arrows highlight the axis location of two north-trending synclines.

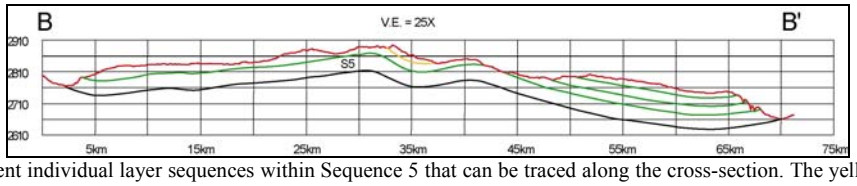

Figure 3. Green lines represent individual layer sequences within Sequence 5 that can be traced along the cross-section. The yellow line is drawn to highlight bedding orientations where the SPLD crosses an east-trending ridge. The PLD descend over 200 m towards the margin of Planum Australe and the average bed dip angle is ~0.5°.

References: [1] Koutnik M.R. et al., (2003) 6th Intl. Mars Conf. #3134 [2] Hourmark-Nielson, M. et al., (2001) Paleo-Ice Stream International Symposium. Pg. 35 [3] Fisher, D. A. (1993) *Icarus* **34**, 501-511. [4] Howard, A.D. (2000). *Icarus* **144**, 267-288.

INTERCRYSTALLINE SWELLING OF STRATIFIED SILICATES EXPOSED TO NEGATIVE TEMPERATURES.

I.A. Komarov Department of Geocryology, Faculty of Geology, Moscow State University, Vorob'evy Hills, Moscow, 119899, Russia. ilya_komarov@mail.ru

ABSTRACT: Theoretical calculations based on a thermodynamic model together with experimental results based on differential scanning calorimetry are used to test whether intercrystalline swelling occurs in montmorillonite under negative temperatures.

Introduction

The analysis of adsorption properties of expandable stratified silicates, exposed to positive temperatures, provides the basis of proposing the existence of intercrystalline swelling caused by the interaction of silicates with water or other polarizing liquids. Swelling produces characteristic peaks (figure 1) on curves relating differential heat adsorption Q_v and moisture W when observing isotherms for the sorption of water vapor by montmorillonite and vermiculite clays. In particular, the heat of adsorption Qw for askangel drops as a result of saturation with water. Two maxima on the Q_w =F (W) curve at W≈10 % and W≈23% are associated with the intrusion of water between silicate layers of askangel. Minimums on the Q_w =F (W) curve are associated with loss of heat due to expansion of the mineral skeleton during adsorption [5]. Similar maxima and minima are observing for oglanlin and pigew Na-montmorillonite, kovdor vermiculite, and Ca montmorillonite. It is proposed, therefore, that intercrystalline swelling could also take place at negative temperatures, because of presence of unfrozen water near sediment and rock surfaces. Signs of swelling at negative temperatures should be evident from differential thermal analyses (DTA) of temperature curves and heat capacities because water between silicate layers could liberate heat. I examine this problem theoretically using thermodynamic equations for a range of temperature and moisture conditions.

Oservation

1.1. Thermodynamic model.

Proposed swelling of stratified silicates at negative temperatures is based on the calculations developed from a model of phase and adsorption equilibrium for water in unsalted and salted frost rocks proposed by Komarov (2001). The basis for this model is that pore liquids are part of a multi-component solution. This point of view is obvious for salted rocks. For unsalted rocks H_2O can occur in a solid, liquid or gaseous phase. A wide range of experimental data derived by various authors using various techniques (e.g. nuclear magnetic resonance (NMR), X-ray, calorimetric) show that unfrozen water is structurally and energetically non-homogeneous [2]. It is proposed, therefore, that water act as a binary solution even without presence of soluble ions in the liquid. Furthermore, I propose that individual H_2O molecules do not associate with the surface of rock particles. Instead water molecules next to the rock surface occur as monomers, which are 5^{th}-8^{th} layers of single water molecules with a thickness of 15 - 25 Å. These monomers are the first pseudo-component of Komarov's [3] model. Moving away from the rock surface, the next layer occurs in a field that is influenced by long distance forces associated with the rock surface. As the distance from the rock surface increases rock-induced forces are diminished such that forces associated with interactions between water molecules and structures within associated polymers dominate. This part of pore liquid is the second pseudo-component of the Komarov [3, 4] model.

The thermodynamics of this model requires that the first component of water have strong adsorption that is localized in the surface layer of the rock particles. This will stratify the solution creating a border between the first component and other components further from the rock surface. This border is characterized by a dynamic equilibrium between water monomers and associated polymers. The ice solution in the binary pore solution is representing by two processes, thawing of ice and mixing of the two determinate components of unfrozen water.

The main preconditions for model construction are in the labour [3, 4]. Evaluation of phase equilibrium parameters of water in salted and unsalted rocks follows Komarov [3]:

$$\sum_i^2 [\ln(m_j f_j)_i]_{T=T_f} =$$

$$\sum_i^2 [-\frac{L\theta_i}{RT_0^2}\sum_1^n (\frac{\theta_i}{T_0})^{n-1}] + \sum_i^2 [\frac{\alpha_i\theta_i^2}{RT_0^2}\sum_1^n \frac{n}{n+1}(\frac{\theta_i}{T_0})^{n-1}] +$$

$$\sum_1^2 [\frac{\beta_i\theta_i^3}{RT_0^2}\sum_1^n \frac{n}{n+2}(\frac{\theta_i}{T_0})^{n-1}] + \sum_i^2 [\frac{\gamma_i\theta_i^4}{RT_0^2}\sum_1^n \frac{n}{n+3}(\frac{\theta_i}{T_0})^{n-1}]$$

$$+\frac{I}{R}[\frac{(T_v - T_0)+\theta_i}{T_v(T_0-\theta_i)}]\sum_i^2 (H_j^0 - H_j)_i, (n=1,2..n) \quad (1)$$

where: m_j , f_j - mole concentration and coefficient of activity; j – component (solution); $\theta = T_f - T_o$ – freezing point temperature (T_f – K degrees); L – molar latent heat of crystallization of water in the volume; R – gas constant; α_i, β_i, γ_i - coefficients determined from the heat capacity of ice and unfrozen water for single temperatures in unsalted rocks and from salt concentrations and compositions for salted rocks; T_v - the temperature of experiment; (H^o_j - H_j) – the difference in enthalpies, which is the value of differential heat of adsorption and moistening with back sign for unsalted rocks, and it is the differential heat of solution for salted rocks; i = 1 for unsalted pore solutions, i = 2 – for pore solutions with soluble ions, n – the number of the member of sum (n=1, 2, … n).

Equation (1) is a generalization of methods obtained by authors [6]. These authors considered single unsalted rocks where unfrozen water occurs in one of the three phases of H_2O and water properties correspond to the properties of deep cool water in freezing volume. This approach is less physically based. In contrast, properties of the solution in the freezing volume in my model are peculiar to the second conditionally determinate component, which is the solvent. Specific interactions between the surface of rock particles and adjacent layers of pore liquid, which do not freeze even under low negative temperatures, is not taking into account in previous approaches. The value for moisture of first component in my current analyzes varies from 0.45 to 0.7 which corresponds to maximum hygroscopic moisture. Transfer to the real surface layers of water is accomplished by adding a coefficient of surface activity for active salt ions.

1.2.The results of simulation.

The temperature curve of unfrozen water for askangel, calculated by equation (1) for unsalted rocks (i=1) and corresponding adsorption data are presented in Figure 1. Parameters used in equation (1) to generate the figure are described by Komarov [4]. Theoretical calculations (Fig. 1) are within 10-15% of experimental results (Figure 2). Data received from labours [2] derived using a variety of methods (e.g. nucleus magnetic resonance (NMR), calorimetry, contact and cryoscopic methods) produce characteristic peaks for calculated curves in temperature ranges of –16 to÷ –18 ^{0}C and - 45 to÷ - 47^{0}C (Figure 2).

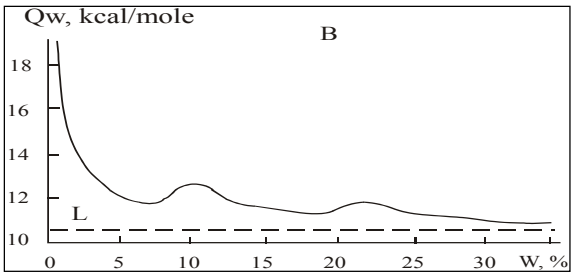

Figure 1. Dependence of differential adsorption heat Q_w on humidity W for the samples of montmorillonite [5].

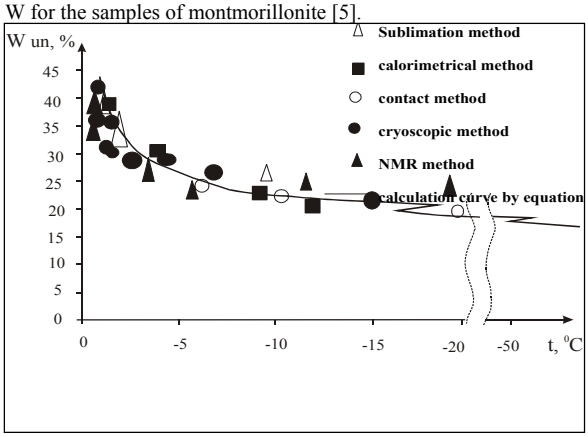

Figure 2. The comparison of calculated curve and experimental (obtained with different methods) data of volume of unfrozen water Wun for the samples of Na – montmorillonite.

These peaks are influenced by the interdependence of Qw = f(W) (Figure 1) and uncertainty that arises when the same value of heat adsorption can result from moisture with three possible phases moisture. Researchers have not previously considered this type of temperature dependence of unfrozen water. In my view this dependence is sensitive to small changes in the quantity of unfrozen water and considerable precision is required when using methods for determining phase consistence. This results in the smoothing of estimated adsorption on the graph. I suspect that this dependence of phase consistence on temperature is related to the intrusion of water between stratified silicate layers and expansion the lattice. Peaks in calculated curves are likely caused by the using of thermodynamic calculations to generate adsorption data. This would require that the surface of the rock not be deformed. However, the results of some work [8, 7] shows that this proposition is not correct even for rocks with inflexible cell structures (e.g. kaolin, talk and pyrophyllite). In particular, parameter B of cell structure changes as water is incorporated. The epitaxial growth of water films creates tension which drives mechanical deformation of particles. As a result, changes in phase consistence are gradual.

1.3. Experimental data.

Thermal capacity and enthalpy was determined by low-temperature differential scanning calorimetry (DSC) (calorimeter "Mettler TA-2000B"). This method is explained at length by Komarov [4]. Hysteresis was fixed for cycles of heating and cooling using the curves of DSC for heat capacity. Shifts in emission peaks varied from 10 to 17 degrees. Circumstantial evidence supporting the existence of crystal swelling in montmorillonite at negative temperatures is obtained by measuring heat capacity, which is a subtle indicator of structure deformations. There are three peaks in the plot of experimental data that relates heat capacity Cp and temperature C_p= f (t) (Figure 3).

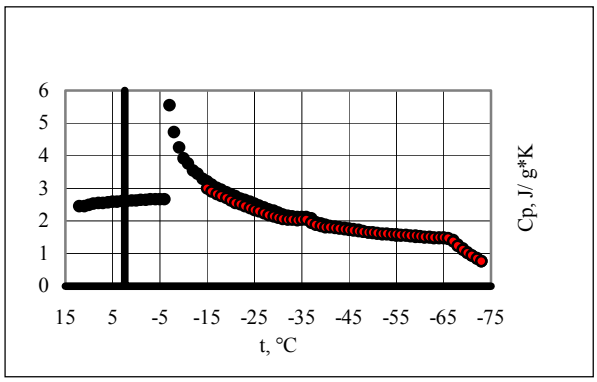

Figure 3. Experimental temperature curves of heat capacity for two samples of Na – montmorillonite (W=15%).

Two of these peaks are likely caused by gradual intrusions of the first and second layers of water between silicate layers in montmorillonite. The range of these peaks corresponds to predicated values that take into consideration shifts in peak caused by changing temperature. These structural reformations cause heating that can be recognized on the DSC curves. In fact, these peaks fix for Li, Na, K, and Ca – montmorillonite [1] .

The origin of these peaks was not explained by the original authors. We present our DSC curve in the labour (Komarov 2001, 2003), that we use to evaluate heat effects Q_{11} of the intrusion of second water layer into silicate structures. However, the sensitivity of calorimeters was insufficient to quantity the effect for first layer. It is Q_{11} = 0.11-0.13 j/g (related on gram of weight of sample of rock). It use calculated curve (Figure 2), which let to evaluate the quantity of unfrozen intruded water, that is necessary for evaluation of Q_{11} meaning on gram of unfrozen water. It is 1.2 ÷ 1.5 %. Then the heat effect for gram of water is Q_{11} = 20÷30 j/g. This meaning is close to experimental data in positive range of temperatures, the valuations of heat of moistening of second water layer, which intrude to inter layer space of Na – montmorillonite and come to Q_{11} =12÷20 J/g [8]. The evaluation is less on order as latent heat, which is emitted during the freezing of water. The fundamental interpretation of this effect with help of modeling, x-ray analyses transgress from borders of this paper and was discussed in the labour [4].

It is reasonably to appoint two ideas as applied to Martian conditions: a) taking into account the discussed phenomena lets to correct in the side of increasing adsorption moisture content in the regions with stratiform silicates in the surface layer; b) As the water evaporation heat could exceed ice sublimation heat in 1,5 times and more under low humidity, so ice existence in the rock leads to ice sublimation or its thawing and next adsorption of formed moisture as these processes are more thermalphysically efficiently.

Reference: 1. Anderson, D. M. and Tace, A. R. (1971). *Soil Science Society of America Proceedings, ,vol.35*, no.1, pp. 47-54

2. Ershov, E. D. et. al. (1979). Phase compound of moisture in frozen rocks. MSU.pp.189

3. Komarov, I. A. (2001), *7-th International Symposium on Thermal Engineering and Sciences for Cold Regions*, Seoul ,Korea.

4. Komarov I.A., (2003), Thermodynamic and heat mass transfer in disperse frozen grounds, Moscow, *Scientific world*, pp.608.

5. Korolev, V. A. (1983), The collection of scientific works. Moscow. *MSU Publishing, Vol. 5.*

6. Low, P. F., Anderson, D. M., Hoekstra P. , (1968), *Water Resources Researchv.4, N 2*, p. 379-394.

7. Osypov, V. I. (1979), The origin of mechanical and deformation properties of clay rocks. Moscow. *Nedra*

8. Tarasevich, J. M. Ovcharenko, F. D. (1975), Kiev. *Scientific thought*, pp.351.

PROPERTIES OF DISPERSE FROST ROCK IN THE RANGE OF LOW NEGATIVE TEMPERATURES.

I.A. Komarov, V.S.Issaev, L. V. Mel'chakova
Geological Department, Moscow State University, Vorob'evy Hill, Moscow, Russia,119899
tpomed@garnet.ru

Abstract: this paper presents experimental data for thermophysical properties of disperse terrestrial soils in the wide range of negative temperatures from 0 to –120 ^{0}C. We represent results of comparision with data of thermal lag of Marthian surface.

Introduction

Frozen soils are multi phases and multi component systems in the thermodynamic sense. As heat capacity is an additive amount, so its value is the sum of the heat capacities of its constituents: minerals of rock skeleton and organic components; pore solutions; pore ice; pore gases. Heat capacity of rocks was studied mainly for a range of positive and comparatively high negative temperatures [2].

Observation

Experimental researches were surveyed on the basis of adiabatic and differential scanning calorimetry. Methods are described in the labours [5].Experiments measuring heat capacity of rocks on using calorimetry were made for quartz sand, loam-sand and clays: kaolin, hydromicaceous. The samples were dried at a temperature of 105 ^{0}C.

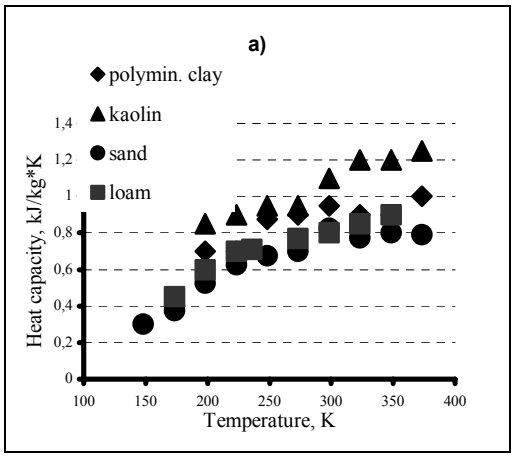

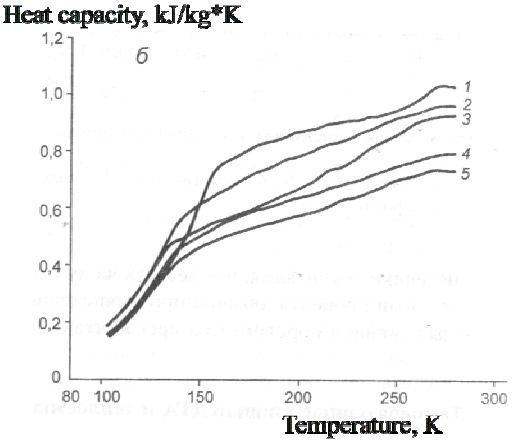

Figure 1. Dependence of heat capacity of skeleton mineral material of various grain size and mineral composition on temperature: a – the data has received with adiabatic calorimeter, b – the data has received with differential scanning calorimeter "Mettler TA-2000B".

In accordance with Figure 1-a specific heat of the skeleton mineral material C_{sk} of soils varies with temperature: it changes little in the range of temperatures from –25 to 100 ^{0}C; C_{sk} falls with temperature decrease to –100 ^{0}C (30% for hydromicaceous clay). Satisfactory agreement (less 5-10% difference) is observed with similar data from [4] for calorimetric experiments in the range of temperature from 223 to 318 K with temperature steps of 15º and data of [7], who did experiments using a massive calorimeter. It is necessary to consider temperature dependence of heat capacity of skeleton minerals for a wider range of negative temperatures. The influence of mineral grain size in the range of temperatures from 100K to 140K correlates to notions about behavior of the heat capacity of minerals.

Results of experimental investigation of temperature dependence of heat conductivity coefficient of clay loam and quartz sand with fractions of 0.1 -0.25 mm under different values of moisture are given in Figure 2 a,b.

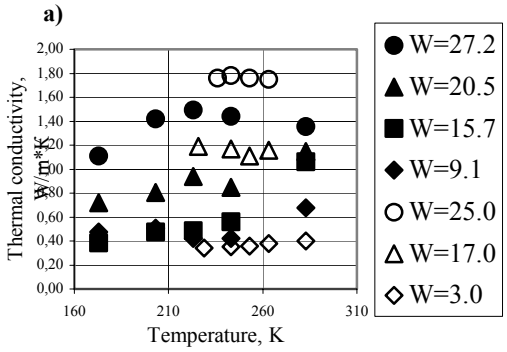

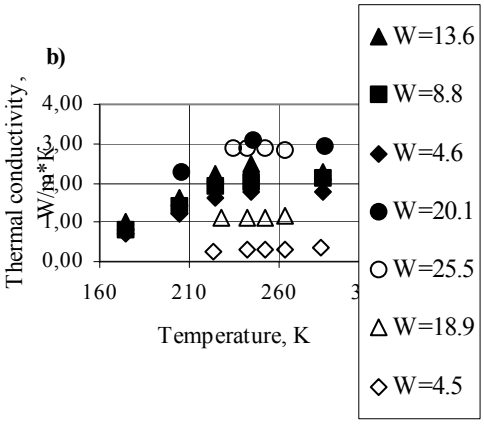

Figure 2. Dependence of thermal conductivity on temperature of various moisture contents: a - of quartz sand (fr.0.1-0.25); b - of clay loam. Unfilled badges are experimental results, filled budges are data from [4].

The coefficient of heat conductivity has inconsiderable dependence on temperature for the air-dry rocks in the light of represent dependencies. These data are comparable with data from [4] for the samples of soils with different dispersion in a more narrow range of temperature about -50^{0}C (Figure 2 a, b). The sum of heat conductivity of soil in an air-dry state has to increase with decreasing temperature, as a result of increasing of heat conductivity of the mineral skeleton.

There is temperature dependence of coefficient of heat conductivity λ of quarts sand of two fractions (0.1 -0.25 mm and 0.25- 0.5 mm) form moisture on the Fig. 2 a. We observe considerable decreasing of λ value under temperature decreasing from -30 to -100 ^{0}C, that has confirmed with data for more narrow interval of temperature (to -50^0 C) [4]. It conflict with assumption that summary coefficient of heat conductivity λ of ice-saturated rocks have to increase with decreasing of temperature. This assumption is based on the character of temperature dependence of thermal conductivity of separate rock's components. λ value of ice increase twice in the temperature range from 0 to –110^{0}C. λ value of organic-mineral rock's skeleton in the same temperature range is not changed. λ value of loamy rocks in air-dry state also isn't related to the same temperature change. We supposes that the causes of λ decreasing are 1) micro-cracks formations in the pore ice (for temperature below –12 ^{o}C); 2) micro-cracks formations on the pore ice - rock particle's boarder contact as the cause α values differences of phases; 3) micro-cracks formations in the organic-mineral skeleton of rock as the cause α values differences of minerals. Structure's formation leads on decreasing of λ as the cause of increasing of pore gas contents. Comparison of calculation and experimental data with data of distance probe and of morphometric analyses of Martian surface. Data of thermophysical properties for surface layer of Mars could be received from the values of thermal lag I. These values are transmitted from landing space modules. The value $I = (\lambda C\rho)^{1/2}$ equals to 0.004÷0.017 cal/cm sec$^{1/2}$ K, and rock's density ρ is from 1 to 1.6 g/cm^3 [6]. λ value changes from 0.2 to 0.12 W/m K for C = 0.42 kJ/kg K. λ values for sandy rocks are in this range. It received from calculation of experimental data for terrestrial atmosphere's conditions with correction to the value of Martian atmosphere's pressure on the surface (6 mm of mercury) Figure 5. It is based on the method [1] for conditions of gaseous phase flowing $22 \geq Kn \geq 0.1$, where Kn is Knudsen's criterion. Accommodation coefficient is chosen for CO_2-quarts system.I value changes from 0.004 to 0.006 cal/cm sec$^{1/2}$(Kuzmin, 1983)· K. It corresponds to λ values from 0.05 ÷ 0.12 W/m K. This range for Martian atmosphere corresponds to thermal conductivity of dusty particles.

The reason for non increase of heat conductivity of mineral skeleton is heterogeneity of mineral composition and differences in coefficient of linear growth which leads to formation of micro cracking in organic mineral skeleton of rocks. The summary effect of these processes could be dominant and could lead to a decrease in the value of heat conductivity. The reason of this is increasing of gaseous phase content. Micro cracking process was proved by micro photograph researches, which were done on the basis of the replica method [5]. These effects are more clearly revealed in the analyses of the behavior of heat conductivity of wet soils (Figure 2 a, b). As the temperature dependence of the coefficient of heat conductivity of air-dry soil sand of ice shows by its behavior (abruptly increase of coefficient of heat conductivity with decreasing of temperature about 50 K, so it is reasonable to propose that the sum effect of heat conductivity will increase with fall of temperature for wet rocks. It confirms by experimental data of linear expansion α received on the basis of laboratory work with Japanese dilatometer "Sinky-Rico" model DL-150LS [3].

Nevertheless experimental data does not prove this suggestion. Heat conductivity of kaolin changes inconsiderable with temperature decreases under moisture content of 20%. Heat conductivity firstly decreases and later inconsiderably increases for rocks with moisture content of less than 20%. Heat conductivity falls under temperature decreases from –30 to-100^{0}C for sand samples, which have some individual differences for each sand fraction.

The reasons, which are determined experimentally for decreasing of the value of coefficient of heat conductivity under decreasing of temperature, are the following: formation of micro cracks inside pore ice; formation of micro cracks on the particle – ice interface; existence of micro cracking in organic mineral skeleton. The sum effect of these processes became dominant and leads to decreasing of value of coefficient of wet rock heat conductivity.

References

1. Dulnev, G.N. & Zarychnyak, Y.P. (1974). Leningrad, *Energy*, p. 264

2. Ershow, E. D. (1996). Moscow: *MSU*. p. 397.

3. Ershow, E.D., Komarov, I. A., Brushkow A.V., Hors M.N., (2001), *Proceeding of 2 conference of Russian geocryologists, . V.1*, pp 81-88.

4. Haynes, F. D., Carbu, D. L. & Van Pett D.J.(1991). *United State army. Corps of engineers. Cold regions research and engineering laboratory. Hanover*, New Hampshire, USA, Ser Crel.

5. Komarov, I.A. (2003). Thermodynamics и thermomasse transfer and frozen disperse rocks. *Scientific world*, Moscow.pp608

6. Kuzmin, R. O. , (1983), Moscow, *Science Press*. 144 p.

7. Shusherina, E. P. (1973), *Proceeding of 1 All union symposium of rheology of rocks*: 282-292. Erevan: Erevan University.

SEASONAL MELTING OF SURFACE WATER ICE CONDENSING IN MARTIAN GULLIES.. K. J. Kossacki, *Institute of Geophysics, Warsaw University, Pasteura 7, 02-093 Warsaw, Poland, (kjkossac@fuw.edu.pl)*, W. J. Markiewicz, *Max-Planck-Institute for Aeronomy, Max-Planck-Str. 2, 37191 Katlenburg-Lindau, Germany*.

Abstract

In this work we consider when and how much liquid water during present climate is possible within the gullies observed on the surface of Mars. We analyze the conditions for melting of H_2O ice, which seasonally condenses within the troughs of the gullies. The model includes both an approximate topography of the gullies as well as the inclination of the slope where the gullies appear. We have found, that water ice condensed in winter on the walls of gully-like troughs can undergo transition to the liquid phase after complete sublimation of CO_2 ice. The amount of liquid water obtained in this way, depends on several parameters but is most likely to be very small.

Introduction

The gullies are one of the most intriguing features discovered with the recent high resolution orbiter imaging of the surface of Mars. They are mostly found on slopes of craters but also on sides of isolated knobs. The gullies are believed to indicate recent surface flows, presumably of liquid water. To date, the details of the formation process of the gullies are not known. Several authors considered creation of gullies by seasonal melting of ice condensing on the surface ((2), (7), (1), (3)). However, these authors assumed flat surface, or at best smooth crater slope without local topography. According to (3) the conditions for melting of water ice can be satisfied on preferentially insolated slopes almost everywhere on Mars, but only at the surface. On the other hand, (1) has shown possibility of water ice melting to a depth of some meters below the appropriately inclined slopes, but not at the present obliquity.

In this paper we address the problem of the role of the shape of the gullies in the diurnal and seasonal cycles of the surface temperature in the present Mars climate conditions. The local topography needs consideration, because the exact slope of the local surface is of key importance for the energy balance and hence for quantifying the conditions for the possible condensation and melting of water ice. We try to answer the question, when and how much liquid water is it possible to form within the gullies on poleward directed slopes. The first condition for this is that the surface has to be above the melting temperature of water ice. At current obliquity, even at high latitudes Martian surface can warm up to temperatures allowing melting of water ice, but only in a very thin surface layer. The second condition is that the atmospheric pressure is above the triple point of water which is 6.1 mbar. In the north hemisphere pressure is high enough for this even at high latitudes, but in the south only at low and regionally middle latitudes.

Model

We analyze heat transport and evolution of ice distribution in the near surface layer of the regolith, in the vicinity of the north-south oriented trough located on a slope, as are most of the the gullies in the south hemisphere (1). The model includes diurnal and seasonal variations of the position of the Sun as well as seasonal variations of atmospheric pressure and composition. Surface condensation and sublimation is calculated for CO_2 and H_2O, on all facets of the troughs. Condensation and sublimation of H_2O is calculated accounting for the temperature dependence of the sublimation/condensation coefficient correcting Hertz-Knudsen equation (5). The model used in this work is based on that presented in (6). The current version differs from the previous one by allowing local inclination of the surface, accounting for the condensation of atmospheric water and including a more consistent way of treating the scattering of light in the atmosphere toward the surface (4).

Results and conclusions

We present the results obtained for two example locations at middle latitude in both hemispheres. They are 50° S, 50° E and the region of Viking 2 landing site at 48° N, 134° E. The surface density of the condensed water ice strongly depends on the atmospheric conditions, in particular strength of the local eddy diffusion which in turn can be parameterized in terms of the speed of the surface wind. For the volcano slopes (8) predict wind speeds reaching 40 m/s. We performed simulations with wind speed 5 m/s and 30 m/s. Toward the end of winter, more and more of the interior facets of the trough become exposed to the direct light. However, the walls receive significant flux of energy only when they are insolated at small angle to the local normal, in the morning at about 6:00 and in the afternoon about 18:00 LST. Thus, seasonal CO_2 ice remains on the walls for some time after the end of winter. When the trough is located on a slope at 50°S, 50°E the middle parts of the walls remain covered by CO_2 ice until $L_s \sim 250^\circ$. Rapid warming of the surface free of CO_2 ice leads to an almost immediate melting of H_2O ice. In the trough located at 48°N, 134°E melting process starts several sols after the complete sublimation of CO_2 ice, when the layer of H_2O ice is thin enough to have no significant influence on the albedo. Fig.1 displays model results for the Viking 2 landing site at 48°N, 134°E. The gully is assumed to be on a slope inclined by 30°. The curves show the evolution of the diurnal maximum of amount of water ice and liquid water on the middle of the west wall of the trough. Thus, the vertical distance to the surface of the slope from this point is 1m. In this place the surface density of ice reaches the maximum value of about $0.7\ kg\,m^{-2}$, at $L_s \sim 69^\circ$. After this date diurnal maximums of surface

water ice decreases with the rate depending on the chosen form of the sublimation/condensation coefficient α. When $\alpha = 1$ (classical approach), water ice disappears within one sol. When α is a function of temperature (5), water ice persists until $L_s \sim 73^\circ$. The amounts of liquid water, which may appear,

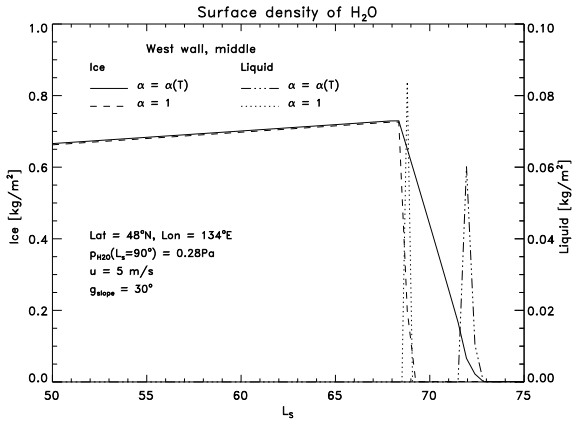

Figure 1: Daily maximum of the surface density of water ice and liquid water, on the middle part of the west wall of the gully-like trough at 48°N, 134°E. The seasonal maximum of vapour pressure is 0.28Pa. The curves are for the sublimation coefficient α = 1, and for $\alpha = \alpha(T)$.

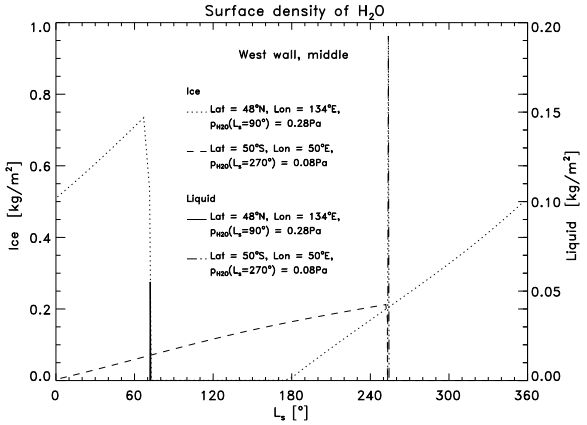

Figure 2: As Figure 1 but for both areographic locations: 48°N, 134°E and 50°S, 50°E, and for a whole Martian year with $\alpha = \alpha(T)$.

are shown as dotted and dashed-dotted lines. The curves are for the diurnal maximum of the surface density of liquid water, again for both forms of the coefficient α. In both cases amount of liquid is less then 0.1 $kg\,m^{-2}$, significantly smaller than the seasonal maximum of the accumulated amount of ice. This is because the surface covered by thick layer of ice has high enough albedo for the water ice to absorb enough energy to significantly sublime but not to melt. Ice can start melting only when the amount of surface ice is so small, that it does not affect the optical properties of the surface (in our model 100μm). For the trough located in the southern hemisphere, at 50°S, 50°E the spring time insolation is higher and the albedo enhanced due to presence of ice does not prohibit warming of the surface to the melting temperature. This results in the surface density of liquid water being comparable to that of the accumulated water ice, Fig. 2. During the day when the liquid appears in a given place, maximum local temperature greatly exceeds boiling point under low pressure of the Martian atmosphere. Thus, no moisture is likely to remain on the surface until next day. The maximum surface density of liquid water for this location is 0.2 $kg\,m^{-2}$.

We analyzed the seasonal cycle of condensation and sublimation of CO_2 and H_2O in the gully like troughs, about ten meters wide. Our simulations show that the H_2O ice deposited in seasonal (winter) cycle on the walls can undergo transition to the liquid phase in spring. When the trough is on the slope at 50°S, 50°E and inclined by 30°, the amount of moisture resulting from our simulations is only about 0.2 $kg\,m^{-2}$ and can appear in a given place during one day only. The rate of condensation is proportional to the wind speed so that simulations with winds of 30 m/s result in about 1 $kg\,m^{-2}$ of liquid water. This amount is probably still not enough to cause surface flow.

References

[1] Costard, F.,F. Forget, N. Mangold and J. P. Peulvast, Formation of Recent Martian Debris Flows by Melting of Near-Surface Ground Ice at High Obliquity, *Science*, *295*, 110–113, 2002.

[2] Haberle, R. M., C. P. McKay, J. Schaeffer, N. A. cabrol, E. A. Grin, A. P. Zent, and R. Quinn, On the possibility of liquid water on present-day Mars, *J. Geophys. Res*, *106*, 23,317–23,326, 2001.

[3] Hecht, M., Metastability of liquid water on Mars, *Icarus*, *156*, 373–386, 2002.

[4] Kieffer, H. H., T. N. Titus, and K. F. Mullins, Mars south polar spring and summer behavior observed by TES: Seasonal cap evolution controlled by frost grain size., *J. Geophys. Res*, *105*, 9653–9699, 2000.

[5] Kossacki, K. J., W. J. Markiewicz, Y. Skorov, and N. I. Kömle, Sublimation coefficient of water ice under simulated cometary-like conditions, *Planet. Space Sci.*, *47*, 1521–1530, 1999.

[6] Kossacki, K. J., and W. J. Markiewicz, Surface temperature of Martian regolith with polygonal features: influence of the subsurface water ice., *Planet. Space Sci.*, *51*, 569–580, 2003.

[7] Mellon, M. T., and R. J. Philips, Recent gullies on Mars and the source of liquid water., *J. Geophys. Res*, *106*, 23,165–23,180, 2001.

[8] Rafkin, S. C. R. and Sta. Maria, M. R. V. and T.I. Michaels, Simulation of the atmospheric thermal circulation of a martian volcano using a mesoscale numerical model., *Nature*, *419*, 697-699, 2002.

SURFACE FEATURES OF THE SOUTH POLAR LAYERED DEPOSITS OF MARS AND POSSIBLE TERRESTRIAL ANALOGUES M. R. Koutnik[1], S. Byrne[2], and B. C. Murray[2], [1]University of Washington (Box 351310, Seattle, WA 98195, mkoutnik@geophys.washington.edu), [2]California Institute of Technology (shane@gps.caltech.edu, bcm@gps.caltech.edu).

Introduction: Data from the Mars Orbiter Camera (MOC) and the Mars Orbiter Laser Altimeter (MOLA) aboard the Mars Global Surveyor (MGS) mission have provided important new clues to the past history of the South Polar Layered Deposits (SPLD). There are distinct features presented here that have been observed almost exclusively with these data sets and are unique to the south polar region of Mars. Although we do not conclusively know the origin of these features and don't rule out other interpretations, we consider here the possiblity that relatively recent subglacial volcanism and possibly the influence of ice flow may have been active in their formation.

Regional Description: We focus primarily on one region of the SPLD, approximately 190° - 230° W, 85° - 87°S (no MGS coverage south of 87°), where nearly all the features discussed here are found. Most extensive in this area are enigmatic large-scale grooves, termed here the "Wire Brush" terrain. Coverage of the Wire Brush terrain in the MOLA shaded relief map are showin in Figure 1. This region can be identified in Viking coverage of this area and shows that the grooves possibly have a connection with the current residual cap. Poleward of Chasma Australe and possibly one area off the cap are the only other locations where we see this grooved pattern at the south pole.

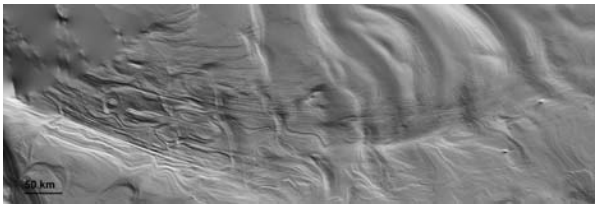

Figure 1. MOLA shaded relief map of the full extent of the Wire Brush Region, 190° - 230° W, 85° - 87°S.

The overall grooved pattern of the Wire Brush region is continuous for more than 300 km, though tracing of individual grooves is difficult to do with certainty for more than about 50 km. The grooves do continue linearly across local topography and are several hundreds of meters across with vertical relief of only a few tens of meters. The slope over the extent of the wire brush terrain is very slight and the grooves to do not seem to be influenced by any larger scale topography.

Near to the Wire Brush terrain there are numerous other unique features that may provide clues to the origin and timing of formation of the large-scale grooves.

Sinuous Ridges and Enclosed Chasma: There are sinuous ridges cross-cutting the Wire Brush which we have termed "Snakes". The Snakes are up to 2 km in width and tens of km long, although they are only a few tens of meters high. The presence of such vertical features is unusual. It could imply an episode of deformation or fracturing that has been filled subsequently with more resistant material than the surrounding layered deposits. The Snakes are found primarily within the Wire Brush but do extend out from this region as well. At least one Snake extends into an adjacent elongated depression and can be seen to interact with layering in this chasma. The enclosed chasma, shown in Figure 2, is a significant feature in association with the Wire Brush terrain. Unlike Chasma Australe, this chasma does not cut all the way through the layered terrains to the underlying basement rock and does not have an outlet. Given the positions of these two chasmas, on both sides of the Wire Brush Terrain, it is possible that all of these features may be related.

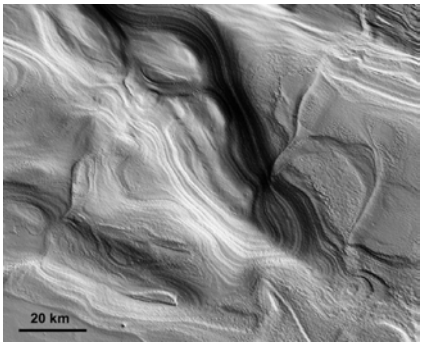

Figure 2. Enclosed depression adjacent to the Wire Brush region (seen in upper right). The Snake features can be seen cutting into the chasma from the right of the image.

Polar Potholes: Another interesting component of the Wire Brush and surrounding region is the presence of small, circular pits. They are found distinctly in the regions 190° - 230° W, 85° - 87° S (within the Wire Brush terrain) and 135°-175° W, 85°-87° S and can be roughly distinguished by orientation and morphology within these two regions. All of the individual polar potholes in both regions are approximately 50-100 m

in diameter. The potholes found within the Wire Brush region are circular, distinct forms. An interesting grouping of potholes is shown in Figure 3 where they are clustered in local circular depressions. The entire population of potholes is found only on the south polar layered deposits and these clustered forms are only in the Wire Brush region.

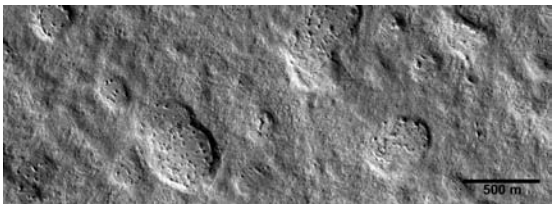

Figure 3. MOC NA m1102900 showing a distribution of potholes in the Wire Brush terrain that are grouped in larger circular depressions.

Mounds: North along the direction which the grooves trend in the Wire Brush terrain, there is a clustering of distinctive mounds, shown in Figure 4 and can also be seen in the far right of Figure 1. The mounds are few km in diameter and all have similar topographic features as observed from MOLA. The occurrence of these mounds in this location (and nowhere else we have found) and that they share a similar shape leads us to believe they could have a volcanic origin.

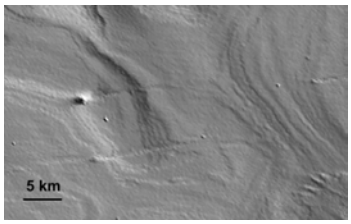

Figure 4. Two of the mound features associated with the Wire Brush region. They appear to act as obstructions, as evidenced by the linear "tail".

Interpretations: The Wire Brush region and associated features could conceivably be the signature of unusual past winds, ancient ice sheet motion, or episodes of catastrophic flooding originating from beneath earlier residual caps. We have explored these interpretations [1] and now look for a mechanism or combination of mechanisms that can best explain all the features we have presented here near to the Wire Brush terrain. Assuming the features we see in this localized region of the SPLD originate from the same or a similar event in south polar history, the interpretation of subglacial volcanism is favored here. As the clustered mounds, enclosed chasma, and sinuous ridges are especially supportive evidence for volcanism. As well, elsewhere in the south polar region, Ghatan and Head [2] have proposed a past episode of subglacial volcanism of Hesperian age. We do not attempt to explain why there would be a period of increased heat flux in this region but acknowledge that an event like this cannot be completely ruled out.

We will also assess the possiblity of ice sheet motion driven by basal melting from changes in cap configuration, not from increased heat flux, active at the south pole in the Martian past. Basal melting beneath the Martian polar caps has been considered possible but is highly sensitive to surface temperature, cap thickness, thermal conductivity, and heat flux [3, 4]. With a heat flux one-third to one-half the terrestrial value [3] basal melting can most easily occur when the ice cap is thick and the conductivity is low, assuming negligible heat production from internal deformation [4]. If basal melting or meltwater generation occurred in the past without increased heat flux, it is assumed that the south polar cap was more extensive or there was a warmer climate. We look at the cap configurations and timing necessary to produce meltwater at the base for the south polar cap.

If the base was lubricated (by cap configuration or increased heat flux) it could be possible to produce large grooved features in the layered terrain by ice flow, analogous to terrestrial ice streams. We also consider the possiblity of a large outburst flood occurring, as seen in Icelandic jokulhlaups. It has been proposed that Chasma Australe was formed by a large outburst flood [5] and, given the possible relation of these features to the Chasma, these same arguments could apply for the Wire Brush region.

We consider the processes of subglacial volcanism and ice sheet motion to be possibly active in forming the enigmatic surface features seen in this region of the Martian south pole. The unique location of all these features is evidence of a significant event in the Martian past that had a considerable influence on the SPLD.

References: [1] Koutnik, M., et al. (2003) 6th Internation Mars Conference. [2] Ghatan, G. and J. Head (2002) *J. Geophys. Res.* 107, E7, 2002. [3] Clifford, S. (1987) *J. Geophys. Res.* 92, B9, 9135-9152. [4] Larsen and Dahl-Jensen (2000) *Icarus* 144, 456-462 [5] Aquita, F. et al. (2000*) Icarus* 144, 302-312.

POLAR WANDER IN THE GEOLOGICAL HISTORY OF MARS: CONSTRAINTS FROM TOPOGRAPHY STATISTICS. ***M. A. Kreslavsky***[1,2] and ***J. W. Head***[1], [1]Dept. Geological Sci., Brown University, Providence, RI 02912-1846, USA; misha@mare.geo.brown.edu, [2]Astronomical Institute, Kharkov National University, Ukraine.

Introduction: True polar wander (that is change of position of the spin axis of a planet relative to the crust) has been hypothesized for Mars long ago (see [1] for review). The general idea is the formation of Tharsis rise should shift any initial spin axis position so that the rise is centered at the equator.

P. Schultz and A. Lutz [2,3] presented two principally different lines of observational evidence for true polar wander in the past. First, they found [2] a significant excess of large impact craters made by grazing impacts, and attributed them to impacts of tidally decelerated former satellites of Mars, which dynamically could only orbit Mars close to its equatorial plane; location and orientation of such craters suggested a position of the equator very different form that of the present-day. Second [3], Schultz and Lutz found concentration of specific deposits in Arabia Terra and on the opposite side of the planet (Medusae Fossae Formation) which they interpreted as remnants of former layered terrain similar to the present-day polar caps.

Recently, analysis of strong magnetic anomalies in the southern highlands of Mars provided some new evidence for the polar wander in the past. J. Arkani-Hamed [4] showed that if one suggests that the crustal magnetization reflects the extinct planetary dipole magnetic field at some moment in the past, then inferred positions of the magnetic dipole axes are clustered in a 30° wide area around 130°W 25°N. Since the deflection of the magnetic dipole axis from the spin axis is not high (at least for the same mechanism of magnetic field generation as on the Earth), the inferred pole position in the Early Noachian is close to this point. This point does not coincide with, but is rather close to, the former pole location proposed in [3].

Analysis of the current topography and rotation state of Mars led B. G. Bills and T. S. James [5] to the conclusion that the present-day rotation of Mars is secularly unstable. If the data used for the inference are accurate, than the spin axis can wander at a rate defined by the characteristic time scale of relaxation of elastic stresses in the lithosphere.

Our recent studies showed pronounced latitudinal zonality of the statistical characteristics of the kilometer-scale topography of Mars [6-8]. Here we analyze constraints that our findings put on the hypotheses of past true polar wander.

Observations: Statistical analysis of martian topography along topographic profiles obtained with MOLA altimeter [9] onboard MGS showed [6] that the circumpolar regions (above 60° latitude) are consistently smoother at kilometer and subkilometer scales than the equatorial zone (below 30° latitude) with a gradual transition with some statistical peculiarities [7] between them. Recently we found [8] that the latitudinal trend of roughness is accompanied by even more pronounced latitudinal trend of steep slope occurrence. **Fig. 1** shows the relative frequency of slopes steeper than 20° as a function of latitude for typical southern highlands in Terra Cimmeria. It is seen that the steep slopes practically disappear above 50° latitude. **Fig. 2** shows locations of the steepest slopes on Mars. The paucity of extremely steep slopes at high latitudes is obvious. (Detailed analysis of the steepest slope occurrence will be published elsewhere).

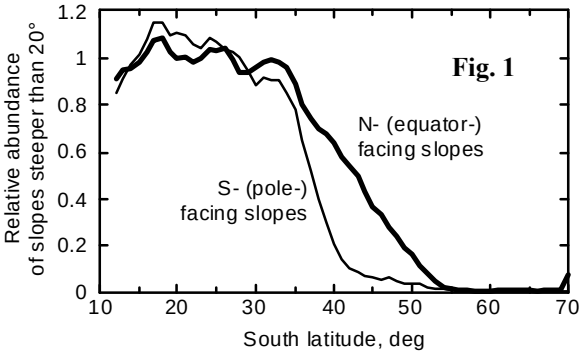

When we move from the equator to the poles, the abundance of steep slopes drops down sooner for the pole-facing slopes and later for the equator-facing slopes (Fig. 1). This produces a strong asymmetry in steep slope abundance at 40-50°S.

Fig. 3 shows the map of normalized median differential slope at 0.3 km baseline inferred from along-profile statistics. This parameter is a characteristic of the north - south slope asymmetry (see [8] for details). Fig. 3 shows two distinctive belts around 45° latitude in both hemispheres with the opposite sign of the asymmetry parameter, which shows that the equator-facing slopes in both bands are systematically steeper than pole-facing slopes. Note that the map in Fig. 3 reflects the behavior of typical (a few degree steep) slopes, while Fig. 1 and 2 are related to the steepest slopes on the planet. (For discussion of other features seen in Fig. 3 see [8].)

Both belts of slope asymmetry (Fig. 3) show a small deflection from ~45° parallel to the south in the western hemisphere and to the north in the eastern one. The

bands are well approximated by minor circles with 45° radii and the centers shifted ~5° from the poles toward 60-90°W in the northern hemisphere and to the opposite direction in the southern hemisphere.

Interpretation: The approximate symmetry relative to the equator strongly suggests that the role of insolation was important in the formation of the observed trend and the anomalous belts. F. Costard and co-authors [9] have pointed to the possibility of melting of thick layers of ground ice at higher obliquity. Their calculations showed that starting at ~35° obliquity, the summertime day-average surface temperature reaches 0°C at high (>~60°) latitudes; for higher obliquity the zero summer isotherm shifts toward the equator. The day-average temperature can exceed the ice melting point down to ~40° latitude at 45° obliquity, but only on steep pole-facing slopes.

We suggest that transient melting of ground ice in summer during periods of high obliquity promotes downslope movement of material and lowers steep slopes. Over geological time scales, this process removed almost all steep slopes above 50° latitude. At 40-50° latitude, the summertime melting and related movement can occur only on pole-facing slopes, making these slopes less steep. The equator-facing slopes in this zone remain intact. This produces the observed latitudinal trend and strong asymmetry of the steepest slopes.

Implications for past polar wander. Well preserved steep slopes in the equatorial highlands are mostly related to impact craters. If our interpretation of the latitudinal trend of the steep slope occurrence and the slope asymmetry bands is correct, the preservation of steep slopes in the equatorial highlands means that the day-average temperature have never exceed 0°C in these regions. Hence, these regions have never been at high latitudes during the time comparable to the highland crater population age. This constrains the true pole position during the whole Amazonian (and probably the Hesperian; more detailed analysis is necessary) to the vicinity of the present poles.

The deflection of the belts from 45° latitude might be related to effects of persistent atmospheric circulation or albedo patterns during the high obliquity epochs. We believe that it is more plausible that the current pole position is shifted ~5° from a formerly stable or long-term-average position. The direction of this shift is neither similar nor opposite to the shift of the geometric centers of the present-day polar layered deposits [10]. The same is true for the platy unit, a geologically older layer of the northern polar deposits [11]. Thus, we see not too strong, but positive evidence for polar wander of ~5° amplitude around its average position, which is determined by the centers of the slope asymmetry belts. The dynamic plausibility of such a process is the subject of a separate study.

Thus, we conclude that planetary-scale polar wander has not occurred since the Hesperian. The topographic information about the Noachian is more obscured, because of the large number of steep slopes produced by cratering and tectonics since that time. However, some information could survive in the topographic record of the Noachian-age highlands. We are presently analyzing this information to test the hypothesis of a different location of the spin axis in the Noachian.

References: [1] Ward, W. R. (1992) In *Mars*, Univ. Arizona Press, 298-320. [2] Schultz, P., and Lutz-Garihan A. B (1982) *Proc. LPSC XIII*, A84-A96. [3] Schultz, P., and Lutz A. B. (1988) *Icarus 73*, 91-141. [4] Arkani-Hamed, J. (2001) *GRL 28*, 3409-3412. [5] Bills, B. G., and T. S. James (1999) *JGR 104*, 9081-9096. [6] Kreslavsky, M. A. and J. W. Head (2000) *JGR 105*, 26695-26712. [7] Kreslavsky, M. A. and J. W. Head (2002) *JGL 29*, 1719, 10.1029/2002GL015392. [8] Kreslavsky, M. A. and J. W. Head (2003) *JGL 30*, 10.1029/2003GL017795 [9] Costard, F. et al. (2002) *Science 295*, 110-113. [10] Fishbaugh, K. E., and J. W. Head (2001) *Icarus 154*, 145-161. [11] Byrne, S. and B. C. Murray (2002) *JGR 107*, 10.1029/2001JE001615.

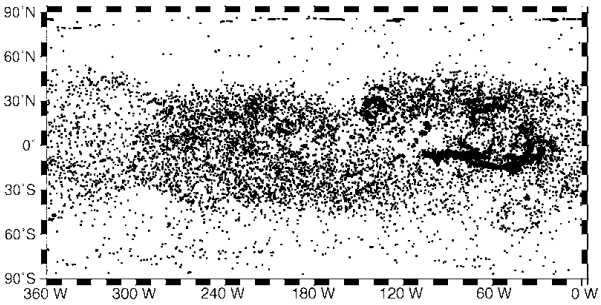

Fig. 2. Distribution of the steepest slopes on Mars. Each dot denotes a 300 m long segment of MOLA profile with slope steeper than 30°. In high-concentration areas the dots strongly overlap.

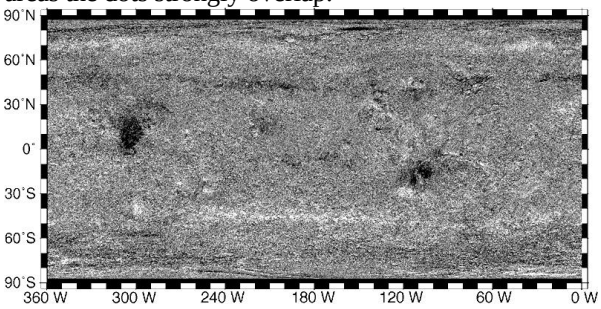

Fig. 3. Distribution of slope asymmetry parameter. Brighter (darker) shades mean that north- (south-) facing slopes are steeper.

DETERMINING STRUCTURAL AND MECHANICAL PROPERTIES OF SNOW WITH A HIGH-RESOLUTION PENETROMETER. K. Kronholm[1] , J. B. Johnson[2] and M. Schneebeli[1], [1]WSL Swiss Federal Institute for Snow and Avalanche Research SLF, Flüelastrasse 11, CH-7260 Davos Dorf, Switzerland, kronholm@slf.ch, [2]Cold Regions Research and Engineering Laboratory CRREL, Fairbanks, Alaska.

Introduction: On Earth, and possibly in extraterrestrial environments, the snow cover consists of individual snow layers that metamorphose over time. The stratigraphic record of snow layers is the result of erosional and depositional events. Adjacent layers differ in terms of their structural and mechanical properties. The structural properties of the upper snow layers are important for the chemical exchange between the atmosphere and the snow cover, snow hydrology, and the spectral properties of the snow cover. The mechanical properties are relevant for over-snow trafficability of vehicles and animals, and for avalanche release. Traditionally, snow is characterized by subjective measures of grain shape and size, and hardness [1]. Until recently, no fully automatic and objective methods to describe snow microstructure were available. The recent development of a snow micropenetrometer (SMP) now provides an objective way to measure the structural and mechanical properties of snow layers at different spatial scales [2, 3]. The SMP interpretation methods used for snow have also been used to objectively characterize soil [4].

Methods: With the SMP, we measured the penetration resistance of a seasonal snow cover. The force-distance signal had a sampling interval of 4 µm. The microstructural properties (microstructural element length and mean grain size) were derived from the signal by relating each force spike to a fracture of a microstructural element. The distance between fractures is directly related to the size of the microstructural elements [5]. Mechanical properties (compressive strength and elastic modulus) were derived using a mechanical theory developed for cohesive granular materials [5]. For comparison, a traditional stratigraphic profile with grain shape, size and hand hardness was done in addition to the SMP measurements. Snow samples were taken from individual layers. The spatial variation of structural and mechanical properties was analyzed for individual layers using geostatistics.

Results: The microstructural element length and the mean grain size derived from the penetrometer signal corresponded well with the results from the traditional methods. The derived compressive strength was within the previously reported ranges [Fig. 1]. The derived elastic modulus was a factor two lower than previously reported values. The mechanical properties of individual layers showed a large spatial variation on a single slope. The spatial variation in microstructure was not as large. Large spatial variation in structural and mechanical properties of individual layers was mainly found in layers deposited during windy conditions.

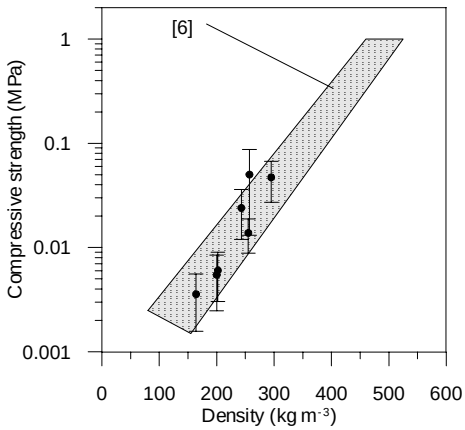

Fig. 1. Compressive strength of snow layers as a function of bulk density. Previously reported values are indicated by the grey area.

Discussion: The large spatial variation found in a terrestrial snow cover emphasizes the need to carry out multiple measurements to accurately characterize the three-dimensional variations of the snow cover properties. The representativity of a single measurement depends on the influence of wind in the snow stratigraphy. On Earth, a single measurement is usually not representative for a large area. The SMP can be used to derive important structural and mechanical properties of individual snow layers in a natural setting. An accurate description of the structural and mechanical properties of the upper snow layers and low density layered deposits on the polar areas of Mars could be obtained with a micropenetrometer mounted on a rover. Measurements could be done at certain intervals as the rover explores the Martian surface.

References: [1] Colbeck S. C. et al. (1990) *IAHS-ICSI Publ.* [2] Johnson, J. B. and Schneebeli M. (1998). Snow strength penetrometer, United States Patent 5,831,161, U. S. Patent Office. [3] Schneebeli M. and Johnson J. B. (1998) *Ann. Glaciol. 26*, 107-111. [4] Johnson, J. B. (2000). *Transportation Research Record, 1714*, 83-88. [5] Johnson J. B. and Schneebeli M. (1999) *Cold Reg. Sci. Technol. 30*, 91-100. [6] Mellor M. (1975) *IAHS Publ. 114*, 251-291.

PRELIMINARY CHARACTERIZATION OF A MICROBIAL COMMUNITY OF ROCK VARNISH FROM DEATH VALLEY, CALIFORNIA. K. R. Kuhlman[1], M. T. La Duc[1], G. M. Kuhlman[1], R. C. Anderson[1], D. A. Newcombe[1,2], W. Fusco[2], T. Steucker[2], L. Allenbach[2], C. Ball[2], and R. L. Crawford[2], [1]Jet Propulsion Laboratory, California Institute of Technology, 4800 Oak Grove Dr., Pasadena, CA 91109, kkuhlman@jpl.nasa.gov; [2]Environmental Research Institute, University of Idaho, Moscow, ID 83844, crawford@uidaho.edu.

Introduction: Rock varnish (also referred to as desert varnish in the literature because it is particularly noticeable in desert environments) is a dark, thin (typically 50-500µm thick), layered veneer composed of clay minerals cemented together by oxides and hydroxides of manganese and iron [1-4]. Some scientists suggest that varnish may provide a historical record of environmental processes such as global warming and long-term climate change. However, despite more than 30 years of study using modern microanalytical and microbial culturing techniques, the nucleation and growth mechanisms of rock varnish remain a mystery [4,5].

Rock varnish is of interest to the Mars science community because a varnish-like sheen has been reported on the rocks at the Viking Lander sites [6,7]. It therefore important for us to understand the formation mechanisms of terrestrial varnish – abiotic, biotic, or a combination of the two -- as this understanding may give us clues concerning the chemical and physical processes occurring on the surface of Mars. It is strongly believed by some in the biogeochemistry community that microbes have a role in forming rock varnish, and iron- and manganese-oxidation by microbes isolated from varnish has been extensively investigated [815-16]. Only two of these studies have investigated the microbial genetics of varnish [16,16]. These studies examined the morphological, physiological and molecular characteristics of microbes that had previously been cultured from various rock varnishes and identified the cultivars using 16S rDNA sequencing techniques. However, it is well known that most of organisms existing in nature are refractory to cultivation [17-20], so many important organisms would have been missed.

The currently described work investigates the genetics of rock varnish microbial community from a site in the Whipple Mtns., south of Death Valley, CA, near Parker, Arizona (Figure 1). We employed both cultural and molecular techniques to characterize the microorganisms found within the varnish and surrounding soil with the objectives of (a) identifying microorganisms potentially involved in varnish formation, and (b) discovering microorganisms that simply use the varnish as an extreme habitat.

Varnish collection: Since we are investigating the biocomplexity of the microbial communities of rock varnishes, it was critical that the samples be collected aseptically as possible. The samples were approached from the downwind direction, photographed *in situ*, picked up at arm's length using sterile gloves, placed within sterile Whirl-paks™ and sealed. Loose dirt on the undersides of the varnished rocks has proven to be a contamination problem during storage and harvesting of the varnish in the laboratory. The samples were then wrapped in protective material to prevent damage. In future collections, glass containers will be used to prevent the deposition of polymers from the Whirl-paks™ on the surface of the varnish, thus contaminating the surface for microanalytical work [21].

The varnish was harvested from the host rock in a laminar flow bench. A Dremel tool with a coarse bit that had been flame sterilized was used to grind the varnish off the host rock and into a sterile container [22]. For use as controls we also collected soil samples adjacent to some of the varnished clasts.

Figure 1. Macro photograph of a varnished clast used in our study. The underlying grid has 10 divisions per inch.

Microbial Enumerations: Powdered rock varnish (0.1 gram) was added to 1 milliliter of sterile double-distilled H_20. The samples were then stained with a stock DAPI (or Acridine Orange) (50mg/mL) solution. Samples were filtered onto 25mm Millipore Isopore 22µm pore size black polycarbonate filters with Whatman 25mm GF/F filters used for support. Fluorescing cells were counted on a Zeiss Research epifluorescence microscope equipped with an Osram

Xenon short arc photo optic lamp XBO 75W, and Chroma #31000 filter set for DAPI/Hoechst/AMCA.

The mean field (n) counted per sample was 57.16. The field standard deviation per sample was 7.48. The rock varnish had an average DAPI direct count of $9.0x10^7$ cells $gram^{-1}$ (standard deviation = 1.2E+07). There was no determinable difference between DAPI and Acridine Orange direct counts.

Cultivable UV-resistant microorganisms: Five distinct colony types were purified from TSA plates after exposure to the UV irradiation treatment. These strains were examined microscopically using both a standard light and a transmission electron microscope (TEM). The 16S rDNA gene of each isolated was amplified by PCR, cloned and sequenced for comparison to the RDP phylogenetic database.

We examined each cultivated strain for its resistance to UV(C) irradiation. The strains were quite resistant, and still showed growth on TSA plates after exposure for five minutes at UV(C) intensities that readily killed E. coli. Affiliations were estimated for three of the strains to genus level only using a similarity level of >98%.

Strain RV1 (white colony). Multiple *Arthrobacter* strains were found in a white colony (*A. polychromogenes, A. ramosus, A. oxidans, A. globifromis, and* unspeciated *A. spp.* show 99% sequence similarity with this isolate). Eppard, et al. (1996) reported the culturing of three strains highly related to *Arthobacter agilis* from rock varnish in the Mojave desert, but did not report UV resistance. [13].

Strain RV2 (orange colony). Various strains of *Curtobacterium flaccumfaciens* (e.g., AY273208.1) and an unidentified glacial ice bacterium (AF479342.1) show 98% sequence similarity to this isolate. Thus, this strain could be a candidate for survival in conditions such as those found in the polar regions of Mars.

Strain RV4 (black colony). This strain shows 16S rDNA sequence similarities of 98% (forward primers) and 99% (reverse primers) to a *Geodermatophilus obscura* originally isolated from soil samples from the Amargosa Desert of Nevada by Luedemann (1968) [20] and found in Negev desert soil and monuments by Eppard, et al., (1996) [13]. The strain's morphological and growth characteristics fit the description of *Geodermatophilus obscura* cluster I as described by Eppard, et al. (1996).

The uncultivable microbial community: We generated three rDNA libraries from the Death Valley rock varnish community DNA and two control libraries from soil adjacent to the varnished rock and lacking varnish. Varnish 16S rDNA libraries were prepared for Eubacteria and Archaea, and an 18S rDNA library for Eukarya. The control soil libraries were prepared for Eubacteria and Archaea. An 18S rDNA control library for Eukarya was not obtained for the soil despite six attempts. Between 100-200 clones were prepared for each library.

The clones within each library have been arranged into related subgroups through examination of their RFLP patterns, and 16S rDNA PCR products of representative members of each subgroup were sequenced.

Acknowledgements: This work was sponsored by the Jet Propulsion Laboratory (JPL) Director's Research and Development Fund and carried out at JPL, California Institute of Technology, under a contract with the National Aeronautics and Space Administration.

References: [1] Potter, R.M. and G.R. Rossman (1977) *Science*, 196(4297), 1446-1448. [2] Potter, R.M. and G.R. Rossman (1979) Chemical Geology, **25,** 79-94. [3] Perry, R.S. and J.B. Adams (1978) *Nature*, **276**(5687) 489-491. [4] Broecker, W.S. and T.Z. Liu (2001) *Geology Today*, **11**(8) 4-10. [5] Dorn, R.I. (1998) *Rock Coatings. Developments in Earth Surface Processes*. Vol. 6, Amsterdam: Elsevier. [6] Guinness, E.A., R.E. Arvidson, et al. (1997) *Journal of Geophysical Research-Planets*, **102**(E12) 28687-28703. [7] Israel, E.J., R.E. Arvidson, et al. (1997) *Journal of Geophysical Research-Planets*, **102**(E12) 28705-28716. [8] Dorn, R.I. and T.M. Oberlander (1981) *Science*, **213**(4513) 1245-1247. [9] Krumbein, W.E. and K. Jens (1981) *Oecologia*, **50**(1) 25-38. [10] Staley, J.T., M.J. Jackson, et al. (1983) *Bmr Journal of Australian Geology & Geophysics*, **8**(1) 83-87. [11] Taylor-george, S., F. Palmer, et al. (1983) *Microbial Ecology*, **9**(3) 227-245. [12] Palmer, F.E., J.T. Staley, et al. (1986) *Geomicrobiology Journal*, **4**(4) 343-360. [13] Hungate, B., A. Danin, et al. (1987) *Canadian Journal of Microbiology*, **33**(10) 939-943. [14] Grote, G. and W.E. Krumbein (1992) *Geomicrobiology Journal*, **10**(1) 49-57. [15] Eppard, M., W.E. Krumbein, et al. (1996) *Archives of Microbiology*, **166**(1) 12-22. [16] Perry, R.S., J. Dodsworth, et al. (2003) *NASA Astrobiology Institute Annual Meeting*, NASA Ames Research Center, Moffet Field, CA. [17] Amann, R.I., W. Ludwig, and K.H. Schleifer (1995) *Microbiological Reviews*, **59**(1) 143-169. [18] Barns, S.M., R.E. Fundyga, et al. (1994) *Proceedings of the National Academy of Sciences of the United States of America*, **91**(5) 1609-1613. [19] Ward, D.M., R. Weller, and M.M. Bateson (1990) *Nature*, **345**(6270) 63-65. [20] Torsvik, V., J. Goksoyr, and F.L. Daae (1990) *Applied and Environmental Microbiology*, **56**(3) 782-787. [21] Perry, R.S., (2002) Personal communication. [22] Luedemann (1968) Journal of Bacteriology, 96(5), 1848-1858.

PRELIMINARY RESULTS FROM A SURVEY OF CANDIDATE PERMAFROST AND PERIGLACIAL FEATURES ON MARS. D. W. Leverington[1], [1]Center for Earth and Planetary Studies, Smithsonian Institution, Washington, DC 20560; leveringtond@nasm.si.edu.

Introduction: Several studies have noted that high-resolution images acquired by the Mars Observer Camera (MOC) may be used to identify candidate Martian permafrost and periglacial features at scales more consistent with their terrestrial counterparts. In the present research, a comprehensive survey of Martian candidate features is being conducted.

Background: Typical terrestrial permafrost and periglacial features (where "periglacial" refers here to environments where frost action dominates) include frost mounds, earth hummocks, ice wedges, sorted circles, thermokarst features, and features produced by gelifluction. Terrestrial *frost mounds* are mound-shaped landforms that are produced in a variety of ways by the combined processes of ground freezing and groundwater movement [1]. Although large frost mounds such as pingos [2,3] are greater than 10 m in height and 100 m in horizontal dimension, frost mounds can be as small as several meters across. *Earth hummocks* are hummocks that have a core of silty and clayey mineral soil and show evidence of cryoturbation [1,4]. On the Earth, these features are believed to form only in permafrost regions; individual earth hummocks are typically 50 to 150 cm across, and often occur in dense clusters. *Ice wedges* are formed mainly in zones of continuous permafrost through the combined and repeated processes of thermal contraction cracking and the penetration of surface water into these cracks by water flow and by the formation of hoar frost [5,6]. Terrestrial ice wedges can be about 10 cm to 3 m in width at the surface, tapering to zero width at a depth of 1-20 m. Ice wedges, and their sand wedge counterparts [7], are typically expressed at the surface in plan view as a network of polygons. *Sorted circles* are tightly-spaced circular domains of fine-grained materials surrounded by gravel ridges, and are formed by freeze-thaw action [8]. On the Earth, the circular domains are typically about 2-4 m across, and the gravel ridges are about 20 cm high [9]. *Thermokarst features* are caused by changes in ground thermal regimes that result in ice thaw and ground subsidence [10-12]. *Gelifluction features* are formed by downslope creep of frozen ground; individual terrestrial lobes can be up to tens of meters wide and hundreds of meters long.

Permafrost and Periglacial Features on Mars: Near-surface ice is stable at latitudes poleward of about 40 degrees [13-15]. Features cited in the Viking era as possible indicators of near-surface ice included alas-like flat-floored depressions [16-18], grooved and lobate landslide and valley deposits that implied processes of rock-glacier flow and gelifluction [19-23], crater ejecta blankets with lobate margins and radial flow patterns [16,24-25], and mid-latitude terrain softening [26]. Examples of patterned ground, most notably networks of relatively large polygons, were cited as possible indicators of near-surface ice and the activity of periglacial processes [16,20,24,27-29]. Clusters of small circular to elongated mounds were observed in Gusev crater and hypothesized to be related to terrestrial frost mounds [30].

The availability of high-resolution MOC images over widely-distributed locales on Mars provides an excellent opportunity for identifying possible periglacial and permafrost features on scales comparable to terrestrial features. For example, tongue-shaped lobes on Mars have now been identified as likely near-surface ice-rich sediment bodies within which processes related to terrestrial rock glaciers may be operating [31,32]. A widespread mid-latitude surface unit has been identified as a possible mantle of ice-rich materials [33]. Local-scale polygonal terrains have been identified [34-36] at latitudes consistent with regions where near-surface water may have been detected [37].

A Survey of Small-Scale Hummocky and Polygonal Features on Mars: High-resolution MOC images are being examined for features that have morphological similarities with terrestrial permafrost and periglacial features. To date, over 250 images have been found that show features considered to be good candidates for Martian analogs of terrestrial hummocks, ice-wedge networks, and gelifluction and thermokarst features. Consistent with other studies [36], these features have been found to predominantly exist at latitudes poleward of about 55 degrees.

Both hummocky and polygonal terrains are prevalent in a number of high-latitude regions on Mars. High-latitude hummock features are often found in large groups of uniformly-sized (~10 m across) and spaced (~20 m) hummocks. Local-scale Martian polygonal networks have been found with a wide variety of geometries, including rectangular, random orthogonal, simple polygonal, and radial orthogonal; the dimensions of individual network units vary widely, with apparent sizes as small as ~10 m or less. While

polygonal features are often clearly evident (Fig.1), they are sometimes relatively subtle features due to factors such as stripping or burial of materials (Fig.2). Dark polygonal features are found on a small proportion of polar dunefields (Fig.3), although most or all of these features may simply be the temporary product of aeolian and defrosting processes. Permafrost-related polygons would be useful for constraining the recent mobility of polar dunes and associated materials.

Conclusions: Strong candidates for Martian analogs of terrestrial permafrost and periglacial features exist in high-latitude regions of Mars. Features such as hummock fields, local-scale polygonal networks, and potential gelifluction and thermokarst features continue to be identified and examined.

References: [1] ACGR (1988) NRC, Tech. Mem. 142. [2] Mackay, J.R. (1977*) Can. J. Earth Sci., 14*, 209-222. [3] Mackay, J.R. (1990) *Can. J. Earth Sci., 27*, 1115-1125. [4] Mackay, J.R. (1980) *Can. J. Earth Sci., 17*, 996-1006. [5] Mackay, J.R. (1974) *Can. J. Earth Sci., 11*, 1366-1383. [6] Burn, C.R. (1990) *Perm. Peri. Pro., 1*, 3-14. [7] Murton, J.B., French, H. M. (1993) *J. Quat. Sci., 8*, 185-196. [8] Kessler, M.A., Werner, B.T. (2003) *Science, 299*, 380-383. [9] Hallet, B. (1990) *Can. J. Phys., 68*, 842-852. [10] Mackay, J.R. (1970) *Can. Geotech. J., 7*, 420-432. [11] French, H.M. (1974) *Can. J. Earth Sci., 11*, 785-794. [12] Burn, C.R., Friele, P.A. (1988) *Arctic, 42*, 31-40. [13] Jakosky, B.M., Farmer, C.B. (1982) *JGR, 87*, 2999-3019. [14] Clifford, S.M., Hillel, D. (1983) *JGR, 88*, 2456-2474. [15] Mellon, M.T. *et al*. (1997) *JGR, 102*, 19,357-19,369. [16] Rossbacher, L.A., Judson, S. (1981) *Icarus, 35*, 39-59. [17] Costard, F.M. (1990) *LPI Tech. Rep. 90-06*, 114-115. [18] Costard, F.M., Dolfus, A. (1987) *LPI Tech. Rep. 87-02*, 16-17. [19] Carr, M.H. (1984) NASA SP-469, 207-263. [20] Lucchitta, B.K. (1981) *Icarus, 45*, 264-303. [21] Squyres, S.W. (1978) *Icarus, 34*, 600-613. [22] Colaprete, A., Jakosky, B.M. (1998) *JGR, 103*, 5897-5909. [23] Mangold, N., Allemand, P. (2001) *Geophys. Res. Lett., 28*, 407-410. [24] Carr, M.H., Schaber, G.G. (1977) *JGR, 82*, 4039-4054. [25] Horner, V.M., Greeley, R. (1987) *LPI Tech. Rep. 87-02*, 25. [26] Squyres, S.W., Carr, M.H. (1986) *Science, 231*, 249-252. [27] Rossbacher, L.A. (1987) *LPI Tech. Rep. 87-02*, 38-39. [28] Mellon, M.T. (1997) *JGR, 102*, 25,617-25,628. [29] Lucchitta, B.K. (1983) *4th Int. Conf. on Permafrost*, 744-449. [30] Cabrol, N.A. *et al*. (2000) *Icarus, 145*, 91-107. [31] Marchant, D.R., Head, J.W. (2003) *6th Int. Conf. on Mars*, #3091. [32] Howard, A.D. (2003) *LPS XXXIV*, #1065. [33] Mustard, J.F. *et al*. (2001) *Nature, 412*, 411-4114. [34] Seibert, N.M., Kargel, J.S. (2001) *GRL*, 28, 899-902. [35] Yoshikawa, K. (2000) *2nd Mars Polar Sci. Conf*., #4045. [36] Kuzmin, R.O. Zabalueva, E.V. (2003) *LPS XXXIV*, #1912. [37] Boynton, W.V. *et al*., (2002) *Science, 297*, 81-85.

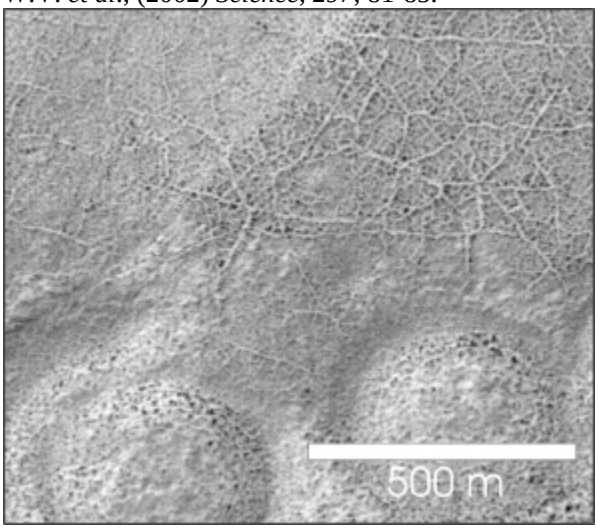

Figure 1 (MOC M0807668)

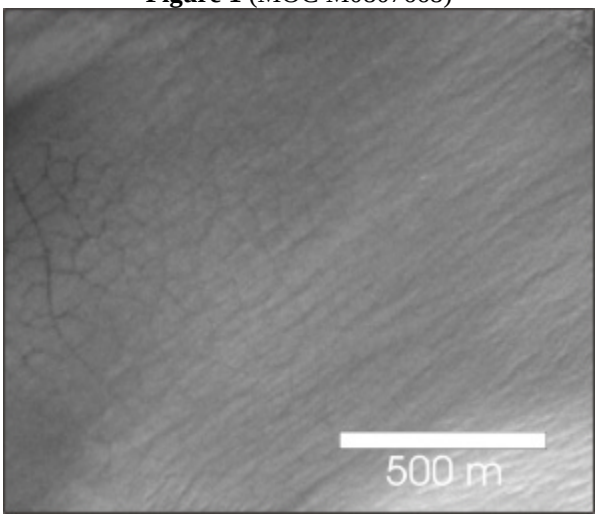

Figure 2 (MOC E1300770)

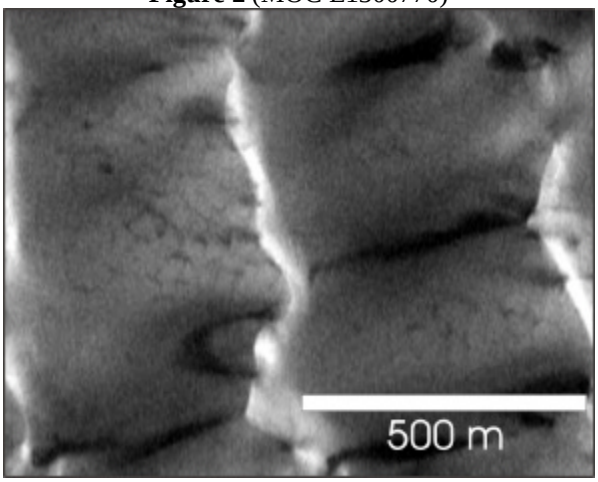

Figure 3 (MOC SP249004)

A GCM RECENT HISTORY OF THE NORTHERN MARTIAN POLAR LAYERED DEPOSITS. B. Levrard, J. Laskar, *Institut de Mécanique Céleste et de Calculs des Ephémérides, Observatoire de Paris, 77, Avenue Denfert-Rochereau, 75014, Paris, France. (blevrard@imcce.fr)*, F. Forget, *Laboratoire de Météorologie Dynamique, Paris VI, 4, pl. Jussieu, T. 15-25, 75252 Paris Cedex 05-France,* F. Montmessin, *Space Science Division, MS 245-3, NASA/Ames Research Center, Moffett Fild CA, 94035.*

Introduction: The polar layered deposits are thought to contain alternate layers of water and dust in different proportions resulting from the astronomical forcing of the martian climate. In particular, long-term variations in the orbital and axial elements of Mars are presumed to generate variations of the latitudes of surface water ice stability and of the amount of water exchanged in the polar areas.

At high obliquity, simplified climate models [1] and independent general circulation simulations suggest a transfer of water ice from the north polar region to tropical areas [2, 3], whereas at lower and present obliquities, water ice is expected to be stable only at the poles. If so, over obliquity cycles, water ice may be redistributed between the surface water reservoirs leading to their incremental building or disintegration depending on the rates of water transfer. If only a relative limited amount of the available water is exchanged on orbital timescales, this may provide an efficient mechanism for the formation of the observed polar deposits.

Within this context, GCM simulations of the martian water cycle have been performed for various obliquities ranging from 15° to 45° and for a large set of initial water ice locations to determine the rate of water exchange between the surface water reservoirs as a function of the obliquity. Propagating these rates over the last 10 Ma orbital history gives a possible recent evolution of these reservoirs.

Recent obliquity history: The martian obliquity is chaotic between 0° and 60° [4] but regarding the uncertainties on the present precessional martian parameters, the chaotic behaviour is only significant beyond $\sim$ 10 Ma. Over the last 10 Ma, a new accurate obliquity solution has been recently computed (Figure 1) [5]. It shows the presence of a low mean obliquity regime ($\sim 25^\circ$) during the recent 0-5 Ma interval before a marked transition toward a higher mean obliquity regime $\sim 35^\circ$ with frequent excursions beyond 40°. Since it may represent a critical obliquity for the stability of a northern pure water cap [2], the dissymetric behaviour of the obliquity between the two regimes may have had a large impact on the recent northern terrains history.

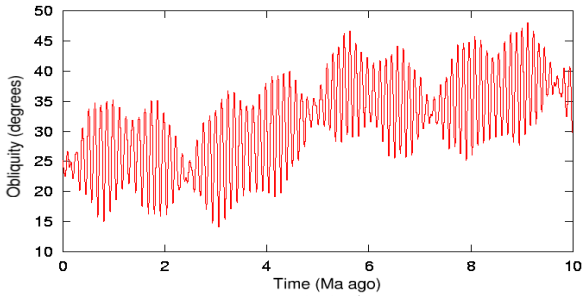

Figure 1: **Evolution of the martian obliquity over the last 10 Ma. From [5].**

Model description: We used the GCM developped in the French laboratory (LMD) for terrestrial climate simulations, which has been modified to incorporate physical parameters consistent with Martian processes and constants [6]. The model resolution is 48 longitudinal points-32 latitudinal points and 25 vertical levels. It provides a full simulation of the martian water cycle which includes the transport and seasonal exchange between surface water ice, atmospheric vapor and water cloud ice [6, 7]. The local albedo is set to 0.4 wherever an ice layer thicker than 5 μm is predicted by the model, which permits ice-albedo feedback process. In all the simulations, the eccentricity has been set to zero and the total available amount of CO_2 is kept constant with obliquity changes with respect to the present value. No permanent CO_2 ice cap or south water reservoir are initially present. All the runs start with a dessicated water vapor and cloud ice reservoir and surface water ice is thus the only initial water source. The stability of water-ice and the rate of movement of water are determined when the water cycle reaches an apparent steady state. In that case, the water vapour and cloud ice budgets comes to an interannually repeatable state. Radiative effects of vapor and clouds that might be important at high obliquity are not considered and largely unknown processes in other orbital conditions (dust storm frequency, cap albedo, atmospheric pressure) may affect the present results.

Results: In a first set of simulations, the stability of a north polar ice cap is studied for obliquities ranging from 15° to 45° with a 5° step. As in [2], we found that the residual nature of the north polar cap is lost between 35° and 40°. The annual loss rate of the northern polar water enhances with the obliquity due to increasing summer sublimation. It reaches $\sim$ 2.7 cm/yr for 40° and $\sim$ 6.9 cm/yr for 45°. We found that water ice mainly accumulates in the equatorial areas of the Tharsis Montes (Arsia, Pavonis, Ascraeus and Olympus Mons) where it becomes stable. However, unlike [2], no accumulation of water has been found in the northern high latitudes for an obliquity equal to 35°. Moderate changes in the initial cap size do not significantly affect these results. At lower obliquities, formerly stable low-latitude deposits become unstable with respect to the poles. In a second set of simulations, the water ice cap has been removed and the stability of an initial water source located on Arsia and Pavonis Mons has been investigated for the same range of obliquities. No change to polar albedo and thermal inertia has been made. Interestingly, we found an increasing accumulation of water in the latitudes higher than $\sim 60^\circ$ both in the north and south polar areas. This may be correlated with the existence of massive water deposits inferred in the near-sub surface by the Mars Odyssey

Gamma-Ray Spectrometer (GRS) at these latitudes [8]. At the lowest obliquity 15°, the maximum accumulation rate is close to 0.15 cm/yr at the north pole, whereas it reaches $\sim$ 0.05 cm/yr at the south pole. Note that these rates are one order of magnitude smaller than the previous opposite situation. It may illustrates an important dissymetric evolution of the northern cap during the two obliquity regimes. We are presently undertaking additional simulations to estimate the speed of water exchange for other initial water-ice locations and final results will be reported at the meeting.

Conclusion: Considering the present evolution of the water reservoirs on the $15^\circ - 45^\circ$ recent obliquity excursion, our results suggest two significant conclusions. First, we found that for obliquities higher than 40°, the annual loss rates of the northern polar cap towards tropical areas are about one order of magnitude higher than the opposite situation (only tropical sources at obliquities lower than 40°). If no interaction with the dust cycle (possible formation of a residual lag deposit which inhibits the sublimation of water ice from the surface) is considered, the model thus predicts (1) a possible quick disintegration of a $\sim$ 3-km thickness polar cap during the high obliquity excursion of the 5-10 Ma recent time interval (2) a recent averaged accumulation of the northern cap during the lower mean obliquity regime ($\sim 25^\circ$) of the 0-5 Ma interval from equatorial areas and also probably at the expense of the south polar area. Second, the slow rates of water accumulation in south and north polar areas on orbital timescales may provide, coupled with dust accumulation, a possible mechanism for the formation of $\sim$ 10-50 m thickness polar layers.

References: [1] Jakosky, B.M. and Carr, H.H. (1985) *Nature*, *315*, 559-561. [2] Mischna, M.A. et al., 2003, *JGR*, in press. [3] Haberle, R.M. et al., 2003, this issue. [4] Laskar, J. and Robutel, P. (1993) *Nature*, *361*, 608-612. [5] Laskar, J., Levrard, B. and Mustard, J.F., (2002) *Nature*, *419*, 375-377. [6] Forget F. et al. (1999), *JGR*, *104*, 24155-24179. [7] Montmessin, F., Ph.D dissertation, 2002, Université Paris VI.[8] Boyton, W.V. et al., 2003, *Science*, *297*, 81-85.

THE USE OF PALEOLIMNOLOGY FOR TRACKING CLIMATE CHANGE IN THE CANADIAN HIGH ARCTIC – ANALOGIES FOR MARS EXPLORATION. D. S. S. Lim[1] and M. S. V. Douglas[1], [1] Paleoenvironmental Assessment Laboratory (PAL), Dept. of Geology, University of Toronto, Toronto, Ontario, Canada M5S 3B1; lim@geology.utoronto.ca.

Tracking Climate Change in the High Arctic: The Canadian High Arctic is a distinct region of our planet in the way that it supports life, responds to shifts in the climate, and affects the environments of the rest of the globe. High Arctic characteristics such as low incoming radiation, small land mass (one tenth the size of tropical regions), and high-albedo surfaces (as a result of the longevity and high reflectivity of the snow and ice cover) exacerbate the effects of hemispheric temperature trends and contribute to the environmental vulnerability of this area of our globe [1, 2]. Over the last hundred years, an arctic warming trend has been recorded with increases in average arctic temperatures exceeding those recorded for the hemisphere as a whole [3]. High arctic environmental changes are not, however, isolated to this region, since they are strongly tied to general circulation patterns due to its inherent role as an energy sink [4]. For example, changes to the High Arctic's climate, such as increases in river run-off as a result of warming effects, may result in the alteration of global thermohaline circulation patterns and eventually lead to changes in low latitude climate systems [3].

Further investigation of high arctic climate and environmental change is still needed to better understand their widespread effects, which necessitates (a) the acquisition of baseline ecological data and (b) long-term monitoring efforts. A paucity of long-term environmental data exists for the High Arctic, due largely to the logistical difficulties and constraints associated with field expeditions in this remote polar region. The physical, biological and chemical limnological and paleolimnological data from the lakes and shallow ponds that dot the High Arctic tundra can provide a means of efficiently and economically meeting both of these requirements. These water bodies are both sensitive and vulnerable to such environmental influences as global warming [5], increased UV-B penetration [6], and local pollution inputs [7]. Furthermore, these lakes and ponds contain both ecological and genetic information that may help to expand our understanding of such basic biological concepts as speciation, and top-down trophic control, and, as a result, assist in the refinement of eco-management techniques used on temperate lakes [8].

Paleolimnological Investigations in the High Arctic: The Paleoenvironmental Assessment Laboratory (PAL) at the University of Toronto, working in partnership with the Paleoecological Environmental Assessment and Research Laboratory (PEARL) at Queen's University in Kingston, Ontario, focuses on acquiring both baseline and historical limnic data from the High Arctic using paleoenvironmental techniques. Fossilized freshwater algal remains of diatoms (class *Bacillariophyceae*), in particular, are used as bioindicators in our investigations of past physical and chemical limnic conditions. In the oligotrophic lakes and ponds of the High Arctic, diatoms typically form a significant proportion of the algal community [9]. Furthermore, they are ecologically diverse and respond rapidly to changes in environmental conditions, making them robust bioindicators in reconstructing such variables as salinity, pH, nutrient fluxes and lake levels [10]. PAL and PEARL have targeted sites throughout the High Arctic for paleoenvironmental investigations. Sites are found on such High Arctic islands as Banks, Bathurst, Cornwallis, Devon, Ellef Ringnes, Northern Ellesmere, Prince Patrick, and Victoria. Our work continues to expand throughout the High Arctic with the goal of creating both a spatial and temporal map of environmental data from this sensitive region of the world.

Implications for the Exploration of Mars: The application of paleolimnological techniques to climate change issues in the Canadian High Arctic has implications for future geobiological research on Mars. Specifically, ancient lake deposits on Mars have become a strategic focus for geobiological and astrobiological studies on the Red Planet. For example, Cabrol and Grin [11], Grin and Cabrol [12], and Wharton et al. [13] describe observational evidence for martian paleolakes, including in Gusev Crater [12], target site of the 2003 Spirit Mars Exploration Rover Mission. Paleolimnological investigations on Mars may lead to the acquisition of critical historical climate data from this planet, and paleolimnological research in polar settings such as the Canadian High Arctic may act as an analogue for future lacustrine investigations on Mars. Comparability in climate regimes, depositional processes, dearth of long-term environmental data, and other characteristics have led to a growing interest in polar paleolimnological studies as analogues to potential paleolake deposits on Mars. Furthermore, many of the tools and techniques that have been refined over the years for use in high arctic paleolimnological investigations will no doubt play a role in the future development of investigative strategies for the exploration of Mars paleolakes. The interesting physical,

chemical and potentially biological characteristics of high latitude water bodies may be analogous to the paleolakes that the early climate regime on Mars may have supported. Therefore, the lessons and experiences garnered in these remote regions may serve as a foundation for future robotic or human-led geobiological exploration on the Red Planet.

References: [1] Roots E. F. (1990) In *Artic and Global Change, J. A. W. McCulloch (ed.)*, 6-31. [2] Rouse W. R. (1994) In *Canada's Cold Environments*, H. M. French and O. Slaymaker (eds.) 65-92. [3] Overpeck, J. et al. (1997) *Science, 278*, 1251-1256. [4] Ledrew, E. F. (1993) In *Artic and Global Change, J. A. W. McCulloch (ed.)*, 271-290. [5] Smol J. P. et al. (1991) *Verh. Internat. Verein. Limnol,24*, 1240-1246. [6] Vincent W. F. and Pienitz R. (1996) *Geoscience Canada*, *23*, 231-236. [7] Douglas M. S. V. and Smol J. P. (1999) In *The Diatoms: Applications for the Environment and Earth Sciences*, E. Stoermer and J. P. Smol (eds.) 227-244. [8] Hammar J. (1989) *Ambio, 16*, 6-22. [9] Douglas M. S. V. and Smol J. P. (1993) *Nova Hedwigia 57(3-4)*, 511-552. [10] Dixit S. S. et al. (1992) *Environ. Sci. Technol. 26(1),* 23-32. [11] Cabrol N. A. and Grin E. A. (1999) *Icarus*, *142*, 160-172. [12] Grin E. A. and Cabrol N. A. (1997) *Icarus*, *130*, 461-474. [13] Wharton Jr. R. A. et al. (1995) *Journal of Paleolimnology*, *13,* 267-283.

COMPARISON BETWEEN NORTH AND SOUTH NEAR POLAR REGIONS OF MARS FROM HEND/ODYSSEY DATA. M.L. Litvak[1], I.G. Mitrofanov[1], A.S. Kozyrev[1], A.B. Sanin[1], V. Tretyakov[1], W.V. Boynton[2], D.K. Hamara[2], C. Shinohara[2], R. S. Saunders[3], D. Drake[4], [1]Space Research Institute, RAS, Moscow, 117997, Russia, max@cgrsmx.iki.rssi.ru, , [2]University of Arizona, Tucson, AZ 85721, USA, [3]Jet Propulsion Laboratory, Pasadena, CA 91109, USA, [4]Lansce 3, Los Alamos Nat'l Lab. Los Alamos, NM and TechSource Inc, Santa Fe, NM 87594, USA.

Introduction: The two years of neutron mapping measurements onboard Mars Odyssey spacecraft are presented based on High Energy Neutron Detector (HEND) observations. HEND instrument is a part of GRS suite responsible for registration of epithermal and fast neutrons originating in Mars subsurface layer [1,2]. The scattering of fast neutrons in Mars surface caused by primary cosmic rays is strongly sensitive to presence of hydrogen atoms. Even several percents of subsurface water significantly depress epithermal and fast neutron flux [3,4]. It turns orbit neutron spectroscopy into one of most efficient methods for finding distribution of subsurface water.

There is direct correspondence between energy of registered neutron and depth where it was produced. The production rate of fast neutrons has maximum at depths less than tens of centimeters while the epithermal neutrons originate in layer placed 1-3 m below the surface. Combining measurements in epithermal energy range with measurements above 1 MeV one may reconstruct the water abundance distribution at different depths starting from thin subsurface layer and going down to several meters depths. It allows to check simple model describing layered structure of regilith.

It is known that North and South near polar regions are affected by global redistribution of atmospheric CO_2. The maximal thickness of CO_2 snow depth may be as high as 1 m at latitudes close to martian poles[5]. It explains why neutron flux above martian poles significantly varies from summer to winter seasons. It occurs because CO_2 frost hides upper surface layer from the orbit observations. This fact was used to estimate thickness of CO_2 deposit at different latitudes[6,7]. Here we suggest to make comparison between martian near polar regions in both ways as in terms of subsurface regolith structure as in terms of distribution of CO_2 deposits.

Data Analysis. To realize this approach we split our study in two steps. On first one the summer data were processed when surface was free from seasonal CO_2 frost. It helps us to find best fit parameters describing regolith structure in given region. To do it two layers model was applied to the data. It consists of relative dry (~2% of water) upper soil layer covering the bottom water ice rich layer. The thickness of upper layer and content of water in bottom layer were used as free parameters. To convert orbital measurements to real values of neutron flux near Mars surface we should to take into account atmosphere thickness above observed region. The orbital measurements are accumulated each ~ 20 sec and gathered from large surface area. The sizes of this footprint area may be as large as 600 km x 600 km. To avoid complicated model-dependent analysis how neutron flux is distributed inside footprint area we split Mars near polar regions into large areas with sizes which are more than HEND footprint. The thickness of martian atmosphere was taken from Ames Global Climate Model.

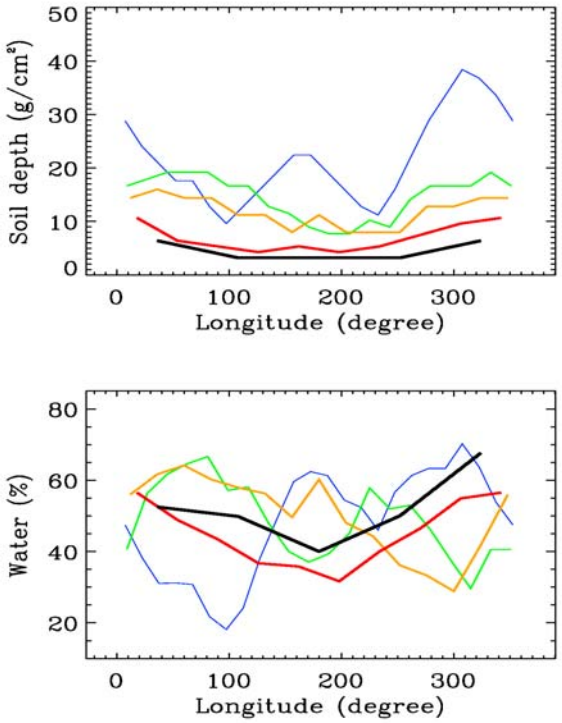

Fig 1. The content of water ice and thickness of soil deposit above it are shown for North region. Black color corresponds to 80°-90° latitude belt. The red, yellow, green and blue colors correspond to 75°-85°, 70°-80°, 65°-75°, 60° -70° latitude belts.

In this study we restrict ourselves by studying regions near Mars poles above 60 degrees for each hemisphere. It was done by two reasons. At first, observation of these regions demonstrates presence of enormous amount of water in subsurface layer [1,2,8,9]. At

second, The south and north regions are highly affected by seasonal CO_2 global circulation process. The CO_2 snow depth varied from tens of cm up to ~1m at the selected latitudes.

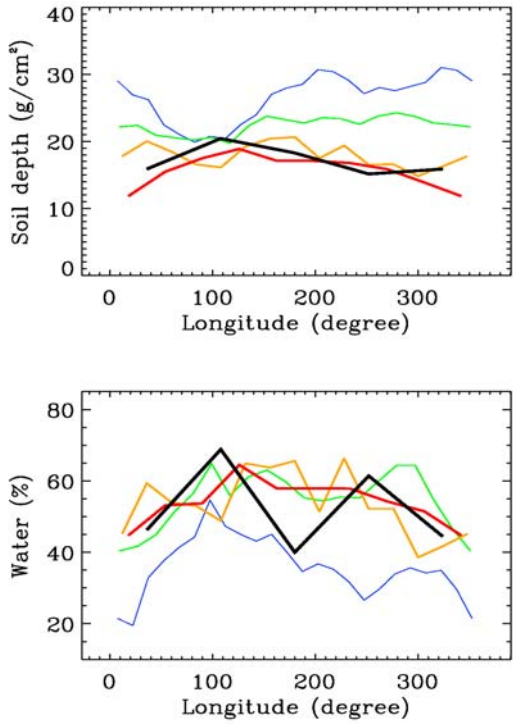

Fig 2. The content of water ice and thickness of soil deposit above it are shown for South region. Black color corresponds to 80°-90° latitude belt. The red, yellow, green and blue colors correspond to 75° -85°, 70° -80°, 65° -75°, 60° -70° latitude belts .

On second step of our study we fixed best fit parameters for each selected area and implemented additional layer of neutron production which should simulate CO_2 deposit. Fitting the HEND data for different winter seasons we tried to find the best fit thickness of this layer.

Conclusions: Comparison between north and south regolith structures show that south and north near polar regions contain comparable content of subsurface water ice. But on south the ice rich layer is placed significantly deeper in comparison with north areas (see fig 1 and fig 2). The minimal depth of bedding of water ice for North was founded equal ~ 3 g/cm^2. For south region this value was estimated more then 10 g/cm^2.

Model estimations of winter CO_2 deposit shows that thickness of snow layer may achieve up to 1 meter on South while snow depth on North do not exceed 80-85 cm. The distribution of south CO_2 deposit also shows more complicated and irregular behavior then on north.

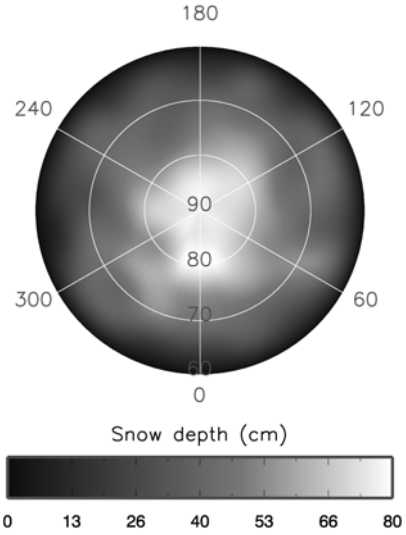

Fig 3. The Map of CO_2 deposit are shown for north region of Mars.

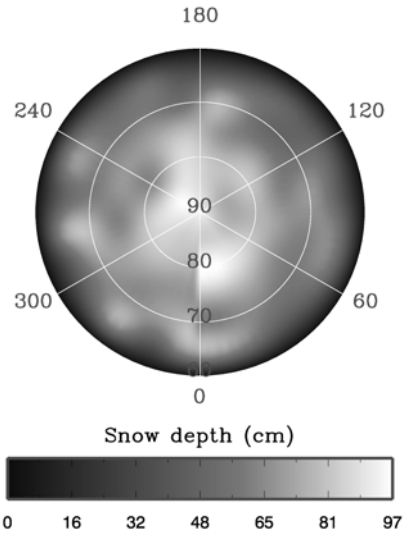

Fig 4. The Map of CO_2 deposit are shown for south region of Mars.

References:

[1] Mitrofanov I.G. et al. (2002) *Science*, 78-81. [2] Mitrofanov I.G. et al. (2003) *LPS XXXIV*, Abstract # 1104. [3] Drake D.M. et al. (1988) *JGR*,V.93, 6353-6368. [4] Feldman W.C. et al. (1993) *JGR*, V.98, 20855-20870. [5] Smith D.E. et al. (2001) , 294, 2141-2146. [6] Mitrofanov I.G. et al. (2003) *Science*, 2081-2084. [7] Litvak M.L. et al. (2003), 6th conference on Mars, Pasadena 2003. [8] Boynton W. et al. (2002) *Science*, 81-85 [9] Feldman W.C. et al (2002) *Science*, 75-78

SOME APPLICATIONS OF CO2-H2O PHASE EQUILIBRIA TO THE COMPOSITION AND EVOLUTION OF THE MARTIAN POLAR ICE CAPS. J. Longhi , Lamont-Doherty Earth Observatory, Palisades, NY 10964 (longhi@lamont.ldeo.columbia.edu)

Preferential melting of CO2 ice and clathrate layers within polar ice caps during periods of low obliquity may lead to sequestration of liquid CO2 in the Martian crust.

Fig. 1 is an update of the P-T projection of the CO2-H2O phase diagram [1,2] showing the approximate location of the solid state breakdown of CO2 clathrate (H) to water ice (I) and solid CO2 (S). Because of extremely limited solubility of H2O in CO2 liquid and gas at low temperatures, binary equililibria ***1*** and ***5*** are virtually equivalent to the sublimation and boiling curves for pure CO2, respectively.

Little solubility data are available with which to draw temperature composition diagrams, but some of the extent data [4] are shown in Fig. 2, which is a 2-bar T-X section. This diagram is relevant to putative ancient greenhouse atmospheres [5]. For a calculated surface temperature of 240° K the average atmosphere would have been in equilibrium with ice at saturation, similar to the present. However, the concentration of H2O would have been > 50 times the present average, and because of the higher atmospheric pressure the actual mass of atmospheric water could have been ~ 18,000 times the present amount. The evaporation rate in equatorial regions would have been much higher and Mars would appear more arid than today.

It is widely noted that ground ice is stable poleward of ~ 40° latitude and that night frosts occur even where no ice is present [6]. This implies that the martian atmosphere is on average saturated with ice (or close to it), and that the atmospheric composition (0.0067 wt% H2O) and frost point (198° K) [6] can be employed to construct a diagram analogous to Fig. 2 for martian surface pressure. Fig. 3 illustrates a T-X section drawn for the average surface pressure (6 mb – solid curve). The diagram predicts that water ice will be the first phase to precipitate upon cooling, that ~ 50° additional cooling is needed before the precipitate changes to clathrate, and that an additional 10° cooling is needed before CO2 and clathrate precipitate together (S >> H). Two other curves are also shown for the extremes of surface pressure (10 mb for the north polar regions and 2 mb for the south polar region and the higher portions of Tharsis). In the 10 mb section the atmospheric composition is farther into the gas + ice field (GI); at 2 mb the average atmospheric composition just intersects the ice field; however, water abundances are typically much lower in the southern hemisphere [7], so clathrate is probably the first phase to precipitate in the south polar region, followed by CO2 after ≤ 10 ° cooling. In fact the lowest water contents in the southern hemisphere are stable for months [7], suggesting that atmospheric water may be buffered by the solid-CO2 + clathrate "eutectic". These diagrams are consistent with observations that the northern ice cap is water-rich, whereas the southern ice cap has a residual CO2-rich top layer [8].

Basal melting has been suggested for both ice caps [9,10]. Fig 4 illustrates a schematic polybaric section along the temperature gradients calculated by [10]. Depths are given in km. Because ice is a much better conductor than solid-CO2 or clathrate [10], greater thicknesses are possible for water-rich ice caps before basal melting ensues. It is believed that in periods of low obliquity the polar ice caps tend to thicken with the addition of solid CO2 [11]. Because the dry ice and clathrate are much better insulators than water ice, the thermal gradient would have increased until melting began. The diagram predicts that mixtures of dry ice and clathrate melt at much lower temperature than water ice + clathrate. Therefore, generation of CO2-rich melts is likely, and because liquid CO2 is denser than water or water ice, it is likely to percolate into the crust This process, which sequesters CO2 in the crust, may be a major agent of atmospheric evolution.. Migration of subsurface liquid CO2 toward the equator may have led to explosive encounters with ground water or ice.

REFERENCES: [1] Longhi J. (2000) *Lunar and Planetary Science XXXI,* Abstract #1903, Lunar and Planetary Institute, Houston.. [2] Longhi J. (2001) *Lunar and Planetary Science XXXII,* Abstract #1955. [3] Zureck R.W., Barnes J.R., Haeberle R.M., Pollack J.B., Tillman J.E., and Leovy C.B. (1992) in *MARS*,H. H. Kieffer, B. M. Jakosky, C. W. Snyder, and M. S. Matthews eds., pp. 835-933, Univ. of Arizona Press, Tuscon. [4] Wiebe R. (19390 *J. Am. Chem. Soc. 61*. [5]] Fanale F.P., Postawako S., Pollack J., Carr M.H., and Pepin R.O.

(1992) in *MARS,* pp. 1135-1179. [6] Carr M.H. (1996) *Water on Mars*. Oxford Univ. Press, New York, 229 pp. [7] Jakowsky B.M and Haberle R.M. (1992) in *MARS,* pp. 969-1016. [8] James P.B, Kieffer H.H., and Paige D. A. (1992) in *MARS,* pp. 934-968. [9] Clifford S.M. (1993) *J. Geophys. Res. 98,* 10,973-11,016. [10] Mellon M.T. (1996) *Icarus 124,* 268-279.[11] Kieffer H.H. and Zent A.P. in *MARS,* pp. 1180-1218.

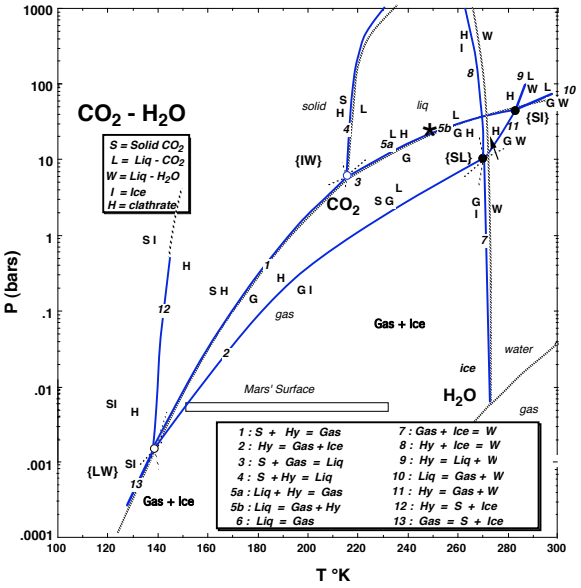

Fig. 1.Low-temperature portion of CO2-H2O phase diagram after [1,2]. Proposed binary invariant points indicated by open circles. Position of low-T stability limit of clathrate (H = S + Ice) is calculated.

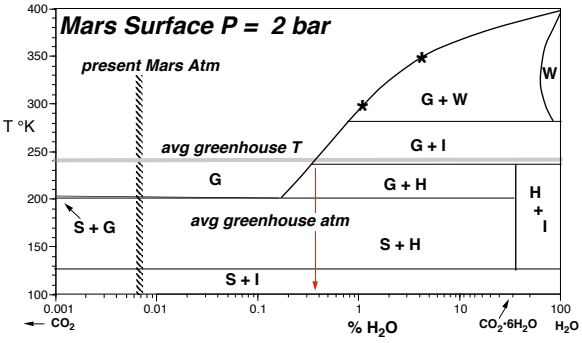

Fig. 2 2-bar isobaric section. Solubility data (*) from [4]. Vertical dashed line indicates present martian atmospheric composition; approx. 240°K greenhouse temperature from [5]. Maximum average H2O in atmosphere would be > 50x present concentration, but > 10000 times present mass.

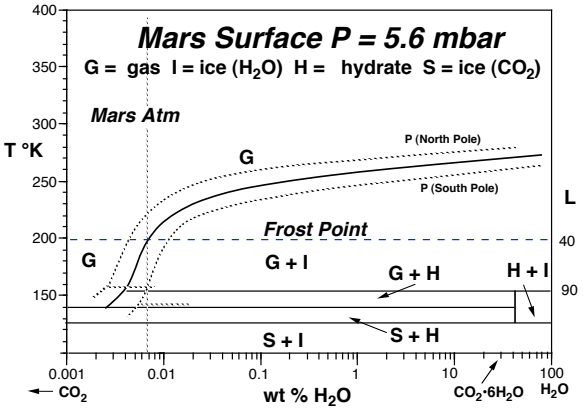

Fig. 3 Schematic isobaric sections based on frost point and atmospheric composition. Ice is first condensate at lower elevations; clathrate may be first at higher elevations

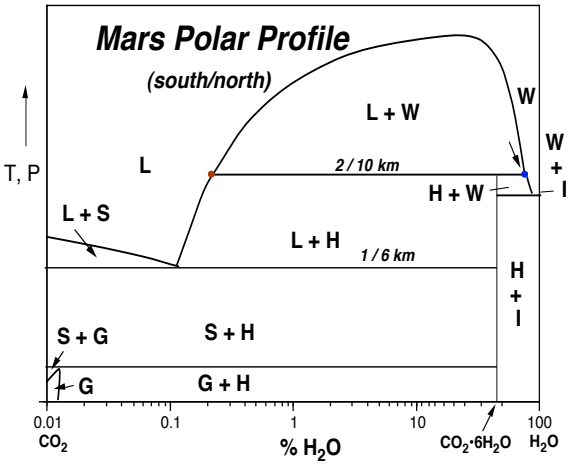

Fig. 4 Schematic profile along polar P-T profiles after [10]. Numbers are depths in km along thermal profiles calculated by [10]: dry ice/water ice.

AN INVESTIGATION OF AEROSOL DYNAMICS IN THE ATMOSPHERE OF MARS. A. Määttänen, H. Korhonen, K. E. J. Lehtinen, H. Vehkamäki, M. Kulmala, *Division of Atmospheric Sciences, FIN-00014 University of Helsinki, FINLAND, (Anni.Maattanen@helsinki.fi)*.

Atmospheric models are developed and used for several purposes. The research of climate change is a hot topic at the moment, and global climate models produce results about past and future climates. Numerical weather prediction models are well-known in the sense that they are used to produce the everyday weather predictions for e.g. television. Both model types can be converted to other planetary atmospheres as well, to describe their weather and climate.

Aerosol models have recently been incorporated as components in atmospheric models; detailed microphysical models describe microscale aerosol size distribution and processes in the atmosphere. When used together with or inside an atmospheric model, e.g. cloud and rain particle formation are defined and described in great detail. Aerosol particles affect radiative transfer in the models because they absorb and scatter radiation thus influencing the net radiative forcing of the atmosphere.

In the Martian atmosphere dust and other types of aerosol particles (most importantly carbon dioxide and water ices) scatter and absorb both short- and longwave radiation. This affects the thermal structure of the atmosphere and flow fields therein. Flow patterns affect the aerosol particle distribution by lifting dust from the surface and advecting dust and ice particles in the atmosphere. This feedback between aerosols and flow patterns may, for example, have a great influence in the onset of global (and also local) dust storms.

In the polar areas atmospheric temperatures are low enough for extensive ice nucleation to occur, since e.g. clouds are regularly observed. Aerosol processes may also have some influence in the formation of the polar layered deposits; the mixture of ice and dust is probable also in the atmosphere (via heterogeneous nucleation) from where it can sedimentate to the surface.

Our goal is to build a microphysical aerosol model for the Martian atmosphere. So far we have studied homogeneous and heterogeneous nucleation of carbon dioxide based on the work by Wood (1999). Homogeneous nucleation of CO_2 is very unlikely to happen in the Martian atmosphere because of the very high supersaturation required (10^8), but instead heterogeneous nucleation seems very probable in temperatures below 178 K. Model simulations have been conducted in average atmospheric near-surface conditions for a 100% CO_2 atmosphere (the Martian atmosphere is 95.3% CO_2). Unary nucleation of H_2O will also be studied in the same way. The binary nucleation of carbon dioxide and water will also be investigated.

Future work includes modelling the growth of the aerosol particles by condensation and coagulation using a box model (spatially 0-dimensional). Eventually, when all the components are together and working, the aerosol model will be incorporated into the Mars atmospheric models of the University of Helsinki (Savijärvi 1995, 1999, Savijärvi and Siili, 1993). Thus the microphysical aerosol model will be improving the atmospheric models by, for example, describing cloud formation and aerosol size distribution more precisely and thus improving the accuracy of the radiation schemes.

This work was supported by the *Academy of Finland*, which is gratefully acknowledged.

References

[Savijärvi, 1995] Savijärvi, H. (1995). Mars boundary layer modeling: diurnal moisture cycle and soil properties at the Viking Lander 1 site. *Icarus*, 117:120–127.

[Savijärvi, 1999] Savijärvi, H. (1999). A model study of the atmospheric boundary layer in the Mars Pathfinder lander conditions *Quarterly Journal of the Royal Meteorological Society*, 125:483–493

[Savijärvi and Siili, 1993] Savijärvi, H. and Siili, T. (1993). The Martian slope winds and the nocturnal PBL jet. *Journal of Atmospheric Sciences*, 50:77–88.

[Wood, 1999] Wood, S. E. (1999). Nucleation and growth of CO_2 ice crystals in the Martian atmosphere. Ph.D. thesis

ASTROBIOLOGY EXPLORATION STRATEGIES FOR THE MARS POLAR REGIONS USING BALLOON PLATFORMS. P. R. Mahaffy[1], S. A. Atreya[2], D. A. Fairbrother[3], W. M. Farrell[1], S. Gorevan[4], J. Jones[5], I. Mitrofanov[6], and J. Scott[7], [1]NASA Goddard Space Flight Center, Greenbelt, MD 20771, Paul.R.Mahaffy@gsfc.nasa.gov, [2]University of Michigan, Ann Arbor, MI, [3]Goddard Wallops Flight Facility, [4]Honeybee Robotics, New York, New York, Wallops, MD, [4]Jet Propulsion Laboratory, Pasadena, CA, [5]Space Research Institute, Moscow, Russia, [6]Carnegie Institution, Washington, DC.

Introduction: Montgolfiere balloons can provide a unique near-surface platform for an extended traverse over the polar regions of Mars. During the polar summer, such solar powered balloons would remain in the constant sun of the polar summer and could remain airborne for many weeks or even months as the atmospheric circulation would drive the balloons around the polar region many times before the balloon would cross the terminator. Such a platform for scientific measurements could provide in situ sampling of the atmosphere for trace disequilibrium species that might be indicators of present geological or biological activity in this region. It could furthermore provide high resolution imaging, deep electromagnetic (EM) sounding for subsurface stratigraphy and liquid water, and high spatial resolution neutron measurements of subsurface ice. Technologies for robust balloon deployment on entry and controlled encounters with the surface and near subsurface for sample acquisition in otherwise inaccessible regions (Figure 1) are presently being studied and developed with support from NASA.

Pointers to Past or Present Life on Mars: Potential indicators or pointers to ***present life*** in the Martian polar region might be found in the atmosphere in the form of non-photochemically produced species such as trace levels of methane or formaldehyde that might be produced by low levels of near-surface biological activity. The near-surface cryosphere and subsurface aquifers, if they were to exist in the polar region, might provide ecological niches for hardy microbial life. Pointers to ***past conditions on Mars that might have been more conducive to the nourishment of life*** may also be measured in the atmosphere in the form of isotope ratios of light isotopes of carbon, nitrogen, and the noble gases. Their isotopic composition address mechanisms of obtaining the present atmosphere through loss to the surface and space and production through infall and volcanic activity. Likewise, the surface stratagraphic record of the near polar region might be able to reveal elements of its glacial, geological, and climate history[1]. All of these diverse measurements could be implemented from a balloon platform in a future mission to this region.

Unique Characteristics of a Balloon Platform: Key mission elements to complete the astrobiology related science objectives sketched in the previous paragraph are (1) regional mobility over; (2) proximity to; and (3) long duration over the volatizing polar cap. A balloon can float just kilometers above the surface with slow speeds of several m/sec providing the needed mobility, proximity, and dudration. There is a substantial usable science mass with such a platform and platform-unique science features. With an appropriate complement of space-proven instruments these could include:

- An in situ atmospheric chemistry laboratory to search for local sources of anomalous trace species in an extended region over a summertime volatile-producing ice cap.
- A platform positioned well below the attenuating ionosphere to perform radio sounding of the ice cap and the polar layered terrain.
- Imaging with better than 11 cm resolution from an altitude of 4 kilometers and higher resolution in near surface flights.
- Higher order magnetic moments beyond dipole values, of surface magnetic features.

Figure 1. Balloon sampling may enhance our ability to carry out exploration over rugged landscapes on Mars such as the polar caps and erg. Under development for solar driven Montgolfiere balloons is the ability to approach the surface for rapid acquisition with a “touch-and-go” sampler.

- The ability to perform targeted stratagraphic studies of erosion features like Chasma Boreale.
- Neutron mapping of shallow water ice with <3 km horizontal resolution from a balloon at 4 km altitude, ~200 x better spatial resolution than the Odyssey global map.

Balloon Technology Studies: Key balloon technology elements to insure robust implementation of such an investigation continue to advance.

Balloon Deployment Studies. Recent tests at JPL have demonstrated balloons autonomously deployment from the ground or while falling from high altitudes[2,3]. The stratospheric deployment tests, which are more likely anticipated for Mars (Figure 2), are still ongoing, but have been generally successful for polyethylene balloons, although there have been two failures of large balloons due to deployment issues. For these stratospheric tests, a packed Montgolfiere balloon is lifted to 36 km altitude (4 mbar) by a helium balloon. The packed Montgolfiere is then allowed to fall on a parachute at 50 m/sec and is deployed from the bottom of the bag. For a a double Montgolfiere deployment, the empty Montgolfieres fill while falling and are rapidly heated by the Sun, thus providing buoyance. Current development activities include selection of optimal balloon materials, balloon fabrication techniquess, and packing as well as optimization of the deployment sequence to increase the robustness of the deployment.

Controlled Surface Access. Several altitude-controlled tests have also been successfully conducted using black plastic Montgolfiere balloons. In the first field test in California's Mojave Desert in 1998, a radio-controlled vent was placed at the top of the balloon. When the vent was opened, hot air was released and the balloon descended. Conversely, closing the vent caused the balloon to ascend. This initial successful flight of about 15 minutes was followed by a much longer flight over the Pacific Ocean later that year. During this ocean test, the balloon was allowed to climb to about 1 km altitude, and the vent periodically opened to allow descent. The balloon payload was actually soft-landed on the ocean several times before the test was terminated. Post-flight thermal analysis very closely agreed with actual balloon behavior during the entire flight. Development of the next generation autonomous altitude control mechanism is underway.

Sample Acquisition Studies. A rapid "touch & go" sample acquisition system has been developed[4] and is being tested and refined. This device is is specifically designed to be deployed from a moving platform such as a balloon to provide very rapid acquisition of material from the surface and to some depth below the surface of Mars. Such a balloon/sampler system could enable collection of materials for analysis from a variety of sites in otherwise difficult to reach locations.

References: (1) Clifford, S. M., et al., "The State and Future of Mars Polar Science and Exploration," Icarus, 144, 210-242. (2000). (2) J. A. Jones and J. J. Wu, "Solar Montgolfiere Balloons for Mars", AIAA #99-3852, 1999. (3) J. A. Jones, "Mars Rover Balloon Launch", JPL Video#9910_06, October 1999. (4) S. Rafeek, K. Y. Kong, S. P. Gorevan, and M. A. Ummy, A Balloon Delivered Subsurface Sample Acquisition and Transfer System, Concepts & Approaches for Mars Exploration, Lunar and Planetary Institute, Houston, TX, July 18-20, 2000.

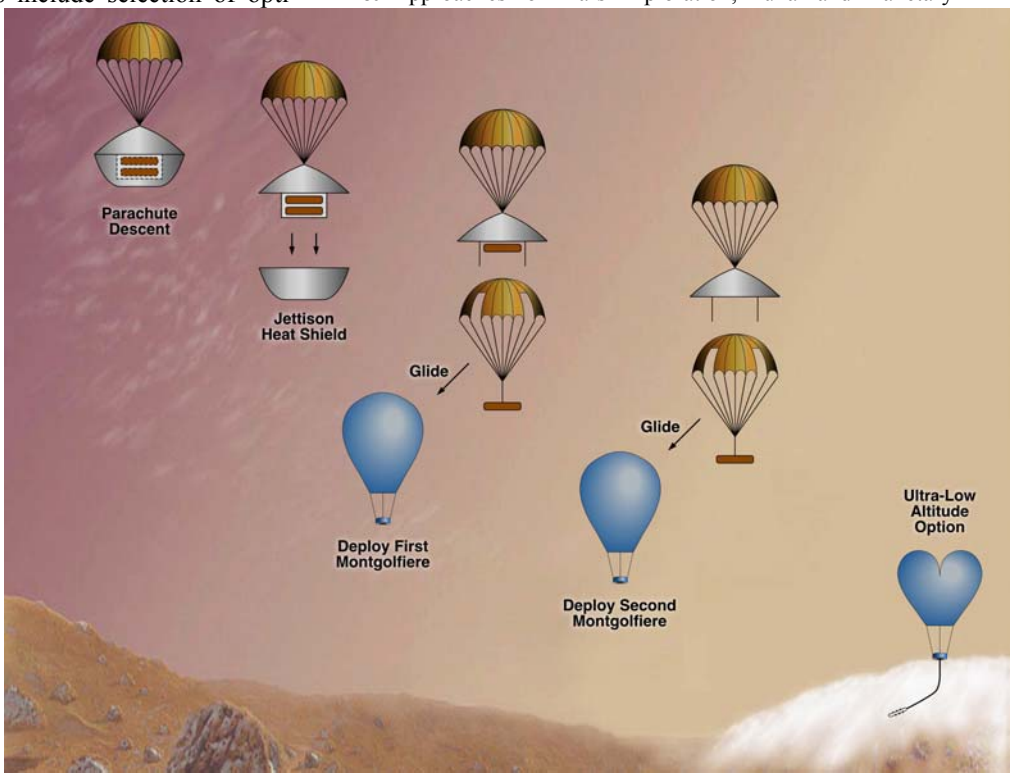

Figure 2. In a deployment scenario studied for a future Mars mission, two Montgolfiere balloons rapidly fill and heat while falling through the atmosphere. Altutude control devices may allow surface soil and ice sampling.

DISTRIBUTION AND CLIMATIC CONTROL OF SMALL SCALE POLYGONS ON MARS N. Mangold, Orsay-Terre, Equipe Planétologie, UMR 8616, CNRS et Université Paris-Sud, Bat. 509, 91405 ORSAY Cedex, France, mangold@geol.u-psud.fr

Introduction:
On the Earth, the formation of patterned ground occurs in periglacial or alpine regions submitted to permanent or transient freezing temperatures. Two climatic effects control their formation: (1) Freeze-thaw cycles which form sorted polygons, hummocks or stripes from ice segregation in lenses and concentration of stones or pebbles and (2) thermal contraction which forms crack networks by volume decrease of the ground during winter (Fig. 1). Ice-wedge polygons are due to a combination of thermal contraction and seasonal melting because meltwater freezes in the cracks in winter and creates a weakness that is reused for cracking [e.g. 1]. The occurrence of polygons on Mars similar to those found on Earth in periglacial regions is thus interesting to study recent modifications of ice distribution and climate. Here, I detail the classification of polygons on Mars and focus on one type of the polygons located close to the south ice cap.

Classification of different type of polygons:
The systematic study of patterned ground on the whole planet Mars has been done using MOC images M01 to E06. Large crack networks observed in NW Elysium and Utopia regions [2,3] as well as those from Athabasca Valles, are not taken in account in the study for a reason of chronology. Indeed, these polygons, although sparsely cratered, show 100 m large craters on about all MOC images [see example on fig.2 of 2]. Despite being Late Amazonian, they are significantly older than the polygons of this study which are almost completely devoid of craters.
We classed patterned grounds using 4 criteria: *(1) Homogeneous or various width*: Polygons are listed as "homogeneous" polygons if they have a regular width and as "various " in the contrary case. (2) *Small or large polygons*: In the case of homogeneous width, polygons are listed as "large" if they are more than 40 m wide and as "small" if they are less than 40 m wide. (3) *Identification of cracks*: The presence of cracks indicates processes involving volume contraction either by freezing, desiccation or tectonic stress. (4) *Topographic control*: We observe that patterned ground are sometimes systematically associated to topography such as crater interior or hillslopes.
Using these criteria we find that polygons of more than 500 images can be listed in 4 main types and 8 subtypes (see whole map of polygons in companion paper, Mangold et al, Geographical relationships between small scale polygons and ground ice distribution from Neutron Spectrometer on Mars). Images with small crack networks (S1) are in very low number (33) compared to the 151 images containing (S2) regular polygons devoid of cracks (Fig. 2A) and 250 images of (S3) regular pattern of hummocks. Large polygons are all formed by cracks identified by their straight shape. There are only two classes of large and homogeneous polygons among which one (Fig. 2B) is found in connection to topography (LT) and the other one (Fig. 2C) in connection to the south polar cap (LPC). The polygons of various sizes (V), divided in complex, fractal and random, consist of a total number of 38 images which are strictly restricted to the southern hemisphere at latitudes from 55 to 80° with a maximum near 70°. 4 subtypes of polygons are found in both hemispheres at the same latitudes. Their distribution thus likely corresponds to climatic effects. Different interpretations of these networks can be given in terms of climate control involving thermal contraction or freeze-thaw cycle like on Earth. Here, I detail the case of polygons (LPC) that are only observed around the south CO_2 cap (Fig. 3).

Interpretation of polygons around the south CO_2 cap by recent variations of the polar cap extend:
Polygons (LPC) have size of 50 to 300 m and they are exclusively at more than 80° of latitude south. Cracks have not the typical morphology of ice-wedge cracks because they are very straight and thin compared to the width of polygons and they are often longer than 1 km. Such regular geometry is more typical of polygons formed by a single and strong episode of contraction. I propose to explain such large and narrow cracks by thermal contraction due to variations in the extent of the CO_2 permanent cap. Indeed, cracking of the ground occurs during the decrease of temperature. Such decrease could be related to the blanketing of the polar deposits by the CO_2 cap. In that case, the surface blanketed by CO_2 is no more heated by the sun in summer and the surface freezes at the temperature of CO_2 around -125°C. A cold thermal wave can propagate even deeper as the duration of the blanketing is long. After that period of expansion, the polar cap would retreat and cracks would become visible at the surface without being completely closed by the thermal expansion. The retreat of the polar cap could correspond to what may be currently observed over MOC images [4]. This scenario is consistent with the lack of similar features in the polar deposits of the North hemisphere because there is no permanent CO_2 polar cap in the North pole. Thus, if this scenario is true, a better understanding of the distribution and formation of these cracks could permit to reconstruct past extent of the CO_2 cap and to identify regions of terrains containing water ice versus those containing CO_2.

References: [1] French, H. M., The periglacial environment, 2nd ed., Longman, 1996 [2] Seibert, N. M. and J. S. Kargel, *Geophys. Research Let.*, 28 (5), 899-902, 2001. [3] Kuzmin, R. O., E. D. Ershow, I. A. Komarow, A. H. Kozlov and V. S. Isaev, *LPSC 33th*, abstract #2030, 2002. [4] Malin et al., *Science*, 2001.

Acknowledgement: The author acknowledges the use of Mars Orbiter Camera images processed by Malin Space Science Systems that are available at http://www.msss.com/moc_gallery/ and the USGS MOC images web graphical assistant available at http://ida.wr.usgs.gov/. This study is supported by the Programme National de Planétologie (PNP) of Institut National des Sciences de l'Univers (INSU), France.

Fig. 1: Patterned ground on Earth (a) About 1 m large sorted polygons in Greenland (photo J.-P. Peulvast) (b) About 30 m large ice wedges polygons (Canada, GSC photograph).

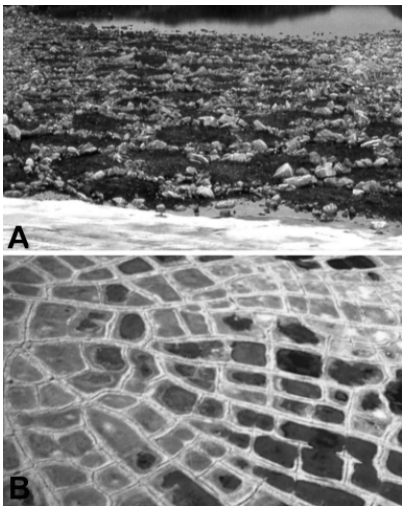

Fig. 3: MOC image of the front of the south polar cap of CO2 with swiss cheese features. Polygons LPC are observed below these swiss-cheese terrains in what is likely ice-rich terrains devoid of permanent CO2 ice.

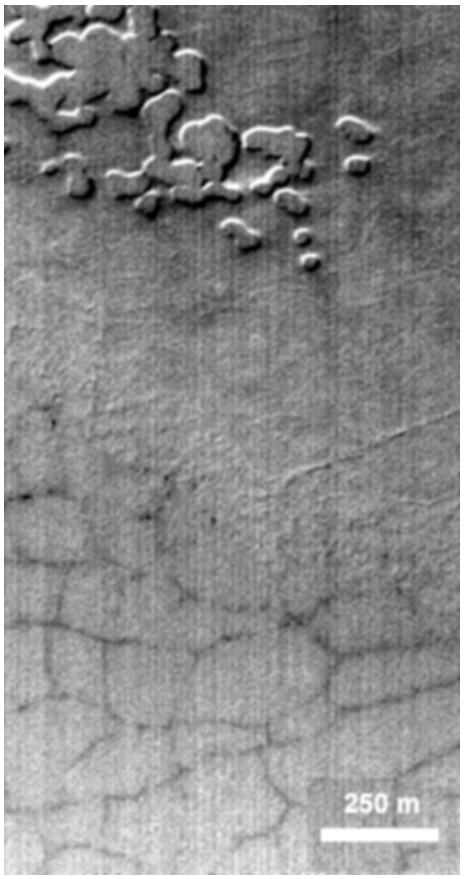

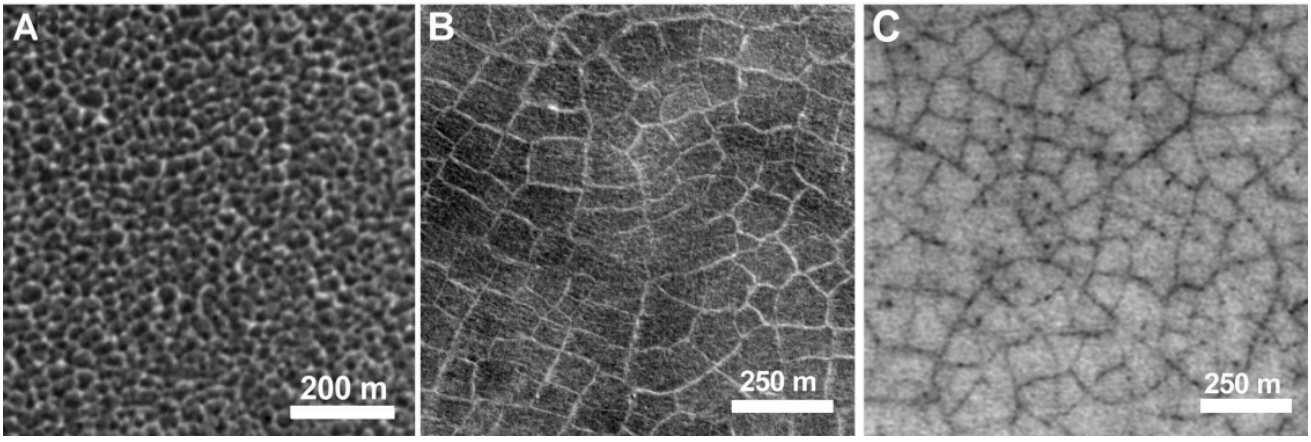

Fig. 2: MOC images of small polygons (S2), large homogeneous polygons (LT) and polygons closed to CO_2 cap (C).

GEOGRAPHICAL RELATIONSHIPS BETWEEN SMALL SCALE POLYGONS AND GROUND ICE DISTRIBUTION FROM NEUTRON SPECTROMETER ON MARS. N. Mangold[1], S. Maurice[2], W. Feldman[3], F. Costard[1], F. Forget[4], [1] Orsay-Terre, Equipe Planétologie, UMR 8616, CNRS et Université Paris-Sud, Bat. 509, 91405 ORSAY Cedex, France, mangold@geol.u-psud.fr, [2] Observatoire Midi-Pyrénées, Toulouse, [3] Los Alamos National Laboratory, New Mexico, USA, [4] Lab. Météorologie Dynamique, Jussieu, Paris.

Introduction:

The occurrence of polygons on Mars similar to those found on Earth in periglacial regions is the subject of debates since three decades. Large polygonal systems have been identified on Viking images of the Northern plains [1]. New high resolution images of the Mars Observer Camera MOC of Mars Global Surveyor (MGS) show small-scale polygons much more similar in size to terrestrial patterned ground [2-5]. The necessary element to the formation of polygons, either by thermal contraction or by freeze-thaw cycles, is the presence of ice in the ground [6]. Our study shows that the global distribution of small-scale polygons on Mars is correlated with the distribution of near-surface ice obtained from the Neutron Spectrometer (NS), one of the component of the Gamma Ray Spectrometer (GRS) aboard Mars Odyssey. This correlation favors the periglacial origin of these polygons which can thus be used as indicators of ground ice and climate variations.

Distribution of polygons on Mars:

The classification of polygons is detailed in the companion abstract (Mangold, Distribution and climatic control of polygons on Mars). These polygons are similar in shape to polygons formed on the Earth by thermal contraction, with seasonal thaw possible in addition. They are classed in polygons smaller than 40 m (S) apparently devoid of cracks (Fig. 1), homogeneous polygons formed by crack networks larger than 40 m (L) and polygons formed by crack networks of heterogeneous size (V). All of these polygons are located in regions of high latitudes poleward of 55° in both hemispheres (Fig. 2). Small polygons (S) and most homogeneous large polygons (L) are found symmetrically in both hemispheres making a climatic control in their formation likely. Nevertheless, the subtype of large homogeneous polygons (LPC) is observed specifically around the polar cap (see companion abstract for explanation). The complex polygons of heterogeneous sizes (V) are located in the southern hemisphere only in the latitude of 65-80 with a gap between 120-220°E. There is no relationship between the distribution of polygons and the Martian stratigraphy: polygons exist in Noachian, Hesperian or Amazonian units. The reason is that the youthful deposits in which they are found is also independent of the stratigraphy established at Viking scale. This young layer is likely composed by a mantling of smooth deposits of dusty, loess like material, containing ice in large amount [7].

Correlation with Neutron Spectrometer data:

The new data from the Gamma Ray Spectrometer (GRS) onboard Mars Odyssey shows that the ground is strongly enriched in ice in polar regions [8]. The ground poleward of 60° may contain proportions of ice of more than 50% in volume whereas the top 10 or 20 cm remains desiccated [8,9]. The Neutron Spectrometer (NS) measures the distribution of hydrogen, supposed to be in the form of ground ice in the latitudes poleward of about 50-60° (Fig. 2). There is a correlation between the distribution of polygons and the distribution of ground ice from NS. Such correlation confirms a periglacial origin for the patterned grounds observed. Looking more in details, small polygons (S) and homogeneous large polygons (L) follow accurately the limit at 55-60° like if they were directly dependent on the occurrence of near-surface ice at these latitudes. The limit is much more equivalent in the south hemisphere than in the northern. Regional differences exist locally. On the NW of Tharsis volcanoes the NS detects near-surface ice down to 45° of latitude whereas polygons seems to exist only at 55° of latitude. By contrast, polygons are found in the latitudes 50-60°N at longitudes of 80-100°E whereas the NS data indicate a limit of ice around 60°.

Interpretation:

The two processes able to produce polygons on the Earth, thermal contraction or freeze-thaw cycles, affect both only the top few meters of the ground because they are the consequence of the propagation of seasonal or diurnal thermal waves. Daily temperature changes produce polygonal features but the maximum propagation depth of the thermal wave is limited to the top 10 cm [10]. In the case of seasonal thaw, the layer which thaws each summer is typically of 1 m thick on the Earth. Seasonal thaw is not possible on Mars currently but obliquity variations may have permitted to thaw the ground down to several tens of centimeters in the recent past [11]. On the other hand, thermal contraction produces crack networks by seasonal changes of temperatures. Seasonal temperature changes induce cracking down to 1 or 2 meters depending on thermal properties of the ground [10]. These depths are similar to the depth of hydrogen possible to be detected by NS which is of about 2 m at maximum. Ground ice may exist deeper than 2 m in regions equatorward to 60° of latitudes without being detected by NS data. However, polygons may not exist at these latitudes because the

depth of this ground ice is not reached by the seasonal thermal waves. Polygons thus correlate to the presence of near-surface ground ice detected by NS probably because periglacial processes like seasonal thermal contraction exist only if water ice is present in the top 1 or 2 m of the ground as detected by Neutron Spectrometer.

Fig; 1: (left) MOC images of small polygons (S). Cracks are not visible but scale limits the identification of geomorphic parameters. (right) MOC image of large polygons (L) very similar to such of high latitudes region of Earth.

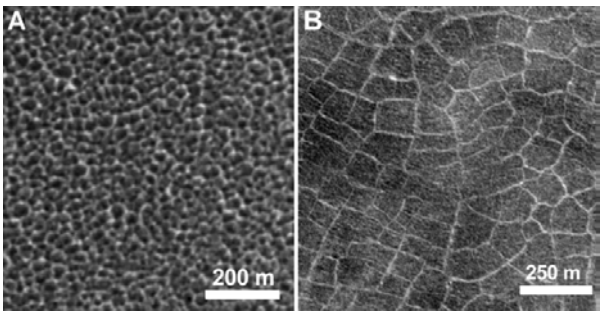

References: [1] Pechmann, *Icarus*, 42, 185-210, 1980. [2] Malin M. C. and K. S. Edgett, *J. Geophys. Res*., 106, E10, 23,429-23,570, 2001. [3] Seibert, N. M. and J. S. Kargel, *Geophys. Research Let.*, 28 (5), 899-902, 2001. [4] Kuzmin, R. O., E. D. Ershow, I. A. Komarow, A. H. Kozlov and V. S. Isaev, *LPSC 33th*, abstract #2030, 2002. [5] Mangold, N., F. Forget, F. Costard et J.-Peulvast, *LPSC*, *33th*, #1912, Houston, USA, 2002. [6] French, H. M., The periglacial environment, 2nd ed., Longman, 1996. [7] Tokar, R. L., W. C. Feldman, T. H. Prettyman, K. R. Moore, D. J. Lawrence, R. C. Elphic, M. A. Kresvalsky, J. W. Head III, J. F. Mustard, W. V. Boynton, *Geophys. Res. Let*., 29, 19, doi10.1029/2002GL015691, 2002. [8] Boynton, W. V. and the GRS team, *Science*, 297, 71-75, 2002. [9] Feldman, W. C., and the GRS Team, *Science*, 297, 76-80, 2002. [10] Mellon, M. T., *J. Geophys. Res*., 102 (E11), 25,617-25,628, 1997.[11] Costard F., Forget F., Mangold N. and J.-P. Peulvast. *Science*, 295, 110-113, 2002.

Acknowledgements: The authors acknowledge the use of Mars Orbiter Camera images processed by Malin Space Science Systems that are available at http://www.msss.com/moc_gallery/ and the USGS MOC images web graphical assistant available at http://ida.wr.usgs.gov/. This study is supported by the Programme National de Planétologie (PNP) of Institut National des Sciences de l'Univers (INSU), France.

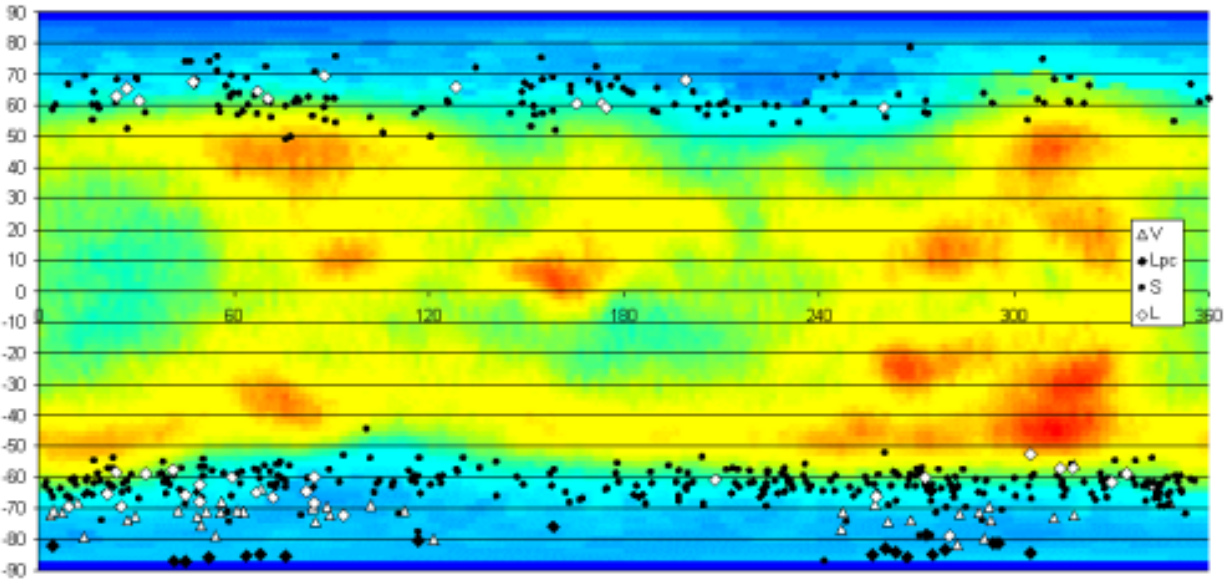

Fig. 2: Distribution of polygons over map of ground ice distribution by the Neutron Spectrometer of GRS onboard Mars Odyssey (Arabia is at left). Most polygons of all types are found in regions where hydrogen is detected at depth of less than 1-2 meters. Equatorial regions with detection of hydrogen have been interpreted as clay rich regions by recent studies.

TONGUE-SHAPED LOBES ON MARS: RELATION TO ROCK GLACIER DEPOSITS AND LONG-TERM HISTORY OF EMPLACEMENT. D. R. Marchant[1], J. W. Head[2], and M. A. Kreslavsky[2,3]. [1]Department of Earth Sciences, Boston University, Boston, MA 02215 marchant@bu.edu; [2]Department of Geological Sciences, Brown University, Providence, RI 02912; [3]Kharkov National University, Kharkov, Ukraine.

Introduction: Recent work based upon Mars Global Surveyor (MGS) data [1,2], in conjunction with previous analyses of Viking data [3], suggests that rock glaciers, similar in form to those found in polar climates on Earth, have been an active erosional feature in the recent geologic history of Mars. A wide range of literature exists describing rock glacier characteristics, form, and distribution, but diversity of opinion exists on rock glacier nomenclature and genesis.

We previously outlined the two-fold genetic classification of *Benn and Evans* [4] for terrestrial rock glaciers, and then proposed a non-genetic descriptive set of terms to be applied to martian features [5] (Fig. 1,2).

Different processes and environments could produce similar or gradational landforms and thus the landforms themselves might not be unequivocal indicators of a specific origin. Thus, we follow *Whalley and Azizi* [1] and suggest that non-genetic descriptive terms be used for the martian features.

We call on established anatomical morphology for nomenclature (Fig. 1,2). The tongue-shaped lobe can be divided into the tip, or *apex*, the *blade* (the flat surface just behind the tip), the body and its rear part (the *dorsum*), and the tongue *root*. Ridges along the edges are called marginal ridges and those concave outward ones at the tongue apex are called *apical ridges*. Within the tongue body and in the dorsum area occur a series of *chevron-shaped ridges* with the apex of the chevrons pointing toward the tongue apex. The central part of the tongue is depressed. The tongue root zones occur in the upper parts of crater walls in subdued alcoves. The tongue width narrows by at least a factor of two from the root zone toward the tongue body. Chevron ridges occur primarily within this transition zone. Surrounding the tongue-shaped lobes are linear to elongate smoothed and subdued ridges and mounds, some with scalloped margins. The scalloped margins occur on the inside and the broad structure often mimics the tongue shape. In Fig. 1, subdued channels emerge from the apices of these broad features. We interpret these broad features to be remnants of earlier larger and more extensive lobes.

On the basis of the characteristics of the tongue-shaped lobes on Mars, their associated features, and comparison to features in the Antarctic Dry Valleys of known origin, we can reach the following conclusions: 1) A variety of features on Mars are very similar to features on Earth that form in glacial and periglacial environments; 2) Confusing nomenclature, genetic classifications, possible form convergence or equifinality, and uncertain origins of many of the terrestrial examples all make direct application of general Earth morphological comparisons to Mars difficult; 3) We therefore have developed a descriptive and non-genetic nomenclature for these features; 4) Careful comparison of the Mars features to well-studied Earth analogs in the Mars-like environment of the Antarctic Dry Valleys can lead to insights into the origin of these features on Mars; 5) The morphology and characteristics of the Mars features examined in this study have been carefully compared to three types of features in the Antarctic Dry Valleys: a) gelifluciton lobes, b) rock glaciers, and c) alpine glaciers; 6) The tongue-like lobate, concave nature of these features is very similar to alpine glaciers and debris-covered glacier deposits. In these cases, the percentage of ice in the original deposit was very high, and sublimation and melting led to retreat, and subsidence and downwasting of any debris cover, leaving marginal morainal ridges as a main feature; 7) The presence of fainter, broad lobe-like features with scalloped margins of similar orientation suggest the former wider extent of such activity; 8) The lack of cross-sectional convexity in these tongue-shaped lobes and related deposits suggests that the ice involved in their formation is now largely gone. This suggests that conditions in the past favored the formation of active glaciers and glacial landforms, and that the present time is more equivalent to an interglacial period; 9) The presence of these features on pole-facing interior crater walls suggests that this micro-environment is very favorable for the accumulation of snow and the initiation of local glaciation; 10) This type of glaciation appears to be a significant process in the modification of crater walls and floors.

We now turn to an analysis of the interior of a crater wall located at 44.4S, 195.3W and illustrating a longer-term evolution than those in Figures 1 and 2. This region lies on the north (pole-facing) wall of a crater in the southern hemisphere and shows a variety of features that contrast radically with the features seen on the southern (equator-facing) wall. Average slopes on the northern wall are ~16° and the floor of the crater slopes about 2-3° to the south.

Figure 3 illustrates the features and facies that have been mapped in this area. First the floor of the crater is marked by extensive dune deposits that cover broad ridges that partly mimic the wall-facing scarp that is seen at point 1. Secondly, the scarp along point 1 is broadly cuspate and separates the south-tilting floor from the base of the wall. Inward of this are observed more arcuate patterns (2) that are very similar to the apical ridges and scalloped margins seen in Figure 1 and 2. Northward of this (3) are much more continuous apical ridges and marginal ridges that appear to be very similar to those seen in Figures 1 and 2. Separating these are broader scalloped margins comparable to those in Figure 1 and 2. The characteristics of these deposits and structures, and their location on pole-facing slopes is consistent with many observations of similar features related to ice-rich features and accumulations [6-10]. We interpret these to be related to a former period of ice accumulation and downslope flow onto the crater floor to produce the asymmetric crater interior slopes and southward-tilting floor. Note the differences between the features and structures in Figures 1 and 2 interpreted to be related to the formation of rock and debris covered glaciers. In the case of Figure 1 we concluded that although morphologically fresh, the morphology of these lobate tongues suggested that they were in a state of wasting and retreat, rather than accumulation and advance.

In contrast to the features seen in Figures 1 and 2, the area in Figure 3 is characterized by fan-shaped deposits superposed on the lobate deposits (4). The apices of these fan-shaped deposits extend up into discrete and rough-textured alcoves on the upper parts of the crater walls. These deposits are interpreted to be talus cones that are derived from erosion of debris from the alcove, and channeling of the debris to form talus cones below the alcoves. Note their clear superposition on the underlying units and features related to rock and debris covered glacial emplacement. The superposition of these features strongly suggests that the environment characteristic of this crater wall in earlier history was climatically capable of supporting sufficiently continuous snow accumulation to create an accumulation zone and produce rock and debris covered glaciers. A summary of these conditions is shown in Figure 3 (right). With time, these conditions changed sufficiently to cause retreat of the glacier, localization into discrete tongue-shaped lobes, and then ultimately to loss of most of the volatiles and topography typical of these lobes elsewhere (compare Figure 3 to Figures 1 and 2). These changing conditions then resulted in the formation of discrete chutes and gullies that fed the

large talus aprons that characterize the most recently detectable geological activity at this scale.

In conclusion, this mapping, superposition relationships, and correlation between different examples of comparable crater wall settings strongly suggest that there is a record of changing climate conditions and microenvironments. We have mapped multiple examples of these deposits and are currently assessing variations in space and time to help map out the recent climate history of Mars, and to distinguish long-term climate change from microenvironments.

References: **[1]** Whalley, W. B. and Azizi F. (2003) *JGR, 104 (E4),*8032, doi: 10.1029/2002JE001864. **[2]** Head J. W. and Marchant, D.R. (2003) *Geology, 31*, 641. **[3]** Lucchitta, B. K. (1981) *Icarus,* 45 (2), 264-303. **[4]** Benn, D.I. and Evans, D.J.A. (1998) *Glaciers and Glaciation*, Arnold Publishers, London. **[5]** Marchant, D. R. and Head, J. W., Mars 6, #3091, 2003. **[6]** Malin, M. and Edgett, K, JGR, 106. 23429, 2001. **[7]** Milliken, R. et al., JGR, in press, 2003. **[8]** Howard, A., LPSC 34, #1065, 2003. **[9]** Reiss, D. and Jaumann, R. LPSC 34, #1821, 2003. **[10]** Kargel, J. et al., LPSC 34, #2092, 2003.

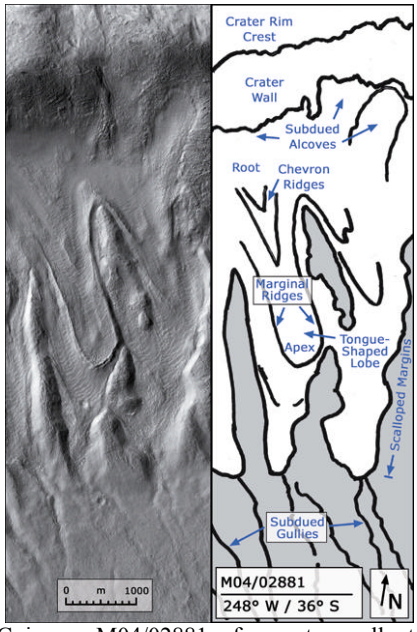

Figure 1. MOC image M04/02881 of a crater wall at 248°W/36°S, Mars. North is at the top of the image, and illumination is from the northwest.

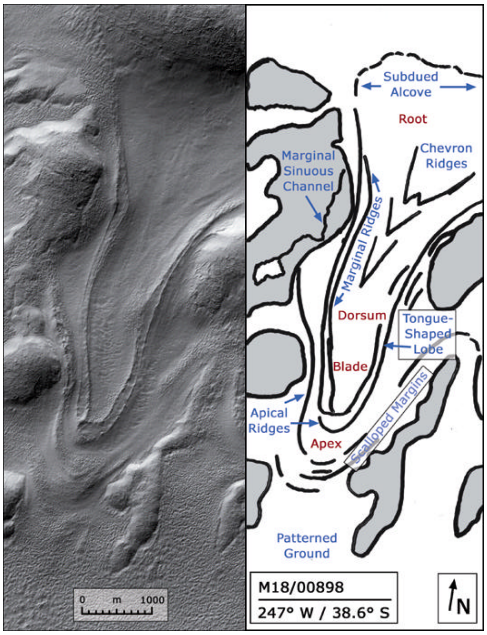

Figure 2. MOC image M18/00898 of a crater wall at 247°W/38.6°S, Mars. North is at the top of the image, and illumination is from the northwest.

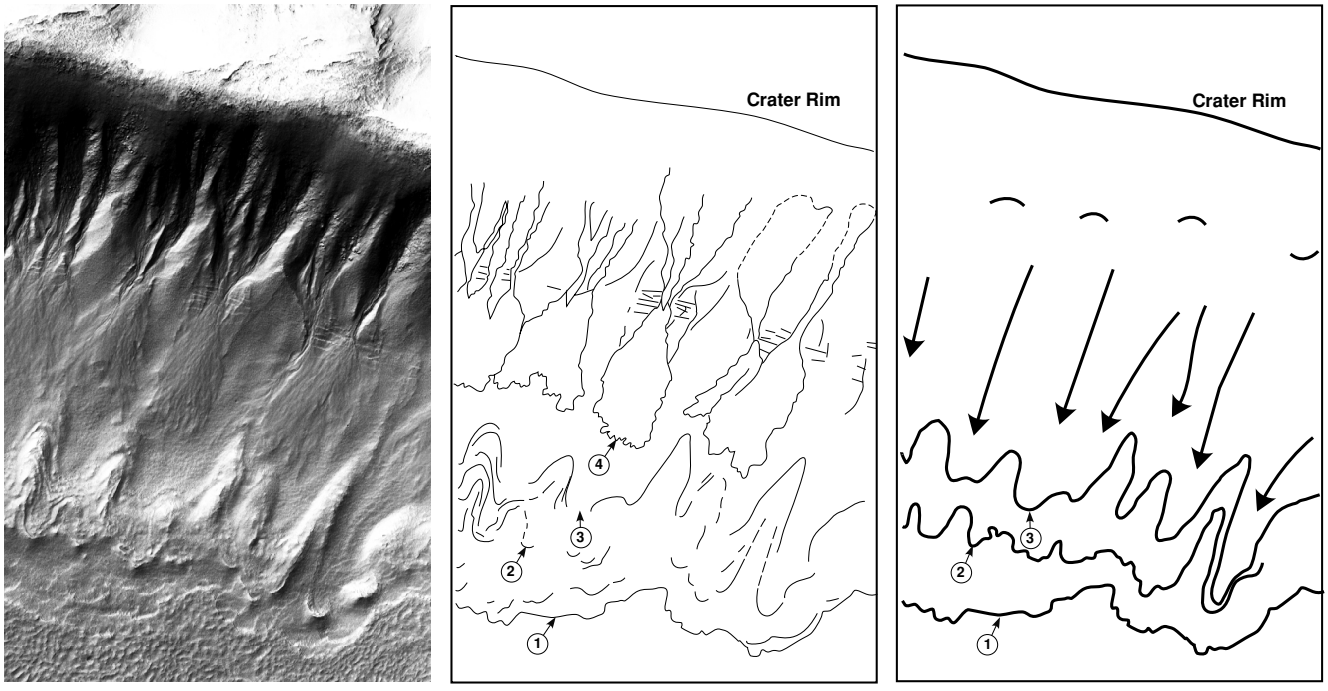

Figure 3. Portion of north (pole-facing) slope of impact crater at 44.45, 195.3W. Left, MOC Image E14 101929. Image is ~3 km in width. Middle, sketch map of features in MOC image. Right, interpreted directions and sequence of glacial advances represented by the deposits and structures.

CO_2 Ice in Polygonal Troughs in Malea Planum, Mars: Sub-Surface H_2O Ice, MOC Images and TES Surface Temperature. W.J. Markiewicz[1] and K.J. Kossacki[2], [1]Max-Planck-Institute for Aeronomy, Max-Planck-Str 2, D-37191 Katlenburg-Lindau, Germany, markiewicz@linmpi.mpg.de, [2]Institute of Geophysics of Warsaw University, Pasteura 7, 02-093 Warsaw, Poland.

Introduction: In this work we analyse the diurnal and seasonal changes of the surface temperature in the south polar region of Mars. This work is a continuation of that presented in [1] were we have modelled the seasonal cycle of CO_2 surface ice within the polygonal features in the Malea Planum region. Our present goal is to investigate the influence of the physical and topographical properties of the polygonal features and the subsurface permafrost on the spatially averaged regolith (surface) temperature. We compare the results of simulations to the seasonal profile of surface temperature derived from the data obtained with the Thermal Emission Spectrometer (TES) on board of the Mars Global Surveyor (MGS). Polygonal patterns were observed with the Mars Orbiter Camera (MOC) also on board of the MGS. An example of such an image, together with the wide angle MOC context image is shown in Fig. 1. The image was taken during early southern spring, L_s=224.96º, the image is centred on 67.71º S and 303.77º W. The high albedo material within the polygonal troughs is interpreted as remnant seasonal CO_2 ice. Formation of the troughs on Mars was analysed in [2].

Surface temperature: The influence of the polygonal features on the average surface temperature can be due to the shadowing of the troughs, but it is also due to the delayed spring sublimation of CO_2 ice deposited within the troughs. Wherever the CO_2 ice is present, the temperature remains close to that of the phase equilibrium of about 145º, significantly lower than the temperature of the surface not covered by the CO_2 ice. During spring the average surface temperature in regions covered by the polygonal patterns will rapidly increase when the surface CO_2 ice disappears. This will be followed by an additional increase starting when the bottoms of the troughs become partially free of the CO_2 ice and continuing until all of the CO_2 ice sublimes away. The magnitude of this secondary increase is most directly dependent on the fraction of the surface covered by the troughs which is in the considered region up to about 10%. This evolution of temperature is seen in the TES data shown in Figure 2. The initial rapid increase at about L_s=220º marks when surface CO_2 is sublimated away. The secondary increase appears around L_s=245º, and can be clearly seen in the detailed plot in Figure 4.

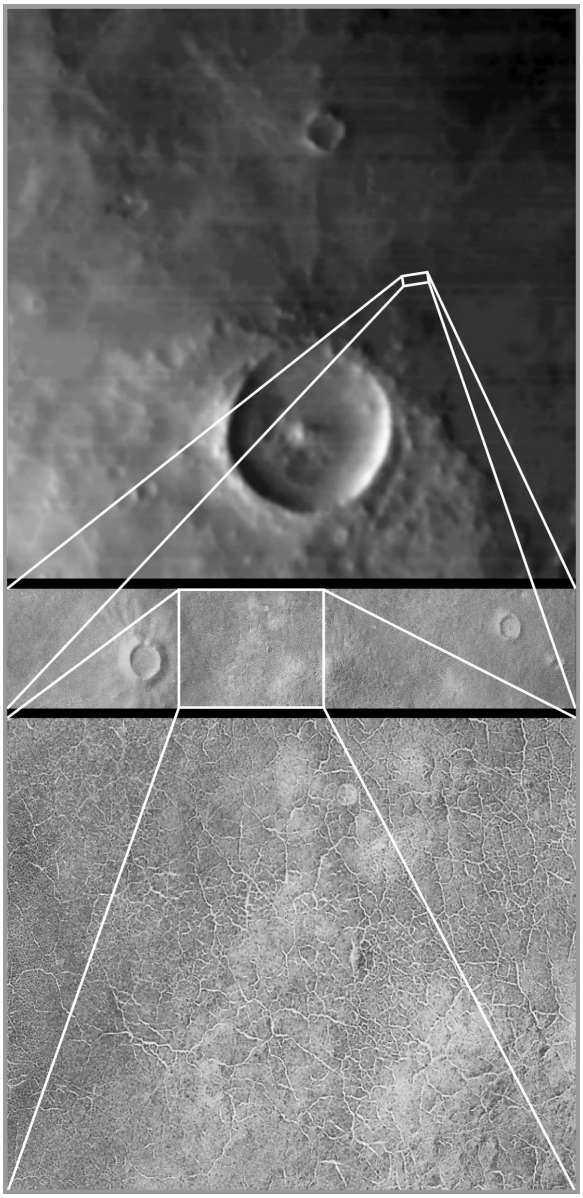

Figure 1 MOC image of the polygonal features with a context image (top). The middle image is 1.5 km across (short side). Resolution is 3 m px^{-1}.

Model: The model used in this work is almost the same as in [1], where the interested reader can also find its full mathematical description. Here we just underline the main features of the model. We analyse heat transport and evolution of water ice distribution in the subsurface vicinity of a trough in the Martian soil.

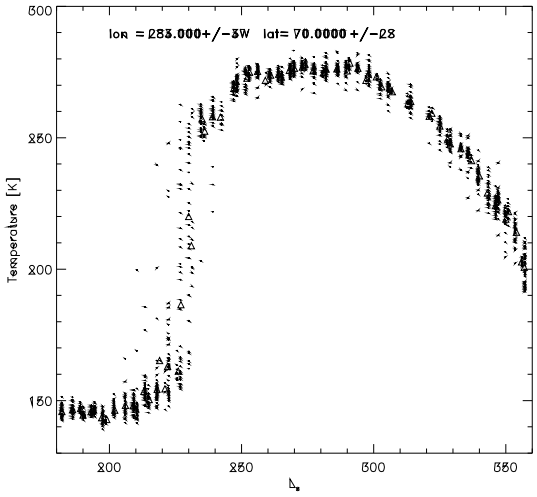

Figure 2 Surface temperature derived from the Thermal Emission Spectrometer data. Dots mark the individual TES footprints and triangles are sol averaged values.

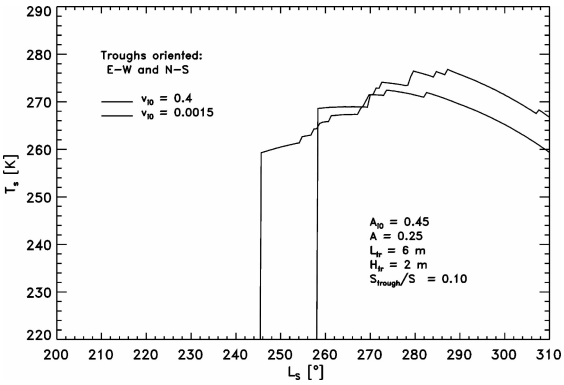

Figure 3 Influence of the content of the subsurface H_2O ice on the average surface temperature. The solid line corresponds to the model with water ice rich regolith, and the dashed line to the model with water free regolith.

The model also includes seasonal variations of the zenith angle of the Sun as well as seasonal variations of atmospheric pressure and composition. We also include sublimation and condensation of CO_2 ice in the trough. The topography considered has spatial scale of meters. This is small enough to assume that the presence of a trough does not have an effect on the diurnal, nor seasonal evolution of atmospheric density and composition which are taken from results of GCM [3]. Most importantly we have looked at two different models of the initial subsurface water ice distribution. One with water rich permafrost and one with effectively dry regolith. Our 2-D model includes condensation and sublimation of the CO_2 ice and a self consistent treatment of variations of the thermal properties of the regolith.

Results: Our primary interest is the amount of water ice that is present in the regolith. In Fig. 3 the surface temperature profiles are plotted for two models of the water ice content in the regolith. One model has volume ice content, v_{i0}=0.4 and the other assumes a dry regolith. When the regolith is rich with water ice, growth of the surface temperature following recession of the seasonal ice cap starts at L_s=245°, about 25 sols earlier than predicted by simulations assuming regolith free of water ice. This is due to the relation between winter condensation rate of CO_2 and the saturation of regolith with water ice. When the concentration of water ice is high, heat flux from regolith reduces winter

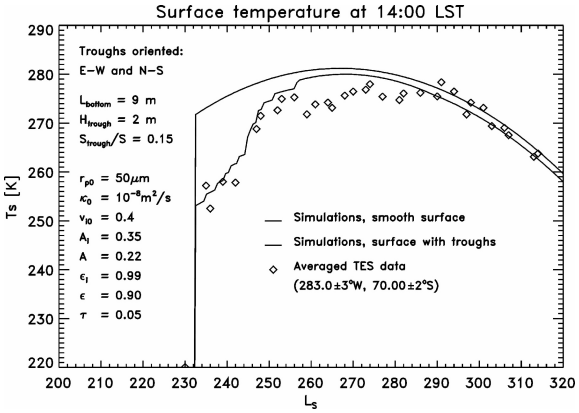

Figure 4 Comparison of the spatially averaged surface temperature from TES data with simulation.

condensation of CO_2 [1] . Resultant thinner deposit of CO_2 ice sublimes away earlier. Subsurface water ice also reduces significantly the maximum summer surface temperatures. This is because the water ice increases the thermal conductivity of the regolith, increasing the inward heat flux and in turn cooling the surface. Clearly only the model with water ice rich regolith can be fitted to the data as finally shown in Figure 4. Further details can be found in [4].

References: [1] Kossacki K.J. and Markiewicz W.J. (2002) *Icarus*, **160**, 73-85. [2] Mellon, M.T. (1997) *JGR*, **102**, 24,177-24,194. [3] Forget F. et al. (1999) *JGR*, **104**, 24,155-24,176. [4] Kossacki K.J. et al. (2003) *Planet. Space Sci.*, **51**, 569-580.

COMBINING MICRO-PENETROMETER AND NEAR-INFRARED PHOTOGRAPHY TO MEASURE PHYSICAL PROPERTIES IN SNOW PROFILES. M. Matzl[1] and M. Schneebeli, [1] WSL Swiss Federal Institute for Snow and Avalanche Research (SLF), Flüelastr. 11, CH-7260 Davos Dorf, Switzerland, matzl@slf.ch

Introduction: The description of layered snow profiles bases mostly on morphological methods. Physical properties are then correlated to the morphology and density of the snow. Different layers and horizons in the snowprofile are classified according to a set of features, most of them by manual and visual inspection [1]. Basic physical parameters, as density, are measured within the layer, assuming no spatial variability within the classified layer. Planar vertical sections allow for higher resolution, but are only feasible for small areas (up to 0.07 m vertical extension). This type of snowprofile has several drawbacks: the features (e.g. hand hardness, grain size, snow type) are measured at discrete locations, the description is one-dimensional and the level of discrimination of layers is subjective. A notable exception is the translucent profile, which is used sometimes for illustration. A quantitative analysis of this type of profile is difficult because transmittance of light is not only dependent on density, but also on grain size. The correlation of physical properties of the snow to density and grain type is incomplete, as is shown by the extensive field measurements of thermal conductivity by Sturm et al. [2]. We developed two new methods, which measure directly with high spatial resolution physical and mechanical properties of a snowpack. The micro-penetrometer measures the strength of bonds between structural elements ("grains") [3]. Near-infrared photography [4] maps the distribution of the specific surface area of a snowprofile with a resolution of about 4 x 10^{-6} m^2. Here we try to combine the signals of these complementary methods.

Methods: The micro-penetrometer (SnowMicroPen) measures the penetration resistance with a sampling distance of 4 µm and a layer resolution of about 1 mm (no thinner layers of snow were observed until now). Based on a mechanical model compressive strength can be calculated directly from the signal [5]. Density and textural information are derived by statistical models. The horizontal spacing of the measurements in the field is for practical reasons about 0.5 m, in the laboratory 0.05 m, each measurement takes about 3-4 minutes. For the near-infrared photography we used a modified digital camera with a CCD sensible in the near infrared. The pitwall is resolved with a resolution of about 1 mm / pixel, effective spatial resolution is about 4 mm^2. Targets of barium-sulphate paper or Teflon were inserted in the profile wall to rectify and calibrate the image. The micro-penetrometer measurements were about 0.05 m behind the profile wall. Details of the methods are described in [6] for the micro-penetrometer and [4] for the NIR-photography.

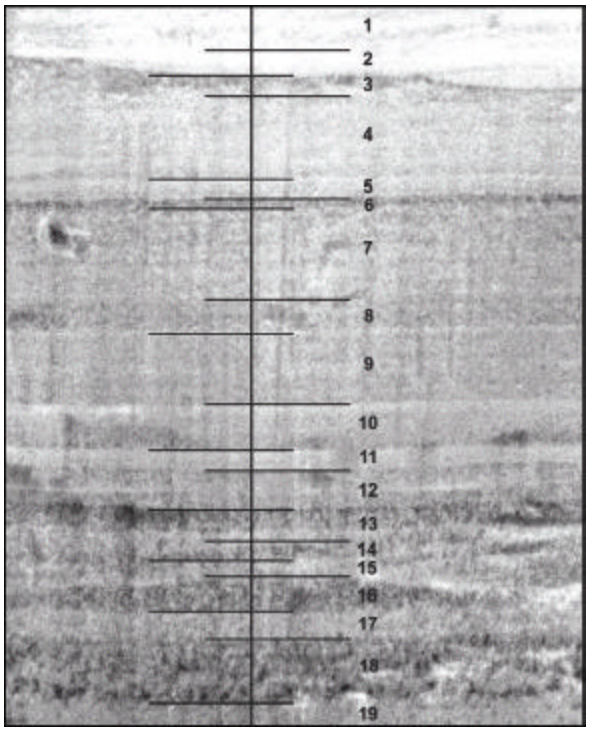

Fig. 1 Corrected near-infrared photography.

Results: A snow profile on a flat area was photographed, rectified and radiometrically corrected. Layers are visually determined and the position of the micro-penetrometer measurement is indicated with a black line (Fig. 1). Similar patterns of change are observed at horizon boundaries for the micro-penetrometer signal and the near-infrared reflectivity (Fig. 2). This shows that similar boundaries are represented in both methods. However, the two signals are not correlated, and are thus representing different properties of the snowpack. Both methods show substantial variability within one horizon.

Discussion: Near-infrared reflectivity, expressed as specific surface area, and penetration resistance measure at high spatial resolution mechanical and physical parameters in a snowpack. The two methods are supplementary. Snowpacks observed with these methods show much more complexity than observed in a classical snow profile, and have the advantage that an objective and persistent record of the snow profile can be

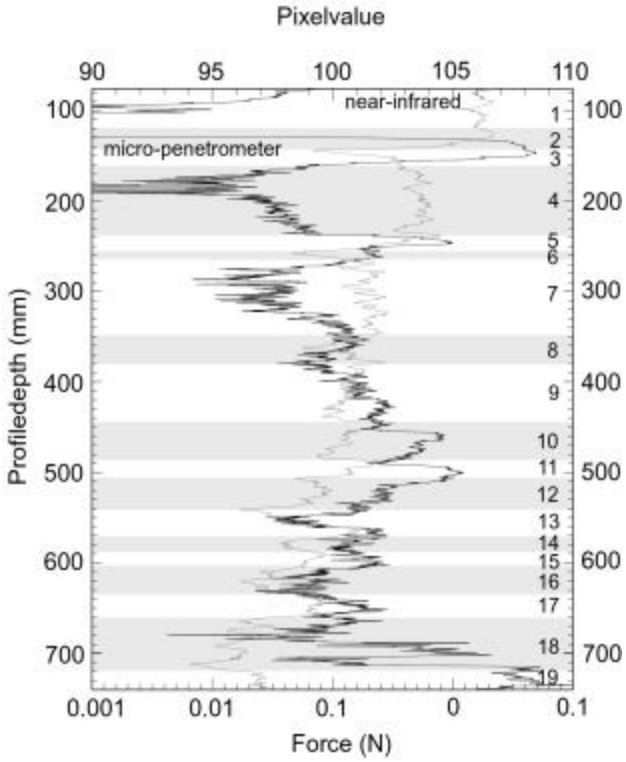

Fig. 2 Comparison of micro-penetrometer resistance and near-infrared reflectivity. Visually determined layers are indicated as grey and white bars.

kept. Additional research has to go in the physical interpretation of the signals and the statistical evaluation of the data. This will be done also by the use of geostatistical methods. The method has a large potential for calibrating radar spectra in the snow cover and to improve correlating chemical and physical and climatologically relevant properties of the snowpack.

References: [1] Colbeck, S. C. et al. (1990) *IAHS-ICSI Publ.* [2] Sturm, M. et al. (1997) *J. Glac. 26*, 209-216. [3] Schneebeli, M. et al. (1999) *Cold Reg. Sci. Technol. 30*, 101-114. [4] Schneebeli, M. and Matzl, M. (2003) *Geophysical Research Letters, submitted*. [5] Johnson, J. B. and Schneebeli, M. (1999) *Cold Reg. Sci. Techno. 30*, 91-100. [6] Pielmeier, C. and Schneebeli, M. (2003) *Cold Reg. Sci. Technol, in press*.

SCOUT MISSIONS AND FUTURE EXPLORATION OF THE MARTIAN POLES. K.S. McBride, Mars Program Directorate, Code SM, NASA Headquarters, Washington, DC 20546 USA, <kmcbride@hq.nasa.gov>.

Introduction: NASA's Mars Exploration Program, (MEP) complemented by missions in operation by ESA and the Japanese space agency, is revolutionizing the study of Mars as a planet and potential home for life, past, present or future. Within the MEP there are a number of significant opportuntieis for the study of the Mars polar regions—from the ongoing Mars Global Surveyor and Odyssey missions, the upcoming Mars Reconnaissance Orbiter, and the soon-to-be-defined Mars Science Laboratory. As an internal complement to the Mars missions being developed by JPL for the MEP, Mars Scout investigations can provide substantial future opportunities to study the polar regions of Mars. These relatively small, PI-led missions provide substantial flexibility within the overall MEP, providing the capability to respond to scientific targets of opportunity in Mars science, with special-interest small missions, or to be developed to respond to instrument opportunities for missions developed by international partners.

Status and Future Plans: In the summer of 2003, NASA will select the Scout investigation planned for the 2007 mission launch opportunity. For future opportunities, Scout will respond to pathways of Mars exploration that are being studied by NASA and others, with the expectation that a Scout mission will be launched approximately every other launch opportunity during the next decade. Such mission opportunities are also anticipated to be supplemented by future instrument opportunities that will both make use of new technologies and to provide US participation on missions now being studied by ESA and CNES.

Irrespective of the opportunities in question, a rigorous selection process that includes both science evaluation and a detailed technical, management, and cost analysis will be applied to all Scout proposals. Through ongoing Scout investigations, the MEP should provide a substantial source of competitive opportunities for PI-led teams to participate in the future exploration of Mars and its polar regions.

MRO's HIGH RESOLUTION IMAGING SCIENCE EXPERIMENT (HiRISE): POLAR SCIENCE EXPECTATIONS. A. McEwen[1], K. Herkenhoff[4], C. Hansen[2], N. Bridges[2], W.A. Delamere[3], E. Eliason[4], J. Grant[5], V. Gulick[6], L. Keszthelyi[4], R. Kirk[4], M. Mellon[7], P. Smith[1], S. Squyres[8], N. Thomas[9], and C. Weitz[10]. [1]LPL, University of Arizona, [2]JPL, [3]Ball Aerospace and Tech. Corp., [4]USGS, [5]CEPS, Smithsonian Ins., [6]NASA Ames/SETI, [7]University of Colorado, [8]Cornell University, [9]University of Bern, Switzerland, [10]PSI/NASA HQ.

Introduction: The Mars Reconnaissance Orbiter (MRO) is expected to launch in August 2005, arrive at Mars in March 2006, and begin the primary science phase in November 2006. MRO will carry a suite of remote-sensing instruments and is designed to routinely point off-nadir to precisely target locations on Mars for high-resolution observations. The mission will have a much higher data return than any previous planetary mission, with 34 Tbits of returned data expected in the first Mars year in the mapping orbit (255 x 320 km).

The HiRISE camera [1] features a 0.5 m telescope, 12 m focal length, and 14 CCDs (Table 1).

Table 1. HiRISE Capabilities

Ground Sampling Dimension (GSD)	30 cm/pixel (at 300 km altitude)
Swath width (Red bandpass)	6 km (at 300 km altitude)
3-Color swath width	1.2 km (at 300 km)
Maximum image size	20,000 x 65,000 pixels
Signal:Noise Ratio (SNR)	>100:1
Color Bandpasses	Red: 550-850 nm Blue-Green: 400-600 nm NIR: 800-1000 nm
Stereo topographic precision	~20 cm vertical precision over ~1.5 m^2 areas
Pixel binning	None, 2x2, 3x3, 4x4, 8x8, 16x16; each CCD separately commanded.
Compression	Fast and Efficient Lossless Image Compression System (FELICS)

We expect to acquire ~10,000 observations in the primary science phase (~1 Mars year), including ~2,000 images for 1,000 stereo targets [2]. Each observation will be accompanied by a ~6 m/pixel image over a 30 x 45 km region acquired by MRO's context imager. Many HiRISE images will be full resolution in the center portion of the swath width and binned (typically 4x4) on the sides. This provides two levels of context, so we step out from 0.3 m/pixel to 1.2 m/pixel to 6 m/pixel (at 300 km altitude). We expect to cover ~1% of Mars at better than 1.2 m/pixel, ~0.1% at 0.3 m/pixel, ~0.1% in 3 colors, and ~0.05% in stereo. Our major challenge is to find the key contacts, exposures, and type morphologies to observe.

Landing Site Safety and Trafficability. A prime objective of HiRISE is to characterize landing sites and identify potential hazards to landed missions. The size and shape of boulders and other topographic obstacles considered dangerous varies from mission to mission, but, for example, 0.5-meter high boulders were considered potentially fatal to the 2001 lander (which may land in the north polar region via the Mars Scout mission called Phoenix [3]). MOC is able to detect giant boulders or detached chunks of bedrock larger than ~5 m diameter, but boulder counts are probably incomplete for objects smaller than ~10 m. Such large objects only occur in limited geologic settings such as near the base of steep slopes that are less than a few km high or near the rims of impact craters. For MER landing site studies it has been necessary to rely on extrapolations based on observed giant boulders using the size-frequency distribution of boulders at previous Mars landing sites and at Earth analog terrains, along with estimates of rock abundance from thermal models [4]. HiRISE will directly map out the distribution of boulders larger than 1 m diameter (typically 0.5 m high).

Mars Polar Science Issues. HiRISE will address many important polar science issues; a few examples are given below.

How recently did the mid-latitude gullies form?
Malin and Edgett [5] proposed that the gullies are young (probably less than 10^6 yrs) because there are usually no superimposed impact craters and because gully materials are superimposed over dunes and polygonally-patterned ground, which are young features on Earth (10^3 to 10^6 yrs for patterned ground [6]). This leaves open the possibility that gullies are forming today, and that liquid water may exist very near the surface. HiRISE can search for changes in the surface topography (compared with previous MOC or HiRISE images) that would indicate current activity of gullies. Evidence for current formation of dunes (possible) or patterned ground (less likely) would also help address this issue.

How can we use small craters for age constraints? There are almost no resolved craters on some polar deposits and high-latitude units such as gullies and debris flows, suggesting that they are extremely young. However, there are several major problems with the statistics of small craters: (1) primary craters may be confused with secondary craters [7]; (2) small craters are easily eroded or buried by eolian processes; (3) small craters may have endogenic origins, and (4) the atmosphere must screen out small and/or low-density bodies and affect the crater distribution. The improved spatial resolution and topographic capability of HiRISE will help address these issues via better discrimination between primaries and secondaries, improved understanding of eolian processes, and improved ability to discriminate between impact and endogenic craters. Extending crater counts to smaller diameters may also reveal clear evidence for atmospheric screening of small bodies, perhaps varying with surface elevation or time (e.g., climate change).

Were there vast ice sheets? Kargel and Strom [8] first proposed that thick, continent-sized ice sheets were present over the polar regions of Mars. If correct, this hypothesis has major implications for paleoclimates. Glacial moraines are characterized by poorly-sorted mixtures of particle sizes up to large boulders, so HiRISE should see clear evidence for this type of deposit, as well as the rich suite of other meter-scale morphologies associated with glaciers.

What was the origin of the Vastitas Borealis Formation? The northern plains are covered by poorly-understood materials; one interpretation is that these are ocean sediments [e.g., 9]. If correct, the sediments should have fine grain sizes except for widely scattered ice-rafted boulders. The detection of abundant boulders in these deposits might favor direct deposition from floods or mudflow deposits. HiRISE will certainly provide a rich set of observations on periglacial processes in the northern plains [10]. It may be possible to correlate morphologies to surface ice abundances mapped by other experiments.

What is the recent climate history recorded in polar layered deposits? MOC images resolve beds in the polar layered deposits (PLD) down to the resolution limit of the camera [11]. HiRISE images of the PLD are therefore likely to show stratigraphy at finer scales than previously observed, potentially addressing the major uncertainty in the timescales of layer formation. Similarly, higher-resolution images of the PLD will be useful in studying the deformation (faulting and folding) of the PLD [12]. Brightness variations in polar ice could be due to dust load or ice-grain size variations, which the color imaging should distinguish.

What is the efficacy of current eolian activity? Dune migration has not been seen in MOC-Mariner 9 comparisons over several decades [13] nor in MOC-MOC comparisons over a few years [14]. Failure of slip faces of the dunes has been noted [11]. With higher resolution, we might very well see dune motion, thereby providing calibration of the efficacy of eolian processes on Mars in the present day.

What is the polar CO_2 inventory? The "swiss cheese" terrain on the residual south polar ice cap has been observed to retreat 1 to 3 meters in 1 Mars year, apparently via sublimation of CO_2 ice [15]. Continued monitoring of these changes and high-resolution topographic measurements will enable us to better quantify rates of CO_2 loss and the total CO_2 inventory available to facilitate periodic climate change.

Monitoring seasonal change. HiRISE has the ability to image in very low light levels. With pixel binning up to 16x16 combined with 128 lines of Time Delay Integration (TDI), HiRISE can acquire good images under twilight conditions, thus better monitoring the polar regions during their winters.

References. [1] Delamere, W.A. et al. (2003), 6th Int. Mars Conf. [2] Eliason, E.M. et al. (2003), 6th Int. Mars Conf. [3] Smith, P.H. (2003) LPSC abstract 1855. [4] Golombek. M.P. et al (2003) LPSC abstract 1778. [5] Malin. M.C., and K.E. Edgett (2000) Science 288, 2330-2334. [6] Sletten, R.S., et al. (2003) JGR-Planets 108, No. E4, paper GDS25. [7] McEwen A.S. (2003), 6th Int. Conf. Mars. [8] Kargel, J.S., and Strom, R.G. (1992) Geology 20, 3-7. [9] Kreslavsky, M.A., and Head, J.W. (2003) JGR-Planets 107, paper 4. [10] Mellon, M.T. (1997) JGR-Planets 102, 25617-25628. [11] Malin, M.C. and Edgett K.S. (2001), J. Geophys. Res. 106, 23,429-23,570, 2001. [12] Murray, B. C. et al. (2002). *Icarus* **154**, 80. [13] Zimbelman, J.R., Geophys. Res. Lett., 27, 1069-1072, 2000. [14] Williams, K.K. et al., in press at Geophys. Res. Lett., 2003. [15] Malin, M.C., et al. (2001) Science 294, 2146-2148.

THE POLAR REGIONS AND THE SEARCH FOR EVIDENCE OF LIFE ON MARS. C. P. McKay[1]. [1]NASA Ames Research Center, Moffett Field, CA, 94035, cmckay@mail.arc.nasa.gov.

Introduction: The search for life on Mars and evidence for past life connects to polar exploration in two important ways. First the polar regions on Mars are sites of possible liquid water today, and hence possible locations for extant life. Secondly, ancient permafrost may preserve evidence of the nature of martian life.

Polar Life: There is direct evidence that Mars had liquid water early in its history. A plausible comparison with the early Earth and evidence that life appeared quickly on the Earth have lead to a focus on the search for life on Mars. However, on Mars today the presence of liquid water is the limiting ingredient for a favorable environment for extant life. The northern polar regions in the summer are arguably the best location for finding liquid water on the surface of Mars today. This is due to the low altitude (2 to 4 km below the datum and hence the surface pressure in the north polar regions is always above the triple point of water), the presence of massive exposed ice, and the continuous sunlight available for heating the polar ice. If a case is to be made for liquid water and life on the surface of Mars today the northern PLD are probably the best location.

Permaforst Preservation: The microbiology of permafrost locations on Earth have been investigated and it has been shown that viable microorganism can be recovered from Siberian permafrost that is ~3.5 Myr old [1]. New work in Beacon Valley, Antarctic indicates the presence of recoverable microorganisms in ice that is thought to be 8 Myr old.

On Mars there may be extensive permafrost that dates back 3 to 4 Gyr. Recent data from the Mars Oddessy spacecraft have confirmed the suggestion that the polar regions of Mars are rich in ground ice [2]. The south polar regions, but not the polar cap deposits themselves, are of particular interest because this region contains ancient cratered terrain presumably dating back to the end of the heavy bombardment, 3.8 Gyr ago. The actual polar cap deposits are probably much younger. One region of particular interest is centered on 80°S, 180°W. Here the terrain is heavily cratered, there is ground ice present and furthermore there is strong crustal magnetism in the surface materials [3,4]. The presence of strong crustal magnetism confirms the antiquity of these terrains and suggests that they have been relatively unaltered since their initial deposition. This location may represent the site of the oldest, coldest, undisturbed permafrost on Mars. Martian microorganisms may be trapped and preserved in this permafrost.

References: [1] Gilichinsky, D.A., E.A. Vorobyova, L.G. Erokhina, D.G. Fyordorov-Dayvdov, and N.R. Chaikovskaya, Long-term preservation of microbial ecosystems in permafrost, Adv. Space Res., 12(4), 255-263, 1992. [2] Feldman, W.C., W.V. Boynton, R.L. Tokar, T.H. Prettyman, O. Gasnault, S.W. Squyres, R.C. Elphic, D.J. Lawrence, S.L. Lawson, S. Maurice, G.W. McKinney, K.R. Moore, R.C. Reedy, Global distribution of neutrons from Mars: Results from Mars Odyssey, Science, 297, 75-78, 2002. [3] Acuña, M. H., J. E. P. Connerney, N. F. Ness, R. P. Lin, D. Mitchell, C. W. Carlson, J. McFadden, K. A. Anderson, H. Reme, C. Mazelle, D. Vignes, P. Wasilewski, and P. Cloutier, Global Distribution of Crustal Magnetism Discovered by the Mars Global Surveyor MAG/ER Experiment, Science, 284, 790-793, 1999. [3] Connerney, J. E. P., M. H. Acuña, P. Wasilewski, N. F. Ness, H. Reme, C. Mazelle, D. Vignes, R. P. Lin, D. Mitchell, and P. Cloutier, Magnetic Lineations in the Ancient Crust of Mars, Science, 284, 794-798, 1999.

NORTH POLAR CAP OF MARS: CORRELATION OF LAYERS WITHIN AND BETWEEN TROUGHS. S. M. Milkovich and J. W. Head, III, Department of Geological Sciences, Brown University Box 1846, Providence, RI, 02912. Sarah_Milkovich@brown.edu

Introduction: Layered deposits exist within the northern residual cap of Mars exposed on the walls of the dark lanes or troughs seen cutting into the cap (Figures 1 and 2). These deposits consist of extensive lateral layers of ice and dust and are found throughout the polar cap. They were first identified in Mariner 9 images [1, 2] and later studied in detail with the Viking orbiters [e. g. 3, 4, 5, 6]. Recent images from Mars Global Surveyor show that the layers have a range of thicknesses and albedos, and are not continuous throughout the cap [7, 8]. Formation theories regard the layers as products of climate change due to orbital cycles [9, 4, 5], similar to climate changes caused by Milankovitch cycles on Earth [10], although the details of the formation processes remain unknown.

Characterization of the layered deposits is key to understanding the details of the layer formation process as well as understanding the processes which shape the polar regions and the martian climate as a whole. This study quantitatively correlates layers in images in order to assess variations within the layered deposits. Such variations can provide constraints for layer formation; for example, how widespread and how uniform is layer deposition on an individual layer scale, and how well do layers correlate within and between troughs?

Method: Many studies of terrestrial climate change are in the field of paleoceanography. Thus, we have adapted a paleoceanographic technique for studying correlations and variations between ocean drill cores. By matching distinctive shapes in the data sets under examination, one can establish correlations and then see how much one data set (the signal) needs to be adjusted to look like the other data set (the target). In this way, one can get a sense of the correlations and changes in accumulation rate between the two sites. By adapting this method to study the stratigraphy of the polar layered deposits we are able to assess correlations and get a sense of the variations between two location within the cap.

Profiles of grayscale intensity, or digital number (DN), taken from MOC images are compared using Match 1.0, a program developed by Lisiecki and Lisiecki [11] to compare sets of paleoceanographic data. This program uses dynamic programming to minimize the square of the differences between the data sets in order to adjust one data set to fit as close as possible to the other set. This method has been used to compare changes in $\delta^{18}O$ values down a core at multiple locations; we use it to compare changes in DN value down a trough wall at multiple locations. In this way, it is possible to measure quantitatively how similar two stratigraphic sequences are.

Prior to comparing profiles from two images, the images must be calibrated and corrected for the slope of the trough wall. To do so, images are calibrated and the associated MOLA data retrieved using programs from the ISIS image processing package. The MOLA data is interpolated between shots to provide an elevation value for each pixel of the image. Thus, the exposure of layers in the image is projected back onto the vertical wall of the trough. The DN profile is then adjusted to run perpendicular to the layer margins. In this way, the data from an overhead image is adjusted to be more like the data from a core sample perpendicular to the cap surface. The profiles are also normalized before they are run through Match 1.0; this entails subtracting the mean from each series and then dividing by the standard deviation. Thus, the data series for each profile will have a mean of 0 and a standard deviation of 1, which improves the ability of Match 1.0 to compare similar data series.

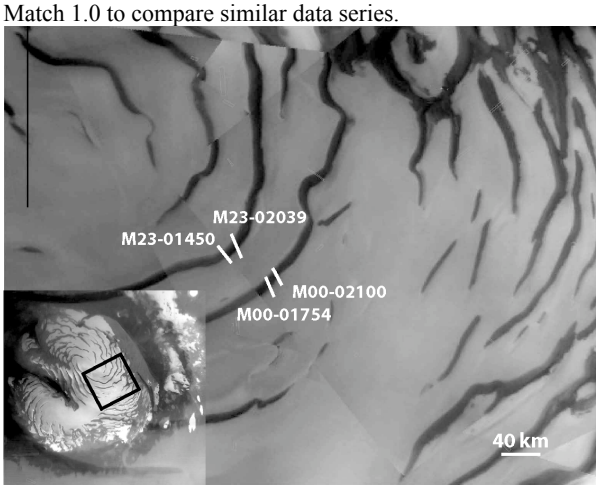

Figure 1. Location of images used in this analysis. Inset box shows location within the cap.

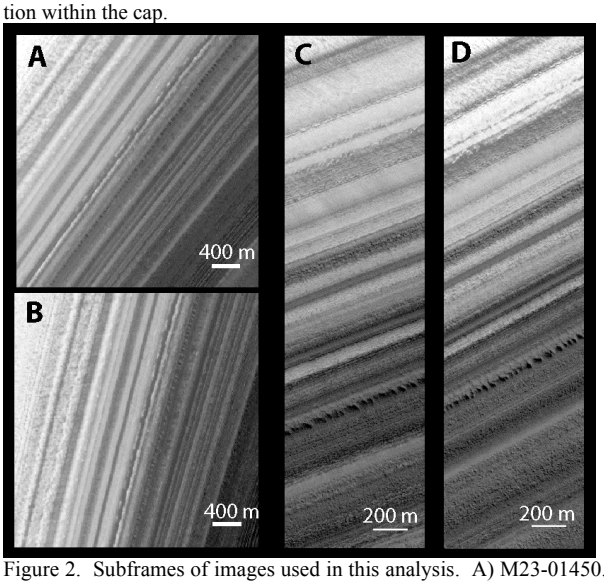

Figure 2. Subframes of images used in this analysis. A) M23-01450. B) M23-02039. C) M00-01754. D) M00-02100. Illumination from the upper right in all images.

The four images selected for this analysis (Figure 2) were taken in the same Ls range (northern summer) to minimize the effects of seasonal frost. M00-01754 and M00-02100, from the southern trough, both have resolutions of 1.8 m/pxl while M23-01450 and M23-02039 have resolutions of 12.1 m/pxl.

Results: Figures 3, 4, and 5 show the results of the matching analysis. In each figure, the top graph shows the normalized, corrected profiles plotted with depth before being matched. The signal is the DN profile which was adjusted to match the target DN profile. The middle graph in each figure plots the results of the matching analysis. The bottom graph shows how much the signal needed to be adjusted along the profile to match the target; this is in essence a relative net accumulation rate (NAR). If no adjustment was necessary, the relative rate is 1.

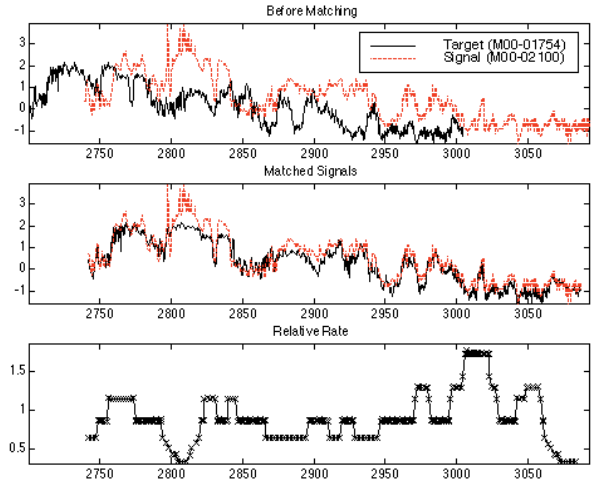

Figure 3. Results of matching M00-01754 and M00-02100. The coefficient of determination (r^2) for this match is 0.9036; 90.36% of the variation in the datasets is related. This indicates a good match between the datasets.

The preliminary results of this analysis are 1) that there is reasonable good correlation between layers in different areas of one trough and between troughs, and 2) that the accumulation rate along a trough varies considerably. Images M00-01754 and M00-02100 are about 18 km apart, and the NAR varies between them up to a factor of two. Additionally, the NAR does not increase systematically – at times one location has the higher NAR while at other times the other location has the higher rate.

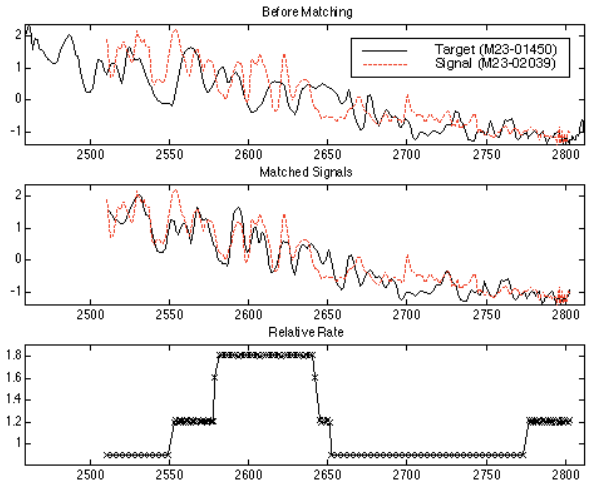

Figure 4. Results of matching images M23-01450 and M23-02039. The coefficient of determination (r^2) for this match is 0.8619; 86.19% of the variation in the datasets is related. This indicates a good match between the datasets.

Additionally, the net accumulation rates do not change in the same manner between the two troughs. The relative rates between M00-01754 and M00-02100 are very different than those between M23-01450 and M23-02039. This implies that there is a great deal of local variation in the layer accumulation process. This can clearly be seen in Figure 5, in which an image from each trough is compared. There is good correlation between the two troughs, with relative accumulation rates again below 2. But the shape of the relative rate curve is different from the relative rate curves of the comparisons of images within a single trough.

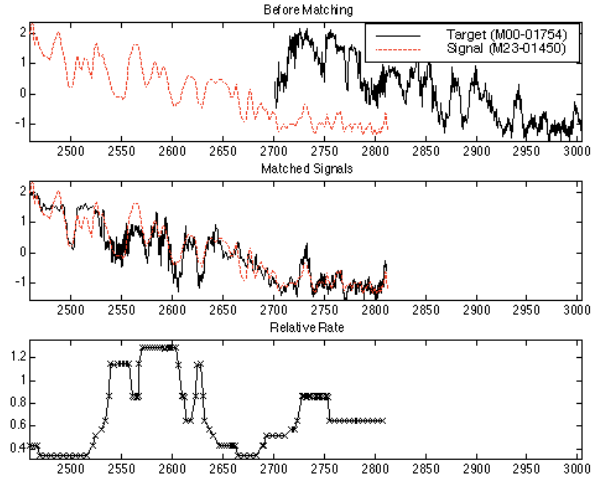

Figure 5. Results of matching M00-01754 and M23-1450. The coefficient of determination (r^2) for this match is 0.8965; 89.65% of the variation in the datasets is related. This indicates a good match between the datasets.

Discussion. Laskar et al [12] examined M00-02100, one of the images used in this study. They compared cycles identified in the image with calculated insolation cycles to find NAR for this area. For the top 250 m the calculated NAR was 0.05 cm/yr. Below that the NAR slowed to 0.025 cm/yr. In order to test these results, it is necessary to determine if these rates remain reasonable for the region. Based on our matching analysis, we find that the DN profile from this image is quantitatively comparable to the three other images in this study. Therefore, under this set of assumptions it is possible to extrapolate NAR to the rest of the region.

The relative rates between the images remain within a factor of 2; therefore, the NAR for this region should be between 0.025 and 0.1 cm/yr for the uppermost section of the region. Estimates of the resurfacing rate for the north polar region based on cratering rates have values as high as 0.1-0.2 cm/yr [13], so the variations on the Laskar et al values are within current estimates. Further studies within this region of the polar cap are required to see if the rates remain plausible.

The fact that the profiles correlate well between two troughs indicates that layers are deposited over a large area, greater that just one trough. However, because the relative rates are not constant, this deposition is not uniform; nor does it change systematically between images or between troughs.

Acknowledgements: The authors gratefully thank Tim Herbert and Lorraine Lisiecki for helpful discussions and assistance with the computer programs.

References: [1] Soderblom, L. A., M. C. Malin, J. A. Cutts, and B. C. Murray.(1973) *J. Geophys. Res.,78,* 4197-4210. [2] Cutts, J. A., (1973) *J. Geophys Res., 78*, 4231-4249. [3] Kieffer, H. H., et. al, (1976) , *Science, 194*, 1341-1344. [4] Blasius, K. R., J. A. Cutts, and A. D. Howard (1982) *Icarus, 50*, 140-160. [5] Howard, A. D., J. A. Cutts, and K. R. Blasius.(1982) *Icarus 50*, 161-215. [6] Thomas, P. et al, (1992) In *Mars*, H. H. Kieffer et al ed. Univ. of Arizona Press. [7] Malin M. C. and Edgett K. S. (2001) *J Geophys Res, 106*, 23429-23570. [8] Milkovich, S. M. and J. W. Head (2001) *LPSC 32* , 1976. [9] Squyres, S. W. (1979) *Icarus 40*, 244-261. [10] Imbrie, J. (1982) *Icarus 50*, 408-422. [11] Lisiecki, L. E. and P. A. Lisiecki (2002) *Paleoceanography, 17*, art no. 1049. [12] Laskar, J. et al. (2002) *Nature, 419*, 375-377. [13] Herkenhoff, K. and J. J. Plaut. (2000) *Icarus 144,* 243-253.

POLAR AND NON-POLAR LAYERS ON MARS: A SINGLE MECHANISM FOR FORMATION? M.A. Mischna[1,2] D.J. McCleese[2,3], M.I. Richardson[2], A.R. Vasavada[1], and R.J. Wilson[4], [1]University of California, Los Angeles, Los Angeles, CA 90095, [2]California Institute of Technology, Pasadena, CA 91125, [3]Jet Propulsion Laboratory, Pasadena, CA 91109, [4]Geophysical Fluid Dynamics Laboratory, Princeton, NJ 08542.

Introduction: The recent discovery of vast quantities of near-subsurface ice in both polar regions of Mars by the Mars Odyssey Gamma Ray Spectrometer (GRS) [1-4] has presented us with an interesting quandary. On one hand, these deposits, found poleward of 60° in both hemispheres, are consistent with thermal models suggesting ice will be best protected in these regions during periods of high obliquity [5-7]. On the other hand, the current paradigm regarding the placement of these deposits, *i.e.*, diffusive deposition of water vapor, appears to be inconsistent with the large volume mixing ratios (~90%) inferred from the GRS data. This incongruity argues that diffusion alone cannot be the primary mechanism for the creation of these reservoirs, and that an alternate, large-scale process should be considered.

Spacecraft Observations: Maps generated by the Mars Odyssey GRS team reveal the presence of massive ice deposits ubiquitously poleward of 60º in both the north and south, well beyond the extent of the observable surface polar layered terrain. We can infer from the GRS data that such deposits may be found only a few to a few tens of centimeters below the surface, and are likely covered by a desiccated surface layer [1].

The GRS results show a distribution of near-surface ice quite similar to the results of [5-7], based on the physical and thermophysical properties of the regolith. One key assumption of these models is the porosity of the soil, which, even for poorly-consolidated regolith, never exceeds ~40%. In other words, the available volume for water vapor within the pore space is limited to 40%. The GRS data, however, yields abundances that are extremely high—as much as 90% by volume, and therefore emplacement via diffusion does not seem wholly consistent with GRS observations.

Further, MGS images of mantled, fretted and otherwise disaggregated, layered terrain are restricted to latitudes just equatorward of these subsurface ice deposits. The suggestion has been made [8] that this distinct "latitude-dependent" morphology is a result of sublimation-driven cementation of the surface material, and hence that these regions, too, must have, at one time, been quite volatile-rich.

Ice Deposition Model: We propose that these observed deposits result from dusty ice sheets formed at the surface, with diffusion into the subsurface being of only secondary importance. Results from a full general circulation model (GCM) [9] support this contention. Whereas presently ice is stable year-round only at the poles (Figure 1a), under periods of higher obliquity, the latitudes of stable, perennial ice change. An increase in obliquity to 35º—approximately that reached at the last obliquity maximum—shifts this zone of stable water ice towards the mid-latitudes, between 50º and 70ºN (Figure 1b). Ice will be deposited in large, localized sheets, predominantly during the wintertime, and in locations of favorable surface properties (*i.e.* high thermal inertia) and favorable atmospheric dynamics. This ice, deposited at a rate of several millimeters to a centimeter per year, will survive through the summer. Over time, ice in such regions may accumulate to potentially significant depths—model results indicate up to several tens of meters may be deposited locally over the course of a single high obliquity excursion.

Increasing obliquity to 45º, which is representative of the high obliquity excursions of 5-10 million years ago, will push this region of stable water ice into the tropics, equatorward of 30º latitude. Under such extreme conditions, the deposition and accumulation of ice is even more substantial, and may, in fact, be limited by the amount of volatiles available for sublimation and transport towards the tropics.

Based upon these model results, it seems possible that the GRS signature we are observing outside the present-day polar deposits is not the present-day diffusion and freezing of water ice in pore space below a preexisting surface, but rather the remnant of a deposited ice sheet(s) during past high obliquity phases, covered by a sublimation lag.

We have developed a simple mechanism to explain the global distribution of water ice by invoking only orbital parameters and the thermophysical conditions of the surface, which is illustrated in Figure 2. The deposition of a layer of dusty ice at a given location will commence once ice at that latitude becomes thermally stable (b). The period of time for which ice will be deposited is clearly dependent on the length of time that obliquity is above some "critical" value, which is different for each latitude. Once Mars' obliquity drops below this "critical" value, ice at lower latitudes is thermally unstable, and will quickly sublime (c), leaving behind the residual lag deposit. For the remainder of the obliquity cycle, ice beneath this lag is quasi-stable and will remain at least until the following obliquity cycle (d). At this point, we argue that one of

two processes may occur. If obliquity again rises above the "critical" value, a new layer of ice and dust may form on the new surface. Such behavior may already be seen in the PLD, for which exposed layers of alternating ice and dust are readily apparent. If, however, obliquity does not again rise above the "critical" value, subsequent mechanisms may act to modify the surface and near surface, including the deposition or removal of dust or sand, and other processes responsible for creating the surface morphology observed in these regions. Such behavior may possibly be observed in the latitude-dependent layer.

Discussion: The advantage of the layering mechanism discussed above is its simplicity. A single mechanism for ice distribution can be used to explain both layered volatile and layered sedimentary deposits presently observed in both the polar and non-polar regions of Mars [10]. This argument is consistent with the observed latitudinal distribution of the dissected terrain being the result of mid-latitude ice deposition at a once higher (~35°) obliquity. It requires no *ad hoc* assumptions about the properties of the surface, or the presence of liquid water. Indeed, the only assumption we must make (which is well grounded) is that dust must be present along with the water ice during deposition.

References: [1] Boynton, W.V. *et al.* (2002) *Science, 297,* 81-85. [2] Feldman, W.C. *et al.* (2002) *Science, 297,* 75-78. [3] Mitrofanov, I. *et al.* (2002) *Science, 297,* 78-81. [4] Mitrofanov, I. *et al.* (2003) *Science, 300,* 2081-2084. [5] Mellon, M.T. and Jakosky, B.M. (1993) *JGR, 98,* 3345-3364. [6] Mellon, M.T. and Jakosky, B.M. (1995) *JGR, 100*, 11,781-11,799. [7] Mellon, M.T. (2003) LPSC XXXIV Abstract #1916. [8] Mustard *et al.* (2001) *Nature, 412,* 411-414. [9] Mischna, M.A. *et al.* (2003) *JGR, 108(E6),* 5062. [10] Malin, M.C. and Edgett, K.S. (2001) *JGR, 106,* 23,429-23,570.

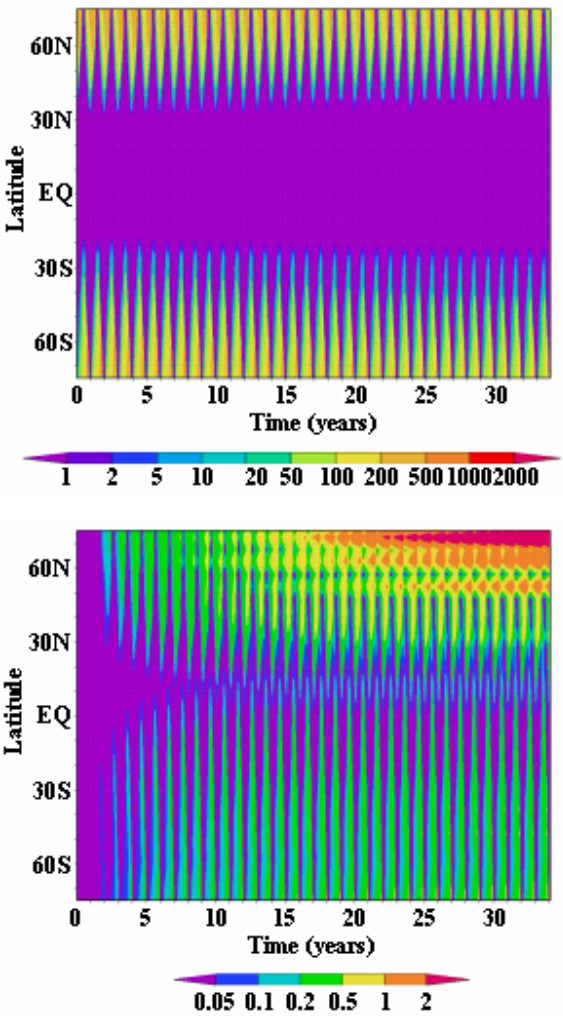

Figure 1: (a) Zonally-averaged surface ice (±75° latitude) at 25º obliquity run for 34 simulated martian years. Ice abundance is in µm. **(b)** Same as (a) but for 35º obliquity. Ice abundance is in cm. Surface ice predominantly located in high mid-latitudes, between 50º-70ºN latitude.

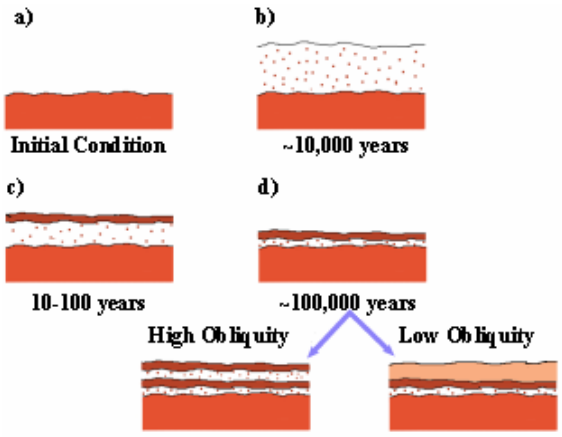

Figure 2: Timeline of surface layering mechanism over obliquity timescales (indicated times are phase durations, not accumulated time during process). **a)** initial exposed regolith **b)** becomes site for residual ice deposition due to variation in astronomical elements. Accumulation goes on for ~10^4 years before **c)** elements change again, area becomes unstable for water ice and net sublimation occurs. However, dust in ice accumulates during sublimation, and generates an isolating lag within 10^1-10^2 years that can **d)** greatly reduce ice loss over an astronomical cycle. The cycle can continue, developing layers, or area may become buried in unconsolidated dust.

NEUTRON DETECTOR FOR MARS ROVER MISSIONS. J.E. Moersch[1] and D.M. Drake[2], [1]Department of Earth and Planetary Sciences, University of Tennessee, Knoxville, TN 37996, [2]221 LA Cruz Rd., Santa Fe, NM 87501, ddrake@cybermesa.com.

Introduction: Recent results from the Mars Odyssey orbiter mission have added immensely to our understanding of the distribution of water ice in the Martian polar deposits. Regional-scale mapping (~300-km resolution) by Odyssey's Gamma Ray Spectrometer [1] and its two neutron detector subsystems [2,3] has revealed shallow (~1m deep) subsurface deposits of water ice in concentrations ranging from 35-100% in the south polar region [4] and 50-75% in the north [5]. Odyssey's Thermal Emission Imaging System has also found thermal evidence for water ice exposed at the surface of the permanent southern cap, mapable at the 100-meter scale [6]. The next step in studying ice deposits in the polar regions of Mars will be to visit them on the surface with mobile robotic explorers. Rover missions offer the opportunity to map the small-scale distribution of water ice, study its mode(s) of deposition and removal, and perhaps gain insight into the climatic history of Mars.

When galactic cosmic rays interact with planetary material nuclei, a variety of particles are produced, including neutrons. Most of the neutrons produced in these interactions are characterized by energies in the 0.5-6 MeV ("fast") range. These neutrons lose energy by scattering from the nuclei in the surrounding medium. In general, neutrons lose more energy in collisions with lighter nuclei. Thus, the energy of neutrons that leak out of the surface is very sensitive to the presence or absence of hydrogen. The most likely reservoir of hydrogen in the Martian surface is water or water ice, although hydrated minerals (e.g. clays) may also account for some Martian H.

The primary signature of the presence of hydrogen in the regolith is carried by epithermal (0.3 eV-0.5 MeV) neutrons, because in this energy region a small amount of hydrogen is extremely effective on moderating the energy of the neutrons. The thermal neutron (<0.3 eV) flux is also related to the hydrogen content in that the neutrons that leave the epithermal flux end up becoming thermal neutrons. Thus, the ratio of thermal to epithermal neutrons leaking out of the Martian surface provides the best indicator of hydrogen content. Monte Carlo simulations suggest that in typical Martian soil, a range of water concentration from 0-5% (by mass) gives rise to ratios of thermal/epithermal neutron counting rates that vary by a factor of ~6.

Instrument Design: We have been funded by the Mars Instrument Development Program to adapt and optimize existing neutron detector designs that have flown on orbiter missions for use on future Mars rover missions. We have recently finished building our first prototype instrument. The instrument design we have selected is based on dual ^{3}He proportional counter tubes, an approach that has heritage from Lunar Prospector [7] and other orbiter missions. One tube is covered in a cadmium jacket, which absorbs incident thermal neutrons, blocking them from being counted. The other tube is left bare, making it sensitive to both thermal and epithermal neutrons. The difference in count rate between the two tubes gives the thermal count rate. The ratio of this rate to the count rate from the Cd-covered tube is the desired thermal/epithermal ratio. This type of instrument is uncollimated, so its effective sensing footprint is determined by the height of the instrument above the surface. Mounted on a rover, the instrument would be able to map subsurface ice abundances at the ~1-meter scale.

The active volume of each counter tube in our design is 20-cm long by 2.5-cm in diameter, a size chosen to balance the trade between keeping instrument mass and volume low versus minimizing the integration time needed to determine hydrogen abundance. Our calculations indicate that a 1-minute integration time on the Martian surface with this size tube gives an error in the thermal/epithermal ratio of about 4%, which gives a corresponding error in the determination of H-abundance of less than one percent.

The signals from each counter tube are fed to pulse-shaping electronics and then to a multichannel analyzer (MCA), which facilitates rejection of higher-energy pulses from gamma rays. The MCAs bin counts from each tube for a user-specified integration time. The MCAs are controlled and read via serial port connection to a laptop computer. In current form, all of the support electronics for the instrument fit in a volume about half the size of a shoe box, although this size could be greatly reduced using custom electronics.

Preliminary Tests: We are currently executing a series of tests with our instrument at Los Alamos National Laboratory to verify it performs as expected (Figure 1). On Earth, the thick atmosphere shields the surface from galactic cosmic rays, so a ^{252}Cf fast neutron source is used to simulate Martian fast neu-

tron production. Dry Martian soil is simulated with glass bricks. In some experiments, glass pans filled with liquid water were used to measure instrument sensitivity to hydrogen. In other experiments, slabs of polyethylene were used; polyethylene has about the same density of hydrogen as water and is easier to work with because it is solid.

Figures 1 and 2 show results from two sets of initial instrument evaluation experiment runs. The points in Figue 1 were obtained by measuring thermal/epithermal count ratios with varying amounts of liquid water at the surface of our soil simulant. As expected, the thermal/epithermal ratio increases as more water is available to moderate high energy neutrons from the source. The points in Figure 2 were obtained by burying different amounts of polyethylene under soil simulant. Once again, the thermal/epithermal ratio increases as more hydrogen is added.

In the near-future, additional lab tests will be performed to further characterize and quantify instrument performance. We will also experiment with different types of shielding (which would be used to block the signal from hydrogen sources on board the rover), instrument placement, and detector tube size.

Field Tests: After we are satisfied with our instrument design based on laboratory evaluations, we will subject it to a series of field tests intended to help us further refine the design and learn how to most effectively work with data from the instrument. In late 2003, we plan to install the instrument on the NASA Ames K-9 rover and perform simple tests with it using buried polyethylene slabs in the new outdoor "Marscape" test facility at Ames. In 2004, our instrument will be fully-integrated into the K-9 rover instrument suite for full-up Mars mission simulations with a "blind" science team remotely directing the rover and interpreting the data it returns. Our hope is that these simulations will demonstrate the utility our instrument would have for upcoming Mars rover missions.

References: [1] Boynton, W.V. et al. (2002) *Science, 297*, 81-85. [2] Mitrofanov, I. et al. (2002) *Science, 297,* 78-81. [3] Feldman, W.C. et al. (2002) *Science, 297,* 75-78. [4] Tokar, R.L. et al. (2002) *Geophys Res. Let., 29*, art. no. 1904. [5] Mitrofanov, I. et al. (2003) *Science, 300*, 2081-2084. [6] Titus, T.N. et al. (2003) *Science, 299*, 1048-1051. [7] Feldman, W.C. et al. (1999) *Nucl. Inst. Meth. Phys Res., 422*, 562-566.

Figure 1: Prototype instrument undergoing first tests. The two 20-cm long ^{3}He detector tubes are visible near the top of the image, held in place on vertical posts. Between the two tubes is a ^{252}Cf fast neutron source. Three layers of glass bricks under the tubes simulate martian soil. In this particular experiment, two glass pans containing water were placed between the first and second layer of glass bricks.

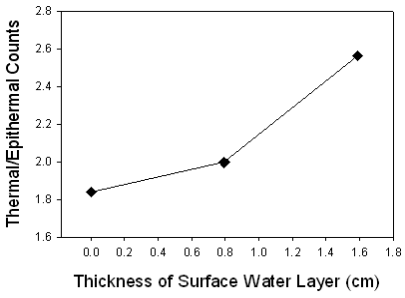

Figure 2: Ratio of thermal to epithermal neutron counts for different depths of water at the surface of our soil simulant. Integration times of 200s were used. As expected, the thermal/epithermal ratio increases with increasing water abundance. These counts are raw (not background-subtracted) and no error bars have yet been assigned.

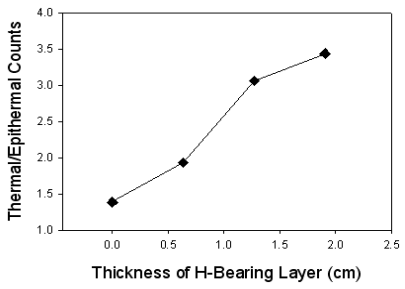

Figure 3: Ratio of thermal to epithermal neutron counts for varying amounts of polyethylene buried under 7.3 cm of soil simulant (which is equivalent to at least 15 cm of real soil because of the difference in density). Integration times of 200s were used. As expected, the thermal/epithermal ratio increases with increasing abundance of buried hydrogen. These counts are raw (not background-subtracted) and no error bars have yet been assigned.

DESCRIBING THE COMPONENTS OF THE WATER TRANSPORT IN THE MARTIAN ATMOSPHERE.. F. Montmessin, R. M. Haberle, *NASA Ames Research Center - Moffett Field*, F. Forget, *Laboratoire de Meteorologie Dynamique-France*, P. Rannou, M. Cabane, *Service d'Aeronomie-France*.

Introduction: In this paper, we examine the meteorological components driving water transport in the Martian atmosphere. A particular emphasis is given to the role of residual mean circulation and water ice clouds in determining the geographical partitioning of water vapor and frost.

Model description: For our simulations, we use the General Circulation Model (GCM) developped at Laboratoire de Meteorologie Dynamique (Paris/France) [1] to simulate Martian hydrological cycle for various orbital configurations. The model includes usual representations of processes like surface sublmation, cloud formation and sedimentation (with predicted cloud particle sizes) [2]. Most of our simulations

Water cycle and circulation: Using the same decomposition as that found in [3], it is possible to recast the water transport in terms of circulation components. Indeed, it is staightforward to demonstrate that the total meridional transport of a tracer species includes the contribution of the mean meridional circulation, that of transient eddies and that of stationary waves.

Following this approach, we express the total transport of water vapor at a given latitude and at a given height as $[\bar{qv}]$, where the $\bar{qv}$ symbol denotes the time average and [] symbols denotes the zonal mean of the product qv, q being the mass mixing ratio of water and v the meridional wind. According to [3], $[\bar{qv}]$ can be written as:

$$[\bar{qv}] = [\bar{q}][\bar{v}] + [\bar{q'v'}] + [\bar{q^*v^*}] \quad (1)$$

with the prime symbol $'$ expressing the departure from the time average ($q' = q - \bar{q}$ and $v' = v - \bar{v}$) whereas the star symbol being related to the departure from the zonal average ($q^* = q - [q]$ and $v^* = v - [v]$).

In short, total water transport $[\bar{qv}]$ is the sum of the mean meridional circulation component $[\bar{q}][\bar{v}]$, that of transient eddies $[\bar{q'v'}]$ and that of non-travelling waves $[\bar{q^*v^*}]$. Eq. (1) can be integrated over height to yield

$$\int_{p_s}^{0} [\bar{qv}]\frac{dp}{g} = \int_{p_s}^{0} [\bar{q}][\bar{v}]\frac{dp}{g} + \int_{p_s}^{0} [\bar{q'v'}]\frac{dp}{g} + \int_{p_s}^{0} [\bar{q^*v^*}]\frac{dp}{g} \quad (2)$$

The latter equation, akin to a zonal- and vertical-mean expression of the water meridional transport, synthetizes the general behavior of the meridional flux fields. Given that q is the sum of both atmospheric water vapor and water ice (clouds), eqs. (1) and (2) can be further recasted to yield the respective contributions of vapor and clouds. Most of the water cycle studies to date [4,5] have focused on the sole role of the Hadley cell in cross-equtorial flows of moisture. However, [4] and [5] have shown that baroclinic activity plays a key role in cycling water in and out the north residual cap. Indeed, [6] concluded that the observed extraction of water from the north polar cap can not be reproduced with a two-dimensionnal circulation model. According to [5], horizontal mixing of moisture between high and mid-latitudes precedes the incorporation of water within the ascending branch of the Hadley cell in the northern tropics. Likewise, the mechanism by which water returns to the north residual cap includes water trapping in the seasonal CO_2 cap, thanks to an intense mixing of air masses across the cap edge. During the recession of the cap, seasonal water frost is carried poleward by a succession of sublimation/recondensation processes occuring within poleward warm fronts and equatorial cold fronts.

With this in mind, describing water transport in terms of its meteorological components becomes a necessary task in order to fully appreciate the mechanisms controlling the Martian water cycle stability.

Results of our analysis on an annual average and at specific seasons will thus be presented.

Water cycle and clouds: Following their first observation of what has been since called the "Aphelion cloud belt", i.e. a cloudy structure encircling the equator during northern spring and summer, [7] proposed a mechanism, involving clouds, to predict preferred storage location of water with changes of perihelion date. The so-called *Clancy effect* comes from the potential ability of clouds to sequester water below the returning branch of the equinoctial Hadley cell if the latter is synchronized with the aphelion season. In practice, aphelion season implies decreasing atmospheric temperatures in the tropics and thus lower levels of condensation/precipitation. Perihelion season, on the contrary, comes with enhanced solar forcing and warmer temperatures which allow water to be carried by the Hadley cell towards the winter hemisphere without experiencing the effects of cloud sedimentation.

On an annual average, [7] suggests a net flux of water towards the hemisphere for which summer is timing with aphelion. Whereas the current orbital configuration should therefore favor the northern hemisphere, it also implies that this situation is reversed when the perihelion is shifted of 180^o.

[7] even suggested that the current position of the permanent water ice cap is a consequence of this effect. Accordingly, the permanent water ice cap should move to the south pole when aphelion occurs during southern summer.

On the other hand, [8] showed that, regardless of excentricity and aphelion date, the south to north topographic slope applies a major component to the general circulation biasing cross-equatorial mass flows towards the north hemisphere.

The purpose of our study is to confront the *Clancy effect* to that induced by topographic forcing within the context of GCM simulations. Ultimately, we will discuss the stability of a permanent cap in the south pole that recent observations may confirm [9].

Reference

[1] F. Forget et al., *JGR* **104**, 24155 (1999)

[2] F. Montmessin et al., *proceedings of the mars VI conference*, Pasadena (2003)

[3] J. P. Peixoto and A. Oort, *Physics of Climate*, Amer. Inst. of Physics (1992)
[4] H. Houben et al., *JGR* **102**, 9069 (1997)
[5] M. Richardson and J. Wilson, *JGR* **107**, 10.129/2001JE001536 (2002)
[6] R. Haberle et B. Jakosky, *JGR* **95**, 1423 (1992)
[7] T. Clancy et al., *Icarus* **122**, 36 (1996)
[8] M. Richardson and J. Wilson, *Nature* **416**, 298 (2002)
[9] T. Titus et al., *Science* **299**, 1048 (2003)

DEVELOPMENT OF A MARS GENERAL CIRCULATION MODEL. Y. Moudden[1], S. R. Beagley, V. Fomichec, J. C. McConnell, A. Akingunola, A. Garcia Munioz. [1]York University Petrie Bldg 4700 Keele St, Toronto ON M3J 1P3 Canada (youssef@numbus.yorku.ca).

Efforts are underway in the Department of Earth and Atmospheric Science at York University to develop a General Circulation Model for Mars. The model, which we call MGEM, is based on the dynamic core of the Meteorological Service of Canada's weather forcast model GEM (Global Environmental Multiscale Model) and is a multiscale grid point semi-Lagrangian semi-implicit model, with a non-hydrostatic option. The multiscale option allows for a horizontal resolution that will enable us to address the mesoscale issues in the Mars atmosphere such as dust lifting mechanisms. The dynamical core has already been tested using TES temperature and surface pressure fields and MOLA topography from MGS. Appropriate changes to the physics parameterizations are being made to deal with the major components of Mars climate. These consist of solar and IR radiative scheme including a non-LTE package, a large scale carbon dioxide condensation scheme and its interaction with the total mass, a dust lifting and transport scheme with its effect on the energy budget. A comprehensive description of the water cycle including the subsurface transport in the regolith, the surface fluxes and the atmosphere transport and condensation is also being developed. The model also is capable of transporting species and chemical and aerosol packages will be added. Other groups within Canada, viz. at Dalhousie University, University of Toronto, University of Western Ontario and University of British Columbia, are planning to contribute to the effort.

We believe that MGEM will be a useful tool for the Martian scientific community, and with the increasing interest in the Mars exploration, MGEM will be useful for instrument design and planning for the future missions.

GEOLOGICAL OBSERVATIONS, CLIMATE MODELING, AND ICE STABILITY: EVIDENCE FOR RECENT MARTIAN ICE AGES J. F. Mustard[1], J. W. Head[1], M. A. Kreslavsky[1,2], R. E. Milliken[1] and D. R. Marchant[3], [1]Department of Geological Sciences, Brown University, Providence RI 02912 USA, John_Mustard@brown.edu, [2]Astronomical Institute, Kharkov National University, Kharkov, Ukraine, [3]Department of Earth Sciences, Boston University, Boston MA 02215 USA.

Introduction and Summary: Recent exploration of Mars has revealed abundant water ice in near-surface deposits of the mid-to high latitudes in both hemispheres. Here we show evidence that these near-surface, water-ice rich units represent a mixture of ice and dust that is layered, meters thick, and latitude dependent. These units were formed during a geologically recent major martian ice age, and were emplaced in response to the changing stability of water ice and dust on the surface during variations in orbital parameters. Evidence for these units include a smoothing of topography at subkilometer baselines from about 30° north and south latitudes to the poles, a distinctive dissected texture in MOC images in the +/-30°-60° latitude band, latitude-dependent sets of topographic characteristics and morphologic features (e.g., polygons, 'basketball' texture, gullies, viscous flow features), and hydrogen concentrations consistent with the presence of abundant ice at shallow depths above 60° latitude. The most equatorward extent of these ice-rich deposits was emplaced during the last major martian ice age between 0.4 and 2 Myrs, down to latitudes of 30°. Mars is currently in an "interglacial" period and the ice-rich deposits between 30-60° are presently undergoing reworking, degradation and retreat in response to the current stability relations of near-surface ice. Unlike Earth, martian ice ages are characterized by warmer climates in the polar regions and the enhanced role of atmospheric ice and dust transport and deposition to produce widespread and relatively evenly distributed smooth deposits at mid-latitudes during orbital extremes.

Geological Observations: A number of geological observations made with new data from the Mars Global Surveyor and Mars Odyssey missions show features that are latitude dependent. These build on the latitude dependent features observed with Viking and Mariner data [1, 2, 3]. Kreslavsky and Head [4, 5] investigated the roughness and concavity (Figure 1) of the martian surface with the full resolution Mars Orbiter Laser Altimeter (MOLA). These analyses showed a pronounced smoothing of the 0.6 km baseline topography beginning around 30° N and S and extending to the polar regions. They also showed that the topography showed a distinct reduction in concavity in the 30-60° N and S latitude bands. They attributed these observations to the presence of a meters thick mantle that was continuous poleward of 60° but discontinuous in the 30-60° latitude bands. Mustard et al [6] mapped the presence-absence of a unique meters-scale morphology in Mars Orbiter Camera (MOC) images. The morphology indicated the presence of a meters-thick surface deposit that was in a state of partial degradation. A survey of 15,000 images revealed that this unique morphology was restricted to the 30-60° latitude bands (Figure 1). They interpreted this to indicate the presence of a formerly ice-cemented dust deposit from which the ice had sublimated and that was now being disaggregated and degraded. Other investigators have noted latitude dependence in the presence of unique morphologies such as viscous flow features, gullies, and periglacial-like morphologies [e.g. 7, 8, 9, 10]

A remarkable result of the Mars Odyssey Gamma Ray Spectrometer (GRS) is the high concentration of hydrogen beneath a thin layer of dry soil in the top two meters of the martian soil at latitudes greater than 60° N and S [11, 12]. Modeling suggests that the concentration of hydrogen would require 35-50% by mass of water ice, which would correspond to an even greater amount by volume. The present equatorward limit of the these high hydrogen concentrations match extremely well the predicted latitude where ice would be in equilibrium with present-day atmospheric conditions

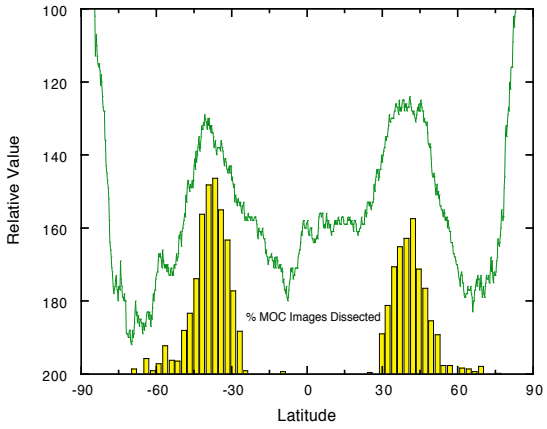

Figure 1: Example of the correspondence among geological observations. The line shows the latitude dependence of topographic concavity while the bars show the precent of MOC images showing dissection. They both show a high correlation in the mid-latitude regions.

[13]. Figure 1 shows the latitude distribution of a subset of these features to illustrate their compelling latitude dependence.

Climate Models: The obliquity, eccentricity, and longitude of perihelion of Mars are known to have varied dramatically over the last 10 Myrs [14] and these changes will have important consequences for the martian climate and the distribution of volatiles. Recent modeling of the behavior of the martian climate under different orbital configurations and its effects on the distribution of volatiles [15, 16] predict that at an obliquity of 35°, 10s of meters of water-ice can be sublimated from the poles over an orbital cycle (10s of thousands of years) and redeposited in the mid-latitudes resulting in a meters-thick deposit in these regions. With an obliquity of 45° this process is more vigorous, and in fact deposits of perennial ice are predicted at the equator. Ice deposited by this process is likely to be dust rich.

Orbital Cycles: Ice stability in the near surface of Mars is most strongly controlled by obliquity [13]. When obliquity exceeds approximately 30°, then ice stability moves towards the equator and is stable to within 30° of the equator. Over the past 400 kyrs, the

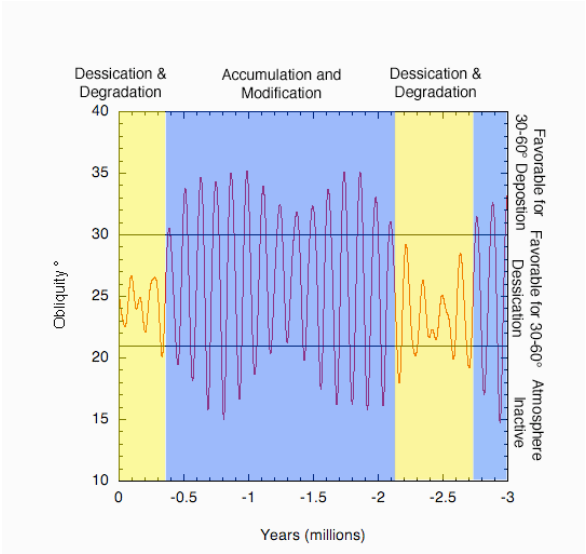

Figure 2. Schematic showing the relationship between obliquity cycles over the last 3 Myrs and deposition-erosion of latitude dependent surface deposits. The blue regions mark martian ice ages, the yellow regions interglacial periods

obliquity has remained within a relatively narrow range (22-26°, Figure 2), while eccentricity and precession have varied strongly. If eccentricity and precession controlled the formation of the geologic observations, then we would expect an asymmetric distribution reflecting the most recent conditions. Clearly the geologic observations are almost perfectly symmetric about the equator. Between 400 and 2000 kyrs ago the obliquity regularly exceeded 30°. This would have facilitated the transport of water ice from the poles to the mid-latitudes and be co-deposited with dust. During the brief low obliquity periods between these highs, water ice would sublimate from these deposits. However, surface lags of dust would form, similar to the Fox Permafrost tunnel in Alaska [17] retarding sublimation and preserving aspects of the deposit.

Martian Ice Ages: The remarkable congruence between geological observations over a range of scales and type with predictions of ice stability over orbital time scales and climate models are strong evidence that the last several million years have witnessed the deposition and reworking, multiple times, of a meters-thick ice-dust deposit in the mid-latitudes of Mars (Figure 2). These are the deposits of the martian ice ages and have significantly affected surface processes in these regions. It is likely that there are remnant deposits beneath surface lags in regions close to the equator.

References:

[1] Squyres, S. W. and M. H. Carr, *Science, 231*, 249-252, 1986; [2] Soderblom et al., *JGR, 78*, 4117-4122, 1973; [3] Squyres, S. W., *Icarus, 34*, 600-613, 1978; [4] Kreslavsky, M. A. and J. W. Head, *JGR, 105*, 26695-26711, 2000; [5] Kreslavsky, M. A. and J. W. Head, *GRL, 29,* 2002; [6] Mustard et al., *Nature, 412*, 411-414, 2001; [7] Malin, M. C. and K. S. Edgett, *JGR, 106*, 23429-23,570, 2001; [8] Carr, M. H., *JGR, 106*, 23,571-23,593, 2001; [9] Milliken et al., *JGR, in press*, 2003; [10] Mangold et al., *LPSC 33*,2002; [9] [11] Boyton W. V., et al., *Science 297*, 81-85, 2002; [12] Feldman W. C., et al., *Science 297*, 75-78, 2002; [13] Mellon, M. and B. Jakosky, *JGR 100*, 11,781-11,799; [14] Laskar J. et al., *Nature 419*, 375-377, 2002. [15] Richardson M. I. and R. J. Wilson, Nature 416, 298-301, 2002. [16] Mischna et al., *JGR 108*, doi:10.1029/2003JE002051, 2003. [17] Johnson, J. J. and R. D., Lorenz, *Geophys. Res. Lett. 27*, 2769-2772 2000;

ALBEDO FEEDBACK IN THE PATTERNING MECHANISMS OF MARTIAN POLAR CAPS. Felix S. L. Ng, Maria T. Zuber, *Department of Earth, Atmospheric and Planetary Sciences, Massachusetts Institute of Technology, Cambridge MA 02139, USA (felix@mit.edu)*.

Introduction. Both the north and south polar caps on Mars display conspicuous patterns of spiraling troughs on the surface (Fig. 1), and their origin is largely unexplained. Here we examine the hypothesis that such morphology could be the result of a spatial instability. By modeling the interaction of polar ice with the Martian atmosphere, we show that an albedo feedback (associated with dust) can lead to relaxation oscillations in the coupling between surface mass exchange, radiative heat balance and air moisture regulation. Under favourable conditions, this temporal behaviour is manifest on the surface of the residual ice caps as alternating domains of sublimation and condensation, whose evolved forms mimic the observed (dark) troughs and their adjacent (light) smooth terrains; their expected orientation and topography are broadly consistent with the actual pattern. The mechanism finds observational support from stratigraphic relationships in the cap deposits [1] and recently inferred wind patterns, and may offer useful insights for developing more complex models.

Background. Understanding large-scale patterning of the Martian ice caps is an important step towards deciphering their history, because it reflects the unique conditions under which the exchange of volatiles (CO_2 and H_2O) and dust between ground and atmosphere occurred in the polar regions. In addition, ice cap internal layers exposed on the equator-facing trough walls (or 'scarps') may contribute a valuable record of Martian climate cycles [2,3]. The age and rate of pattern formation can also be used to constrain other polar processes.

It is generally thought that the observed system of troughs migrates poleward due to isolation-driven ice sublimation at the scarps, while ice accumulates on inter-trough areas [4]. Previous studies explored the role of these processes in creating the spiral planform [5] and their effect on ice cap internal stratigraphy [6,7], but it remains unclear as to how the troughs were initiated and maintained, and what governs their spacing.

It is likely that the troughs developed via a positive feedback resulting from surface processes rather than from ice flow, for the latter has the tendency to suppress surface undulations. This idea is supported by steady flow modeling of the north polar cap [7]: to sustain scarps, ablation at their base and accumulation at their top must be imposed. Presumably, wave-like propagation of the scarp topography requires a similar mass balance configuration.

Mathematical Model. The feedback studied here connects the regulation of surface albedo a to the direction of mass transfer at the ice surface — that is, whether $\dot{m} > 0$ or $\dot{m} < 0$, if $\dot{m}$ denotes the rate of sublimation. Drawing on an earlier description of radiative energy balance and the sublimation process [8], we calculate $\dot{m}$ from the equations

$$I_n(1-a) = \sigma T^4 + \dot{m}L, \tag{1}$$

$$\dot{m} = D(p_s - \phi)\sqrt{\frac{M_w}{2\pi k T^{1/2}}}, \tag{2}$$

in which I_n is the incident solar flux (corrected for surface slope), T is the surface temperature, ϕ is the partial vapour pressure of CO_2 or H_2O in the atmosphere (whichever ice-type is being considered), and p_s is the saturation vapour pressure, $= c_0 e^{-c_1/T}$. Model constants are explained in ref. [8].

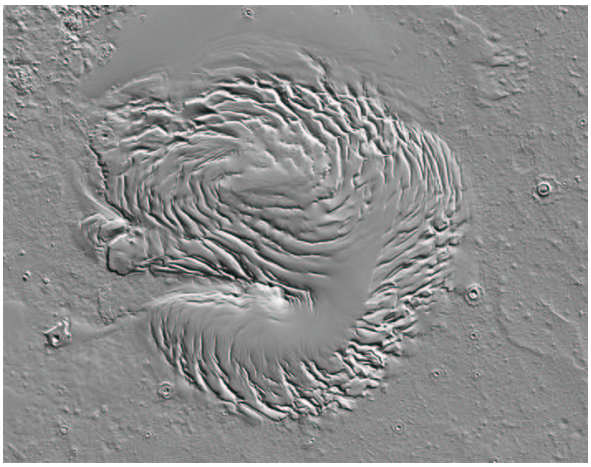

Figure 1: *Shaded relief image of the Martian northern polar region, showing spiral chasms. Courtesy of MOLA Science Team.*

A crucial control on the surface albedo is the dust content of the dirty ice. We envisage sublimation to promote a low albedo ($a = a_1$) by exposing dust at the surface, and condensation to have the opposite effect through burial of the dust (raising a to a_2). While this process can be modeled in detail, here it is sufficient to suppose that such albedo change can be achieved by removing/depositing an ice or snow layer of thickness Δ, and then an appropriate description is

$$\frac{\Delta}{|\dot{m}|}\frac{da}{dt} + a = \frac{a_2 + a_1}{2} - \frac{a_2 - a_1}{2}\mathrm{sgn}(\dot{m}). \tag{3}$$

Analysis of Equations (1)–(3) shows that for a given insolation, the function $\dot{m} = \dot{m}(\phi)$ that characterises

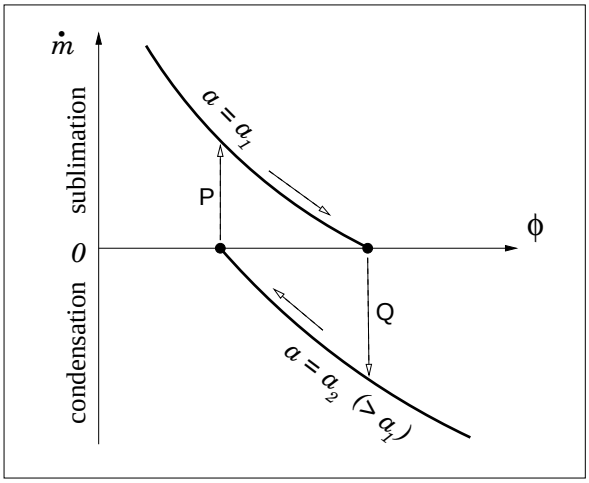

Figure 2: *Albedo-controlled oscillations in ice sublimation rate $\dot{m}$ and partial vapour pressure ϕ.*

the system at equilibrium is multi-valued, with stable branches representing high and low albedo states (Fig. 2). Essentially, a surface on which ice condenses would continue to experience condensation because its high albedo maintains a low surface temperature, keeping the atmosphere over-saturated with vapour at that temperature (Fig. 2, lower curve). Another way of stating the feedback is that T is kept below the frost point for a given ϕ. In contrast, if ice sublimates, the surface will remain dark (and above the frost point), reinforcing sublimation (Fig. 2, upper curve).

The two states do not last indefinitely. Owing to vapour depletion or enrichment, the atmosphere evolves towards saturation (with diminishing $\dot{m}$), at which point each state becomes unstable and switches into the other (described by Eqn. (3)), leading to an oscillatory cycle (Fig. 2, dashed arrows). In the presence of wind, an air packet will undergo the same transitions as it moves along the surface to produce light and dark regions, which we liken to the smooth terrain and troughs/ scarps, respectively. Due to the alternating accumulation and ablation in these regions, an undulating topography will develop that migrates and self-organises (via slope control on I_n). If u is the windspeed and x is distance downwind, mass conservation for an ideal-gas atmosphere of effective height h would imply $u d\phi/dx \approx kT\dot{m}/(hM_w)$, so that a length-scale for the spacing between troughs is $x \sim uh\phi M_w/(kT\dot{m})$. For the north polar cap and with H_2O, we obtain $h \sim 10$ to 10^3 m if (as observed) $x \sim 50$ km. (The large uncertainty arises from the poorly-known constant D; see [8]). Similar mechanisms known as Belousov-Zhabotinskii reactions have been studied in the field of biological pattern formation [9].

Discussion. Although our model is simple, the proposed mechanism is robust and points to interesting comparisons with observations. (1) The distinction between two kinds of terrain in terms of topography, albedo, and accumulation–ablation regime supports a bistable mechanism. (2) The model-predicted trough axes align in a normal direction to wind transport, such that, under a radial wind pattern modified by the Coriolis effect at both poles, large-scale spiraling of the troughs in the observed orientation would occur (anti-clockwise going out in the north, clockwise in the south). (3) The model can simulate the small width ratio of the troughs vs. smooth terrain, because the atmospheric flow attains saturation over short distances on warm, sun-facing scarps. (4) If, contrary to what is often assumed [10], the surface winds are directed *poleward*, the simulated topography would best fit the observed. This is because high ablation occurs at the base of scarps where vapour-depleted air first encounters the troughs (corresponding to transition P, Fig. 2), and high accumulation occurs atop scarps where vapour-laden air encounters smooth terrains (Q, Fig. 2). With this mass balance configuration, our model is consistent also with the stratigraphy of layered ice deduced by [1]. It can explain the extension of 'layered terrain' over the bottom of troughs, and the irregular edges of the 'banded terrain' (which mark the place where moisture can no longer condense out of the air, sensitive to atmospheric fluctuations).

Regarding the last point above, although the notion of winds flowing up the ice caps seems counter-intuitive, evidence from MOLA-detected cloud features (see [11], Figs. 9A,B) indicates that such conditions happen at least some of the time in the north. To further our study, we have begun incorporating a more detailed atmosphere, as well as the effects of seasonal and long-term cycles of wind and volatile transport, into our model simulations.

References. [1] A. D. Howard et al., *Icarus*, **50**, 161, 1982. [2] J. A. Cutts & B. H. Lewis, *Icarus*, **50**, 216, 1982. [3] J. Laskar et al., *Nature*, **419**, 375, 2002. [4] A. D. Howard, *Icarus*, **34**, 581, 1978. [5] D. A. Fisher, *Icarus*, **105**, 501, 1993. [6] D. A. Fisher, *Icarus*, **144**, 289, 2000. [7] C. S. Hvidberg, *Ann. Glaciology*, **37**, 2003 (in press). [8] A. B. Ivanov & D. O. Muhleman, *Icarus*, **144**, 436, 2000. [9] J. D. Murray, *Mathematical Biology. I: An Introduction* (3rd ed.), Springer-Verlag, 2002. [10] A. D. Howard, *Icarus*, **144**, 267, 2000. [11] M. T. Zuber et al., *Science*, **282**, 2053 ,1998.

GEOPHYSICAL INVESTIGATIONS AT A MARS ANALOG SITE: DEVON ISLAND, NUNAVUT. Nieto, C.E.[1] and Stewart, R.R.[1], [1]Dept. of Geology and Geophysics, The University of Calgary (GLGP, 2500 University Dr., N.W., Calgary, Alberta, Canada T2N 1N4. cenieto@ucalgary.ca, stewart@ucalgary.ca).

Abstract

The Haughton meteorite impact structure, located on Devon Island, Nunavut is one of the most Mars-like places on Earth. The Haughton crater is cold (average temperature –17°C), dry, rocky, dusty, and windy. As part of the effort at NASA SETI Institute Haughton Mars Project (HMP), the University of Calgary Applied Geophysics Group conducted geophysical surveys, both ground-penetrating radar (GPR) and high-resolution seismic, in the summer of 2002. Objectives of the geophysical work were to image the permafrost layer as well as assess deeper geologic horizons.

GPR data were acquired using Sensors & Software NOGGIN 250 MHz system and PulseEKKO devices with 50 and 100 MHz antennae. These surveys imaged depths from about 0.5m to 3 m and indicate layering and permafrost events. High-resolution seismic results, recorded with a Geometrics 60-channel recording system and accompanying 28 Hz omni-directional geophones, also show the permafrost layer.

Shallow excavations, seismic refractions, and GPR reflections at the site all proved useful and indicate that the permafrost layer is at a depth of about 60cm. We also tested geophysical operations in prototype spacesuits and found the suits to be manageable although cumbersome. We plan on returning to the Haughton crater in the summer of 2003 for further geophysical surveying and system testing.

Introduction

The Haughton meteorite impact structure on Devon Island, Nunavut in the high Canadian Arctic is one of the most Mars-like places on Earth. The Haughton structure, at 75°22'N longitude and 89°41'W latitude, is a 23 Ma old impact crater about 20 km in diameter [1], [2]. Host rocks of the structure are of Ordovician and Silurian age, mostly of the Allen Bay formation [3]. The impact has left a very impressive scar on the landscape as seen from an airborne radar image.

The northwest region of the outer middle rim hosts the base camp for the Haughton Mars Project [4], [5], [6], [7]. Geophysical surveying can be difficult, even in the summer on Devon Island, due to the high winds of the polar area (up to 70 km/hr during this field survey), low summer temperatures (-5°C to +5°C), sleet, rain, snow - even though this is characterized as a desert [8], and significant ultraviolet radiation [9].

The site chosen for the GPR and seismic surveys was located near the base camp in the "Von Braun Valley" (VBV). We conducted another series of surveys several kilometres away at the "Gemini Hills", but only the VBV surveys will be discussed here. We dug several test pits near the base camp to investigate the composition of the near surface. We found a tan-coloured, saturated silt with small clasts down to depths of about 45 – 65 cm. We then encountered solid and uniform permafrost with the appearance of frozen silt.

Seismic and GPR surveys

We used a Geometrics Strata View 60-channel seismic recorder with 28Hz omni-geophones (planted in vertical and horizontal configurations). One of the seismic micro-spreads is shown in Figure 1. A small sledgehammer was employed as a source striking a base plate in either a vertical or horizontal direction.

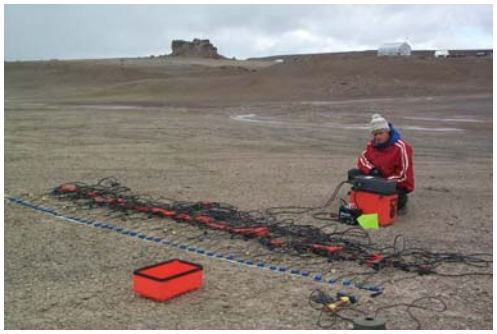

FIG. 1 Photograph the 3-C micro-seismic line in the "Von Braun Valley" at the HMP base camp.

We conducted a number of surveys using a variety of source-receiver combinations. That is, vertical source strikes and vertical receivers, horizontal hammer blows and transverse receivers, etc. A data example for a vertical hammer strike with horizontal, inline receivers (the P-S configuration) is shown in Figure 2.

We are still analysing the seismic data, but have determined very low preliminary P and S velocities in the near-surface silts (260m/s and 168m/s, respectively) with very high velocities in the permafrost (P-wave velocity = 3100m/s, S-wave velocity = 2060m/s).

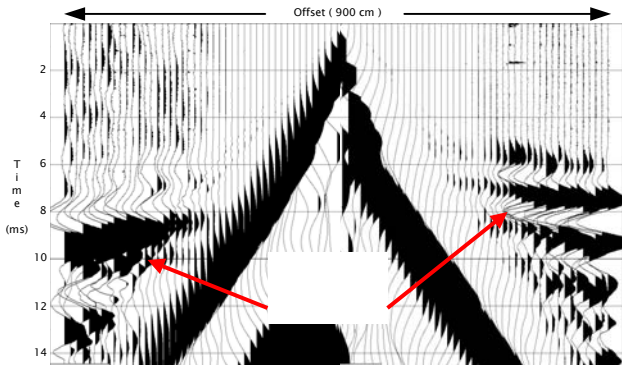

FIG. 2 Vertical hammer blow with inline (horizontal) receivers showing a high amplitude PSS refracted at the top of permafrost.

We processed the PP and PSS refracted data (as it has very high amplitude) into stacked sections that are shown in Figure 3. Since the velocity contrast between the permafrost and silt layer is so high the obtained sections correspond to a zero – offset stacked section. We interpret the dominant event on both sections to be the top of the permafrost [10].

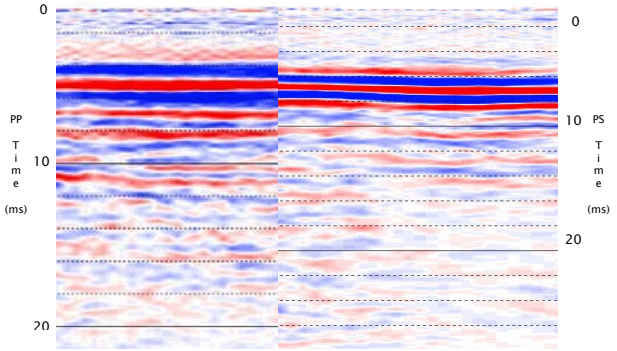

FIG. 3 Vertical hammer blow with inline (horizontal) receivers showing a high amplitude PSS refracted at the top of permafrost.

We also acquired a number of GPR lines in the Von Braun Valley. Use of the Sensors and Software NOGGIN SmartCart greatly simplified acquisition as one just rolls it across the surface and provides a real-time display of the radar arrivals. Having a similar acoustic system would be a great stride forward in subsurface imaging.

We also used a Sensors and Software 250 pulse EKKO system with 50 MHz and 100 MHz antennae in a walk-apart manner to determine radar velocity values. To assist with interpretation of the GPR data, we dug a trench down to the permafrost and pounded a 1m length of rebar into the end of the trench on top of the permafrost. We then surveyed orthogonally across the undisturbed ground above the rebar. This gave a strong diffraction from the rebar and helped determine which event to interpret as the permafrost top (Figure 4). We have experimented with a number of processing flows to find optimal filter, deconvolution, and migration parameters for the GPR data.

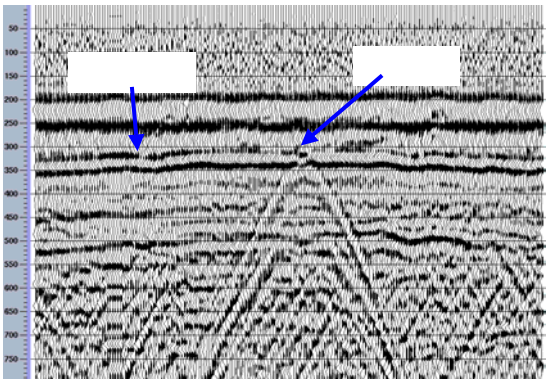

FIG. 4 GPR line from the NOGGIN 250 MHz System in the Von Braun Valley.

Conclusions

This paper provides a preliminary report of some of the geophysical findings of the HMP-2002 field surveys. Both seismic and GPR systems worked well in the field, under some harsh conditions, and provided useful information. Using test pits, reflected GPR data, and refracted seismic energy, we found the permafrost layer to be at about a 60 cm depth. Conducting field operations in prototype spacesuits was cumbersome, but manageable. We plan to return to HMP in the summer of 2003 for further surveys and analysis.

References

[1] Osinski, G.R. and Spray, J.G. (2001) *Eath and Planetary Science Letters, 194, 17-29.* [2] Osinski, G.R., Spray, J.G., and Lee, P. (2001) *Meteoritics and Planetary Science, 36, 731-745.* [3] Scott, D. and Hajnal, Z. (1988) *Meteoritics, 23, 239-247.* . [4] Lee, P. (2002a) *National Space Society, 14, 12-17.* [5] Lee, P. (2002b) *The Planetary Report, v. 1.* [6] Lee, P. (2002c) *The Planetary Report, v. 1.* [7] Long, M.E. (1999) *National Geographic, 196, 34-51.* [8] Cockell, C.S., Lee, P., Schuerger, A.C., Hidalgo, L., Jones, J.A., and Stokes, M.D. (2001) *Arctic, Antarctic, and Alpine Research: 33, 306-318.* [9] Cockell, C.S., Scherer, K., Horneck, P., Rettberg, P., Facius, R., Gugg-Helminger, A., Driscoll, C., and Lee, P. *(2002) Photochemistry and Photobiology, 74, 570-578* [10] Nieto, C. and Stewart, R.R. (2003) *2003 CSPG/CSEG Annual Meeting.*

Acknowledgements

We express our appreciation to the NASA Haughton-Mars Project and especially its principal investigator, Dr. Pascal Lee of NASA Ames. Thank you to Sensors and Software Inc. for GPR support. Many thanks to Mssrs. Eric Gallant and Henry Bland of the CREWES Project at the University of Calgary who provided logistical help. We thank the University of Calgary (especially former Department Head, Dr. Don Lawton) for equipment support. We are grateful to NSERC for providing financial assistance for University of Calgary student, Mr. Robert Birch, via a summer fellowship. University of Calgary graduate students Ms. Julie Aitken and Ms. Monica Moldoveanu have capably assisted in the analysis of these data. Geo-X Systems Ltd. of Calgary has generously provided further processing of the HMP GPR data.

Testing the SHARAD experiment of Mars Reconnaissance Orbiter with a flight balloon over polar regions.
G. G. Ori[1], E. Flamini[2], R. Seu[3], L. Marinangeli[1], [1]IRSPS (Universita' d'Annunzio, Viale Pindaro 42, 65127 Pescara Italy, ggori@irsps.unich.it), [2]Agenzia Spaziale Italiana (ASI, Solar System Exploration, Via di Villa Grazioli, 00100 Roma Iatly, enrico.flamini@asi.it), [3] INFOCOM (Universita' La Sapienza, Via Eudossiana, 00100 Roma Italy, robeto.seu@uniroma1.it)

Introduction: SHARAD is a subsurface penetrating radar that will be onboard the Mars Reconnaissance Orbiter (MRO) NASA mission. SHARAD [1] is a facility instrument provided by Agenzia Spaziale Italiana for a NASA mission and the PI is R. Seu (INFOCOM Dept., Univ. Roma "La Sapienza). SHARAD is the direct evolution of MARSIS [2, 3], the subsurface penetrating radar on board the European mission Mars Express. MARSIS has a strong penetration power (a few kilometers) and lower vertical resolution, whereas SHARAD will penetrate only several 100s meters but its data will have high-resolution range. This is achieved with the use of different hardware and different frequencies. One of the goals of MARSIS and SHARAD data is to understand the nature of the signal and compare it with the geological nature of the subsurface.

The two instruments have been not tested yet in flying conditions on Earth. The Agenzia Spaziale Italiana has set up a test campaign in order to evaluate and validate the operation and data of the SHARAD experiment. The Agenzia Spaziale Italiana is planning a test programme in order to evaluate and validate the operation and data of the SHARAD experiment. Possibly, two experiments are envisaged one in Antarctica and the other in the Artic. At present, only one flight will be performed. According to the results of the first test a decision to carry out another test will be taken. The first experiment is scheduled in 2004.

Rationale and operations: Testing a subsurface sounder orbiting radar on Earth is a difficult challenge. The most difficult problem is the presence of interstitial water that, even in small concentration, will strongly attenuate the signal. The consequence is to not have reliable data from most part of the planet. However, the polar areas are good candidates for this kind of test due to the presence of thick cover of ice, as well as the extensive presence of permafrost. A stratospheric balloon flaying at about 35 km above sea level will carry the experiment. The balloon will carry a model of SHARAD with some capability and electronics scaled to the experiment parameters. Both polar regions (the Arctic and Antarctica) are under considerations. The Arctic experiment will be launched from Svalbard where the facility of the Italian base will be used. Simulations of the balloon trajectory show a circular shape with a landing area within 100 km from the launch pad. During the flight the balloon will get data from northern Greenland the Canadian Archipelago and part of northern Siberia and adjoining islands. The experiment will be able to investigate thick ice sheets, permafrost areas, seasonally snow covered zones and sea ice. The Antarctica experiment will flight from the US McMurdo base and the Italian base at Terra Nova Bay will provide the support. Even in this case the trajectory will be circular with the landing near the launch location. In this experiment the balloon will chiefly flight over the thick Antarctic ice sheet.

Preliminary work and data: The selection and timing of the experiment is still under consideration. A preliminary scenario suggests the Arctic flight in summer 2004 with a possible second experiment in winter (Austral summer) 2004.

Fieldwork will be carried out in order to analyse the surface properties along with the gathering of previous data. The ground penetrating radar data already obtained from the surface in the past years by several institutions are of particular interest, because they will be used to control the SHARAD signal when operating on Mars.

Several simulations of the radar signal have been performed in order to model the response of the SHARAD model to the polar environment. Some examples are provided in Figure 1. The ice has been modeled as a layered unit composed of strata of pure ice and ice with silicoclastic detritus. The layer thickness varied according to the simulation experiment ranging from a few tens of cm to a few meters. When a basal layer of melt water is present the bedrock is not recorded. Possible lakes of liquid water will produce, as expected, the same effect with the disappearance of the signal below the water layer.

Conclusion: The experiment with a model of the SHARAD radar on earth will provide useful clues in understanding the signal behaviour and will give some know-how about the geological and glaciological interpretation of the data. This experiment will support the analysis of the SHARAD data and will provide some clues on the use of a similar instrument on the icy satellites.

References: [1] Seu R. et al. (2003) *PSS, in press*. [2] Picardi et al. (1999) *INFOCOM Tech. Rep., n*.007/005/99 [3] Biccari et al. (2003) *PSS., in press*.

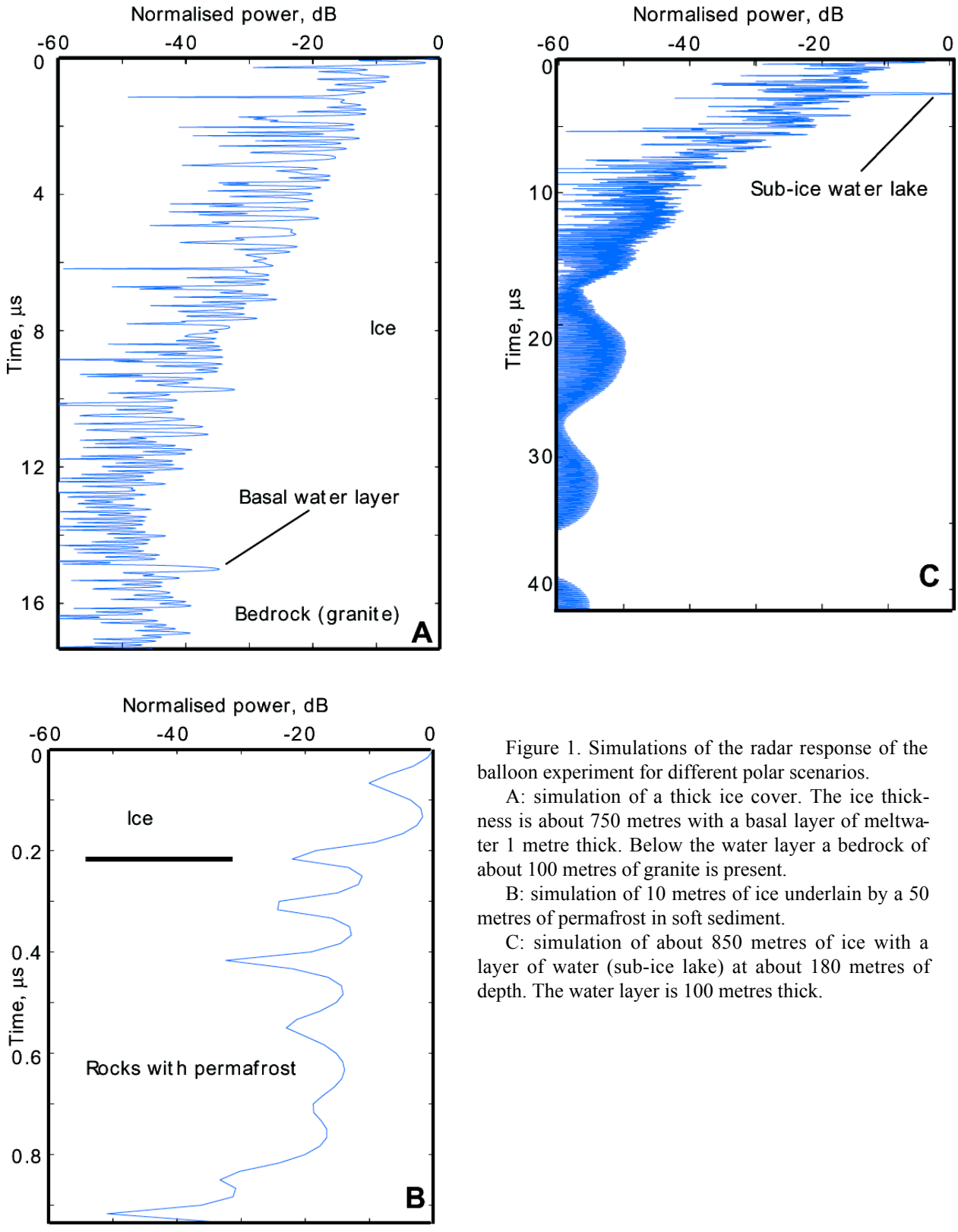

Figure 1. Simulations of the radar response of the balloon experiment for different polar scenarios.

A: simulation of a thick ice cover. The ice thickness is about 750 metres with a basal layer of meltwater 1 metre thick. Below the water layer a bedrock of about 100 metres of granite is present.

B: simulation of 10 metres of ice underlain by a 50 metres of permafrost in soft sediment.

C: simulation of about 850 metres of ice with a layer of water (sub-ice lake) at about 180 metres of depth. The water layer is 100 metres thick.

HUBBLE SPACE TELESCOPE SEARCH FOR LOCALIZED OUTGASSING ON MARS

T. Ouvarova and J. Caldwell[1]; S. Atreya, A. Wong, and N. Renno[2]; P. James[3]
[1] York University (Earth and Space Science), 4700 Keele St.,Toronto, ON, Canada, M3J 1P3
[2] University of Michigan, Ann Arbor, MI, USA
[3] University of Toledo, OH, USA

Introduction: Evidence of recent groundwater seepage and surface runoff [1] (at mid and high latitudes) may suggest that current outgassing from small, localized sources on Mars is possible. Further, formaldehyde (CH_2O) has been tentatively detected in the equatorial region of Mars [2]. If this detection is confirmed with future observations, it would give more evidence to support the possibility of present-day localized outgassing occurring on Mars.

Photochemical models [3], based on terrestrial analogues, have identified methane (CH_4), sulfur dioxide (SO_2), and hydrogen sulfide (H_2S) as plausible outgassing products on Mars. Two of these gases have strong bands in the UV (SO_2) and near IR (CH_4) in the range of Hubble Space Telescope's (HST) detectors, however H_2S does not.

HST has obtained spectra of Mars from the UV (with its STIS – Space Telescope Imaging Spectrograph – instrument) to the near IR (by NICMOS – Near Infrared Camera and Multi-Object Spectrometer) in 1997 and 2001. We will analyze the archived data to search for evidence of these outgassing products.

Improving Detection Limits: Although these minor constituents have not been detected in global observations so far, localized outgassing sources concentrations may have been diluted in global averages, by as much as a factor of 10^8. To date, the current global average upper limits, obtained by the IRIS instrument on Mariner 9[4], are 0.02ppm (CH_4) and 0.1ppm (SO_2) at the surface. HST's high spatial resolution may help to detect these gases in local concentrations higher than their global average upper limits.

We are first analyzing STIS spectral data of Mars, to be followed with NICMOS data analysis. The angular resolution of the STIS CCD spectra of Mars is set the by the CCD's pixel size (0.05 arcseconds on the sky) and telescope's point-spread-function (0.1 arcsecond radius for 70% energy inclusion from a 'point source'). The spatial resolution (linear dimensions) is dependent on the distance of HST to Mars at the time of observation and the spectrograph slit width (4 or 10 pixels). For the data from 1997 and 2001, distance to Mars varied from 0.58AU to 1.79AU. This results in HST resolving regions on Mars from 14,000km² to 840,000km², or a 'resolved fraction' of 0.0004 to 0.024 of Mars' cross-section (global average), significantly improving upon the detection thresholds set by Mariner 9.

Data Characteristics: In the UV range of STIS, there is a significant grating scatter effect in the wavelength region below 2,200A. This instrumental effect causes the spectrum to appear to increase towards the lower-wavelengths (see Figure 1), compromising the data below 2,200A.

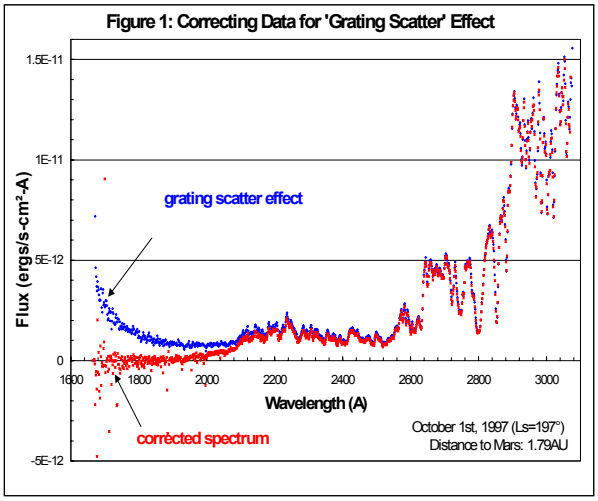

Complementary Images: With each set of spectral observation sets by STIS or NICMOS, typically HST's WFPC2 (Wide Field Planetary Camera 2) obtained images of Mars, within 2-3 hours of the spectral observations. Figure 2 shows one such image taken on October 1st, 1997, when Mars was 1.79AU from the HST, and the planetary disc spanned about 5.2 arcseconds in diameter.

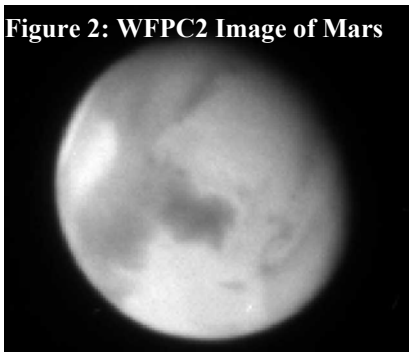

Mars Brightness Profile: STIS has the advantage of observing Mars simultaneously with spectral resolution (across the slit width) and spatial resolution (along the slit length). The disk of Mars, from pole to pole, is completely 'imaged' along the slit, and presents a 'brightness profile', averaged over eight pixels across the slit, in Figure 3.

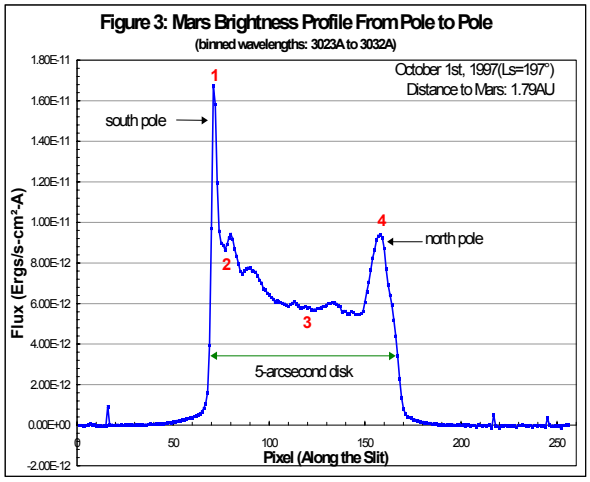

Four regions of interest are identified: the south pole (1), high latitude region close to south pole (2), equatorial region (3), and the north pole (4).

Spectra of Four Regions: UV Spectra, averaged over four pixels (along the slit), of the four regions of interest (as identified in Figure 3), are shown in Figure 4.

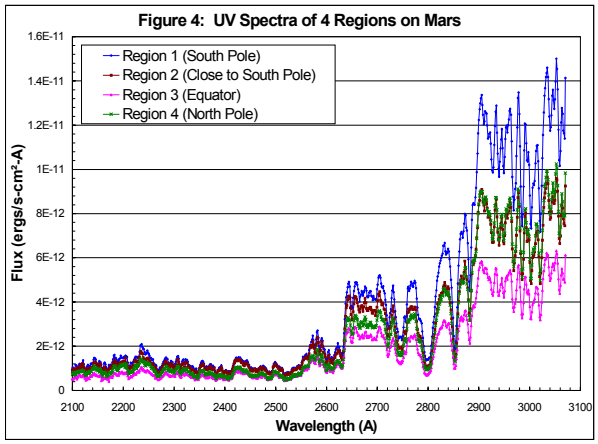

The spectra shown in Figure 4 (same observation, on October 1, 1997) have been corrected for the grating scatter effect. Spectral resolution is approximately 11A.

Analysis Plans: We plan to perform extensive analysis of the available spectral data of Mars, from both the STIS and NICMOS instruments on the HST. The spectra will be compared to the known absorption bands of CH_4 and SO_2. Adjacent spectra, along the slit, will be compared to each other, for any regional variations in the absorption features. A STIS spectrum of the Moon, taken with same instrument settings as the Mars spectra, will be used as a solar surrogate spectrum. This will produce Mars albedo spectra independent of any instrument aliasing effects that could occur when comparing spectra taken with different instruments. Figure 5 shows an image of the Moon taken by the HST, contemporaneous with the STIS spectral data.

Figure 5: HST Image of Moon (1999)

We will correlate any evidence of the signature gases found during the analysis with the available high-resolution images of Mars taken by the Mars Global Surveyor (MGS) during the observation runs.

Detailed Observations in the Future: Even if no conclusive evidence of CH_4 and H_2S is found, the HST spectral data will improve the upper abundance limits on these gases. The STIS exposure time calculator will be used to estimate possible improvements in the data with the STIS MAMA detectors, which have higher sensitivity and do not suffer the grating scatter effect in the UV region.

References:

[1] Malin, M.C. and Edgett, K.S. (2000) *Science, 288,* 2330-2335

[2] Korablev et al. (1993) *Plant. Space Sci., 41*, 441-451

[3] Wong, A.-S., Atreya, S.K. and Encrenaz, T. (2003) *J. Geophys. Res., 108(E4)*, 5026, doi: 10.1029/2002JE002003

[4] Maguire, W.S. (1977) *Icarus, 32*, 85-97

Further Information:

Please contact Tatiana Ouvarova by email: tats000@yorku.ca

THE SUBLIMATION AND RELAXATION OF TROUGHS AND SCARPS WITHIN THE MARTIAN NORTH POLAR LAYERED DEPOSITS. A. V. Pathare[1] and D. A. Paige[2]. [1]Division of Geological and Planetary Sciences, California Institute of Technology (avp@gps.caltech.edu), [2]Dept. of Earth and Space Sciences, University of California, Los Angeles, CA (dap@ucla.edu).

Summary: The kilometer-scale topography of the North Polar Layered Deposits (NPLD) is dominated by troughs and scarps: Fig. 1 shows both (a) the ubiquity of troughs throughout the NPLD, and (b) the enhanced steepness of scarps at the margins of the NPLD (e.g., along the inner wall of the channel-like reentrant, Chasma Boreale). Although the surface slopes and total depths of NPLD troughs and scarps are widely presumed to result from surface ablational processes, here we propose that an alternative mechanism, viscous relaxation of subsurface water ice, governs the morphological evolution of NPLD troughs and scarps.

Topography: Using the 64 pixel/degree MOLA altimetry grids, we constructed eight radial profiles spaced at 45° longitudinal intervals through the North Polar Dome. Along each profile, we have identified all interior troughs and marginal scarps with depths greater than 200 m located between 80°N and 87°N. Fig. 2 plots maximum 1.6-km baseline surface slopes observed along the equatorward-facing (EWF) walls of troughs and scarps, as well as upon the poleward-facing (PWF) walls of troughs.

As previously noted [1], most NPLD troughs are asymmetric: our measurements (Fig. 2A) indicate that maximum EWF slopes (α_ε) are on average 75% steeper than maximum PWF slopes (α_ρ). Although primary scarps at the periphery of the NPLD are generally at least twice as steep as interior troughs, we find that there is no significant dependence of trough slope (Fig. 2A) or depth (not shown) upon latitude. Interestingly, the slopes and depths of NPLD troughs and scarps are strongly correlated with one another (Fig. 2C).

Sublimation: The most widespread theories of PLD evolution [1,2] presume that the asymmetrical slopes of most NPLD troughs ($\alpha_\varepsilon > \alpha_\rho$) result from preferential H_2O sublimation from EWF trough walls. However, our modeling indicates that there is no long-term sublimation advantage of EWF trough walls, due to the effects of obliquity upon the slope dependence of sublimation rate (Fig. 3). We define a parameter *R* comparing the sublimation rates from the mean EWF and PWF trough wall slopes of $\alpha_\varepsilon = 5.4°$ and $\alpha_\rho = 3.1°$, respectively; at the present obliquity ($\theta = 25.2°$), the relative sublimation ratio $R = 1.33$.

However, the sublimation enhancement of EWF slopes is limited to lower obliquities, since as obliquity increases and the average solar zenith rises, the benefit of being tilted towards the sun close to local noon is

Fig. 1. Overlay of an NPLD Viking image mosaic upon MOLA topography, created by the GSFC Scientific Visualization Studio and the MOLA Science Team. Vertical exaggeration ~ 300x.

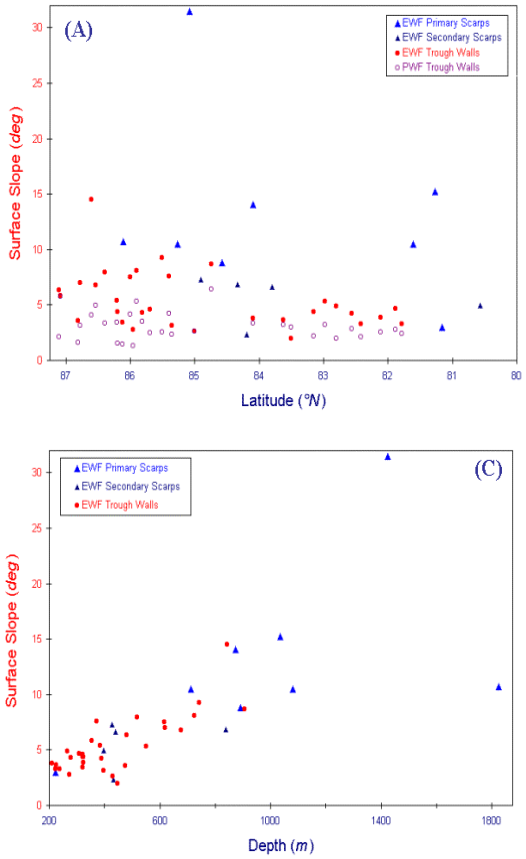

Fig. 2. Dependence of the maximum surface slopes of NPLD trough and scarp walls upon (a) latitude and (c) depth. Surface slopes are calculated over an approximate 1.6-km baseline.

offset by the disadvantage of being tilted away from the sun during the now brighter nighttime hours. Thus at obliquities of θ = 32.1° / 37.5° / 45.0°, the relative sublimation ratio R = 1.06 / 1.00 / 0.98. (Note that sublimation is actually slightly enhanced from PWF trough walls at near-maximum obliquities).

Since 80% of NPLD sublimation over the last 10 Myr takes places at obliquities above the median θ = 32.1°, our calculations demonstrate that EWF trough wall sublimation, when integrated over an obliquity "cycle", is not much greater than that from PWF trough walls (R = 1.02 since t = 10 Ma). Hence we conclude that, contrary to expectations, the steeper EWF slopes of NPLD trough walls do not result from long-term preferential sublimation driven by insolation variations.

Relaxation: But then what causes the slope asymmetry of opposing trough walls? We propose that viscous relaxation of subsurface water ice—which we have previously shown to be important to South PLD crater morphology [3]—may also govern NPLD trough and scarp evolution. Although [2] suggested that the continued presence of troughs argues against PLD flow, our trough simulations of NPLD troughs with the finite element model Tekton [4] predict trough closure times of approximately several million years.

Furthermore, Fig. 4 shows that if the EWF half of the trough is just 2 K warmer than the PWF half—which is consistent with the slope-dependent temperature variation over the last few Myr predicted by our subsurface thermal modeling—then maximum EWF slopes will become significantly steeper than maximum PWF slopes (Fig. 5), due to the slower rate of uplift of the inner PWF trough walls (which can be attributed to the increased subsurface viscosity below the colder PWF slopes). Additionally, we show that relaxation of NPLD trough and scarps can readily account for the correlation of surface slope and total depth (Fig. 2C), an observation that is particularly difficult to explain via sublimation or eolian erosion.

Conclusions: (1) The slope asymmetry of PLD troughs does not result from preferential sublimation but rather from differential relaxation of opposing trough walls. (2) Present-day NPLD troughs have formed since 5 Ma, and are not sites of long-term deposition. (3) Glacial flow probably governs the large-scale evolution of the North PLD.

References: [1] Thomas P. *et al.* (1992) in Mars, Ed. H. Kieffer *et al.*, Univ. Arizona Press, Tucson, 767-795. [2] Clifford S. *et al.* (2000) *Icarus* **144**, 210-242. [3] Pathare A. V. *et al.* (2002) *LPSC XXXIII*, Abstract #1972. [4] Melosh H. J. and Raefsky A. (1980) *Geophys. J. Royal Astron. Society* **60**, 334-354.

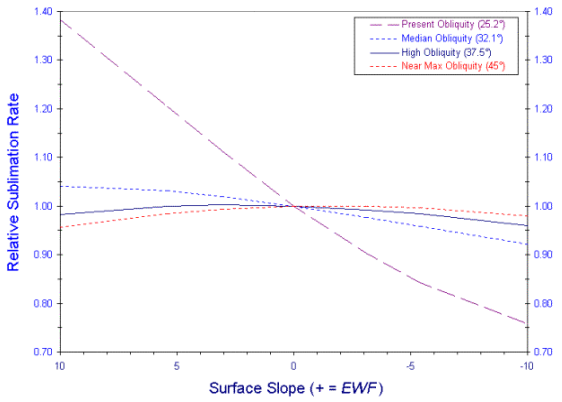

Fig. 3. Dependence of sublimation upon EWF surface slope, expressed relative to the net annual sublimation rate at α_ε = 0°, for four different obliquities and nominal North PLD conditions.

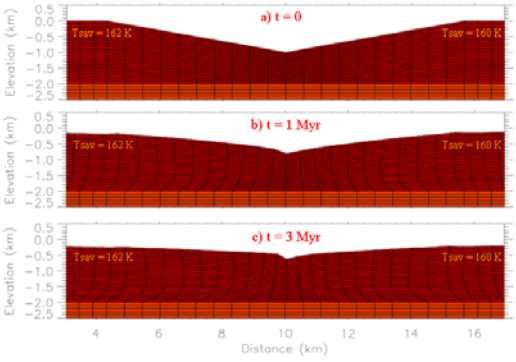

Fig. 4. Relaxation history at time steps of t = 0 / 1 / 3 Myr for baseline simulations of an North PLD trough characterized by T_{sav} = 162 K upon the EWF wall and T_{sav} = 160 K upon the PWF wall. A total PLD thickness of Z = 2 km is assumed.

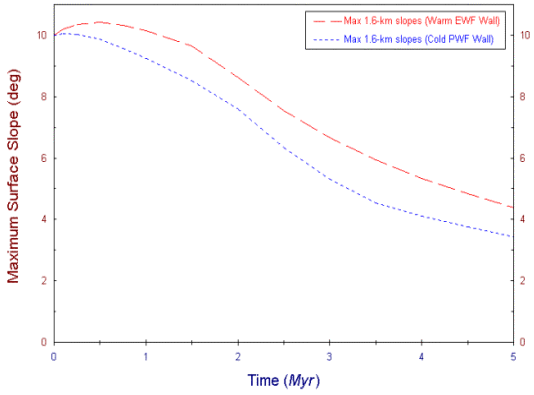

Fig. 5. Temporal dependence of maximum 1.6-km surface slopes for both EWF and PWF trough walls, derived from baseline North PLD trough simulations for differential thermal conditions shown in Fig. 4.

PRESERVATION OF ANCIENT GLACIAL ICE BELOW SUBLIMATION TILL IN THE DRY VALLEYS OF ANTARCTICA: IMPLICATIONS FOR MARS. A. V. Pathare[1], D. R. Marchant[2], and J. W. Head[3], [1]Division of Geological and Planetary Sciences, California Institute of Technology (avp@gps.caltech.edu), [2]Department of Earth Sciences, Boston University (marchant@bu.edu), [3]Department of Geological Sciences, Brown University (James_Head@brown.edu).

Introduction: Recent observations of circumpolar Martian terrains by the Gamma Ray Spectrometer are most consistent with the presence of widespread water ice in the uppermost meter of the near-surface blanketed by a thin dusty mantle [1]. A key question for Martian climatology concerns the stability of this buried ice: most models presume that the rate of exchange with the atmosphere is primarily a function of near-surface and atmospheric temperatures [e.g., 2].

However, the preservation of buried glacial ice in the dry valleys of Antarctica suggests a more complex mantle-dependent process. Within Beacon Valley, a thin till layer known as "Granite drift" that is less than one meter thick overlies stagnant Miocene glacier ice, the minimum 8.1 Ma age of which is derived from $^{40}Ar/^{39}Ar$ analyses of volcanic ash deposits within Granite drift that appear to lie conformably above the ice [3]. Furthermore, the concentration of cosmogenic ^{3}He in dolerite cobbles within the till exhibits steadily decreasing values that are most consistent with drift formation via sublimation of underlying ice [4].

If Granite drift is a layer of sublimation till, then the Antarctic paleoclimate has likely been relatively stable for several million years, since any significant climatic fluctuations would probably have melted the underlying remnant ice. Moreover, the long-term stability of Antarctic ice would suggest that much colder Martian ice could persist beneath similarly thin layers for even longer periods of time. Thus it is important to fully understand the reasons for Antarctic ice stability.

Sublimation of ice through an overlying mantle can be expressed as a combination of Fickian diffusion of concentration gradients and pressure-driven Darcian transport [5]:

$$q_v = -bD\phi\frac{\partial C}{\partial z} + \frac{k}{\mu}\frac{\partial p}{\partial z}C$$

where q_v is the vapor flux, C is the gas concentration, D is the diffusion coefficient, ϕ is the porosity, b is the tortuosity (which provides a measure of the complexity of transport paths within the mantle), k is the permeability, μ is the viscosity of the atmosphere, and p is the atmospheric pressure. Boundary conditions at the ice- mantle interface can be derived from saturation vapor pressure curves, while those at the surface are dictated by atmospheric humidity.

Hindmarsh *et al.* [5] showed that for typical Antarctic ice and till conditions, the sublimation flux into a dry atmosphere is $q_v = 10^{-3}$ m/yr, which is three orders of magnitude greater than the 10^{-6} m/yr required to preserve Miocene ice in Beacon Valley. They also showed that the near-saturation conditions proposed by [3] to inhibit sublimation should result in water ice condensation throughout the overlying till layer; such widespread icing is not observed in Granite drift [4]. Therefore, Hindmarsh *et al.* [5] concluded that the ice beneath Granite drift could only be over 8 Myr old if the porosity or tortuosity of the till layer is significantly lower than the combined value of $b*\phi = 0.2$ suggested by laboratory analogues.

Salinity: We propose that the presence of salts—which are particularly prominent in Antarctic soils [6]—may reduce sublimation rate in the dry valleys. Salt has two potential inhibiting effects, both related to brine formation due to the lowering of the melting point. First, the saturation vapor pressure of a solution decreases linearly with salt content as per Raoult's Law (indeed, this decrease is what lowers the melting point). Secondly, tortuosity varies inversely with liquid water content; hence, formation of thin briny films at temperature well below the pure ice melting point could greatly impede water vapor flow.

We will test this hypothesis by incorporating the effects of salt solutions into a finite difference vapor transport model similar to that of Hindmarsh *et al.* [5], and comparing our results to profiles of salt content through Granite drift that we obtained earlier this year in Beacon Valley.

Martian Implications: Interestingly, Mars may also provide a test of our hypothesis, for if the Gamma Ray Spectrometer detects a correlation of near-surface water ice content to the constitiuent elements of salts suchs as sulfates and nitrates, then this would strongly suggest that a common process is occurring in both Mars and Antarctica. GRS correlations observed in equatorial regions would be especially important, since the stability of non-polar ice deposits is difficult to explain with standard Martian diffusion models [2].

References: [1] Boynton W. et al. (2002) *Science, 297,* 81. [2] Paige D.A. (1992) *Nature, 356,* 43. [3] Sugden D.E. (1995) *Nature, 376*, 412. [4] Marchant D.R. (2002) *GSAB, 6,* 718. [5] Hindmarsh R.C. et al. (1998), *Geog. Ann*., *80A*, 209. [6] Claridge, G.G. et al. (1977), *Soil Sci.*, *123*, 377.

USING MARS ORBITER LASER ALTIMETER DATA TO DETECT SUBGLACIAL FEATURES AT THE RESIDUAL NORTH POLAR ICE CAP. M. C. Payne[1] and J. D. Farmer[1], [1]Department of Geological Sciences, Arizona State University (PO Box 1404, Tempe, AZ, 85287, USA, mcpayne@asu.edu, jfarmer@asu.edu).

Introduction: Digital Elevation Models (DEMs) constructed from Mars Orbiter Laser Altimeter (MOLA) data are a valuable tool in the analysis of surface geomorphic features. When formatted for use in a Geographical Information Systems (GIS) software package, such as ESRI's ArcView, MOLA data can be used to compose DEMs. In turn, the DEMs can be used to create contour maps, to create profiles through features of interest, and to generate hill-shaded views that provide an image-like perspective of selected areas. Furthermore, DEMs eliminate many problems associated with photographic images, such as over- or underexposure, sun angle, and high albedo.

In this study, we examined an area near the margins of the north polar cap in Olympia Planitia, using MOLA DEMs. We show that in marginal glacial areas where the ice is thin, MOLA detects variations in subglacial land surface topography, including a variety of distinctive geomorphic features (e.g. impact craters, fluvial channels, coniform features of probable volcanic origin, etc.). We offer a simple model to explain why MOLA is sensitive to subglacial geomorphology, and then demonstrate the potential for determining important aspects of the geologic history of polar regions obscured by surface ice and snow, using superpositional relationships apparent in MOLA DEMs.

Study Area: The region of study is located along the margin of the Martian north polar cap. This broad area, named Mare Boreum, consists of a perennial polar cap of H_2O ice, underlying CO_2 ice [1], surrounded by four distinct polar sand seas [2, 3] and a remnant polar cap margin extending from ~ 80°-75° N latitude and ~ 105°-255° W longitude.

The site discussed here is centered at ~77° N, 183° E. A feature resembling a small volcano, and a bifurcated valley, are visible in Viking images of this area. MOLA data for the site were used to test hypotheses for the origin of these features. In the process of that work on surface features, a number of subglacial geomorphic features were also detected in DEMs.

Methods: MOLA data points were input into ESRI's ArcView GIS software to create digital elevation models (DEMs) that offer an image-like view of the study site (Figure 1). The craters visible in the DEMs are actually subglacial features not visible in Viking or MOC images (Figures 1). Clearly, these subglacial features were detected by MOLA, establishing that DEMs can be used to see the geomorphology of the sub-ice features in this marginal region of thin ice (average ice thickness at the site ~100-300 m). Furthermore, the DEMs allow geomorphic measurements (such as topographic profiling) of the observed features, further facilitating their characterization.

Figure 2 explains why MOLA data is sensitive to sub-ice features in polar cap margin environments. As ice and snow accumulate over a topographical surface, the surface topography of the ice mirrors the underlying topography. As ice/snow cover increases in thickness, the underlying topography is progressively damped out, becoming more subdued. When the accumulated ice/snow cover has reached a significant thickness relative to the total relief of the underlying topography, sub-ice topography is no longer expressed at the surface. Altimetry data and DEMs of the surface of the north polar cap revealed that MOLA is indeed very sensitive to subglacial topographic features, such as the craters and channels shown in Figure 1. The form of the features is easily discernable in DEMs, as are superpositional relationships of the features. We conclude that the technique of using MOLA data to study subglacial features in marginal polar regions where ice thicknesses are less than the relief of the buried surfaces, provides a new way of mapping geomorphic units in such regions, and for reconstructing geologic history.

Age relationships/Geologic history: The subglacial craters and channels documented in the present study lie within the "mantled smooth plains material" mapped by Dial [4], which was assigned the age of mid-Amazonian. More recently, Herkenhoff and Plaut [5] used crater-counting techniques to derive an age for the north polar-layered deposits and residual cap of between 74 ka and 147 ka. Therefore, it may be concluded that the features discussed here are certainly younger than mid-Amazonian, and may be much younger.

Cross-cutting relationships of geomorphic features observed in the hill-shaded DEMs suggest that the 18 and 44 km diameter craters are the oldest features observed in the study area. Although glacial advances and retreats of the north polar ice cap are likely to have substantially modified the overall morphology of these craters, their characteristic form is obvious. Cross-cutting relationships suggest that the channels that breach these craters are younger.

Subglacial fluvial activity (e.g. basal melting environments of Clifford [7]) typically creates positive-relief, ridge-like features (e.g. eskers). However, most

of the channels observed in the region of study are interpreted to be pre-glacial and could have been formed by either: 1) fluvial systems associated with impact-generated hydrothermal systems (e.g. [6]) or 2) surface flows unrelated to impact hydrothermal processes. It may be noted that the northern channel has a more pristine appearance than the sinuous channel to the south and therefore may be younger.

A sinuous ridge found at the study site is the strongest candidate for an earlier period of subglacial fluvial activity and could be as young as the last glacial advance in this area. A pristine impact crater appears to be superimposed on this feature and is likely a post-glacial occurrence. This impact crater (and several nearby impact craters) overlie all other features in the region, and thus, are the youngest features observed.

Coniform features in the study are interpreted to be small volcanoes. This interpretation is supported by the presence of summit craters in profiles of these features. The concentration of these features in one area may indicate the presence of a single volcanic field. The timing of observed coniform features is difficult to assess. They predate the pristine impact craters, but post-date the heavily degraded 18 and 44 km diameter craters. However, their age relationship to the channels is ambiguous. It is possible that their formation overlapped with the channels, although they could also be younger.

Summary: The analysis of MOLA DEMs of ice-covered regions marginal to the north polar cap has proven useful for interpreting the geologic history of the region beyond that based on imaging alone. Superpositional relationships suggest that an ancient cratered terrain, formed during a pre-glacial era, underlies the area of the remnant north polar ice cap.

To summarize the characteristics of the region of study, the presence of subglacial channel-forms revealed by MOLA data almost certainly indicates that the surface underlying the remnant cap was modified by flowing surface water in the distant past. The presence of a sinuous ridge interpreted to be an esker suggests that subglacial fluvial activity continued in the region through the most recent glacial advance. Coniform features in the area are interpreted to be of volcanic origin, suggesting that subsurface magmatic sources could have sustained subsurface hydrothermal systems and surface outflows for some time.

The valley forms observed in DEMs suggest that they formed by surface flows of water during a pre-glacial epoch subsequent to the formation of the oldest craters. The coniform features, interpreted to be volcanic constructs, likely formed around the same time.

An analysis of the geomorphic features in this area (utilizing MOLA data) suggests that liquid water has existed in this region for a long time. This observation is particularly relevant for NASA's exploration strategy to "follow the water" as a basis for understanding the potential for past of present habitable environments for Martian life.

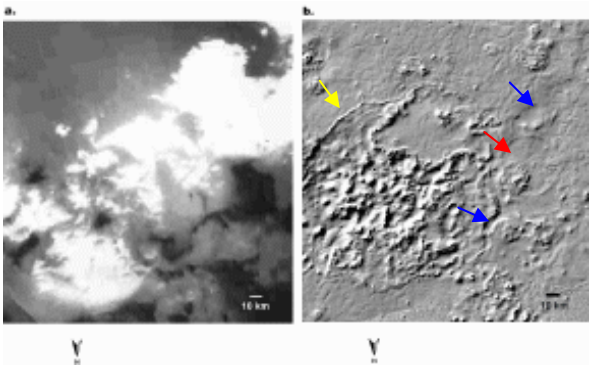

Figure 1. The study site is shown above using a) MOC wide angle visible image data, and b) a hill-shaded view of a DEM constructed from MOLA point data. The scales and areas of figures a and b are identical. It is obvious that the MOLA data provides a wealth of geomorphic information (such as the revelation of craters (red arrow), channels (blue arrows), and other landforms such as a possible esker feature (yellow arrow)) which is obscure or invisible in camera images.

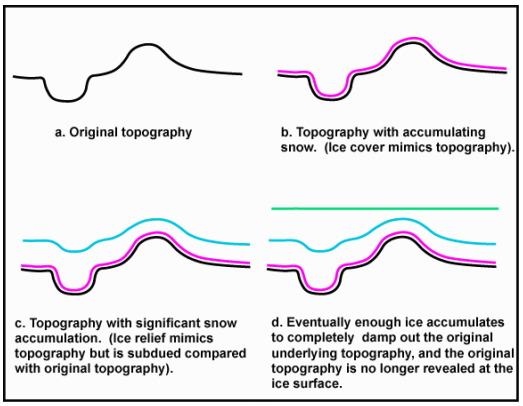

Figure 2. Graphical representation of how ice mimics topography allowing detection of subglacial features by MOLA.

References: [1] Thomas P. et al. (1992) *Polar deposits of Mars*, in *Mars*, H.H. Kieffer et al., Editors, 767-795. [2] Tsoar H. R. et al. (1979) *JGR, 84,* 8176-8180. [3] Lancaster N. and Greeley R. (1990) *JGR, 95,* 10,921-10,927. [4] Dial A. L. (1984) *Geologic map of the Mare Boreum area of Mars; scale 1:5,000,000*, United States Geological Survey. [5] Herkenhoff K. E. and Plaut J. J. (2000) *Icarus, 144,* 243-253. [6] Brakenridge G. R. et al. (1985) *Geology, 13,* 859-862. [7] Clifford S. M. (1987) *JGR, 92,* 9135-9152.

ELECTROMAGNETIC PROPAGATION MODELLING FOR GPR EXPLORATION OF MARTIAN SUBSOIL. E. Pettinelli[1], P.Burghignoli[2], A.Galli[2], A.R.Pisani[1], F. Ticconi[2], D. Del Vento[3] and A.Cereti[3], [1]Università Roma Tre - "E.Amaldi" Physics Department - Via della Vasca Navale, 84 00146 Rome, Italy, e-mail: pettinelli@fis.uniroma3.it, [2]Università La Sapienza – Electronic Engineering Departement – Via Eudossiana, 18 00184 Rome, Italy, [3] IFSI-CNR, Via del Fosso del Cavaliere, 100 00133 Rome, Italy.

Introduction: The use of GPR for Mars exploration has been suggested by several authors in the past ten years [1-5]. Some of the instruments proposed in the late 90s were designed to investigate the subsurface at great depth (thousands of meters)[1,2,4] and therefore implemented a measurement technique quite different from traditional GPR [6,7]. The interest toward a detailed investigation of the first few meters of Mars subsurface, linked to the exploration of past or present life on the planet, requires, however, the use of such a traditional technique, which is well established and has been widely applied on the Earth [7].

It is well known that GPR performance is maximized when it is applied in a very 'resistive' environment, like that expected in a cold and dry planet. Very little is known on the electromagnetic properties (permittivity, permeability, and conductivity) of the Martian soil [8], but the absence of liquid water on surface and in the shallow subsurface should in principle assure a good penetration of the signal.

Both Viking and Pathfinder missions have shown, however, that strongly magnetic mineral phases are present in the Martian dust [9,10] and therefore highly magnetic phases are also expected in the soil. Moreover, measurements from the Gamma Ray Spectrometer (GRS) experiment onboard the *Mars Odyssey* spacecraft [11-13] support the existence of significant quantities of shallow subsurface water ice in certain parts of the planet. The highest concentrations occur pole-ward from about 60° N and 60° S, as interpreted on the basis of the specific patterns of detected neutrons and spatial correlations with regions where ground ice has been predicted to be stable. The presence of both icy soil and magnetic materials may significantly affect the attenuation values and thus the achievable GPR penetration depth.

The main scope of the present work is to predict GPR propagation and attenuation features at 225 MHz and 900 MHz in Martian-like materials on the basis of the electromagnetic parameters measured in the laboratory, and also to evaluate the effect of volumetric scattering for possible in homogeneities (intrusions) in the planetary subsurface.

Laboratory measurements Dielectric measurements on different soil samples and mixtures have been performed in the frequency domain (20 *Hz* – 1 *MHz*) using a capacitive cell [8], while magnetic measurements have been performed in the same frequency range using a toroid. Table 1 summarizes the results at 1 *MHz* for the materials used in the simulations.

Note that CO_2 powder and CO_2 powder plus volcanic sand have also been included because they are common materials in the Martian polar caps, whereas the sample with magnetite has been considered in order to investigate the effect of a soil having a high iron oxide content.

Table 1

Martian soil simulants	ε'	ε"	μ'	μ"	σ (*S/m*)
CO_2 Powder	1.4	0.002	1.0	-	$1.0x10^{-7}$
CO_2 Powder+Volcano Sand	2.1	0.018	1.0	-	$1.0x10^{-6}$
Dry Volcano Sand	3.0	0.018	1.01	0.00056	$1.0x10^{-6}$
Icy soil (20% wt ice)	5.0	0.540	1.0	-	$3.0x10^{-5}$
Basalt	6.2	0.026	1.0	-	$1.0x10^{-6}$
Glass beads+Magnetite (15% wt)	4.54	0.043	1.3	0.006	$2.4x10^{-6}$

It should be underlined that the values at 1 *MHz* might represent an overestimation of both permittivity and permeability with respect to the values obtainable at hundreds of *MHz*, while the values for conductivity may be underestimated. However, these materials have shown a rather nondispersive behaviour at lower frequencies, and their values at 1 *MHz* were not very different from those measured at higher frequencies with a TDR (time domain reflectometry) technique [8].

Attenuation of GPR signals In order to evaluate the attenuation of the electromagnetic waves in the first few meters of the Martian soil, taking into account both the presence of the ice and the iron oxides, some calculations have been developed. Table 2 summarizes the attenuation and the skin depth obtained in the materials presented in Table 1 at two different frequencies.

Table 2

Martian soil simulants	**225 *MHz***		**900 *MHz***	
	Attenuation (*dB/m*)	Skin depth (*m*)	Attenuation (*dB/m*)	Skin depth (*m*)
CO_2 Powder	0.02	357.1	0.10	89.4
CO_2 Powder+Volcano Sand	0.51	16.9	2.06	4.2
Dry Volcano Sand	0.65	13.3	2.61	3.3
Glass beads+Magnetite (15 *wt%*)*	0.81	10.7	3.25	2.7
Magnetite grains (100%)*	5.51	1.6	22.06	0.4
Icy soil (20 *wt%* H_2O ice)	5.23	1.7	20.92	0.4
Basalt (dry)	0.21	40.6	0.86	10.2
*Grain size range: 200-500 μm				

In addition to the intrinsic attenuation of the involved media, the effect of scattering by small particles randomly distributed inside a host material has also been considered. In particular, a model of composite materials with spherical inclusions has been developed, and the resulting attenuation has been calculated on the basis of Mie theory of plane-wave scattering by dielectric spheres. Typical behaviours of total attenuation as a function of particle dimensions are shown in Figs. 1(a) and (b), for basalt spherical inclusions embedded in dry volcano sand and in CO_2 powder, respectively. It can be observed that maxima and minima may occur in the attenuation curve, especially at high frequencies, connected with free resonances of the inclusions.

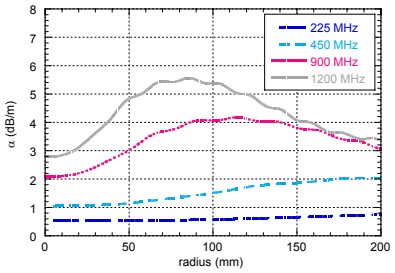

Fig. 1a

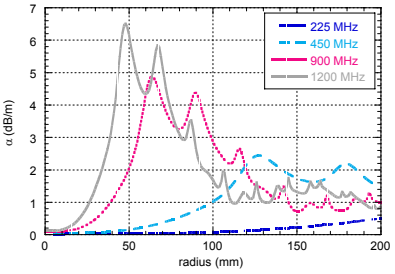

Fig. 1b

Maximum penetration depth The maximum depth of a detectable interface has been calculated using the radar range equation [6] and the *PulseEkko* Software version 4.2 (Sensors and Software Inc., Mississauga, ON, Canada). Table 3 shows the L values obtained for rough interfaces between different materials, where a two-layered soil model has been considered.

Table 3

Material interfaces	L_{max} (*m*) 225 *MHz*	L_{max} (*m*) 900 *MHz*
CO_2 Powder+Volcano Sand/ Volcano Sand	13.6	3.4
Glass Beads+Magnetite (15 *wt%*)/Icy soil	7.7	1.9
Magnetite grains (100%)/Icy soil	3.6	0.9
Icy soil/Basalt	2.7	0.7
Dry Volcano sand/Icy soil	12.5	3.1

Finally Figs. 2(a) and (b) show the maximum penetration depth achievable respectively with 225 and 900 MHz antennas as a function of the magnetite content (with a basalt as a bottom layer).

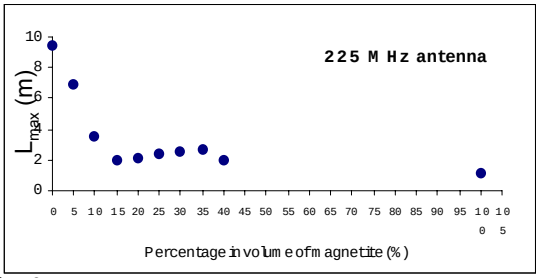

Fig. 2a

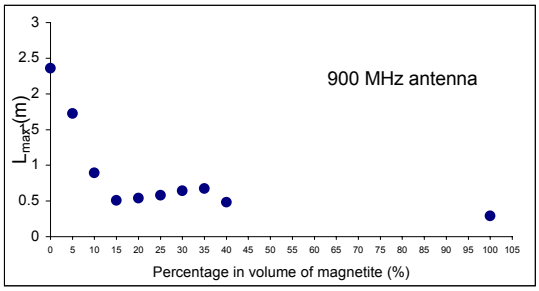

Fig.2b

References

[1] Barbin Y.et al., (1995*), JAG, 33*, 27-37
[2] Berthelier, J.J. et al. (2000), *PSP, 48,* 1161-1180
[3]Grant J.A. et al., (2003), *JGR, 108,* 1856-1865
[4]Berthelier J.J. et al., (2003) *JGR, 108*, 1866-1875
[5] Leuschen C. et al., (2003*) JGR, 108*, 1876-1885
[6] Annan A. P. (1992), Sens. and Soft., Canada
[7] Daniels D. J. (1996), Surface-Penetrating Radar
[8] Pettinelli E. et al., (2003) *JGR, 107*, 8029-8040
[9] Hargraves R.B. et al., (1979) *JGR, 84*, 8379-8384
[10] Madsen M.B. et al., (1999) *JGR, 104*, 8761-8779
[11] Boynton W. V. et al., (2002) *Science, 297,* 81-85
[12] Feldman W. C. et al., (2002) *Science*, *297,*75-78
[13] Mitrofanov I.et al., (2002) *Science*, *297,* 78-81

THEMIS VISIBLE IMAGING OF THE SOUTH POLAR LAYERED DEPOSITS, MARTIAN SOUTHERN SPRING, 2003. J. J. Plaut[1], P. Christensen[2], K. Bender[2], J. Bell[3], L. Cherednik[2], A. Ivanov[1], H. Kieffer[4], T. McConnochie[3], M. Richardson[5], and T. Titus[2], [1]Jet Propulsion Laboratory, California Institute of Technology, Mail Stop 183-501, 4800 Oak Grove Dr., Pasadena, CA 91109, plaut@jpl.nasa.gov, [2]Department of Geological Sciences, Arizona State University, [3]Department of Astronomy, Cornell University, [4]U. S. Geological Survey, Flagstaff, AZ [5]Division of Geological and Planetary Sciences, California Institute of Technology.

Introduction: The polar layered deposits (PLD) of Mars have attracted considerable attention since their identification in Mariner 9 images, largely due to the possibility that these finely layered, volatile-rich deposits hold a record of recent eras in Martian climate history. The PLD have been a target of imaging and other sensors in the last several decades, but only recently has it been possible to obtain a moderately high resolution image map, using the visible sensor on 2001 Mars Odyssey's Thermal Emission Imaging System (THEMIS). We report here on the acquisition of a 36 meter/pixel contiguous single-band visible image data set of the south polar layered deposits (SPLD), obtained during early southern spring in 2003. The data will undoubtedly be applied to many problems in Mars polar studies. We will discuss here, and in more detail at the Conference, the use of these images to further characterize the population of impact craters on the SPLD, and the implications of the observed population for the age and evolution of the SPLD.

Data: An imaging campaign with the goal of obtaining complete coverage of exposures of SPLD during early southern spring began in late April, 2003, just prior to the southern vernal equinox ($L_S = 180$). Most of the SPLD during this time of year is covered with CO_2 frost, giving a uniform albedo, and a view of the landforms that is dominated by local topographic slope. While this remained the case on surfaces close to the pole, higher latitude SPLD exposures showed surprisingly early changes in albedo, particularly in the so-called "cryptic" region [1,2]. The visible camera mode chosen was single band (0.654 microns) at 36 m/pixel resolution, which is twice the minimum pixel size of the visible camera. This allowed collection of a nearly contiguous data set in just two 30-sol Odyssey near-repeat orbital cycles. Each image is approximately 18 km by 260 km. Figure 1 shows the coverage after about 50 sols. The final data set consists of about 1000 images. Images were targeted at all longitudes between –78° and –87° latitude (areas poleward of –87° are inaccessible to THEMIS in the nadir-pointed attitude). The sector containing the Ultimi lobe, between longitudes 130° and 230° E was also targeted up to –70° latitude. At high latitudes, the Odyssey orbit track "walks" ~15 km every two sols, allowing collection of adjacent swaths closely spaced in time. Selected images are retargeted every 30 sols, to monitor changes associated with the retreat of the seasonal CO_2 frost. Simultaneous THEMIS infrared images are also acquired with selected visible images to monitor surface temperatures associated with the visible changes in surface albedo.

Impact Craters: One key objective of the SPLD imaging campaign was to obtain a new inventory of the population of impact craters on the SPLD. Studies using Viking orbiter images [3] and Mars Global Surveyor laser altimeter data [4] determined that the SPLD contained ~10 to 100 impact craters with diameters >800 m. These crater abundances are consistent with a surface age ~10s of My [5]. The THEMIS visible data set at 36 m/pixel allows identification of impact craters as small as about 200 m (~6 pixels). Many such craters have been identified in the THEMIS data. Current models of the size frequency distribution of martian impact craters predict that craters with D>200 m should be at least an order of magnitude more abundant than craters with D>800 m on a surface purely in crater production. Preliminary examination of the new SPLD images suggests that the small craters are not as abundant as expected for a production surface, implying efficient processes of small crater removal, as postulated by [4]. A complete inventory of impact craters on the THEMIS SPLD images will be presented at the Conference.

References: [1] Kieffer, H. et al. (2000) *JGR, 105,* 9653. [2] Titus. et al. (2003) this volume. [3] Plaut, J. J. et al. (1988) *Icarus 75,* 357-377. [4] Koutnik, M. et al. (2002) *JGR 107*, doi:10.1029/2001JE001805, [5] Herkenhoff and Plaut (2000) Icarus 144, 243-253.

(See next page for Figure 1)

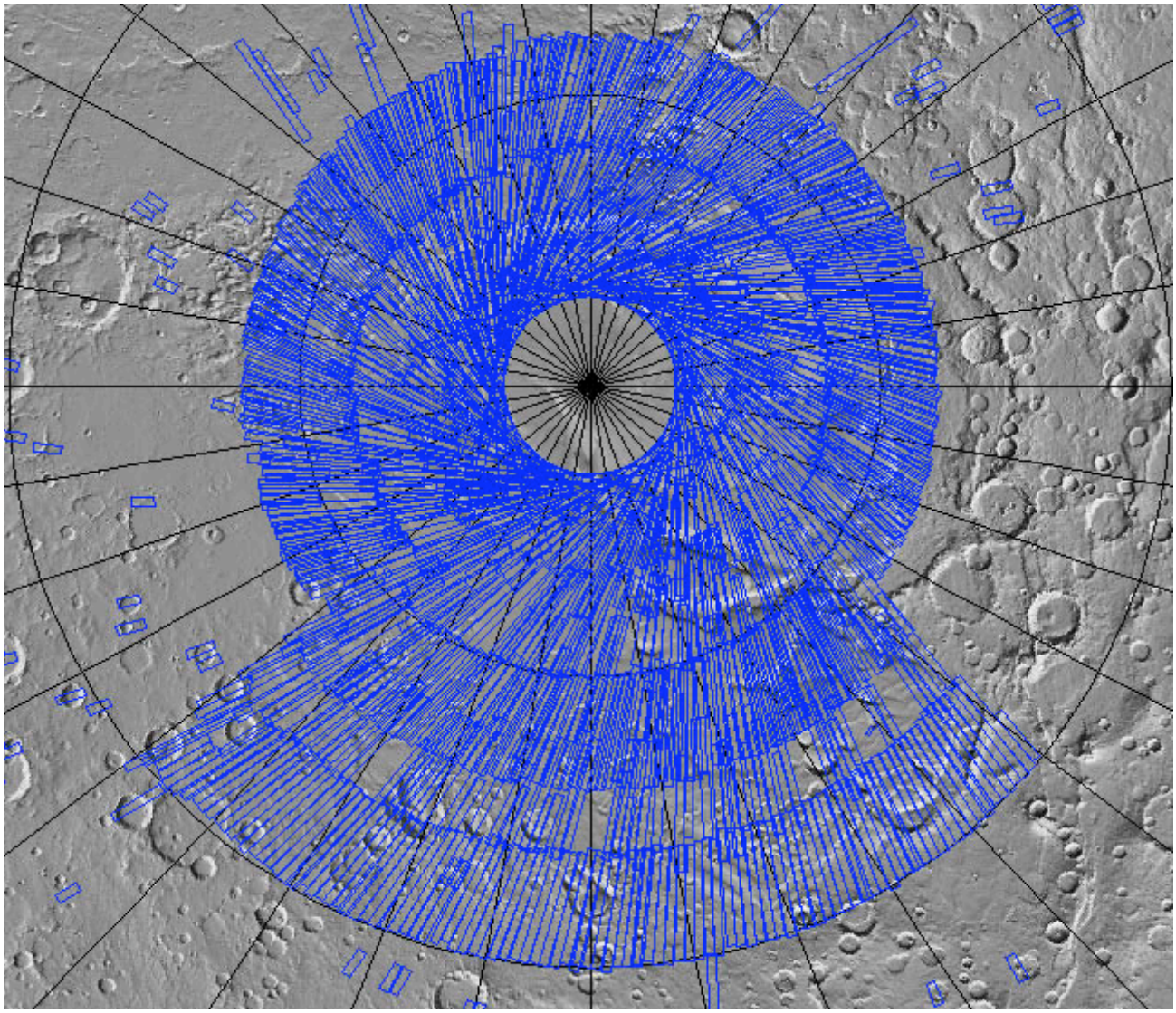

Figure 1. The south polar region of Mars, showing coverage of THEMIS visible images (blue outlines) after ~50 sols of the springtime imaging campaign. Background image is MGS MOLA topography. Latitude rings are 10 degrees. The area poleward of –87° is not accessible to THEMIS.

PROBING THE SUBSURFACE OF THE MARTIAN POLAR REGIONS WITH MARSIS ON MARS EXPRESS. J. J. Plaut[1], G. Picardi[2], and the MARSIS Team. [1]Jet Propulsion Laboratory, California Institute of Technology, Mail Stop 183-501, 4800 Oak Grove Dr., Pasadena, CA 91109, plaut@jpl.nasa.gov, [2]INFO-COM Department, University of Rome "La Sapienza", Via Eudossiana, 18, 00185 Rome, Italy.

Introduction: The European Space Agency (ESA) is currently conducting a mission to Mars known as Mars Express. The orbiter carries an instrument called the Mars Advanced Radar for Subsurface and Ionospheric Sounding (MARSIS). The MARSIS experiment is a joint project between NASA and the Italian Space Agency, and is being carried out by the University of Rome, the Jet Propulsion Laboratory, Alenia Aerospazio, and the University of Iowa. This paper describes the science objectives of the experiment, the instrument characteristics, and applications of the MARSIS investigation to studies of the martian polar regions.

Science Objectives: The primary objective of the MARSIS experiment is to detect, map and characterize subsurface material discontinuities in the upper portions of the crust of Mars. These may include boundaries of liquid water-bearing zones, icy layers, geologic units and geologic structures. Secondary objectives include characterization of the surface topography, roughness and reflectivity, and passive and active ionospheric sounding. Detection of water and ice reservoirs will address many key issues in the hydrologic, geologic, climatic and possible biologic evolution of Mars, including the current and past global inventory of water, mechanisms of transport and storage of water, the role of liquid water and ice in shaping the landscape of Mars, the stability of liquid water and ice at the surface as an indication of climatic conditions, and the implications of the hydrologic history for the evolution of possible Martian ecosystems.

Instrument Description: MARSIS is a multi-frequency, coherent pulse, synthetic aperture radar sounder/altimeter. The instrument features flexibility in frequency selection for adaptation to the Mars environment, and a secondary, receive-only antenna and data channel to minimize the effects of surface "clutter" on subsurface feature detection. The instrument will acquire echo profiles of the subsurface of Mars at a lateral spacing of approximately 5 km and a vertical (depth) resolution of 50-100 m. Four frequency channels will be available for use: 1.8, 3.0, 4.0 and 5.0 MHz. The lower frequency channels, which are likely to penetrate more deeply, will be used during night-side operations, when the ionospheric plasma frequency is lowest. The primary antenna consists of a simple dipole with a total length of 40 m. An impedance matching system is used to improve antenna efficiency across the range of frequencies. The secondary antenna is designed with a null in its pattern at the spacecraft nadir, and will therefore primarily detect echoes from off-nadir surface structure (clutter). On-board digital processing will generate coherently summed echo spectra for both the primary and secondary receive streams, at two frequencies. When data bandwidth is limited, or clutter cancellation is not needed, single frequency and/or single antenna data can be acquired. Post-processing on Earth will include convolution of the primary and secondary antenna profiles for surface clutter cancellation, and compilation of map products showing, for example, the depth to detected interfaces.

Detection of Subsurface Interfaces: A number of factors affect the ability of a radar echo sounder such as MARSIS to unambiguously detect a subsurface interface. A boundary must separate two materials of contrasting real dielectric constant, occur over a lateral length scale at least comparable to the sounder footprint (5 km), and over a vertical length scale smaller than the vertical resolution (50 m). The portion of the crust that lies between the surface and the interface must be sufficiently transmissive to allow a round-trip of the radar signal that is still detectable at the receiver on orbit. Scatterers comparable in scale to the radar wavelength (50-150 m) will disperse energy away from the nadir direction; these scatterers may occur at the surface, within the intervening crust, and at the subsurface interface. Larger-scale roughness (100s of m to km) of the terrain can introduce "clutter" that can mask the echo from a subsurface interface. Such topographic undulations (e.g., crater rims, cliff faces, etc.) may contribute echoes from off-nadir positions that correspond in time-delay to the subsurface region being probed. To minimize the effects of off-nadir scattering, a synthetic aperture approach is applied to isolate echoes in the along-track direction (effectively narrowing the footprint), and the secondary, nadir-null antenna is used to identify (and subsequently remove) off-nadir echoes.

A model of surface and subsurface scattering is developed to evaluate the depths and types of interfaces that may be detected. Crustal rocks are represented by two end-members: a low-loss, moderate dielectric andesite, and a lossier, higher dielectric basalt. The porosity is assumed to be filled by one of three materials: martian atmosphere, water ice or liquid water. Near-surface porosity values of 20% and 50% are used, with an exponential decay with depth. The surface roughness is described by a two-scale model, to take into account wavelength-scale scattering and quasi-specular effects.

Model results show that substantial penetration of the signal can be expected for many reasonable cases of surface roughness, crustal composition and volatile content. The primary "noise" factor above which a subsurface reflection must rise is competing signals from off-nadir. Use of the secondary antenna can lower the off-nadir clutter by 10 dB or more. At the lowest frequency (1.8 MHz), an interface between ice-saturated and water-saturated basaltic crust is detected at depths of 4 km, except for the roughest surface models. In the andesite crust, detection is expected at depths > 5 km. At the higher frequencies, detection depths are less (1-2 km in basalt at 5.0 MHz). An interface between dry rock and ice-saturated rock, which might be expected at moderate depths at low latitudes, is more difficult to detect than an ice-water interface, due to smaller dielectric contrasts between the pore-filling material. However, under favorable conditions of roughness and rock composition, such an interface should be detectable in the upper several kilometers of the crust.

If aquifers occur only at great depth (> 5-10 km) in the martian crust, they may elude detection by MARSIS. However, shallower reservoirs of liquid water, perhaps associated with thermal anomalies or an insulating upper stratigraphy, should detectable. Many other stratigraphic and structural boundaries are expected to be identified by the radar sounding, providing a view into third dimension of the geology of Mars.

Applications in Polar Regions: Data from MARSIS can potentially address several critical issues in Mars polar studies. Of particular interest is the depth and character of the "bed" of the polar layered deposits. If attenuation of the signal by the layered materials is not too great, it may be possible to map the base of the deposits, and detect basal melting zones, should they exist. Detection of pockets of liquid water beneath the layered deposits would be a dramatic result, with implications for possible ecosystems, and regional or global hydrologic systems. Strong discontinuities in dielectric properties may also be detected within the layered deposits, and may be indicative of major climate shifts. It may be possible to measure the thickness and electrical properties of the residual ice (high albedo unit thought to be water ice in the north and CO_2 ice in the south). Recent observations by the 2001 Mars Odyssey gamma and neutron detectors indicate the presence of ice-rich soil in the upper meter of the surface poleward of about 60° latitude. Analysis of the initial reflected pulse in MARSIS profiles should provide an estimate of the bulk dielectric constant of the upper ~50 m, possibly constraining the thickness of the ice-rich zone. If this zone extends to depths of 100s of m, MARSIS profiles may show its base. The thickness of the low-latitude desiccation zone may also be measurable. Properties of other high latitude terrains will be studied, including the thickness of the north polar erg, and possible subsurface stratigraphic contacts among sedimentary and volcanic units in both polar regions. Detection of shallow (< 5 km) aquifers would revolutionize our ideas on the current state of water on Mars, and provide targets for future biologic searches and a possible sustained human presence.

MODEL FOR FORMATION OF SPIDER PATTERNS IN THE CRYPTIC REGION. G. Portyankina and W.J. Markiewicz, Max Planck Institut für Aeronomie, Max-Planck-str., 2, Katlenburg-Lindau, 37191, Germany

Introduction: The cryptic region is one of the most dominant albedo features in data from Thermal Emission Spectrometer (TES) onboard of the Mars Global Surveyor (MGS). It is situated between latitudes 73°S and 81°S and longitudes 175°W and 225°W. Its main characteristic is that it remains cold well after it attains an albedo similar to the Martian soil. This low albedo is in contradiction with the low temperature that is close to that of CO_2 ice. One possibility to resolve this paradox is to assume that a large fraction of the solar flux passes through a surface layer of CO_2 ice and is absorbed by the dust underneath it. This is possible if the ice is slab CO_2 ice. Within this cryptic region Mars Orbiter Camera also onboard of MGS has taken images of radially converging dendritic patterns example of which is shown in Figure 1.

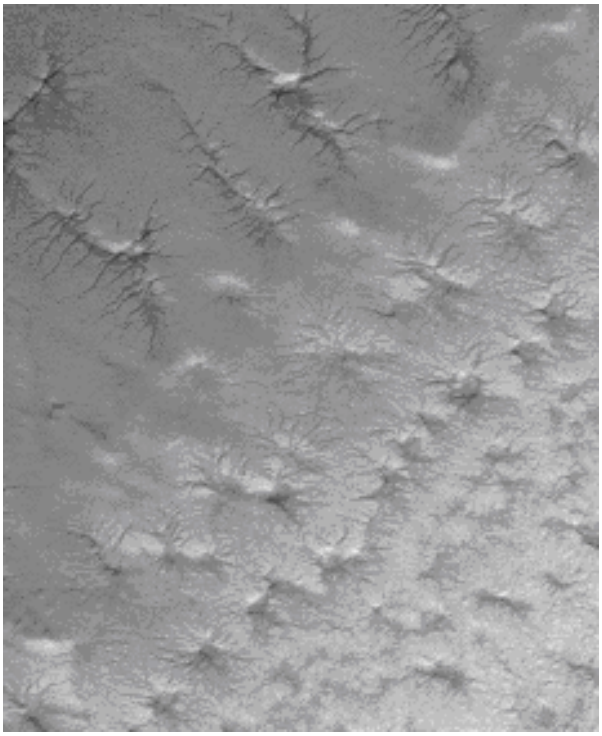

Fig. 1 MOC image showing an example of spider ravins.

These spiders are unique patterns of South Polar Regions. They have never been seen before neither in other regions on Mars nor on other Solar System bodies. A descriptive model for formation of such a patterns was proposed by [1]. The winter condensation of CO_2 includes atmospheric dust in roughly its average atmospheric mass fraction. The CO_2 slab ice is virtually transparent to solar radiation with 72% of solar energy reaching the bottom of a 1 metre thick layer [2]. Dust will modify the depth of penetration of sun light but can not influence the basic aspects of the model as long as the solar penetration is greater than the thermal flux attenuation length [1]. Dust grains embedded in the CO_2 slab will absorb solar radiation on a time scale of less than one second [3] and form individual gas pockets around themselves. The grains will rest in a gas layer, continue to sublime the ice underneath it, and "sink" downwards. Net result should be clean CO_2 ice with dust accumulating at the bottom. The transparent layer of the slab CO_2 ice will have low temperature and the underlying dust low albedo - the situation observed in the cryptic region. With increasing solar radiation flux during spring, the temperature of dust in and under the ice will increase raising the sublimation rate of CO_2 ice. The gas formed during sublimation at the bottom of the slab layer cannot diffuse through the CO_2 deposit and localized escape pathways should develop. Those of them large enough to carry adequate warm gas from the sub-layer to remain open will grow into vertical columnar vents. Mixture of fine dust grains and CO_2 gas can be ejected through them and redistributed according to wind direction to form patterns of spiders. In this model these patterns represent channels formed by sub-slab channelized flow of the sublimation gas towards the vents.

Model of cleaning CO_2 ice: The modeling of spiders' formation should include mechanism of cleaning dusty CO_2 ice to produce an ice slab transparent for most of the solar radiation that can reach the surface of Mars through its atmosphere. As a first step we calculated the timescale for this cleansing process. We consiered two types of shapes for dust grains: spheres and cylinders with the ratio height/radius = 1/10. Dust grains receive Solar radiation amount of which depends on time of day, season and and latitude of the place inside cryptic region. All radiation received by the dust grain is assumed to go into sublimation of the ice underneath it; the grain sinks to the bottom of sublimed volume – and in such a way moves downward inside the ice. Time needed for cleaning of 1-meter thick CO_2 slab ice by such a process was calculated for different particle shapes and orientations. Plots in Figure 2 show distance from the top of slab to the dust grain center (grain radius is 2.5 μm) versus time (starting with the southern spring at $L_s = 150^o$) for spherical grains and differently oriented cylinders. Curves are: cylindrical dust particle tilted by 10^o from vertical (1), 30^o (2), 60^o (3), 90^o (5), and spherical dust particle (4).

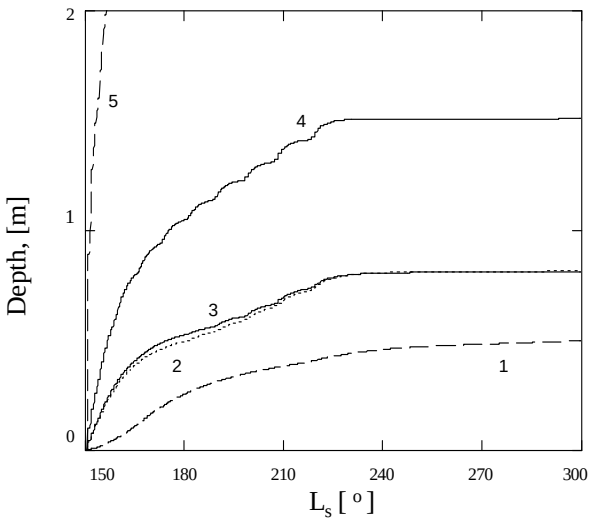

Figure 2 Depth to wich particles sink as a function of time

As the CO_2 ice evaporates, the boundary atmosphere-ice will move downward as well as dust particles. The comparison of the rates of two processes is shown at Figure 3. The dashed lines show the depth of boundary atmosphere-ice, curves are shown for several values of albedo, line 1 – depth of cylindrical dust particle tilted by 10^o from vertical and line 2 – depth of spherical dust particle.

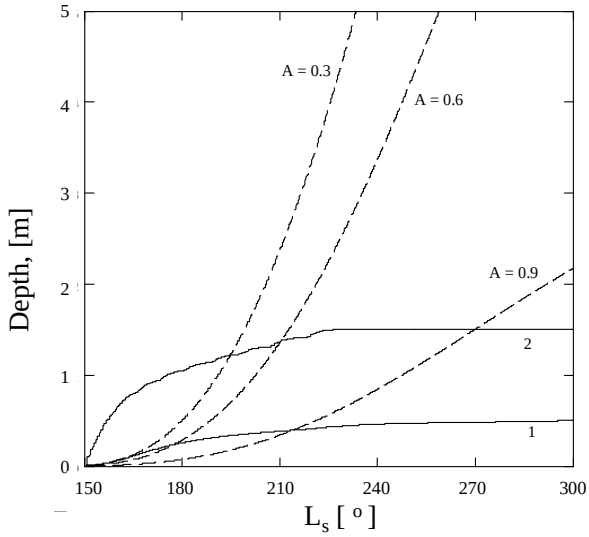

Figure 3 The comparison of particles sinking rate and the rate of ice sublimation.

Our initial estimates of the time scales critical for the cleaning process show that this aspect of the model is feasible.

Future work: We plan to create a physical model for the formation of spiders including elements such as: absorption of solar flux by dust imbedded in the CO_2 ice, sinking of the dust particles, and build up of pressure at the bottom of the CO_2 slab.

References:

[1] Kieffer, H.H. (2000) International Conference on Mars Polar Science and Exploration, p. 93. [2] Hansen, Gary B. (1997) *JGR*, *102*, 21569-21587. [3] Kieffer, H.H. ; et al. (2000) *JGR*, *105*, 9653-9699.

SEASONAL ADVANCE AND RETREAT OF MARS' SOUTH POLAR CAP AS MEASURED BY THE MARS ODYSSEY NEUTRON SPECTROMETER. T. H. Prettyman,[1] W. C. Feldman,[1] J. R. Murphy,[2] H. O. Funsten,[1] D. J. Lawrence,[1] R. R. Linn,[1] S. Maurice,[3] and R. L. Tokar,[1] [1]Los Alamos National Laboratory, Los Alamos, New Mexico, [2]New Mexico State University, Las Cruces, New Mexico, [3]Observatoire Midi-Pyrenees, Toulouse, France.

Introduction: The Martian seasonal polar caps consist of CO_2 frost deposits that advance towards lower latitudes during fall and winter and retreat toward the poles during spring and early summer in response to seasonal changes in insolation [1]. Because a large portion of the atmosphere is cycled in and out of the seasonal caps during the year, the frost deposits play a significant role in regional and global atmospheric circulation. Surface thermal properties as well as local atmospheric temperature and pressure influence the onset of frost deposition. The presence of dust in the atmosphere affects the polar energy balance, and can influence the rate of deposition and sublimation of frost [2]. During southern summer, the south polar cap is covered by residual CO_2 frost [3].

In this study, we determine the spatial distribution, areal density, and total inventory of the seasonal CO_2 frost in the southern hemisphere using neutron spectroscopy. In contrast to telescope observations and orbital photography, neutrons provide a direct measurement of the areal density (with units of g/cm^2) of CO_2 surface ice, which we refer to as "thickness" in this abstract. However, the surface spatial resolution that can be achieved by neutron spectroscopy is coarse, on the order of 600 km full-width-at-half-maximum. Nonetheless, the regional-scale resolution of neutron spectroscopy is sufficient for validation of circulation models and for comparison with previous observations.

Results reported in this abstract were obtained using data acquired by the neutron spectrometer subsystem of the Mars Odyssey gamma ray spectrometer while in mapping orbit during the years 2002 and 2003, from L_S=330° through L_S=180°. This period of time includes the advance of the seasonal frost in the south. By mid-September (L_S=260°), the frost will have fully retreated, exposing the residual terrain. Consequently, we will report details of the advance and retreat of the frost at the conference.

Advance of the seasonal frost: A map of thermal neutron count rates in the high southern latitudes obtained during southern summer (330°<L_S<0°) is shown in Fig. 1. Thermal neutrons are the portion of the population of neutrons produced by cosmic ray interactions with Mars that achieve thermal equilibrium with the surface. The relatively low count rates poleward of -55° observed during summer correspond to a terrain rich in water-equivalent hydrogen that was recently discovered by Mars Odyssey [4,5].

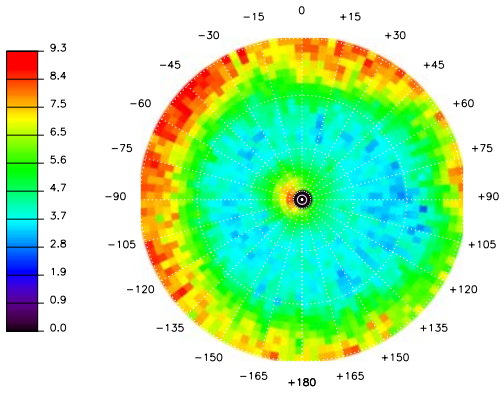

Fig. 1. Map of thermal neutron count rates in the southern high latitudes (poleward of -45°) during late summer. The units are counts per second.

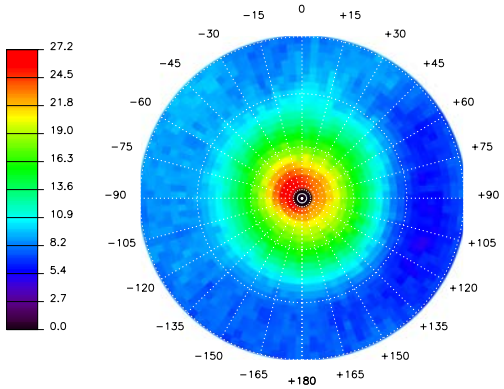

Fig. 2. Map of thermal neutron count rates in the southern high latitudes (poleward of -45°) during late winter. The units are counts per second.

The population of neutrons in thermal equilibrium with the surface is very sensitive to the presence of CO_2 frost, which is an excellent neutron moderator that is also a poor thermal neutron absorber. Consequently, the seasonal deposition of frost causes the output of thermal neutrons to increase. For this reason, the south polar residual cap, which is covered by CO_2 ice, is associated with enhanced thermal neutron count rates relative to the surrounding water-rich terrain, which can be seen in Fig. 1 [6]. The residual cap is centered at about -50° east longitude and is offset approximately 3° from the pole.

As the southern winter progresses, CO_2 frost deposits form and advance equatorward. Fig. 2 shows

the thermal neutron map late in the southern winter ($140°<L_S<180°$) as the frost is approaching its maximum coverage. Note that the region of enhanced count rate has expanded around the residual cap to produce an irregular boundary that extends equatorward beyond -60°. The maximum count rate, which corresponds to maximum frost thickness, is roughly centered on the location of the residual cap.

Thickness of the seasonal frost: We developed an algorithm to determine the distribution and thickness of the seasonal CO_2 frost from thermal neutron count rates. The neutron output observed during summer was used to minimize the sensitivity of the thickness determination to variations in the composition of the underlying terrain. The effect of possible enrichment of N_2 and Ar, which are strong thermal neutron absorbers, in the polar atmosphere during winter was ignored in the present analysis [7]. Consequently, lower bounds on frost thickness are presented.

The time-evolution of CO_2 frost thickness determined from longitudinally-averaged thermal neutron count rates is shown in Fig. 3. The time interval for each measurement was 5° of L_S. The measurements can be compared to frost thicknesses calculated by the Ames Research Center General Circulation Model (ARC-GCM). The ARC-GCM is a comprehensive model of the Martian atmosphere that treats the seasonal condensation and sublimation of CO_2 frost to and from the surface, taking into account the dynamics of the atmosphere, surface thermal properties and the effect of atmospheric dust on the rate of frost deposition and sublimation [8.9]. Calculated frost thicknesses are shown in Fig. 4 for latitudes that fall within four of the zones defined in Fig. 3. When comparing Figs. 3 and 4, note that the L_S scales are different.

Predictions of frost thickness by the ARC-GCM are similar in magnitude and shape to the measured values. The measurements indicate that frost forms later and achieves maximum thickness earlier at lower latitudes than near the poles, which is predicted by the model. The measured times of peak frost thickness, however, are slightly later than predicted and the frost recession is not as rapid as modeled. The relatively slow frost recession may be caused by increased atmospheric dust compared to the model. The measured inventory of CO_2 frost in the southern seasonal cap achieves a maximum value of 8×10^{18} g between 160° and 170° L_S, which is slightly more than 30% of the established value for total atmospheric mass (2.5×10^{19} g).

This comparison demonstrates the utility of thermal neutron count rates for determining absolute frost thickness with high temporal resolution. Further work is being carried out to improve the spatial resolution of the measurements using forward models of the instrument response, and spatial deconvolution techniques. Corrections for atmospheric composition will also be implemented. A comparison of our measurements to the ARC-GCM and observations of the seasonal frost in previous years will be presented.

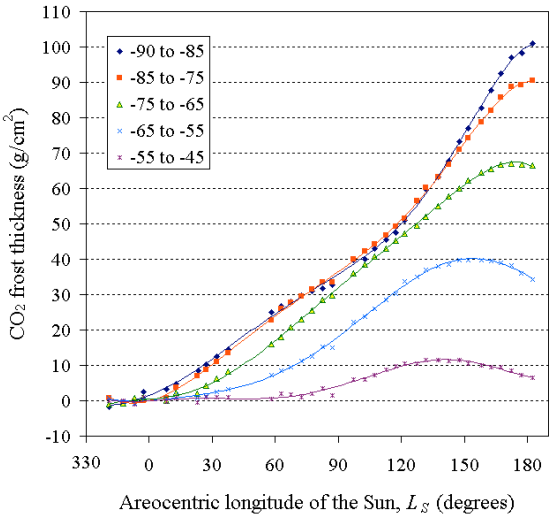

Fig. 3. Seasonal CO_2 frost thickness determined from longitudinally-averaged thermal neutron count. Latitude ranges for each zone are shown in the legend.

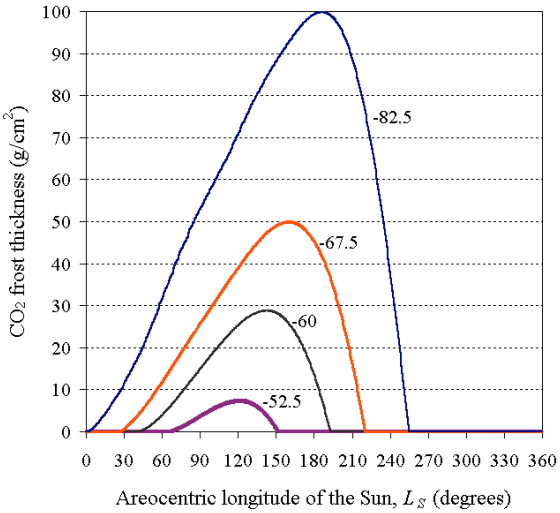

Fig. 4. Seasonal frost thickness in the southern latitudes predicted by the ARC-GCM for four latitudes (-82.5°, -67.5°, -60°, and -52.5°).

References: [1] Neugebauer, G., et al., *Astron. J.* 76, 719-749, 1971. [2] James, P. B., et al., *JGR* 84 (B6), 2889-2922, 1979. [3] Kieffer, H. H., *JGR* 84 (#SI), 8263-8288, 1979. [4] Boynton, W. V., *Science* 297 (#5578), 81-85, 2002. [5] Feldman, W. C., *Science* 297 (#5578), 75-78, 2002. [6] Tokar, R. L., et al., *GRL* 30 (#13), 1677, doi:10.1029/2003GL017316, 2003. [7] Feldman, W. C., et al., JGR in press, 2003. [8] Pollack, J. B., et al., *JGR* 95 (#B2), 1447-1473, 1990. [9] Haberle, R. M., *JGR* 104 (#E4), 8957-8974, 1999.

PLANETARY PROTECTION FOR POLAR MARS MISSIONS. J. D. Rummel, Office of Space Science, Code S, NASA Headquarters, Washington, DC 20546 USA, <jrummel@hq.nasa.gov>.

Introduction: The picture of Mars that is emerging from the Mars Global Surveyor and Odyssey results (1,2) contrasts markedly from that portrayed shortly after the Viking missions ended (cf., 3). Particularly intriguing is the abundance of water ice seen both in the polar caps themselves, and in lower latitudes outside of the polar regions. Along with the new data comes a heightened consideration of the potential for biological contamination that may be carried by future missions, and its possible effects. Particularly challenging are scenarios where missions carrying perennial heat sources of high capacity and longevity (e.g., Radioisotope Thermoelectric Generators) could, by non-nominal landings or other mission operations be introduced to close contact with water ice on Mars—-potentially forming Earthlike environments that could accommodate the growth of contaminant organisms.

Standards and Consequences: The likelihood of impinging on those environments and situations, and the potential mitigations available to mission planners, are of critical importance to the future success of Mars polar science and exploration. Recently, the ICSU Committee on Space Research (COSPAR) has published an international consensus planetary protection policy (4) that provides a standard to address the prevention of biological contamination in sensitive areas on Mars. As Mars exploration proceeds, new data will drive future planetary protection concerns, and a framework for assessing required contamination control measures will need to be developed to be responsive to the evolving understanding of the planet.

References: [1] Christensen P. R. (2003) *Nature, 422,* 45–48. [2] Mitrofanov I. G. et al. (2003) *Science, 300,* 2081-2084. [3] Horowitz, N. H. (1986) *To Utopia and Back*, W. H. Freeman [4] COSPAR (2002) *COSPAR Planetary Protection Policy*, Paris.

VOLATILE-RICH CRATER INTERIOR DEPOSITS IN THE POLAR REGIONS OF MARS: EVIDENCE FOR ICE CAP ADVANCE AND RETREAT Patrick S. Russell[1], James W. Head[1], Michael H. Hecht[2], [1]Geology. Dept., Brown Univ., Providence, RI 02912 USA, [2]JPL, Pasadena, CA, USA. Patrick_Russell@Brown.edu.

Introduction: Many craters on Mars are partially filled by distinctive material emplaced by post-impact processes. This crater fill material is an interior mound which is generally separated from the walls of the crater by a trough that may be continuous along the crater circumference (i.e. a ring-shaped trough), or which may only partially contact the crater walls (i.e. a crescent-shaped trough). The fill deposit is frequently offset from the crater center and may be asymmetric in plan view. Populations of such craters include those in the circum-south polar cap region, in Arabia Terra, associated with the Medusae Fossae Formation, and in the northern lowlands proximal to the north polar cap. We focus on those craters in circum-polar regions and assess their relationship to polar cap advance and retreat, especially the possibility that fill material represents remnants of a formerly larger contiguous cap.

Motivated by assessment of the martian hydrological cycle, especially the groundwater system, we have previously examined northern lowlands craters for signs that the impacts may have interacted with the groundwater system [4]. Given the physical and thermal disruption of the ground associated with impact, disruption of the subsurface cryosphere could have allowed effusion of sub-cryosphere confined groundwater into the crater under artesian-like conditions [4,5]. In a globally interconnected hydrosphere-cryosphere system [5], this process would be favored in the northern lowlands, where hydraulic pressure head of groundwater should be greatest [4]. Such a scenario presents an alternative hypothesis for volatile-rich crater fill in northern lowlands craters, but impacts into high-elevation circum-south polar terrain would not be expected to have accessed subsurface water. In addition, the only large craters in the northern lowlands containing significant fill material (e.g., Korolev) are those closest to, but isolated from, the north polar cap [6]. Unless these impacts were very recent, such that the volatile fill had not yet sublimated away [7], this non-random clustering near the north pole suggests that there has been either preferential deposition by polar-like processes in isolated craters, or deposition contiguous to, or part of, a formerly more extensive polar cap [e.g., 3] and subsequent preferential removal of material in intercrater plains. Fill deposits in some craters around the south pole are contiguous with south polar layered material [1], which argues for a similar process of deposition with possible later exhumation or flow into the crater [2].

Volatile-rich deposits have the property of being modifiable by the local stability of the solid volatile, which is governed by local energy balance. Here we test the hypothesis that asymmetries in volatile fill shape, profile, and center-location within a crater result from asymmetries in local energy balance within the crater, due mainly to variation of solar insolation and radiative effects of the crater walls over the crater interior. Model profiles of crater fill are compared with MOLA topographic profiles to assess this hypothesis. If asymmetry in morphology and location of crater fill are consistent with radiative-dominated asymmetries in energy budget within the crater, then 1) the volatile-rich composition of the fill is supported (this process should not be effective at shaping volcanic or sedimentary deposits), and 2) the dominant factor determining the observed shape of volatile-rich crater fill is the local radiative energy budget (and erosive processes such as eolian deflation are secondary or unnecessary).

We also use a geographic and energy model approach to specifically test the idea that material in partially filled craters around the south pole may once have been contiguous to the cap and may have been sustained and modified by radiative processes specific to the crater environment (as opposed to the surrounding plains) as the cap retreated.

Korolev Crater: Korolev crater (~80 km diameter; [6,8]) is superposed on Amazonian mantle material surrounding north polar terrain [1]. While the crater is circular, rim height is not uniform around its circumference. The smooth-surfaced, roughly circular fill deposit within Korolev does not extend completely to the interior walls of the crater, leaving an intervening ring-shaped trough. Relative to the crater's center, the fill deposit is displaced to the north and east, where it reaches closer to and higher up the crater walls. The highest point of the fill deposit is also displaced in the same sense. Based on rim-to-floor depths expected at a fresh, unfilled crater of Korolev's diameter [8,9] the actual deepest point of the crater is not much deeper than the observed elevation. The maximum thickness of the fill mound is then ~1.5 km [8].

Circum-South Polar Craters: There are many craters with fully or partially visible rims within the polar layered terrain of the south polar cap, especially on the half oriented towards 180° (e.g., Fig. 1). Around the fringes of the cap, northern parts of crater rims are fully exposed, while on pole-ward sides crater fill material is still clearly contiguous with polar material (e.g., Fig. 2; [10]). Up to ~ 12° of latitude from the edge of the polar layered terrain are craters with fill material isolated from polar material (e.g., Fig. 3). This isolated fill appears to become less circular and symmetric at greater distances, often located in the northern portions of the crater (e.g., Fig. 4). These materials have been mapped as extensions of polar layered material (Apl; [1]) or as ice and fine dune material possibly derived from polar layered terrain and possibly covering polar layered terrain material deposited in areas of low wind velocity (Ad; [1]).

Based on morphologic and topographic similarity, and in some cases contiguousness, of crater fill with polar layered deposits, we hypothesize that fill material either 1) was deposited preferentially in craters rather than on surrounding plains, or 2) was once present in the plains as well, as part of a larger continuous polar cap, and preferentially remains in the craters today as polar material has retreated from the plains. Fill material in craters partially visible around the edges of the polar layered terrain appears to be maintained by the same conditions as the surrounding, extra-crater polar layered terrain, unless both materials are being deflated and the craters are being exhumed. In some cases there is evidence that physical flow of polar layered material contributed to crater fill deposits [2,10]. Further north, craters not physically connected to the polar layered terrain contain less fill, and this is generally in the form of a circular mound. Yet further north, crater fill is significantly less, occurring only locally within craters. The observed trend of decreasing fill amount with increasing northerly latitude suggests that either deposition and equilibrium-amounts of fill are less at more northern latitudes, or erosive, sublimation, or ablation processes have been more severe at more northern latitudes.

Energy Balance Model: Our approach to determine where and how much modification of an assumed existing water-ice

crater-fill occurs is to calculate the main energy input and output pathways for a patch of the surface and assume any excess input energy is available for sublimation. The main processes involved are as follows: 1) solar insolation, including shadowing effects of the crater walls, 2) temperature-dependent reradiation from the surface, including the geometric effects of the crater walls on reducing emittance to the sky, 3) diffusion of heat into or out of the body of ice below the surface, and 4) energy, if any, available for phase change and sublimation of CO_2 and H_2O [11]. By iteratively calculating the energy balance of these processes at different points within the crater, we determine the relative amount of sublimation at each point. The same is done for a point in the plains, outside a crater environment. As an observed proxy for evolution of the modification process, we use characteristic fill morphologies at increasing distance from the south polar cap terrain. If actual fill shape is largely consistent with these modeled processes, then 1) the deposit is likely largely ice-rich, 2) radiative effects likely dominate over wind effects, for example, in the size, location, and shape of such fill, and 3) the retreat (in the plains) of a formerly larger polar cap is supported.

We are interested in timescales less than those of eccentricity and obliquity variations, given the rapid rates of sublimation expected on Mars [7], so we hold orbital parameters constant during each trial. However, the stability of ice changes drastically at different orbital configurations [e.g., 12], so we test several combinations of obliquity and eccentricity. The sensitivity of the model and resulting crater-fill morphology and asymmetry is assessed with respect to physical and geometric parameters such as albedo, emissivity, slope angle, atmospheric scattering (based on [13]), proximity to the crater wall, and crater wall height.

The relative role of incident solar radiation on differently-facing slopes is dramatic. As expected at the high northern latitude of Korolev, south facing slopes receive more total yearly insolation, yet the maximum daily insolation occurs on north-facing slopes due to obliquity effects. With a nominal, non-dust storm, atmospheric optical depth of 0.5, incident insolation is reduced by 10-30% when the sun is more than 10° above the horizon [13]. Albedo can vary by a factor of 4 [11], which directly effects absorbed insolation. The latter two effects affect the total amount of insolation, while the first, and the geometry of the crater, affect the relative distribution of insolation. Asymmetry in insolation is clearly a candidate for being the major control on volatile fill asymmetry, which is supported by observation in a north-south profile across Korolev showing a strong asymmetry in which fill is concentrated to the north, consistent with more yearly energy input from southerly insolation [6].

A nearby high rim, however, will also decrease radiative heat loss by reducing the angle of sky seen by a surface [11]. Due to a thin atmosphere that is ineffective at convecting heat, the sky on Mars is very cold relative to these crater walls. Thus, the greater the visible angle of sky, the more energy can be radiated away, and the more the crater wall fills the field of view, the less the effective emissivity [11]. This concept of effective emissivity is summarized in the following equation: *radiated energy* = :

$$(E\sigma T_{surf}^4 - \sigma T_{sky}^4) * skyfraction + (E\sigma T_{surf}^4 - \sigma T_{cwall}^4) * cwallfraction \quad (1)$$

where E is emissivity of the surface, σ is the Stephan-Boltzman constant, and T is the temperature of the surface, sky, and crater wall, respectively. The hemisphere centered on the normal to the surface is divided into that fraction which is open to the sky and that which is filled, or "blocked" by the crater wall.

Conduction of energy into the subsurface is represented simply by a one-layer slab the thickness of the skin depth. It is assumed that, at each iteration of time, this slab changes temperature based on its heat capacity and the difference between its temperature at the previous time iteration and the temperature at the surface.

The amount of CO_2 deposited and sublimated each season, which we take to be a relatively thin cover over the H_2O ice-rich fill material, is tracked over the interior of the crater based on the latent heat available and assuming the surface temperature never drops below the CO_2 frost point of 148K.

At current orbital configuration, significant energy for sublimation of water ice is not available, thus evolution of deposits may not be currently active. If outlier fill material between ~150° and 240° W longitude was once part of a larger contiguous southern cap, we estimate that on the order of 0.5-2 x 10^6 km^3 of material has since been removed. We are further testing a variety of orbital configurations which will reveal under what conditions, when, and for how long, evolution of ice-rich crater deposits will occur. This will help constrain the relationship of fill material to polar cap material over geological history.

References: [1] Tanaka, K.L., and D.H. Scott (1987) USGS Map I-1802-C. [2] Head, J.W. (2001) *JGR 106*, 10075-10085. [3] Fishbaugh, K.E., and J.W. Head (2000) *JGR 105*, 22455-22486. [4] Russell, P.S., and J.W. Head (2002) *GRL 29*, 17, doi:10.1029/2002GL015178. [5] Clifford, S.M. (1993) *JGR 98,* 10973-11016. [6] Russell, P.S., et al. (2003) *LPSC XXXIV*, #1249. [7] Kreslavsky, M.A., and J.W. Head (2002) *JGR 107*, E12, doi:10.1029/2001JE001831. [8] Garvin, J.B. et al. (2000) *Icarus 144*, 329-352. [9] Pike, R.J. (1988) in *Mercury*, F. Vilas et al., eds., Univ. Arizona Press, 165-273. [10] Pratt, S., and J.W. Head (2002) *LPSC XXXIII*, #1866. [11] Hecht, M.H. (2002) *Icarus 156*, 373-386. [12] Mellon, M.T., and B.M., Jakosky (1995) *JGR 100*, 11781-11799. [13] Pollack, J.B. et al. (1990) *JGR 95*, 1447-1473.

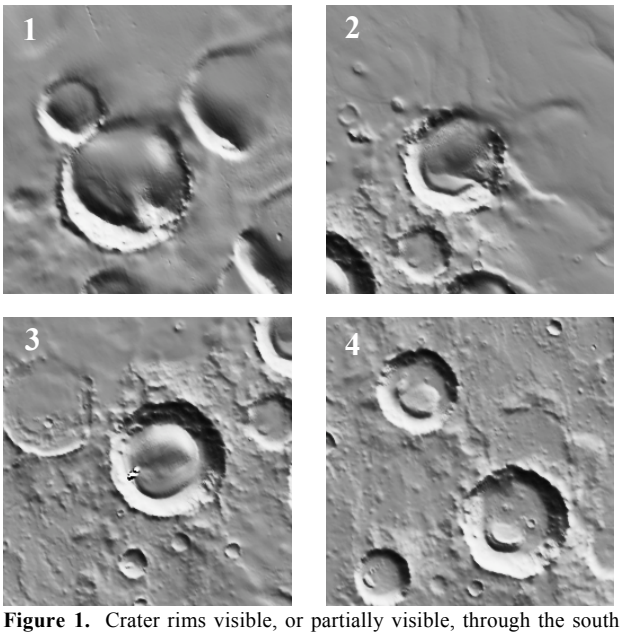

Figure 1. Crater rims visible, or partially visible, through the south polar layered terrain. 75°S, 120°W. All figures at roughly same scale: ~200 km wide. **Figure 2.** Crater mostly exposed, but still half surrounded with south polar layered terrain. Fill material is still contiguous with polar terrain. 80°S, 124°W. **Figure 3.** Crater isolated from south polar layered terrain, with circular fill material. Nearby fringes of polar layered terrain visible at top. 78°S, 126°W. **Figure 4.** Craters with local, isolated, irregularly-shaped fill material. These craters are furthest from the polar layered terrain. 74°S, 131°W.

Martian North Polar Impacts and Volcanoes: Feature Discrimination and Comparisons to Global Trends. S. E. H. Sakimoto[1] and S. L. Weren[2,1], [1] GEST at the Geodynamics Branch, Code 921, NASA Goddard Space Flight Center, Greenbelt, MD 20771, sakimoto@geodynamics.gsfc.nasa.gov, [2]Geoscience Department, Franklin and Marshall College, P.O. Box 3003, Lancaster PA, 17604, serena.weren@fandm.edu.

Introduction: The recent Mars Global Surveyor and Mars Odyssey Missions have greatly improved our available data for the north polar region of Mars. Pre-MGS and MO studies proposed possible volcanic features [e.g., 1, 2] , and have revealed numerous volcanoes and impact craters in a range of weathering states that were poorly visible or not visible in prior data sets. This new data has helped in the reassessment of the polar deposits [e.g. 3, 4, 5] From images or shaded Mars Orbiter Laser Altimeter (MOLA) topography grids alone, it has proved to be difficult to differentiate cratered cones of probable volcanic origins from impact craters that appear to have been filled. It is important that the distinction is made if possible, as the relative ages of the polar deposits hinge on small numbers of craters, and the local volcanic regime originally only proposed small numbers of volcanoes. Therefore, we have expanded prior work on detailed topographic parameter measurements and modeling for the polar volcanic landforms [e.g. 6-10] and mapped and measured all of the probable volcanic and impact features for the north polar region as well as other midlatitude fields, and suggest that 1) The polar volcanic edifices are significantly different topographically from midlatitude edifices, and have steeper slopes and larger craters as a group, 2) the impact craters are actually distinct from the volcanoes in terms of the feature volume that is cavity compared to feature volume that is positive relief, and that 3) there are actually several distinct types of volcanic edifices present, and that 4) these types tend to be spatially grouped by edifice. This is a contrast to many of the other small volcanic fields around Mars, where small edifices tend to be mixed types within a field.

Approach: For topographic measurements, we use the released MOLA profiles to grid 30 degree regions at 128 pixels per degree longitude and 256 pixels per degree latitude (approximately 460 m/pixel by 230 m/pixel) using G. Neumann's crossover correction approach to gridding [11] and the publicly available GRIDVIEW software [12]. We measure parameters such as those in [13-14] and [6] for impact craters and volcanoes, respectively. For craters, this includes crater width, depth, rim height, ejecta thickness, rampart height, cavity volume, ejecta volume, etc… For volcanoes, this includes height, diameter, mean flank slope, max flank slope, crater depth, diameter, and volume, edifice volume, area, basal elevation, and locations. The volcano modeling includes the hydrostatic head models used in [7,8]. Examples of some of the features measured are shown in Figure 1 and include impact craters with a relatively fresh cavity, impact craters with filled cavities, cratered cones, steep near-polar cratered cones, and a field of steep cratered cones. The features in this region are compared to those in Tempe Mareotis, Syria, Tharsis, Elysium, the South Polar region, and others.

Figure 1. High resolution MOLA topography shown as shaded relief for A) a fairly fresh polar impact crater, B) a group of partially filled polar impact craters, a C) large cratered cone, D) a group of several near polar cap cratered cones, and E) A field of steeper cratered cones.

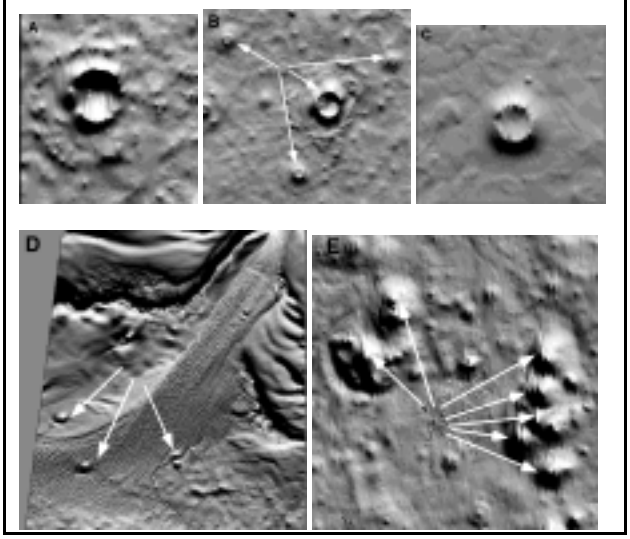

Results:

Polar and Mid-latitude differences. The higher resolution measurements support earlier conclusions that the polar volcanoes are systematically different than the midlatitude volcanoes in flank slope, crater sizes, and other parameters, and that their flank slopes as a group continue the global trend of increasing average flank slope with increasing latitude [e.g. 7, 8].

Impact Crater or Volcano?? While the cratered cones of presumed volcanic origin [e.g. 2, 6] have craters perched above the surrounding plains, local impact –craters with readily apparent ejects ramparts also have craters perched above the surrounding plains, and for those craters with minimal eject ramparts, the volcano/crater distinction is not always obvious in images or topographic grids. Additionally, the volume/diameter versus flank slope that helps differenti-

ate between volcano types sometimes yields overlapping impact and crater field plots (see Fig. 2).

Figure 2. This plot shows feature volume/diameter versus average flank slope in log-log axes for Tempe small volcanic features (in gray for comparison), polar small volcanic features (red triangles), and polar impact craters (blue circles).

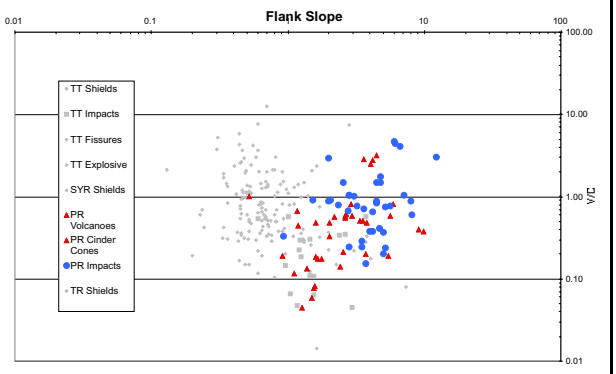

However, the readily identifiable impact craters with remnant ejecta blankets and topographically visible ramparts have a larger fraction of the landform occupied by the crater cavity than the features mapped as probable volcanoes do. We use this observation as the basis of plotting newly identified probable volcanoes and possible volcanoes with the impact craters in Figure 3, as crater cavity volume/edifice volume versus crater diameter. This plot tends to show fairly distinct impact and volcanism fields may hat help separate enigmatic features by most likely origins.

Volcanic Types and Origins. With the higher resolution topographic data, the prior suggestion of several different volcanic types within the polar volcanic landforms [e.g. 8, 10, 15] appears much more robust. The large cratered cones identified by several authors as probable volcanics are distinct from the steeper (< 7 degrees flank slope) cratered cones found closer to the polar cap, and these are also distinct from the cluster of steep cratered cones found directly between the polar cap and Alba Patera. The latter features overlap significantly, range in sizes, and are quite numerous within a defined region, while the near polar steeper cones tend to be more isolated, or are found in small groupings.

Conclusions: 1) Polar and mid-latitude volcanoes are fundamentally different in topography, thus and presumably eruption style, 2) Careful parameter measurements appear to assist in differentiating between impact and volcanic features, and there are several probable volcanic edifice types present in the north polar region, with the implication that eruption styles by sub-region tend to be distinct.

References: [1]Tanaka, K. L. and Scott, D. H. (1987) USGS Map I-1802-C. , [2] Hodges, C. A. and Moore, H. J. (1994) USGS Prof. Pap. 1534. [3] Tanaka et al., JGR-Planets, *108* (E4), GDS 24-1, CiteID 8043, DOI 10.1029/2002JE001908, 2003. [4] K.L. Tanaka, and E.J. Kolb, Regional Geologic History of the Polar Regions of Mars, *International Conference on Mars Polar Science and Exploration,*, p 168-169, 2000.[5] Plaut, J. J. et al. (1988) Icarus 73, 357-377. [6] Garvin J.B. et al., (2000), *Icarus*, 145, 648-652. [7] Sakimoto S.E.H. et al., (2002) *LPSC XXXIII*, Abstr.#1717. [8] Sakimoto S.E.H. et al., (2001) *LPSC XXXII,* Abstr.#1808. [9] Wong, M.P. et al., (2001) *LPSC XXXII,* Abstr.#1563. [10] Weren, S.L. and S. E. H. Sakimoto, Abstract #66446, submitted to GSA Fall meeting, 2003. [11] Neumann, G.A., et al., JGR, *106* (E10), p. 23573-23768, 2001. [12] Roark, J., et al., *LPSC XXI, Houston, TX*, *CDROM*, Abstract # 2026, 2000. 13] Garvin, J.B., et al., *LPSC XXI, Houston, TX*, *CDROM*, Abstract # 1619, 2000. [14] Garvin, J.B., et al., *Icarus*, *144* (April), 329-352, 2000. [15] Sakimoto, S.E.H., et al., *LPSC XXI, Houston, TX*, *CDROM*, Abstract #1971, 2000.

Acknowledgements: This research was supported in part by funding from the Mars Data Analysis Program and the MOLA Scence Team. Essential software support from J. Roark, helpful discussions and support from J. Garvin, and supplemental funds for S. Weren from H. Frey and Franklin and Marshall College are gratefully acknowledged. We thank E. King and J. Chadwick for assisting with collection of high-resolution mid-latitude volcanism data.

Figure 3. This plot shows crater cavity volume/edifice volume versus diameter for polar features. Polar impact craters (filled blue circles), large cratered cones previously mapped as volcanoes (large open red triangles), small cratered cones that are probable volcanis features (large filled red triangles) andsome enigmatic features that appear to be possibly volcanic (small filled red triangles) so far tend to be fairly distinct groupings. We are in the process of adding more complete data.

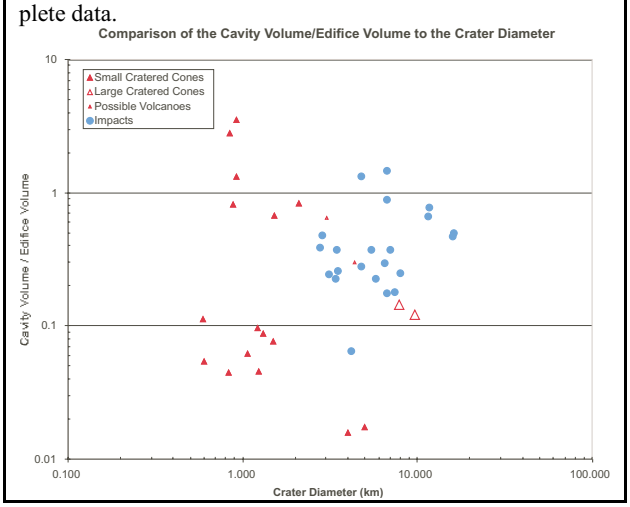

INVESTIGATION OF EXCHANGE PROCESSES IN THE MARTIAN WATER CYCLE. K. G. Schmidt, *Center for Planetary Science, University of Copenhagen, Denmark (kgs@gfy.ku.dk)*.

Introduction

Water is found on Mars in the three reservoirs: The polar caps, the permafrost, and the atmosphere. We focus on the processes of mass exchange of water between the atmosphere and the polar caps as well as exchange with the regolith in order to investigate the relative importance of the two surface reservoirs to the present water cycle on Mars.

The polar caps of Mars are believed to consist mostly of water ice with large amounts of dust in both of them and some CO_2 ice. On images from space crafts stripes or layers are seen on the slopes of the polar caps facing the equator, which may be related to climate changes in the history of Mars, just as the climate history of the Earth is captured in the ice caps of Greenland and Antarctica.

A characteristic feature of the north polar cap is a spiralling pattern of scarps and troughs organised around the pole. Horizontal or north-facing areas appear white, while the scarps expose the dark layers. The alternating white polar ice and exposed layers suggest that the cap interacts with the atmosphere through deposition and sublimation processes and plays an active role in the current water cycle on Mars. The spiralling scarps and troughs are thought to be formed in a combination of sublimation, wind effects, deposition and ice flow [1,2].

In the northern summer, water may sublimate both from the North polar cap and from the northern lowlands, which were recently shown to contain large amounts of water beneath the surface [3]. This water may be stored as permafrost, adsorbed water, or water of hydration, depending on the latitude. However, a surface dust cover would protect subsurface ice from sublimating, e.g. as observed on terrestrial glaciers. The polar cap may thus be the dominant source of water vapour with its white surface and exposed ice deposits.

The spatial and temporal distribution of water vapour in the atmosphere has been measured by the Mars Atmospheric Water Detector (MAWD) on the Viking Orbiters [4, 5] and extracted from the Thermal Emission Spectrometer (TES) on the Mars Global Surveyor (MGS) [6].

Results

The model couples a simple atmospheric model with transportation of water by eddy diffusion and a sublimation and deposition model for the surface.

The sublimation rate of water from the ice surface is controlled by the saturation pressure of water vapour over an ice surface, which is a function of temperature, and the partial pressure of water vapour in the atmosphere, which varies in time. For the lower latitudes models for permafrost and adsorbed water are used.

Datasets for temporal and spatial water vapour abundance in the atmosphere and spatial distribution of water in the surface reservoirs are combined with model results in order to obtain understanding of the water exchange and circulation.

References

[1] Howard, A.D., et al., (1982). *Icarus*, 50, 161–215.

[2] Fisher, D.A. (1993). *Icarus*, 105, 501–511.

[3] Odyssey data: Boynton, W.V., et al., (2002). *Science*, 297, 81–85, (10.1126/science.1073722). Feldman, W.C., et al., (2002). *Science*, 297, 75–78, (10.1126/science.1073541). Mitrofanov, I., et al., (2002). *Science*, 297, 78–81, (10.1126/science.1073616).

[4] Farmer, C.B., et al., (1977). *JGR*, 82, 4225–4248.

[5] Jakosky, B.M. and C.B. Farmer, (1982). *JGR*, 87, 2999–3019.

[6] Smith, M.D., (2002). *JGR*, 107 (doi:10.1029/2001JE001522).

THE FORMATION AND DETECTABILITY OF CO_2 CLATHRATE HYDRATE ON MARS. B. Schmitt, L. Mulato and S. Douté. Laboratoire de Planétologie de Grenoble, UJF/CNRS, Bât. D de Physique, B.P. 53, 38041 Grenoble Cedex 9, France. E-mail: Bernard.Schmitt@obs.ujf-grenoble.fr

Introduction: CO_2 clathrate hydrate is suspected to be present near the surface of the south polar cap of Mars, and covered by seasonnal CO_2 frost during winter. After sublimation of this frost during summer times, it may be locally present at the surface where it may eventually decompose [see e.g. 1]. However there are currently no direct proof of its existence. Very limited laboratory spectral data are available in the mid-infrared and none in the near-infrared. Thermodynamical data on the formation, stability and decomposition rates are also sparse.

Clathrate Formation: Kinetic experiments have been performed on the formation of CO_2 clathrate by direct interaction of CO_2 gas with water ice grains at low temperature (195-213 K) [2]. We show the effects of several gas and solid phase parameters on the clathrate hydrate formation rates: temperature, pressure difference with dissociation pressure, specific surface area and surface stability of water ice, ... The stability of the CO_2 clathrate and its decomposition kinetics have been also studied. Microphysical mechanisms for both formation and decomposition processes are proposed.

CO_2 clathrate on Mars. The conditions for CO_2 clathrate formation and stability in the atmosphere and at the surface of Mars are discussed and the formation rates are estimated from the extrapolation of our laboratory data to the relevant Mars conditions.

Clathrate IR spectrum: We are currently performing laboratory experiments on the spectroscopic properties of CO_2 clathrate hydrate in the fundamental modes region (mid-infrared) and in the combination and overtone bands region (near-infrared).
We will present the result of this study focusing on the spectral signatures that may allow us to discern between pure CO_2 ice and CO_2 clathrate in the reflectance spectra of the polar caps.

Detectability of CO_2 clathrate. Using the optical constants of water ice [3], CO_2 ice [4] and those we expect to obtain for CO_2 clathrate hydrate we are performing radiative transfer calculations [5] to assess the detectability of CO_2 clathrate in reflectance spectra of Mars polar caps for different microphysical situations: 1) "pure" CO_2 clathrate; 2) mixed with CO_2 frost; 3) overlying water ice; 4) with a CO_2 frost layer on top; 5) thin water ice layer (from clathrate decomposition) overlying CO_2 clathrate. This study is performed at full spectral resolution (1 cm^{-1}) as well as at the resolution of the OMEGA spectro-imager (Mars Express mission).

References: [1] Kargel J. and Lunine J.I. (1998) *Solar System Ices,* Kluwer, 97-117. [2] Schmitt B. (1986) *Thesis, UJF-France,* 201-230. [3] Grundy W. and Schmitt B. (1998) *JGR E,* 103, 25809-25822. [4] Quirico E. and Schmitt B. (1997) *Icarus,* 127, 354-378. [5] Douté S. and Schmitt B. (1998) *JGR E,* 103, 31367-31390.

SUBLIMATION AND CONDENSATION FLOWS IN CHASMA BOREALIS: A SENSITIVITY STUDY USING A 2-D ENSEMBLE MESOSCALE CIRCULATION MODEL. T. Siili, *Finnish Meteorological Institute / GEO, FIN-00550 HELSINKI, FINLAND, (Tero.Siili@fmi.fi)*, A. Määttänen, *Division of Atmospheric sciences, FIN-00014 University of Helsinki, FINLAND.*

Introduction and background The University of Helsinki's 2-D Mesoscale Circulation Model (MCM) [1] has been adapted for Martian conditions in early 1990s [2] to create the University of Helsinki (UH), Division of Atmospheric Sciences (ATM) 2-D Mars MCM (MMCM). The model has since been used and developed at both UH/ATM and Finnish Meteorological Institute (FMI), Geophysical Research (GEO) to study a number of martian mesoscale circulations, especially so-called *surface-induced* phenomena. Among the forcing and circulation types are [2–5]:

- slope winds,
- (CO_2 and H_2O) ice edge winds,
- winds driven by horizontal variations in albedo, thermal inertia and horizontal dust optical thickness.

The model also incorporates a basic H_2O transport scheme, but no dust transport as of yet. A fairly comprehensive description of the model can be found in, *e.g.* [6].

Ensemble approach To our knowledge, until recently this and other MMCMs have been used in what might be called *single-forecast* mode, producing a single simulation result or a forecast from essentially a single set of initial and boundary conditions [7]. As those conditions are bound to have errors and the models are sensitive to initial conditions, *ensemble*-type approaches have, however, been and are being introduced to terrestrial operational numerical weather prediction systems in the recent years. In these approaches a set of simulations with varied and disturbed initial or boundary conditions is run and the forecast and a confidence estimate are derived from the set of results using, *e.g.*, statistical analyses. These approaches provide improved confidence in the range of and perhaps better robustness of the results obtained. Such multi-run approaches do multiply the requirements for computational resources and are hence in many cases prohibitively costly, even in terrestrial operational applications. For an introduction of the ensemble approaches, *see, e.g.*, the Web site (and links and references therein) of the European Centre for Medium-range Weather Forecasts (ECMWF) at `http://www.ecmwf.int/`.

For Mars research purposes the 3-D MMCMs are much more realistic, but at least in the near future probably remain computationally much too expensive for such systematical and more comprehensive statistical studies. The computational cost of the 2-D MMCM is only a fraction of a contemporary 3-D MMCM; hence a 2-D MMCM is a much more feasible tool for use in (at least initial) studies using ensemble approaches with reasonable set or sample sizes: in this early phase a typical sample size has been 5–50 runs.

At least two main sub-approaches to the ensemble approach can be identified: *parameter space mapping* and *Monte Carlo*-approach. Parameter space mapping implies a set of simulations run using, *e.g.*, systematically and deterministically varied initial or boundary values of some parameters (essentially using a parameter space grid) to investigate and analyse — also with statistical methods — the domain and range of the results. The Monte Carlo approach includes in addition or in stead introduction of (correlated or uncorrelated) random variations in selected parameters.

An environment enabling the use of an ensemble approach with the UH/ATM 2-D MMCM has recently been implemented and is currently being further developed at FMI/GEO. This environment comprises simulation preparation (including selection of variables to-be-perturbed as well as perturbation types and magnitudes) and statistical analysis tools — the latter providing statistical quantities such as pointwise set average, range, variance as well as distributions of the solutions included in a simulation set. Our first application of the system has been an idealised sensitivity study of mesoscale circulation and water transport phenomena occurring and emerging in a polar cap region where H_2O ice is being exposed in the springtime from under the wintertime CO_2 cover — perhaps in a patchy and irregular fashion [8].

Case study: influence of sublimation and condensation flows on regional circulation patterns in the Chasma Borealis area In this work we expand on earlier 2-D simulations of Martian winds across an idealised valley geometry. The geographical context is the northern polar terrain — especially the Chasma Borealis region and its section close to the pole. In this region the valley axis is directed approximately along a latitude circle. Our primary interest is in the interactions between the larger-scale sublimation and condensation flows and the regional flows up and down the valley walls, with secondary interest in the influence of the shape and dimensions of the valley cross section on the ensuing circulation patterns. In the geographical area of study the sublimation and condensation flows are expected to have substantial across-valley components.

In Chasma Borealis we have a varied topography due to the valley combined with seasonally varying coverages of H_2O and CO_2 ices. The topography drives slope winds and the ice coverage variations and the associated albedo and thermal inertia contrasts drive sea-breeze type thermal circulations. Hence, in a configuration and situation such as this a complex set of circulation patterns is expected to occur due to the combined slope, sea-breeze type and large-scale sublimation/condensation flow forcings. Since in our earlier works the large-scale influences have been studied less, we have here focussed thereon, corresponding to both spring/summer/sublimation as well as autumn/winter/condensation situations. Both parameter space mapping and the Monte Carlo approaches have been used.

Our goals here include: further testing of the feasibility of the ensemble approach as well as provision of improved (and perhaps more robust) insight into this type of regional features

of the Martian mesoscale circulations and the associated water cycle.

Funding for this work was provided by the Academy of Finland (project 51441) and is gratefully acknowledged.

References

[1] Alpert P, Cohen A, Neumann J and Doron E, 1982. A model simulation of the summer circulation from the Eastern Mediterranean past Lake Kinneret in the Jordan valley. *Mon. Wea. Rev.*, **110**:994–1006.

[2] Savijärvi H and Siili T, 1993. The Martian slope winds and the nocturnal PBL jet. *J. Atmos. Sci.*, **50**:77–88.

[3] Siili T, 1996. Modeling of albedo and thermal inertia induced mesoscale circulations in the midlatitude summertime Martian atmosphere. *J. Geophys. Res.*, **101**:14957–14968.

[4] Siili T, Haberle R M and Murphy J R, 1997. Sensitivity of Martian southern polar cap edge winds and surface stresses to dust optical thickness and to the large-scale sublimation flow. *Adv. Space Res.*, **19**:1241–1244.

[5] Siili T, Haberle R M, Murphy J R and Savijärvi H, 1999. Modelling of the combined late-winter ice cap edge and slope winds in Mars' Hellas and Argyre regions. *Planet. Space Sci.*, **47**(8-9):951–970.

[6] Siili T, 1999. *Two-dimensional modelling of thermal terrain-induced mesoscale circulations in Mars' atmosphere*. Ph.D dissertation, Helsinki University of Technology. Available as Finnish Meteorological Institute Contributions No. 27, Helsinki, Finland.

[7] Siili T, Savijärvi H, Määttänen A and Kauhanen J, 2003. Two-dimensional simulations of martian mesoscale circulation phenomena: a review and future role. In Desjean M C, Forget F, Lopez-Valverde M and Newman C, eds., *Proceedings of the workshop on Mars atmosphere modelling and observations*, pp. 6–4. Centre national d'etudes spatiales, European Space Agency, Instituto de astrofisica de Andalucia, Laboratoire de meteorologie dynamique / Centre national de recherches scientifiques, University of Oxford.

[8] Siili T, 2003. Simulations of mesoscale circulations and water transport in regions of water ice being exposed: first 2-D ensemble results. In *Proceedings of the 6th international conference on Mars*. Lunar and Planetary Institute, Houston, TX, USA.

THE APPLICATION OF THE ELECTRIC SOUNDING TECHNIQUE TO THE SEARCH FOR WATER AT SHALLOW DEPTHS WITH PLANETARY LANDERS AND ROVERS: A SURVEY OF THE RSSD-ESA ACTIVITIES

Fernando Simoes, Roland Trautner and Rejean Grard
Planetary Mission Division
Research and Scientific Support Department
European Space Agency
ESTEC, Keplerlaan 1, PO Box 299
2200 Ag Noordwijk, The Netherlands

The possible presence of subsurface solid or liquid water can be detected *in-situ* by measuring the electric properties of the soil. The Research and Scientific Support Department (RSSD) of the European Space Agency (ESA) has been engaged in the design of dedicated space instruments since 1990, when we first proposed a technique for measuring the complex permittivity of solid or liquid materials with multipolar arrays. In short, an alternating current is injected in the ground by means of two transmitter electrodes and the induced differential voltage is measured by two receiver electrodes. Information about the electric properties of the medium is derived from the voltage/current ratio, or mutual impedance of the quadrupole.

We shall review the specificity and complementarity of the various ongoing and planned activities, which form this line of research at RSSD in partnership with other laboratories.

(1) Laboratory characterization of the electric properties of water, and water mixtures, at low frequencies
The conductivity and permittivity of any material is strongly influenced by the presence of water and by temperature. This feature can serve as an indicator of water but is not well understood.

(2) Design and realization of space instrument concepts.
Prototype arrays with different configurations are designed and tested for specific applications and integration on platform, rover and drill systems.

(3) Laboratory and field tests:
The purpose of laboratory and field tests is twofold. They provide, on the one hand, information about possible planetary soil characteristics, e.g. the properties of Mars simulants as functions of temperature and water content. They serve, on the other hand, to validate the performances of candidate instruments in given environments.

(4) Numerical simulation and modeling.
The interpretation of results obtained with a mutual impedance probe in homogeneous media is rather straightforward, but deciphering the response of a layered or inhomogeneous environment is more intricate. A three-dimensional numerical code, presently under development, will simulate the response of composite terrains in general, and the effect induced by the presence of buried rocks and cavities, in particular.

(5) Experiment proposals and development of flight instruments:
Quadrupolar probes are parts of the scientific payloads carried by Huygens, which will land on Titan in January 2005, and the Rosetta lander, which will make contact with the nucleus of comet Churyumov-Gerasimenko in November 2014. Similar instruments have been proposed for Mars missions (e.g. Exomars).

LONG DAY'S DRIVE: AN ALTERNATIVE PARADIGM FOR MARTIAN ROBOTIC EXPLORATION. M. H. Sims[1] and C. P. McKay[2], [1]NASA Ames Research Center, Moffett Field CA, 94035, Michael.H.Sims@nasa.gov. [2]NASA Ames Research Center, Moffett Field CA, 94035, cmckay@mail.arc.nasa.gov.

Introduction:. The Log Day's Drive proposed Martian polar exploration rover mission represents a different place in the space of designs from previous missions including MER, and in part represents an alternative to future deep drilling missions. This mission design is characterized by:

-High power and continuous power afforded by the northern polar region in summer sunlight.

-No nighttime operations; small thermal variability over the day.

-Rapid acquisition of data by virtue of instrument selection - the full suite of instruments can collect their data in under an hour. Stylized transects and previously demonstrated pattern recognition algorithms (e.g., the recognition of rock like objects in a terrain) will be used.

-Mobility during a large fraction of the Martian day

-Vehicle self-safing. This is the fundamental technology needed for long range mobility. This ability of the vehicle to be responsible for its own well being is commonly used on earth based autonomous vehicles and is the crucial element for long traverses.

-Sufficient mobility in rover design to allow access beyond the landing ellipse. Hence, specific locations are then targetable.

-Excellent access to orbital communication facilities

Mission Overview: LDD will investigate the north polar layered deposits (PLD). The overarching science rationale for LDD is the belief that the PLD preserve within their stratigraphy an interpretable record of recent climate and geologic history for Mars. Our primary goal is to obtain data that can provide a basis for interpreting that record. In addition, we will test the hypothesis that the ice of the PLD contains organics at higher concentrations than the aeolian dust sampled at the two Viking sites. Finally, we seek to contribute to the understanding of Mars' total volatile inventory by detailed determination of the ice content of the PLD over the traverse

Science Goals: It is widely believed that the Martian polar layered deposits record climate variations over at least the last 10 to 100 million years, but the details of the processes involved and their relative roles in layer formation and evolution remain obscure.

Variations in axial obliquity and orbital eccentricity are thought to influence the climates of both Earth and Mars, but are of greater amplitude in the Martian.

A common presumption among Mars researchers has been that the polar layered deposits are the result of variations in the proportions of dust and water ice deposited over many climate cycles but their density and composition are poorly constrained. There is evidence for both topographic and albedo variations between layers in the north polar layered deposits, based on analysis of springtime images.

Traversing the PLD over the surface is the most effective way to collect a long-term record of their variation. If the LDD rover traverses 10 km up or down a 5% slope, perpendicular to the layering we could have a record corresponding to a drill depth of 500 m. If the nominal deposition rate of dust on Mars is of order a few microns per year, then the climate history captured by the layers covered would be about 10 to 100 M-yr. This time scale is significant because variations in Mars' obliquity, eccentricity, and phase of perihelion vary significantly on time scales of millions of years. As the obliquity changes the total radiation received at the polar regions changes and this changes the amount of CO_2 in the atmosphere and the amount of water vapor released in the summer from the polar deposits. Changes in the pressure of CO_2 and the annual water cycle should both change the amount of dust and ice deposited in the winter in the PLD. This climate record is preserved in the PLD layering and the LDD traverse will be able to document this recored.

Organics. detection for organics on Mars would have important implications for astrobiology and future Martian missions. Any future search for organics on Mars must follow up from the Viking results. The Viking results were puzzling in three respects. First, was the total absence of organics as measured by the GCMS. The second unexpected result was the rapid release of O_2 when soil samples were exposed to water vapor in the Gas Exchange Experiment (GEx) at levels of 70 - 770 nanomoles per gram. The third unexpected result was that organic material in the Labeled Release (LR) Experiment was consumed as would have been expected if life was present --- the presence of life being in apparent contradiction with the results from the GCMS.

Currently, the most widely held explanation for the reactivity of the Martian soil is the presence of one or more inorganic oxidants.

It has been observed that the level of oxygen release from the GEx experiment was lower at the northernmost Viking site and suggested that the oxidant might decrease systematically toward the poles with a concomitant increase in the stability of organics. Chemically this might be due to the role of ice and thin films of water in destroying oxidants.

Thus we hypothesize that organics may be present in the PLD at concentrations significantly higher than the upper limit determined at the Viking sites.

Ice content. A recognized goal for Mars exploration is to map the 3D distribution of water in all its phases. We propose to contribute to the understanding of Mars' total water inventory by detailed determination of the ice content of the PLD over the length of our traverse.

Proposed payload: The proposed payload consisted of

- copy of MER PanCam system
- one shot panoramic camera (fish eye or mirrored sphere lens for panorama)
- Distant microscopic imager – By using telescopic optics creating microscopic quality images from a few inches to a meter or more distant
- Laser Induced Breakdown Spectrometer – Los Alamos to generate elemental analysis quickly and up to 10's of meters distant
- Raman spectrometer integrated into above Laser Induced Breakdown Spectrometer allows for organic detection
- Neutron spectrometer
- Ground penetrating radar

THE MASSES OF MARS/SEASONAL POLAR ICECAPS. David E. Smith[1] and Maria T. Zuber[2], [1]Laboratory for Terrestrial Physics, NASA Goddard Space Flight Center, Greenbelt, MD 20771, e-mail: David.E.Smith@nasa.gov, [2]Dept of Earth Atmospheric and Planetary Sciences, Massachusetts Institute of Technology, 77 Massachusetts Ave., 54-918, Cambridge, MA 02139-4307, e-mail: zuber@mit.edu.

Introduction. Radio tracking of the Mars Global Surveyor spacecraft has revealed temporal changes in the long-wavelength gravity field of Mars that correlate, to first order, with the pattern expected for the seasonal redistribution of carbon dioxide between the atmosphere and surface. Detecting these gravity field changes requires isolating very small perturbations in the velocity of the spacecraft and estimating the very low degree zonal coefficients of the field. A comparison of these coefficients determined every 5 days for a period over 2 Mars years shows annual and semi-annual variations that are similar to those predicted by a General Circulation Model simulation [1]. These changes result from the redistribution of the mass of the planet by the exchange of carbon dioxide between the surface and the atmosphere through deposition and sublimation of CO_2 in the polar regions. A simple time-dependent model for the icecaps enables an estimate to be made of the mass of carbon dioxide at each pole as a function of the seasonal parameter, L_s.

Temporal Variations in Gravity. The gravity field of Mars is typically represented by a series of spherical harmonics [2] of which the largest are the low degree zonal terms. These terms represent the basic gravitational shape of Mars and, in combination with the rotational potential, largely define the long wavelength areoid. The redistribution of atmospheric material, particularly the pole-to-pole transport of carbon dioxide on the surface, causes these low degree terms in the description of the gravity field to change with time. In addition, when the CO_2 is deposited on the surface, the rest of the planet (mantle, core, etc. that is not changing in mass) moves slightly in position in order to maintain the center of mass of the whole planet in the same position in inertial space. This motion, and its gravitational effect, is a $C_{1,0}$ term in the gravity potential of the solid part of the planet. In addition, motion of material in the atmosphere that is deposited at the poles causes a change in the flattening of Mars that is manifest as a change in the $C_{2,0}$ gravitational coefficient. Similarly, there are changes in $C_{3,0}$ and all the higher degree and order terms, although the largest changes are in the first few low degree coefficients.

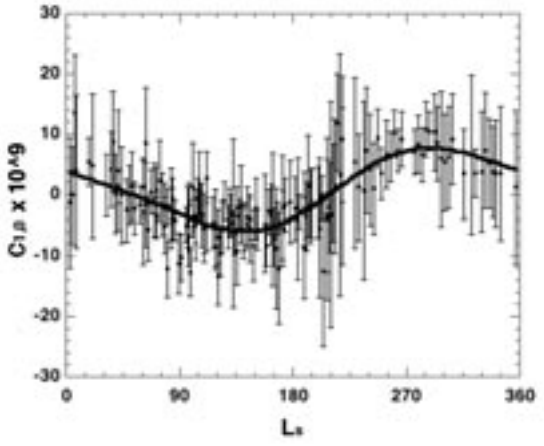

Fig. 1 *The variation in the degree 1 term of the solid part of the planet (core, mantle, $C_{1,0}$, e, crust) that arises because the deposition of carbon dioxide at the poles is balanced by a small motion of the rest of the planet.*

We have estimated the changes in the first 3 gravity coefficients by analyzing the small changes in the orbit of the MGS spacecraft [3]. Figure 1 shows the variation in the degree 1 coefficient of the gravity field of the solid part of the planet.

Note that the magnitude of the variation of the $C_{1,0}$ term is of order 10^{-9}, equivalent to a few centimeter movement of the solid component of the planet from its mean position.

Estimating the Seasonal Mass. If we make the assumption that the seasonal polar icecaps can, to first order, be represented as point masses at each of the poles, then it can be shown [4] that the mass of the north seasonal polar cap, *m(n),* can be written

$$m(n) = (1/2)(C_{1,0} + C_{2,0}) \times M,$$

and the mass of the south seasonal polar cap, *m(s),* as

$$m(s) = (1/2)(- C_{1,0} + C_{2,0}) \times M,$$

where $C_{1,0}$ and $C_{2,0}$ are the un-normalized first and second degree zonal coefficients in the expansion of the gravity field, and M $(=6.42 \times 10^{23}$ kg) is the mass of Mars.

The results for each pole for approximately two Earth years (one Mars year) are shown in Figure 2 where the mass in kg is plotted vs. L_s. Both datasets have been fit with annual (L_s), semi-annual $(2L_s)$, and tri-annual $(3L_s)$ periods. The annual period dominates for each pole as a result of the $C_{1,0}$ variation (Fig. 1) being much larger than the variation in the planetary flattening, $C_{2,0}$. Evident in Figure 2 is the suggestion of slow sublimation $(L_s \sim 270^o - 140^o)$ and rapid deposition $(L_s \sim 180^o - 260^o)$ in the northern hemisphere. In the south the accumulation and sublimation appear to be of equal length when measured against L_s. The pattern of mass exchange shows differences in comparison to the temporal pattern of latitudinal brightening due to the seasonal changes in frost deposition [5], suggesting that at least some aspects of reflectivity change are not associated with significant mass exchange.

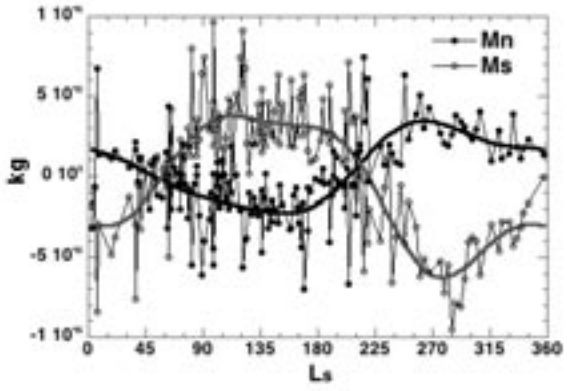

Fig. 2. *Estimated seasonal mass at each of the Martian poles based on a point mass model for the seasonal icecaps. Note that (1) sublimation begins in the southern hemisphere as soon as the sun reaches its maximum northerly latitude ($L_s=270^o$), and (2) the rapid rise and slow fall of deposition in the north.*

References. [1] Smith D. E. et al. (1999) *JGR, 104,* 1885-1899. [2] Lemoine F. G. et al. (2001) *JGR, 106*, 23,359-23,376. [3] Smith D. E. and Zuber M. T. (2003), submitted to *JGR*. [4] Zuber M. T. and Smith D.E. (2003) in prep. [5] Zuber M.T. and Smith D.E. (2003) this volume.

THE PHOENIX SCOUT MISSION. P. H. Smith, Lunar & Planetary Lab, University of Arizona, 1629 E. University Ave, Tucson, AZ 85721, psmith@lpl.arizona.edu.

Introduction: In December 2002, four Scout missions to Mars, proposed in response to a NASA Announcement of Opportunity (AO), were selected to proceed to Phase A. Phoenix was one of the missions selected. All missions were required to launch in 2007 and meet a cost cap of $325M (FY03$) that encompasses all mission costs including the launch vehicle and a healthy reserve. A Concept Study report was submitted May 15 after a 5-month Phase A study; it completely describes the technical approach and management plan. The cost plan with reserves ensures that the mission can meet all its science goals within the cost cap.

This abstract is being submitted prior to the selection announcement in August 2003. The strategy and goals for exploring subsurface ice layers in the northern plains will still be valid in spite of any negative decision that delays the mission.

Strategy: From the beginning our strategy has been to capture the low cost, low risk, and good science corner of the proposal range. Clearly, low cost comes from building on structures created for previous missions. The AO allowed the use of the 2001 lander that was canceled after the loss of two spacecraft in 1999. The spacecraft was four months into final assembly and test (ATLO) and many instruments were already delivered; the spacecraft and instruments have been mothballed ever since waiting for an opportunity for flight. The name Phoenix symbolizes the rebirth of a new project from the ashes of the canceled mission.

In addition, the Mars Polar Lander with its MVACS instrument package failed to land safely after completion of integrated testing, a Ground Data System (GDS) development, and the mission sequences. The knowledge to rebuild the MVACS instruments still exists. The challenge that faced the Phoenix team was choosing among the wealth of existing hardware and knowledge to produce a scientific mission capable of meeting NASA goals for exploring Mars (MEPAG), a mission exciting both to the public and our team. We have succeeded in this goal by virtue of the exciting discovery of abundant ice in the circum-polar regions.

Phoenix science goals. Phoenix truly 'follows the water' by landing on an ice-rich region and digging up to a meter into the icy soil. The Odyssey Gamma Ray Spectrometer (GRS) team announced in Spring 2002 the discovery of large amounts of water ice poleward of -60 degrees latitude within a few 10s of centimeters of the surface [1,2]. Recently, the ice abundance in the northern plains during summer has been measured and mapped [3]; it appears to contain an even higher abundance of near surface ice than the southern pole. Mellon and Jakosky [4] and other scientists had predicted for some time that ice would be stable near the surface in balance with water vapor diffusion through an overburden of regolith. The actual measurement of ice with 3 independent instruments allowed the GRS team to estimate the depth and abundance of ice with a simple two-layer model. The amount of ice is on the border of being too large for vapor diffusion appearing more like a dirty-ice layer than icy dirt.

Of all the accessible sources of water on Mars this near surface icy layer represents the greatest potential for finding evidence of near surface liquid water. Recent work has verified our hopes [5] that periodically, through variations in obliquity and precession of the polar axis, the temperature of the ice-soil boundary exceeds –20 C and melting can occur. The influence of liquid water on the soil chemistry and mineralogy should be measurable by Phoenix instruments. Granted the melting may only produce a monolayer of water on crystalline surfaces, but this is enough to allow mobility and maintenance in biologic communities on Earth. Higher temperatures will allow reproduction and growth.

Goal #1: Study the history of water in all its phases in the northern polar region. Phoenix will land in the northern near-polar region and dig through the dry regolith searching for an ice-soil boundary. Instruments on the deck will receive samples and analyze the chemistry, the volatile inventory, isotopic ratios, and grain morphologies. Altered minerals created through the weathering of the soil grains in a periodically moist environment will be measured as a function of depth beneath the surface. Samples taken at several depths will also be mixed with water to test the aqueous chemistry of the wet soil. Knowledge of the wet chemistry allows creating similar environments in Earth laboratories and at analog field sites to help understand the properties of the Martian soil.

Even if the ice layer cannot be reached at our landing site, Phoenix will become the first scientific station in the important polar regions to return useful data. Not only will the soil be trenched and surface features examined for evidence of a freeze-thaw cycle, but the weather throughout the polar summer and fall will be monitored. Temperature, pressure, and winds will be measured on an hourly basis. In addition, humidity will be tracked using a mass spectrometer. A lidar will make measurements of the boundary layer for the first time to be compared with mesoscale models that are now becoming an important tool in predicting near-surface weather.

The geomorphology studied over the last 6 years from orbit will be augmented with Phoenix images and will allow visualization of the site in an unprecedented manner. During descent a wide-field camera will produce a set of nested images surrounding the landing site. After landing, these will be compared to panoramic images so that the exact distances (and therefore the size) to features of interest can be computed. The panoramic camera is also stereoscopic and multispectral throughout the sensitive range of the CCD detector; its resolution is equivalent to the PanCam on MER, about 0.25 mrad/pixel. A camera on the robotic arm that digs the trench continues to reduce the scale at which we examine the scene; closeup images of the trench walls will provide insight into the layered structure and grain size of the soil. Samples will be provided to an optical microscope housed on the deck; images of the tiny grains in 4 colors will be taken through focus with a resolution of 4 microns per pixel. Finally, an Atomic Force Microscope has been developed to enlarge our view of selected objects on the microscope stage to resolve structures at the 10 nm scale.

Goal #2: Assess the biologic potential of the subsurface environment. Although there are no "life-detection" instruments on board, we suspect that a long term active biological community will leave observable signatures in the soil horizons and chemical tracers in the ice. The TEGA instrument can detect small abundances of organic molecules in the gases that are driven off of samples as they are heated above

300° C. The association of organic compounds with subsurface layers will indicate the likely origins of these compounds. In addition, the wet chemistry of the soils will test whether any hazards exist that preclude a habitable zone at these latitudes.

To summarize, our goals are to understand the near surface chemistry, hydrology, climatology, and geology of a polar landing site. We will examine the ice-soil boundary for periodic melting and biologic potential, our goal is to detect an accumulation of organic molecules. The hazards to life that exist in the ice layer, particularly salts and oxidants, will be quantified. Finally, we will characterize the polar weather throughout northern summer and fall with particular attention to the distribution of water in all its phases.

Implementation. Phoenix will modify the 2001 lander according to the recommendation of the Young commission [6] and the Casani JPL review board [7]; this lander has probably endured more reviews than any other. The lander has been stored for 2 years at the Lockheed Martin Astronautics facility in Denver; they will be responsible for refurbishment and improvements along the lines of the review boards. Guided entry, a hazard avoidance system, and full communications during entry and descent will reduce the risks to an acceptable level. Communications will include UHF relay to orbiting assets (MGS, Odyssey, and MRO) and a high gain antenna for a direct-to-Earth link.

Many of our instruments are already delivered. The descent imager (MARDI) is already bolted on the lander, the robotic arm with its camera is in bonded stores at JPL, and so is the MECA instrument with its wet chemistry cells and microscopes. Other instruments are build to print from the Mars Polar Lander (MPL): the panoramic camera (SSI), and TEGA. New instruments include the MET station with a lidar, and a mass spectrometer.

The Phoenix project is led by Peter Smith as PI with a 25-member science team. Leslie Tamppari has been chosen as the Project Scientist at JPL. Several of the science team members are also responsible for instrument performance: William Boynton for TEGA at the University of Arizona (UA), Michael Hecht for MECA at JPL, Michael Malin for MARDI at MSSS, Horst Keller for RAC from the Max Planck Institute for Aeronomy in Germany, Alan Carswell for the MET package in Canada, Mark Lemmon for the camera systems at the UA, and Ray Arvidson for the robotic arm at JPL.

An important aspect of any mission is the Education and Public Outreach portion. Two percent of our budget is devoted to this part and all activities will be led by a manager at the UA who reports directly to the PI. Each member of the science team will contribute to the EPO activities. Other important elements contribute to the training of teachers, curriculum support, provide exhibits to museums and science centers, and create exciting visual products that illustrate the mission.

Mission scenario: After a launch in August 2007, Phoenix will land in late May 2008 at Ls=78 (late spring). The engineering data acquired during descent and the descent images plus the first panoramic images will be returned immediately. A successful landing will give the Mars program a much needed landing vehicle for future missions. The first week will be reserved for examination of the landing site with the remote sensing cameras and calibration of the instruments.

The digging phase (first 90 sols). After surface samples are collected and verified, trench digging begins. The sampling strategy requires surface samples, samples from within the dry regolith and samples from the ice-soil boundary. If the robotic arm is capable of digging into the icy soil, another sample will be collected from within the ice. To be sure of getting an ice sample, ripper tines and scrappers are added to the back of the scoop. The digging and sampling activities have been grouped into 8-sol cycles that include 4 days of digging and monitoring the trench and 4 days of examining samples with TEGA and MECA. Seven of these cycles are baselined with adequate reserve added in case digging is more difficult than planned.

Polar climate phase. As the season turns to fall and winter, Phoenix will continue to operate until the Sun is too low on the horizon to charge the batteries. This is period when power must be conserved. Limited imaging will look for the first carbon dioxide frost deposits as the seasonal cap approaches. The MET instruments will record the decrease in temperature and pressure as fall turns to winter and humidity sensors will record the transport of water vapor. We do not expect that the lander will survive the winter and have no plans for its recovery in the spring.

References: [1] Boynton, W. V. et al. (2002) *Science*, *297*, 81. [2] Feldman, W. C. et al. (2002) *Science, 297*, 75-78. [3] Mitrofanov et al. (2003) *Science, 300*, 2081-2084. [4] Mellon, M. T. and Jakosky, B. M. (1993) *JGR, 98,* 3345-3364. [5] Jakosky, B. M. et al. (2002) *Astrobiology.* [6] Young, T. et al. (2000) "Mars program independent assessment team (PRIAT) summary report." [7] Casani, J. et al. (2000) "Report on the loss of the MPL and DS-2 missions."

INTERANNUAL COMPARISON OF WATER VAPOR IN THE NORTH POLAR REGION OF MARS. L. K. Tamppari[1], M. D. Smith[2], A. S. Hale[3], and D. S. Bass[3], [1]NASA Jet Propulsion Laboratory (4800 Oak Grove Drive, Pasadena, CA 91109 leslie.k.tamppari@jpl.nasa.gov), [2]NASA Goddard Space Flight Center (Michael.D.Smith.1@gsfc.nasa.gov), [3]NASA Jet Propulsion Laboratory (MS 264-235, 4800 Oak Grove Drive, Pasadena, CA 91109 amy.s.hale@jpl.nasa.gov), [4]NASA Jet Propulsion Laboratory (MS T1722, 4800 Oak Grove Drive, Pasadena, CA 91109 deborah.s.bass@jpl.nasa.gov).

Introduction: The Martian water cycle is one of the three annual cycles on Mars, dust and CO2 being the other two. Despite the fact that detailed spacecraft data, including global and annual coverage in a variety of wavelengths, have been taken of Mars spanning more than 25 years, there are many outstanding questions regarding the water cycle.

There is very little exposed water on Mars today, in either the atmosphere or on the surface [1] although there is geological evidence of catastrophic flooding and continuously running water in past epochs in Mars' history [2] as well as recent (within about 10,000 years ago) evidence for running water in the form of gullies [3].

The north polar cap region is of special interest as the residual cap is the main known reservoir of water on the planet today. The south polar residual cap may contain water, but presents a CO2 ice covering, even during southern summer. This hemispheric dichotomy is unexplained and is especially puzzling due to the fact that the Martian southern summer is much warmer (due to Mars' eccentricity) than the northern summer. Recently, water has been found in the top meter of the surface in both the northern and southern high latitude regions [e.g. 4-5] indicating an even greater amount of water on Mars than previously known.

Background: In order to better understand the current climate of Mars, we seek to understand atmospheric water in the north polar region. Our approach is to examine the water transport and cycling issues within the north polar region and in/out of the region on seasonal and annual timescales. Viking Mars Atmospheric Water Detector (MAWD) data showed that water vapor increased as the northern summer season progressed and temperatures increased, and that vapor appeared to be transported southward [6]. However, there has been uncertainty about the amount of water cycling in and out of the north polar region, as evidenced by residual polar cap visible brightness changes between one Martian year (Mariner 9 data) and a subsequent year (Viking data). These changes were originally thought to be interannual variations in the amount of frost sublimed based on global dust storm activity [5-7]. However, Viking thermal and imaging data were re-examined and it was found that 14-35 pr □m of water -ice appeared to be deposited on the cap later in the summer season [9], indicating that some water may be retained and redistributed within the polar cap region. This late summer deposition could be due to adsorption directly onto the cap surface or due to snowfall. We seek to understand what happens to the water on seasonal and interannual timescales. We address these issues by examining water vapor in the north polar region of Mars during the north spring and summer period from MGS TES data and by comparing these results to the Viking MAWD results.

Method:

Water vapor. Smith *et al.* [10] have performed retrievals for the column-integrated abundance of water vapor using the rotational water vapor bands at 220-360 cm^{-1}. Atmospheric temperatures are first retrieved using the 15-□m CO_2 band (Conrath *et al.*, 2000). Next, a forward radiative transfer computation is used to find the column-integrated water abundance that best fits the observed water vapor bands. At this time water is assumed to be well-mixed up to the condensation level and then zero above that. A total of six water vapor bands between 220 and 360 cm^{-1} are observed in TES spectra and the widths and relative depths of all six bands are very well fit by the synthetic spectra. Because the spectral signature of water vapor is spectrally very distinct from those of dust and water-ice, we can easily separate the relative contributions from each component (dust, water-ice, and water vapor) on a spectrum-by-spectrum basis.

Recent analysis with MGS TES data has shown evidence for water vapor "pulses" as the seasonal north polar cap sublimes [15]. This could be linked to the previous late-summer season deposition, discussed above. There appear to be significant differences in the details of the water vapor as a function of latitude and season between the Viking era and the current era (Figure 1). These differences may be a degree of interannual variability in the water vapor or a result of the coverage differences (Figure 2). Note that in Fig. 2, there are large differences in the MAWD coverage between the Ls=80°-95° bin (bin 7) vs. the Ls=95°-110° bin (bin 8). The TES coverage is much more uniform over time due to its orbit. An understanding of these possible interannual differences is important in several ways: (1) to understand the Martian climate, (2) to characterize the extent of interannual variability or lack thereof , and (3) to understand water-cycling within the north polar region and potentially in/out of the region. We will present our results of the investigation of the differences in these water vapor column amounts.

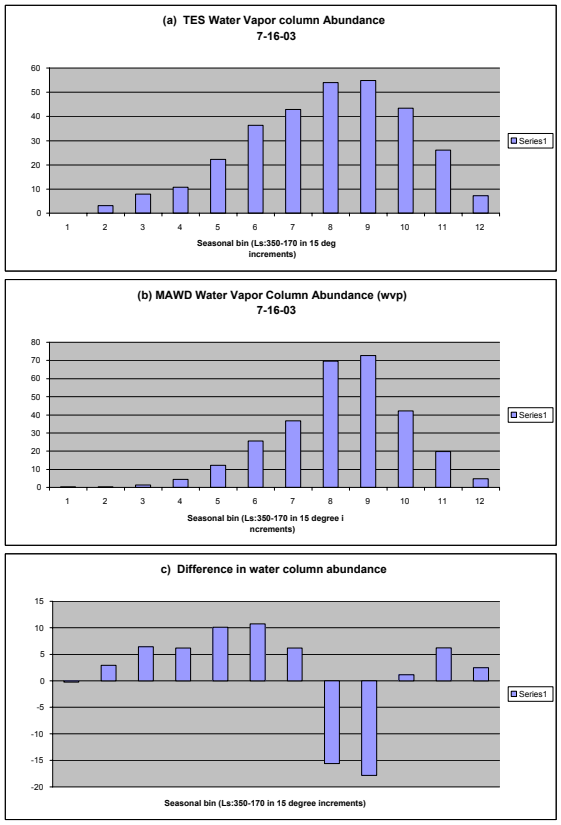

Figure 1. (a) TES water vapor column abundance in pr microns for the north polar region (60°-90°N). The seasonal binning is plotted Ls=15° increments, beginning at Ls=350° and ending at Ls=170°. Note that there is no TES data plotted for the first seasonal bin, Ls=350°-5°. (b) MAWD water vapor column abundance for same region and seasonal bins. MAWD data are shown for Ls=350°-5°. (c) The difference between the TES water vapor column abundance amount and the MAWD water vapor column abundance amount as a function of season.

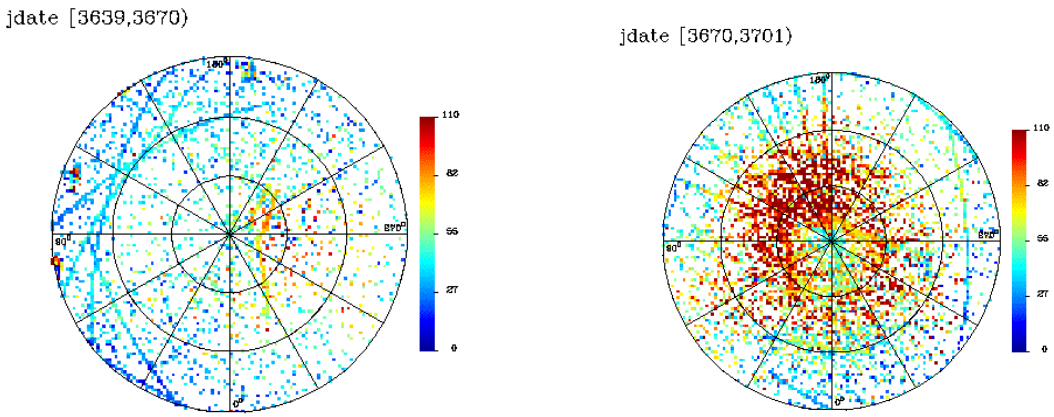

Figure 2. (Left) MAWD water vapor coverage shown for the Ls=80°-95° bin (bin 7). (Right) Similar for the Ls=95°-110° bin (bin 8). Note that the coverage near the cap center is much denser for the later season, possibly explaining the greater amount of water vapor measured during that season than in the previous season.

References: [1] Keiffer H. H. et al. (1976) *Science*, 194, 1341-1344 [2] Carr, M. H. (1998) *Water on Mars* [3] Malin M. C. and Edgett, K. S. (2001) *JGR* 106, 23429-23570. [8] Feldman W. C. et al., (2002) *Science* 297, 75-78 [4] Boynton W. V. et al., (2002) *Science* 297, 81-85 [5] Jakosky, B. M. (1985), Space Sci. Rev. 41, 131-200. [6] James P. B. and Martin L. (1985) *Bull. Amer. Astron. Soc., 17,* 735. [7] Kieffer H H. (1990) *JGR, 96,* 1481-1493. [8] Tamppari L. K. and Bass D. S. (2000) *2nd Mars Polar Conf.* [9] Tamppari L. K. et al. (2002) *Bull. 34th Am. Astron. Soc.,* 845. [10] Smith M. D. et al. (2000), *Bull. AAS*, 32(3), 1094.

THE SOUTH POLAR RESIDUAL CAP OF MARS:LAYERS, EROSION, AND STRATIGRAPHY. P. C. Thomas[1] [1]Center for Radiophysics and Space Research, Cornell University, Ithaca NY, 14853.

The south polar residual cap (sprc) of Mars is a group of thin layers degraded into unique topography resting on the flatter portions of the main polar layered deposits. This is a summary of the characteristics of these layers and their degredation that impacts the interpretation of the history of the martian polar environment..

Residual cap layers: There are two primary sets of depositional units in the sprc: 1) An older unit, approximately 10 m in thickness with four or five included layers, widely distributed over the sprc, and expressed as mesas or broad surfaces cut by a variety of circular to linear depressions, and commonly having polygonal troughs on the uppermost surface. Shadow and MOLA measurements show these layers are ~2 m in thickness. The layers can be exposed in scarps over 30° in slope, but commonly the lower portions of exposed layers are covered by debris with much lower slopes, and also commonly display a patterned surface that can be confused with layering.

2) One or more younger units, approximately 1-2 m thick, that have superposed and filled depressions formed in the older unit, and also formed in local discrete deposits. This unit also has a wide variety of depression types.

Both units show scarp retreat of up to a few m over one Martian year [1].

Erosion and other modification forms: The sprc topography has unique erosional topography [2,3]. Large circular depressions 300 –1000+ m across that cut two to four (perhaps 5) of the layers occur across the sprc. Linear depressions, asymmetric in cross section, usually cutting two-three layers, occur in the central portion of the sprc. Their trends suggest some underlying structural control, while the cross sectional asymmetry may be related to insolation asymmetry. Curled depressions grade into other forms, and show a preferred opening direction toward the north. Other depressions can be irregularly-shaped, and some areas have been largely stripped of the sprc layers by merging depressions. Moat-like depressions occur within some nearly circular forms as well as bounding a variety of mesas and other remnant topography. Moats within depressions show two distinct widths: ~20 m and ~70 m. The latter is indistinguishable from moat widths around mesas and other remnants.

Development of the depressions and deposits: Initiation of many of these forms appears to involve sag and collapse (Fig. 1a,d). Backwasting of the steeper slopes then enlarges the depressions. Changes between 1999 and 2001 indicate some backwasting of the forms of order 1-4 m/ Mars year [1], with a few instances over 5 m. Development sequences of curled depressions can be found, and examples of enlargement almost entirely by collapse are also found (Fig. 1a,d). The sag and collapse features may explain the development of "escher" terrain, whereby an upper surface appears contiguous between different cycles of erosion (Fig. 1d,e).

Most interesting is the development of inverted relief (Fig. 1f-h). The large, scalloped mesas have in some instances collapsed below the level of embaying deposits that in most other instances are lower than the mesa remnants. Different stages of this development can be found in the sprc. The preferred collapse of some materials suggests significant variations in the susceptibility to sublimation of these deposits.

Thin layers preferentially develop pits and other depressions over underlying topography, and on some upper convex slopes. These pits, "peels", and moats indicate modification of overlying deposits by exposure of relief or a critical layer thickness.

Non-uniform deposition is also found in some tongues of material several m in depth and a few hundred m long in restricted areas of the sprc. These appear to be part of the later deposits.

Interpretations: Several different cycles/changes in polar depositional and sublimational regime are indicated:

1). Change from main polar layered deposits to deposition of the sprc: H_20 rich deposits to CO_2 rich ones.

2) Cycles producing layering within the 10 m stack, about 4-5 cycles. Some differences in physical characteristics/ composition.

3) Significant erosion of the deposits in the form of merging depressions and sag and collapse modification.

4) Before or during the subsequent steps, development of polygonal troughs in much of the surface of the thick deposit.

5) Deposition of one or two, ~1- 2 m layers in the erosional topography of the thick deposits, and/or smoothing of surface of a lag deposit left by collapse and backwasting of the layers.

6) Renewed sublimation and collapse of both deposits. Included in this step is the scattered development of inverted relief. This activity may continue at present.

The evident variety of layer types, thicknesses, and cycles of deposition and erosion show there are several combinations of composition and/or texture within these deposits. The sag and collapse suggest a possible role for either absorption of insolation at depth, or a geothermal role in sublimation or other modification of the layers. Loss of substantial porosity might be a part of the collapse sequence. The inverted relief and the other forms surrounding mesa remnants indicate at least one major change in the thermal environment of the layers since major sublimation loss began.

References:

[1] Malin, M. C., M. A. Caplinger, and S. D. Davis (2001). *Science, 294*, 2146-2148. [2] Thomas, P. C. et al. (2000). *Nature 404*, 161-164. [3] Byrne, S., and A. P. Ingersoll (2003). *Science 299*, 1051-1053.

Acknowledgements: Help was provided by Mike Malin, Ken Edgett, Scott Davis, Bruce Cantor, Brian Carcich, Rob Sullivan, Karla Consroe, and Lisa Wei.,.

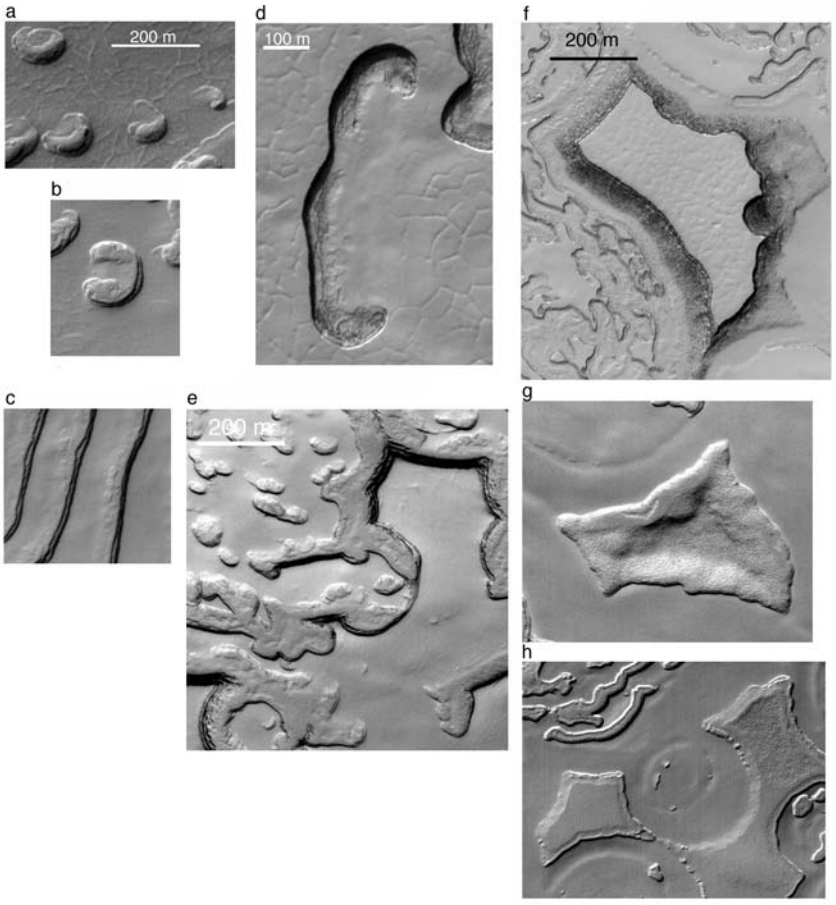

Figure 1a. Sequence of development of curl depressions by collapse and fracture. Illumination is from lower right. b. Curl depression showing ramp from upper surface. Illumination is from lower right. c. Fingerprint depressions; steep on right side, gentle slope on left. Sun is from lower right. Compare gentle slope on left to ramp in Fig. 1b. d. Depression at margin of sag in upper surface. Compare Fig. 1b. Illumination is from upper left. e. Remnant of several layers, near upper right, which tapers to feather edge at lower right. Possible later deposit embays the scalloped margin of the tapering set of layers. Illumination is from lower right. f. Typical remnant of layers, about 10 m above surroundings. Edges are patterned debris. g. Patterned debris from near complete collapse of material such as that in 1f, with overlying deposit (or, less likely, a different form of collapse material). Illumination is from lower right. h. Inverted relief. The scalloped topography of mesas (such as 1f.) has collapsed to a level lower than occupied by embaying materials (note circular feature in middle is high relative to surroundings, illumination is from lower right).

DUST FLUX INTO THE GRÍMSVÖTN SUBGLACIAL LAKE, VATNAJÖKULL ICE CAP, ICELAND, ESTIMATED FROM ICE CORE DATA. Th. Thorsteinsson[1], T. Jóhannesson[2], G. Larsen[3], O. Sigurdsson[1], K.G. Schmidt[4] and M. Forwick[5]. [1]Hydrological Service, Orkustofnun (National Energy Authority), Grensasvegi 9, IS-108 Reykjavik, Iceland. E-mail: thor@os.is, [2]Icelandic Meteorological Office, Bustadavegi 9, IS-150 Reykjavik, Iceland, [3]Science Institute, University of Iceland, Dunhaga 3, IS-107 Reykjavik, Iceland, [4]Niels Bohr Institute, University of Copenhagen, Juliane Maries Vej 30, DK-2200 Copenhagen O, Denmark, [5]Geology Department, University of Tromsoe, N-9037 Tromsoe, Norway.

Introduction. The center of hot-spot volcanic activity in Iceland is located beneath the NW-part of the Vatnajökull ice cap. Continuous melting of the ice cap from below sustains the Grímsvötn subglacial lake; the source of large jökulhlaups which regularly flood regions south of the ice cap [1]. The lake is covered by an ice shelf with an area of 25 km^2 and thickness varying between 100 and 300 m. The bottom of the subglacial lake is covered with sediments of volcanic origin [2], and dust released into the lake by melting of the ice shelf from below is continually being deposited at the lake bed. The Grímsvötn lake has recently attracted the interest of researchers investigating the possible existence of microbial life in Antarctic subglacial lakes and ice covered oceans in the solar system [3].

Ice core study. A 115 m ice core was drilled on the ice shelf in June 2002, concurrently with a thermal drilling that penetrated the ice shelf for geochemical and biological sampling of the subglacial lake [4]. A new core barrel and chips collecting system designed for use in core drilling below the water table in temperate ice was tested with success, and ice core processing involving density measurements, visual-stratigraphic observations, dust measurements and thin section analysis of crystal size was carried out on site.

Density measurements show that the transformation of snow to glacier ice (ρ = 830 kg/m^3) is completed by 16 m depth in the ice shelf, in less than 10 years. The water table in the ice shelf coincides with this transition. Stratigraphic observations reveal the presence of numerous bubble-free melt layers in the core, up to 60 cm in thickness. A 20 cm thick tephra layer from the December 1998 eruption in Grímsvötn was found at 4 m depth, beneath the 2001-2002 winter snow layer, indicating that the entire accumulation of the years 1999-2001 melted during summer. It is thus clear that hiatuses can exist in the annual-layer sequence present within the ice shelf.

The dust concentration of melted 20 cm samples was measured continuously on the core with a *Monilog L* turbidity meter, manufactured by Metrisa Inc. The instrument calculates dust concentrations in ppmv from the intensity of infrared light scattered off dust particles at a 90° angle. Results show that the background dust concentration is in the range 0.3-2.5 ppmv, but peak concentrations of 3-33 ppmv occur at depth intervals varying between 0.5 and 5 m in the core. In most cases, the dust producing the peaks seems to be concentrated in < 1 cm thick layers, which often are visible to the naked eye. Studies on a 100 m core drilled at 1800 m elevation on the Hofsjökull ice cap in Central Iceland [5] have shown that dust peaks in that core are due to windblown dust which originates in nearby deserts and is deposited on the ice cap in late summer. The situation in Grímsvötn is more complicated, since dust from a local source (Mt. Grímsfjall, 2.5 km from the drilling site) can probably be deposited on the ice shelf at all times of the year. Thus, the interpretation of the 40+ dust peaks found in the Grímsvötn core is not straightforward in terms of annual layering, but tephra layers of known ages and a 50 year time-series of winter accumulation from the ice shelf help constrain age vs. depth estimates. The tephra layer from the 1934 eruption is known to lie at ~120 m depth, indicating that the average thickness of annual layers in the uppermost 120 m is 1.8 m. Due to the complicated dynamics of the ice shelf [6], it is not clear how the thickness of the annual layers varies with depth in the lower part, but it seems reasonable to assume that 100-200 annual layers are present within the 280 m thick ice shelf at the drilling site.

The average dust concentration in the ice core is 3.9 ppmv, excluding very high concentrations in layers adjacent to the 1998 tephra layer at 4 m depth. We thus take 4 ppmv (~ 10 ppm by weight) as the average dust concentration in the entire ice shelf, and it seems realistic to assume a similar dust content in the ice within the entire Grímsvötn catchment area. This value is comparable to the dust concentration in Greenland ice dating from the Last Glacial Maximum [7].

From mass-balance considerations, it has been estimated that $4*10^{11}$ kg of ice melt annually by geothermal heat within the Grímsvötn drainage basin, which has an area of 160 km^2 [8]. This corresponds to an ice layer of thickness 2.8 m, melted annually from the base of the glacier. Given the average dust concentration of 10 ppm by weight, the amount of dust released from the melting ice within the entire Grímsvötn drainage basin is $4*10^{11}$ kg$*10^{-5}$= $4*10^6$ kg dust/year. The lake area is ~25 km^2; i.e. ~15% of the area of the entire drainage basin, and thus $0.15*4*10^6$ kg dust/year = $6*10^5$ kg dust are released into the lake

from the shelf per year on average, according to these estimates. The corresponding areal flux is $6*10^5$ kg/$25*10^6$ m^2/year = 0.024 kg/m^2/year.

SEM images of particles from dust peaks in the Hofsjökull ice core show particles mainly in the size range 1-50 μm, made of basaltic volcanic glass together with basaltic crystalline materials and porous tephra grains. No such images are presently available of the Grímsvötn dust particles, but because of the proximity to the subglacially erupted Mt. Grímsfjall and recent eruption products, the proportion of basaltic glass and tephra particles is likely to be high in the Grímsvötn core.

The thin section studies show that average crystal size increases gradually with depth, from ~3 mm just below the firn-ice boundary to ~3 cm in the lowest part of the core. This trend is interrupted in layers containing high amounts of dust, showing that grain-boundary pinning by dust particles, which is commonly observed in polar ice [9], occurs in temperate ice as well. The data on crystal size changes in the core are currently being analysed in the light of new ideas suggesting that habitats for psychrophilic bacteria are present in interconnected liquid veins along three-grain boundaries in ice [10].

References: [1] Björnsson H. (2002) *Glob. Planet. Change*, 35, 255-271. [2] Gudmundsson M.T. (1989) *Jökull*, 39, 1-19. [3] Gaidos E.J. et al. (1999) *Science*, 284, 1631-1633. [4] Lanoil B. et al. (2002) Abstract 03-GM-A-3497-ASM (Am. Soc. Microbiol.). [5] Sigurdsson O. et al. (2002) *NHP Report*, 47, 17-22. [6] Jóhannesson T. (1984). *M.Sc. thesis*, U. Washington, 79 pp. [7] Ruth U. et al. (2003) *JGR*, 108 (D3), 4098. [8] Björnsson H (1988) *Soc. Sci. Isl.*, 45, 139 pp. [9] Thorsteinsson Th. (1997) *JGR*, 102 (C12), 26,583-26,599. [10] Buford Price P. (1999) *PNAS*, 97 (3), 1247-1251.

SOUTH POLAR CRYPTIC REGION REVISTED: THEMIS OBSERVATIONS. T. N. Titus[1], H. H. Kieffer[1], J. J. Plaut[2], P. R. Christensen[3], A. B. Ivanov[2], and the THEMIS Science Team[3], [1]USGS, 2255 N. Gemini Dr., Flagstaff, AZ 86001; email: ttitus@usgs.gov, [2] JPL, Pasadena, CA, [3] ASU, Tempe, AZ.

Introduction: The early part of the Mars Global Surveyor mission provided good TES coverage of the Mars south polar region. These data allow mapping of the polar cap recession, surface and atmospheric temperatures, and albedo features found within the seasonal cap itself [1,2] over L_s = 180° – 270°. During this period, the seasonal south polar cap retreated continuously and asymmetrically around the geographic pole, similar to the observations of Viking in 1976-1977 [3]. A prominent albedo feature on the seasonal cap is a region that appears almost as dark as bare ground, yet remains cold. (See Figure 1.) We refer to this region, generally located between latitudes 85°S and 75°S and longitudes 150°W and 310°W, as the Cryptic region.

Past Observations: A re-examination of the IRTM data revealed that the Cryptic Region was not unique to the TES era, but also was apparent during the Viking IRTM era. (See Figure 2.) Interestingly, Antoniadi [4] observed dark regions forming on the seasonal cap that loosely correlate to the Cryptic region: Depressio Magna (1909) and Depressio Parva (1929). These *depressios* were located at 270° W, 78°S and 166° W, 76°S, respectively.

Analysis of both the TES and IRTM data indicate that the Cryptic region is unique in its thermophysical properties relative to the rest of the cap. The region occupies the same general area from year to year. It is darker and slightly warmer than the rest of the south polar cap. Even though the Cryptic region is slightly warmer, it must still be CO_2-buffered since it remains "cold" for several days.

Spectral analysis of the TES data longward of the 15-micron atmospheric band shows that the Cryptic Region shows less spectral contrast than the rest of the polar cap. This suggests that the region may be composed of "ice," as opposed to snow or frost [5].

The Vent Hypothesis: Since the initial discovery of the Cryptic Region, several surface features, referred to as spiders, fans, and Dalmatian spots on the basis of their appearance, have been seen. The fans and spiders correlate to the location of the Cryptic Region [6]. Kieffer [7,8] suggested that the spiders, fans, and Dalmatian spots are the result of CO_2 vents, caused by basal heating of CO_2 deposits. This can only be possible if the CO_2 is at least partially transparent to visible solar radiation and opaque to thermal IR, thus creating a solid greenhouse effect. The CO_2 would sublimate from the bottom of the ice slab, thus building up pressure until the gas can be released through a vent. The gas would transport dust from underneath the ice, through the vent, resulting in dust plumes. This hypothesis is consistent with past observations.

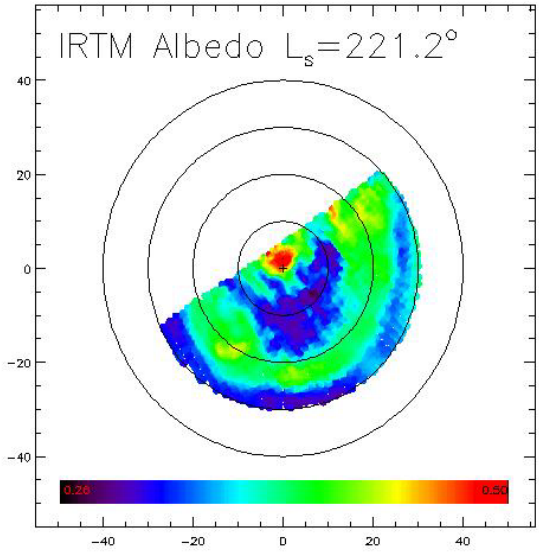

Figure 1: Viking IRTM Albedo Mosaic. This is a mosaic of IRTM visible data taken at L_s = 221.2°. The dark blue feature near the center of the image is the Cryptic region. The latitude lines are drawn at 10° intervals and 0° longitude is up. The region poleward of 65°S is at CO_2 temperatures.

THEMIS Results: THEMIS has the advantage over previous observations in being capable of taking VIS and IR images simultaneously at 18-meter and 100-meter resolution, respectively. Early in the spring, THEMIS observations of Dalmatian spots showed no thermal structure that differentiated the dark albedo areas from the rest of the surrounding seasonal cap. However, by L_s = 206°, thermal structure could be seen. (See Figure 2.) The warmer areas have an increase in brightness temperature of only 5 K over thermally bland areas that are covered by seasonal CO_2 deposits, which is consistent with TES observations at the 3 km scale [9]. These warm areas loosely correlate to the darker albedo areas, as seen in Figures 2 and 3. The spectra of a thermally bland area and an area interior to the three-legged "starfish" show an increase in brightness temperature over the spectral range of 9 μm to 12.5-μm. There are two possible causes for the increase in brightness temperature between these two areas: either the "starfish" surface is warmer than

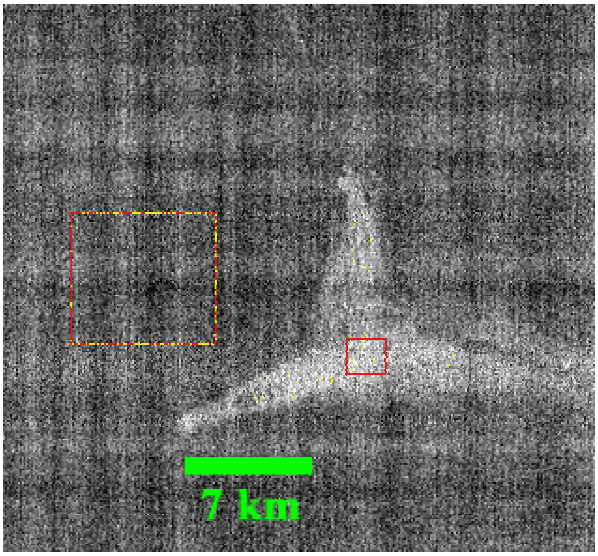

Figure 2: THEMIS IR Image I06707008 (Band 9). This THEMIS IR image shows thermal structure on the seasonal CO2 cap. Spectra were extracted from two locations, the center of the "starfish" and a thermally bland region, representative of seasonal CO_2.

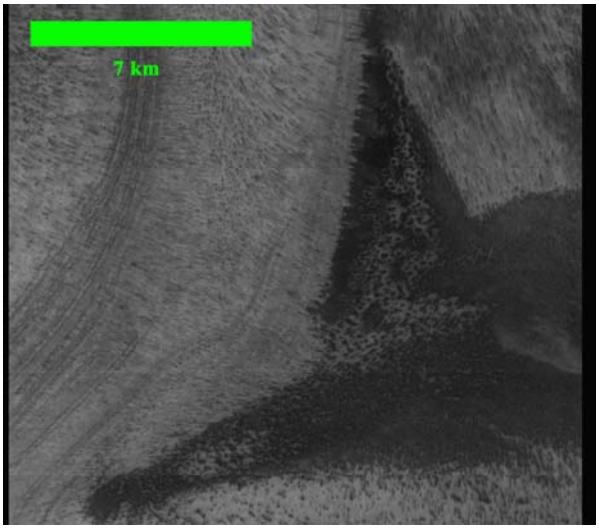

Figure 3: A THEMIS VIS Image V06707009. This THEMIS VIS image shows the same location as the IR image in Figure 2. Notice that the dark albedo region only loosely correlated to the thermal structure seen in Figure 2.

the surrounding area or the local atmospheric opacity is greater than the surrounding atmosphere. If the increase in brightness temperature is due to an increase in the kinetic temperature of the surface, then the spectra have an absorption feature at 11-12 µm. However, if the increase in brightness temperature is due to in increase of atmospheric opacity, perhaps from a nearby dust plume, then the spectra have emission features at 9-10 µm and 12.5 µm. The 9-10 µm spectral region is where atmospheric dust has a peak in opacity. The 12.5-µm region is where water ice clouds have a peak in opacity. The combination of these two spectral peaks in brightness temperature is suggestive of water ice-coated dust grains. Atmospheric emission features are a more plausible explanation of the THEMIS spectra than is an absorption feature at 11-12 µm. The atmospheric opacity explanation of the THEMIS spectra is consistent with the geyser hypothesis.

Summary: We will present the most current THEMIS observations of the Cryptic region. These data, combined with TES data and MOC imaging, will be used to test the Kieffer geyser model.

References: [1] Kieffer, et al. (1998) In LPSC XXIX, Abstract #1481. [2] Titus, T., et al. (1998), BAAS, vol. 30, no. 3, 1049-1050. [3] Kieffer, H.H. (1977) JGR, 82, 4249-4291. [4] Blunck, J (1977) "Mars and its Satellites: A detailed Commentary on the Nomenclature". [5] Hansen,G. (1998) JGR, 104 , 16,471. [6] Piqeux, S. (2003) JGR, Submitted. [7] Kieffer, H. H. (2001) Second International Conf. On Mars Polar Sci. and Exploration, #1057. [8] Kieffer, H. H. (2003), Sixth International Conference on Mars, #3158. [9] Kieffer, H. H. et al. (2000) JGR, 105, 9653.

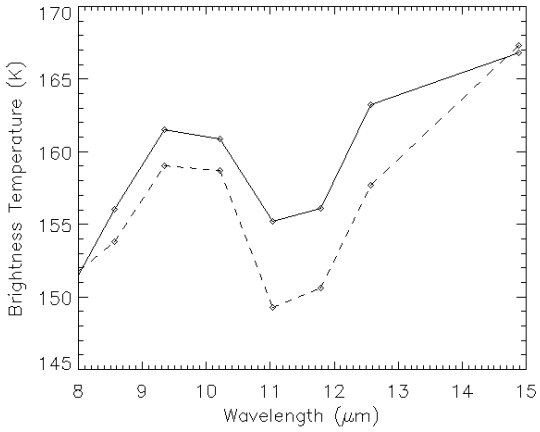

Figure 4: THEMIS IR Spectra. This is a plot of two spectra extracted from THEMIS image I06707008. The solid line is the spectrum extracted from the area inside the small red box (Figure 2). The dashed line is the spectrum extracted from the area in the larger red-yellow box (Figure 2). The 15 µm brightness temperature is an atmospheric temperature.

MODELING THE DEFORMATION OF LOBATE DEBRIS APRONS ON MARS BY CREEP OF ICE-RICH PERMAFROST. E.P. Turtle[1,2], A.V. Pathare[1], D.A. Crown[1], F.C. Chuang[1], W.K. Hartmann[1], J.C. Greenham[3] and N.F. Bueno[2], [1]Planetary Science Inst., 620 N. 6th Ave., Tucson, AZ, 85705, [2]Lunar and Planetary Lab., Univ. of Arizona, Tucson, AZ, 85721-0092 (turtle@lpl.arizona.edu), [3]California Inst. of Technology, Pasadena, CA.

Introduction: A wide variety of mid- to high-latitude surface features on Mars has long been attributed to viscous creep and flow phenomena associated with near-surface ground ice. On the basis of Viking Orbiter images, Squyres [1] identified two classes of creep-related landforms: (1) softened terrain, which results from *in situ* viscous deformation and is particularly evident in impact craters with degraded rims and flattened topographic profiles, and (2) debris aprons, which are produced by mass wasting along escarpments, *e.g.*, lobate debris aprons, lineated valley fill, and concentric crater fill. Such features have been attributed to kilometer-thick layers of permafrost (with upper boundaries less than 200 m deep) at higher latitudes [2], an interpretation that is consistent with recent *Mars Odyssey* GRS observations indicating a high water content very close to the Martian surface [3].

We are using *MGS* MOC and MOLA data to document the structural and topographic characteristics of softened landforms and debris aprons in the Hellas and Noachis regions. By comparing the observed landforms to the results of finite-element models of viscous creep relaxation, which incorporate recent laboratory measurements of ice/rock mixtures [4-6], we can constrain the conditions necessary to allow such deformation on Mars [7,8].

Observations: Debris aprons are broad, gently sloping (~1°-14°) accumulations of material at the bases of escarpments (*e.g.*, Fig. 1). They often exhibit convex-upward topographic profiles (Fig. 1B) and relatively young crater retention ages (1-100 Myr). One concentration of these features is found east of the Hellas impact basin [9]. To look for patterns between the location or nature of mountains and whether or not they exhibit debris aprons, we have characterized debris aprons in a region east of the Hellas impact basin: 30° - 40° S, 240° - 280° W. Using MOLA data we quantified a variety of attributes of mountains in the study region: latitude, longitude, maximum flank slope, total slope, total height, total width perpendicular to the long axis, and basal altitude.

Within this region the only attributes that showed even weak correlations to the existence of debris aprons were latitude and slope, and these were not statistically significant. Debris aprons are more abundant to the south of our study region, which seems consistent with the lower average annual temperatures and annual insolation if near-surface ice (the stability of which is strongly temperature dependent) plays a large role in debris apron formation. Similarly, a correlation between the existence of debris aprons and basal altitude was expected. However, despite a depletion of debris aprons in the portion of the study area within Hellas (westward of ~270°W) no correlation with altitude was observed.

We are in the process of expanding our study area down to 50° south to further investigate the effect of latitude. In this area no debris aprons are found around mountains at low elevation or west of 265° W, *i.e.*, within Hellas. We are evaluating the characteristics of mountains with and without debris aprons outside of Hellas and will combine these observations with those for mountains between 30° and 40° to look for other factors that may control ground ice distribution.

Figure 1: Example of a debris apron around a mountain near Hellas at 45ºS, 255°W. (A) MOC image (M0204416) with the approximate location of the MOLA groundtrack. (B) MOLA topographic profile (orbit 15221), vertical exaggeration ~10.

(A)

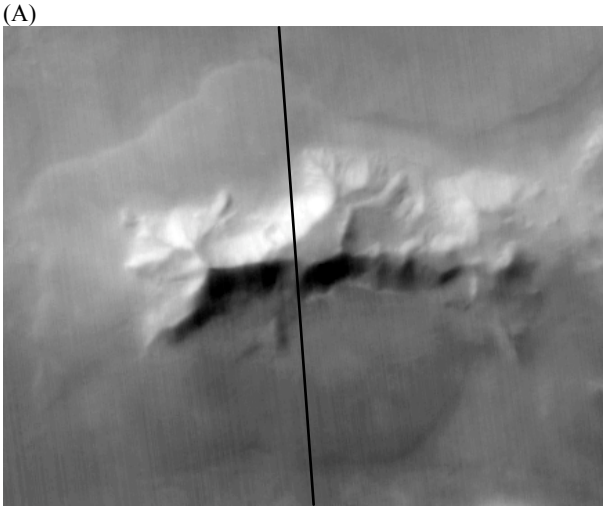

(B)

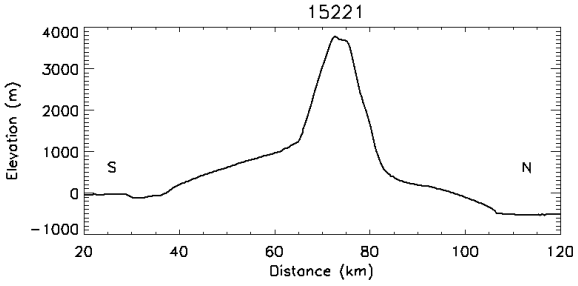

Modeling: We have applied finite-element analysis to investigate the deformation of debris aprons by creep of an ice-rich surface layer. Our models incorporate laboratory measurements of the rheological parameters for dust/water-ice mixtures undergoing dislocation creep and grain size dependent creep [4,5]; both of which are relevant under present Martian conditions: T_{surf} = 200 K [10]; dT/dz = 15 K/km [11,12]. We have built models with initial slopes ranging from 5° - 45° (*e.g.*, Figs. 2-5); slopes as shallow as ~1° have been observed for Martian debris aprons [13,9].

Fig. 2: Cross section of a finite-element model of a 45° scarp with a 1 km thick layer of 30% ice by volume (dark red), before (top) and after (bottom) 1000 yr of dislocation creep.

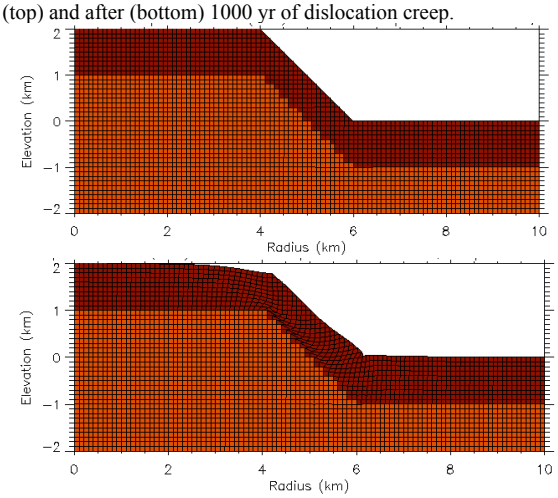

Our simulations demonstrate that the final morphology is very dependent on the initial distribution of the ice-rich material (*cf.* Figs. 3, 4) as well as on the conditions applied at the base of the ice-rich debris. Furthermore, even under present Martian conditions, viscous creep can occur quite rapidly; on timescales of 10^3-10^4 years (Fig. 5). However, if the mobility of the ice is restricted by a surface layer that resists deformation, or the high volume fractions of ice inferred to be present within a ~1 m surface layer [3] does not continue to significant depths, the deformation timescales could be significantly longer. We are also investigating the extent to which blocks of intact rock distributed within the ice-rich regolith [*e.g.*, 14] could serve to increase the deformation timescales.

Fig. 3: Cross-section of a slope of ice-rich material (uniform composition of 30% ice by volume and frictionless basal boundary) after 7500 yr of dislocation creep (basal boundary is frictionless). The solid diagonal line illustrates initial topography which is 34°, near the angle of repose.

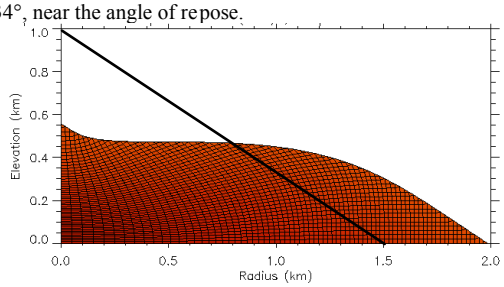

Fig. 4: Cross-section of a 500 m surface layer of ice-rich material (30% ice by volume, dark red) after 7500 yr of dislocation creep (basal boundary is frictionless). The solid diagonal line illustrates initial topography (34°).

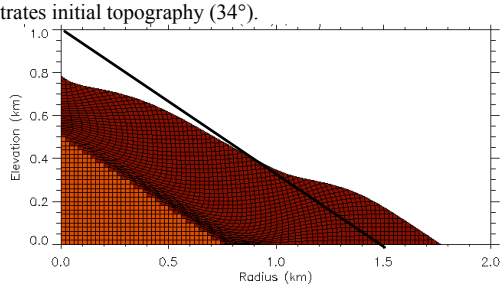

Fig. 5: This (log-log) plot of height-to-length ratio *vs.* time illustrates the rapid evolution of wedge-shaped aprons with initial slopes of 5°, 10°, and 20°. Even slopes as low as ~1° (indicated by the solid horizontal line), which are achieved in significantly less than 10^5 years, continue to deform rapidly.

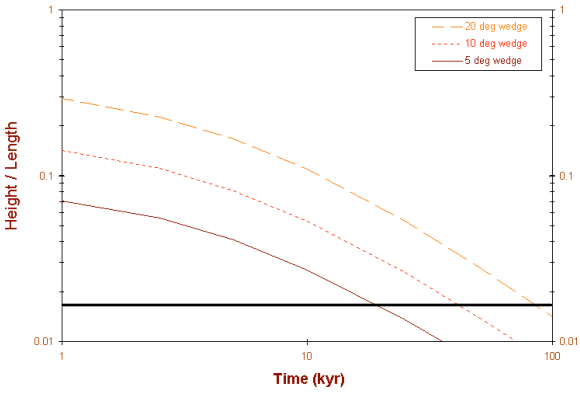

References: [1] Squyres S. (1989) *Icarus* **7**, 139-148. [2] Squyres S. *et al.* (1992) in Mars, Ed. H. Kieffer, Univ. Arizona Press, Tucson, 523-554. [3] Boynton W.V. *et al.* (2002) *Science* **297**, 81-85. [4] Durham W.B. *et al.* (1997) *JGR* **102**, 16293-16302. [5] Durham W.B. *et al.* (2000) Second Intl. Conf. on Mars Polar Sci. and Exploration, LPI Contribution #1057, 28-29. [6] Mangold N. *et al.* (2002) *Planet. Space Sci.* **50**, 385-401. [7] Turtle E.P. *et al.* (2002) *Eos. Trans. AGU, 83*, Spring Meet. Suppl., Abstract #P42A-10. [8] Turtle E.P. *et al.* (2003) *EGS/AGU* EAE03-A-07809. [9] Pierce T.L. and Crown D.A. *Icarus* **163**, 46-65. [10] Martin T.Z. (1981) *Icarus* **45**, 427-445. [11] Schubert G. *et al.* (1992) in Mars, Ed. H. Kieffer, Univ. of Arizona Press, Tucson, 147-183. [12] Clifford S.M. (1993) *JGR* **98**, 10973-11016. [13] Mangold N., Allemand P. (2001) *GRL* **28**, 407-410. [14] Whalley W.B., Azizi F. (2003) *JGR* **108**, 2002JE001864.

SIMULATION OF ATMOSPHERIC CIRCULATIONS OVER THE SUMMERTIME NORTH POLE USING THE OSU MARS MM5. D. Tyler[1] and J. R. Barnes[2], [1]College of Oceanic and Atmospheric Sciences, Oregon State University, dtyler@coas.oregonstate.edu; [2]College of Oceanic and Atmospheric Sciences, Oregon State University barnes@coas.oregonstate.edu.

Introduction: It is important to develop a more thorough knowledge of mesoscale circulations over the residual polar ice caps of Mars. Mesoscale circulations, forced by topography and gradients in the thermal properties of the surface, can significantly modify surface energy fluxes throughout these regions on relatively small scales. Efforts to more completely describe polar weather and climatology, at resolutions greater than those of present day General Circulation Models, must account for the importance of mesoscale circulations. Moreover, a greater understanding of polar mesoscale circulations will assist other investigations into polar processes. This research is the first comprehensive high-resolution attempt to understand the dynamics of the north polar summertime circulation

Mars MM5 Simulations: We have used the OSU Mars MM5 (MMM5) [1] to simulate atmospheric circulations, for northern hemisphere summertime conditions, over the north residual ice cap and southward into midlatitudes. The model was run hydrostatically using a semi-global mother domain, and two-way nesting was used to resolve circulations over Chasma Boreale to a resolution of ~6 km. Three simulations (14 sols each) were performed for L_s values of: 90°, 135° and 160°. Only the final eight sols of each simulation (output centered on L_s values) were used for analysis. Together these simulations allow an examination of how atmospheric circulations change during the entire season that the north residual ice cap is exposed to the atmosphere.

Both the MMM5 and the NASA Ames Mars GCM [2], which is used for boundary and initial conditions, utilize the most current thermal inertia [3], albedo [4] and topography [5] data that is presently available. Our model was tuned to match Radio Science temperature profiles for Ls=135° [6]. The MMM5 was tuned by first setting the visible dust opacity in the model to coincide with TES IR opacities for dust [7], and then by fixing the deepest soil model temperature for ice surfaces (dependent upon albedo) to an appropriate mean climatological temperature (175 K). Subsurface heat flux can play an important role in the residual cap energy budget [8], and this change in the initialization routines of the MMM5 yields simulated residual cap temperatures that match quite favorably with the TES observations without modifying albedo values.

Results: At the time of this writing an analysis of model results is in progress. With three runs, each at multiple resolutions (nesting), we have a 6-D data set. However, there are some results from this analysis that deserve preliminary comment.

Zonal means. Zonal Mean fields from the MMM5 are quite similar with those from the NASA Ames Mars GCM in the lower to middle atmosphere, especially over polar regions when comparing with the coarse resolution results of the MMM5 mother domain (~162 km). At a resolution nine times that of the mother domain (~18 km, two nests in), the winds over the residual cap become well resolved, with zonal mean values at L_s=90° that exceed 10 ms^{-1} near the surface over much of the cap, see Fig. 1. Such wind speeds have been suggested as possibly being required to move the amount of water off the residual cap that was measured by MAWD [9]. By late summer, Ls=135°, mean wind speeds drop to ~5 ms^{-1}, significantly reducing the wind stress on the residual cap.

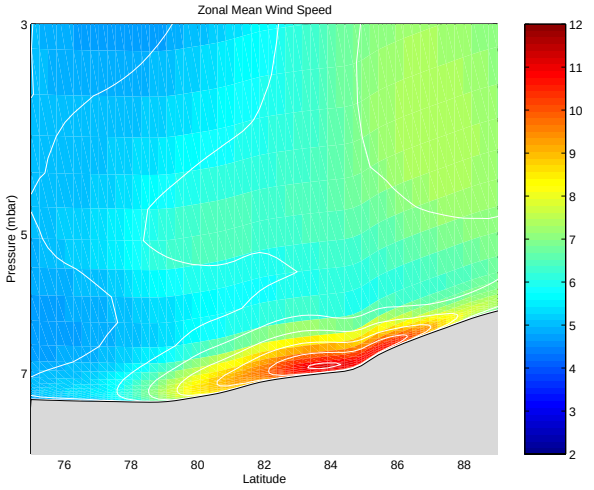

Figure 1: Eight-sol zonal mean wind speeds, for L_s=90°, over the north residual ice cap. The plot was constructed by averaging data on sigma surfaces and then converting the vertical coordinate of the average to pressure. The resolution of this nest is ~18 km.

The zonal mean meridional wind field over the residual cap is weak, as is the zonal mean zonal wind field. At the surface we do observe a weak and fairly shallow off-cap flow, with speeds of ~3 ms^{-1}. Zonal winds contribute most significantly to the zonal mean

wind speeds near the residual cap surface. Aloft, above the residual cap, the zonal mean meridional and zonal winds are negligible, suggesting there is little meridional mixing of the polar atmosphere into lower latitudes. This is only correct in terms of the zonal mean wind fields. For diurnal mean slices at specific longitudes, or for instantaneous meridional winds throughout the course of the day, the results differ dramatically from the zonal means.

Diurnal means and diurnal cycles. Diurnal mean meridional slices of meteorological fields (T, U and V) exhibit a substantial amount of asymmetry from their respective zonal means. As would be expected, we find that some of the strongest off-cap meridional flows are concurrent with Chasma Boreale.

Asymmetries from the zonal mean winds can become surprisingly large at latitudes just south of the residual cap. Certain longitudes exhibit fairly deep northerly or southerly diurnal mean flow (~5 ms^{-1}). At higher altitudes in the modeled atmosphere, asymmetries from the zonal mean meridional flow are also quite pervasive.

Presently we are investigating dynamical mechanisms to better understand the causes for these asymmetric features of the polar circulation in our model. Larger scale dynamics are presumably involved, possibly related to the proximity of Alba Patera and the Tharsis massif. This seems the single most impressive topographical feature that is close enough to be dynamically significant in the polar circulation. A working hypothesis is that stationary features of a larger scale circulation are influencing the smaller scales.

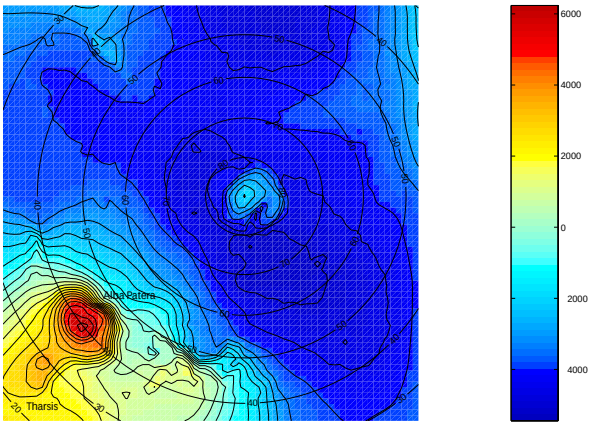

Figure 2: Topography of the ~54 km nest that was used in these simulations (76x76).

An interesting aspect of the polar circulation that we hope to understand is what we have described as "tidal sloshing" [10]. Meridional winds, in the bulk of the atmosphere above the residual cap, reverse direction over the course of the diurnal cycle with a dominant diurnal period. The strength of this effect has longitudinal preference, but it is a pervasive phenomenon over the entire north polar cap in these simulations. The image in Fig. 2 shows topography of the first nest below the mother domain (~54 km); the image is suggestive of why we are suspicious of large-scale dynamical influences related to the proximity of Alba Patera and Tharsis.

Future Direction: This work, when finalized, will complete my Ph.D. studies. Our next effort in this research will be to activate water transport in the MMM5, correctly configure the associated water routines in the model, and revisit these same simulations with the objective of developing a better understanding of the atmospheric pathways through which water is transported southwards off the north residual cap in northern hemisphere summer. There is much to be learned about the present day stability of the residual ice caps using such models, and we look forward to working closely with others interested in investigating the stability and evolution of polar ice deposits.

References: [1] Tyler D. and Barnes J. R. (2002) *JGR, 107,* 10.1029/2001JE001618. [2] Haberle R. M. et al. (1999), *JGR*, *104*, 8957-8974. [3] Mellon M. T. et al. (2002) *LPS XXXIII, Abstract #1416*. [4] Christensen P. R. et al. (2001) *JGR*, *106*, 23,823-23,871. [5] Smith D. E. et al. (1999) *Science*, *284*, 1495-1503. [6] Hinson D. P. et al. (2001) *JGR*, *106*, 1463-1480. [7] M. Smith, *Submitted to Icarus*, (2003). [8] Paige D. A. and Ingersoll A. P. (1985) *Science*, *228*, 1160-1168. [9] Haberle R. M. and Jakosky (1999), *JGR*, *102*, 9069-9083. [10] Tyler D. and Barnes J. R. (2003), *Granada Mars Workshop*.

CHASMA AUSTRALE, MARS: FORMATION BY SUCCESSIVE HEADWARD THERMO–EROSIONAL COLLAPSES.

S. van Gasselt, R. Jaumann, *German Aerospace Center, Institute of Planetary Research (Stephan.vanGasselt@dlr.de)*.

Abstract: The development of the south polar Chasma Australe re-entrant has been discussed for several years and a variety of theories including eolian, aquatic, subglacial and tectonic mechanisms have been proposed for its formation. Morphological observations and studies of recent imagery support the idea of successive headward erosion and removal of volatile–rich sub–surface material combined with collapse and eolian blow–out processes.

Introduction: The south polar Chasma Australe is a prominent arcuate elongated trough. Discussed models are formation by eolian processes [2, 3], aqeuous carving [4, 5], subglacial volcanic processes [5, 6] as well as tectonically triggered catastrophic outflow events [1] and basal melting [13]. In this work we provide some aspects to contribute to the understanding of its development. We have mapped the circum–Chasma Australe region on the basis of available imagery (Viking, Global Surveyor MOC, Odyssey THEMIS) at all resolutions and performed morphometric measurements on the basis of Laser Altimetry topographic data (MOLA) to evaluate outflow models proposed for the Chasma Australe development. A detailed description of the general morphology of the Chasma Australe has been provided by [1].

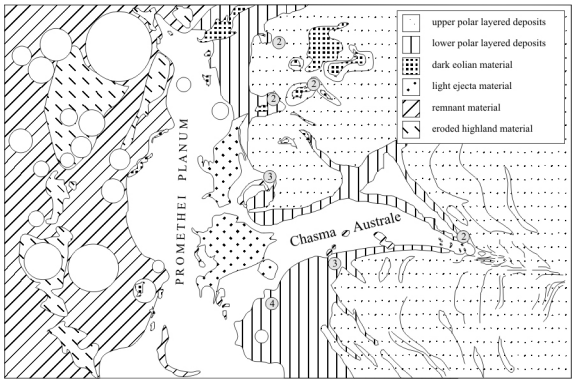

Fig. 1: Map of geomorphologic units of the Chasma Australe region, Promethei Planum and adjacent units. The Chasma Australe system is accompanied by several unlabeled Chasmata (2-4) to the east and west. Several elliptical and circular shaped depressions are located near the heads of secondary (2) re–entrants which indicate identical formation processes. Earlier stages of development (3-4) are presented by small third generation re–entrants. Light material near the terminus of Chasma Australe is connected to impact ejecta, which might be rich in volatiles, as lobate ejecta blankets indicate as well. Lineations south of the head of Chasma Australe.

Geomorphologic and geologic setting: The Chasma Australe is an arcuate and elongated steep sided depression with a length of ≈500 km and a width of 16.5 km at its head and 93 km at its terminus. The Chasma head begins near $-82°$S/90°E and reaches down to 71°S/86°E with an opening angle of $\approx 30°$. It terminates in the Promethei Planum, a large circum-polar basin. The head of Chasma Australe is a well–defined, almost circular depression at an elevation of 2500 m with a depth of 950 m. Inside the U–shaped depression a secondary almost circular depression with a depth of ≈100 m and a diameter of ≈5 km appears. The Chasma terminus is situated at an elevation of ≈1060 m and is marked by a lobate–shaped remnant of possible base rock material.

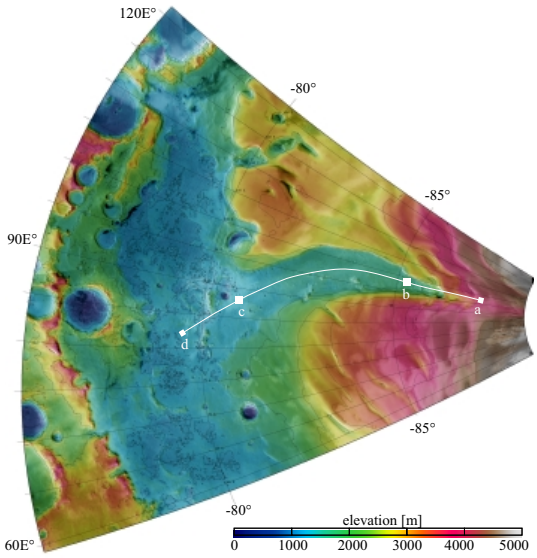

Fig. 2: Topographic map of Chasma Australe, Promethei Planum and adjacent units. Line a-b-c-d marks the profile discussed in the text.

The trough cuts into the Amazonian aged polar layers (Apl), which have been exposed mainly on the eastern flank. The basis of the re–entrant consists of the Hesperian aged Upper and Lower Dorsa Argentae Formations (Hdu and Hdl) [7].

Observations: From its head to its terminus the Chasma covers an area of $\approx 93.6 \cdot 10^3$ km^2. MOLA measurements have shown that $\approx 28.4 \cdot 10^3$ km^3 of material have been removed from the trough. The main trough (profile b:c) has a length of $\approx$ 300 km and slopes with an average angle of $0.06°$ ($S = 0.00112$) (see fig. 3). For comparions reasons we estimated discharge values Q[1] with the help of eight Chasma cross–sections and obtain values ranging from $3.67 \cdot 10^8 m^3 s^{-1}$ to $4.73 \cdot 10^9 m^3 s^{-1}$, depending on the Manning coefficient n (0.03-0.05 [11]) and the definition of the hydraulic radius R. For velocities v we obtained values ranging from $37 ms^{-1}$ to $68 ms^{-1}$. The values show a larger range of estimated peak discharges but they are of the same order as calculations by [1] and estimations for outflow systems in mid latitudes [9]. We obtained higher velocities and slightly larger discharge values. The Chasma floor has a rough small–scale surface texture.

[1](using $v = \left[(g_m RS) / \left(g_e n^2 R^{-1/3}\right)\right]^{1/2}$according to [11], with velocity $v[ms^{-1}]$, Mars/Earth gravity $g_{m/e}[ms^{-2}]$, hydraulic radius $R[m]$, bed slope $S[-]$, Manning coefficient $n[-]$).

Except for several crater chains in East–West direction only elongated ridges almost perpendicular to the proposed outflow can be observed. We find no streamlined islands as classic features for mid–latitude outflow channels and we have no evidence for outflow–parallel ridges and terraces as a high energetic flow would have caused.

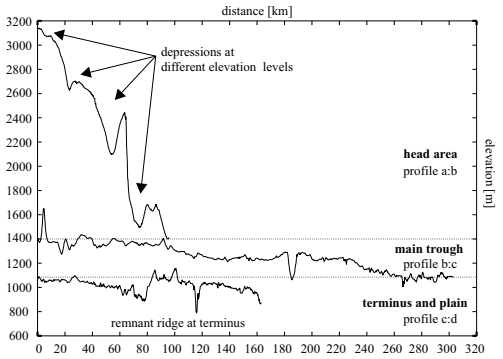

Fig. 3: Length profile of the Chasma Australe head, the main trough and the southern parts of the Promethei Planum.

In an abundance of MOC–NA imagery we observe a pattern of linear, radial and polygonal crack patterns [10] accompanied by cicular and elongated depressions in the vicinity of the Chasma walls and other re–entrants of the south polar region. The crack pattern is aligned parallel to the polar layer outcrops and becomes more densely spaced towards the Chasma walls. These fractures occur mainly near to the southern and eastern (steeper) walls. Linear fracture are connected to elongated depressions and radial fractures are connected with circular depressions. In lower resolution imagery (MDIM resolution) we observe a set of lineaments and large circular depressions south of the Chasma Australe head. The lineaments are exposed polar layer deposits and circum polar troughs which seem to bend in the headward direction of the Chasmata. Fig. 3, profile a:b shows several depressions south of the Chasma head. Each base is situated on a higher elevation level which indicates a headward progressing process of material removal. Near the western walls of Chasma Australe several remnants break through a mantling deposit (s. fig. 2). Between remnant rock and Chasma wall the polar layered deposits remain completely intact.

Conclusions: For the Chasma Australe we propose a successive headward thermo–erosional formation which has been initiated at the Promethei Planum boundary. Sapping processes due to subsurface removal of volatiles could be responsible for collapses and depressions which are aligned in the main directions of several observed Chasmata. Material has been removed afterwards in the direction of the Promethei Planum during several stages similar to the model of supra–glacial erosion by [8]. (1) Although discharge quantities are similar to mid–latitude outflow channels, the general morphology (smoothness, curvature, profile) differs immensly from the well defined known outflow channels. (2) Polar layers remain intact near crucial locations, we have no signs for streamlined islands, groove casts, secondary inner–valley channels or deposits at the terminus towards the Promethei Planum. We find some hints for (3) volcanic influence (crater chains on the Chasma basis and volcanic remnants [12]). Cracks, fissures and small basins near the walls indicate subsurface instabilities in the proximity of the Chasma. The fracture pattern favours the idea of contraction cracking of the surface material, either due to dessication or due to freezing processes of the surface as analogue to terrestrial ice wedge polygonal nets. The depressions indicate either removal of surface material due to deflation, similar to terrestrial pans, sublimation processes or subsurface removal of volatiles and subsequent collapse.

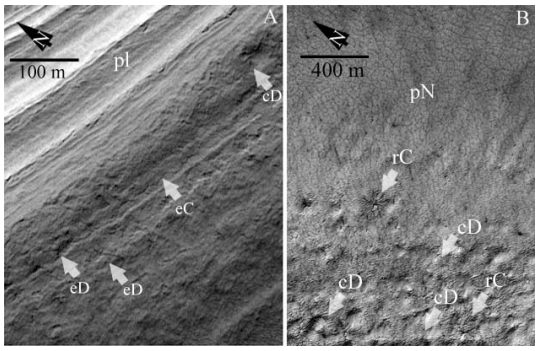

Fig. 4: Selected MOC–NA images at the head of Chasma Australe. (A) E12/02439: The eastern wall shows the layered units (Apl) and presents a pattern of elongated (eD) and circular depressions (cD), as well as elongated cracks (eC) parallel to the layering. (B) E11/01508: Image south of the Chasma's circular head. The polygonal network (pN) is gradually changing to aligned circular depressions and some occurences of radial cracks (rC).

Volcanic processes could be main trigger mechanisms for volatile removal in the subsurface, contraction–cracking and collapse might be bound to this process. Furthermore, eolian transport has a major influence on erosion and mantling the topography. Small–scale cracking and collapse structures are not mantled by eolian material although the overall surface appears very deflated, so even processes of contraction cracking and collapse could occur at present time. Open questions are adressed to the nature of cracking origin (dessication or (CO_2)ice wedges) and the removed material below collapse structures.

References: **[1]** Anguita, F. et al. (2000) *Icarus* **144**, 302-312. **[2]** Cutts, J. A. (1973) *J. Geophys. Res.* **78**, 4211-4221. **[3]** Howard, A. D. (1980) *Icarus* **50**, 161-215. **[4]** Wallace, D. and C. Sagan (1979) *Icarus* **39**, 385-400. **[5]** Clifford, S. M. (1987), *J. Geophys. Res.* **92**, 9135-9152. **[6]** Benito, G. et al. (1997) *Icarus* **129**, 528-538. **[7]** Tanaka K. L. and D. H. Scott (1987) *US Geolog. Surv.*, Map 1-1802-C, Washington D. C. **[8]** Costard, F. et al. (2003) *Lun. Planet. Sci. Conf. XXXIV, #1354*, Houston. **[9]** Komatsu and Baker (1997) *J. Geophys. Res.* **102**, 4151-4160. **[10]** van Gasselt, S. et al. (2003) *3rd Mars Polar Sci. Conf., this volume*. **[11]** Komar, P. D. (1979) *Icarus* **37**, 156-181. **[12]** Ghatan, G. J. and J. W. Head (2002) *J. Geophys. Res.***107**, 10.1029/2001JE001519. **[13]** Fishbaugh, K. et al. (2000) *Lun. Planet. Sci. Conf. XXXI, #1206*, Houston.

DISTRIBUTION AND MORPHOLOGY OF POLYGONS, SOUTH POLAR REGION, MARS. S. van Gasselt, D. Reiß, R. Jaumann, *German Aerospace Center DLR, Institute of Planetary Research, D-12489 Berlin, Germany (Stephan.vanGasselt@dlr.de)*.

Abstract: In this work we present a mapping of polygonal patterns at the south pole of Mars between 80°-90°S on the basis of all MOC narrow angle images (up to the current release of E18). We found 750 (out of 6000) MOC narrow angle images showing a variety of polygonal patterns resmebling terrestrial ice wedge polygons. They occur predominately inside circular depressions of the polar layered deposits, circum polar troughs and re–entrants or below slopes.

Introduction: Small–scale polygonal patterns have been observed in Viking Lander imagery [1]. Their morphology and development have often been ascribed to contraction cracking processes, analogous to terrestrial ice wedge polygons and are an indicator for the presence of subsurface water [e.g., 2]. With high resolution imagery from the Mars Orbiter Camera the features have been mapped and classified on a global scale by [3] and [4]. The main focus on analyzing the origin of polygonal patterns has been put on their distribution at southern and northern latitudes of $> \pm 40°$N. In this work we provide a detailed mapping of polygonal patterns at the south pole of Mars (s. fig. 2). The patterns are described on the basis of morphology and distribution.

We have mapped polygonal crack patterns on MOC narrow–angle imagery (up to E -18 release) and combined the results with color–coded MOLA digital elevation models superimposed on the MSSS MOC wide–angle MC–30 imagemosaics.

Geologic Setting and Observations: According to the geologic mapping of [5] the south polar region between 80°S and 90°S consists of the residual ice cap (Api) shifted towards longitudes between 0°W and 90°W. The remaining area is mainly covered by the Amazonian aged polar layered deposits (Apl) with small patches of non–polar related plains unit (s. fig. 1). At longitudes between 265°W and 90°W parts of the upper and lower Hesperian aged Dorsa Argentae Formation are exposed (Hdu, Hdl). The lateral distribution of this unit is equivalent to the area of low elevation (1200 m, blue color, s. fig. 2). At 10°W and between 70°W to 95°W remnants of the undivided Hesperian and Noachian material (HNu) which has undergone degradation processes by removal of ground ice, mass wasting and eolian removal occur.

We observe several regions (marked A–E, s. fig. 1) with clusters of polygonal patterns in MOC imagery. The distinct circum polar distribution (D) of polygonal patterns at 87°S is due to the dense coverage of imagery. The circum polar distribution at 87°S does not continue on the surface of the residual polar cap but spreads along circum polar troughs (C). Especially at longitudes >270°W the polygons are bound to the polar troughs, where (a) the trough material is older than the polar layers at the surface, (b) degradation and removal

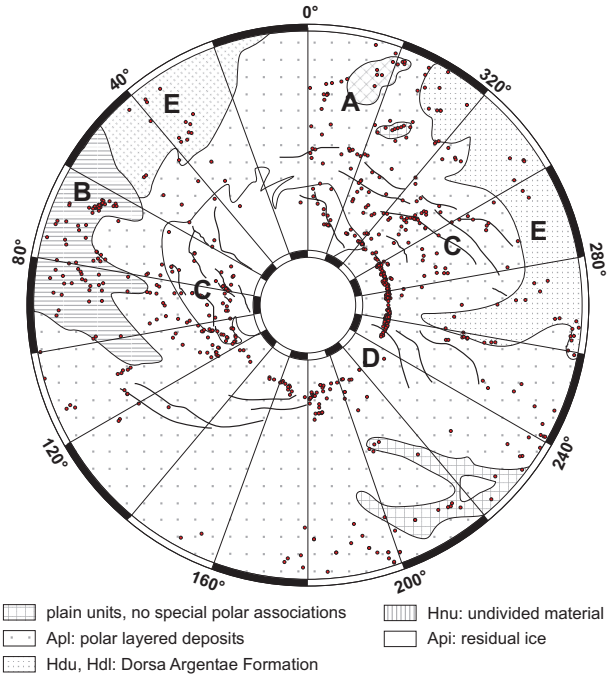

Figure 1: Simplified geologic map of the south polar region between 80°S and 90°S (after [5]) with polygonal crack patterns outside the polar cap. Letters represent areas discussed in the text.

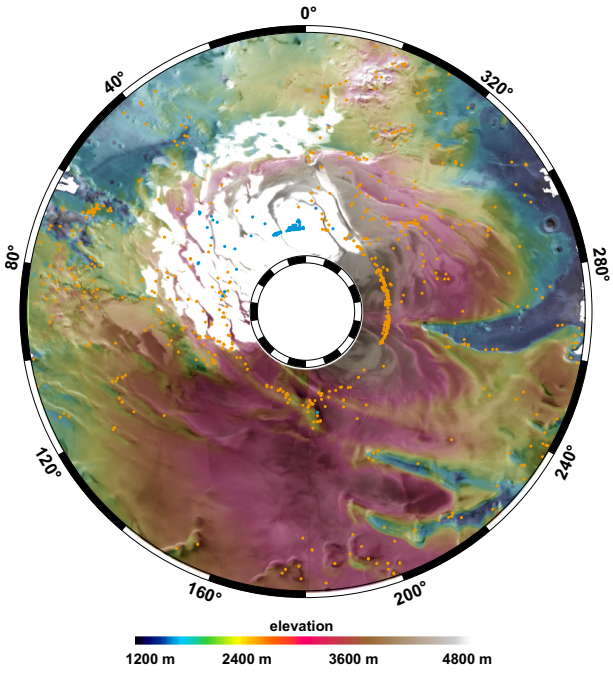

Figure 2: South polar topography and distribution of polygonal crack patterns at the south pole between 80°S and 90°S. Blue dots represent polygonal patterns associated with circular depressions [6] on the residual polar cap.

of material has not yet advanced as far as at the surface, and (c) only a few layers of the polar layered deposits show the typical polygonal pattern. The layers containing polygons are exposed at the Chasma Australe walls, the eastern chasmata, and inside depressions of the polar layered deposits at 180°W to 200°W. At 80°W the circum polar distribution furcates to the north and presents a large cluster of polygonal patterned ground in undivided Hesperian aged units (B).

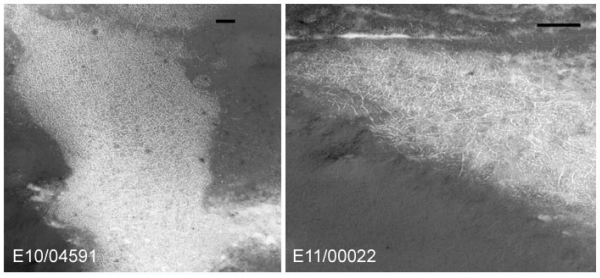

Figure 3: Plains units polygons at 80°S (A on fig. 2). The black bar represents 200 m, north is up. Polygons of the south polar plains units occur predominately in sheltered places at slopes and inside of depressions.

Small quantitites of polygonal terrain is visible on material of the Dorsa Argentae Formation (E), where it is bound to small depressions and rough terrain. Minor clusters of polygonal terrain is exposed adjacent to undivided plain units (A). Polygons related to plains units (A) are randomly orthogonal and highly complex shaped (s. fig. 3). They are degraded and occur south of sheltered slopes or inside depressions. Their diameter varies between 10 to 50 m but reaches up to 80 m. The polygonal troughs are filled with bright material, which might be associated with CO_2 frost [7]. Towards the pole polygons are orthogonal and their shape becomes more distinct with a preferred N–S direction. The polygonal troughs are filled with dark eolian material. Their diameter increase up to 100 to 200 m. Polar troughs related polygons (s. fig. 5) occur on the slopes and inside the troughs.

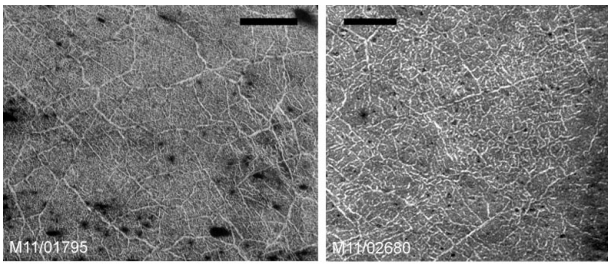

Figure 4: Randomly orthogonal and complex polygons of the Dorsa Argentae Formation (Hdl, Hdu) near 84°W and 80°S. The black bar represents 200 m, north is up.

They have an orthogonal shape and diameters between 10 m to 20 m. Outside the troughs the polygons dissappear below eolian material. Polygons of undivided material near 84°W and 80°S are, similar to the plains units, more complex shaped and randomly orthogonal (s. fig. 4). Polygons exposed at the eroded wall material of the polar layered terrain occur on a few layers only. These polygons are partly degraded but show a distinct orthogonal pattern and sizes in a range of 20-40 m.

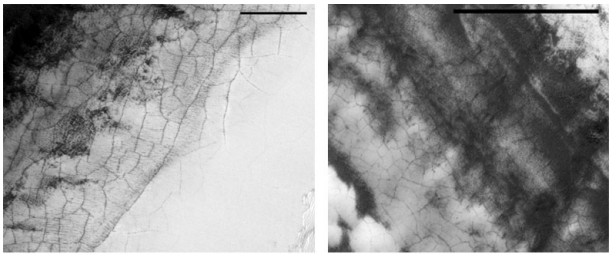

Figure 5: High resolution imagery of polar trough related polygonal networks near 85°W and 86°S. The black bar represents 200 m, north is up.

Conclusions: The distribution of south polar polygons is bound to circum polar troughs, polar re–entrants and depressions where polar layers are exposed (Apl). Polygonal patterns associated with circular depressions can be observed on the polar residual cap. Furthermore, clusters of polygonal patterns are distributed at undivided (HNu) and unclassified plains material. Polygons have a distinct shape and morphology according to their geologic and geomorphologic setting, although transitional morphologies occur in all units. As the distribution is not random at all, surfaces (especially few marker horizons of the layered terrain) showing polygonal patterns might have ages which are valuable to for implications on the past climate. Further research regarding ages is under way.

As far as insights have been provided by MOC, there are major dependencies on parameters like topography, homogeneity of (sub-)surface material, temperature changes, and exogenic degradation processes. Changes in these parameters will affect the growth, size, pattern and distribution of the polygonal networks [8]. Providing a complete coverage, color, and stereo information at high resolution, Mars Express will help to close the remaining gaps and to determine surface and morphologic properties to rule out some of the unknown parameters.

References: [1] T. A. Mutch et al. (1977), *J. Geophys. Res.*, **82**, 4452-4467. [2] M. T. Mellon (1997), *J. Geophys. Res.*, **102**, 25617-25628. [3] R. O. Kuzmin and E. V. Zabalueva (2003), *Lun. Planet. Sci. Conf.*, Houston, #1912. [4] N. M. Seibert and J. S. Kargel (2001), *Geophys. Res. Let.*, **28**, 899-902. [5] Tanaka K. L. and D. H. Scott (1987) *US Geolog. Surv.*, Map 1-1802-C, Washington D. C. [6] Thomas et al. (2000), *Nature*, **404**, 161-164. [7] K. J. Kossacki and W. J. Markiewicz (2002), *Icarus*, **160**, 73-85. [8] A. H. Lachenbruch (1962), *GSA papers*, **70**, New York.

THERMOPHYSICAL PROPERTIES OF MARS' NORTH POLAR LAYERED DEPOSITS AND RELATED MATERIALS FROM MARS ODYSSEY THEMIS. A. R. Vasavada[1], M. I. Richardson[2], S. Byrne[2], A. B. Ivanov[3], P. R. Christensen[4] and the THEMIS Team, [1]Department of Earth and Space Sciences, Box 951567, University of California, Los Angeles, CA 90095-1567, ashwin@ess.ucla.edu, [2]Division of Geological and Planetary Sciences, Mail Stop 150-21, Caltech, Pasadena, CA 90025, [3]Jet Propulsion Laboratory, Mail Stop 168-416, Pasadena, CA 91106, [4]Department of Geological Sciences, Arizona State University, Tempe, AZ 84287.

Introduction: The presence of a thick sequence of horizontal layers of ice-rich material at Mars' north pole, dissected by troughs and eroding at its margins, is undoubtedly telling us something about the evolution of Mars' climate [1,2]—we just don't know what yet. The North Polar Layered Deposits (NPLD) most likely formed as astronomically driven climate variations led to the deposition of conformable, areally extensive layers of ice and dust over the polar region. More recently, the balance seems to have fundamentally shifted to net erosion, as evidenced by the many troughs within the NPLD and the steep, arcuate scarps present near its margins, both of which expose layering.

Viking Orbiter imaging of the NPLD revealed that dark, dune-forming material is spatially associated with NPLD scarps [3]. This material may be liberated from an ice matrix by thermal erosion of the NPLD, either as sand particles or sand-sized aggregates of dust [4]. In either case, the NPLD seems to be a source of material similar in particle size and color to that present in the vast, circumpolar sand sea [3].

Recently, the stratigraphy of the NPLD has been subdivided into two distinct units [5-10]. The upper unit appears to consist of horizontal layers of water ice and a small fraction of dust. Layers are exposed within gently sloping, spiral troughs cut into the cap complex. The lower unit consists of thicker, darker layers with an irregular, platy appearance. It crops out near the margin of the NPLD and within Chasma Boreale. When troughs cut deeply enough to encounter the lower unit, the trough forms are replaced by steep, arcuate scarps. Edgett *et al.* attribute the change in morphology to a lower unit that is less resistant to wind erosion [7].

This stratigraphic sequence has been observed at widely separated locations within the NPLD [6]. If the layering is truly horizontal over the pole, such that the lowest portions of the stratigraphic column crop out in the marginal scarps, it suggests that the erosion of the platy unit uniquely contributes the dark, dune-forming material. Indeed, the platy unit may be an ancient sand sea now covered by the ice-rich, finely layered unit [6], although no bedforms have been found upon it [7].

Optical and thermal infrared (IR) measurements have been used to infer and compare the properties of the different polar materials. For example, Thomas and Weitz compared the color of the dark material near NPLD scarps to material within NPLD layers and within the circumpolar sand sea [3]. Herkenhoff and Vasavada used Viking IR measurements to determine the nature of the dune-forming material and its relationship to other dark, dune-forming materials at lower latitudes [4]. However, such investigations have been limited by the relatively low spatial resolution of Viking color imagery and IR data compared to the spatial dimensions of layers, troughs, scarps, and dune fields. We hope to take advantage of the unprecedented spatial resolution of Mars Odyssey Thermal Emission Imaging System (THEMIS) visible and IR imagery in order to make these inferences and comparisons with the highest possible accuracy (e.g., Figure 1).

THEMIS Observations: To address this science goal, we defined a number of Regions of Interest (ROI) for THEMIS to target as part of the Mars Odyssey Participating Scientist program. We gratefully acknowledge the THEMIS science team and operations staff for acquiring ~100 visible and IR image cubes during Mars' northern summer (L_s 110-160) as orbit tracks intersected our ROIs. The visible image cubes in our data set have five wavelength bands, along-track lengths of ~1000 pixels, and a spatial resolution of 19-38 m/pixel. The IR image cubes have ten wavelength bands and a spatial resolution of 100 m/pixel. The along-track footprint of the IR cubes often begins < 80° latitude, crosses the pole, and terminates < 80° latitude.

Visible Data Analysis: We use these THEMIS data in order to understand the morphology and color/thermal properties of the NPLD and related materials over relevant (i.e., m to km) spatial scales. We have assembled color mosaics of our ROIs in order to map the distribution of ices, the different layered units, dark material, and underlying basement. The color information from THEMIS is crucial for distinguishing these different units (Figure 1), which are less distinct on Mars Orbiter Camera images.

We wish to understand the nature of the marginal scarps and their relationship to the dark material. Co-registered Mars Orbiter Laser Altimeter (MOLA) data provides a measure of scarp morphologies and may help identify the process(es) eroding the NPLD (e.g.,

mass wasting, wind, sublimation). The dark material (or perhaps the platy unit in planar configuration) is present at the feet of many scarps, but does not express dune bedforms there. However, dark material has barchan-type formations when present tens of kilometers away from the scarps [3]. MOLA will help identify the relationship between the spatial distribution of dark material, the presence of bedforms, and the influence of topography.

Thermal Data Analysis: Our next, more ambitious goal is to derive the thermophysical properties of the different geologic materials using THEMIS and Mars Global Surveyor Thermal Emission Spectrometer (TES) data. Such analyses are complicated by the need for atmospheric correction (of both radiatively active CO_2 and dust) and accurate, representative surface temperatures. The latter may be compromised by the footprint size (compared to the areal extent of the material of interest), the influence of topography, and the absolute calibration of the measurement. However, the THEMIS data offer the promise of extending our previous analyses [4] to finer spatial scales and effort will be made to overcome these challenges. In order to derive thermal inertias and thermally derived albedos, we will employ a 1-D, radiative-convective thermal model of Mars surface, subsurface and atmosphere. The model will use simultaneous (or seasonally relevant) TES atmospheric dust opacities, and where possible, include the effects of surface slopes on insolation using MOLA topographic data.

Summary: We hope to understand the geologic evolution of the north polar region by studying the optical and thermophysical properties of polar materials. The primary questions include: what processes control the morphology of the troughs and scarps within the NPLD? What is the nature of the upper and lower NPLD units, as inferred from their thermophysical properties? And finally, what is the nature and source of the dark, dune-forming material?

References: [1] Murray, B. C. et al. (1972) *Icarus*, *17*, 328. [2] Cutts, J. A. (1973) *J. Geophys. Res*., *78*, 4231. [3] Thomas, P. C. and Weitz C. (1989) *Icarus*, *81*, 185. [4] Herkenhoff, K. E. and Vasavada A. R. (1999) *J. Geophys. Res*., *104*, 16,487. [5] Malin, M. C. and Edgett, K. S. (2001) *J. Geophys. Res*., *106*, 23,429. [6] Byrne, S. and Murray, B. C. (2002) *J. Geophys. Res*., *107*, 11-1. [7] Edgett, K. S. et al. (2003) *Geomorph*., *52*, 289. [8] Kolb, E. J. and Tanaka, K. L. (2001) *Icarus*, *154*, 22. [9] Tanaka, K. L. et al. (2003) *J. Geophys. Res.*, *108*, 24-1. [10] Fishbaugh, K. and Head, J. W. (2003), *6th Intl. Conf. on Mars*, abstract 3137.

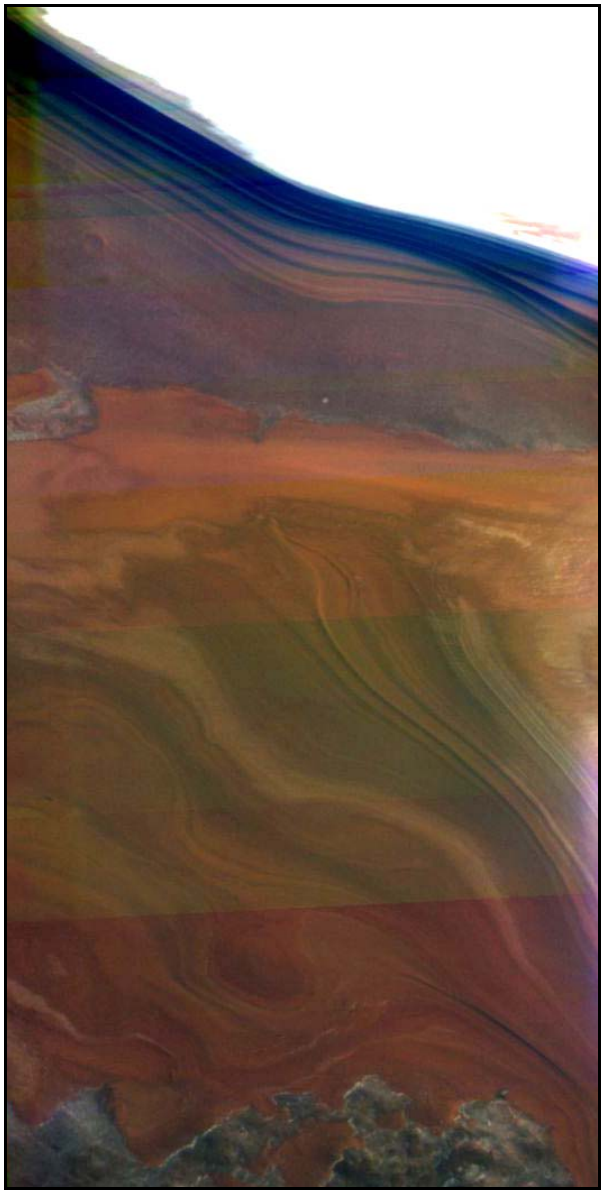

Figure 1. Color composite of THEMIS visible image data showing the north polar residual ice cap (top) and layered materials near the margin of the NPLD. Here the erosion of the deposits appears to "bottom out", exposing the basement terrain underneath the NPLD (best seen along the lower edge of the image). The color information greatly aids this interpretation.

LOW-TEMPERATURE, AQUEOUS ALTERATION OF SOIL IN WRIGHT VALLEY, ANTARCTICA, COMPARED WITH AQUEOUS ALTERATION ON MARS. S. J. Wentworth,[1] E. K. Gibson, Jr.,[2] and D. S. McKay[2], [1]Lockheed Martin Space Operations, C23, 2400 NASA Rd. 1, Houston, TX, 77058 (susan.j.wentworth@jsc.nasa.gov), [2]NASA Johnson Space Center, Houston, TX, 77058.

Introduction: The Dry Valleys of Antarctica are possibly one of the best analogs on Earth of the environment at the surface of Mars. Many types of research have been focused on the Dry Valleys, partly because of the potential application to Mars, and also because of the importance of the Dry Valleys in understanding the characteristics and development of terrestrial polar deserts. In 1983, we published a detailed study [1] of weathering products and soil chemistry in a soil pit at Prospect Mesa, Wright Valley, as a possible analog to Mars. Much more is now known about Mars, so we are re-examining that earlier work and comparing it with newer martian data. The Mars information most pertinent to this work includes (**A**) the strong evidence for recent aqueous activity on Mars reported by [2], along with more recent evidence for present-day, near-surface water ice on Mars [3, 4]; and (**B**) the identification of meteorites from Mars [5] and the subsequent, definitive proof that low-temperature, aqueous weathering has occurred in these meteorites prior to their ejection from Mars [6-8].

Soil column, Wright Valley: The samples used in the Dry Valleys study [1] were taken at irregular intervals from the soil pit shown in Fig. 1. The soil column consists of a permanently frozen zone below ~40 cm depth overlain by an active/seasonally frozen zone.

Results of the Wright Valley work seem to be consistent with what is now known or postulated about Mars. Orbital data indicate the presence of water ice just beneath the martian surface, especially at high latitudes [2, 3].

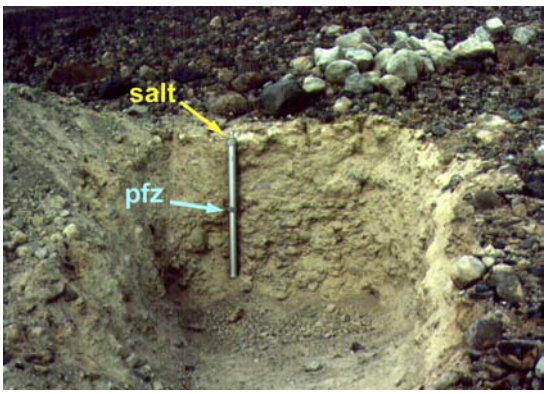

Figure 1: Soil pit, Prospect Mesa, Wright Valley, Antarctica. Drive tube=78 cm long. Yellow arrow points to salt-rich zone just beneath surface (~2-4 cm depth). Top of permanently frozen zone (pfz) is at ~40 cm depth; after [1].

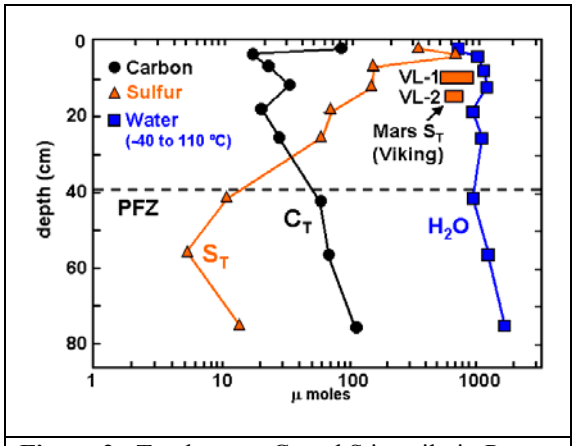

Figure 2: Total water, C, and S in soil pit, Prospect Mesa, Wright Valley; dashed line marks top of permanently frozen zone (pfz); after [1].

Similarly, Fig. 2 demonstrates that the water content (from -40 to +110 deg C) of the Wright Valley soil is much lower at the surface than at depth. This upward decrease in water occurs even within the permanently frozen zone.

In the Wright Valley soil column, water-soluble (salt-forming) species generally increase upward, with a salt-rich zone at ~2-4 cm depth and a dramatic decrease in salts at the surface of the soil (Fig. 3). Mars remote sensing data suggest that total amounts of alteration of original igneous rocks on Mars may be low [3]. The duricrust found just beneath the surface during Viking lander experiments, however, indicate that subsurface salts analogous to those in the Wright Valley soils are likely present on Mars although their possible abundance and distribution are unknown.

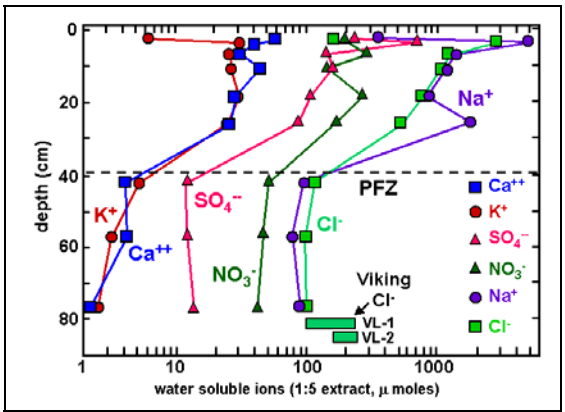

Figure 3: Water-soluble ions in soil pit, Prospect Mesa, Wright Valley; after [1].

Aqueous alteration and secondary phases: SEM studies of the Wright Valley soils [1] showed that aqueous alteration of detrital silicate grains and the formation of secondary phases occurred throughout the soil column, including the permanently frozen zone. Similar features are also present in martian meteorites, and various lines of evidence have shown that some of this alteration occurred on Mars [8, 9]. Examples of typical silicate dissolution in the Dry Valleys soil and a Mars meteorite (Shergotty) are shown in Fig. 4. These features are quite similar to each other. They are typical of chemical weathering of such silicates but are not diagnostic of the mode of alteration. Note that the Wright Valley grain (Fig. 4A) came from the permanently frozen zone of the soil, demonstrating active, although probably slow, alteration processes.

The Wright Valley soil (again, including the permanently frozen zone) and the martian meteorites also contain secondary salts. Secondary carbonates, Ca-sulfate, and halite are found in the Wright Valley soils and the martian meteorites, although not all the meteorites contain all these minerals. A martian origin has been well established for some, but not all, of the secondary phases in martian meteorites. Various means have been used to determine a martian origin for secondary phases; e.g., carbonates in meteorite ALH84001 were quantitatively identified as martian because of their ~3.9 Ga age (ALH84001 itself is 4.5 Ga old) [7]. The origin of many other secondary phases in other meteorites is less certain, however.

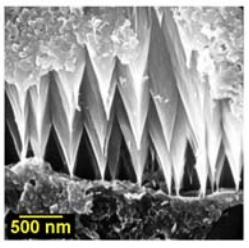

Figure 4A: SEM image of amphibole from Wright Valley soil pit sample WV-221 (permanently frozen zone) showing dissolution features typical for silicates; after [1].

Figure 4B: SEM image of pyroxene from martian meteorite Shergotty (observed fall) with dissolution features and incipient phyllosilicates.

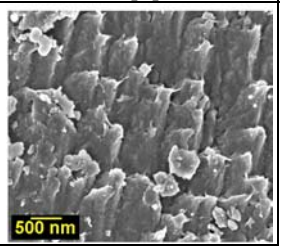

Recent orbital data have suggested the possible presence of a zeolite such as chabazite in Mars dust [10]. Chabazite is present as an authigenic mineral throughout the Wright Valley soil column (Fig. 5) in the Antarctic soil. This is consistent with the suggestion by [11] that chabazite may store water on Mars, especially near the equator. More work is needed to determine whether zeolites are not present in the existing martian samples, or whether they simply have not been found yet.

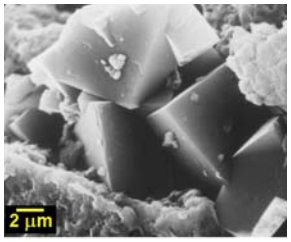

Figure 5: SEM image of authigenic chabazite in Wright Valley soil pit sample WV-221 (permanently frozen zone); after [1].

Conclusions: Aqueous alteration in Mars meteorites and the Wright Valley soil are quite similar with respect to type and degree of weathering of the primary silicates, and also to the nature and distribution of secondary phases. Alteration in the Dry Valleys soils occurs even in the permanently frozen zone, suggesting that similar alteration probably occurs on Mars. Alteration can occur gradually in permanently frozen material because of a liquid-like thin film of water that seems to persist at very low temperatures [12]. Freezing-point depression in brines could also cause weathering at low-temperatures; the salts in the Mars meteorites point to the existence of such brines. The low total amount of alteration of the martian meteorites, along with the presence of secondary phases only in trace amounts, seems consistent with such a process. Transient heating events (e.g., impacts and volcanic activity) have probably been responsible for some weathering on Mars. The Mars meteorites probably do not reflect strong heating events because significant alteration would be expected, at least in close proximity to the heated areas. The seasonal behavior of water ice at the martian poles and possibly elsewhere indicates that water (liquid or vapor) is available for periodic episodes of weathering, even if effects are concentrated mostly on wind-blown dust. Whether or not Mars was once wet and warm, or if it was always cold and dry as suggested by [13], it is clear that weathering and salt deposition have occurred in some form. If the cold, dry Mars model is correct, then the Dry Valleys of Antarctica may be a good analog for most of Mars for most of geologic history.

References: [1] Gibson et al (1983) Proc. LPSC 13, A912-A928; [2] Malin and Edgett (2000); [3] Boynton et al. (2002) Science 297, 81; [4] Christensen (2003) 6th Mars Conf. #3126; [5] Bogard and Johnson (1983) *Science*, 221, 651; [6] Gooding et al. (1988) *GCA* 52, 909; [7] Borg et al. (1999) *Science* 286, 90; [8] Wentworth et al. (2003) *Astrobio*, in revision; [9] Gooding et al. (1991) *Meteoritics* 26, 135; [10] Ruff (2002) *Eos* 83, 1059; [11] Bish et al. (2003) *LPS XXXIV*, 1786; [12] Anderson (1981) *NASA TM 84211*, 292.

LIFE IN PERENNIALLY ICE COVERED LAKES ON MARS - AN ANTARCTIC ANALOGUE

Alex T. Wilson Dept of Geosciences, University of Arizona, Tucson, AZ 86721, USA. (520) 298 5446, email atwilson@U.arizona.edu.

Introduction: As a past member of the New Zealand Antarctic Program, the author spent many summers studying the perennially ice covered lakes in the cold and arid regions of the Antarctic [1 – 5]. This presentation will review what is known about such lakes and conclude that versions of them may exist on Mars. If indeed this proves to be the case, they would be prime sites to look for life. They might also be suitable sites for the construction of a research base, since they would provide a good landing site, water and building material.

Fresh Water Perennially Ice Covered Lakes: It may come as a surprise that large bodies of fresh water can exist in regions where the mean annual temperature is –20 C and below. In the Antarctic, such lakes are possible because some water enters the perennially ice covered lake during a few days each summer. This water flows under an ice cover, which is many meters thick. Water can only be frozen on the bottom of the ice if its latent heat of fusion can be conducted through the overlying ice cover.

The water that enters the perennially ice covered lake flows into the lake and fingers into its appropriate density level. The maximum density for pure water is 4.1 C, which is the temperature of the bottom waters of many of these lakes. For a steady state situation, the amount of water in such lakes (on average) must equal the amount of water sublimed from the ice surface each year, or the lake level will rise or fall until it comes into balance.

During late winter, ice freezes onto the bottom of the perennial ice cover to replace the ice lost during the year. It follows that the thinner the ice, the more ice can freeze onto the bottom of the ice cover. In effect, the ice thickness is a measure of the aridity of the area. Thus the heat input to the perennially ice covered lake comes from the latent heat of fusion of the inflow water and from solar heating.

The very clear ice on perennially ice-covered lakes makes them appear blue. Such an unusual ice cover will give the lakes a low albedo and a "blue ice" color. The ice crystals in the ice cover have been growing for thousands of years. In the case of Lake Vanda [1], perhaps the most studied perennially ice covered lake, the ice crystals are 10 cm across and 3.6 meters long with the c-axis vertical. These crystals act as light pipes and allow the 12 ft ice cover on Lake Vanda to transmit 6% of the total incident solar energy [1]. Because of the unusual crystal orientation of the ice cover, it may be possible to develop methods to confirm the existence of perennially ice covered lakes on Mars.

Can Perennially Ice Covered Lakes Exist On Mars?: The situation on Mars is like the cold arid ice-free areas of Antarctica – only a more extreme version. The temperatures on Martian polar regions are clearly much colder but the relative humidities may be higher. The problem is to find a source of water for Martian perennially ice covered lakes which would replace the sublimation losses from the lake surface. One possibility would be the brine that would be flowing into the sides of the lakes – see discussion below. The origin of the brines entering Antarctic lakes will be discussed and is published [2] [3]. A saturated solution of sodium chloride has a freezing point of –20.7 C and an equilibrium relative humidity of 75%. A better candidate might be calcium chloride: a saturated solution has a freezing point of -50 C (223 absolute) and an equilibrium relative humidity of 45%. Of course in practice, any brine would be a complex mixture. However, it seems feasible to have a situation where in the warmer times of the annual cycle (or at some time in the past) salt brines would flow into a perennially ice covered lake and sink to finger into an appropriate density layer. During the late winter, relatively pure water would freeze onto the bottom of the ice to make up for sublimation from the ice surface. During the summer, the solar radiation would melt voids in the ice, particularly in places where any biological colonies intercept solar radiation. This happens on perennially ice covered Antarctic lakes - see for example references [4] and [5].

Origin Of Brine Needed To Feed The Ice Covered Lakes: The Northern Martian Ice Sheet has probably been in existence for a very long time. The surface of the ice sheet has been losing water by sublimation. This has been made up by the precipitation on the surface by ice crystals. This ice would not be pure water, but would contain small quantities of inorganic salts – e.g. calcium, magnesium and sodium chlorides. Where are these salts today? It is proposed that the more deliquescent of these salts have taken up water and have flowed down-slope into the topographically enclosed drainage basins associated with the ice sheet. Some of these might be expected to contain perennially ice-covered lakes. These lakes may have living things associated with their ice cover, since there would be relatively fresh liquid water at least for part of the annual cycle.

Direct Evidence Of The Existence Of Lakes Associated With The Northern Ice Sheet: Viking Surveyor color satellite photos will be shown (see below) in which a number of ice-blue lakes can be seen occupying the bottom of various enclosed basins. There may even be different kinds of Martian perennially ice covered lakes. For example, one lake appears to be a circular lake analogous to the lakes found on terrestrial icesheets and might be expected to have an ice bottom. Such a lake would be able to acquire water by melting the underlying ice and may contain fresh water. An interesting point is that there appear to be several lakes associated with the Northern Ice Sheet but none are observable in the South Polar Region.

[1]Wilson A.T. and H.W.Wellman Nature **196** 1171-1173.[2]Wilson A.T. Nature **280** 205-208.[3]Wilson A.T. J.Geoph. Rev.,D.V.D.P.,**33** 185-192.[4]Wilson A.T. Ecology **46** 376.[5]Wilson A.T. and H.W.Wellman Nature **196** 1773.

THE NORTHERN ICE SHEET OF MARS WITH FOUR OF THE LAKES ENLARGED

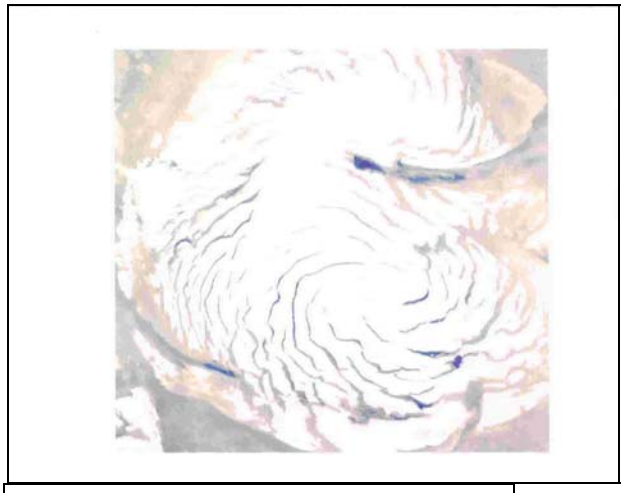

_____100 km_____

_____100 km_____

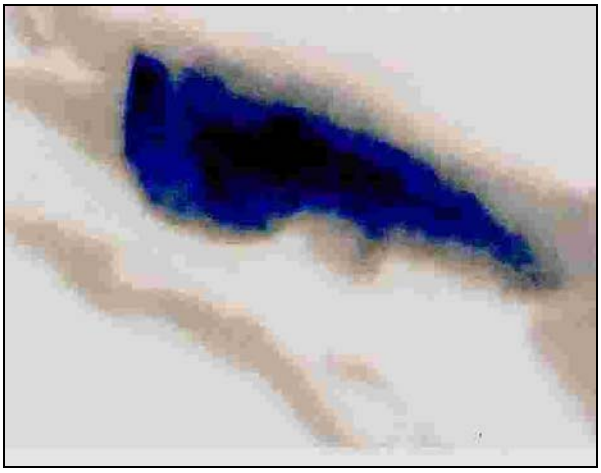

_____100 km_____

THE POLAR REGIONS AND MARTIAN CLIMATE: STUDIES WITH A GLOBAL CLIMATE MODEL. R. J. Wilson[1], M. I. Richardson[2], and M. D. Smith[3], [1]Geophysical Fluid Dynamics Laboratory, Princeton, NJ 08542 (rjw@gfdl.gov), [2]Division of Geological and Planetary Sciences, MC 150-21, California Institute of Technology, Pasadena, CA 91125 (mir@gps.caltech.edu), [3]NASA Goddard Space Flight Center (Michael.D.Smith@gsfc.nasa.gov).

Introduction: Much of the interest in the polar regions centers on the fact that they likely contain the best record of Martian climate change on time scales from years to eons. This expectation is based upon the observed occurrence of weathering product deposits and volatile reservoirs that are coupled to the climate. Interpretation and understanding of these records requires understanding of the mechanisms that involve the exchange of dust, water, and carbon dioxide between the surface and atmosphere, and the atmospheric redistribution of these species. We will summarize our use of the GFDL Mars general circulation model (MGCM), to exploration aspects of the interaction between the global climate and the polar regions. For example, our studies [1] have shown that while the northern polar cap is the dominant seasonal source for water, it can act as a net annual source or sink for water, depending upon the cap temperatures and the bulk humidity of the atmosphere. This behavior regulates the annual and global average humidity of the atmosphere, as the cap acts as a sink if the atmosphere is too wet and a source if it is too dry. We will then focus our presentation on the ability of the MGCM to simulate the observed diurnal variations of surface temperature. We are particularly interested in assessing the influence of dust aerosol and water ice clouds on simulated surface temperature and the comparison with observations. Surface thermal inertia and albedo are critical boundary inputs for MGCM simulations. Thermal inertia is also of intrinsic interest as it may be related to properties of the surface such as particle size and surface character.

Model: The GFDL Mars general circulation model simulates the circulation of the Martian atmosphere from the surface to roughly 90 km [2]. The MGCM includes parameterizations for radiative transfer associated with CO_2 gas and for aerosols. An arbitrary number of aerosol populations can be transported by the simulated circulation. Dust may be injected at the surface using a prescribed rate and spatial distribution. We have recently added a dust source scheme that associates injection with resolved wind stresses and parameterized dust devil activity. This scheme allows the seasonal cycle of air temperatures and dust to match observations well at times when large-scale dust storms are not occurring. The model has also proven capable of simulating global dust storms with interannual variability in size and timing of occurrence. A potential source of memory for interannual variability is the spatial distribution of dust on the surface, as suggested by spacecraft and telescopic observations of interannual albedo variations. An ongoing line of research is considering the coupling of injection and sedimentation to the surface budgets of dust to investigate their role in interannual variability and assess net transport of dust onto the polar caps.

The water cycle is represented by surface ice and regolith water reservoirs, atmospheric transport and ice cloud formation [1,3]. The optical properties of predicted ice clouds can be passed to the radiative heating codes, allowing cloud radiative feedbacks and dust-water ice interactions to be examined.

Surface Temperature:

The daily and seasonal variation in surface temperature is a central element in the description of the martian climate. In the case of an optically thin atmosphere, surface temperature provides the bottom boundary condition that fundamentally influences the profile of overlying atmospheric temperature. The low thermal inertia of the Mars surface allows for the large seasonal variation in diurnal-mean surface temperature that reflects the seasonal migration of the subsolar latitude and the annual variation in insolation due to the eccentric orbit. We have used MGS TES surface temperatures and thermal inertia estimates [4,5] to derive thermal inertia and albedo maps suitable for use in the MGCM. It is important to note that estimates of thermal inertia must account for atmospheric opacity due to dust and water and CO_2 ice clouds. These effects are significant in the polar regions and will influence the characterization of the polar surfaces. By using relatively coarse spatial resolution compared to [4], we can more readily trade off spatial resolution for temporal resolution and relate the evolution of observed morning and afternoon temperatures (and thermal inertia estimates) to variations in atmospheric opacity.

Figure 1 shows the seasonal evolution of zonally-averaged daytime (2pm) surface temperature (contoured) from a reference simulation representing relatively clear sky conditions. There is a large seasonal variation in temperature that reflects the seasonal migration of the subsolar latitude and the annual variation in insolation due to the eccentric orbit. The advance and retreat of the polar CO_2 ice caps approximately follows the 150 K isotherm. It is apparent that very strong temperature gradients develop along the retreating edge of the polar caps as spring advances into summer in each hemisphere. These gradients likely give rise to

strong local thermal wind systems that evidently are associated with observed local dust storm activity along the cap boundaries [*6*].

Figure 1 also shows the difference between zonally-averaged TES surface temperatures and those from a reference MGCM simulation. This figure clearly highlights the seasonal changes of observed temperatures that may largely be attributed to variations in atmospheric opacity. Temperature differences are minimal during the relatively clear NH spring/summer season when the atmospheric opacity assumed in the simulation most closely approximates that of the actual Mars atmosphere. The effects of a regional scale dust storm at L_s=225° in the first mapping year and a major, planet-encircling dust storm at L_s=185° in the second year are evident. A dusty atmosphere leads to an increase in morning temperature and a decrease in afternoon temperature.

There are systematic temperature differences in the vicinity of the polar caps. These are due, in part, to errors in simulating the polar cap latitude. Significant temperature differences are also due to the presence of dust and polar hood clouds in the vicinity of the polar caps. The aphelion season tropical water ice cloud has a clear influence on apparent tropical nighttime temperatures. We will show how simulated temperatures depend on atmospheric opacity. In a related manner, we consider how atmospheric opacity affects the determination of surface thermal inertia.

References: [1] Richardson, M. I. and Wilson, R. J. (2002) *JGR 107(E5)*. [2] Wilson, R. J. and Hamilton, K. (1996) *J. Atmos. Sci., 53*, 1290-1326. [3] Richardson, M. I., Wilson, R. J. and Rodin, A.V. (2002) *JGR 107(E9)*, 5064. [4] Mellon et al., (2000), *Icarus, 148*, 437-455. [5] Christensen et al. (2001) *JGR 106*(E10), 23823-23872. [6] *Cantor et al*. (2001), JGR 106, 23653-23687.

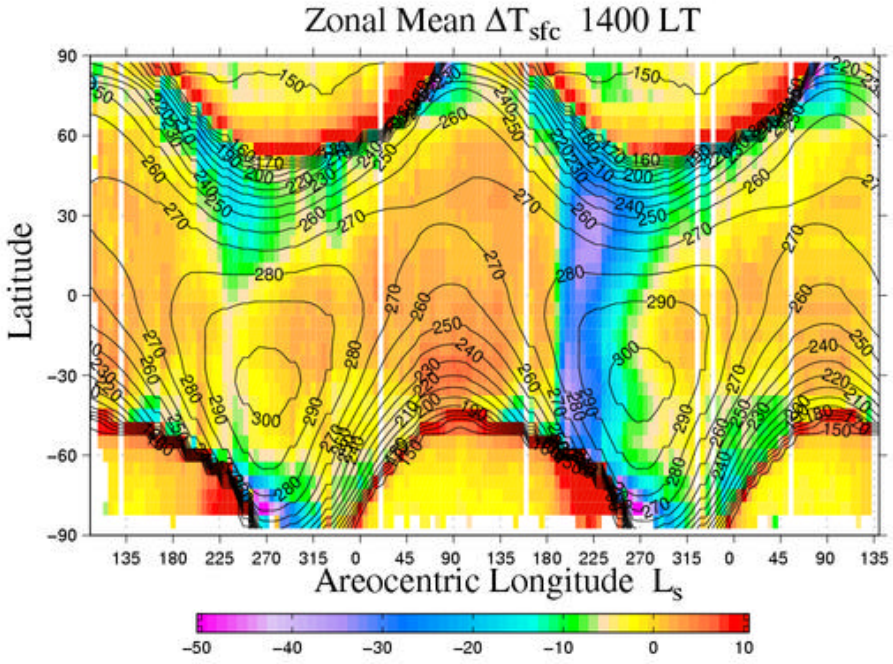

Figure 1. The seasonal evolution of zonally-averaged afternoon surface temperature anomaly derived from TES spectra. Afternoon temperatures nominally correspond to 1400 LT. Predicted surface temperatures from a MGCM simulation employing a low (τ=0.1) atmospheric dust column have been subtracted from the observed surface temperatures to highlight changes in surface temperature due to atmospheric opacity. The simulated surface temperature is contoured. A dusty and/or cloudy atmosphere leads to a decrease in observed afternoon temperature (and an increase in observed morning temperature) relative to the reference simulation. The effects of a regional scale dust storm in the first year (L_s=225°) and a major, planet-encircling dust storm in the second year (L_s=185°) are evident.

ICE KEEL SCOUR MARKS AND ICE FLOE GROUNDING STRUCTURES IN KASEI VALLES AND ECHUS CHASMA. Christopher Woodworth-Lynas and Jacques Yves Guigné, Guigné International Ltd. 685 St. Thomas Line, Paradise, Newfoundland, CANADA A1L 1C1 709 895 3819 chriswl@guigne.com

Introduction: We present further new observations from analyses of Mars Global Surveyor Mars Orbiter Camera images of surficial features interpreted to be the result of interactions between the keels of floating ice masses on submerged sediment [1]. The surface morphology of scour marks typically comprises a curvilinear trough from which seabed material has been ploughed to the sides by the entrenched, moving ice keel, to form two co-linear berms of excavated material.

Background: Scour marks are the seafloor tracks made by floating ice masses as their keels mechanically plough into soft sediments of lake, river or ocean floors. On Earth scour marks are ubiquitous features on the seafloors of the modern Arctic and sub-arctic regions and on the seafloor of the continental margin of Antarctica.

Scour marks commonly survive the transition from submergence to exposure above water level and ancient features are commonly seen, over large areas of southern Manitoba and parts of southern Ontario formerly occupied by glacial Lake Agassiz and glacial Lake Iroquois [2,3]. They are also found on several large islands of the Arctic Archipelago (e.g. King William Island, Victoria island) and are readily identified from aerial photographs. The relic Arctic features were formed in areas formerly submerged below sea level some 10,000 years ago. Scour marks preserved in Pre-Cambrian, Ordovician and Carboniferous/Permian age glacimarine sediments have also been identified on exposed bedding plane surfaces in several localities worldwide [4].

On Earth scour marks form today in water depths from < 5 - 500 m, and fall in the range < 100 m to several kilometers long, 5 - 100 m wide and < 1 - 5 m deep (exceptionally 25 m).

In a preliminary analysis [1] we examined several hundred high-resolution narrow angle images acquired by the Mars Orbiter Camera (MOC). We searched for ice keel scour marks to the margins of Chryse Planitia in the vicinity of an ancient shoreline, Contact 2, proposed by [5] and largely substantiated [6], and to the valley floor regions of the six great valley systems that empty into Chryse: the Mawrth, Ares, Tiu, Simud, Maja and Kasei Valles systems. We chose these regions because floating ice masses, either river ice from the valleys, or sea ice would likely ground and scour in the littoral waters of a river mouth and near-shore region, and that traces of this activity may be preserved on bedding surfaces.

Present work and description of Martian features: We have extended our analysis and interpretation to include much of Echus Chasma (Figure 1) where we have identified features interpreted as multi-keeled scour marks and in one place a zone of multiple, parallel scour marks related to the movement of ice keels locked in a floating ice canopy (Figure 2).

***Networks of Parallel sided Troughs with Berms*:** On the flat valley floor of Kasei Valles and in Echus Chasma we have found networks of curvilinear, intersecting, parallel-sided troughs that meander and intersect with no consistent orientation. The troughs typically are at least 1 km long and some exceed 3 and 4 km and range in width from 10 – 50 m. By observing sun shadows it is possible to distinguish narrow ridges, or berms, on one or both sides of most troughs. In places *multiple, overlapping sub-parallel trough*s coalesce into wide (100 - 300 m), irregular-sided grooved and ridged surfaces.

***Ridge-bounded regions*:** Associated with the troughs are poorly- to moderately well-defined irregular to rounded, smooth, low albedo regions, the margins of which are defined by low continuous ridges. These ridge-defined smooth areas range in size from 200 to 600 m, exceptionally up to 950 m. They may occur as solitary features, but more commonly occur in groups forming jig-saw-like ridge networks. In Echus Chasma these ridge-defined features are larger (in the range 0.5 to 1.0 km) and individual features may contain smaller, well defined jigsaw-like groups of sub-circular regions, that are also defined by ridges of a smaller scale than the larger feature in which they are contained.

In Kasei Valles the *parallel-sided troughs with berms*; the *multiple, overlapping sub-parallel troughs*; and smooth *ridge-bounded regions* are restricted in their occurrence to the lowest and flattest portion of the valley floor (Figure 1) and do not occur at or east of the vicinity of Sharanov crater and are not found on any of the elevated, older grooved surfaces of the Kasei system.

Ridge-defined smooth areas are considerably more common, and of larger scale, in the much wider, flat regions of Echus Chasma. Parallel-sided troughs with berms are less common but multiple troughs (Figure 2) and closely-spaced parallel troughs were found here.

Interpretation: We interpret the small-scale troughs on the floor of the Kasei Valles system as ice keel scour marks made by the bottom-touching keels of floating ice floes. We interpret the associated ridge-defined low albedo regions as grounding pits made by stranded tabular floes. The megaripple-like surfaces on

which the scour marks and grounding pits appear to have formed in the lower Kasei Valles during a period of strong unidirectional down-valley currents. There may have been floating ice present and ice scouring may have occurred during megaripple formation but all traces have been erased by the migrating ripples. As the strong currents associated with the megaripples waned, ice scour marks and ice floe grounding pits formed and were preserved. The meandering tracks of the scour marks point to a significant decrease in unidirectional flow, and suggest that winds may have played a significant role in driving the scouring floes.

We interpret the wide lanes of multiple, overlapping sub-parallel troughs as zones of linear shear in the ice canopy (Stamukhi zones), which are typically regions of intense ice keel scouring of the seafloor e.g. [7, 8].

Discussion and implications: The preserved traces of ice keel scour marks and ice floe grounding pits are restricted to the surface of stratigraphic Kasei unit 2. The scour marks are therefore of early Amazonian age. Scour marks demonstrate:

1. the former presence of a water body;
2. the water body must have been at least seasonally, or perhaps permanently, covered by ice floes;
3. the water area must have been large enough for wind and current to drive the floes forward during ice/seabed interaction.

References:

[1] Woodworth-Lynas, C.M.T. and J.Y. Guigné. 2003. Ice keel scour marks on mars: evidence for floating and grounding ice floes in Kasei Valles. 6th International Conference on Mars. Pasadena, July 20-25th.

[2] Gilbert, R.J., Handford, K.J. and Shaw, J., 1992. Ice scours in the sediments of glacial Lake Iroquois, Prince Edward County, eastern Ontario. Geographie physique et Quaternaire v. 46, 189-194.

[3] Woodworth-Lynas, C.M.T. and J.Y. Guigné. 1990. Iceberg scours in the geological record: examples from glacial Lake Agassiz. In, Glacimarine environments: processes and sediments (J.A. Dowdeswell and J.D. Scourse, eds.). Geol. Soc. Spec. Pub. No. 53: 217-233.

[4] Woodworth-Lynas, C.M.T. and J.A. Dowdeswell. 1994. Soft-sediment striated surfaces and massive diamicton facies produced by floating ice. In: Earth's Glacial Record (Eds. M. Deynoux *et al*.) Cambridge University Press: 241-259.

[5] Parker, T.J. , D.S. Gorsline, R.S. Saunders, D.C. Pieri and D.M. Schneeberger. 1993. Coastal geomorphology of the Martian northern plains. JGR, 98: 11061-11078.

[6] Ivanov, M.A. and J.W. Head. 2001. Chryse Planitia, Mars: Topographic configuration, outflow channel continuity and sequence, and tests for hypothesized ancient bodies of water using Mars Orbital Laser Altimeter (MOLA) data. JGR, 106 (E2): 3275-3295.

[7] Barnes, P.W., D.M. Rearic, and E. Reimnitz. 1984. Ice gouging characteristics and processes, In, The *Alaskan Beaufort Sea - Ecosystems and Environments.* Academic Press, Orlando: 185-213.

[8] Reimnitz, Erk, and P.W. Barnes. 1974. Sea ice as a geologic agent on the Beaufort Sea shelf of Alaska: In, *The Coast and Shelf of the Beaufort Sea*, edited by J.C. Reed, and J.E. Sater, Arctic Institute of North America, Arlington, VA: 301-351.

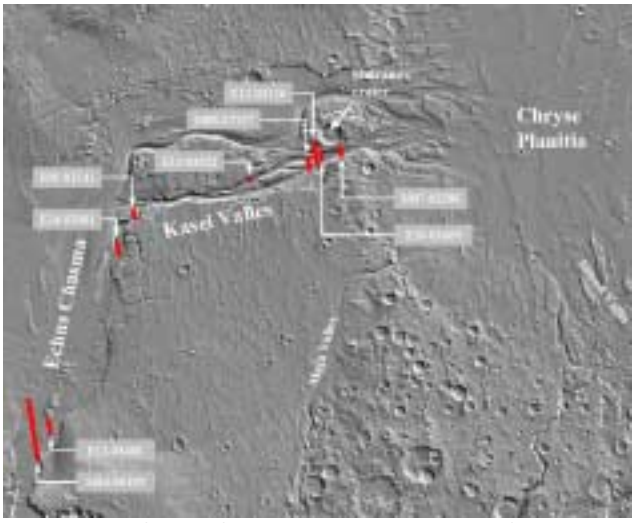

Figure 1 Relief map of Kasei Valles with location of selected MOC images that show ice scour marks and ice floe grounding pits. Context relief image from the Mars 2001 Odyssey THEMIS website (http://themis-data.asu.edu/).

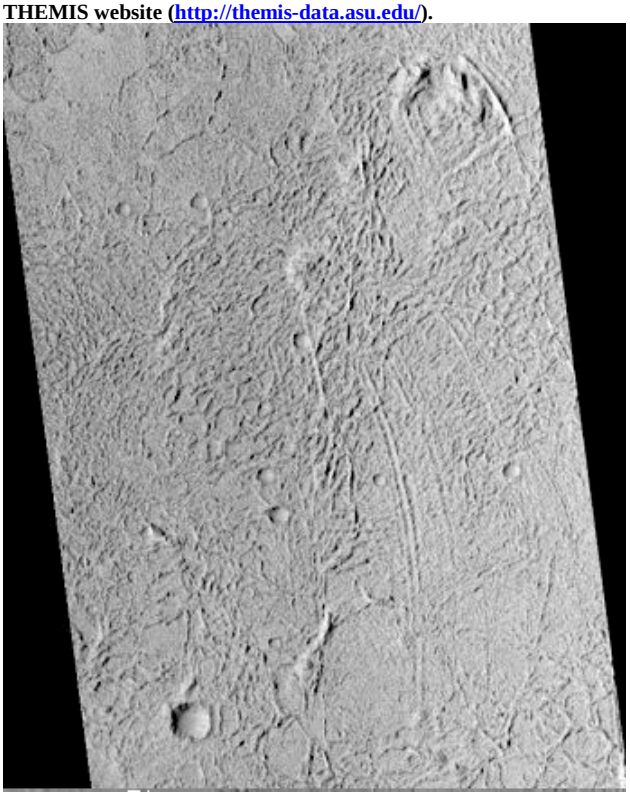

Figure 2 MOC image (southern Echus Chasma) of a 2 km-wide group of curved, wind-driven ice keel scour marks terminating in transverse ice-push ridges. MOC image M14-00193. Scaled pixel width: 11.6 m; Scaled image width: 2.96 km.

ORIGIN OF MGS-TES SURFACE COMPOSITIONS IN THE NORTHERN PLAINS AND POLAR REGION OF MARS. M. B. Wyatt[1] and K. L. Tanaka[2], [1]Department of Geological Sciences, Arizona State University, Tempe, AZ 85287 (michael.wyatt@asu.edu), [2]U.S. Geological Survey, Flagstaff, AZ 86001 (ktanaka@usgs.gov).

Introduction: The largest extent and highest concentrations of the MGS-TES derived Surface Type 2 (ST2) spectral unit, interpreted as an andesitic [1,2] and/or partly altered basaltic composition [3], are mapped in the low-albedo northern lowlands and circumpolar sand seas of Mars [1]. In this study, we examine the relationships between distributions of TES-derived surface compositions and mapped geologic units in the northern polar regions of Mars and integrate Viking, MGS-MOC and -MOLA and MO-THEMIS datasets to constrain theories of the composition, origin, and evolution of these materials.

MGS-TES Background: Studies of low-albedo regions on the martian surface using atmospherically corrected thermal emissivity data from the MGS-TES have identified two distinct global surface spectral signatures [1, 4-6]. The Surface Type 1 (ST1) spectral end-member has been interpreted as an unaltered basalt [1-2, 4], while the ST2 spectral end-member has been variously interpreted as an andesitic [1,2] and/or partly altered basaltic composition [3]. The ST1 surfaces roughly form an equatorial band, restricted to southern highlands and Syrtis Major regions and a few local depostis in the northern plains, capped with ST2 surfaces at mid-latitudes and high-latitudes [7,8]. The transition from ST1 to ST2 compositions at southern high-latitudes appears gradual with no obvious distinguishing boundaries, unlike the topographic dichotomy to the north where plains materials are dominated by ST2 compositions [8]. Detectable abundances of local hematite [e.g. 9], orthopyroxene [e.g. 10], and olivine [e.g. 10] have also been identified in equatorial regions where ST1 basaltic compositions dominate surface units. The mapped distributions of ST1 and ST2 materials indicate that surface compositions are not well correlated with crustal thickeness [8,9].

Northern Plains Geologic Relations: The ST2 surfaces in the northern lowlands correspond with the distribution of low-albedo surfaces, which surround Planum Boreum, cover vast expanses of Vastitas Borealis, and extend in some regions south of 30°N. These surfaces occur on a variety of geologic units, including the VBF, other plains materials, dissected and rugged volcanic flows of Tharsis and Elysium,and circumpolar dunes (Fig. 1).

Part of the ST2 signature in the northern lowlands may be related to chemical weathering caused by water at the surface during periods of high obliquity. The high southern latitudes of Mars (>30°S) also display ST2 materials and do not appear to be generally related to outcrops of volcanic rocks. The correlation with high latitudes may be indicative of modest chemical weathering of basaltic rocks (type ST1) in which liquid water has been present on and near the surface at least periodically, perhaps at times of high obliquity beneath snow packs [11]. The same explanation may hold true for basaltic rocks in the northern plains. However, the TES signature in the northern plains indicates a higher ST2 abundance than the south polar region. Given also the relative youth of northern plains surfaces vs. the southern highlands, it would appear that this obliquity-related mechanism cannot fully explain the northern plains ST2 signature.

In the plains surrounding Planum Boreum, Viking and MOC images show low-albedo dune fields, including the vast Olympia Undae (unit d in Fig. 1), and others near the mouth of Chasma Boreale. These dunes appear to originate from a dark unit containing uneven bedding that forms the base of Planum Boreum and has been interpreted as a sand sea deposit [12]. Geologic mapping of this Boreum unit indicates that it approaches 1000 m in thickness west of Chasma Boreale, was emplaced during the Early Amazonian, and was extensively eroded prior to emplacement of north polar layered deposits that bury much of the unit [13]. The original volume of the dark Boreum unit may have approached that of Planum Boreum, or ~10^6 km^3. If the Boreum unit consists of relatively unaltered andesite, this would suggest a highly eroded, andesite bedrock source. Maximum transport distances for basaltic sand grains on Mars based on models of abrasion and TES observations for saltating materials on Mars indicate maximum transport distances of a few hundred kilometers [8] (we also note that the dark ST1 dunes apparently derived from the ST1 Syrtis Major volcanic flows near Isidis Planitia have not produced a ST1 signature significantly beyond the occurrence of the flows).

The only major source of sand in the vicinity of Planum Boreum is the VBF and associated materials of the Scandia region (unit vb). The VBF materials are generally thought to be clastic sediments derived from catastrophic fluvial erosion of martian highland rocks, (unit f), perhaps emplaced within a temporary, plains-filling ocean [14-15]. Structures within the VBF and Scandia region, including polygonal troughs, pitted and pancake domes, terraces, and depressions, suggest reworking of the VBF materials by near-surface, volatile-driven processes [13]. Because the highland materials have a ST1 TES signature, it would appear that the Boreum unit's ST2 signature must originate by alteration of ST1 rocks, which is consistent with the apparent water-associated emplacement and reworking history of the VBF. The VBF also may likely be the

source of most of the ST2 material throught the northern plains (Fig. 1), because the limited eolian transport distances noted previously preclude an origin from potential dust-covered ST2 highland and volcanic rocks (units h and v) in surrounding terrains.

Early Amazonian volcanic outcrops with ST2 signatures in and near the northern plains include rugged flows in northern Amazonis Planitia that originated near Olympus Mons (unit fr in Fig. 1) and dissected flow deposits in central and eastern Utopia Planitia originating from the Elysium rise thought to be lahars [13,16]. Some have argued that the pitted cones that occur along the margins of the VBF may be silicate volcanoes [e.g., 17], but their geologic associations seem to be more consistent with a sedimentary volcanic origin [13]. In any case, these materials all could have interacted significantly with water during their formation, resulting in weathered basaltic material. Alternatively, the ST2 signatures could result from saltation of VBF fines onto the outcrops or from an original andesite composition for the material.

Origin of the ST2 spectra. The ST2 unit displays the highest concentrations in the northern lowlands regions of Acidalia Planitia and the circumpolar sand seas [1]. Alteration rinds or coatings (i.e., sheet silicates, palagonites, and zeolite) are probably too fragile to resist much eolian abrasion. Silica coatings, however, may be sufficiently resistant to mechanical weathering to survive as coatings or cementing agents that can account for the ST2 spectral shape. Recent work by [18 and references therein] summarizes evidence for the probability of sedimentary silica existing on Mars and emphasizes the highly mobile nature of silica during near surface alteration of basaltic rocks under a wide variety of temperature, pressure, and fluid conditions. Palagonitization is a commonly proposed alteration process for the martian surface and the production of palagonites and secondary clays, both of which have been shown to be spectrally similar to high-silica volcanic glass, result in a high degree of silica mobilization [18 and references therein]. The geologic context of the VBF within a sedimentary basin with either transported or indigenous materials having interacted with surface or near-surface volatile-rich materials [13-14] supports an altered basalt classification for the TES ST2 unit in the northern lowlands.

References. [1] Bandfield J. L. et al. (2000) *Science*, 287, 1626-1630. [2] Hamilton et al. (2001) *JGR*, 106, 14733-14746. [3] Wyatt M. B. and McSween H. (2002) *Nature* 417, 263-266. [4] Christensen P. R. et al. (2000) *JGR*, 105, 9609-9622. [5] Bandfield J. L. et al. (2000) *JGR*, 105, 9573-9587. [6] Smith M. D. et al. (2000) *JGR*, 105, 9589-9609. [7] Bandfield J. L. (2002) *JGR* 107 (E6), 10.1029/2001JE00151. [8] Rogers D. and Christensen P. R. (2003) *JGR*, 108, 10.1029/2002JE001913. [9] Christensen P. R. et al. (2000) *JGR*, 105, 9632-9642. [10] Hamilton V. E. et al. (2002) *LPSC XXXIII*, Abs #1937. [11] Christensen P. R. (2003) *Nature*, 422, 45-48. [12] Byrne S. and Murray B.C. (2002) *JGR* 107, 10.1029/2001JE001615. [13] Tanaka K. L. et al. (2003) *JGR* 108, 10.1029/2002JE001908. [14] Parker T.J. et al. (1989) *Icarus*, 82, 111-145. [15] Baker V. R. et al. (1991) *Nature,* 352, 589-599. [16] Christiansen E. H. (1989) *Geology,* 17, 203-206. [17] Frey H.V. and Jarosewich M. (1982) *JGR,* 87, 9867-9879. [18] McLennan S. M. (2003) *Geology,* 31, 315-318.

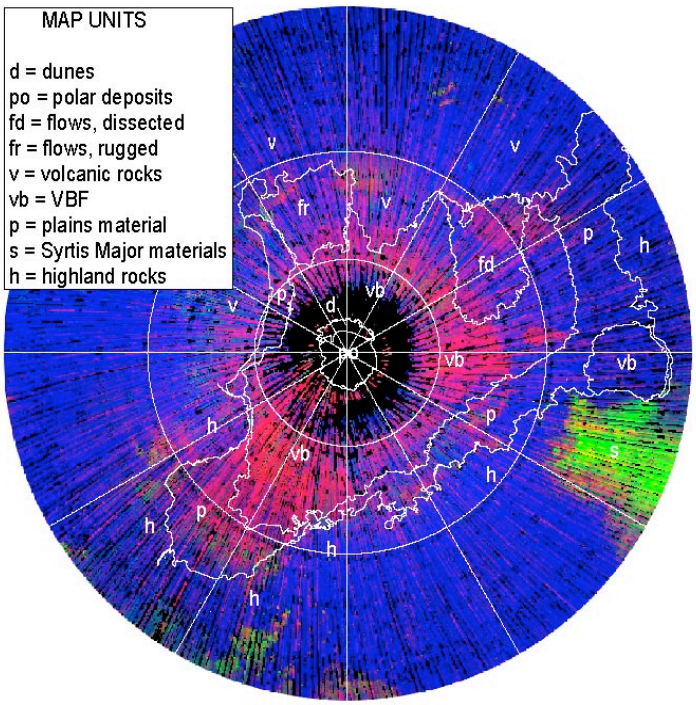

Figure 1. MGS-TES composition map of the northern hemisphere of Mars showing surfaces dominated by ST1 (green; basaltic spectra), ST2 (red, andesitic/weathered basalt spectra), and dust (blue). White lines outline geologic units described in text and generalized from [13].

OBSERVATIONS OF THE SEASONAL POLAR ICECAPS OF MARS AT 1064 nm.
Maria T. Zuber[1] and David E. Smith[2], [1]Dept of Earth Atmospheric and Planetary Sciences, Massachusetts Institute of Technology, 77 Massachusetts Ave. 54-918, Cambridge, MA 02139-4307, e-mail: zuber@mit.edu, [2]Laboratory for Terrestrial Physics, NASA Goddard Space Flight Center, Greenbelt, MD 20771, e-mail: David.E.Smith@nasa.gov.

Introduction. The Mars Orbiter Laser Altimeter (MOLA) [1, 2] is routinely making radiometric observations of Mars at a wavelength of 1064 nm. Although the altimeter function is no longer operational, the MOLA detector [3] continues to measure the reflectivity of the surface. Observations have been obtained almost continuously since the beginning of the Mars Global Surveyor (MGS) [4] mapping mission in February 1999, and are providing measurements relevant to understanding the seasonal cycling of CO_2 surface frost.

Radiometer Data. The field of view of the MOLA detector is approximately 800 μrad and from an altitude of 400 km receives reflected solar radiation from a roughly circular spot ~300 m in diameter. The data are acquired at a rate of 8 Hz and with a ground track velocity of the spacecraft of about 3 km s^{-1} the along-track resolution is slightly less than 400 m, thus providing an almost continuous profiling measurement of Martian surface brightness.

To determine reflectivity, the received optical power can be estimated by a mathematical model that utilizes the MOLA threshold setting and noise counts [5, 6]. Utilizing the link equation [7], observations are normalized to a constant mean solar flux assuming Lambertian scattering to yield a spectral radiance *(I/F)*.

For the purposes of this analysis the data were binned in 1 second time intervals representing a pixel size of 300 m x 3 km. The detector operates at 1064 ± 1 nm and measures the reflected signal strength to about 1%, and the receiver performance closely matches pre-launch testing. For the seasonal variations of interest in the present analysis the stability of the measurement is more important than the absolute calibration.

In this passive mode the radiometry is only obtainable when the surface of Mars is illuminated by sunlight. Further, since the orbit of the spacecraft is approximately sun-synchronous with a 2:00 PM local time the data are generally acquired under similar lighting conditions.

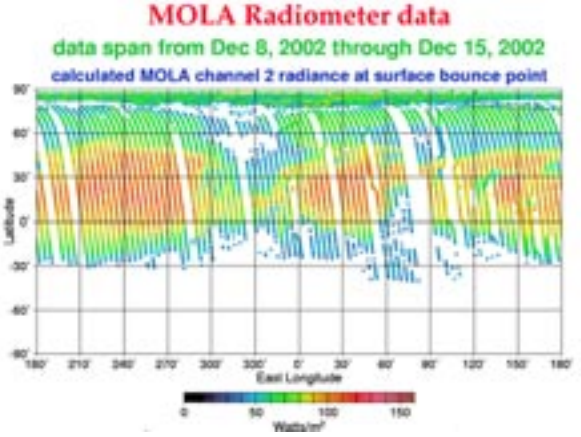

Fig. 1. *Uncalibrated passive radiometry observations acquired by MOLA between Dec 8 and 15, 2002. During the observation period the season was northern summer, with the sun illuminating the northern hemisphere of the planet. An example of the spacecraft being pointed off-nadir is evident in the figure at lat 25° N, 55° E. The spacecraft was traveling from south to north.*

However, the spacecraft instrument deck is not always pointed toward nadir and for much of the last year has been tilted off-nadir

by approximately 16^o in order to save on propellant used for attitude control. Further, the spacecraft is frequently rolled and pitched toward a particular target for camera observations, and the MOLA detector field of view follows the same path (Fig.1).

Seasonal Changes. The radiometry data show clear seasonal brightness changes in the polar regions that are a result of the deposition and sublimation of CO_2 on the surface at the onset of fall and in early spring. Fig. 2 shows the reflectivity at 1064 nm at the beginning of spring and early summer in the 2 hemispheres. Generally, the frost deposition in the north is distributed uniformly in longitude except on the polar cap itself, where the deposition and the sublimation appear to be related to the topography of the cap. In general areas that are less bright are lower in elevation and receive less solar illumination.

In the south the frost covering varies significantly with latitude and longitude (Fig. 2) and some regions appear even in early spring to have lost all their seasonal covering of CO_2. In contrast to the north polar region, the brightest regions do not correspond to those of highest elevation. The residual cap remains bright throughout the year and is probably a result of the exposure of water ice under the seasonal frost.

Seasonal frost on the southern polar residual cap is brighter than in the north and lasts longer in the spring. Both seasonal caps brighten as winter proceeds, and the brightness of both caps oscillates just before the frost sublimates back to the atmosphere, most markedly in the north. This phenomenon is observed in consecutive Martian years.

Observations of the process of frost deposition are more difficult to obtain due to most of the frost at high latitudes being deposited when the region is in darkness. However, the radiometry data do suggest that frost at the higher latitudes actually starts to form on the surface before the end of summer when the sun is approaching the equator but the pole is still illuminated. For the high northern latitudes this appears to begin around L_s= 150^o. The frost covering at both poles appears to have been similar, but not identical, in the two successive Mars years so far studied.

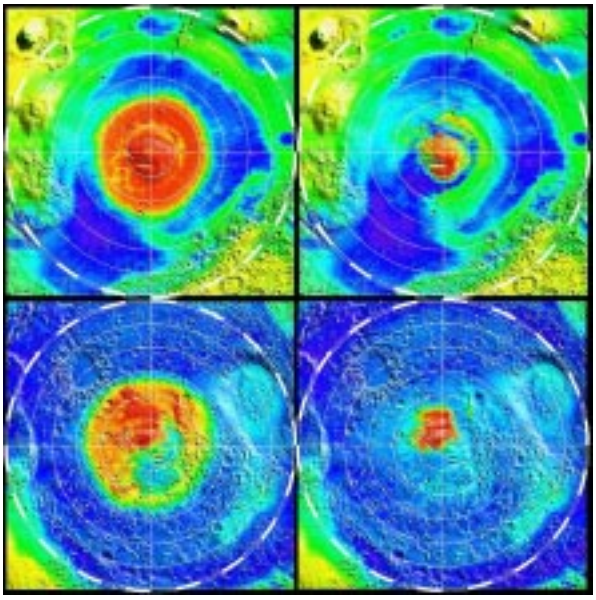

Fig. 2. *Seasonal images of the 1064-nm reflectance in the polar regions in early spring and early summer. The top 2 images are of the northern hemisphere (30^{o}N to pole) for L_s= 32^o (left) and L_s= 12^o (right). Bottom 2 images are of the southern hemisphere (30^o S to pole) for L_s= 212^o (left) and L_s= 272^o (right).*

References. [1] Zuber M.T. et al. (1992) *JGR, 97,* 7781-7797. [2] Smith D.E. et al. (2001) *JGR, 106,* 23,689-13,722. [3] Abshire J.B. et al. (2000) *Appl. Opt., 39, 90,* 2440-2460. [4] Albee A. et al. (2001) *JGR, 106,* 23,291-23,316. [5] Sun, X., et al. (1992) *IEEE Trans. Aero. Elec. Syst.,28,* 268-274. [6] Sun X. et al., (2001) *EOS Trans. Am. Geophys. Un.* [7] Gardner C.S. (1992) *IEEE Trans. on Geosci. Rem. Sens., 30,* 1061-1072.